Nuclear Science

OECD

Utilisation and Reliability of High Power Proton Accelerators

Workshop Proceedings
Daejeon, Republic of Korea
16-19 May 2004



NUCLEAR • ENERGY • AGENCY

Nuclear Science

Utilisation and Reliability of High Power Proton Accelerators

Workshop Proceedings
Daejeon, Republic of Korea
16-19 May 2004

© OECD 2005
NEA No. 6003

NUCLEAR ENERGY AGENCY
ORGANISATION FOR ECONOMIC CO-OPERATION AND DEVELOPMENT

ORGANISATION FOR ECONOMIC CO-OPERATION AND DEVELOPMENT

The OECD is a unique forum where the governments of 30 democracies work together to address the economic, social and environmental challenges of globalisation. The OECD is also at the forefront of efforts to understand and to help governments respond to new developments and concerns, such as corporate governance, the information economy and the challenges of an ageing population. The Organisation provides a setting where governments can compare policy experiences, seek answers to common problems, identify good practice and work to co-ordinate domestic and international policies.

The OECD member countries are: Australia, Austria, Belgium, Canada, the Czech Republic, Denmark, Finland, France, Germany, Greece, Hungary, Iceland, Ireland, Italy, Japan, Korea, Luxembourg, Mexico, the Netherlands, New Zealand, Norway, Poland, Portugal, the Slovak Republic, Spain, Sweden, Switzerland, Turkey, the United Kingdom and the United States. The Commission of the European Communities takes part in the work of the OECD.

OECD Publishing disseminates widely the results of the Organisation's statistics gathering and research on economic, social and environmental issues, as well as the conventions, guidelines and standards agreed by its members.

* * *

This work is published on the responsibility of the Secretary-General of the OECD. The opinions expressed and arguments employed herein do not necessarily reflect the official views of the Organisation or of the governments of its member countries.

NUCLEAR ENERGY AGENCY

The OECD Nuclear Energy Agency (NEA) was established on 1st February 1958 under the name of the OEEC European Nuclear Energy Agency. It received its present designation on 20th April 1972, when Japan became its first non-European full member. NEA membership today consists of 28 OECD member countries: Australia, Austria, Belgium, Canada, the Czech Republic, Denmark, Finland, France, Germany, Greece, Hungary, Iceland, Ireland, Italy, Japan, Luxembourg, Mexico, the Netherlands, Norway, Portugal, Republic of Korea, the Slovak Republic, Spain, Sweden, Switzerland, Turkey, the United Kingdom and the United States. The Commission of the European Communities also takes part in the work of the Agency.

The mission of the NEA is:

- to assist its member countries in maintaining and further developing, through international co-operation, the scientific, technological and legal bases required for a safe, environmentally friendly and economical use of nuclear energy for peaceful purposes, as well as
- to provide authoritative assessments and to forge common understandings on key issues, as input to government decisions on nuclear energy policy and to broader OECD policy analyses in areas such as energy and sustainable development.

Specific areas of competence of the NEA include safety and regulation of nuclear activities, radioactive waste management, radiological protection, nuclear science, economic and technical analyses of the nuclear fuel cycle, nuclear law and liability, and public information. The NEA Data Bank provides nuclear data and computer program services for participating countries.

In these and related tasks, the NEA works in close collaboration with the International Atomic Energy Agency in Vienna, with which it has a Co-operation Agreement, as well as with other international organisations in the nuclear field.

© OECD 2005
No reproduction, copy, transmission or translation of this publication may be made without written permission. Applications should be sent to OECD Publishing: *rights@oecd.org* or by fax (+33-1) 45 24 13 91. Permission to photocopy a portion of this work should be addressed to the Centre Français d'exploitation du droit de Copie, 20 rue des Grands Augustins, 75006 Paris, France (*contact@cfcopies.com*).

FOREWORD

These proceedings contain the papers presented at the Fourth Workshop on Utilisation and Reliability of High Power Proton Accelerators (HPPA), organised by the Nuclear Science Committee of the OECD Nuclear Energy Agency (NEA). The first meeting in this series was held in Mito, Japan on 13-15 October 1998, and the second and the third meetings followed in Aix-en-Provence, France on 22-24 November 1999 and in Santa Fe, NM, USA on 12-16 May 2002, respectively. The fourth workshop was held in Daejeon, Republic of Korea on 16-19 May 2004.

This fourth workshop covered issues related to (1) accelerator reliability, (2) target, window and coolant technology, (3) sub-critical system design and ADS simulations, (4) safety and control of ADS, and (5) ADS experiments and test facilities. In addition, three working group discussions were organised on accelerators, on sub-critical systems and interface engineering, and on safety and control of ADS. Both accelerator scientists and reactor physicists participated.

The fifth workshop in the series is planned to be held in spring 2006 in Belgium.

Acknowledgements

The OECD/NEA gratefully acknowledges the Korea Atomic Energy Research Institute (KAERI) for hosting the Fourth Workshop on Utilisation and Reliability of High Power Proton Accelerators. Special thanks are extended to Ms. Amanda Costa and Ms. Andrea Griffin-Chahid for having prepared the proceedings for publication.

TABLE OF CONTENTS

Foreword 3

Executive Summary 11

Welcome 15

D-S. Yoon
Congratulatory Address 17

I-S. Chang
Welcome Address 19

G.H. Marcus
OECD Welcome 21

GENERAL SESSION: ACCELERATOR PROGRAMMES AND APPLICATIONS 23

CHAIRS: B-H. CHOI, R. SHEFFIELD

T. Mukaiyama
Background/Perspective 25

M. Salvatores
Accelerator-driven Systems in Advanced Fuel Cycles 27

S. Noguchi
Present Status of the J-PARC Accelerator Complex 37

H. Takano
R&D of ADS in Japan 45

R.W. Garnett, A.J. Jason
Los Alamos Perspective on High-intensity Accelerators 57

J-M. Lagniel
French Accelerator Research for ADS Developments 69

T-Y. Song, J-E. Cha, C-H. Cho, C-H. Cho, Y. Kim, B-O. Lee, B-S. Lee, W-S. Park, M-J. Shin
Hybrid Power Extraction Reactor (HYPER) Project 81

V.P. Bhatnagar, S. Casalta, M. Hugon
Research and Development on Accelerator-driven Systems in the EURATOM 5th and 6th Framework Programmes 89

S. Monti, L. Picardi, C. Rubbia, M. Salvatores, F. Troiani
Status of the TRADE Experiment 101

P. D'hondt, B. Carluec
The European Project PDS-XADS "Preliminary Design Studies of an Experimental Accelerator-driven System" 113

F. Groeschel, A. Cadiou, C. Fazio, T. Kirchner, G. Laffont, K. Thomsen
Status of the MEGAPIE Project 125

P. Pierini, L. Burgazzi
ADS Accelerator Reliability Activities in Europe 137

W. Gudowski
ADS Neutronics 149

P. Coddington
ADS Safety 151

Y. Cho
Technological Aspects and Challenges for High-power Proton Accelerator-driven System Application 153

TECHNICAL SESSION I: ACCELERATOR RELIABILITY 163

CHAIRS: A. MUELLER, P. PIERINI

D. Vandeplassche, Y. Jongen (for the PDS-XADS Working Package 3 Collaboration)
The PDS-XADS Reference Accelerator 165

N. Ouchi, N. Akaoka, H. Asano, E. Chishiro, Y. Namekawa, H. Suzuki, T. Ueno, S. Noguchi, E. Kako, N. Ohuchi, K. Saito, T. Shishido, K. Tsuchiya, K. Ohkubo, M. Matsuoka, K. Sennyu, T. Murai, T. Ohtani, C. Tsukishima
Development of a Superconducting Proton Linac for ADS 175

C. Miélot
Spoke Cavities: An Asset for the High Reliability of a Superconducting Accelerator; Studies and Test Results of a $\beta = 0.35$, Two-gap Prototype and its Power Coupler at IPN Orsay 185

X.L. Guan, S.N. Fu, B.C. Cui, H.F. Ouyang, Z.H. Zhang, W.W. Xu, T.G. Xu
Chinese Status of HPPA Development 195

J.L. Biarrotte, M. Novati, P. Pierini, H. Safa, D. Uriot
Beam Dynamics Studies for the Fault Tolerance Assessment
of the PDS-XADS Linac 203

P.A. Schmelzbach
High-energy Beat Transport Lines and Delivery System
for Intense Proton Beams 215

M. Tanigaki, K. Mishima, S. Shiroya, Y. Ishi,
S. Fukumoto, S. Machida, Y. Mori, M. Inoue
Construction of a FFAG Complex for ADS Research in KURRI 217

G. Ciavola, L. Celona, S. Gammino, L. Andò, M. Presti,
A. Galatà, F. Chines, S. Passarello, XZh. Zhang, M. Winkler,
R. Gobin, R. Ferdinand, J. Sherman
Improvement of Reliability of the TRASCO
Intense Proton Source (TRIPS) at INFN-LNS 223

R.W. Garnett, F.L. Krawczyk, G.H. Neuschaefer
An Improved Superconducting ADS Driver Linac Design..... 235

A.P. Durkin, I.V. Shumakov, S.V. Vinogradov
Methods and Codes for Estimation of Tolerance
in Reliable Radiation-free High-power Linac 245

S. Henderson
Status of the Spallation Neutron Source Accelerator Complex 257

TECHNICAL SESSION II: TARGET, WINDOW AND COOLANT TECHNOLOGY..... 265

CHAIRS: X. CHENG, T-Y. SONG

Y. Kurata, K. Kikuchi, S. Saito, K. Kamata, T. Kitano, H. Oigawa
Research and Development on Lead-bismuth Technology
for Accelerator-driven Transmutation System at JAERI 267

P. Michelato, E. Bari, E. Cavaliere, L. Monaco, D. Sertore,
A. Bonucci, R. Giannantonio, L. Cinotti, P. Turroni
Vacuum Gas Dynamics Investigation and Experimental Results
on the TRASCO ADS Windowless Interface 279

J-E. Cha, C-H. Cho, T-Y. Song
Corrosion Tests in the Static Condition and Installation
of Corrosion Loop at KAERI for Lead-bismuth Eutectic 291

P. Schuurmans, P. Kupschus, A. Verstrepen, J. Cools, H. Aït Abderrahim
The Vacuum Interface Compatibility Experiment (VICE)
Supporting the MYRRHA Windowless Target Design 301

C-H. Cho, Y. Kim, T-Y. Song
Introduction of a Dual Injection Tube for the Design
of a 20 MW Lead-bismuth Target System 313

H. Oigawa, K. Tsujimoto, K. Kikuchi, Y. Kurata, T. Sasa, M. Umeno, K. Nishihara, S. Saito, M. Mizumoto, H. Takano, K. Nakai, A. Iwata
Design Study Around Beam Window of ADS 325

S. Fan, W. Luo, F. Yan, H. Zhang, Z. Zhao
Primary Isotopic Yields for MSDM Calculations of Spallation
Reactions on ^{280}Pb with Proton Energy of 1 GeV 335

N. Tak, H-J. Neitzel, X. Cheng
CFD Analysis on the Active Part of Window Target Unit
for LBE-cooled XADS 343

T. Sawada, M. Orito, H. Kobayashi, T. Sasa, V. Artisyuk
Optimisation of a Code to Improve Spallation Yield Predictions
in an ADS Target System 355

TECHNICAL SESSION III: SUBCRITICAL SYSTEM DESIGN AND ADS SIMULATIONS 363

CHAIRS: W. GUDOWSKI, H. OIGAWA

T. Misawa, H. Unesaki, C.H. Pyeon, C. Ichihara, S. Shiroya
Research on the Accelerator-driven Subcritical Reactor at the Kyoto
University Critical Assembly (KUCA) with an FFAG Proton Accelerator 365

K. Nishihara, K. Tsujimoto, H. Oigawa
Improvement of Burn-up Swing for an Accelerator-driven System 373

S. Monti, L. Picardi, C. Ronsivalle, C. Rubbia, F. Troiani
Status of the Conceptual Design of an Accelerator
and Beam Transport Line for Trade 383

A.M. Degtyarev, A.K. Kalugin, L.I. Ponomarev
Estimation of some Characteristics of the
Cascade Subcritical Molten Salt Reactor (CSMSR) 393

F. Roelofs, E. Komen, K. Van Tichelen, P. Kupschus, H. Aït Abderrahim
CFD Analysis of the Heavy Liquid Metal Flow Field
in the MYRRHA Pool 401

A. D'Angelo, B. Arien, V. Sobolev, G. Van den Eynde, H. Aït Abderrahim, F. Gabrielli
Results of the Second Phase of Calculations Relevant to
the WPPT Benchmark on Beam Interruptions 411

TECHNICAL SESSION IV: SAFETY AND CONTROL OF ADS 423

CHAIRS: J-M. LAGNIEL, P. CODDINGTON

P. Coddington, K. Mikityuk, M. Schikorr, W. Maschek, R. Sehgal, J. Champigny, L. Mansani, P. Meloni, H. Wider
Safety Analysis of the EU PDS-XADS Designs 425

X-N. Chen, T. Suzuki, A. Rineiski, C. Matzerath-Boccaccini, E. Wiegner, W. Maschek
Comparative Transient Analyses of Accelerator-driven Systems with Mixed Oxide and Advanced Fertile-free Fuels 439

P. Coddington, K. Mikityuk, R. Chawla
Comparative Transient Analysis of Pb/Bi and Gas-cooled XADS Concepts 453

B.R. Sehgal, W.M. Ma, A. Karbojian
Thermal-hydraulic Experiments on the TALL LBE Test Facility 465

K. Nishihara, H. Oigawa
Analysis of Lead-bismuth Eutectic Flowing into Beam Duct 477

P.M. Bokov, D. Ridikas, I.S. Slessarev
On the Supplementary Feedback Effect Specific for Accelerator-coupled Systems (ACS) 485

W. Haeck, H. Aït Abderrahim, C. Wagemans
K_{eff} and K_s Burn-up Swing Compensation in MYRRHA 495

TECHNICAL SESSION V: ADS EXPERIMENTS AND TEST FACILITIES 505

CHAIRS: P. D'HONDT, V. BHATNAGAR

H. Oigawa, T. Sasa, K. Kikuchi, K. Nishihara, Y. Kurata, M. Umeno, K. Tsujimoto, S. Saito, M. Futakawa, M. Mizumoto, H. Takano
Concept of Transmutation Experimental Facility 507

M. Hron, M. Mikisek, I. Peka, P. Hosnedl
Experimental Verification of Selected Transmutation Technology and Materials for Basic Components of a Demonstration Transmuter with Liquid Fuel Based on Molten Fluorides (Development of New Technologies for Nuclear Incineration of PWR Spent Fuel in the Czech Republic) 519

Y. Kim, T-Y. Song
Application of the HYPER System to the DUPIC Fuel Cycle 529

M. Plaschy, S. Pelloni, P. Coddington, R. Chawla, G. Rimpault, F. Mellier
Numerical Comparisons Between Neutronic Characteristics of MUSE4 Configurations and XADS-type Models 539

B-S. Lee, Y. Kim, J-H. Lee, T-Y. Song
Thermal Stability of the U-Zr Fuel and its Interfacial Reaction with Lead 549

SUMMARIES OF TECHNICAL SESSIONS 557

CHAIRS: R. SHEFFIELD, B-H. CHOI

Chairs: A.C. Mueller, P. Pierini
Summary of Technical Session I: Accelerator Reliability 559

Chairs: X. Cheng, T-Y. Song
Summary of Technical Session II: Target, Window
and Coolant Technology 565

Chairs: W. Gudowski, H. Oigawa
Summary of Technical Session III: Subcritical System Design
and ADS Simulations 571

Chairs: J-M. Lagniel, P. Coddington
Summary of Technical Session IV: Safety and Control of ADS 575

Chairs: P. D'hondt, V. Bhatagnar
Summary of Technical Session V: ADS Experiments and Test Facilities..... 577

SUMMARIES OF WORKING GROUP DISCUSSION SESSIONS 581

CHAIRS: R. SHEFFIELD, B-H. CHOI

Chair: P.K. Sigg
Summary of Working Group Discussion on Accelerators 583

Chair: W. Gudowski
Summary of Working Group Discussion on Subcritical Systems
and Interface Engineering 587

Chair: P. Coddington
Summary of Working Group Discussion on Safety and Control of ADS..... 591

Annex 1: List of workshop organisers 595

Annex 2: List of participants 597

EXECUTIVE SUMMARY

Introduction

Accelerator-driven systems (ADS), i.e. a subcritical system driven by an accelerator in order to sustain a chain reaction, are being considered for their potential use in the transmutation of nuclear waste. The performance of such hybrid nuclear systems depends to a large extent on the specification and reliability of high-power accelerators, as well as on the integration of the accelerator with spallation targets and subcritical systems. Much R&D is still required in order to demonstrate the desired capability as a whole system.

A series of workshops on "Utilisation and Reliability of High Power Proton Accelerators" is thus organised by the Nuclear Science Committee of the OECD Nuclear Energy Agency (NEA). The first meeting in this series was held in Mito, Japan on 13-15 October 1998, and the second and third meetings followed in Aix-en-Provence, France on 22-24 November 1999 and in Santa Fe, New Mexico, USA on 12-16 May 2002, respectively. Accelerator scientists and reactor physicists gathered at the NEA workshops to discuss issues of common interest and to present the most recent achievements in their research.

The present workshop (fourth in the series) took place in Daejeon, Republic of Korea on 16-19 May 2004 and was hosted by the Korea Atomic Energy Research Institute (KAERI).

Topics covered by the workshop

The workshop began with a general session involving 15 invited papers covering large national/ international accelerator programmes and ADS applications. Thirty-eight (38) contributed papers were presented during five technical sessions and three working group discussion sessions were organised. Topics covered by the five technical sessions included:

- accelerator reliability;
- target, window and coolant technology;
- subcritical system design and ADS simulations;
- safety and control of ADS;
- ADS experiments and test facilities.

The three working group discussions covered the following topics:

- accelerators;
- subcritical systems and interface engineering;
- safety and control of ADS.

Summary of the technical sessions

Accelerator reliability

Eleven (11) papers were contributed covering issues on ADS accelerator system designs, subcomponent operation, beam dynamics aspects and SNS commissioning. Regarding the ADS accelerator designs, three out of four designs (European PDS-XADS, Japanese and US SC accelerators, FFAG at Kyoto University) presented at the meeting were based on a superconducting linac solution. As for subcomponent operation, high availability of proton sources, RFQs, PSI beam line operation experimental results and test results with spoke cavities were presented. Aspects of fault tolerance in RF and magnets were discussed. Furthermore, it was reported that analytical and numerical methods can be used to assess sensitivity to fabrication tolerances in such devices as RFQ or periodic beam lines.

Target, window and coolant technology

Nine papers were presented. Recent results were obtained from LBE corrosion loops in Japan and Korea. In the windowless target designs, experimental results of vacuum gas dynamics investigations in the TRASCO programme and those of the vacuum interface compatibility experiment in the MYRRHA programme were reported. Concerning target and beam window designs, the performance of a dual injection tube introduced in KAERI's HYPER target and results of the target and window design study for JAERI's ADS were presented. Two papers from China and Japan were presented on calculation methodologies for spallation isotope yield predictions. Finally, CFD analysis results for an XADS target were reported for both steady state and transient cases from FZK.

Subcritical system design and ADS simulations

Six papers were presented covering research/demo facility designs, conceptual design of a full-scale transmuter, ADS component design and benchmark results on beam trips. Core and/or component design studies from the Kyoto University Critical Assembly (KUCA), the TRADE experiment, the MYRRHA programme, a Cascade Subcritical Molten Salt Reactor (CSMSR) were reported showing a visible convergence for Pb-Bi systems but with a large variety of core designs, fuel options and fuel cycle. Calculation results from the second phase of the NEA ADS beam trip benchmark were presented. These benchmark results included a sensitivity analysis on the main parameters.

Safety and control of ADS

Seven papers were presented. Two papers – very design specific – were presented describing the WP2 results of the PDS-XADS project. The two 80 XADS designs were covered, with the conclusion that a Pb-Bi reactor ADS has significant safety characteristics, particularly if it has a low Δp and a high natural circulation flow rate and if a gas-cooled system has a short period for beam shutoff. Any

pump-driven system will lie between these two. A paper reported that the new Pb-Bi loop can provide neutral circulation, etc., which is useful only for a Pb-Bi system. An interesting paper presented a proposal for dynamic control of an ADS by linking. The use of void boxes with mini cycles was discussed in order to control reactivity swings as well as plans to examine burnable poisons. Finally, a paper compared PDS-ADS Pb-Bi 80 MW and the reactor design considered as part of the EU FUTURE project.

ADS experiments and test facilities

Five papers were presented. JAERI reported the current status of the Transmutation Experimental Facility (TEF) within the framework of J-PARC (Japan Proton Accelerator Research Complex). The TEF consists of TEF-P (transmutation physics experiments with MA nitride fuel) and TEF-T (material irradiation tests). The Czech Republic presented the project SPHINX (spent hot fuel incineration by neutron flux), which is based on a subcritical system with liquid molten fluoride fuel. KAERI presented the HYPER system preliminary design features and the performance analysis for the DUPIC fuel cycle. Numerical comparisons between neutronic characteristics of MUSE4 configurations and XADS-type models with different coolants (Na, Pb/Bi, gas) were reported by PSI. Finally, KAERI presented a paper on the Pb bonding reaction between fuel and cladding, which includes the fabrication process and a thermal stability study on U-Zr fuel.

Summary of the working group discussion sessions

Accelerators

Discussions were held on several topics such as availability, reliability, high intensity and efficiency, etc. After having worked out solutions to some of the key questions (such as *What accelerator type is "best"? → Try SC linac; What are the costs? → First estimates available for prototype machines; What is the energy consumption? → Expected energy efficiency is a maximum of ~50%)*, there are still a few remaining open questions and trying to answer them at present would merely be guesswork. Questions such as *When will what accelerator be fully operational?* and *When will the trip rate reach the desired value?* are still waiting to be answered in the future. The prototypes now under construction will help us in providing answers to these questions and many smaller issues. Details on the discussions can be found in the summary of working group discussion sessions at the end of these proceedings.

Subcritical systems and interface engineering

To understand better the current situation and to identify future R&D needs, six questions were raised: (1) the role of P&T vs. deep geological repository; (2) the role of ADS – only for a transitional period between the present LWRs and the future fast reactor-dominated situation; (3) international co-operation for ADS deployment; (4) window or windowless target – which is the best solution; (5) is there a need for a windowless MEGAPIE experiment; (6) what are the consequences of a window break. Various reactions to each question were discussed and the details can be found in the summary of working group discussion sessions at the end of these proceedings.

Safety and control of ADS

Discussions were held on safety activities, safety guidelines for core melt and design basis accidents, and ADS reactivity control (shutdown, burn-up control). Details on the discussions can be found in the summary of working group discussion sessions at the end of these proceedings. In addition, the working group proposed to the OECD/NEA Nuclear Science Committee a safety-related benchmark as a follow-up activity to the ongoing beam trip benchmarks. The proposed benchmark would consider 800 MW transmuters with Pb-Bi coolant and MA load fuel for both BOC and EOC.

Next workshop

A follow-up workshop has been planned for spring 2006 in Belgium.

WELCOME

CONGRATULATORY ADDRESS

Dr. Dae-Soo Yoon
Director-General
Ministry of Science & Technology (MOST), Korea

Dr. Gail Marcus, Deputy Director-General, OECD Nuclear Energy Agency, Dr. In-Soon Chang, President of Korea Atomic Energy Research Institute, and distinguished scientists from many countries:

It is an honour and pleasure for me to deliver a congratulatory address at the 4th Workshop on the Utilisation and Reliability of High-power Proton Accelerators, held under the auspices of OECD/NEA Nuclear Science Committee. On behalf of the Ministry of Science and Technology of the Korean government and all Korean scientists who are associated with this workshop, I would like to express a warm welcome to all those who are attending.

The Korean government has been pushing a long-term R&D programme with a strong commitment to enhance the capability of nuclear technology development in more systematic and effective ways. In July 1994, the Atomic Energy Commission issued the "Direction to Long-term Atomic Energy Policy Towards the Year 2030". The Direction emphasises the safe and peaceful use of atomic energy under a spirit of pursuing "a better life in harmony with nature".

When I was first informed about this workshop, it was clear to me that the topics addressed deserve our attention and are consistent with our future energy policy. In the scientific sense, proton accelerator technology is cutting edge, and it has a high potential to be applicable to various modern science and industries. Particularly when combined with the accelerator-driven system for nuclear transmutation, I understand that enormous synergic effects will be generated. Projects concerning both proton accelerator constructions and accelerator-driven systems have already been initiated at the Korea Atomic Energy Research Institute as of 1997. The Korean government has also paid much attention to the development of these technologies. The information collected through this workshop will be very useful to determine governmental policy regarding this research and development area.

Furthermore, I think Korean scientists will be exposed to many new, advanced technologies through this workshop. Hopefully, this meeting will also be a good opportunity to provide all the international attendees with a good place to enhance mutual understanding, to exchange information and to foster future collaborations.

Once again I would like to extend a welcome to all of you and I hope you enjoy the scientific and social events during this workshop.

Thank you.

WELCOME ADDRESS

Dr. In-Soon Chang
President
Korea Atomic Energy Research Institute (KAERI)

Ladies and gentlemen, it is my honour to give a welcome address at the 4th OECD/NEA Workshop on the Utilisation and Reliability of High-power Proton Accelerators. Also, I am very pleased to be here with Dr. Gail Marcus, Deputy Director-General of OECD/NEA and the many distinguished guests from abroad.

For the last two decades, the Korea Atomic Energy Research Institute (KAERI) has been devoted to renovating our domestic nuclear power technology to the level of being able to design and construct our own nuclear power plant. Today, KAERI is planning to boost its radiation technology for the betterment of our society. Such radiation technology includes applications of radioactive isotopes, protons, neutrons, laser and heavy ions. As our past research achievements have demonstrated the quality of our work, I am confident that the deployment of our radiation technology will be equally successful.

Although we have performed a sort of feasibility research on proton accelerator construction and applications over several years, we have recently launched a new innovative project, known as the Proton Engineering Frontier Project. In this project, we are aiming not only toward high-power proton accelerator construction, but also practical beam applications for various scientific and industrial areas. Accelerator-driven system research that has been initiated at our research institute since 1997 has also been one of our important projects. We have well understood that the combination of these two technologies will produce a highly efficient energy source which reduces environmental pollution as well. Some anti-nuclear crusaders are saying that radiowastes from nuclear power plants are beyond the control of human beings, and that nuclear power is not eco-friendly, embossing difficulties in the radiowaste handling process. No matter their discourse, we must provide a clear solution for handling the radiowastes induced from the nuclear industry. I believe that this should be a firm mission in our generation, along with pursuing the peaceful use of the nuclear technology for future generations. And, I do believe that development of ADS technology will be a backbone of accomplishing this mission. I am sure this workshop will be a good benchmark for Korean nuclear scientists in this R&D area. All the papers that are being presented in this workshop will be precious assets, useful for our ongoing and future researches.

We are very much honoured by your presence today. It is my hope that the various international collaborations and partnerships will ripen through this meeting.

I hope you have a pleasant time during this workshop with the Korea Atomic Energy Research Institute, and that your stay in Korea is enjoyable. Thank you very much for your attention.

감사합니다

OECD WELCOME

Dr. Gail H. Marcus
Deputy Director-General, OECD/NEA

It is my privilege and pleasure to welcome you all, on behalf of the OECD Nuclear Energy Agency, to the 4th International Workshop on Utilisation and Reliability of High-power Proton Accelerators.

Let me start by describing some of the background of NEA's involvement in this area and our activities related to the theme of this workshop.

In nuclear power generation, the efficient and safe management of spent fuel produced during the operation of commercial nuclear power plants is one of the most important issues, not only to the nuclear community, but also to the general public. The partitioning and transmutation (P&T) of nuclear waste (i.e. the separation of minor actinides and long-lived fission products from spent fuel and transmuting them into short-lived or stable radionuclides in appropriate reactor systems for the reduction of the volume and toxic potential) is complementary to the option of long-term geological disposal of spent fuel and other nuclear waste.

Therefore, P&T has gained increasing attention over the past decade. As a result, the OECD Nuclear Energy Agency, in response to the interest of member countries, has included P&T in its Programme of Work since 1989. I am pleased to note that we co-operate with the European Commission and the International Atomic Energy Agency on many of our P&T activities.

Within the NEA, the P&T project is one example of a horizontal activity involving several divisions and committees. Most of the work on P&T has been and is being undertaken under the auspices of the Nuclear Development Committee (NDC) and the Nuclear Science Committee (NSC).

The NEA biennial information exchange meetings on P&T are a key component of our international collaboration, providing experts with a forum to present and discuss current developments throughout the field. As you may remember, the 7th meeting took place here in Korea two years ago in Jeju. We are now preparing for the 8th meeting, to be held in Las Vegas, USA, in November of this year.

After the completion of two system studies, the Nuclear Development Committee set up, in 2002, an Expert Group on the Impact of Advanced Fuel Cycle Options on Waste Management Policies to analyse a range of future fuel cycle options from the perspective of their impact on waste repository demand and specifications.

Under the auspices of the Nuclear Science Committee, since the early 1990s, various scientific activities in P&T have been undertaken covering nuclear data and computer code validations, physics benchmarks, accelerator applications and separation technologies. In 2000, the NSC established a Working Party on Scientific Issues in Partitioning and Transmutation (WPPT) to better co-ordinate its ongoing activities related to P&T.

To cover the wide range of the P&T field, the WPPT comprises four subgroups: accelerator utilisation and reliability for ADS applications, chemical partitioning, fuels and materials, and physics and safety for transmutation systems. Each subgroup will publish a state-of-the-art report on their specialised field by the end of 2004.

This series of workshops on the utilisation and reliability of high-power proton accelerators is one important activity of the NSC in the field of P&T. It provides a forum for addressing ongoing R&D activities and construction plans related specifically to high-power proton accelerators (HPPAs) being considered in various countries to support basic and applied sciences. These include accelerator-driven nuclear energy systems (ADS) for nuclear waste transmutation and/or energy production. The first workshop was held in Mito, Japan in 1998, the second in Aix-en-Provence, France in 1999 and the third in Santa Fe, USA in 2002. The purpose of this workshop is to provide experts from different fields, such as accelerators, reactor physics, target and window technology, and safety, with a scientific forum for discussing common problems and fostering collaborative research in accelerator-driven systems development. In this regard, I am pleased to note that we have participants from over a dozen countries, including countries outside the NEA.

Before finishing my talk, please let me express my gratitude, on behalf of the NEA, to KAERI for hosting this workshop here in Daejeon, Korea, and to all the organisers and participants for their contributions to this meeting, as well as for their collaboration in this important area.

My best wishes to all of you for a most successful meeting.

GENERAL SESSION

Accelerator Programmes and Applications

Chairs: B-H. Choi, R. Sheffield

BACKGROUND/PERSPECTIVE

T. Mukaiyama
JAIF, Japan

No paper was available at the time of publication.

ACCELERATOR-DRIVEN SYSTEMS IN ADVANCED FUEL CYCLES

M. Salvatores
ANL, USA and CEA Cadarache, France

Abstract

Approximately two decades ago, H. Takahashi revived the concept of accelerator-driven systems to propose it for the transmutation of radioactive nuclear wastes.

In parallel, partitioning and transmutation (P/T) strategies have also been revisited, so as to enlarge the options as concerns waste management. At present, after numerous studies and some experimental demonstrations, it is possible to characterise the different options and strategies, in order to put them into perspective and to offer some practical paths towards implementation.

The framework

The increasing urgency to provide robust and acceptable solutions regarding the problem of waste management and the recognised imperative, whatever is the strategy, to implement deep geological repositories, has provided the framework for most P/T studies. Utilities and industries have participated in these studies with some reluctance, as P/T has been perceived as a costly option, projected in an uncertain, far future.

R&D laboratories have provided most of the effort, and international organisations have been active in this field, since there is a widespread consensus that the attempt to find global solutions to the waste management problem, benefits from wide international collaborations.

A turning point

P/T is a multi-disciplinary endeavour. This is a well-recognised characteristic, reflected in the R&D programmes which have been established in the fields of the chemistry of actinide separation, metallurgy of fuels dedicated to transmutation, liquid metal technologies, nuclear physics at intermediate energies, high power proton accelerator technology, waste forms, etc.

The "building blocks" necessary for P/T implementation are:

- Standard spent fuel reprocessing capability with selected isotope or full non-separated TRU recovery.
- Dedicated fuel fabrication capability: MA-dominated U-free/inert-matrix-based fuels or homogeneous non-separated TRU-bearing fuels.
- Transmutation devices (critical or ADS).
- Dedicated fuel reprocessing capability.

The decision to implement P/T must be supported by demonstration experiments at a significant engineering level for each "building block" and by a global cost/benefit analysis.

In the past, P/T has been mostly conceived as a strategy with the objective to cope with the waste legacy from the past development of nuclear energy. In this perspective, the implementation of P/T and its associated costs are perceived in the framework of a "static" environment, dominated by existing technologies and relatively unfavourable to the development of new technologies to complement the inevitable implementation of a deep geological repository.

Recently, a new perspective has emerged, in which waste minimisation is one of the objectives of future nuclear system development, making P/T part of the assessment of the advanced fuel cycles in support of future reactors.

This is a real turning point which can influence specific developments and priorities in the field of P/T.

Transmutation scenarios and advanced fuel cycles

As far as transmutation and the transmutation device, simple physics considerations allow to make unambiguous comparisons among different systems, in terms of impact on the "transmuter" core characteristics, transmutation performance and impact on the fuel cycle. Detailed examples are given in Ref. [1], where the concepts of neutron balance and of neutron consumption/fission, coupled with a generalisation of the Bateman equations to include specific fuel cycle characteristics, are used to intercompare different LWR and FR systems and different multi-recycling strategies (e.g. selective MA recycling).

Moreover, the potential and possible role of accelerator-driven systems (ADS) has also been widely assessed (e.g. Ref. [2]).

In summary, most of the studies devoted to the assessment of the potential of transmutation in the framework of waste management have pointed out the interest of three major scenarios:

1) *Transmutation of not-separated TRU (e.g. as recovered from the reprocessing of spent fuel from LWRs) in fast reactors*. Whatever the coolant, the generic features of a fast neutron spectrum allow the multi-recycling of the TRU. Moreover, the neutron balance feature of a fast reactor allows flexibility in the design in order to achieve a conversion ratio which can be lower, equal or higher than one, according to the specific strategy objectives.

   This scenario meets the requirements of both sustainability and waste minimisation.

   In fact, the inventory of TRU can be stabilised or decreased, according to the choice of the appropriate conversion ratio, and the waste sent to a repository correspond to the losses at reprocessing. A maximum gain is obtained as far as reduction of the potential source of radiotoxicity, heat load in a repository, and even in terms of non-proliferation resistance.

2) *Selective partitioning of TRU, and transmutation of Am (and possibly Np) in MOX-loaded LWRs*. This scenario can be seen as a temporary option. In fact there are several drawbacks to its application: the inventory of Pu can eventually be stabilised, but not that of Am; the build-up of ^{238}Pu is very significant; there is the need to separate Cm and to envisage a strategy for its storage and the further use of the ^{240}Pu built-up in the process. The potential interest is the use of existing reactors and technologies.

3) *Use of accelerator-driven systems (ADS) to transmute TRU*. This can be done for two different objectives: a) to transmute MA in a "double-strata" perspective, and b) to burn all TRU, in a nuclear energy "phase-out" perspective.

Scenario 1 is the preferred one in the new perspective, as indicated earlier, as it is consistent with the sustainable development of nuclear energy and meets the requirement of waste minimisation without significant penalties as regards the fuel cycle, and even providing increased non-proliferation resistance, since it does not require selective TRU separations.

Scenarios 2 and 3 are to be seen as transition options, in order to temporarily stabilise Pu stocks, while reducing the MA impact on a repository.

In comparing these last two scenarios, one relevant factor is the perceived cost of the deployment of new technologies. In fact, as mentioned above, Scenario 2 does allow using present reactor technology, even if adapted to the specific mission of Am recycling, but requires the development of a

sophisticated technology to separate Cm and the development of appropriate installations for Cm storage, decay and re-utilisation, mostly in the form of ^{240}Pu.

The burden of Scenario 3 is the industrial deployment cost of a new reactor concept, the ADS, beyond the proof of principles phase.

In this context, it is interesting to explore a strategy in which international collaboration is extended from the current phase of basic and supporting R&D, to the practical implementation of the scenario at an industrial level.

A "regional" scenario for ADS-based transmutation deployment

Up to now there has been no attempt to consider the deployment of P/T not only as a national endeavour but rather as a "regional" endeavour.

However, one can imagine regional scenarios [3], wherein countries with different policies and objectives could share regional facilities developed with shared resources, appropriately conceived in order to meet the objectives of the different participating countries. An example is given in Figure 1, where the shared deployment of Scenario 3 by two countries (A and B) is shown, Country A being committed to the use of nuclear energy and having developed reprocessing capability in order to use Pu in LWRs at first, and fast reactors in a more distant future. In order to reduce the burden on a waste repository, this country considers the possibility of deploying a "double-strata" approach. Country B has a legacy of spent fuel and wants to avoid a massive storage in a repository.

Regional facilities can be imagined as shown in Figure 1, with mutual benefits. As an example, the type of ADS to be developed in common, would benefit from the different objectives: in fact Country A if alone, would devote some Pu to make a viable fuel for the ADS in order to burn MA, and Country B, if alone, would face the difficulty of designing an ADS with a Pu-dominated fuel.

The values quoted in Figure 1 for this "blend and burn" scenario are indicative, and a detailed scenario study is underway to quantify mass flows and other fuel cycle characteristics. However, previous studies indicate that, if Country A decides upon the multi-recycling of Pu in existing LWRs, an equilibrium will be reached after 5 , 7 recyclings, and the Pu stocks will stabilise. The build-up of separated MA from Country A spent fuel reprocessing and the existing stocks of Pu and MA of Country B will be used to fabricate the fuel for a rather aggressive introduction of medium-power (~300 MWe) ADS. The number of needed ADS, in terms of power, is defined by the need to absorb the MA production of the power fleet of Country A at equilibrium (~3 t/year) and to keep an optimised ratio of Pu to MA in the ADS fuel (Pu/MA $\simeq$1).

The overall need in terms of installed ADS power is sizable: 6 , 8 GWe, of the order of ~10% of the total nuclear power produced in this scenario.

Which type of ADS?

In Figure 1, we have indicated a generic ADS modular system, each module having a power of ~2 , 300 MWe.

In order to get an idea on the required performance of each module, the following simplified considerations can be made:

- *Hypothesis:*
  - Proton beam energy E_p = 600 MeV.
  - Heavy metal spallation target providing $z = \frac{neutrons}{proton} = 16$.
  - G (number of neutrons/fission in the subcritical core due to the external source, if all the energy produced in it is used to feed the accelerator) = 1.06.
  - Thermal power of the subcritical core W = 500 MWt.
  - MA/Pu ratio in the fuel ~1, to which corresponds a ΔK/cycle $\simeq$1%/$\Delta K/K$/year and $\beta_{eff} \simeq$ 0.15%/$\Delta K/K$.
  - j* (ratio of the importance of the source neutrons to the importance of fission neutrons) $\simeq$1.
- *Energy requirements:*

  The fraction f of energy produced in the subcritical core used for feeding the accelerator depends on the subcriticality level:

$$f \simeq \frac{\nu}{G}\frac{1-K}{K}$$

  If ν (average number of prompt fission neutrons per fission) = 2.8:

f = 2.6% if 1 – K = 0.01
f = 5.3% if 1 – K = 0.02
f = 13% if 1 – K = 0.05

- *Current (power) of the proton beam ip (Wp):*

  If E_f (energy released/fission) $\simeq$ 200 MeV:

$$i_p \simeq \frac{G}{z} W \frac{1}{E_f} \quad \begin{cases} 4.3\ mA & if\ \ 1-K = 0.01 \\ 8.6\ mA & if\ \ 1-K = 0.02 \\ 22\ mA & if\ \ 1-K = 0.05 \end{cases}$$

  which correspond, respectively, to:

$$W_p = \begin{cases} 2.5\ MWt \\ 5\ MWt \\ 12.5\ MWt \end{cases}$$

A few comments on the outcome of these simplified evaluations:

- The subcriticality level choice is a crucial parameter. In fact, it is probably difficult to envisage a deep subcriticality level (e.g. $K = 0.95$), in view of the demanding characteristics of the required accelerator (~12.5 MWt in the beam) and the cost of the energy to feed it.

- The appropriate choice of the MA/Pu ratio, made possible by a regional scenario as the one illustrated in Figure 1, can help to optimise the reactivity swing during irradiation (down to $\leq 1\%/\Delta K/K$), and reduce the accelerator current requirement.

- It is clear that the choice of the primary coolant will have an impact on the safety case and on the minimum margin of subcriticality which is allowable.

- A modular architecture, such as the one shown in Figure 2, can provide a significant degree of flexibility, both in terms of deployment and in terms of operation of the overall system (availability).

- The stringent requirements in terms of accelerator reliability have to be met whatever the type of ADS. However, a modular structure can help to optimise the requirements and their cost/benefit impact.

- If the subcritical level is chosen in the range $K = 0.97$, 0.98, it will be very relevant to demonstrate the safe operation of an ADS in the "transition" from a "source-dominated" to a "feedback-dominated" regime.

- The continuous and effective monitoring of the subcriticality level will be mandatory, and appropriate experimental techniques should be developed and demonstrated.

- The overall layout of a modular system, such as the one of Figure 2, will require a careful evaluation and optimisation of the shielding structures to optimise costs.

The European Integrated Project EUROTRANS

European R&D organisations, universities and industries have been co-operating over the past decade in order to assess the potential of ADS-based transmutation, to perform basic research in the different scientific and technological domains of relevance to ADS and to define a common platform for the development of that strategy.

The three major outcomes of these activities are:

- The document *A European Roadmap for Developing Accelerator-driven Systems (ADS) for Nuclear Waste Incineration*, issued by the European Technical Working Group, chaired by Professor Rubbia in 2001.

- Launching of experimental programmes to validate the major ADS components (MUSE for neutronics of the subcritical core, MEGAPIE for flowing Pb-Bi target and IPHI for high power proton accelerator injector, etc.).

- R&D programmes with EU funding in the domains of ADS design, fuel development, HLM technology, nuclear data.

For the Sixth Framework Programme of the EU, a new Integrated Project, IP-EUROTRANS, is being proposed for funding, with the objective to streamline all R&D efforts towards the assessment of the feasibility of a European Facility for Industrial Transmutation.

The proposed project (to be co-ordinated by J. Knebel of FZK-Germany) is structured in DOMAINS (DM, see Table 1), and should start in 2005.

The EFIT ADS could represent the first model of the modular system described in Figure 2.

Conclusions

The perceived role of P/T has evolved from an optional strategy aiming to reduce the burden on a deep geological storage, to an integral component of future nuclear systems. In this new perspective "transmutation" is achieved in an optimum manner in a fast neutron reactor, with the homogeneous recycling of not-separated TRU.

Specialised devices like ADS can play a role in a transition scenario between the present LWR-dominated to a future FR-dominated situation.

In any case, the ADS deployment can hardly be considered by a single country in isolation, and a "regional" approach, wherein countries with rather different policies in terms of nuclear power development can join efforts to develop shared facilities, is a practical solution.

In the case of a regional scenario for ADS-based transmutation, a modular concept seems to be the most promising. Each module could be an ADS of intermediate power (2-300 MWe or lower), fed by a proton accelerator with ~5 MWt of power in the beam.

The decision to go ahead with ADS-based transmutation can only be made if significant demonstrations of feasibility in all the domains (reprocessing and separation of TRU from commercial power plants, ADS design, dedicated fuel, reprocessing of irradiated dedicated fuel) are available to decision makers, accompanied by sound cost evaluations.

The IP-EUROTRANS, proposed for funding to the EU, is an essential initiative to meet that objective.

REFERENCES

[1] Salvatores, M., *et al*., "The Physics of TRU Transmutation – A Systematic Approach to the Intercomparison of Systems", *Proc. Int. Conf. PHYSOR 2004*, Chicago, IL, 25-29 April 2004.

[2] "Accelerator-driven Systems (ADS) and Fast Reactors", *Advanced Fuel Cycles*, OECD Nuclear Energy Agency, Paris, France (2002).

[3] Salvatores, M., "Nuclear Fuel Cycle Strategies Including P/T", *Annual Meeting on Nuclear Technology 2004*, Düsseldorf, Germany, 25-27 May 2004.

Table 1. IP-EUROTRANS structure

DM1 DESIGN	Development of a reference design for a European Facility for Industrial Transmutation (EFIT) with a power of up to several 100 s MW(th). The coolant for the reference design of the core and the spallation target is a heavy liquid metal (Pb-Bi), but Pb and gas cooling are to be considered as back-up solutions for the core as well. An interconnected and consistent objective is to undergo a more detailed design activity leading to a short-term experimental demonstration of the technical feasibility of Transmutation in an Accelerator Driven sub-critical System (XT-ADS), i.e. demonstration starting at the least within the next 10 years. The latter facility is representing the first-of-a-kind of the EFIT system.
DM2 TRADE-PLUS	Design, realisation and operation of the experimental facility TRADE to demonstrate the coupling between proton accelerator, spallation target and subcritical blanket at sizeable power (several 100 kWs) in the presence of thermal reactor feedback effects. The expected outcomes of this domain – in terms of proof of stable operability, procedures for start-up and shutdown, reactivity monitoring, dynamic behaviour, response to accelerator beam trips and definition of licensing issues of an ADS – are crucial for and give input to the future realisation of the EFIT and XT-ADS (see DM1 DESIGN).
DM3 AFTRA	Design development and qualification in representative conditions of a U-free fuel concept for the EFIT, compatible with the reference design studied in DM1 DESIGN. Ranking of different fuel concepts according to their main out-of-pile properties, their in-pile behaviour and their predicted behaviour in normal, transient operating conditions, safety performance in accidental conditions at the end of the project. Recommendations about fuel design and fuel performance of the most promising fuel candidate(s).
DM4 DEMETRA	Improvement and assessment of the heavy liquid metal (HLM) technologies and thermal-hydraulics for application in ADS, and in particular to EFIT and XT-ADS, where the HLM could act both as spallation material and primary coolant; characterisation of the reference structural materials in representative conditions (with and without irradiation environment) in order to provide the data base needed for design purposes (fuel claddings, in-vessel components, primary vessel, instrumentation, target container, beam window, etc.).
DM5 NUDATRA	Improvement and assessment of the simulation tools and associated uncertainties for ADS transmuter core and shielding design. The activity is essentially focused on the evaluated nuclear data libraries and reaction models for materials in transmutation fuels, coolants, spallation targets, internal structures, and reactor and accelerator shielding, relevant for the design and optimisation of the EFIT and XT-ADS.

Figure 1. Regional "blend-and-burn" scenario (R2B)

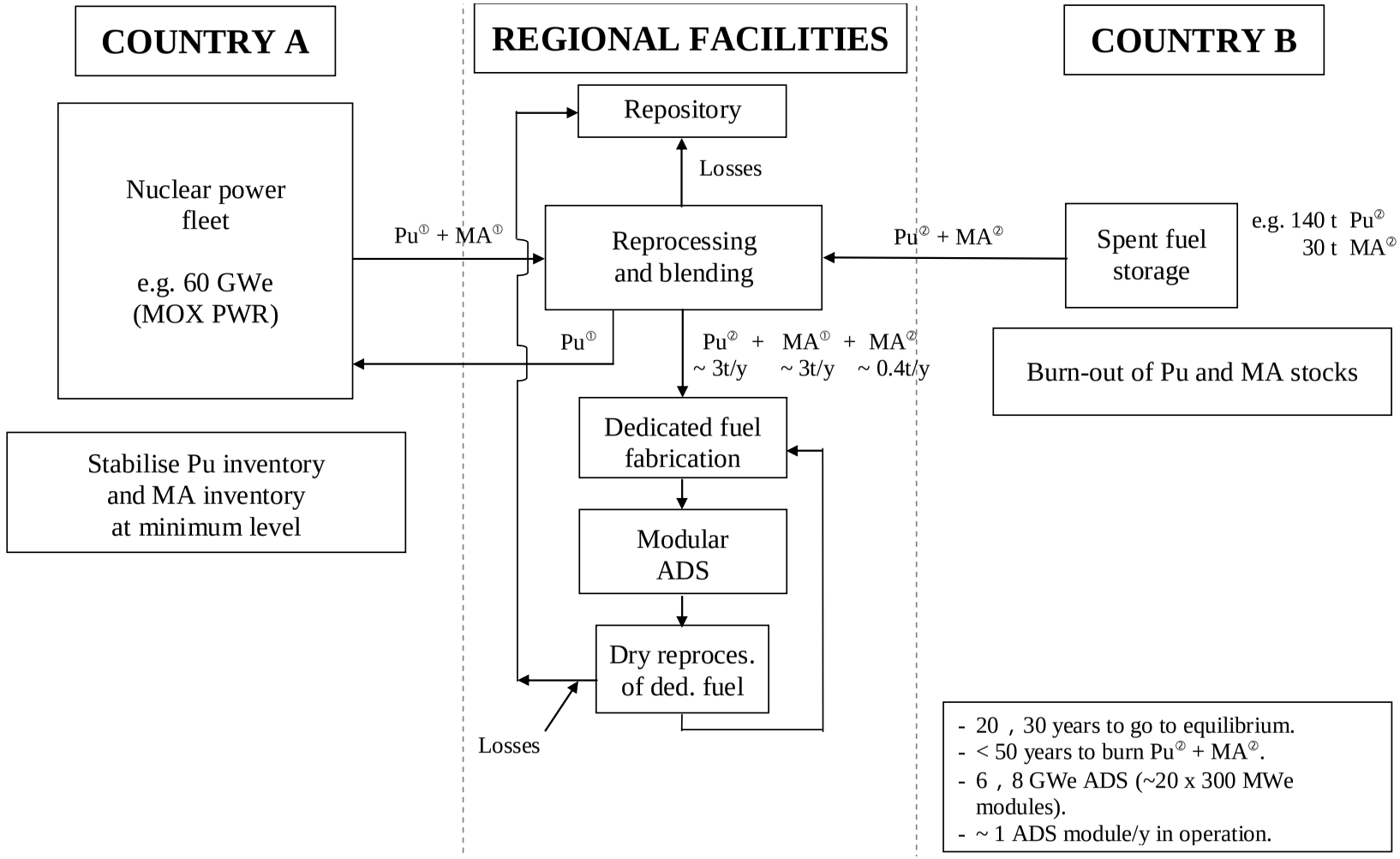

Figure 2. “Regional” concept for waste transmutation with modular ADS

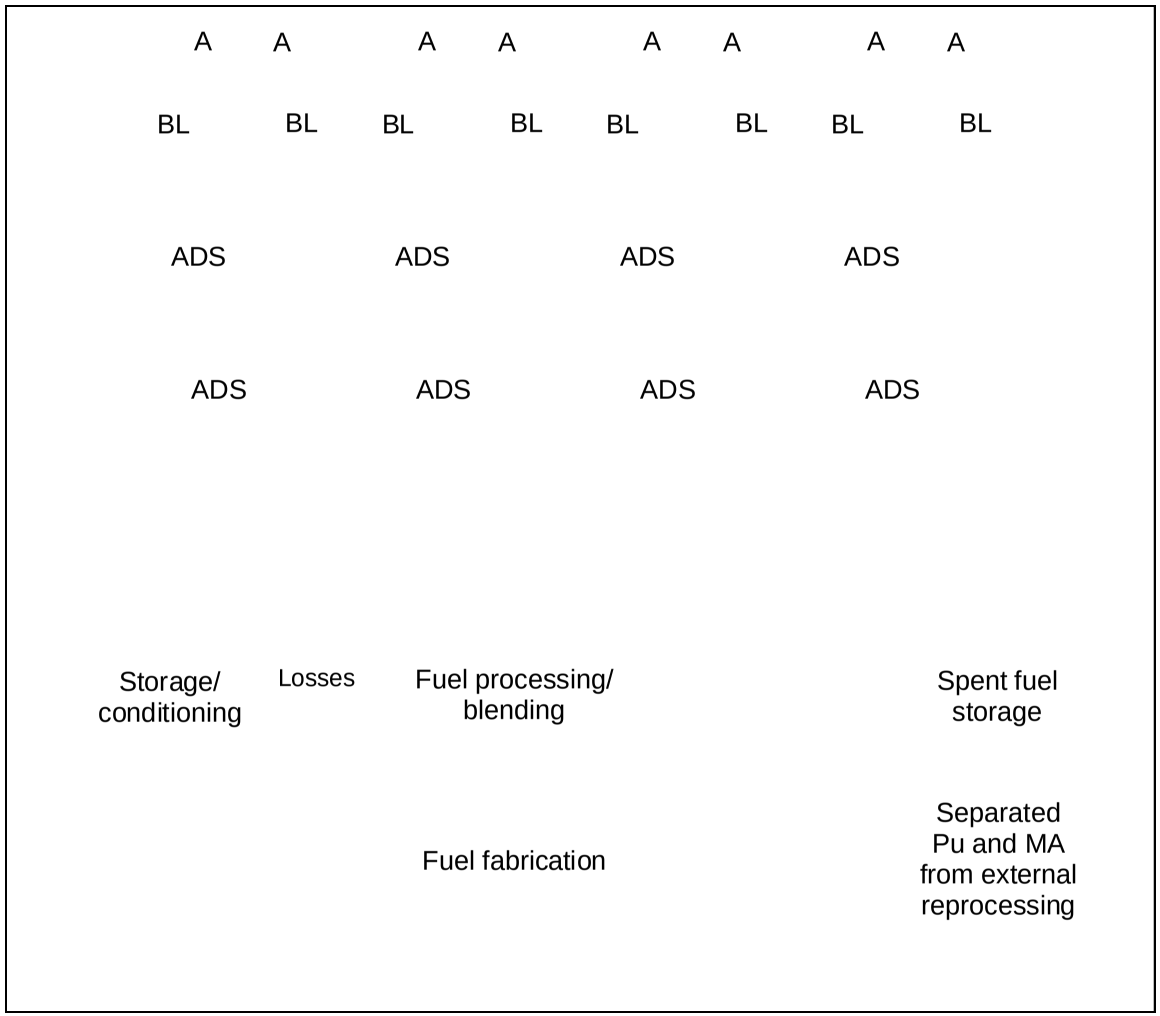

A : Proton accelerator - Ep ≃ 600 MeV
i_p ≃ 5 , 10 mA

BL : Beam transport line

ADS : ~ 500 MWt
K ≃ 0.98 ΔK/cycle ≃ 1 % ΔK/K
f ≃ 5 % (fraction of energy to feed A)
Pu/MA ratio in the fuel ≃ 1.

Total power: ~ 4 000 MWt

fi 2 , 3 of such installations for e.g. Europe?

① COUNTRY B: Spent fuel stock

② COUNTRY A: Nuclear power fleet with minimisation of wastes

PRESENT STATUS OF THE J-PARC ACCELERATOR COMPLEX

Shuichi Noguchi
KEK, High Energy Accelerator Research Organization
1-1 Oho, Tsukuba, Ibaraki, 305-0801, Japan

Abstract

The construction of the J-PARC accelerator complex is proceeding rapidly at the JAERI Tokai site. The key concepts related to this accelerator complex are high power, low beam loss and high availability. A brief description of the project and the status of the construction are presented.

Introduction

Construction of the Japan Proton Accelerator Research Complex (J-PARC) facilities [1] began in 2001 as a joint programme of Japan Atomic Energy Research Institute (JAERI) and High Energy Accelerator Research Organization (KEK), subsequent to their respective efforts on high-intensity proton facilities, JAERI's Neutron Science Project (NSP) in JAERI [2] and the KEK's Japan Hadron Facility (JHF) Project [3,4]. In order to meet a variety of requirements regarding beams, the accelerator complex [5] consists of a 600-MeV linac, a 3-GeV rapid-cycling synchrotron (RCS) and a 50-GeV synchrotron (MR) as shown in Figure 1. The 400-MeV normal-conducting linac is designed so that it can accelerate a beam of 50 mA at 50 Hz and 10% duty. In the second phase of the programme, a 200-MeV superconducting linac (SCL) will be added, which boosts the beam energy to 600 MeV and delivers a beam of 50 mA at 25 Hz to the ADS experimental facility. The 400-MeV chopped beam is injected to RCS at 25 Hz. Then the 3-GeV beam of 333 mA and 1 MW is delivered to the Material and Life Science Experimental Facility (MLF). About 5% of the 3-GeV beam is injected to MR every 3.5 sec. The 50-GeV beam is either slowly extracted to the Nuclear and Fundamental Particle Experimental Facility (NPF) or fast-extracted to the Neutrino Experimental Facility at Kamioka, about 300 km west from Tokai. The accelerator system is really complex. For example, each facility has several modes, where the requirements for the beam are different. The number of combinations of beam delivery modes thus becomes very large.

Figure 1. The layout of J-PARC facilities

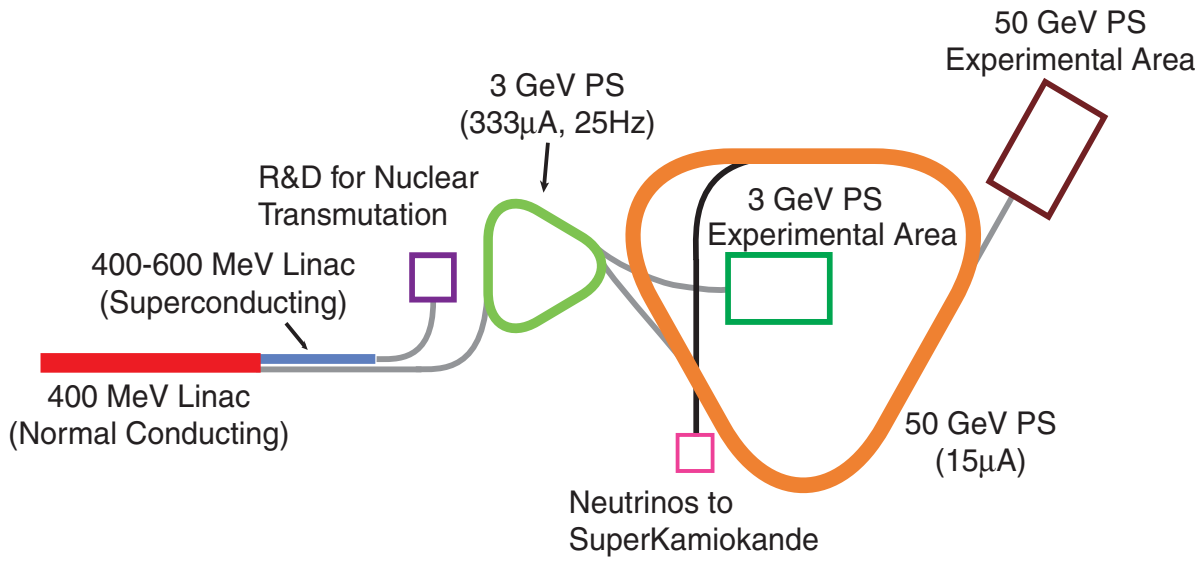

In parallel with civil engineering and hardware components design works and construction, the accelerator design study has been continued extensively and more accurately. As a result, the acceptance, circumference and the injection system of RCS were changed so that it has a greater margin for the allowable beam loss. There are two other important changes as follows:

1) Partly because of the above changes for RCS and cost overrun of various hardware components, the linac energy was lowered to 181 MeV. Thus the target performance of the 3-GeV RCS is now 0.6 MW.

2) The construction of the neutrino beam line was approved as a five-year programme starting in 2004. However, the construction schedule of Phase 1 was delayed by one year.

The present schedule is shown in Figure 2. The contracts for the major accelerator components have been completed and the energy recovery scenario has been established.

Figure 2. Revised construction schedule

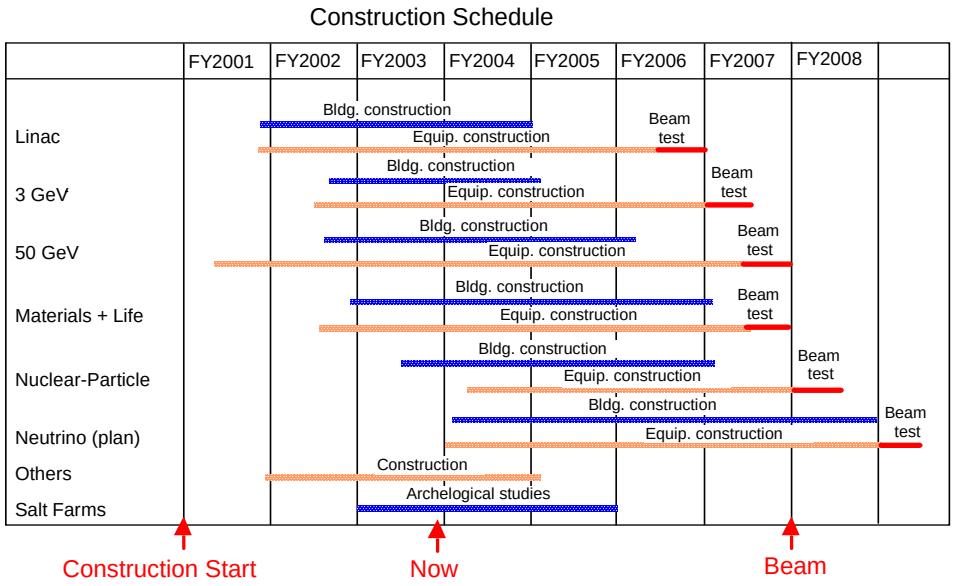

Linac

The layout of the linac is shown in Figure 3. The H^- beam is accelerated by an RFQ, a drift-tube linac (DTL), a separated-type drift-tube linac (SDTL) and annular coupled accelerating structures (ACS). Then the beam is transported to RCS through a long section designated L-3BT. Here the beam momentum is compressed within 0.1% by two debunchers and beam hallow over 4 πmm • mrad (normalised) is scraped. As mentioned before, the construction of ACS is postponed and SCL will be constructed during Phase 2. Since two SDTL tanks are used as debunchers for momentum compression, the linac energy becomes 181 MeV. Frequencies of RF components up to SDTL are set at 324 MHz so that klystrons can be used and electric Q-magnets can be contained in drift tubes of the DTL. The adoption of the electric Q-magnets provides great flexibility as concerns the focusing scheme. Frequencies of ACS and SCL are 972 MHz, and their prototypes are under construction.

Figure 3. Linac layout

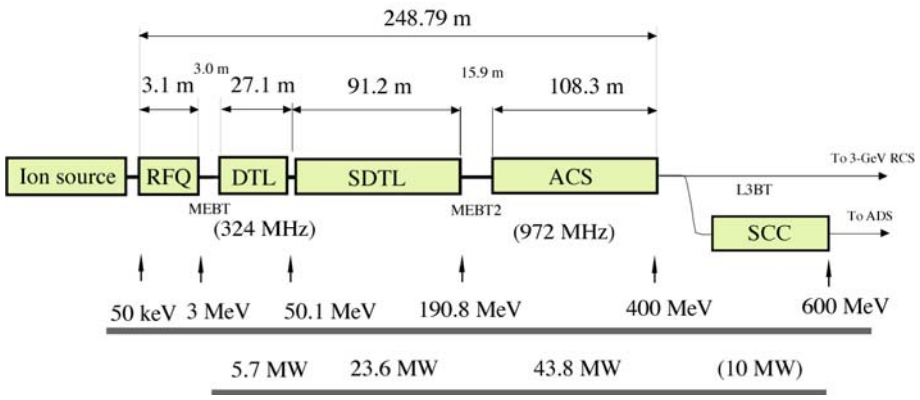

At the commissioning of the linac, the existing H^- ion source and RFQ, which were established for the JHF project and are under beam testing in KEK, will be used. The 50-keV H^- beam is accelerated to 3 MeV by a 3-m long RFQ. The RFQ (Figure 4) is assembled by bolting four machined quadrants, and placed in a vacuum chamber. The mixing of a dipole mode and a quadrupole mode is avoided by perturbing bars called the p-mode Stabilising Loop (PISL). This front-end system has already satisfied the design specification. These will be replaced by a new system being developed for 50-mA operation when the linac energy is recovered to 400 MeV.

Figure 4. Inside view of the RFQ

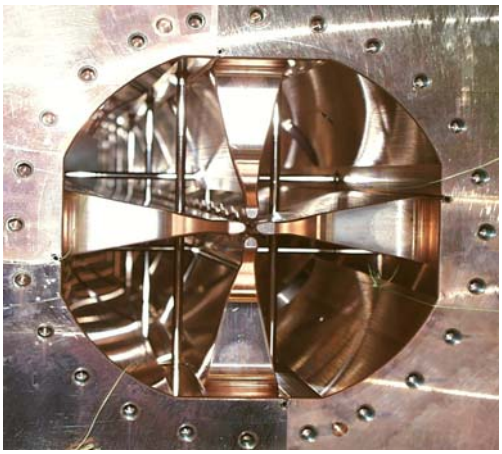

Bunching, chopping and matching of the output beam from RFQ are done in the MEBT-1. The beam is deflected by two RF cavity type choppers by about 10 mrad, and scraped. The chopping factor is 54%, and bunch trains of about 0.5 msec are injected into two RF buckets of RCS. To achieve a sharp cut, the Q-value is lowered by two strong RF coupling loops to about 10. The bunches partially deflected and accepted by DTL (Figure 5) with a rise and fall time of about 15 nsec are scraped by other scrapers set downstream. Pre-chopping is indispensable to lower the heat load to the first scraper. This is performed by accelerating/decelerating the 50-keV beam with an induction cavity and using a transmission property of RFQ.

Figure 5. DTL in the KEK tunnel

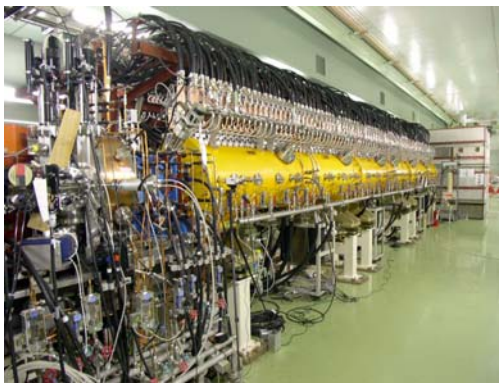

Three DTL tanks accelerate the beam to 50 MeV. They are equipped with post couplers to stabilise the accelerating field. The first tank is being commissioned at KEK. After DTL, 32 SDTL follow. Two SDTL are driven by one klystron. Both DTL and SDTL are made of iron and Cu plated by the periodic reverse method, which gives higher Q-values and less outgas.

RCS

RCS is designed to accelerate $8.3 \cdot 10^{13}$ protons per pulse at a repetition rate of 25 Hz, maintaining a beam loss below hands-on maintenance level (1 W/m). It has a three-fold and mirror symmetric lattice (Figure 6 and Table 1). One of three long straight sections is used for a H^- injection system and a beam collimator system. The other two are used for an RF system and an extraction system, respectively. The main features of the lattice are a higher transition energy than 3 GeV and a wide tuning range for the betatron tune. The high transition energy is realised by a missing bend lattice and the avoidance of possible beam loss at the transition energy. The wide tuning range of the betatron tune is realised by seven independently powered Q-magnet families.

Figure 6. RCS layout

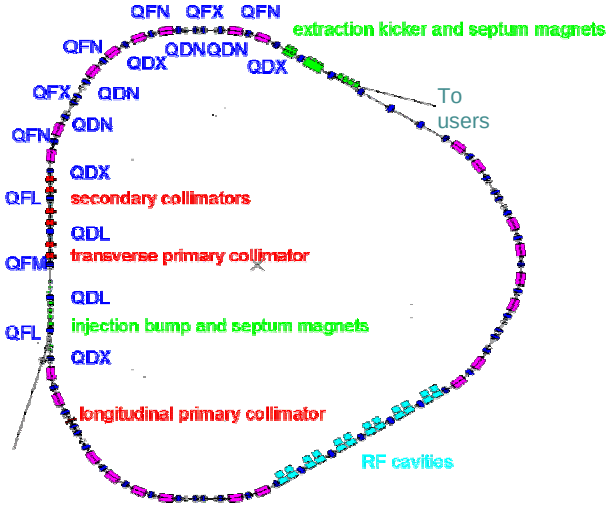

Table 1. RCS main parameters

Beam parameters	
Injection energy	400 MeV
Extraction energy	3.0 GeV
Repetition rate	25 Hz
Harmonics	2
Output power	1.0 MW
Lattice parameters	
Circumference	348.333 m
Cell structure	(6 FODO arc + 3 FODO insertion) · 3
Nominal tune	(6.72, 6.35)
Natural chromaticity	(-8.5, -8.8)
Transition g	9.14
Momentum compaction	0.012

The most important and difficult part of RCS is the injection system shown in Figure 7. In order to maintain the betatron tune shift due to the space-charge effect below the design value (-0.24), a charge exchange and painting injection scheme is adopted. The painting is done in a 6-D phase space. About 500 bunch trains are injected into two RF buckets of RCS during a 500 msec period. Eight bump magnets are used for a horizontal painting. The vertical painting is performed by a pair of pulse steering

Figure 7. Layout of the RCS injection system

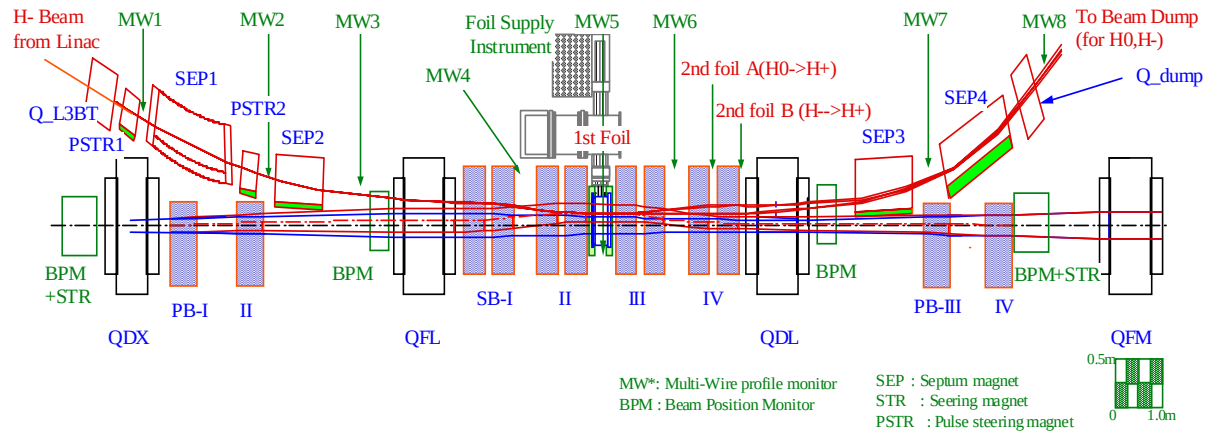

magnets located in the injection beam line. The painting in the longitudinal phase space is undertaken by the sinusoidal magnetic excitation pattern at injection and momentum offset. A carbon foil of ~0.3 mg/cm^2 thick is used to strip electrons of H^-. Escaping H^- and H^0 pass the second foils, are changed to H^+ then led to a beam dump.

Using the Laslett formula for the space charge tune shift, and an expected value of 0.27 for the bunching factor and the design tune shift of -0.24, the painting emittance becomes 216 πmm • mrad (normalised). Taking a margin for the emittance growth or hallow formation, the collimator acceptance and physical aperture are set at 324 and 486 πmm • mrad. If the tune shift is larger and the beam loss is larger than expected, the second harmonic RF will be added to increase the bunching factor. In the case of 181 MeV injection, the number of protons which gives the same tune shift is 1/3 of the 400 MeV case. As radioactivity is proportional to loss power, however, more beam loss is tolerable in the 181 MeV case. The tracking simulation shows that an output power of 0.6 MW can be achieved.

Very rapid acceleration in RCS requires high accelerating voltage, about 500 kV, for an RF system. A usual ferrite-loaded cavity cannot be used at a higher field of ~200 Gauss, so it cannot fit in our straight section. The RF system can be simplified by using magnetic alloy (MA). MA has a constant permeability at higher filed of some kGauss with a reasonably low loss. Moreover, Q is very low, only several, so the second harmonic RF can be superposed. A MA and a MA loaded cavity are shown in Figures 8 and 9. The same type of MA loaded cavities are used in MR. The other problem resulting from rapid ramping is eddy current. All the beam ducts in the magnets are made of Al_2O_3 coated by TiN inside and a Cu strip plated outside for RF shielding. Brazing of 50 cm units is used to make long (~3 m) ducts. For the coil of magnets, aluminium stranded cable made from 72 insulated wires of 3 mm in diameter is used.

Most of the extracted beam is transported to MLF and four pulses (eight bunches) are transported to MR every 3.5 sec. The transport line from RCS to MR is about 200 m long, where the beam is collimated within 54 πmm • mrad and shifted down by 4.3 m.

MR

MR is designed with a similar philosophy as RCS and has a similar shape of 9/2 times larger circumference. The harmonic number is 18, so more bunches can be injected if necessary. Three 120-m long straight sections are used for an injection system, a slow extraction system and a fast extraction

Figure 8. MA core

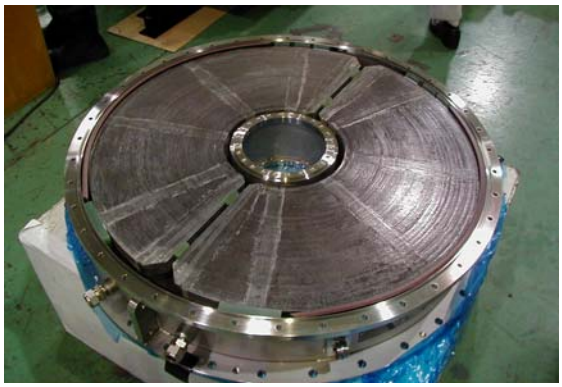

Figure 9. MA-loaded cavity

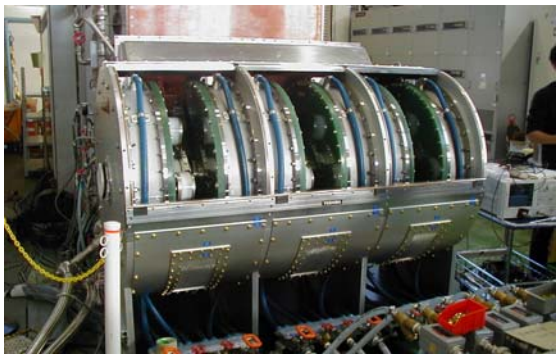

and an RF acceleration system. Because of the very large inductance of the magnet system, both powers necessary for excitation and coming back during fall time are very large. This power variation is not tolerable for the main power line from the power plant, and a fly-wheel system is necessary. The maximum energy of MR is limited to 40 GeV for the fast extraction mode and to 30 GeV for the slow extraction mode until the fly-wheel system is installed in Phase 2. Coasting beam is slowly extracted at the flat top of 0.7 sec by using the third-order betatron resonance. The protons having large betatron amplitude come into the electro-static septum (ESS), where they are kicked by -0.2 mrad then led to septum magnets for extraction. In order to reduce the beam loss by scattering, ESS is made of thin tungsten wires of 100 μm in diameter. The estimated beam loss is ~0.3% for a 1.5-m long ESS.

Superconducting magnets

Twenty-eight (28) combined-type superconducting magnets with an acceptance of 200 πmm • mrad are used in the neutrino beam line. This is the first application in the world and can reduce the cost as compared with the separated function type. The required cooling power is about 1 kW at 4.2 k.

Summary

The construction of the J-PARC accelerator complex is proceeding rapidly. The installation of accelerator components will start in April 2005. Although the completion of Phase 1 was extended by one year, and linac energy was lowered to 181 MeV, the schedule remains tight. Many efforts are necessary to maintain the schedule and achieve the target performance as quickly as possible.

Figure 10. Superconducting magnet

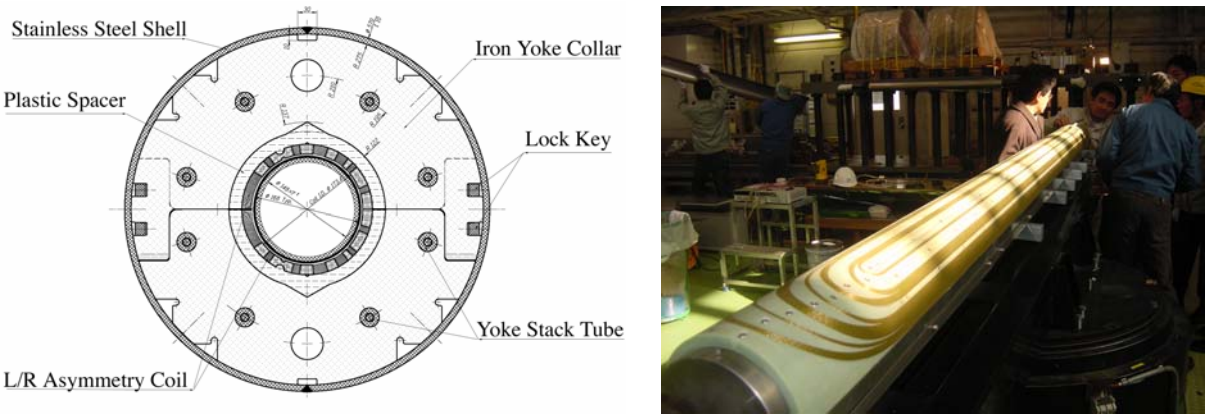

REFERENCES

[1] *The Joint Project for High-intensity Proton Accelerators*, KEK Report 99-4, JHF-99-3 and JAERI-Tech 99-056(1999).

[2] Mizumoto, M., *et al*., "A High Intensity Proton Linac Development for the JAERI Neutron Science Project", *Proc. 1998 Linac Conf*., p. 622 (1998).

[3] JHF Project Office, *Proposal for Japan Hadron Facility*, KEK Report 97-3, JHF-97-1.

[4] JHF Project Office, *JHF Accelerator Design Study Report*, KEK Report 97-16, JHF-97-10.

[5] *Accelerator Technical Design Report for J-PARC*, KEK Report 2002-13, JAERI-Tech 2003-44.

R&D OF ADS IN JAPAN

Hideki Takano
Japan Atomic Energy Research Institute
Tokai-mura, Ibaraki-ken, 319-1195, Japan

Abstract

Under the OMEGA programme, the Japan Atomic Energy Research Institute (JAERI) continues to carry out the development of partitioning processes, nitride fuel technology, and a basic study to support the development of accelerator-driven systems (ADS). The current status of the technical issues to realise ADS are summarised: high-intensity proton accelerator, lead-bismuth technology, subcritical level, power control for the core, beam window and spallation target, and the Transmutation Experimental Facility proposed in the framework of the High-intensity Proton Accelerator Project: J-PARC. Further, the roles of P&T on high-level waste disposal including cost estimate are summarised. Kyoto University and KEK are moving forward with the experimental project Accelerator-driven Subcritical Reactor (ADSR), in which a small proton accelerator called Fixed-field Alternating Gradient (FFAG) will be coupled with a critical assembly, KUCA.

Introduction

By confirming plutonium recycling technology, a long-term sustainable energy of several hundred years could be maintained with the use of underground uranium resources. In addition to underground resources, the feasibility of using huge uranium resource from sea water – in which are stored a diluted, infinite store of uranium of about 45 billion tonnes – should not be discounted. The Japan Atomic Energy Research Institute (JAERI) has developed a reliable technology to extract uranium from sea water, and the natural uranium cost is estimated at five times more as compared with the present uranium ore. Though production countries of the uranium ores are unevenly distributed as are as oil, coal and gas, sea water uranium and thorium resources will bring an equal energy resource to almost countries in the world. As the main impetus for global wars is the deprivation of such resources, such conflict could be avoided with equal access to such a huge and evenly-distribution energy source. Further, population explosions in developing countries would be alleviated once a steady energy source is obtained. Another important property of nuclear energy utilisation is its environmental friendliness with respect to the irrevocable greenhouse problem caused by using oil, coal and gas. The greenhouse problem addressed in the Kyoto Protocol could be solved by utilising a scenario consisting of an optimum mix of the nuclear energy of base load and biomass, natural energy and fossil energy.

The management of high-level radioactive waste (HLW) is one of the most important and difficult issues to be solved for the utilisation of the fission energy. To reduce the burden of the final disposal of HLW, partitioning and transmutation (P&T) technology has been actively studied world-wide. The goal of P&T technology is to optimise the disposal concept by adopting the partitioning of wastes and to reduce the radiological toxicity of HLW by adopting the transmutation of minor actinides (MA) and long-lived fission products (LLFP). By combining these technologies, the period of time during which HLW should be controlled can be significantly shortened and the capacity of disposal sites can be enhanced without derogation of the safety.

JAERI has proposed a P&T technology based on the Double-strata Fuel Cycle Concept [1,2]. Figure 1 displays a schematic outline of this concept. A dedicated transmutation fuel cycle, i.e. the “second stratum”, is established separately from the commercial power generation fuel cycle, i.e. the “first stratum”, where the plutonium and uranium are recycled. The HLW exhausted from the reprocessing plant in the first stratum is treated at the partitioning plant and separated into four groups: transuranic elements (TRU), Tc and noble metals, Sr-Cs and the other elements. The TRU, mainly consisting of MA, namely Np, Am and Cm, is the principal object of the transmutation because these elements dominate the potential radiotoxicity in the HLW for a long-term period – over one hundred years after reprocessing.

In the transmutation fuel cycle, nuclear fuel mainly consisting of MA is used to enhance the transmutation efficiency. Using such MA fuel, the critical reactor would encounter some difficulties as regards safety and controllability. The accelerator-driven subcritical system (ADS) has potential advantages as the dedicated transmutation system in comparison with critical reactors: 1) various fuel compositions are flexibly acceptable since the Doppler effect does not seriously affect the system safety, 2) a small value of delayed neutron fraction is also acceptable since the margin to the prompt critical state can be kept by the subcriticality, 3) ADS is flexible as concerns nuclear waste transmutation in various scenarios of future nuclear reactors, e.g. in the case of advanced Pu utilisation commercial reactors such as HCLWR/FBR, ADSs can transmute MAs from LWRs, and (Am, Cm) from HCLWR/FBR and co-exists with HCLWR/FBR, and 4) partitioning and transmutation technology (P&T) with ADS reduces the twin burdens of economy and safety for commercial reactors, and MAs are confined in one small P&T cycle site. The ADS is, therefore, considered suitable to transmute MAs in the second stratum of the double-strata fuel cycle.

Figure 1. Double-strata Fuel Cycle Concept

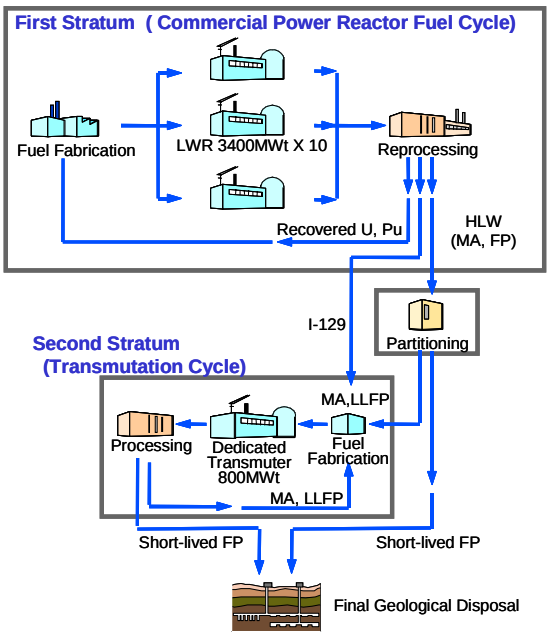

There are, however, several technical issues to be solved for the realisation of a large-scale ADS. At JAERI, various research and development (R&D) activities on the ADS are being conducted in the field of the proton accelerator, lead-bismuth eutectic (LBE or Pb-Bi) and subcritical reactor physics as well as the design study. In this report, these R&D activities in JAERI are reviewed, and the plan for the Transmutation Experimental Facility is also presented. The cost and benefits of P&T technology development are being studied as concerns the following possibilities: reduction of long-term radiotoxicity of high-level waste and inventories of minor actinides, environmental friendliness, treatment for Sr and Cs, effect on a geological disposal capacity, nuclear proliferation and cost estimate.

Kyoto University and KEK are progressing with the experimental project on an Accelerator-driven Subcritical Reactor (ADSR) in which a small proton accelerator called Fixed-field Alternating Gradient (FFAG) will be coupled with a critical assembly, KUCA.

Design study of ADS

The ADS proposed by JAERI is an 800 MWth, LBE-cooled, tank-type subcritical reactor with a spallation target of LBE, as shown in Figure 2, which can transmute 250 kg of MA annually. To optimise the neutronics design of ADS, several critical points must be resolved: reduction of the power peaking factor, reduction of the beam intensity, reduction of the burn-up reactivity swing and maximisation of the transmutation rate. These points are largely dependent on one other. It is important that these critical points should be optimised throughout each stage of the fuel cycle, from the beginning of cycle (BOC) initial loading to the end of cycle (EOC) of the equilibrium cycle.

In the optimisation study [3] on the neutronics of the ADS, the dedicated fuel for MA transmutation without uranium and plutonium shows a rapid increase of the effective multiplication factor (k_{eff}) with fuel burn-up because MA acts as a good fertile material. To mitigate this burn-up reactivity swing, plutonium is added at the initial loading, though not after the second cycle. The initial content of plutonium is one of the important design parameters to be optimised. In addition, inert matrix such as ZrN should also be mixed into the fuel to reduce the power density.

Figure 2. Conceptual view of 800 MWth LBE-cooled ADS

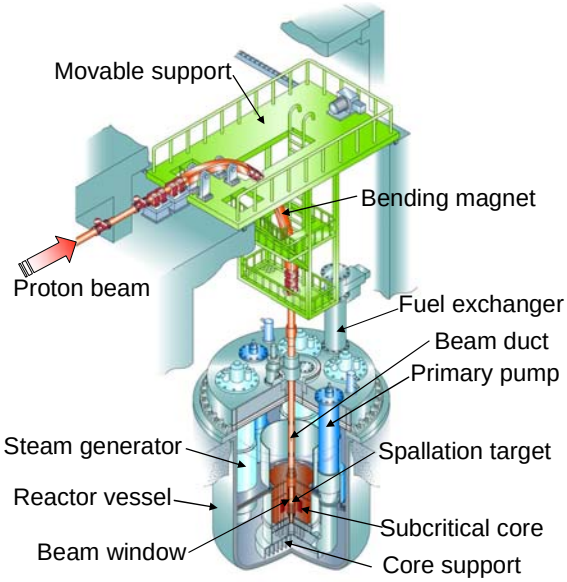

The value of the maximum multiplication factor (k_{max}) is another important design parameter which largely influences all the critical points described above. In the previous neutronics design [4], we had adopted k_{max} = 0.95, taking into account the limitation for the critical safety of fuel fabrication and processing plants. Recently, considering the accidental situations of the ADS, we estimated the marginal subcriticality to avoid the critical accident of the ADS, and it was concluded that a k_{max} of 0.97 can be adopted [3].

Moreover, to reduce the power peaking factor, two-zone fuel loading is adopted in the reference design of JAERI's ADS concept, where initial contents of plutonium are adjusted to minimise the power peaking throughout the entire fuel cycle. The k_{eff} changes from 0.970 to 0.940. According to this reactivity swing, the proton beam power should be adjusted from 12 MW to 27 MW. The optimisation of the neutronics design is ongoing, and will take into consideration the results of the thermal-hydraulic and structural design studies of the beam window and the fuel assembly.

Thermal-hydraulic and structural design of ADS

In terms of thermal-hydraulic and structural design, the critical issues of ADS design concern the engineering feasibility of the beam window for the high power spallation target and the cooling performance of the hot spot fuel pin. Preliminary results of the analysis at JAERI are described below.

In JAERI's reference design, "ductless type" fuel assemblies are adopted to reduce neutron capture reactions by structural material and to enhance the cooling capability of decay heat during fabrication, transportation and storage. The LBE flows into the core bottom structure and is distributed to the target region and the core region. Previous studies of the thermal-hydraulic behaviour showed that cross-flow of LBE between the spallation target and the ductless-type fuel assemblies will occur if there is no partition wall between them [5]. This cross-flow deteriorates the flow speed of LBE around the innermost fuel assemblies, and hence the cooling performance of the hot spot fuel pins is seriously affected. The current design has a partition wall around the spallation target.

Superconducting linear accelerator technology [7]

The proton accelerator for the ADS should be of high intensity, more than 20 MW, with good economical efficiency and reliability. Taking this into account, JAERI regards the superconducting linear accelerator (SCL) as the most promising choice. The SCL consists of a series of cryomodules, which contain two units of superconducting cavities made of high-purity niobium. In the programme, JAERI and KEK are collaborating on the construction of a prototype cryomodule, and examining its performance as concerns the electric field and helium cooling.

The prototype cryomodule manufactured in this programme is designed to accept a 972 MHz radio frequency wave and to be suitable for the acceleration of 424 MeV protons (b = 0.725). The superconducting cavities will be cooled down to 2 K, and the targeted maximum surface electric field is 30 MV/m. The measurement is scheduled in FY2004.

J-PARC project

In addition to the above-mentioned development, JAERI has started the High-intensity Proton Accelerator Project, called J-PARC (Japan Proton Accelerator Research Complex, see Figure 3), in partnership with KEK [8]. In Phase I of this project, a proton linac with 0.33 mA · 200 MeV and two proton synchrotrons with 0.33 mA · 3 GeV and 0.015 mA · 50 GeV, respectively, are under construction and scheduled to be completed by 2007. In addition, the linac's energy will be upgraded to 400 MeV within the framework of Phase I.

Figure 3. Site plan of High-intensity Proton Accelerator Project: J-PARC

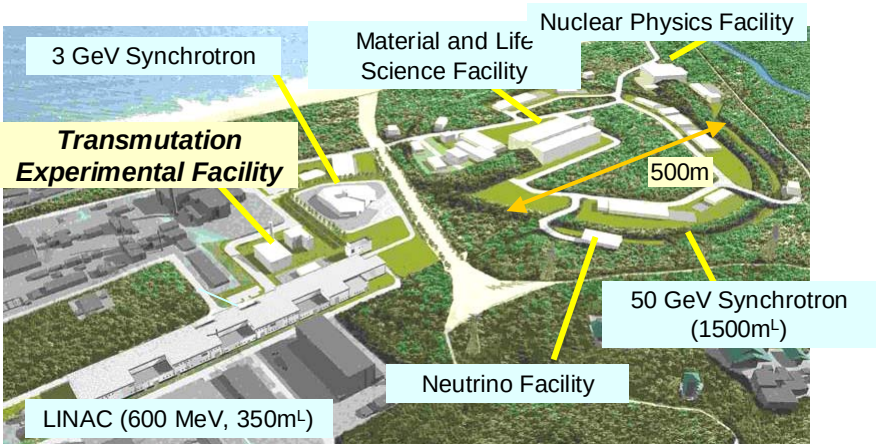

Through the experience of the construction of the 400-MeV linac, we can accumulate technology for the low-energy part of the linac even though it is operated in the pulsed mode. In Phase II of the project, the SC linac will be constructed to upgrade the proton energy from 400 MeV to 600 MeV. Then the 600-MeV proton beam will be introduced into the Transmutation Experimental Facility (TEF).

Experimental facilities for ADS technology demonstration

To study the basic physics and technologies for ADS development and to demonstrate an ADS composed of accelerator, spallation target and subcritical core, the Transmutation Experimental Facility (TEF) [1,2] is planned within the framework of the J-PARC Project. The TEF consists of two buildings,

the Transmutation Experimental Facility (TEF-P) and the Target Test Facility (TEF-T). TEF-P is a zero-power critical facility wherein a low-power proton beam is available to research the subcritical reactor physics and the controllability of ADS. TEF-T is a material irradiation facility which can accept a maximum 600-MeV/200-kW proton beam into the spallation target with lead-bismuth eutectic.

Lead-bismuth eutectic technology and material development

JAERI selects the lead-bismuth eutectic as the first candidate for the spallation target and core coolant materials in the ADS system, because it has some advantageous characteristics such as chemical stability, low-melting and high-boiling temperature, high neutron yield by spallation reaction, small neutron capture cross-section and less positive void reactivity than sodium. However, the lead-bismuth is corrosive for structural materials such as austenite stainless steel for temperatures higher than 500 C and is erosive for materials at a flow speed beyond 2 m/s.

Corrosion of structural materials **[9-11]**

For target, materials and operation of Pb-Bi system, a material test loop and stagnant test devices were installed for Pb-Bi technology development and they were in operation. The statistic corrosion tests were performed after 3 000 h at 450 C. The loop corrosion test was conducted for austenite stainless steel under the temperature of 450 C, EMP power of 5 l/min and a velocity of 1 m/s. This test was conducted without controlling oxygen.

In the present programme, a new corrosion test on austenitic (JPCA) and martensitic (F82H) stainless steel materials is planned under various conditions with oxygen control and lead-bismuth flowing rate. This test will be started in FY2003 and continued in FY2004. The loop will be operated with various temperature differences to study the mass transfer of structural materials caused by solubility difference.

Thermal-hydraulics at beam window

One of the critical problems in the design of the ADS is the viability of a beam window installed under hard conditions. JAERI and MES are collaboratively building a thermal-hydraulic loop so as to investigate the prediction accuracy of heat transfer coefficients of the hemispherical shape of the beam window. The maximum flow rate of lead-bismuth is 500 l/min and the maximum flow speed at the head of the window is 0.8 m/s. The outer diameter of the test vessel is 8.9 cm. A mesh heater with a power density of 63 W/cm^2 is attached on the side wall of the hemispherical shape of the test vessel.

Behaviour of radioactive impurity

When LBE is used as a core coolant, ^{210}Po is produced mainly by a ^{209}Bi(n,γ)^{210}Bi reaction and β decay. ^{210}Po is an α emitter whose half-life is 138 days, and has a volatile property. It is, therefore, important to know the evaporation rate of Po from LBE in order to evaluate the safety of the system. Moreover, when LBE is used as the spallation target, many types of elements and isotopes are produced as spallation products (SPs), some of which should be also taken into consideration to evaluate the safety of ADS. To obtain a better understanding of the behaviour of ^{210}Po in LBE, the Japan Nuclear Cycle Development Institute (JNC), JAERI, Nippon Nuclear Fuel Development Co. Ltd. and Kaken Co. Ltd. collaboratively irradiated solid Pb-Bi at the material test reactor JMTR, and are investigating its thermochemical properties. In this collaborative work, the evaporation rates of Po from LBE are being measured by the transpiration method as a function of the LBE temperature.

As for the SPs, the behaviour of several elements such as gadolinium, samarium and dysprosium in LBE will also be studied. Moreover, the Tokyo Institute of Technology is investigating the prediction accuracy of spallation products yield as a joint study with JAERI.

Research and development on subcritical reactor physics

In the ADS dedicated to the transmutation of MA, a large amount of MA is loaded and ^{238}U is excluded to enhance the transmutation rate. Plutonium is added at the initial loading to mitigate the burn-up reactivity swing, though it is not added on after the second cycle. The chemical form of the fuel is mono-nitride, in which enriched ^{15}N will be used to avoid ^{14}C produced by $^{14}N(n,p)^{14}C$ reactions. The fuel will be diluted with ZrN. The prediction accuracy of the reactor physics parameter, therefore, must be significantly different from that for conventional fast breeder reactors.

After operation during 600 effective full power days (EFPD), the fuel is unloaded and reprocessed to remove fission products using the pyrochemical process. MA is then added to compensate the burnt actinides, and nitride fuel is refabricated. Comparing the homogenised atomic number densities between the beginning of the first cycle and that of the fifth cycle in the single-zone ADS [5], the amount of ^{239}Pu decreases by 1/3, while ^{238}Pu increases significantly. ^{242m}Am is also accumulated during the fifth cycle.

To evaluate the prediction accuracy of reactor physics parameters for ADS, the sensitivity of nuclear data to the reactor physics parameters was analysed [5] using the SAGEP code. Figure 4 shows the obtained sensitivity to the effective multiplication factor. The sensitivity of fission reaction by ^{239}Pu is the largest in the first cycle, while that of ^{238}Pu becomes the largest in the fifth cycle. Fission reactions of ^{237}Np, ^{241}Pu and ^{241}Am are largely influential for both cycles. ^{242m}Am is also considerably sensitive in the fifth cycle. It can be found that the capture reactions of ^{237}Np and ^{241}Am also have large sensitivities on the effective multiplication factor, though that of ^{239}Pu is not so great. It should be noted that the scattering reactions of ^{15}N and the inelastic scattering reactions of Pb and Bi are highly sensitive. The accuracy of the cross-section data of MA, Pu, ^{15}N, Pb and Bi, therefore, are important for the design of the ADS.

Figure 4. Sensitivities of nuclear data to effective multiplication factor of ADS

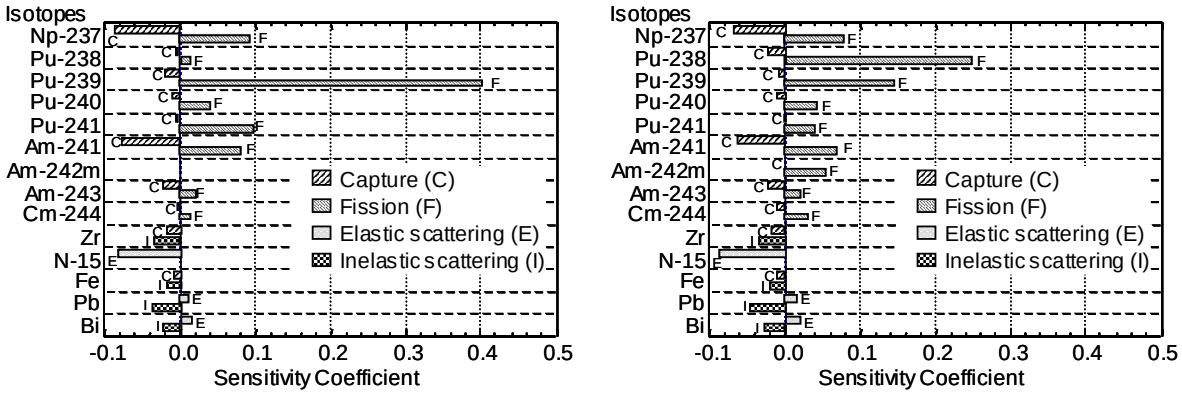

(a) Beginning of 1st. cycle (b) Beginning of 5th. cycle

Reactor physics experiments for the subcriticality monitoring and various physics parameters of ADS are also under way at critical assemblies: Fast Critical Assembly (FCA) in JAERI and Kyoto University Critical Assembly (KUCA) as joint research projects. Nagoya University is studying the subcriticality monitoring method using the reactor noise technique and trying to demonstrate its applicability at KUCA as a joint study with JAERI.

Cost and benefit

Analysis of mass flow and cost on the basis of a double-strata fuel cycle has been examined. As the commercial reactor fuel cycle is assumed to be sustainable over a significantly long term, the following different reactors and fuel cycles are considered: co-existing scheme of ADS in Pu utilisation fuel cycles with MOX-LWRs and FBRs. Additionally, an impact assessment of the P&T cycle on geological disposal is being studied. The performance of the ADS considered here [13] is 800 MWt and can transmute MA and ^{129}I produced per year from about 10 PWRs of 3 400 MWt.

The cost and benefits of P&T technology development are studied and the following possibilities are estimated: 1) the long-term radiotoxicity of high-level waste (HLW) is reduced to a factor of two hundred, 2) the inventories of minor actinides are reduced to a factor of one hundred, meaning that environmental friendliness increases ten-fold, 3) Sr and Cs separated from HLW are intermediately stored and processed, and the geological disposal wastes become a ten-fold reduction, 4) as a result of 2) and 3), a geological disposal site can be used more efficiently at a ten-fold capacity, 5) the transmutation of Pu and Np in HLW can significantly reduce nuclear proliferation, and 6) P&T technology is estimated to add a relatively modest 5-10% to the electricity cost, though these values depend on the cost estimate of geological disposal and fuel cycle.

Roadmap for ADS development

A P&T scenario with an ADS transmutor is an innovative and flexible system (coexisting with Pu-fuelled reactors such as MOX-LWR, RBWR and FBR) for reducing high-level wastes. After the basic R&D mentioned above, an experimental ADS with 80 MW thermal power is considered to be planned in the late 2010s to demonstrate the engineering feasibility of the ADS as shown in Figure 5. The experimental ADS will be operated by MOX fuel at first and gradually altered to MA nitride fuel.

Figure 5. Road map for ADS development at JAERI

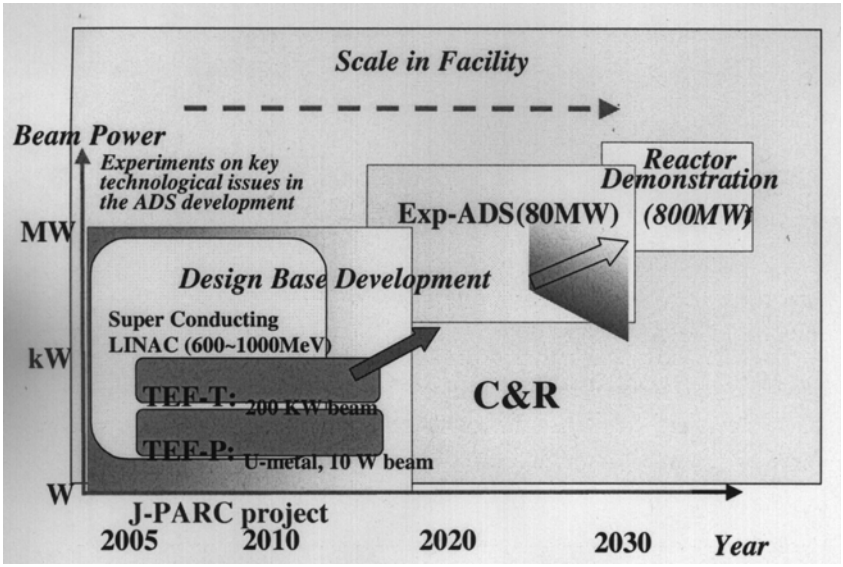

A partition and transmutation (P&T) scenario with ADS transmutor will be one of the most prime candidates for reasonable disposition of nuclear wastes. The ADS is an innovative and flexible system (coexisting with Pu-fuelled reactors such as MOX-LWR, RBWR and FBR) for reducing long-term

radioactive nuclides as shown in Figure 6. Since 2002, JAERI has started a basic R&D programme to validate the engineering feasibility of ADS development. After the basic R&D for subcritical core design and technology, lead-bismuth eutectic technology and superconducting linear accelerator mentioned above, an experimental ADS with 80 MW thermal power is considered to be planned in the late 2010s to demonstrate the engineering feasibility of the ADS. The experimental ADS will be operated by MOX fuel at first and gradually altered to MA nitride fuel.

Figure 6. Scenario of minimising HLW in advanced future fuel cycles in Japan

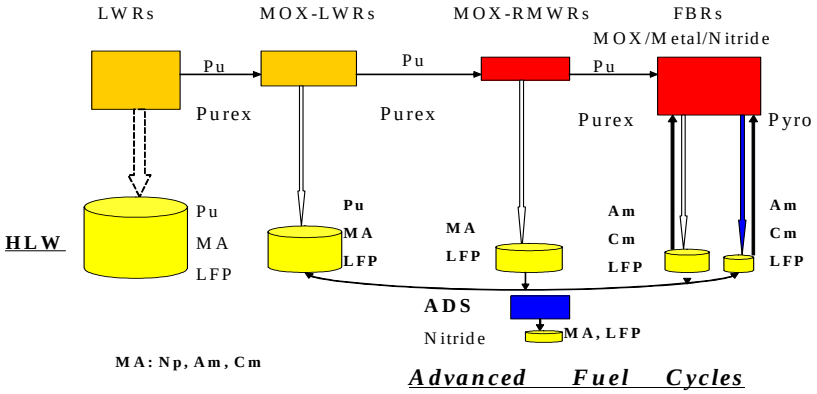

Project on Accelerator-driven Subcritical Reactor (ADSR) at Kyoto University Research Reactor Institute (KURRI) [14,15]

At the Kyoto University Research Reactor Institute (KURRI), an accelerator-driven subcritical reactor (ADSR) is considered to be the final goal of a future plan called the "Neutron Factory" project. It is anticipated that this ADSR will become a substitute for the current Kyoto University Reactor (KUR) of 5 MW established in 1964 for the joint use programme among university researchers in Japan. The Neutron Factory will be a synergistic system of a high-energy proton accelerator and a research reactor, which will allow operation in either independent or combined mode to generate so-called "controlled neutrons" in the energy and time spaces for research purpose.

A conceptual neutronics design study was initiated in 1997 by a working group of a future plan in KURRI, and the MCNPX code was introduced in 1999 to promote this study. A basic experimental study on the ADSR was also formally initiated in 2000 using the Kyoto University Critical Assembly (KUCA), where a subcritical assembly of polyethylene moderated and reflected highly-enriched uranium core can be driven by 14-MeV neutrons from a Cockcroft-Walton type accelerator installed in KUCA. Last year, a new programme of public subscription related with the technology development for the innovative nuclear reactor system has been initiated by the Ministry of Education, Culture, Sports, Science and Technology (MEXT) of Japan. This programme is based on the concept of collaboration among industries, national institutions and universities.

A proposal entitled as "Technology Development for the ADSR Using a Fixed-field Alternating Gradient (FFAG) Synchrotron" was submitted for this programme on the basis of research activities in KURRI and the High Energy Accelerator Research Organization (KEK); the reactor engineering and the accelerator development activities, respectively. This proposal aimed at a feasibility study concerning the ADSR as a nuclear energy system as well as the future neutron source for scientific research.

Conclusions

JAERI has been conducting the study of a dedicated transmutation system using ADS. The design study is under way on LBE-cooled, tank-type ADS with a thermal power of 800 MW. As concerns the feasibility of the beam window, a promising design concept was obtained, though further investigation is still necessary. In the field of the proton accelerator, a prototype cryomodule was fabricated and its performance is being studied. In the field of LBE technology to be used for the spallation target and the core coolant of the ADS, material compatibility, thermal-hydraulics and polonium behaviour are being studied. As for the study on the behaviour of radioactive impurity, Pb-Bi was irradiated at JMTR and the evaporation rates of Po from LBE are going to be measured as a function of the LBE temperature. In the field of the reactor physics of the subcritical core fuelled with MA, the reliability of nuclear data is being examined, and the subcriticality monitoring technique is being investigated. In the framework of the J-PARC project, JAERI plans to construct the Transmutation Experimental Facility (TEF) to demonstrate the feasibility of the ADS using a high-energy proton beam, to accumulate valuable knowledge regarding the reactor physics and operation of ADS, and to establish a database for LBE spallation target and relevant material.

Kyoto University and KEK are progressing with the experimental project on the Accelerator-driven Subcritical Reactor (ADSR) in which a small proton accelerator called Fixed-field Alternating Gradient (FFAG) will be coupled with a critical assembly, KUCA.

Acknowledgements

Part of this work was funded by the Ministry of Education, Culture, Sports, Science and Technology (MEXT) as one of the R&D programmes for innovative nuclear systems. This work is based on collaborations with many institutes, universities and private companies. The author is especially grateful to Dr. H. Oigawa, the leader of Nuclear Transmutation Research Group of JAERI.

REFERENCES

[1] Takano, H., *et al*., "Transmutation of Long-lived Radioactive Waste Based on Double-strata Concept", *Progress in Nuclear Energy*, 37, 371 (2000).

[2] Mukaiyama, T., *et al*., "Review of Research and Development of Accelerator-driven System in Japan for Transmutation of Long-lived Nuclides", *Progress in Nuclear Energy*, 38, 107 (2001).

[3] Tsujimoto, K., *et al*., "Neutoronics Design for Lead-bismuth Cooled Accelerator- driven System for Transmutation of Minor Actinide", *J. Nucl. Sci. Technol*., 41, 21 (2004).

[4] Tsujimoto, K., *et al*., "Accelerator-driven System for Transmutation of High-level Waste", *Progress in Nuclear Energy*, 37, 339 (2000).

[5] Oigawa, H., *et al*., "Research and Development Program on Accelerator Driven System in JAERI", *GLOBAL2003*, New Orleans, USA 16-20 November 2003.

[6] Takizuka, T., *et al*., "Responses of ADS Plant to Accelerator Beam Transients", *Proceedings of the OECD/NEA 2nd Workshop on Utilisation and Reliability of High Power Proton Accelerators*, Aix en Provence, France, 22-24 November 1999.

[7] Ouchi, N., "R&D Status of Superconducting Proton LINAC and KEK/JAERI High Intensity Proton Accelerator Project", 3rd International Workshop on the Utilisation and Reliability of High Power Proton Accelerators (*HPPA2002*), Santa Fe, USA 12-16 May 2002.

[8] The Joint Project Team of JAERI and KEK, *The Joint Project for High-intensity Proton Accelerators*, JAERI-Tech 99-056 (KEK Report 99-4, JHF-99-3) (1999).

[9] Kurata, Y., *et al*., "Corrosion Studies in Liquid Pb-Bi Alloy at JAERI: R&D Program and First Experimental Results", *J. Nucl. Mater*., 301, 28 (2002).

[10] Kurata, Y. and M. Futakawa, "Excellent Corrosion Resistance of 18Cr-20Ni-5Si Steel in Liquid Pb-Bi", *J. Nucl. Mater*., 325, 217 (2004).

[11] Kikuchi, K., "Corrosion-erosion Test of SS316 in Flowing Pn-Bi", *J. Nucl. Mater*., 318, 348 (2003).

[12] Oigawa, H., *et al*., "Conceptual Design of Transmutation Experimental Facility", *International Conference on Back-End of the Fuel Cycle (GLOBAL2001)*, Paris, France, 10-13 Sept. 2001.

[13] Nishihara, K. and H. Takano, "Transmutation of ^{129}I Using an Accelerator-driven System", *Nuclear Technology*, 137, 47 (2002).

[14] Shiroya, S., H. Unesaki, *et al.*, "Accelerator Driven Subcritical System as a Future Neutron Source in Kyoto University Research Reactor Institute (KURRI) – Basic Study on Neutron Multiplication in the Accelerator Driven Subcritical Reactor", *Prog. in Nucl. Energy*, Vol. 37, No. 1-4, p. 357 (2000).

[15] Shiroya, S., H. Unesaki *et al.*, "Experimental Study on Accelerator Driven Subcritical Reactor by Using the Kyoto University Critical Assembly (KUCA)", *Proc. Int. Conf. on the New Frontiers of Nucl. Technol.: Reactor Phys., Safety and High-Performance Computing (PHYSOR 2002)*, Seoul, Korea, 7-10 October 2002, p. 7C-01 1.

LOS ALAMOS PERSPECTIVE ON HIGH-INTENSITY ACCELERATORS

Robert W. Garnett, Andrew J. Jason

Abstract

Los Alamos has been an active participant in the development of high-intensity accelerators, including the RFQ, LAMPF with the innovation of a CCL structure, and more recently, LEDA with a 100-mA CW beam. Participation in technology development related to high-intensity applications such as transmutation of waste, and others, remains a strong interest at Los Alamos. Past efforts leading up to present programmes are discussed. These programmes include development of novel normal and superconducting structures, RF power systems, beam dynamics, beam diagnostics and general system considerations.

Introduction

This paper is divided into two parts. The first part describes the history at Los Alamos of participation in the application of technology to high-intensity accelerators. The second part of this paper is a discussion of the current trends in high-intensity accelerators, specific ADS design challenges, some expectations, and some conclusions as viewed by the authors.

Overview of LANSCE

The Los Alamos Neutron Science Center (LANSCE) is located in the mountains of northern New Mexico. It is a multi-user facility operated jointly by the Department of Energy (DOE) National Nuclear Security Administration (NNSA) and the DOE Office of Science (SC) Office of Basic Energy Science (BES). DOE-NNSA supports accelerator operations, spallation-neutron production and weapons research in support of stockpile stewardship. DOE-BES supports the Manuel Lujan Jr. Scattering Center Experimental User Program, its operations, and condensed matter and materials research [1]. Other major supporters of programmes at LANSCE include the DOE-SC Office of High Energy (HEP) and Nuclear Physics (NP) which support basic nuclear-physics research, and the DOE Office of Nuclear Energy, Science and Technology (NE), which supports the recently commissioned Isotope Production Facility (IPF) and the Advanced Fuel Cycle Initiative (AFCI). Accelerator technology projects have been supported by many of these sponsors, including the US Department of Defense Programs and others.

Figure 1 shows an aerial photo of the LANSCE facility and its associated research areas. Figure 2 shows a schematic overview layout of the LANSCE facility including the accelerator and the various experimental beam lines. At the heart of the LANSCE facility is a high-intensity 800-MeV linac first commissioned in 1972. At present the linac is capable of simultaneously accelerating both protons and H^- ions provided by two 750-keV Cockcroft-Walton DC injectors. Protons up to an average beam current of 1 mA can be delivered to Area A. This area is presently inactive while development of a target test facility for AFCI/ADS applications is in progress. As part of the recent beam line

Figure 1. The Los Alamos Neutron Science Center (LANSCE)

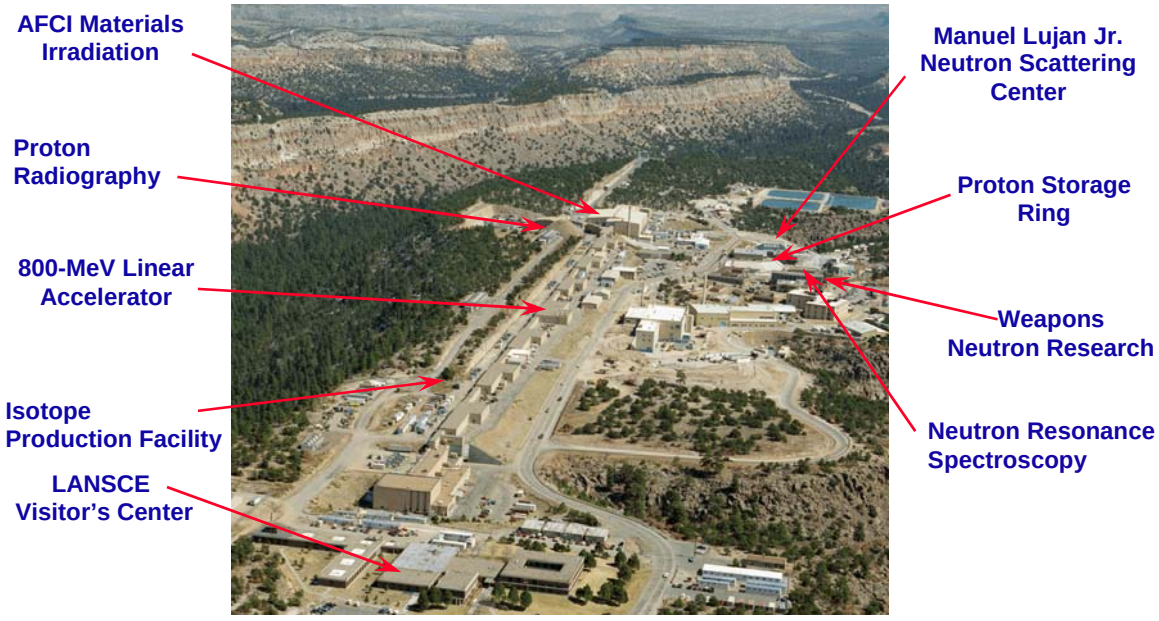

Figure 2. Schematic layout of the LANSCE facility

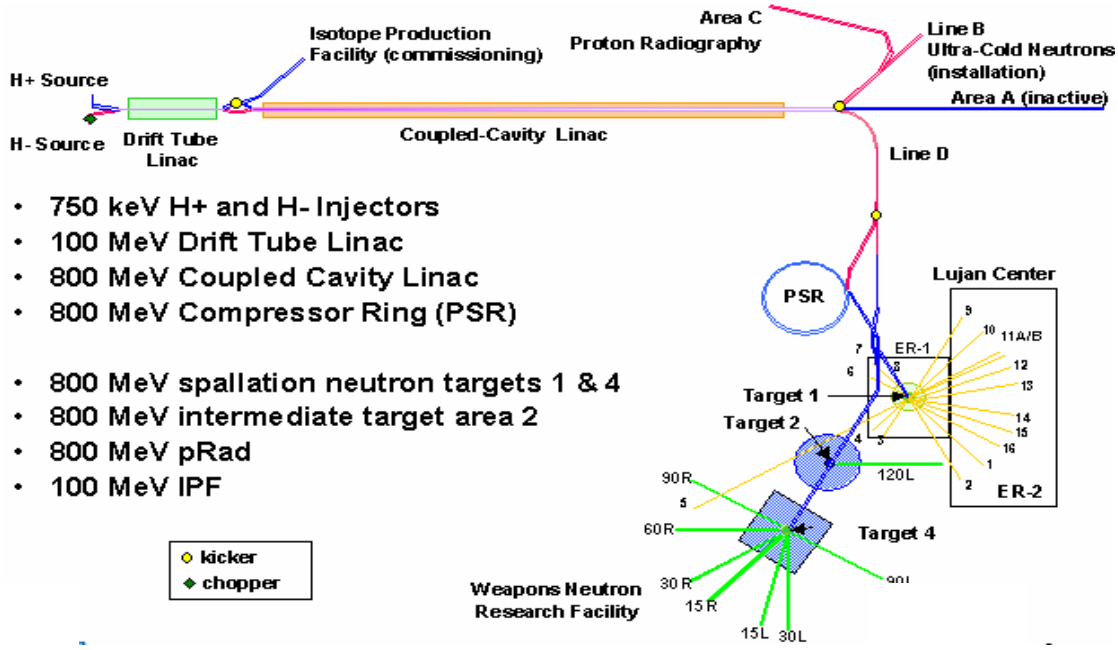

modifications for the IPF, a pulsed kicker magnet was installed to deflect the 100-MeV proton beam from the drift-tube linac into the IPF. This will later allow simultaneous operation of the IPF and the AFCI/ADS test facility. A lower-average-current H^- ion beam can be deflected, again via a pulsed kicker magnet in the beam line, to Line B for ultra-cold neutron production or to Area C for proton radiography. The majority of the H^- ion beam, however, is injected at 800 MeV into the Proton Storage Ring (PSR) and then later sent to the Lujan Center spallation neutron target or various solid targets at the Weapons Neutron Research (WNR) facility. Until full-power operation of the Spallation Neutron Source (SNS) linac at Oak Ridge, LANSCE is the world's highest average power linac and the PSR has the highest-peak pulse.

Los Alamos high-intensity accelerator contributions

Los Alamos has made many major contributions to proton linac technology over the past 35 years, starting with the design and construction of the LANSCE linac. One of the first of these was the invention of the side-coupled accelerating structure for high-velocity beams [2], allowing significantly shorter accelerating structures by moving the coupling cells off-axis. The side-coupled structure has become the structure of choice for small electron and ion linacs for industrial and medical applications. Several other major accomplishments include:

- First high power (~1 MW average beam power) proton linac: 800-MeV LAMPF (first beam in 1972).
- RFQ proof of principle experiment (1980) – enabling higher beam currents.
- RFQs for CERN, FMIT, BEAR (operated in space), GTA and SSC.
- 6.7-MeV 100-mA CW LEDA RFQ (1999).

- Superconducting cavities for medium-velocity protons (1996 on).
- High-current beam dynamics including space-charge, emittance growth and beam-halo physics (~1977 on).
- Accelerator design and simulation codes (~1970 on).
- SNS linac design and construction (1997 on).
- EPICS control system developed (1987 on).

Our accelerator R&D capabilities

Due to our past involvement in many projects, excellent accelerator R&D capabilities have been developed. These include accelerator physics and beam dynamics expertise that allow us to develop new projects from conceptual design onward. Included are linac, circular-machine and beam-transport design, higher-order optics, and design-code and simulation development. As a result of participation in the Accelerator Production of Tritium (APT) Project, superconducting (SC) cavity and power-coupler design capabilities have been developed. Expertise in accelerator-specialised mechanical engineering and design, including cryogenics and prototype fabrication, has also been attained.

Four facilities are operated:

1) A magnet laboratory for fabrication, testing and measurement of accelerator and beam line magnets.
2) An RF accelerating structures laboratory which includes a Class 100 clean room for SC and normal-conducting cavity development and tuning.
3) A beam-diagnostics development facility equipped with automated electromagnetic diagnostics test equipment.
4) A well-equipped machine shop capable of sophisticated accelerator-structure and component fabrication.

Recent high-intensity accelerator projects

Listed below are some of the more recent high-intensity linac projects we have participated in and for which Los Alamos has made contributions that have advanced accelerator technology:

- Accelerator Production of Tritium (APT) – first proposed high-intensity SC proton linac:
  - Low-energy Demonstration Accelerator (LEDA).
  - Superconducting cavity and power coupler development.
- Advanced Accelerator Applications (AAA/AFCI):
  - Accelerator Transmutation of Waste (ATW).
  - Superconducting cavity development.

- Spallation Neutron Source (SNS):
  - LANSCE personnel led physics design and engineering of the linac. LANSCE also inspired the superconducting linac decision.
- Free Electron Laser (FEL) programme development.
- PSR upgrades and instability studies.
- Advanced Hydrotest Facility (AHF) design:
  - Synchrotron.
  - Beam transport.
  - Imaging.
- Proton Radiography (pRad) microscope.
- Los Alamos Accelerator Code Group (LAACG).

Two of these projects in particular, APT and SNS, have resulted in a large number of contributions. Some examples are shown in Figures 3-6. Of particular interest to ADS applications is the successful construction and operation of the LEDA facility at LANSCE. This facility is discussed below.

The LEDA facility

The LEDA facility, shown in Figure 7, was built and tested as a major element of the APT Project Engineering Development and Demonstration (ED&D) programme. It successfully operated at full power operation from 1999-2001, confirming the feasibility of a high-power linac front end, the most technically challenging portion of such a machine [3]. The LEDA accelerator consists of a 100-mA, CW 6.7-MeV proton accelerator that includes a 75-keV H^+ injector coupled to a 350-MHz radiofrequency quadrupole (RFQ) linac. The equipment is presently in a "cold standby" condition and is located in a 143-m long tunnel that is part of the LEDA facility building at LANSCE (shown in Figure 7). The accelerator tunnel and support facilities were originally built to test a neutral-particle beam system for the Strategic Defense Initiative programme in the late 1980s.

Figure 3. APT 1-MW power coupler



Figure 4. Superconducting elliptical-cavity development for APT and spoke-cavity development for AFCI/ADS applications

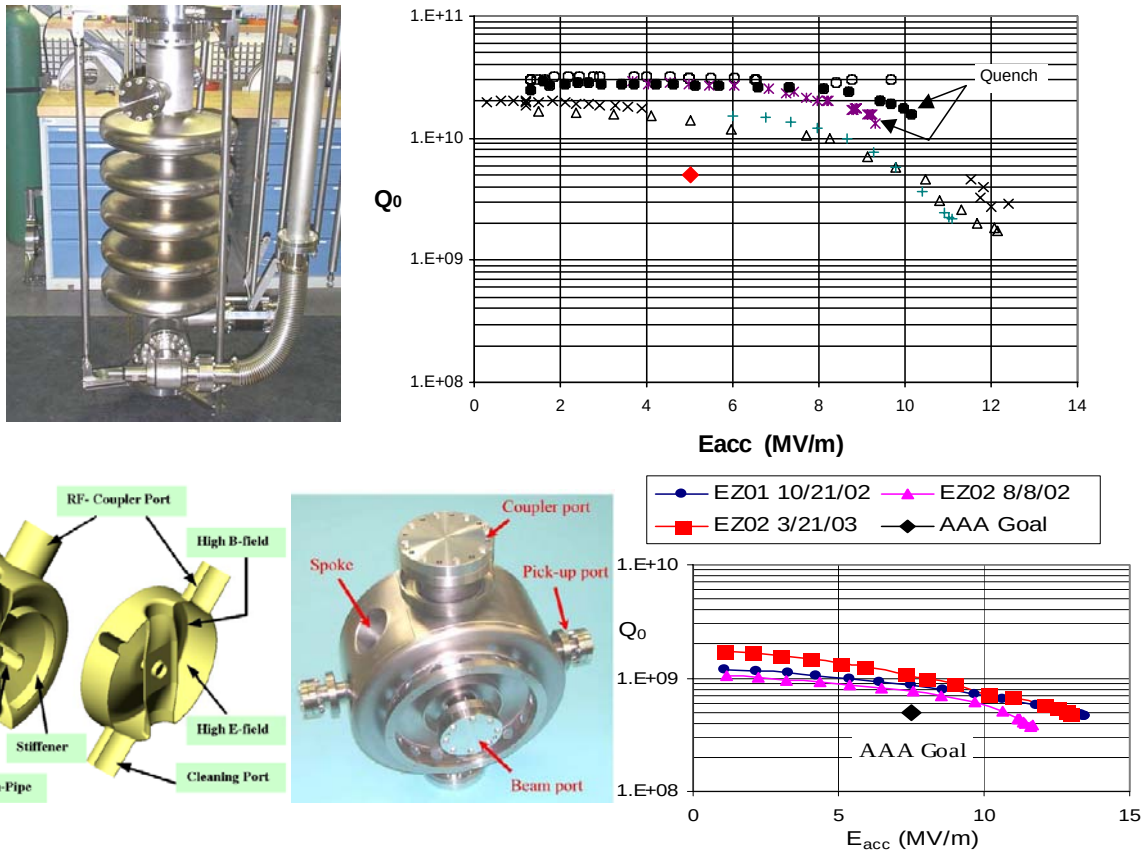

Figure 5. SNS solid-state pulsed converter-modulator

Can operate at up to 140 kV and 11 MW peak power (1.1 MW average). This design is compact and efficient. It requires no capacitor rooms.

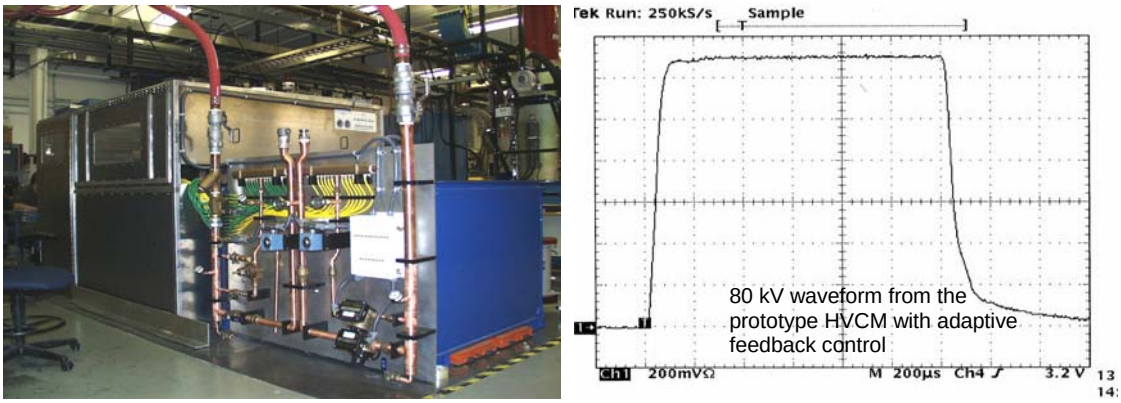

Figure 6. Advanced low-level RF cavity/field controls

Developed for SNS to control pulsed SC cavities. Allows modelling of SC cavity effects such as Lorentz-force detuning, microphonics and effects due to inadequate mechanical damping, etc.

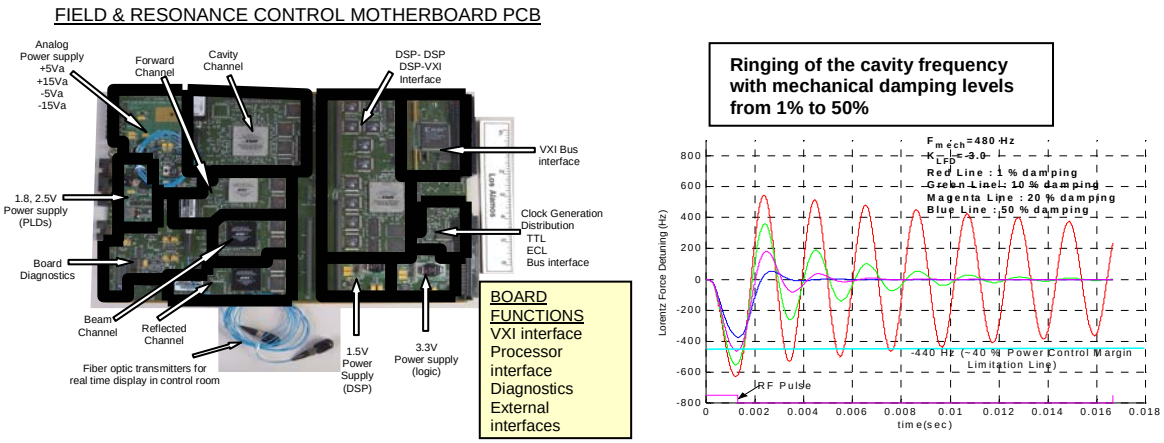

Figure 7. Top: Photograph of the LEDA facility building. Bottom: Layout of the LEDA acclerator including the injector, RFQ, HEBT and beamstop.

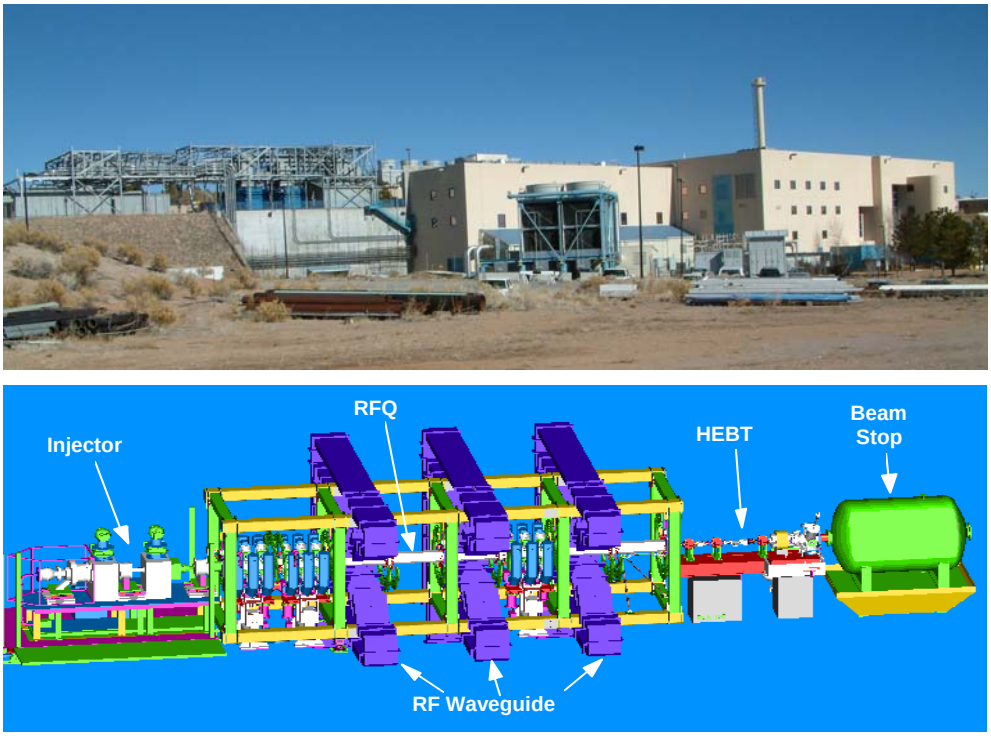

Beam testing with the LEDA RFQ demonstrated not only successful operation with a 100-mA CW beam, but also included the thorough characterisation of the output beam, providing important benchmarks for the structure and beam dynamics design codes. The three years of integrated operation with all of the necessary support systems has demonstrated the device feasibility needed for proposed accelerator-driven “neutron factories” such as ADS.

Figure 8 shows photographs of the LEDA H^+ injector and the RFQ. After beam characterisation experiments, the short high-energy beam transport (HEBT) section seen in Figure 7 was removed and replaced with a longer transport line instrumented to systematically study beam-halo effects [4]. The LEDA halo experiment beam line and some wire-scanner results are shown in Figure 9. Our beam diagnostics team developed a new wire scanner/beam scraper halo diagnostic that allowed beam measurements over an unprecedented 5-order-of-magnitude dynamic range [5].

Figure 8. Left: LEDA H^+ injector including the low-energy beam transport. Right: LEDA RFQ accelerator with the injector rolled back.

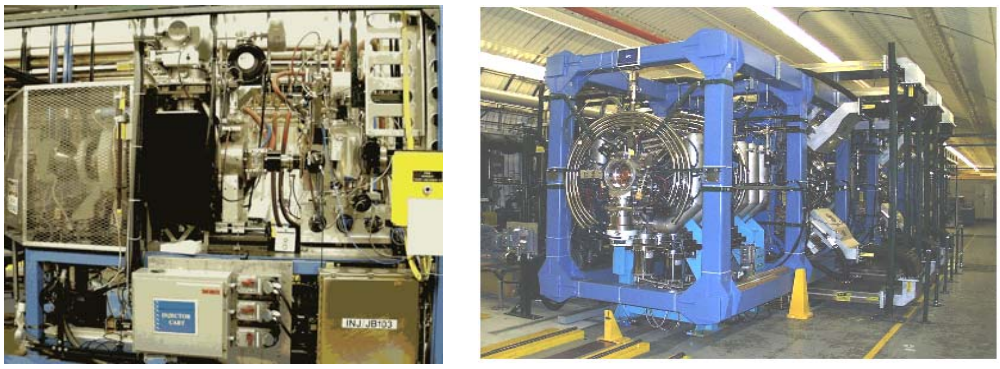

Figure 9. The halo experiment beam line is shown on the left. Numerous wire scanner/scrapers as shown on the right can be seen in the beam line photo. Data for a 75-mA matched beam case is also shown.

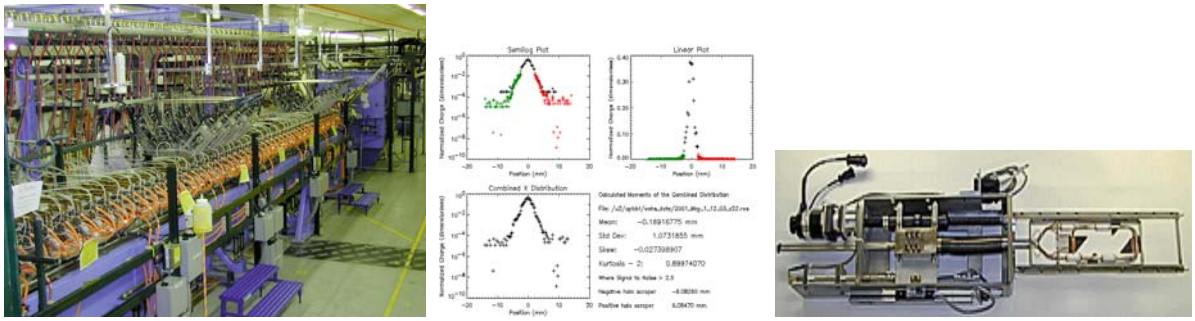

Current LANSCE accelerator technology activities

Somewhat different from the past, many of our current activities are now more focused on LANSCE upgrades and operations. Recently Los Alamos has participated in the development of beam diagnostics for the switchyard kicker and the new IPF facility, structure calculations for the LANSCE drift-tube linac (DTL), magnetic shielding calculations for the neutron beam lines, and several studies for possible beam current and energy upgrades at LANSCE such as for a Long-pulse Spallation Source (LPSS) based on a SC post accelerator that would provide 100-mA 3-GeV beam operation.

Other recent non-LANSCE-related activities include support of the SNS project, a CW injector for a 100-kW US Navy free-electron laser, SC cavity development, compact accelerators for homeland security, SC linac designs for AFCI/ADS, Rare Isotope Accelerator (RIA) beam dynamics and code development, design of the Advanced Hydrotest Facility (AHF) for stockpile stewardship, and continued operation of the Los Alamos Accelerator Code Group.

Current trends in high-intensity accelerators

There is now a trend in new high-power proton-linac projects to use SC accelerator technology almost exclusively. The APT project at Los Alamos in the 1990s established the necessary technology base required for high-power CW SC proton-linac technology by demonstrating the feasibility and advantages of using SC elliptical cavities at high beam velocities. Since then, many around the world have taken advantage of our work on APT. Additionally, as should be expected, other institutions have continued to improve and expand the applications of SC-accelerating structures.

Since about 1995, all new high-power proton-linac projects include SC accelerator sections. It appears that SC is becoming the technology of choice. New applications include accelerator-driven subcritical reactors for nuclear waste transmutation, the neutrino factory, fusion-materials studies, injectors for spallation-neutron sources, and many others. Table 1, although somewhat outdated, shows both the proposed and operating high-power proton, H^- and D^+ linacs worldwide. Most of these are proposing using SC technology.

Table 1. High-power linacs worldwide. Most are proposing using SC technology.

Name	Ion	Pulse length (msec)	Rep rate (Hz)	Duty factor (%)	I_{bunch} (mA)	$I_{Average}$ (mA)	Energy (GeV)	$P_{average}$ (MW)	Start date
LANSCE	H^+/H^-	0.625	100/20	6.2/1.2	16/9.1	1.0/0.1	0.8	0.8/0.08	ON
SNS	H^-	1.0	60	6.0	38	1.4	1.0	1.4	2006
CERN SPL	H^-	2.8	50	14.0	22	1.8	2.2	4.0	?
ESS short pulse	H^-	1.2	50	6.0	114	3.75	1.33	5 + 5	2010
ESS long pulse	H^- or H^+	2/2.5	16.67	4.2	114/90				
FNAL 8 GeV	$H^+/H^-/e^-$	1.0	10	1.0	25	0.25	8.0	2.0	?
KEK/JAERI 400 MeV	H^-	0.5	50/25	25	50	0.7	0.4	0.28/0.14	2006
KEK/JAERI 600 MeV			25	1.25		0.35	0.6	0.21	?
TRASCO	H^+	CW	CW	100	30	30	>1.0	>30	?
IFMIF	D^+	CW	CW	100	$2 \cdot 125$	$2 \cdot 125$	0.040	10.0	2010
KOMAC (KAERI)	H^+/H^-	CW	CW	100	20	20	0.1 (1.0)	2.0 (20)	2011 (?)
ATW	H^+	CW	CW	100	45	45	1.0	45	?

Progress in SC technology is making its application more attractive and broad. Dramatic increases in accelerating gradients are measured each year as a better understanding of the surface physics and cavity processing methods occurs. New types of cavities are being developed. Higher-power RF input couplers are being developed. And finally, more operational experience and data are becoming available at new facilities such as the TESLA Test Facility where they are studying pulsed-beam SC operations. High-intensity pulsed-beam-SC experience will soon also be gained at the SNS, scheduled to be operational in 2006.

Development of high-power accelerator technology is now a worldwide effort. The institutions involved are listed below:

- *US* (LANL, LBNL, LLNL, FNAL) – APT/LEDA, AAA, ATW, ADS, IFMIF, HIF, SNS, neutrino, factories and muon colliders.
- *Europe* (IAP/University of Frankfurt, GSI/TU Darmstadt, CEA/Saclay, CNRS/Orsay, TRASCO/INFN-ENEA, CERN, IHEP/Protvino) – ADS, ESS, IFMIF, Superconducting Proton Linac (SPL), High-intensity Light Source (SILHI), High-intensity Proton Injector (IPHI).
- *Asia* (KEK/JAERI, IAP, KAERI) – Basic Technology Accelerator (BAT), Fusion Neutron Source (FNS), IFMIF, Korea Multi-purpose Accelerator Complex (KOMAC).

What makes SC attractive?

A SC linac provides many advantages for high-intensity applications. First, there is reduced operating cost. Additionally, as achievable accelerating gradients increase and improved design solutions are found to take advantage of these high gradients, significant construction and operational cost savings should be realised. This is due to the reduction in the number of accelerating cavities and associated systems required to accelerate the beam. Tunnel-construction-cost savings should also result.

A SC linac should also offer improved operational flexibility. The short multi-cell cavities of a SC accelerator have larger velocity acceptance for the beam. Independent phasing of the cavities may allow operation even with some RF module failures and the larger cavity bore radius, acceptable for SC cavities, allows off-energy or poorly focused beams after faults to be transported with minimal or controlled losses. Reduced sensitivity to beam trips from thermally induced perturbations to cavity RF fields should result from the more stable operating temperatures.

Finally, over the past 5-10 years the worldwide industrial capability to produce SC accelerating cavities as increased dramatically. There are now more commercial firms building SC cavities and cryostats than there are building normal-conducting accelerating structures.

ADS challenges

Excellent progress has been made in accelerator technology development for ADS applications. The main ADS system design challenges will be at the accelerator and subcritical multiplier (SCM) interface. Reactor designers generally view the accelerator as a “black box” providing neutrons on demand with the expectation that operational availability, and reliability, will be similar to that of a nuclear reactor with few or no interruption in neutron production. By contrast, accelerator designers tend to view the target-multiplier as a modified, special-purpose beam target that should be insensitive to the normal beam trips which occur in most accelerators. Requiring the accelerator to meet “reactor world” operational specifications or, likewise, requiring the SCM to be capable of accepting an erratic beam from an accelerator seem difficult design requirements at present. Beam availability has been the usual requirement for accelerators rather than beam continuity (for example, 90% availability at LANSCE). A major design goal so far for our ADS linac has been to substantially reduce beam interrupts so as to limit thermal stresses in the target. Reduction of beam-interrupt rates, as is presently required, will be very challenging. Future efforts must be to develop reasonable system-level requirements that include compromises between both the driver-linac design and the SCM-system design to reach the goals in the most cost-effective manner. These requirements have yet to be established.

These accelerator-SCM-interface requirements are primarily driven by material-stress limits and safety considerations. Excessive beam trips cause large coolant temperature excursions that in turn cause the surface temperature on structures to change quickly. This results in large transient thermal gradients and high mechanical stresses in the target. Multiple thermal cycles cause fatigue and potential component failure. Safety considerations include a situation where excessive beam power (excessive current or energy) from the accelerator potentially causes a power/flow mismatch in the target or multiplier that could cause catastrophic failure of the SCM. Advanced target and accelerator diagnostics and controls will be required to effectively shut down the beam (i.e. for loss of flow or heat sink) and to control the beam on target (current and energy).

Future expectations and conclusions

Since 1995 there has been a rapid transition to RF superconducting technology world wide. These worldwide efforts in SC technology will no doubt produce many interesting surprises in the future. High-intensity operation of the SNS SC linac, scheduled to start in 2006, will most certainly teach us something about pulsed-mode operations and operations with ion beams. High-power SC linacs are being extended to lower and lower beam velocities, even including SC RFQs at a few MeV beam energy. Alternative superconducting materials (Nb3Sn, MgB2, ...) are being developed. We should also see higher reliability and availability with new computer control and beam diagnostics advances and higher intensity linac beams using multiple beams and funnelling.

Besides the technology advances, much has been learned about high-current beam dynamics. Control of emittance and beam halo will be important for future high-intensity linacs. Accelerator and subcritical multiplier interface issues will probably be the most challenging design issues for an ADS system. Los Alamos has a long history of significant high-intensity accelerator accomplishments and contributions over the last 35 years. Continued technology development related to high-intensity applications like ADS remains a strong interest at Los Alamos.

REFERENCES

[1] *Los Alamos Neutron Science Center Activity Report, January-December 2002*, Los Alamos National Laboratory Progress Report, LA-14036-PR, August 2003.

[2] Knapp, E.A., B.C. Knapp and J.M. Potter, "Standing Wave High Energy Linear Accelerator Structures", *Rev. Sci. Instr*., Vol. 39, 979 (1968).

[3] Vernon Smith, H., Jr., J.D. Schneider and R. Sheffield, "Low-energy Demonstration Accelerator (LEDA) Test Results and Plans", *Proceedings of the 2001 Particle Accelerator Conference*, Chicago, Illinois, 18-22 June 2001.

[4] Allen, C.K., *et al*., "Beam Halo Measurements in High-current Proton Beams", *Phys. Rev. Letters*, Vol. 89, No. 21, 214802-1, 18 November 2002.

[5] Gilpatrick, J.D., *et al*., "Beam Profile Instrumentation for Beam-halo Measurement: Overall Description and Operation", *Proceedings of the 2001 Particle Accelerator Conference*, Chicago, Illinois, 18-22 June 2001.

FRENCH ACCELERATOR RESEARCH FOR ADS DEVELOPMENTS

Jean-Michel Lagniel
CEA – DAM Ile de France, Bruyères-le-Châtel, France

Abstract

Teams from the CEA and CNRS French research agencies are working on high-intensity high-duty factor proton, H^- and deuteron linear accelerators for several applications (waste transmutation, nuclear and high-energy physics, spallation neutron sources, tritium production, materials irradiation facilities...). The R&D programmes undertaken to progress on the different components of such linacs and the simulation tools developed to optimise their design will be described.

Introduction

The CEA and CNRS French research agencies have been [1] and are still involved in the study of high-intensity and high-power proton and deuteron accelerators for several projects:

- TRISPAL: A facility for tritium production based on a 40-mA CW proton linac up to 600 MeV (24 MW beam power) studied from 1992 to 1998.
- IFMIF: The International Fusion Material Irradiation Facility based on two 125-mA CW deuteron linacs up to 40 MeV (2 · 5 MW beam power) since 1994.
- ADS demonstrator since 1994.
- CONCERT: A multi-purpose facility based on a 100-mA high-duty factor proton and H^- linac up to 1.3 GeV (20 MW beam power) studied from 1999 to 2001 [2].
- ESS: The European Spallation Neutron Source using a 100-mA 5% duty cycle H^- linac up to 1.3 GeV studied from 1996 to 2003.
- EURISOL: A European project for a future RIB production facility based on a 5-mA CW 1-GeV proton linac (5 MW beam power) since 1999.
- SPIRAL 2: A GANIL project for a RIB production facility using a 40-MeV, 5-mA CW deuteron beam accelerated up to 40 MeV started in 2002.
- Neutrino production facility projects based on proton drivers, in particular in the framework of the HIPPI joint research activity.

The large domain covered by these projects and the interest, even temporary, attached to each project explain the important and continuous effort undertaken by the two French agencies in collaboration with several laboratories all over the world. It is clear that ADS studies strongly benefit from the synergies with the other projects. The necessity to achieve a very high availability with a reduced number of beam trips for ADS is an additional constraint which renders the R&D effort even more indispensable so as to obtain a realistic view of the new generation of high-power accelerators.

The design and R&D efforts concerning ADS studies are now focused on the XADS accelerator reference scheme shown in Figure 1.

The main parameters of the linac [3] designed to drive a 80-MWth subcritical core are:

- 600-MeV protons nominal energy (800 MeV upgrade).
- 6-mA CW maximum current on target (10 mA rated).
- 200-ms beam interruptions for neutronics measurements.
- Number of beam trips (> 1 sec) lower than five per year.
- Stability: $\Delta W/W < -1\%$ (beam energy) and $\Delta I/I < -2\%$ (beam current).

Figure 1. The XADS linac reference scheme

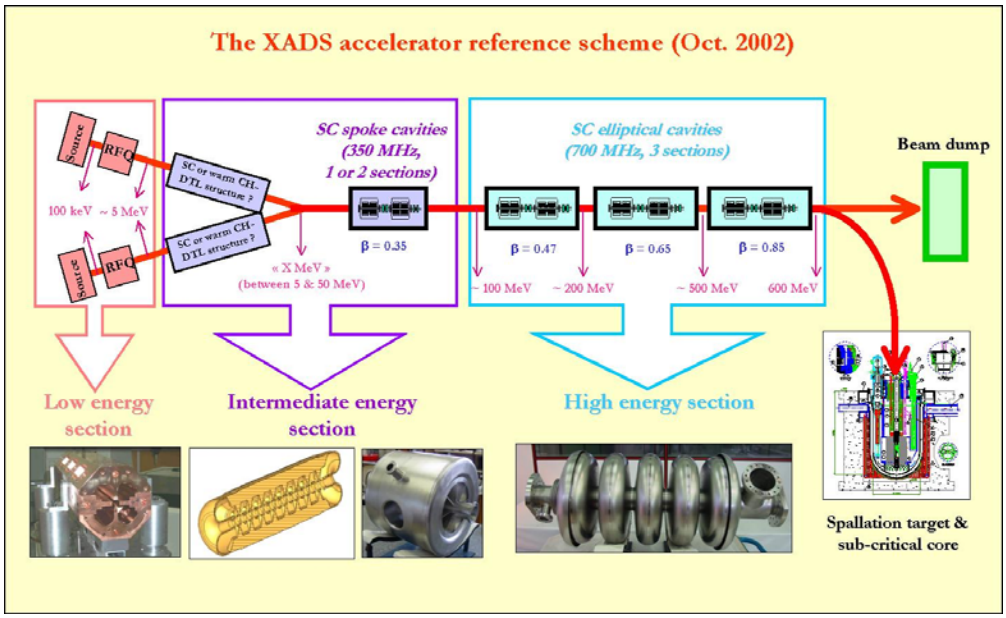

The French laboratories work on the low-, intermediate- and high-energy sections of this linac and have developed the tools needed to design and optimise the whole accelerator. The following sections of this paper will provide a broad but inevitably incomplete overview of the very large amount of work done by the CEA and CNRS teams; the author apologises to those colleagues whose work is not mentioned.

R&D on the accelerator low-energy part

The Injector of Protons for High Intensity (IPHI) demonstrator project is being developed by a CEA/DSM, CNRS/IN2P3 and CERN collaboration. The aim of this project is to build and test an injector made up of the proton source SILHI (*Source d'Ions Légers Haute Intensité*), a low-energy beam transfer (LEBT) line including a fast chopper, a RFQ linac and a high-energy beam transfer (HEBT) line equipped with diagnostics for accurate beam characteristics measurements [4].

The particles are injected from the SILHI ECR source which has been producing CW and pulsed intense proton and deuteron beams since 1996. More than 130 mA CW are now routinely produced at 95 keV with a proton fraction higher than 80%. A continuous effort has been made to improve the beam stability and to reduce the beam losses in the extraction system and beam line. Automatic restart procedures allow minimising the beam off time. Several long-run tests have been performed during a total time of 810 hours to measure the source reliability and to improve the mean time to repair. In 2001, a 104-hour test was successfully achieved with a 75-mA CW proton beam; the source availability reached 99.96% [5].

More recently, a new reliability test dedicated to ADS studies was performed at a lower current [6]. Figure 3 shows the data recorded during a 162-hour period with a 30-mA CW proton beam. This "moderate" beam intensity was obtained through a reduction of the extraction aperture diameter from 8.0 to 4.8 mm (same plasma density and fraction species as for higher currents). A very short spark occurred about 10 hours after the beginning of the run, but no beam interruption during the sampling time was observed.

Figure 2. Scheme of the IPHI installation (top) and IPHI 6-m long RFQ HEBT and beam stop

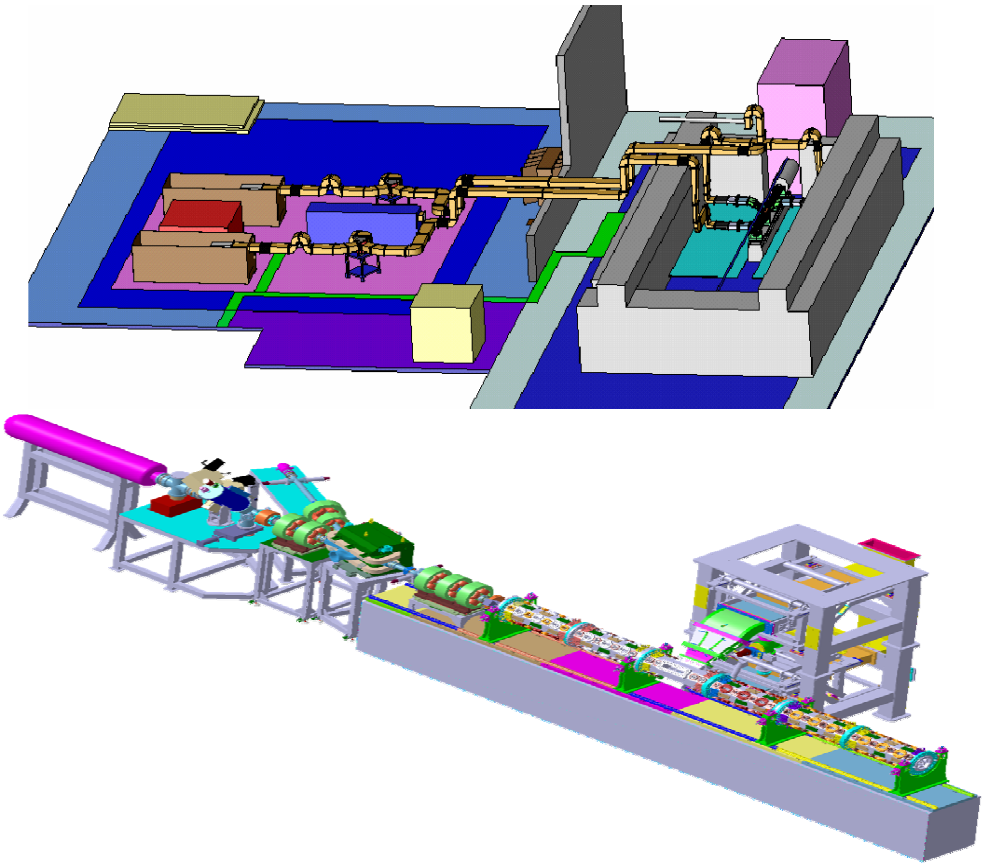

Figure 3. Record of a continuous 162-hour test of SILHI (sampling period = 2 s)

Green – SILHI platform high voltage (95 kV), blue – Extracted beam current (30 mA with some instability)

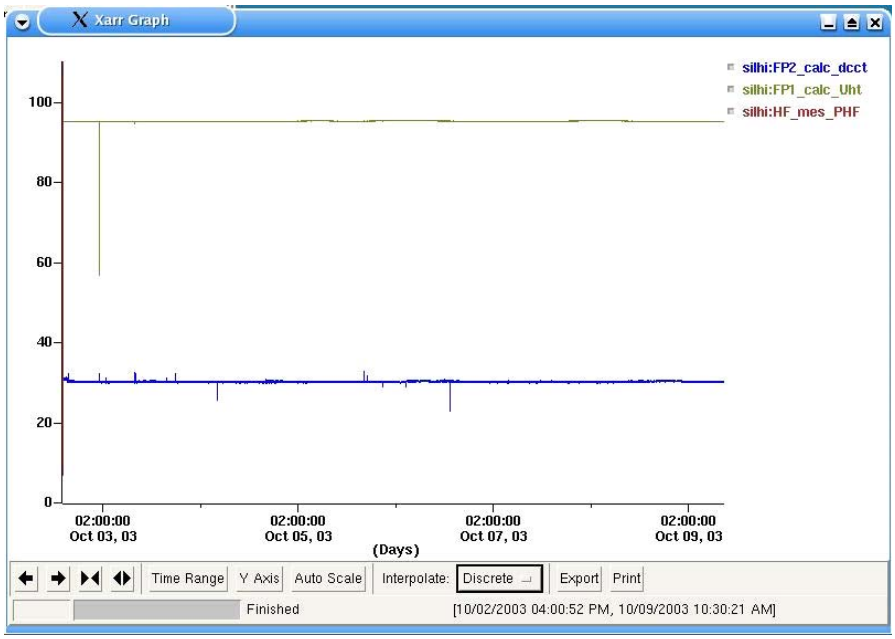

The IPHI RFQ is designed to accelerate a 100-mA CW proton beam from 95 keV to 3 MeV. The construction of the segmented 6-m long RFQ is under progress. Figure 4 shows some pictures of the first RFQ segment machined and brazed recently. The RFQ fabrication will continue up to mid-2006.

Figure 4. Pictures of the first IPHI RFQ 1-m long segment (top). Bottom left: Detail of the vanes modulation. Bottom right: Inside of the cavity with the pumping holes and the slug tuner holes.

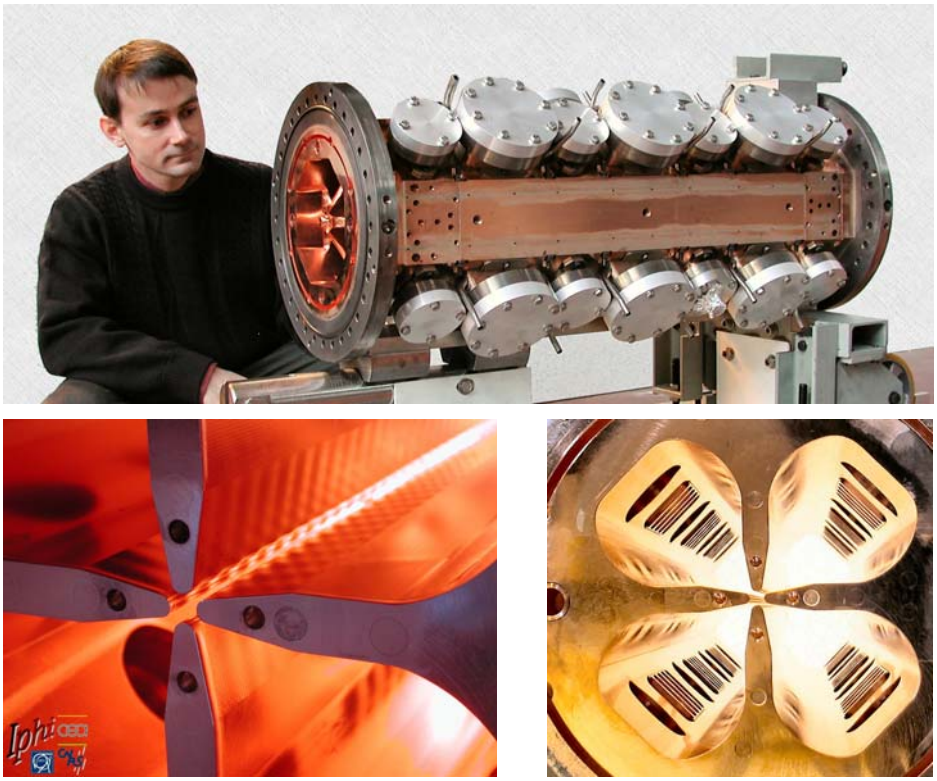

The IPHI test stand installation is progressing rapidly (concrete shielding in place, water cooling system nearly completed…). The RF system based on two LEP klystrons (1.3 MW CW, 352 MHz) shown in Figure 5 will first be tested on a load in October 2004. A new technique of RF coupling has been successfully tested on the 6-m RFQ mock-up (aluminium).

Figure 5. View of the two 352 MHz, 1.3 MW CW RF systems installed in the IPHI test area



IPHI RFQ first beam is scheduled in September 2006. Reliability tests especially prepared in the framework of ADS will be performed up to September 2007, date of the transfer of the installation to CERN.

Research on the accelerator medium-energy part

Room temperature drift tube linac (DTL)

Over the course of the IPHI project, a DTL hot model (Figure 6) was successfully built and tested (CEA-Saclay, CEA-Bruyères-le-Châtel, CNRS-IN2P2-Grenoble, CERN collaboration) [7]. The tests at CERN were made at the nominal power of 40 kW CW for an accelerating field of 1.75 MV/m. Results show that a stainless steel envelope can be used even at this high power density, provided that it is copper-plated both inside and outside to enhance the thermal conductivity. The prototype is a four-gap DTL structure with three full drift tubes, two of them including quadrupole electromagnets. Two types of drift tubes were tested, one using a completely new design with the whole drift tube filled with water cooling both magnet conductor and drift tube body (Figure 7). This design is extremely efficient from the cooling point of view and leads to important cost savings.

The demonstration that a 5-10 MeV CW DTL is a good candidate to follow the RFQ has been made.

Figure 6. View of the 352-MHz CW DTL prototype: Cavity (left) and drift tubes (right)

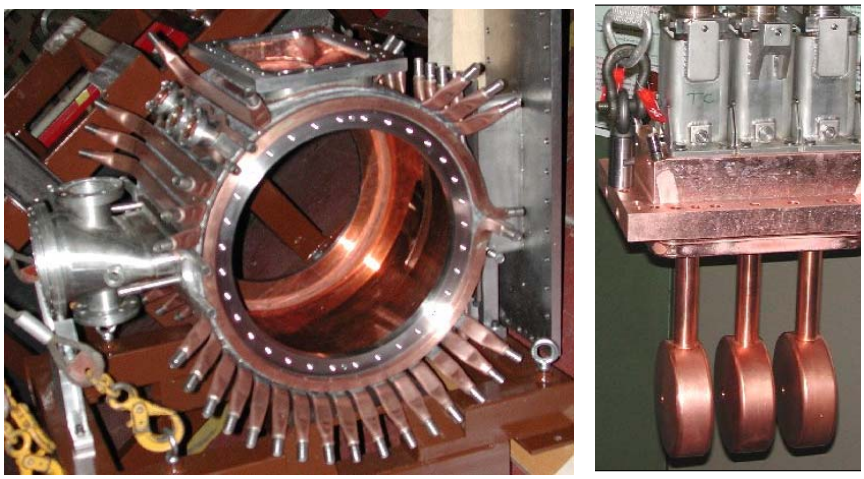

Figure 7. Pictures of the two types of quadrupoles tested in the DTL prototype

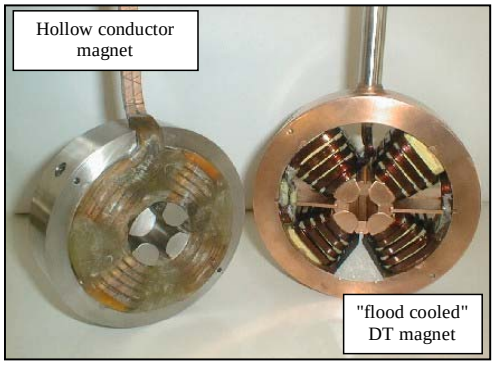

Quarter Wave Resonator (QWR) superconducting cavities

The CEA-Saclay team is studying 88 MHz QWRs for the SPIRAL 2 project (RIB facility, GANIL). The fabrication of a prototype (Figure 8) is in progress, with assembly scheduled next September [8]. RF studies (tuning, couplers…) are also undertaken with a view to the development of technologies which can benefit ADS accelerators.

Figure 8. Views of the 88-MHz Quarter Wave Resonator prototype in construction for the SPIRAL 2 project

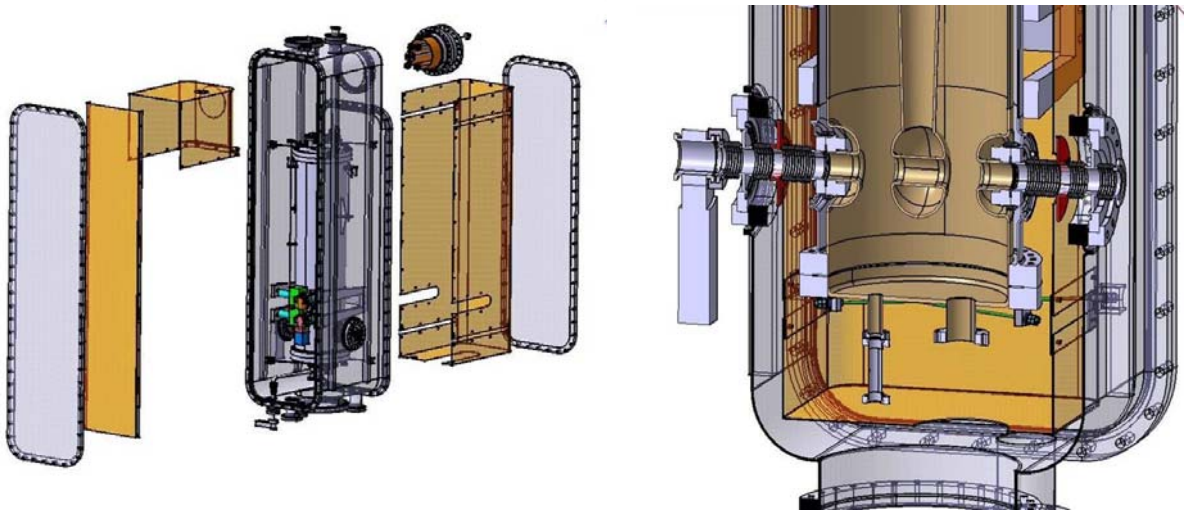

Spoke superconducting cavities

Spoke cavities, more efficient at 352 MHz, have been chosen for the ADS accelerator reference design. A β = 0.35 prototype was studied, built by CERCA and tested at IPN-Orsay [9]. The cavity, which is a 352-MHz two-gap resonator (Figure 9) has shown a good mechanical stability and a low Lorentz force detuning coefficient. The RF tests at 4.2 K (Figure 10) show that the quality factor is above 10^9 for the ADS working point (6.2 MV/m). The maximum accelerating field exceeds 12 MV/m after He processing, providing a large safety margin; high reliability using such cavities can thus be expected.

Figure 9. 3-D drawing (left) and picture of the spoke cavity prototype

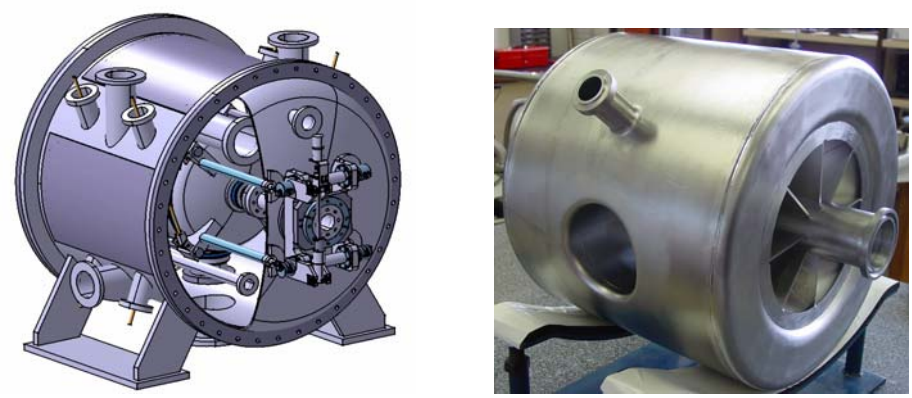

Figure 10. Quality factor vs. accelerating field for the b = 0.35 spoke cavity prototype

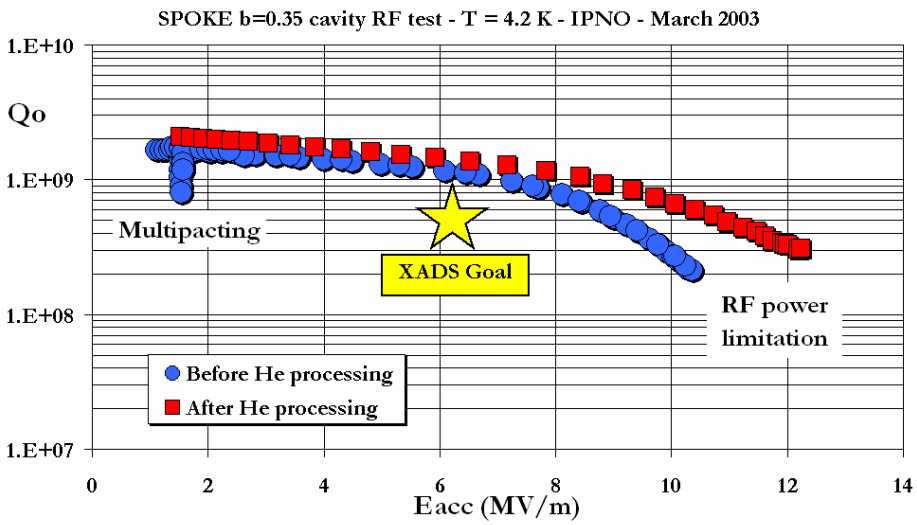

Research on the accelerator high-energy part

The R&D collaboration on 700-MHz superconducting radio frequency (SCRF) cavities between CEA-Saclay and IPN-Orsay started few years ago in the framework of the French Superconducting Accelerator for Hybrid (ASH) reactor project, aborted since then. Nevertheless the study of this kind of cavity is always a topical subject because of its involvement in any proton linear accelerator requiring a high-energy section (Spallation Neutron Sources, EURISOL, XADS, muon colliders and neutrino factories projects).

The first 700-MHz, b = 0.65, five-cell niobium superconducting cavity (Figures 11 and 12) was successfully tested in the horizontal cryostat CryHoLab (Figure 13). Technological choices such as equipment with a stainless steel helium vessel and flanges appeared to be viable for the future. Before this test, several operations were performed: field flatness adjustment, chemical etching, heat treatment and RF measurements in vertical cryostat. Good performances for a multi-cell cavity were obtained. However, field emission and not-yet-elucidated phenomenon limit the accelerating field around 16 MV/m [10-11] (Figure 14). An important R&D effort is also devoted to control of the Lorentz detuning of the cavities (amplitude/phase control) [12-13]. A 150-kW CW RF coupler (KEK, SNS type) will be fabricated and tested this year.

Figure 11. Drawing of the first 700-MHz, b = 0.65, five-cell SCRF cavity

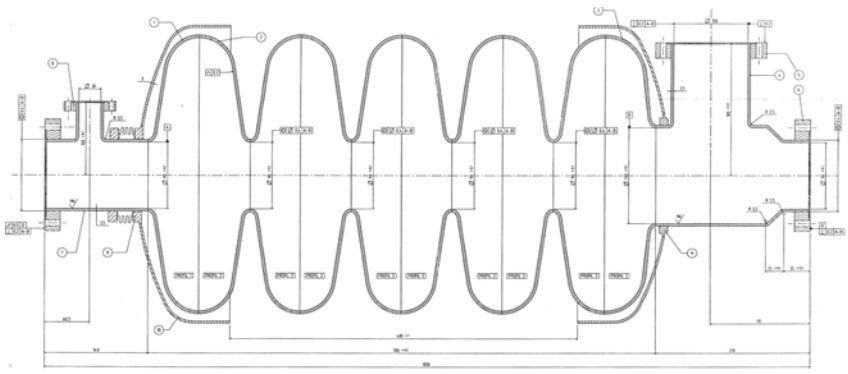

Figure 12. TIG welding (CERCA) of the first 700-MHz, $\beta = 0.65$, five-cell SCRF cavity (left) and picture of the cavity in the clean room (right)



Figure 13. Drawing (left) and picture (right) of the horizontal cryostat CryHoLab used by the CEA-Saclay/IPN-Orsay collaboration to test the SCRF cavities

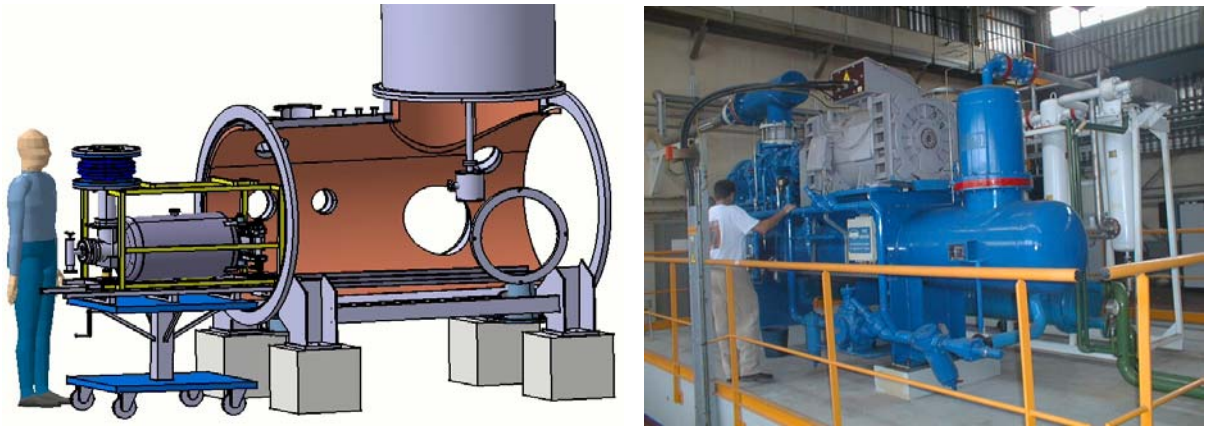

Figure 14. First measurements (2003) of the 700-MHz, $\beta = 0.65$, five-cell SCRF cavity. Multipactor has been observed around 10 MV/m, XADS specs are $Q_0 > 10^{10}$ at 10 MV/m and 2 K.

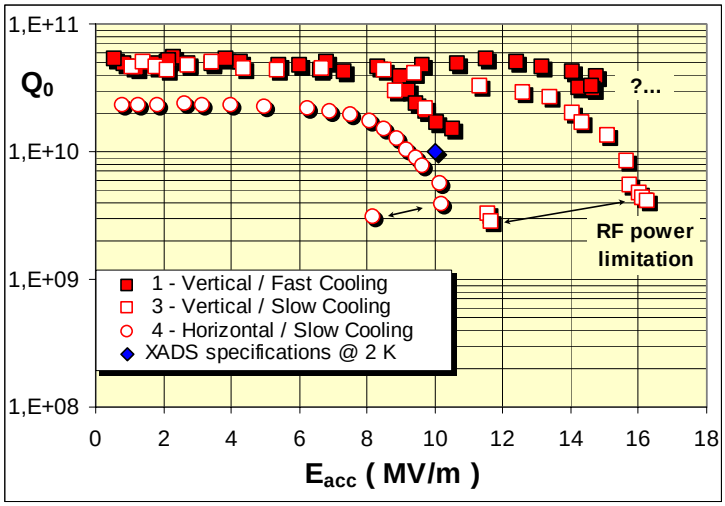

Code developments and accelerator design for ADS

A continuous and important effort is undertaken to develop the tools needed to design and optimise the whole accelerator [14] with two main concerns:

- The level of beam loss during operation must be extremely low (lower than 1 W/m although the beam power exceeds MWs) to allow hands-on maintenance of the equipments. For this purpose, the work is mainly focused on three subjects:

  i) Study of the basic mechanisms leading to "halo formation".

  ii) Development of codes accurate up to very low densities taking into account mechanical and tuning errors from the source to the target.

  iii) Crosschecks with experiments (SILHI, IPHI, ...).

- The design must take into account fault tolerance of accelerator components to achieve the very high reliability level requested for ADS. This new constraint specific to ADS has led to several evolutions of the numerical simulation codes [15].

A complete set of codes for the design and automatic optimisations of the high-intensity linacs is now operational (Figure 15). Accurate space charge computations are performed up to approximately 10^6 macro-particles using multi-grid PIC methods. Beam dynamics studies can be done "from the source to the target" with tools for automatic error studies which can be distributed over several PC computers to allow statistics up to 10^{-7}.

Figure 15. Organisation of the set of codes developed by the CEA-Saclay to design and optimise high-intensity linacs (see [14] for the description of each module)

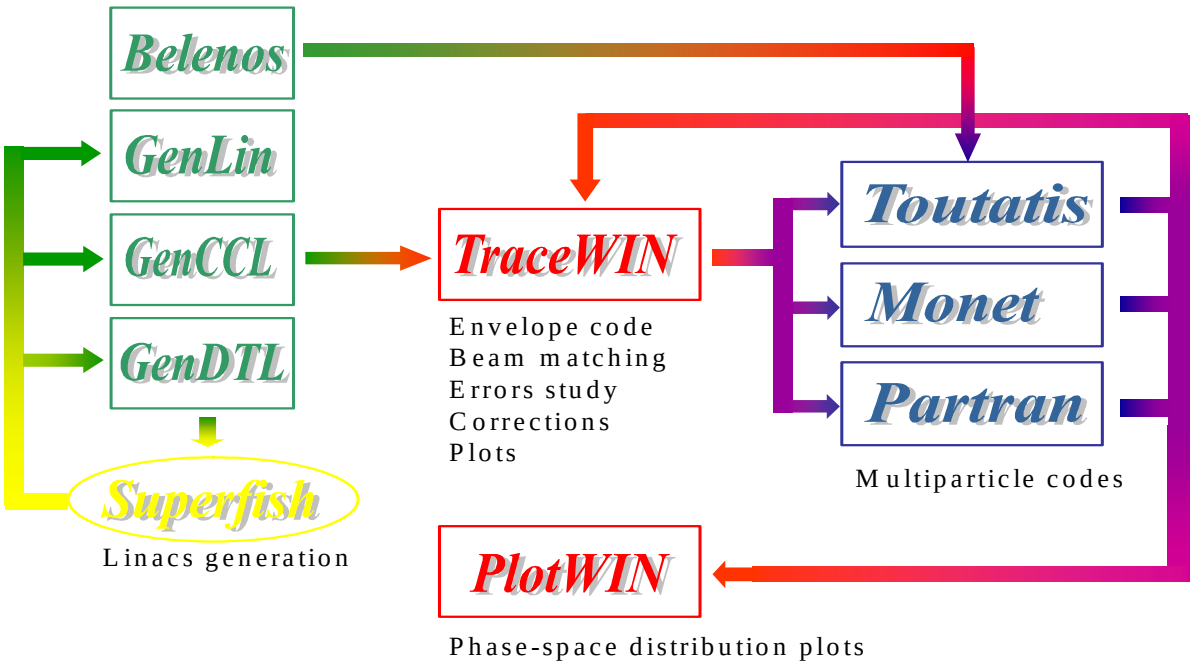

Perspectives

It is proposed to continue the accelerator studies for ADS in the framework of the Integrated Project EUROTRANS (EURATOM 6th F.P. 2nd call) [16]. The project proposal which has been made by about 30 European organisations is divided into five sub-projects, SP1 "DESIGN" being devoted to the "Development and Assessment of a Reference Design of a European Transmutation Demonstrator (ETD) Industrial-scale Prototype of Waste Burner (200-300 MWth)".

The subject of SP1 Work Package #3 (WP3) is "Accelerator Technology Development Focused on the Specific Needs of an ETD: Reliability Issues and Feasibility of Upgrade for Future Industrial Applications". The CEA and CNRS teams have been involved in the proposition of the WP3 tasks:

- Task 1.3.1: Experimentally determine the reliability of the injector part by means of the 3-MeV, 100-mA accelerator IPHI.

- Task 1.3.2: Assess the performance of the subsequent accelerating components (medium energy section) with a quantification and optimisation made with experimental results from three prototypical components.

- Task 1.3.3: Qualify the performance of a high-energy section cryomodule.

- Task 1.3.4: Design and realisation of a prototypical RF control system made to guarantee the fault tolerance of the linac. Final performance tests will include a connection to the cryomodule of Task 1.3.3.

- Task 1.3.5: Ensures the "overall coherence" of this R&D so that the outcome is a frozen design with assessed reliability and costing. It also includes the beam dynamics calculations for the fault tolerance.

Acknowledgements

Many thanks to Alex Mueller, Pascal Debu, Robin Ferdinand, Pierre-Yves Beauvais, Stéphane Chel and Nicolas Pichoff for their help.

REFERENCES

[1] Lagniel, J-M., "High-intensity LINAC Studies in France", *Proc. International LINAC Conference* (1998).

[2] Lagniel, J-M., "High-power Proton Linac for a Multi-user Facility", *Proc. EPAC 2000*, Vienna, Austria.

[3] Vandeplassche, D., “The PDS-XADS Reference Accelerator”, these proceedings. See also Mueller, A., “The PDS-XADS Reference Accelerator”, *Proc. Int. Workshop on P&T and ADS Development (INWOR)*, Oct. 2003.

[4] Beauvais, P-Y., “Status Report on the Construction of the French High Intensity Proton Injector (IPHI)”, *Proc EPAC 2002*, Paris, France. See also Beauvais, P-Y., “Recent Evolution in the Design of the French High Intensity Proton Injector IPHI”, *Proc. EPAC 2004*, Lucerne, Switzerland.

[5] Gobin, R., *et al*., “Reliability Tests of the High Power Proton Source SILHI at CEA/Saclay”, *Proc. NEA Workshop HPPA3*, Santa Fe, NM, 12-16 May 2002.

[6] Ferdinand, R., *et al*., *CEA-DSM-DAPNIA-SACM Contribution to the IFMIF Transition Phase 2003*, DSM/DAPNIA 04-35.

[7] Bernaudin, P-E., *et al*., “Results of the IPHI Drift Tube Linac Hot Model CW Tests”, *Proc. PAC 2003*, Portland, Oregon, USA.

[8] Devanz, G., *et al*., “Quarter-wave Cavities for the SPIRAL 2 Project”, *Proc. SRF 2003*, Luebeck, Germany.

[9] Olry, G., *et al*., “Development of SRF Spoke Cavities for Low and Intermediate Energy Ion Linacs”, *Proc. SRF 2003*, Luebeck, Germany. See also Olry, G., *et al*., “Recent Developments of Superconducting b = 0.35 and b = 0.15 Spoke Cavities at IPN for Low and Medium Energy Sections of Proton Linear Accelerators”, *Proc. EPAC 2004*, Lucerne, Switzerland.

[10] Bousson, S., *et al*., “700 MHz SC Proton Cavities Development and First Tests in the Horizontal Cryostat CRYHOLAB”, *Proc. EPAC 2002*, Paris, France.

[11] Visentin, B., *et al*., “Experimental Results on 700 MHz Multicell SC Cavities for Proton Linacs”, *Proc. PAC 2003*, Portland, Oregon, USA.

[12] Devanz, G., M. Luong and A. Mosnier, “Numerical Simulations of Dynamic Lorentz Detuning of SC Cavities”, *Proc. EPAC 2002*, Paris, France.

[13] Luong, M., M. Desmons, G. Devanz and A. Mosnier, “Minimizing RF Power Requirement and Improving Amplitude/Phase Control for High Gradient SC Cavities”, *Proc. EPAC 2002*, Paris, France.

[14] Duperrier, R., N. Pichoff, D. Uriot, “CEA-Saclay Codes Review for High Intensities Linacs Computations”, *Computational Science – ICCS 2002: International Conference*, Amsterdam, The Netherlands, 21-24 April 2002. Proc. Part III.

[15] Pierini, P., these proceedings, see also Biarotte, J-L., *et al*., “Beam Dynamics Studies for the Fault Tolerance Assessment of the PDS-XADS Linac Design”, *Proc. EPAC 2004*, Lucerne, Switzerland.

[16] Bhatmagar, V., “R&D on ADS in the EURATOM Fifth and Sixth Framework Programmes”, these proceedings.

HYBRID POWER EXTRACTION REACTOR (HYPER) PROJECT

T-Y. Song, J-E. Cha, C-H. Cho, C-H. Cho, Y. Kim, B-O. Lee, B-S. Lee, W-S. Park, M-J. Shin
Korea Atomic Energy Research Institute
P.O. Box 105, Yuseong, Daejeon, 305-600, Korea

Abstract

The KAERI ADS system is known as the *HY*brid *P*ower *E*xtraction *R*eactor (HYPER) project. Research on this project began as a 10-year nuclear research programme in 1997. The conceptual design of the HYPER core is almost complete. HYPER is designed to transmute TRU and some fission products such as ^{129}I and ^{99}Tc. HYPER is a 1 000 MW_{th} system and its k_{eff} is 0.98. The required current is 10.6 mA at BOC and 16.4 mA at EOC. The inventory of TRU is 6 510 kg at BOC, and 282 kg of TRU is transmuted per year. In the case of fission products, ^{129}I and ^{99}Tc are transmuted at the rates of 7 and 27 kg/yr, respectively. Pb-Bi is used as the coolant and target material. The average outlet temperature is 490°C when the inlet temperature of coolant is 340°C. The maximum cladding temperature turned out to be 570°C. It was found that a 2.5-mm thick beam window is needed to sustain the mechanical load. When the inlet velocity of Pb-Bi is 0.95 m/s, the maximum allowable current is 24.1 mA, which is greater than the required current of HYPER. U surrogate fuel was fabricated and tested. KAERI joined the MEGAPIE project in 2001 for Pb-Bi research. KAERI also installed the static Pb-Bi corrosion test device in 2003 and began experiments. KAERI will complete the construction of a Pb-Bi corrosion loop in 2004.

Introduction

KAERI has been working on ADS since 1997. The KAERI ADS system is known as the *HY*brid *P*ower *E*xtraction *R*eactor (HYPER) project. Research on this project began as a 10-year nuclear research programme funded by the government. The ADS research of KAERI consists of three stages. A basic concept of HYPER was established in the first stage (1997-2000) of development. The basic technology related to HYPER was investigated in the second stage (2001-2003) while upgrading the design. The third stage of research began in March 2004. The conceptual design of the HYPER core will be completed during this third stage (2004-2006). The investigation of key technologies will be continued in the third stage.

The conceptual design of the HYPER core was almost finished during the second stage. The upgrade of core design and transient study will be done in the third stage. Regarding experimental research, fuel and Pb-Bi study were performed during the second stage. U surrogate fuel was fabricated and tested. KAERI joined MEGAPIE project in 2001 for Pb-Bi research. KAERI also installed the static Pb-Bi corrosion test device in 2003 and started experiments. KAERI will complete the construction of a Pb-Bi corrosion loop in 2004. The I-NERI programmr, related to lead-alloy experiments, will be launched in 2004. For the fuel/FP target study, KAERI plans to perform fission product irradiation test using KAERI's research reactor HANARO.

In this paper, the results obtained through the research of the first and second stages and plans for the third stage will be described. The results and plans for further research are also discussed, and fall into two categories, one being design and analysis, the other experimental.

Design and analysis

Core

HYPER is designed to transmute TRU and some fission products such as ^{129}I and ^{99}Tc. HYPER is a 1 000 MW_{th} system and its k_{eff} is 0.98. Figure 1 shows a schematic configuration of the HYPER core with 186 ductless hexagonal fuel assemblies. As shown in the figure, the fuel blanket is divided into three TRU enrichment zones to flatten the radial power distribution. In HYPER, a beam of 1-GeV protons is delivered to the central region of the core to generate the spallation neutrons. To simplify the core design, the LBE coolant is used as a spallation target as well. In addition to the ultimate shutdown system (USS), six safety assemblies are placed in the HYPER core in case of an emergency. The safety rods are also used conditionally to control the reactivity of the core. For a balanced transmutation of both TRUs and LLFPs (^{99}Tc and ^{129}I), ^{99}Tc and ^{129}I are incinerated in moderated LLFP assemblies loaded in the reflector zone.

It is well known that the LBE coolant speed is limited (usually <2 m/sec) due to its erosive and corrosive behaviour. Therefore, the lattice structure of the fuel rods should be fairly sparse. In fast reactors, a pancake-type core has been typically preferred mainly to reduce the coolant pressure drop. Unfortunately, it has been found that the multiplication of the external source is quite inefficient in a pancake-type ADS because of the relatively large source neutron leakage. It was shown that the maximum source multiplication can be achieved when the core height is about 2 m [1]. Taking into account the source multiplication and the coolant speed, the core height of HYPER was compromised at 150 cm, and the power density was determined such that the average coolant speed could be about 1.65 m/sec. To reduce the core size and improve the neutron economy, a ductless fuel assembly is adopted in the HYPER system. An advantage of the ductless fuel assembly is that the flow blockage of a subassembly is basically impossible and the production of the activation products in the duct can be avoided.

Figure 1. Schematic diagram of the HYPER core

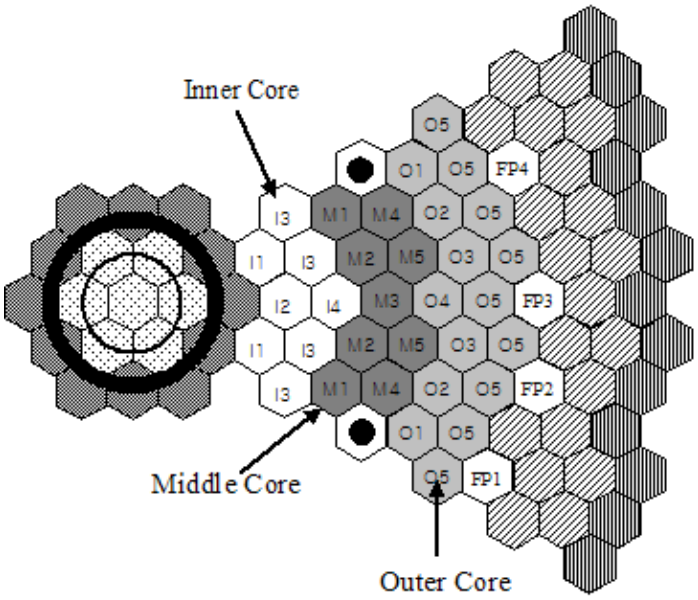

Concerning a TRU-loaded ADS using a fixed cycle length, one of the challenging problems is a very large reactivity swing, leading to a large change of the accelerator power over a depletion period. Even in an ADS loaded with a minor actinide (MA) fuel, the burn-up reactivity swing is found to be fairly noticeable, although it is relatively smaller than that of a TRU-loaded core. The large burn-up reactivity swing results in several unfavourable safety features as well as deleterious impacts on the economics of the system. In the HYPER core, the ^{10}B was also used as a burnable absorber (BA) in a unique way to reduce the reactivity swing and control the core power distribution [2].

The required current is 10.6 mA at BOC and 16.4 mA at EOC. The inventory of TRU is 6 510 kg at BOC and 282 kg of TRU is transmuted per year. In the case of fission products, ^{129}I and ^{99}Tc are transmuted with the rates of 7 and 27 kg/yr, respectively. The fuel cycle is 180 days. HYPER adopts a scattered fuel reloading system.

MC-CARD, REBUS-3 and DIF3D are used for the core analysis. The LAHET code system is used for the target neutronic calculations. KAERI is also developing a kinetics code called Design Evaluation and Simulation of Nuclear Reactor (DESINUR).

Fuel and fission products

In general, a non-uranium alloy fuel is utilised in a TRU transmuter to maximise the TRU consumption rate. Previously, a Zr-based dispersion fuel was used as the HYPER fuel since it was expected that a very high fuel burn-up could be achieved. However, we have found that the dispersion fuel transforms to a metallic alloy during the high-temperature operation. Therefore, in the current design, a metallic alloy of U-TRU-Zr is utilised as the HYPER fuel, in which pure lead is used as the bonding material. As a result, a large gas plenum is placed above the active core.

Each fuel assembly has 204 fuel rods, which are aligned in a triangular pattern with 13 tie rods. A fairly open lattice with a pitch-to-diameter (P/D) ratio of 1.49 is adopted in HYPER. In Figure 2, a schematic configuration of the ductless fuel assembly is shown. The ^{10}B burnable absorber is loaded

Figure 2. Fuel and fission product assemblies

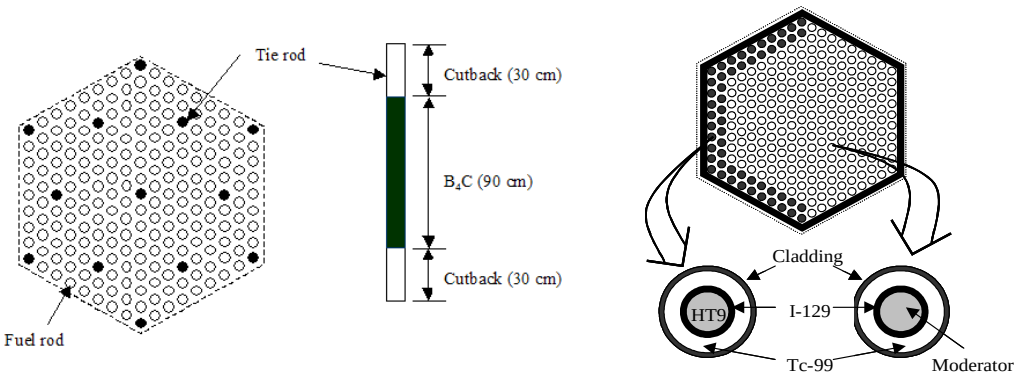

into the tie rods with top and bottom cutbacks in order to enhance the ^{10}B depletion rate and also to flatten the axial power distribution of the core. The BA concept with the cutbacks can effectively mitigate the peak fast neutron fluence of the assembly. The peak fast neutron fluence is a limiting design criterion in LBE-cooled fast reactors.

MACSIS-H (for an alloy fuel) and DIMAC (for a disperison fuel) are being developed as the steady-state performance analysis codes. The main structures of each code consist of the temperature profile calculation routine, the swelling/FGR calculation routine and the deformation calculation routine. The He production rates calculated by the other code are inserted into the swelling/FGR routine of each code. Figure 3 is an example of MACSIS-H calculation. The strain was calculated as a function of burn-up of HYPER fuel. The calculation was performed with and without He generation varying the fission gas rate. The result shows that the maximum strain is lower than the limit at a HYPER average discharge burn-up of 17 at.%.

Figure 3. Strain vs. burn-up for HYPER fuel

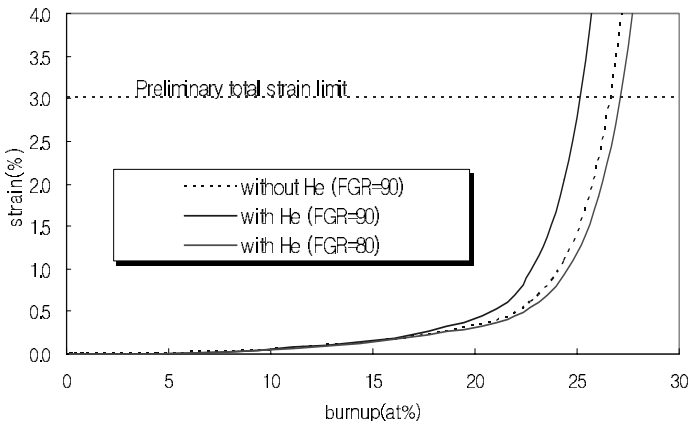

Coolant and target

Pb-Bi is used as the coolant and spallation target material. The coolant is not separated from the target. MATRA and SLTHEN are used for the core thermal-hydraulic calculations. SLTHEN can be used for multi-assembly analysis. Therefore, a 7-assembly and a 45-assembly analysis of HYPER were performed using SLTHEN. MATRA was developed to be used for the ductless assembly with grid

spacer, which is the case of HYPER fuel assembly. The sub-channel analysis was performed using MATRA and the result shows that the average outlet temperature is 490°C when the inlet temperature of coolant is 340°C. The maximum cladding temperature turned out to be 570°C

The cylindrical beam tube and the hemispherical beam window were adopted in the basic target design concept with 1-GeV proton energy, and the thermal-hydraulic and structural analyses were performed with the CFX and ANSYS codes. The target window material is 9Cr steel such as T91 and 9Cr-2WVTa. The beam window diameter and thickness were varied to find the optimal parameter set based on the design criteria: maximum lead-bismuth eutectic (LBE) temperature < 500°C, maximum beam window temperature < 600°C, maximum LBE velocity < 2 m/s and the maximum beam window stress < 160 MPa. The results show that a 40-cm wide proton beam with a uniform beam profile should be adopted for HYPER. It was found that a 2.5-mm thick beam window is needed to sustain the mechanical load. When the inlet velocity of Pb-Bi is 0.95 m/s, the maximum allowable current is 24.1 mA, which is greater than the required current of HYPER.

Figure 4. CFX and ANSYS results of HYPER target calculation

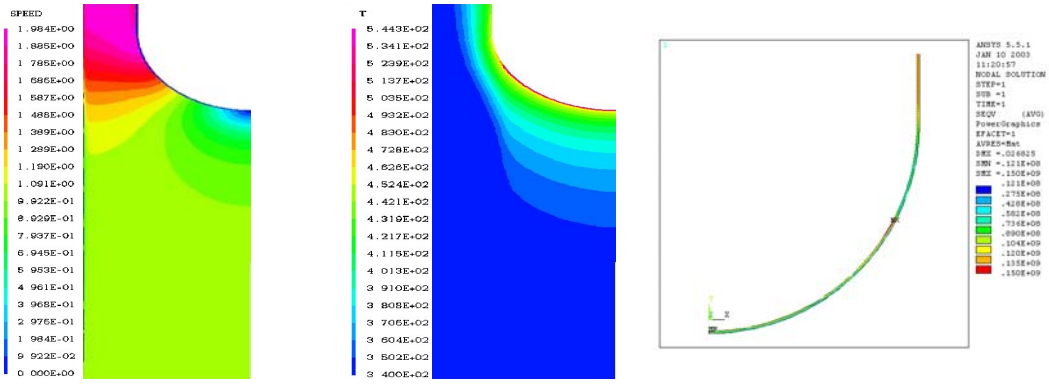

Velocity (Max=1.96 m/s) | Temperature (Max=544 °C) | Stress (Max=150 MPa)

Experiment

Fuel

Two types of metal fuels were considered for HYPER fuel. One is metal alloy type and the other is dispersion type. Both types of U surrogate fuel samples were fabricated and basic characteristics were investigated. It was found that dispersion fuel was not made with good microstructure and the original structure of dispersion fuel was not kept after annealing. Therefore, we chose the metal alloy fuel for HYPER.

The reference blanket fuel pin of HYPER consists of the fuel slug of the TRU-xZr (x = 50-60 wt.%) alloy, and it is immersed in lead for thermal bonding with the cladding. The blanket fuel cladding material is ferritic-martensitic steel HT-9. As a basic study on the HYPER fuel, we fabricated surrogate U-50, 55, 60 wt.% Zr alloy fuel instead of the actual TRU-Zr fuel. The U-Zr metallic fuel was fabricated by mixing, pressing, sintering and extrusion. The sintering temperature and time were 1 500°C and 2 hrs, respectively.

After fabricating the surrogate fuel, thermal properties such as thermal conductivity and thermal expansion coefficient were measured. Thermal stability testing of the surrogate fuel was also performed, so as to investigate volume and microstructure change. The fuel samples were placed in

the furnace for 1 500 hrs with temperatures of 630°C and 700°C. Figure 5 shows volume change as a function of time and microstructure change after annealing. Reaction characteristics were also investigated among Pb bonding, cladding material (HT-9) and U surrogate fuel.

Figure 5. Volume and microstructure change of U-Zr sample after annealing

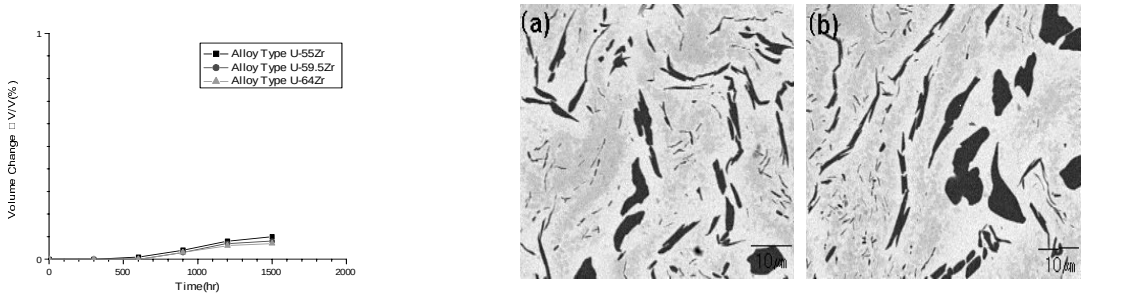

Volume change

Microscopic structure : (a) Before (b) After

Pb-Bi

KAERI joined the MEGAPIE project in 2001 for the experimental study of Pb-Bi. MEGAPIE is the 1-MW proton beam irradiation test of a Pb-Bi target. PSI, CEA, CNRS, FZK, ENEA, SCK•CEN, KAERI, JAERI and LANL are members of the MEGAPIE project. The Pb-Bi target is currently in the stage of fabrication.

The most significant problem in handling Pb-Bi is corrosion. Therefore static corrosion tests were performed at the FZK's facility COSTA to investigate the dissolution effect. KAERI also installed a static corrosion facility in 2003 and began static corrosion tests. Figure 6 shows the schematic diagram of the static corrosion facility. It is mainly composed of tube furnaces, a gas system and a glove box. The furnace has three independent zone heaters to reduce the temperature difference.

Figure 6. Schematic diagram of the KAERI static corrosion facility and test results

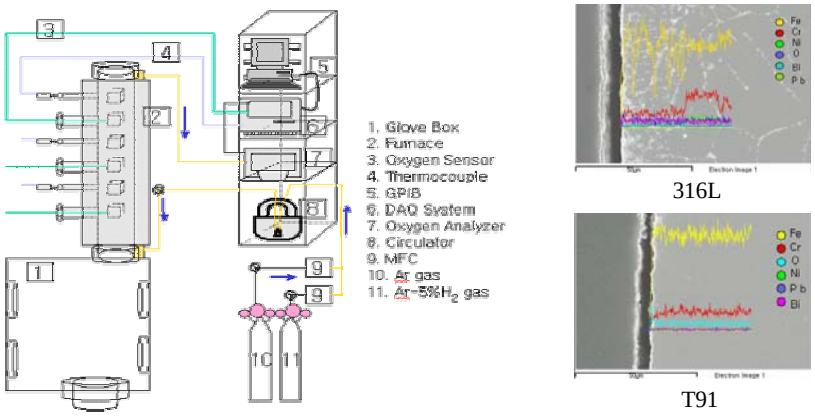

The test materials were 316LN and some ferrite/martensitic steels such as HT-9 and T91. The test was performed under both reduced and oxygen-controlled atmospheres. Part of the test results are shown in Figure 6.

Figure 7 shows the schematic diagram of the dynamic corrosion loop to be installed at KAERI. The LBE loop is an isothermal loop. The flow velocity in the test section was designed to be around 2 m/s in the range of 400~550°C and the charging volume of the LBE is around 0.03 m^3 in the circulation loop.

Figure 7. Three-dimensional schematic diagram of the corrosion loop

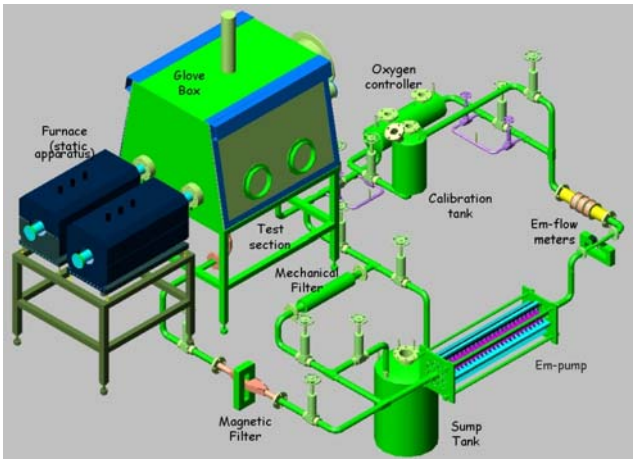

The LBE loop is mainly composed of a main test loop, a bypass loop for filtering the LBE and a mixture gas supplying system. The liquid metal in the main test loop circulates in the following order: EM pump – EM flow meter – oxygen controller – test section – magnetic filter – EM pump. From the analysis of the pressure drop, the specification of the piping system was determined as a 1.5-inch pipe to reduce the pressure drop by a high mean fluid velocity. The pressure drop of the main test loop was estimated at around 3 bar with the flow rate of 60 lpm.

The oxygen concentration in the range of 10^{-7} wt.%~10^{-5} wt.% is controlled by the chemical equilibrium between the mixture gas of hydrogen-argon and the water vapour. At present, the oxygen concentration in the LBE and the mixture gas is measured with an oxygen sensor made of yttria-stabilised zirconia as a solid electrolyte cell and Pt/air as a reference system.

Summary

KAERI has been working on ADS since 1997. The KAERI ADS system is known as the *HY*brid *P*ower *E*xtraction *R*eactor (HYPER) project. HYPER research began as a 10-year nuclear research programme. The ADS research of KAERI consists of three stages. The conceptual design of the core was almost completed during the second stage (2000-2003). The core design will be upgraded and modified in the third stage (2004-2006). For example, the dual annular injection tube will be introduced to reduce the flow rate of Pb-Bi in the target channel. The structural analysis of the HYPER fuel assembly will also be performed. The main work related to the design and analysis, however, is the transient case study. Some core transient cases such as LOHS-WS and LOF-WS will be studied. The transient cases related to target, beam window and fuel assembly structure will also be examined.

KAERI fabricated U surrogate metal fuel and performed tests using U fuel samples to investigate basic characteristics during the second stage of research. The HYPER fission product target includes both ^{99}Tc and ^{129}I in the same rod. The fission product rod will be fabricated and subsequently tested using KAERI's 30-MW research reactor HANARO. A fabrication study of the FP target will be performed in 2004 and irradiation will commence in 2005.

KAERI will complete construction of a corrosion loop in 2004. The oxygen control method is considered to test the protection of the steel structure materials against Pb-Bi corrosion. Therefore, an oxygen sensor will be developed. KAERI will launch the I-NERI programme in June 2004. Lead-alloy corrosion will be investigated through the I-NERI programme. The duration of I-NERI is three years and LANL is the US partner.

Acknowledgement

The Korean Ministry of Science & Technology (MOST) has supported this work.

REFERENCES

[1] Kim, Y., *et al*., "Optimization of Height-to-diameter Ratio for an Accelerator-driven System", *Nuclear Science and Engineering*, 143, 141 (2002).

[2] Kim, Y., *et al*., "Core Design Characteristics of the HYPER System", *Proc. of the OECD/NEA 7th Information Exchange Meeting on Actinide and Fission Product Partitioning & Transmutation*, Jeju, Korea, 14-16 October 2002.

RESEARCH AND DEVELOPMENT ON ACCELERATOR-DRIVEN SYSTEMS IN THE EURATOM FIFTH AND SIXTH FRAMEWORK PROGRAMMES

Ved P. Bhatnagar, Sylvie Casalta, Michel Hugon
European Commission, B-1049 Brussels
E-mail: Ved.Bhatnagar@cec.eu.int

Abstract

A fast subcritical reactor coupled to a particle accelerator is a concept of transmutation system that would allow large quantities of minor actinides to be burned efficiently. The research on transmutation encompassing accelerator-driven systems (ADS) is a part of the EURATOM research and development programme that lies within the area of partitioning and transmutation (P&T) of long-lived radionuclides in nuclear waste. P&T is one of the most notable research areas of the EURATOM Fifth (1998-2002) as well as the Sixth (2002-2006) Framework Programmes (FP). The objective of the research work in this area is to determine practical ways of reducing the amount and/or hazard of the waste to be disposed of. In FP5, there are 13 projects in this area with a total budget of about 69 M€ of which the EU contribution is about 28 M€. In FP6, the research in this area, with a EU contribution of about 30 M€, strengthens the work that has been carried out in FP5 with a view to building a European Research Area (ERA) in this field. This has lead to integrating all EU activities on partitioning into one integrated project, and the same is planned for the transmutation activities. Moreover, a targeted project concerning the impact of P&T on waste management has also been initiated. International co-operation in the area of P&T with non-EU countries (such as Canada, USA and Japan), including the Commonwealth of Independent States (CIS) is also outlined.

Introduction

The priorities for the European Union's research and development activities for the period 1998-2002 are set out in the Fifth Framework Programme (FP5) [1]. To maximise its impact, FP5 has focused on a limited number of research areas combining technological, industrial, economic, social and cultural aspects. FP5 and its predecessors have contributed effectively to the policy of supporting science and technology by encouraging co-operation between research players of the member states. Despite this achievement, no specific European research policy had emerged. National research programmes have been undertaken to a large extent independently of one another.

The primary objective now is to achieve greater co-operation among member states' research strategies and a mutual opening-up of programmes. To this end, the European Commission launched the so-called European Research Area (ERA) initiative in January 2000 [2]. The Sixth Framework Programme (FP6) [3] encompassing the period 2002-2006 is geared toward making ERA a reality [4].

The overall organisation of FP6 reflects the broad avenues of approach that are implicit in the proposed implementation of ERA. FP6 has three main blocks of activities:

- Integrating research in the well-focused research priority areas principally by using new research implementation instruments such as Networks of Excellence (NoE) and Integrated Projects (IP).

- Structuring the ERA through research and innovation, human resources and researcher mobility, research infrastructure and science and society issues.

- Strengthening the foundations of ERA by networking of national research and opening-up of national programmes, closer links between EU and other European organisations (such as CERN), benchmarking of research policies, mapping of excellence, etc.

In this context, the scientific and technical goals of the EURATOM FP6 specific programme "Research and Training Programme on Nuclear Energy" are to help exploit the full potential of nuclear energy, both in the long and short term. Its development and exploitation are to be undertaken in a sustainable manner while combating climate change and reducing the energy dependency of the EU. Research and development activities in this programme have been subdivided into (a) controlled thermonuclear fusion, (b) management of radioactive waste, (c) radiation protection and (d) other activities in the field of nuclear technologies and safety.

The paper briefly recalls the goals of P&T, including ADS, its position in the framework of management and disposal of radioactive waste. The research projects on P&T that are being funded in FP5 are then briefly described. A brief sketch of the P&T research work programme of FP6 is also given where once again the focus is on nuclear waste management. Finally, co-operation in this field with some countries of the Commonwealth of Independent States (CIS) through the International Science and Technology Centre (ISTC) in Moscow is also outlined.

The EURATOM Fifth Framework Programme (FP5) (1998-2002)

The Fifth Framework Programme of the European Atomic Energy Community (EURATOM) has two specific programmes on nuclear energy, one for indirect research and training actions managed by the Research Directorate General (DG RTD) and the other for direct actions under the responsibility of the Joint Research Centre of the European Commission (EC). The strategic goal of the first one,

"Research and Training Programme in the Field of Nuclear Energy," is to help exploit the full potential of nuclear energy in a sustainable manner, by making current technologies even safer and more economical and by exploring promising new concepts [1].

The implementation of the key action on nuclear fission, comprising four areas: (i) operational safety of existing installations, (ii) safety of the fuel cycle, (iii) safety and efficiency of future systems and (iv) radiation protection, was made through targeted calls for proposals. Following the three calls for proposals made since the start of FP5, 278 projects were funded in the area of nuclear fission and radiation protection. In the area of P&T, 13 projects were funded with a total budget of 69 M€ of which the EU contribution is 28 M€.

Partitioning and transmutation (P&T) and accelerator-driven systems (ADS)

Spent fuel and high-level waste contain a large number of radionuclides, from short- to long-lived. The time scales involved are very long before the waste becomes harmless, which raises concerns in guaranteeing the safety of waste disposal in geological repositories. Partitioning and transmutation aims at reducing the inventories of long-lived radionuclides (actinides and some fission products) by transmuting them into radionuclides with a shorter lifetime [6,7]. Partitioning in and of itself can be of help in the disposal strategy by specific conditioning of the minor actinides and long-lived fission products.

Partitioning is the set of chemical and/or metallurgical processes necessary to separate from the high-level waste the long-lived radionuclides to be transmuted. This separation must be very efficient to obtain a high decontamination of the remaining waste. It should also be very selective to achieve an efficient transmutation of the long-lived radiotoxic elements.

Long-lived radionuclides could be transmuted into stable or short-lived nuclides in dedicated burners. These burners could be critical nuclear reactors and/or subcritical reactors coupled to accelerators, the so-called accelerator-driven systems (ADS). An ADS is a concept that would allow large quantities of minor actinide waste to be burned efficiently. In a *sub*critical reactor, additional neutrons are supplied by an external source – from spallation reactions, for instance – in which an energetic proton beam from a particle accelerator impinges on a heavy metal such as lead. Subject to more detailed studies, for minor-actinide-rich fuel, an ADS seems likely to be safer than critical reactors, as the neutron chain reaction can, in principle, be stopped when desired by switching off the additional supply of neutrons (the accelerator). This, however, still leaves the task of removing the decay heat.

If successfully achieved, P&T will produce waste with a shorter lifetime. However, as the efficiency of P&T is not 100%, some long-lived radionuclides will remain in the waste, which will have to be disposed of in a deep geological repository. P&T is still at the research and development (R&D) stage. Nevertheless, it is generally accepted that the techniques used to implement P&T could considerably alleviate the problems linked to waste disposal.

There has been a renewal of interest in P&T worldwide [5], including Japan, Korea, Europe, China and the USA. In Europe, the most notable idea is that of the Energy Amplifier (EA) developed by CERN, Geneva. In addition, there are a number of research activities on ADS going on in several EU countries including Belgium, Czech Republic, France, Germany, Italy, Spain, Sweden as well as in Switzerland. P&T activities are also pursued in Russia.

The interest for P&T in the EU is reflected in the increase of funding in this area over the successive EURATOM Framework Programmes, 4.8, 5.8 and about 28 M€ for the Third, Fourth and Fifth Framework Programmes respectively. In the Sixth Framework Programme (2002-2006), the indicative budget for P&T is about 30 M€.

The research activities on P&T in the EURATOM Fifth Framework Programme

The objective of the research work carried out under FP5 is to provide a basis for evaluating the practicability, on an industrial scale, of partitioning and transmutation for reducing the amount of long-lived radionuclides to be disposed of. The work on partitioning concerns the experimental investigation of efficient hydrometallurgical and pyrochemical processes for the chemical separation of long-lived radionuclides from high-level liquid waste. The work on transmutation is related to the preliminary design studies of an accelerator driven subcritical system (ADS) and acquisition of data, both technological and basic, necessary for its development including the development of fuel and targets for an ADS.

The selected projects in this area address various scientific and technical aspects of P&T and have therefore been re-grouped. A network, ADOPT, co-ordinates the activities of the accelerator-driven system (ADS) design project with those of the four clusters of FP5 projects in the area of P&T (see Figure 1). One cluster concerns chemical separation of radionuclides (PARTITION) and three deal with transmutation: (i) basic studies (BASTRA), (ii) technological studies (TESTRA) and (iii) fuel studies (FUETRA).

Figure 1. FP5 funded projects in the area of P&T under the umbrella of the ADOPT network

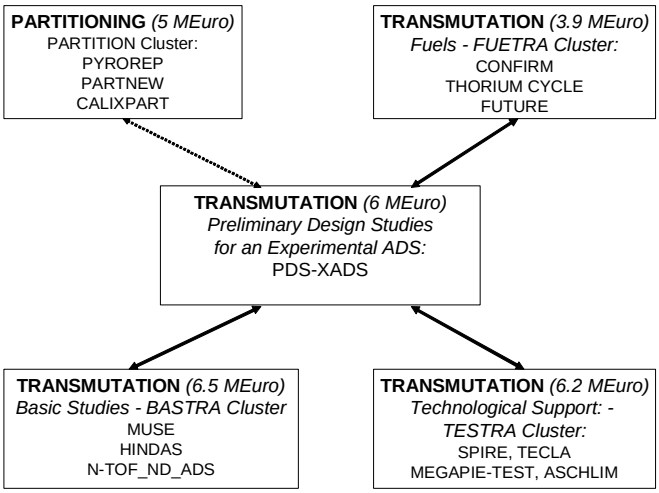

ADOPT network

The objectives of the ADOPT network (see Table 1) are: (i) to formulate actions with a view to promote consistency between FP5-funded projects and national programmes, (ii) to review overall results of the FP5 projects, (iii) to identify gaps in the overall programme of P&T research in Europe, (iv) to provide input to future research proposals and guidelines for R&D orientation, (v) to maintain relations with international organisations and countries outside the EU involved in P&T and ADS development.

Table 1. Advanced options for P&T (ADOPT) network and preliminary design studies for an experimental ADS (PDS-XADS)

Acronym	Subject of research	Co-ordinator (country)	No. of partners	Start date & duration	EC funding (M€)
ADOPT network	Thematic network on advanced options for P&T	SCK•CEN (B)	16	01-11-01 36 m	0.4
PDS-XADS	Preliminary design studies of an experimental accelerator-driven system	FRAMATOME ANP (F)	25	01-11-01 36 m	6.0

Design studies of an experimental ADS

Successful operation of an ADS together with the coupling of an accelerator to the neutron spallation target and the subcritical core is a first step for demonstrating the practicability of this type of transmuter on an industrial scale. The aim of the PDS-XADS project (see Table 1) is to produce a well-documented study with supporting evidence to choose and adopt the most promising technical concepts for ADS. It will also address the critical points of the entire system, identify the research and development (R&D) required in support, define the safety and licensing issues, assess the preliminary cost of the installation and consolidate the road-mapping of the XADS development. The assessment and comparison studies of the different conceptual designs of the main systems (accelerator, spallation target unit, subcritical core, primary system) will allow identifying the most promising solution which could be studied in detail during the next phase of design activities.

FP5 partitioning projects

The PARTITION cluster includes three projects, the main characteristics of which are given in Table 2. The first one, PYROREP, aims at assessing flow sheets for pyrometallurgical processing of spent fuels and targets. Two methods, salt/metal extraction and electro-refining, investigate the possibility of separating actinides from lanthanides. Materials compatible with corrosive media at high temperature will be selected and tested.

Table 2. PARTIONING cluster projects

Acronym	Subject of research	Co-ordinator (country)	No. of partners	Start date & duration	EC funding (M€)
PYROREP	Pyrometallurgical processing research	CEA (F)	7	01-09-00 36 m	1.5
PARTNEW	Solvent extraction processes for minor actinides (MA)	CEA (F)	10	01-09-00 36 m	2.2
CALIXPART	Selective extraction of MA by organised matrices	CEA (F)	9	01-10-00 40 m	1.4

The two other projects deal with the development of solvent extraction processes to separate minor actinides (americium and curium) from high-level liquid waste (HLLW). In the project PARTNEW, the minor actinides are extracted in two steps. They are first co-extracted with the lanthanides from HLLW (using the DIAMEX processes), then separated from the lanthanides (using the SANEX processes). Basic studies are being performed for both steps, in particular synthesis of

new ligands and experimental investigation and modelling of their extraction properties. The radiolytic and hydrolytic degradation of the solvents are also studied and the processes are tested with genuine HLLW.

The CALIXPART project deals with the synthesis of more innovative extractants. Functionalised organic compounds, such as calixarenes, will be synthesised with the aim of achieving the direct extraction of minor actinides from HLLW. The extraction capabilities of the new compounds will be studied together with their stability under irradiation. The structures of the extracted species will be investigated by nuclear magnetic resonance (NMR) spectroscopy and X-ray diffraction to provide an input to the molecular modelling studies carried out to explain the complexation data.

FP5 transmutation projects

BASTRA cluster

Three projects are grouped in the cluster of Basic Studies on Transmutation (BASTRA, see Table 3). The MUSE project aims to provide validated analytical tools for subcritical neutronics, data and a reference calculation tool for ADS study. The experiments are carried out by coupling a pulsed D-T/D-D neutron generator source (GENEPI) to the MASURCA facility loaded with MOX fuel operated as a subcritical system with different coolants (such as sodium and lead). Cross-comparison of codes and data is foreseen. Experimental reactivity control techniques related to subcritical operation are being developed.

The other two projects deal with nuclear data. The objective of the HINDAS project is to collect most of the nuclear data necessary for ADS applications. This is achieved by basic cross-section measurements at different European accelerator facilities, nuclear model simulations and data evaluations in the 20-200 MeV energy region and beyond. Iron and lead (materials used for ADS) and uranium have been chosen to have a representative coverage of the periodic table.

The n-TOF-ND-ADS project aims at the production, evaluation and dissemination of neutron cross-sections for most of the radioisotopes (actinides and long-lived fission products) considered for transmutation in the energy range from 1 eV up to 250 MeV. Measurements are being carried out at the n-TOF facility at CERN, at the GELINA facility in Geel and using other neutron sources located at different EU laboratories.

Table 3. Basic Studies for Transmutation (BASTRA) cluster projects

Acronym	Subject of research	Co-ordinator (country)	No. of partners	Start date & duration	EC funding (M€)
MUSE	Experiments for subcritical neutronics validation	CEA (F)	13	01-10-00 49 m	2.0
HINDAS	High- and intermediate-energy nuclear data for ADS	UCL (B)	16	01-09-00 39 m	2.1
n-TOF-ND-ADS	ADS nuclear data using time-of-flight facility	CERN(CH)	18	01-11-00 49 m	2.4

TESTRA cluster

Four projects are grouped in the cluster of Technological Studies on Transmutation (TESTRA) (see Table 4). This cluster deals with the investigation of radiation damage induced by products of spallation reactions in materials, of the corrosion of structural materials by lead alloys and of fuels and targets for actinide incineration.

The SPIRE project addresses the irradiation effects on an ADS spallation target. The effects of spallation products on the mechanical properties and microstructure of selected structural steels (e.g. martensitic steels) are being investigated by ion beam irradiation and neutron irradiation in reactors (HFR in Petten, BR2 in Mol and BOR60 in Dimitrovgrad). Data representative of mixed proton/neutron irradiation are being obtained from the analysis of the SINQ spallation target at the Paul Scherrer Institute in Villigen (CH).

The objective of the TECLA project is to assess the use of lead alloys both as a spallation target and as a coolant for an ADS. Three main topics are addressed: corrosion of structural materials by lead alloys, protection of structural materials and physico-chemistry and technology of liquid lead alloys. A preliminary assessment of the combined effects of proton/neutron irradiation and liquid metal corrosion is being carried out. Thermal-hydraulic experiments are being performed together with numerical computational tool development.

Table 4. Technological Studies for Transmutation (TESTRA) cluster

Acronym	Subject of research	Co-ordinator (country)	No. of partners	Start date & duration	EC funding (M€)
SPIRE	Effects of neutron and proton irradiation in steels	CEA (F)	10	01-08-00 48 m	2.3
TECLA	Materials and thermal-hydraulics for lead alloys	ENEA (I)	16	01-09-00 39 m	2.5
MEGAPIE-TEST	A megawatt heavy liquid metal spallation target experiment with proton beam	FZK (D)	17	01-11-01 61 m	2.4
ASCHLIM	Computational fluid dynamics codes for heavy liquid metals	SCK•CEN (B)	14	01-01-02 12 m	0.12

The major objective of the MEGAPIE-TEST project is to develop and validate the design and operation of a heavy liquid metal (Pb-Bi) spallation target at a level of a megawatt. The project aims to provide a comprehensive database from single-effect experiments, a full-scale thermal-hydraulic simulation experiment, and the first beam-on experiments. In parallel, numerical computational tools will be validated for Pb-Bi target design. The studies include neutronic calculations, materials, corrosion, thermal-hydraulics, structure mechanics, liquid metal technology, safety and licensing issues. Prospects on the extrapolation and applicability of the obtained results to an ADS spallation target will also be given.

The *AS*sessment of *C*omputational Fluid Dynamics Codes for *H*eavy *LI*quid *M*etals (ASCHLIM) project aims at bringing together various actors (industry, research institutions and university) in the field of heavy liquid metals both in the experimental and numerical fields and creating an international collaboration to (i) make an assessment of the main technological problems in the fields of turbulence, free surface and bubbly flow and (ii) co-ordinate future research activities in this area. The assessment is being made on the basis of existing experiments whose basic physical phenomena are analysed through the execution of calculational benchmarks using commercial and research codes.

FUETRA cluster

There are three projects in this cluster. The objectives of the CONFIRM project are to develop methods for fabrication (such as carbo-thermic reduction process) of uranium-free nitride fuels (Pu,Zr)N and to model and test their performance under irradiation up to 20% burn-up in the Studsvik (Sweden) R2 reactor. Carbo-thermic process will also be used for the production of (Am, Zr)N pellets at ITU, Karlsruhe. Successful high-temperature (≈2 500°C) stability tests of (U,Zr)N have been made and a study of ^{14}C production has been completed.

The objective of the project THORIUM CYCLE is to investigate the irradiation behaviour of thorium/plutonium (Th/Pu) fuel at high burn-up and to perform full core calculations for thorium-based fuel with a view to supplying key data related to plutonium and minor actinide burning. Two irradiation experiments are being carried out: (i) four targets of oxide fuel (Th/Pu, uranium/plutonium, uranium and thorium) will be fabricated, irradiated in HFR in Petten and characterised after irradiation, (ii) one Th/Pu oxide target is also irradiated in the KWO reactor at Obregheim (D). Though this project was accepted for funding in the area of "Safety and Efficiency of Future Systems", it has been grouped with the FUETRA cluster.

Table 5. Fuel Studies for Transmutation (FUETRA) cluster

Acronym	Subject of research	Co-ordinator (country)	No. of partners	Start date & duration	EC funding (M€)
CONFIRM	Uranium-free nitride fuel irradiation and modelling	KTH (S)	7	01-09-00 64 m	1.0
THORIUM CYCLE	Development of thorium cycle for PWR and ADS	NRG (NL)	7	01-10-00 48 m	1.2
FUTURE	Development of transuranic oxide fuels for transmutation	CEA (F)	7	01-12-01 36 m	1.7

The main objective of the FUTURE project is to study the feasibility of oxide compounds $(Pu,Am)O_2$, $(Th,Pu,Am)O_2$ and $(Pu,Am,Zr)O_2$ to be irradiated as homogeneous fuel for an ADS. The R&D programme is largely devoted to the synthesis of the compounds, their characterisation (thermal and chemical properties at relevant temperatures) and the development of fabrication processes. Modelling codes will be developed to calculate the fuel performance. The input data for the codes will be based on experimental results. Assessment of the fuel behaviour under accident conditions will be analysed using the experimental data obtained at high temperatures.

The EURATOM Sixth Framework Programme (FP6) (2002-2006)

Research and development activities of the EURATOM FP6 specific programme "Research and Training Programme on Nuclear Energy" have been subdivided into four areas (a) controlled thermonuclear fusion, (b) management of radioactive waste, (c) radiation protection and (d) other activities in the field of nuclear technologies and safety.

In the area of management of radioactive waste, the priority is to find a more permanent and safe solution for the management of long-lived, high-level waste that is acceptable to society. This includes establishing a sound technical basis for the demonstration of long-lived high-level waste disposal in geological formations. This is to be supported by studies on P&T and further supplemented by exploring the potential of system concepts that would by themselves produce less waste in nuclear

energy generation. Combating the decline in both student numbers and teaching establishments by a better integration of European education and training in nuclear safety and radiation protection is another important aim.

The detailed work programme of EURATOM FP6 has been adopted by the EC [8]. In P&T, the research areas include a fundamental assessment of the system and safety aspects of the overall concept of P&T and, in particular, of its impact on waste management and geological disposal. In the area of partitioning, continued R&D of hydrometallurgical and pyrochemical processes is envisaged with a view to the demonstration of the most promising techniques. In the area of transmutation, the development of basic knowledge and technologies for transmutation and evaluation of their industrial practicability, in particular, of transmutation devices such as accelerator-driven subcritical systems (ADS) is proposed [9].

Two calls for proposals have been made in December 2002 and November 2003 respectively, where the so-called new instruments (such as Integrated Projects) are used as a priority. The Integrated Projects (IP) are designed to give increased impetus to the Community's competitiveness or to address major societal needs by mobilising a critical mass of research and technological development resources and competencies. Avoiding the micro management, increased autonomy will be given to the consortiums in the management (both scientific and financial) of the projects that will be judged on the global end-results. Specific Targeted Research Projects (STREPS) are sharply focused on research and technological development designed to gain new knowledge either to improve or develop new products, processes or services or to meet other needs of society and Community policies.

Studies on the impact of P&T on waste management

RED-IMPACT project

Partitioning, transmutation and conditioning (P&T/C) and waste reduction technologies, if implemented properly and in full consultation with the geological disposal community, are expected to significantly reduce the burden associated with radioactive waste management and disposal. P&T is likely to ease the final repository requirements and it will also contribute to the sustainability of nuclear energy in those countries that pursue this source of energy.

The objectives of this three-year RED-IMPACT project (total budget 4 M€ including an EC contribution of 2 M€) are: (i) to assess the impact of P&T on geological disposal and waste management, (ii) to assess economic, environmental and societal costs/benefits of P&T (iii) to diisseminate results of the study to stakeholders (scientific, general public and decision makers) and get feedback during the course of the study and (iv) to iterate and refine the work based on stake-holders' feedback to achieve the full impact of this study on the implementation of the waste management policy of the European Community.

Partitioning

EUROPART project

The research work in this project (total budget 10.3 M€ and EC contribution 6 M€) concerns the partitioning (chemical separation) of actinides that are contained in the nuclear wastes issuing from the reprocessing of nuclear spent fuel. The selected elements for partitioning are the so-called minor actinides (MA) but in the case of the treatment of dedicated spent fuels or targets the actinides to be separated also include U, Pu and Np. The separation techniques are hydrometallurgy and pyrometallurgy.

In hydrometallurgy, the research is dedicated to the study of partitioning methods mainly based on the use of solvent extraction methods including the development of An co-conversion methods for fuel or target preparation. The research in pyrometallurgy concerns the development of An partitioning methods, and the study of the basic chemistry of transcurium elements in molten salts. Conditioning of the wastes and system studies are also included. Processes for possible industrialisation of partitioning strategies will also be defined.

Transmutation

For this subject matter, the proposal is currently undergoing the evaluation and selection procedure. The objective of the required work is the evaluation of the industrial practicability of transmutation of high-level nuclear waste in a fast neutron burner and development of the necessary basic knowledge and technologies. The focus of research should be on system analysis for an accelerator-driven system (ADS), including more advanced integrated design, cost evaluation of the whole system and safety and licensing issues. Moreover, the work should improve the basic knowledge and technologies required for improving the reliability of high-energy accelerators for ADS applications, coupling of the ADS components (accelerator, spallation target and subcritical core), material and coolant technologies, advanced fuels and targets and basic nuclear data.

ADS-related research activities in the framework of the International Science and Technology Centre (ISTC)

The International Science and Technology Centre (ISTC) was established by an international agreement in November 1992 as a non-proliferation programme through scientific co-operation. It is an inter-governmental organisation grouping the European Union, Japan, the USA, Norway and the Republic of Korea, which are the funding parties, and some countries of the Commonwealth of Independent States (CIS): the Russian Federation, Armenia, Belarus, Georgia, Kazakhstan and Kyrgyzstan. The ISTC finances and monitors science and technology projects to ensure that the CIS scientists are offered the opportunity to use their skills in the civilian fields. A similar organisation, the Science and Technology Centre in Ukraine (STCU) was established in 1995; the EU, Canada, the USA, Georgia and Uzbekistan are involved.

Five topics have been identified by the ISTC Contact Expert Group (CEG) for ADS-related projects: (i) accelerator technology, (ii) basic nuclear and material data and neutronics of ADS, (iii) targets and materials, (iv) fuels related to ADS and (v) aqueous separation chemistry. The EU CEG has started to develop co-operation between ISTC and FP5 EU funded projects especially in the above area (ii) by organising joint meetings of the BASTRA cluster with related ISTC projects and the PARTITION cluster with related ISTC/STCU projects.

Conclusions

Research activities in the field of partitioning and transmutation under the EURATOM Fifth Framework Programme are nearing completion. The research projects have been re-grouped into four clusters, one on partitioning and three on transmutation: basic studies, technological studies and fuel studies. These clusters and the design project form a balanced programme on P&T that is co-ordinated by the ADOPT network. With a view to thoroughly integrate the EU research efforts, a European Research Area (ERA) initiative has been launched. Two calls for proposals have been launched in FP6 making the ERA a reality. One partitioning project and one project on impact studies have begun. The

project on transmutation is undergoing the evaluation and selection procedure. The collaboration of EU-funded FP5 projects and the ISTC/STCU projects on partitioning and basic studies of transmutation is progressing satisfactorily.

REFERENCES

[1] "Council Decision of 25 January 1999 Adopting a Research and Training Programme (EURATOM) in the Field of Nuclear Energy (1998 to 2002)", *Official Journal of the European Communities*, L 64, 12 March 1999, p. 142, Office for Official Publications of the European Communities, L-2985 Luxembourg.

[2] "Towards a European Research Area", Communication from the Commission, COM 2000 6, 18 January 2000, http://europa.eu.int/comm/research/area.html.

[3] "Council Decision of 3 June 2002 Concerning the Sixth Framework Programme of EURATOM for Nuclear Research and Training Activities, also Contributing to the Creation of European Research Area (2002 to 2006)", *Official Journal of the European Communities*, L 232/34, 29-08-2002, Office for Official Publications of the European Communities, L-2985 Luxembourg.

[4] "Making a Reality of the European Research Area: Guidelines for EU Research Activities (2002-2006)", Communication from the Commission, COM 2000 612, 4 October 2000, http://europa.eu.int/comm/research/area.html.

[5] Hugon, M., V.P. Bhatnagar, "Partitioning and Transmutation in the EURATOM Fifth Framework Programme", *Proc. 6th Inf. Exch. Meeting*, Madrid, Spain, 11-13 December 2000, Actinide and Fission Product P&T, OECD/NEA 2001, EUR 19783 EN (2000).

[6] *Actinide and Fission Product Partitioning and Transmutation – Status and Assessment Report*, OECD Nuclear Energy Agency, Paris, France (1999).

[7] *Accelerator-driven Systems (ADS) and Fast Reactors (FR) in Advanced Nuclear Fuel Cycles –A Comparative Study*, OECD Nuclear Energy Agency, Paris, France (2002).

[8] EURATOM FP6 Work Programme 2003 and 2004 (Commission Decision, unpublished), visit: http://fp6.cordis.lu/fp6/calls_euratom.cfm.

[9] Hugon, M., V.P. Bhatnagar, S. Casalta, "Research on Advanced Systems in the EURATOM Framework Programmes", *Proc. GLOBAL 2003*, ANS/ENS International Winter Meeting, New Orleans, Louisiana (USA), 16-20 November 2003.

STATUS OF THE TRADE EXPERIMENT

S. Monti[1], L. Picardi[1], C. Rubbia[1], M. Salvatores[2], F. Troiani[1]
[1]ENEA, Lungotevere Thaon di Revel, I-00196 Rome, Italy
[2]CEA, CEN-Cadarache, F-13108 Saint-Paul-lez-Durance, France

Abstract

The paper describes the status and the main technical achievements in view of the preparation of the TRADE experiment to be performed in the TRIGA reactor of the ENEA Casaccia Centre in Italy. The first beam operation is foreseen for early 2007 and the first operation of the full experiment in TRIGA by early 2008.

Substantial improvements have recently been introduced with respect to the original design developed in 2002-2003, both in the functionality of the components and in the general layout of the experiment, within the main target goals already described in previous papers [1,2].

The main additional elements of TRADE with respect to the already-existing TRIGA-1 MWatt reactor are: (1) a high-energy accelerator with a suitable current and conservative, well-proven technologies, (2) a beam transport line to bring the beam in the TRIGA reactor operated as a subcritical system, (3) a solid target inserted in the core of TRIGA with the purpose of producing an adequate neutron source by the spallation reaction, and (4) additional shielding due to the production and injection of a particle beam in order to conservatively ensure an adequate radiation protection of the above new components.

The accelerator chosen is a compact negative ion (H^-) accelerator with an energy of approximately 140 MeV and a variable current with a maximum of about 300 mA. The beam transport has been drastically simplified with respect to previous designs, reducing the integrated bending power to the minimal 90 required by the difference in orientation of the horizontal accelerator and the vertical access tube to the spallation target. The presence of an extracted proton beam introduces significant contributions in terms of beam losses and additional radioactivity in the immediate vicinities of the accelerator, beam transport and target. To this effect additional shields have been introduced both in the regions immediately adjacent to the active elements and some additional conservative shielding in the form of a full "box" around the full reactor building, but physically well separated from the reactor structure.

The present schedule of TRADE foresees the first accelerator operation by early 2007. A period of one year is foreseen for the operation of the beam transport and the spallation target in the so-called "test station" realised in the accelerator building. When all possible certifications of the operability of the target system have been successfully completed the coupling between the accelerator and TRIGA will become operational.

Outline and general layout of the TRADE facility

The *TR*IGA *A*ccelerator-*D*riven *E*xperiment (TRADE), to be performed in the existing TRIGA reactor of the ENEA Casaccia Centre, is an original idea of Carlo Rubbia aimed at a global demonstration of the ADS concept. TRADE will be the first experiment in which the three main components of an ADS – the accelerator, the spallation target and the subcritical blanket – will be coupled at a power level sufficient to encounter feedback reactivity effects. As such, the TRADE experiment represents the necessary intermediate step in the development of hybrid transmutation systems, its expected outcomes being considered crucial – in terms of proof of stable operability, dynamic behaviour and licensing issues – for the subsequent realisation of an ADS transmutation demonstrator.

As already demonstrated in previous papers [1,2], the experiments of relevance that can be performed in TRADE concern:

- The dynamic system behaviour of an ADS vs. the neutron importance of the external source at different subcriticality levels, providing important information on the optimal subcriticality level.
- Subcriticality measurements at significant power.
- Correlation between reactor power and proton current.
- Reactivity control by different means and possibly by neutron source importance.
- Compensation of power effects of reactivity swing with control rods movements or with proton current variation.
- Start-up and shutdown procedures, including suitable techniques and instrumentation.

The representativity of the TRADE experiment as concerns the validatation of the dynamic behaviour of a subcritical system over a wide range of subcriticality levels (whatever the neutron spectrum in the core), has been demonstrated [1], and has been the subject of an international workshop, held in Rome on 11 March 2004 (presentations available on the Internet site http://www.trade.enea.it).

The overall layout of the facility – determined after a quite comprehensive comparison among others – is shown in Figure 1 [3]. It foresees the erection of a new bunker, close to the existing TRIGA building, to house the accelerator and the test station for proton beam test and adjustment. The proton beam is transferred from one building to the other via a section of the transfer line that is particularly simple, since the cyclotron is at the same level as the top of the reactor. The beam transport line is protected by a massive shielded tunnel which extends into the TRIGA building up to the reactor top. Through the straight section of the transport line, the beam is transferred to the final bending section composed of two magnetic dipoles and three magnetic quadrupoles, which have the duty of directing the beam, with the correct size, to the spallation target placed in the central thimble of the reactor.

As for the accelerator, several configurations were studied for a suitable proton energy beam of 140, 200 and 300 MeV and with a beam current in the range 100-300 ㎃. Taking into account the constraints related to the cost and the relatively short time scale for the implementation of the TRADE experiment, a room temperature H^- cyclotron is considered the most affordable solution. In fact, even if the requested performances for TRADE (140 MeV, 2-300 A㎃) are rather challenging with respect to those of the existing machines, the TRADE cyclotron can be regarded as an evolution of a typical H^- machine for radioisotope production (E_p around 30 MeV) or for hadron therapy (E_p around 60 MeV).

Figure 1. Reference layout of the TRADE facility (vertical section)

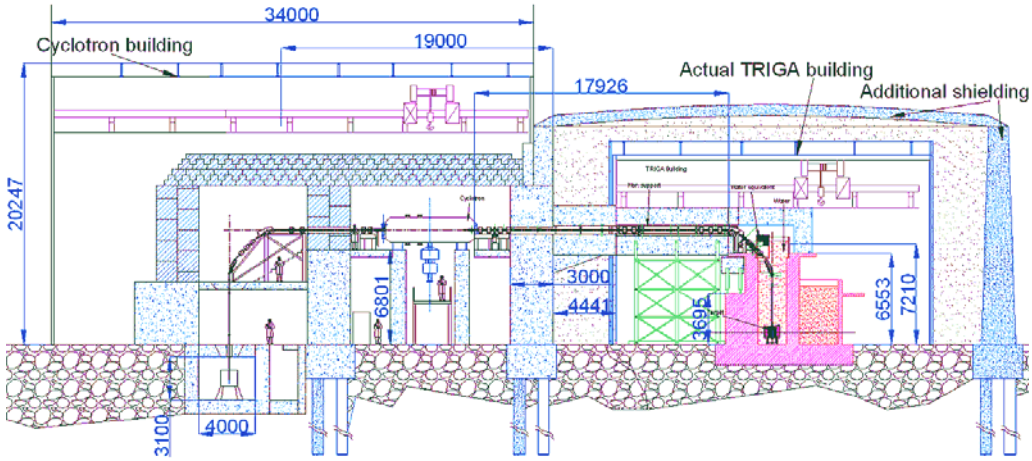

The main reference parameters of the TRADE subcritical core are reported in Table 1.

Table 1. TRADE main reference parameters

Global parameters	Symbol	Reference case
Initial fuel mixture	LEU	UZrH
Initial fuel mass	m_{fuel} (kg)	235.2
Initial U concentration	m_U/m_{fuel} (wt.%)	8.5
Initial fissile enrichment	$^{235}U/U$ (at.%)	20.0
Thermal power output	P_{th} (kWatt)	200
Spallation target		Tantalum
Proton beam energy	E_p (MeV)	140
Spallation neutron yield	$N_{(n/p)}$ (n/p)	0.74
Multiplication coefficient	k = (M – 1)/M	0.94-0.99
Accelerator current	I_p (mA)	215-35
Beam power	P_{beam} (kWatt)	30-5
Core power distributions		
Avg. fuel power density	P_{th}/V_{fuel} (W/cm^3)	4.9
Spec. fuel power density	P_{th}/m_U (W/g HM)	10.0
Max. heat flux	P_h (W/cm^2)	6.0
Max. linear power	P_l (W/cm)	68.0
Radial peaking factor	P_{max}/P_{ave}	1.3

The studies performed so far by a working group of scientists of ENEA (Italy), CEA (France), CERN (Switzerland), CIEMAT (Spain), CNRS (France), DOE (USA) and FzK (Germany) concern:

- The neutronics of selected possible configurations, along with a neutronic benchmark to define codes and tools to be used for the neutronic design and the interpretation of the experimental measurements.

- The core and target thermal-hydraulics, using natural or forced convection, including the target coupling to the reactor at power.

- The target performances and characteristics as well as the conceptual design of the target, its cooling system and the definition of the tests needed for its qualification.
- A conceptual design of the beam transport line.
- The shielding and activation aspects in order to gain insight on the dose issues.
- The safety and licensing aspects related to the plant modifications induced by the TRADE experiment, including considerations on general safety criteria, possible accident initiators and a preliminary hazards analysis.
- The overall experimental programme to be performed in TRADE.
- The representativity of the foreseen experiments in terms of dynamic behaviour, neutron spectrum, reactivity control, proton current/power relation, operation at start-up and shutdown, external source importance measurements, etc.
- A preliminary cost and time schedule evaluation.

Furthermore, a preliminary experimentation in the TRIGA RC1 reactor was carried out in fall 2002 so as to characterise the TRADE reference core; a new experimental phase – which will include measurements in a mock-up of the TRADE core with californium, DD and DT external sources – is being performed over 2003-2004.

The accelerator

Taking into account the constraints related to the cost and the relatively short time scale for the implementation of the TRADE experiment, a H^- machine is considered the most affordable solution. Moreover, the room temperature H^- cyclotron relies on a well-proven technology. The performance both in energy and in intensity for the accelerator of TRADE is significantly higher with respect to those of the presently commercially available units. However, this cyclotron can be regarded as a logical evolution of typical H^- machines for radioisotope production (E_p ~ 30 MeV) or for hadron therapy (E_p ~ 60 MeV), the most challenging upgrade being the need of bringing the energy of the protons up to about 140 MeV with an extracted current of at least 300 mA. Further, the accelerator must guarantee a flawless continuity of the beam to be injected in the subcritical subassembly.

In the past, some concern has been expressed as concerns the possible occurrence of erratic behaviour of the delivered current, which could produce adverse effects on the high-power subcritical core. Therefore, all active components of the accelerator and of the beam transport line must ensure the utmost reliability during operation. The simple cyclotron chosen in the design is characterised by an extremely small number of active, very reliable components, in comparison for instance with the number of elements and the size of a linac accelerator with equivalent performance.

A compact geometry is preferable to an open sector geometry because of the geometrical considerations related to the available space and accessibility, as evident from Figure 1. This type of structure also ensures a better shielding against beam losses, primarily due to stripping of negative ions. Such radiation losses, which occur in a narrow radial segment near the last orbits, could eventually be moderated with the help of dedicated small beam absorbers of suitable material.

An indicative list of parameters for the TRADE cyclotron is given in Table 2. Further details of the proposed cyclotron design are reported in another paper at this conference.

Table 2. Main parameters of the TRADE cyclotron

Parameter	Reference value
Output energy	120-140 MeV
Max. nominal current	300 μA
Normalised emittance at 2σ	1-4 π mm mrad
Injected particles	H^-
Number of sectors	4
Extraction radius	2.2 m
Cyclotron outside diameter	6.5 m
Cyclotron magnet vertical size	= 2.0 m
Total weight	300-400 tonnes
Total power in main coils	~150 KW
Extraction	Stripping (carbon foil 70 μg/cm^2)
Beam losses due to electromagnetic dissociation	= 1%

The beam transport line and the beam diagnostics

The beam transport line (BTL) has two main purposes: (1) to rotate the beam direction from horizontal to vertical (90); (2) to match the beam emittance from the cyclotron to the precisely circular shape of the size required by the subsequent target.

The BTL is characterised by a straight line to transport the beam nearby the target with the help of a small number of quadrupoles, followed by the 90 achromatic final bend, composed of two dipoles and three quadrupoles. The two dipoles, each of 45 , have been chosen with a relatively conservative magnetic field of 1.3 tesla, corresponding to a curvature radius of about 1.3 m.

The second dipole M4 (see Figure 2) is immersed in the pool water of TRIGA in order to shield the neutron back-streaming from the core through the beam pipe (50 mm diameter), by about 2 meters of water. In the present layout, the water level also includes the quadrupole triplet Q7-Q8-Q9. It may be possible, however, to locally replace water with some other equivalently absorbing material (polyethylene?) in order to avoid insulation problems due to the water of the reactor pool.

The design criteria for the final part of the BTL were characterised by the minimum number of components with which one could achieve a circular spot of nominally 40 mm diameter at the target spot, starting from the actual parameters of the accelerator.

The overall layout of the accelerator and of the beam transport line in the final location is shown in Figure 3.

As for the diagnostics of the beam transport line, these are considered crucial for the TRADE experiment, both for the capability of delivering the correct beam to the target and for a very low loss transport in the BTL part sited in the TRIGA building, where shielding may not be as complete as for the cyclotron bunker. These monitors have to quickly react to beam variations and eventually, whenever necessary, shut off the accelerator in a very short time (microseconds).

They are used in a number of critical positions, both when the experiment is in the location of the target mock-up (i.e. in the test station) and in the final TRIGA position. In particular, during the mock-up phase they are necessary in order to experimentally determine the amount and the position of

Figure 2. BTL final section and beam port into the TRIGA core

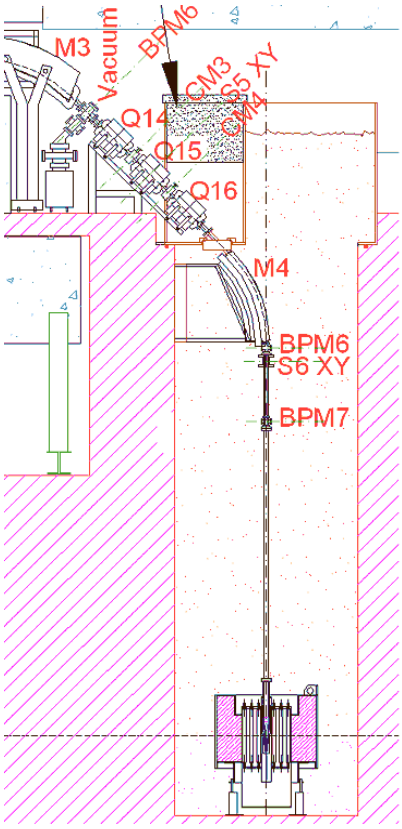

Figure 3. General layout of the accelerator, the beam transport and the TRIGA subcritical assembly with the target inserted in the core

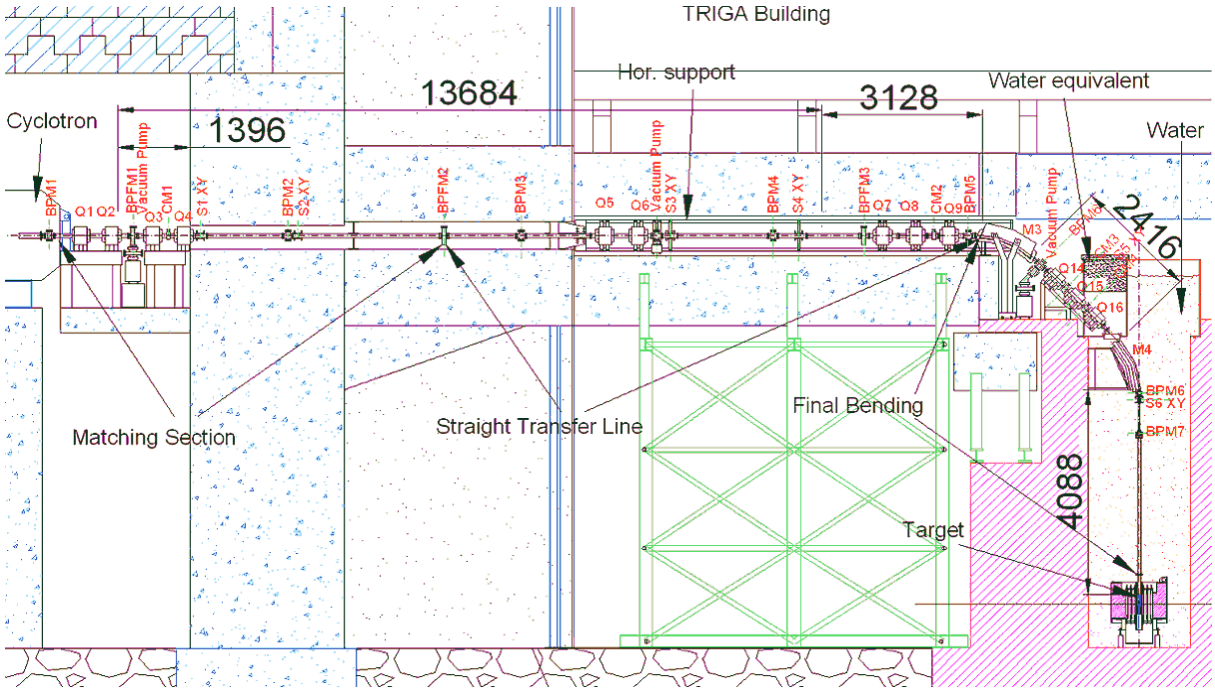

the beam losses, in order to finalise a robust shielding protection. Some of the monitors are still at the detailed design stage, since they have to be checked in particular as to sensitivity and resolution. They are of two types, non-interceptive and interceptive. The non-interceptive are: beam position monitors, current monitors, beam loss monitors and infra-red thermometry.

Most of the beam diagnostics required are of a non-intercepting nature and therefore have straightforward solutions. However, these tools are unable to produce a precise "image" of the proton beam, for which intercepting diagnostics is necessary. In this case the interaction of the proton beam with a suitable detecting method is necessary, with a consequent scattering and hence modification of the beam emittances and eventually of some heat production. Particularly suited are the so-called secondary emission monitors (SEMs), in which secondary electrons, generated by the passage of protons through a thin foil or mesh, are recorded. They are currently under development in several laboratories (CERN, FERMILAB). In our case, however, they must withstand a current which is about an order of magnitude higher (up to 300 mA). These modern methods may replace with significant advantages the classic fluorescent screens viewed by a camera.

The BTL design and its diagnostics are discussed in more detail in another paper of this conference.

The spallation target

The spallation target is the key component of any ADS concept. Even in the TRADE facility, despite the relative small power of the proton beam (< 40 kW), the development and design of the target implies a detailed assessment of different aspects mutually interacting, from the physics of spallation reaction – including neutron generation and distribution, spallation products yields and damage rates – to technological issues, such as choice of the most suitable material, power density distribution, heat removal, thermo-mechanics, fabricability, etc. The guidelines that were followed for the target development, along with the main constraints and interfaces, have been extensively addressed in Refs. [4] and [5]. The target geometry is shown in Figure 4.

The inner geometry is characterised by three conical cavities with different angles and total length equal to the active height of the TRIGA core. The cone tip (lowest cone) is exposed to the highest power density for two reasons:

- The relevant proton current at the centre of the Gaussian distribution.
- The forward scattering of protons as a consequence of the conical angle steepness.

The main choices for the target are the following:

- *Material*: Tantalum has been selected for the spallation target due to its good properties of ductility, machinability and resistance to water corrosion and irradiation.
- *Thermal flux*: It has been decided to maintain the target thermal flux at a level corresponding to one-third of the critical thermal flux.
- *Target cooling mode*: Forced circulation has been selected, rather than natural circulation, in order to facilitate the start-up and shutdown operations as well as to guarantee an efficient heat removal with limited exchange surfaces.

- *Tantalum welding*: No welds are allowed in the zone where spallation reactions occur and/or in high thermal flux regions.

- *Cladding of the target*: No target cladding is foreseen in order to avoid fabrication difficulties and negative effects related to differential thermal expansions of the materials.

Figure 4. Spallation target configuration

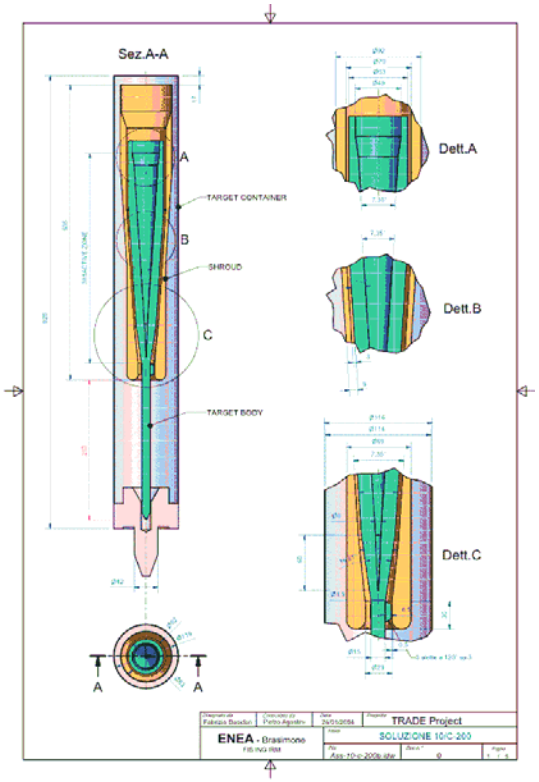

As for maximum admissible loads and the elasto-plastic state of the material, on the basis of the RCC-MR engineering rules for fast reactors, a certain degree of plasticisation of the material is allowed. In any case the licensing of the target is subject to positive results of irradiation integral tests to be performed in the test station.

The thermal performances of the target under the reference operating conditions are reported in Table 3.

Table 3. Operating conditions

Parameter	Value
Power deposited in the target	38.7 kW (0.2857 mA)
Mass flow rate	2.24 Kg/s
Inlet mean velocity	0.728 m/s
Inlet mean temperature	25 °C
Outlet mean velocity	2.78 m/s
Outlet mean temperature	29 °C
Mass-averaged h×mfr i/o diff.	39.1 kW
Total-pressure loss	0.08 bar
Static-pressure loss	0.12 bar

The neutron flux distribution outside the target is reported in Figure 5. Since the region of maximum production lies below the median plane of the core, in order to achieve a greater efficiency in the use of the source neutrons it is necessary to axially shift, by about 4 cm, the target body in the upward direction.

Figure 5. Neutron flux distribution in (n/cm^2/s) per kW of beam

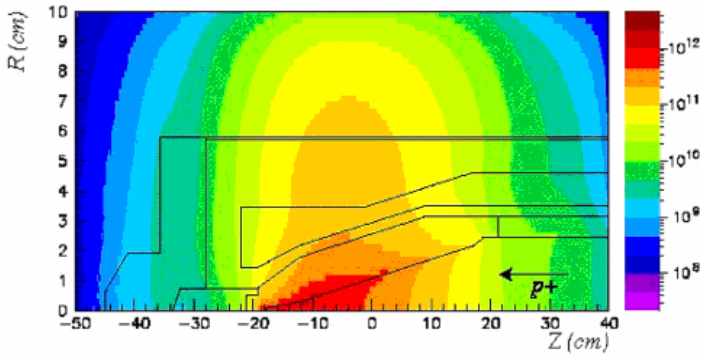

Finally, the primary proton flux distribution for the target is reported in Figure 6. The fraction of protons escaping the target vessel is almost negligible apart from the upper part of the target (direct connection to the beam transport line) where the tails of the Gaussian profile are truncated. In any case the majority of the protons escaping the spallation target are either stopped in the cooling channel (riser) surrounding the target or inside the thick flow guide, none reach the core internal structures and only a few are backscattered into the vacuum beam pipe.

Figure 6. Primary proton flux distribution in (p/cm^2/s) per kW of beam

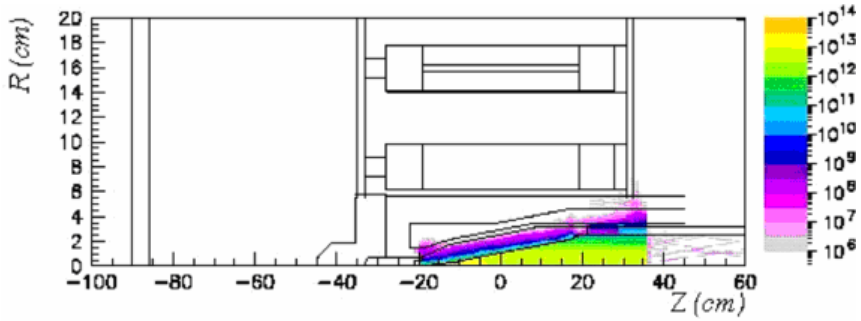

Radioprotection

The design of an ADS experiment in an existing critical facility such as TRADE presents some unusual shielding problems:

- A beam tube line entering from above the reactor that implies the requirement for shielding to be supported at a height in the facility hall.
- A vacuum pipe penetrating to the centre of the subcritical configuration and the subsequent radiation streaming back along this pipe from the core.
- The presence of both fission and spallation radiation components with quite different penetrative characteristics, with the existing shielding dimensioned for the fission component.

In designing the conversion of the TRIGA reactor to a subcritical configuration driven by a spallation source, preliminary solutions have been proposed to these problems. In order to support the shielding design, several Monte Carlo calculations have been performed by both the FLUKA and MCNPX transport codes [6]. These simulations have lead to the definition of the reference design of the BTL shielding and of the cover above the reactor well as well as to the need for two bending magnets in the final section of the beam transport line and an external full box around the reactor building. The reference configuration design has been modelled as shown in Figure 7, where the beam transport line, the core, the primary and the secondary pool and the shielding are shown (ordinary concrete at 2.3 g/cm^3 and barytic concrete at 3.2 g/cm^3).

Figure 7. Vertical section of a schematisation of the reactor building adopted in the Monte Carlo shielding and dose calculations

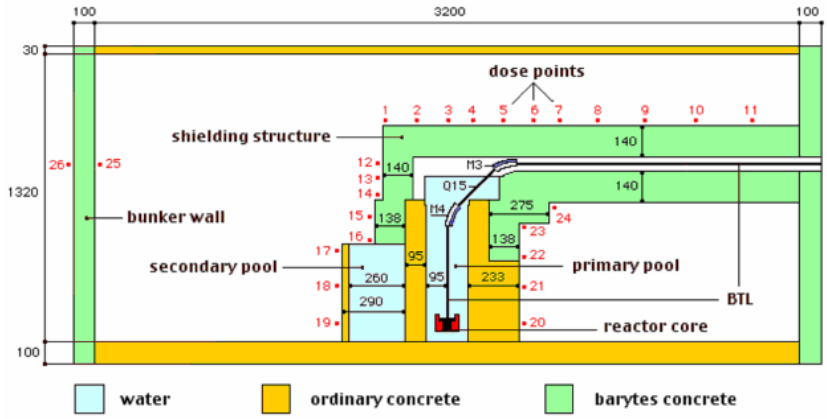

In order to reach dose rates below the limit of 0.5 mSv/h for the population, thicknesses of at least 170 cm barytic concrete would be needed around the BTL; on the other hand such weights might not be supported by the current foundations of the reactor hall. It has therefore been decided to limit the local shielding around the BTL to 140 cm barytic concrete and to introduce shields around the reactor hall (100 cm barytic concrete). Such a configuration produces maximum dose rates of 0.06 mSv/h outside the walls of the reactor building. This value has been evaluated by means of a 3-D mapping of the dose rates. Thus the dose limit to the population (0.5 mSv/h) is respected with a safety coefficient of 8. At the moment this should be adequate, and would possibly allow greater beam losses than those hypothesised (1 nA/m along the BTL and 30 nA for the quadrupole).

Concerning the dose limits inside the reactor hall, the calculational results show a maximum dose rate of 20 mSv/h, well below the allowable limit of 50 mSv/h inside the reactor hall.

The doses due to the streaming along the vertical part of the beam pipe have been calculated outside the shielding in the reactor hall and outside the bunker. Compared with the doses from the hypothesised beam losses, these doses are almost negligible.

Finally, the contribution to the dose rate in the reactor hall due to the spallation neutrons in the target and from the fission neutrons in the core has been evaluated. As the present reactor shielding has been designed for a critical 1 MW core, as expected the fission contribution from the 200 kW subcritical core is already well shielded. Instead the spallation component is far more penetrating, and it turns out that dose levels in the reactor hall are more than 2 orders of magnitude above the current limits of 50 mSv/h, with the fission contribution being negligible with respect to the spallation contribution. Solutions involving extra shielding around the core are currently being examined to reduce these doses.

The experimental programme

TRADE has begun the first phase of its experimental programme, and preliminary results have been described in past papers [7,8]. As discussed, TRADE will ultimately lead to the coupling of a high-energy spallation source to a TRIGA reactor. To ensure a meaningful transition from other preliminary ADS experiments, notably MUSE at Cadarache, an experimental programme has been developed consisting of three phases. In Phase IA, scheduled to extend from May 2003 to June 2004, a number of measurements in a mock-up of the TRADE core will be made, using a californium source. These include precise reactivity determinations, kinetic parameters such as b/L, and certain transient responses important to the safety case. In Phase IB, from June to December of 2004, the measures will be repeated with DD and DT sources, allowing direct comparison to the MUSE programme. Phase II deals with the start-up of the accelerator, and is scheduled for the 2007 time frame, while Phase III, the final TRADE experiments, will begin after.

Conclusions

The general set-up of the TRADE facility is now firmly established. The cyclotron building is separated from the TRIGA building. The geometry of the facility calls for a heavily shielded enclosure for the cyclotron and for the validation tests of the beam transport line and of the full target in water. After validation, the full unit is transferred to the TRIGA building. The beam is sent to the subcritical assembly through a shielded channel. A large external additional shielding externally surrounds the reactor building in order to ensure an adequate radiation protection of the radiation due to the production and injection of the particle beam. The structure of the shielding walls is well separated from the TRIGA building.

In summary, the main conclusions are the following:

- The accelerator is a compact H^- cyclotron of nominal current of approximately 300 mA, preceded by a HV set and an external source.

- The proton beam extraction from the H^- is based on an appropriate target stripper. Two independent extraction lines are foreseen, at about 180 radially from each other. The first line is used to validate the overall performance of the full acceleration system in the cyclotron building. After full certification, the subcritical TRIGA is activated in the final configuration.

- The beam transport line (BTL) has two main purposes: (1) to rotate the beam direction from horizontal to vertical (90), (2) to match the beam emittance from the cyclotron to the precisely circular shape of the size required by the subsequent target.

- An original “zoom” focusing geometry has been introduced in order to ensure with precision the required spot of the beam at the target position, independent of the actual emittances of the produced beam.

- All active components of the accelerator and of the beam transport must ensure the utmost reliability during operation.

- A comprehensive beam diagnostic will permit monitoring of the beam at all times, the main task being that of the observation of the beam shape immediately in front of the spallation target. A fast trip (microseconds) can switch off the cyclotron beam in case of emergency.

- The full subcritical source (spallation) will be evaluated in the test station, including the evaluation of the expected lifetime of individual components; one year operation at representative conditions (e.g. the same number of thermal cycles and same proton fluence); irradiation tests in order to evaluate and eventually optimise their mechanical characterisation and radiotoxicity; experimental determination of the beam losses and spectral measurements in order to optimise the shielding configuration in the final position.

Table 4 shows the relevant activities and milestones for TRADE design, construction and operation.

Table 4. Tentative schedule for the realisation of TRADE

Year	2004				2005				2006				2007				2008			
Main items	3	6	9	12	3	6	9	12	3	6	9	12	3	6	9	12	6	12	6	12
ACCELERATOR			■	■	■	■	■	■	■	■	■	■								
BTL			■	■	■	■	■	■	■	■										
INSTRUMENTATION			■	■	■	■	■	■	■	■	■	■								
TARGET			■	■	■	■	■	■	■	■	■	■								
SHIELDING			■	■	■	■	■	■	■	■	■	■								
CONTROL ROOM			■	■	■	■	■	■	■	■	■	■								
IRRADIATION STATION													■	■	■	■				
EXPERIMENTS																	■	■	■	■
INTERPRETATION													■	■	■	■	■	■	■	■

REFERENCES

[1] Rubbia, C., *et al*., "A Full Experimental Validation of the ADS Concept in a European Perspective", *AccApp2003*, San Diego, California, June 2003.

[2] Salvatores, M., *et al*., "The TRADE Experiment and Progress", *Global 2003*, New Orleans, Louisiana, November, 2003.

[3] Rubbia, C., *et al*., *TRADE: General Lay-out of the Experimental Facility*, TRADE Technical Report, March 2004.

[4] Agostini, P., *et al*., *Design Manual of the TRADE Spallation Target*, TRADE Technical Note, March 2004.

[5] Monti, S., *et al*., "The TRADE Experiment: Status of the Project and Physics of the Spallation Target", *PHYSOR 2004*, Chicago, Illinois, 25-29 April, 2004.

[6] Burn, K., *et al*., "The TRADE Experiment: Shielding Calculations of the Building Hosting the Subcritical System", *ICRS10-RPS2004*, Madiera, Portugal, 9-14 May 2004.

[7] Rosa, R., *et al*., "The TRADE Project: First Results of the Preliminary Experimental Program", *AccApp2003*, San Diego, California, June 2003.

[8] Imel, G., *et al*., "The TRADE Source Multiplication Experiments", *PHYSOR 2004*, Chicago, Illinois, 25-29 April 2004.

THE EUROPEAN PROJECT PDS-XADS "PRELIMINARY DESIGN STUDIES OF AN EXPERIMENTAL ACCELERATOR-DRIVEN SYSTEM"

Pierre D'hondt[1], **Bernard Carluec**[2]
[1]SCK•CEN, MOL, Belgium (Co-ordinator of ADOPT network)
[2]FRAMATOME ANP, Lyon, France (Co-ordinator of PDS-XADS project)

Abstract

During the 1990s, in different European countries, the idea of using accelerator-driven systems as efficient tools for transmutation of radioactive wastes came to the forefront. At the national level, various concepts of accelerator-driven system have also been suggested. In 1998, a Technical Working Group was mandated by the Research Ministers of France, Italy and Spain, to identify the critical technical issues and to prepare a "Roadmap" for a demonstration programme.

The Roadmap, issued in April 2001, defines the main requirements of an experimental accelerator-driven system commonly accepted by the European countries.

Subsequently, certain European research centres, universities and nuclear industry companies decided to merge their efforts on this topic so as to propose a common European experimental accelerator-driven system. One of the first steps towards attaining this objective is to evaluate the different candidates previously developed in Europe in order to select the most appropriate concept. This led to the creation of the *P*reliminary *D*esign *S*tudies of an E*X*perimental *A*ccelerator-*D*riven *S*ystem (PDS-XADS) project performed within the Fifth Framework Programme and supported by the European Commission.

Introduction

In 1998 the Research Ministers of France, Italy and Spain, set up a Ministers' Advisory Group on the use of accelerator-driven systems (ADS) for nuclear waste transmutation. This led to the creation of a Technical Working Group (TWG) consisting of representatives from Austria, Belgium, Finland, France, Germany, Italy, Portugal, Spain, Sweden and the European Joint Research Centres, whose task was to identify critical technical issues and to prepare a Roadmap [1] for a demonstration programme.

The goals of the Roadmap were to propose a technological route for the transmutation of nuclear waste in ADS; to prepare a technical programme which will lead to the realisation of an e*X*perimental *ADS* (XADS); to co-ordinate the human resources and experimental facilities in Europe and to identify the possible synergies in the scientific community.

In order to be able to define a consistent view of the programme needed for supporting the development of an XADS, it appeared necessary to establish a minimum detailed design of the XADS. The design activities initially performed in the European countries have been merged in a common European project named "Preliminary Design Studies of an XADS" (PDS-XADS), partially funded by the European Commission within the Fifth Framework Programme. The project rallies the main European organisations involved in partitioning and transmutation studies, both industrial companies and research institutes. The duration of the project is three years (2002-2004); its budget is 1 034 persons months.

The PDS-XADS project is consistent with various other activities performed within the framework of partitioning and transmutation studies supported by the European Commission (Figure 1).

Figure 1. Projects on *AD*vanced *O*ptions for *P*artitoning and *T*ransmutation (ADOPT)

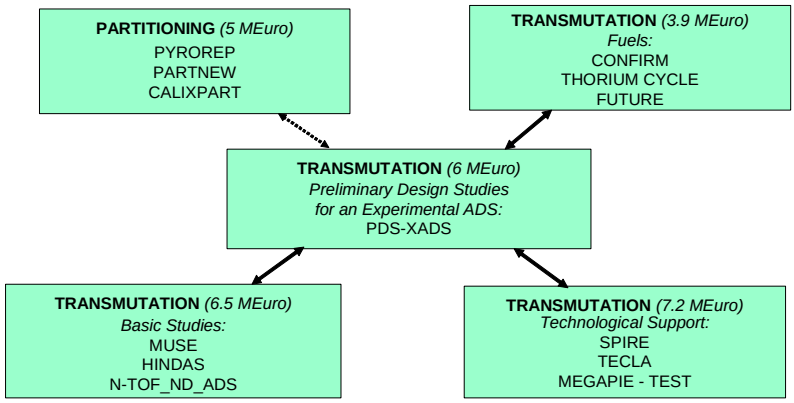

In contrast to conventional nuclear reactors in which there are enough neutrons to sustain a chain reaction, subcritical systems used in ADS require an external source of neutrons to sustain the chain reaction. These external neutrons are provided by the spallation source in which high-energy protons produced by an accelerator interact with the spallation source.

ADS is considered for the transmutation of minor actinides (Np, Am and Cu). Because of their characteristics, cores loaded with high contents of minor actinides could not be burnt in critical reactors. These characteristics are especially a low fraction of delayed neutrons and a low Doppler effect. Under critical conditions, the control of such cores could not be safely maintained.

Previous studies have concluded that the most efficient transmutation of minor actinides requires a fast neutron spectrum, for which the ratio between fission and capture is the highest.

The mission of XADS is to demonstrate the safe and efficient operation of the XADS concept dedicated to the transmutation of long-life highly-radioactive wastes. The demonstration requests a significant neutronic power of several tens of megawatts.

Concerning the accelerator, the studies conclude that the demonstration might be achieved with a proton beam of several hundreds MeV, up to one GeV, and a few milliamps. The main requirement concerning the accelerator is its reliability, which must be very much higher than that observed for existing accelerators dedicated to physic experiments. The objective for the accelerator is a number of beam trips, the duration of which lead to the shutdown of the plant, lower than a few per year. Beam trips of short duration might be acceptable if the thermal loadings on the reactor structure, the fuel and the spallation target are not penalising. A duration lower than some hundreds milliseconds has been assessed acceptable *a priori*. Both cyclotron and linac concepts are assessed.

The efficiency of the spallation target in term of neutrons generated per proton is maximum if heavy metal is used. The reference solution is to use liquid metal (e.g. the lead-bismuth eutectic), which tolerates high-power density. The window separating the accelerator-end and the spallation target is a very highly loaded structure. Therefore a spallation concept without a physical window is also considered.

The XADS concepts investigated in the PDS-XADS project

Research and engineering activities have been performed in the European countries to integrate basic aspects of the ADS and to define conceptual XADS configurations. Several technological options have been considered. These options are oriented to the basic characteristics of the ADS concept dedicated to the transmutation of nuclear wastes:

- Fast spectrum subcritical core leading to use gas or liquid metal as coolant.
- No requirement concerning the conversion of the generated energy (no need for electrical production).
- The objective of demonstration of the operability of the ADS concept need not use cores having a high content of minor actinides, therefore in order to be consistent with the time schedule defined in the European Roadmap, the investigated fuels of XADS are classical MOX fuels (e.g. similar to the Superphénix fuel).
- Due to the innovative technological aspects of XADS, the operational criteria (temperature, pressure…) are selected as low as possible, but consistent with the objective of operability demonstration.

Three XADS concepts are studied:

- Two lead-bismuth eutectic (LBE)-cooled concepts:
  - An 80 MW concept.
  - A smaller concept (50 MW): MYRRHA.
- A gas-cooled concept (80 MW).

The main purpose of the PDS-XADS project is to develop the three concepts using common rules and objectives, to a level sufficient to precisely define the supporting R&D needs, to perform objective comparisons and eventually to recommend the solution to be engineered in detail and realised.

In the following sections we highlight the main characteristics of the different concepts studied as well as for the accelerator. More ample information on the XADS concept investigated in the PDS-XADS project can be found in the proceedings of the International Workshop on P&T and ADS Development (InWor), organised by SCK•CEN, Mol, Belgium on 6-8 October 2003 [2-5].

An 80-MW lead-bismuth-eutectic-cooled concept by Ansaldo

The primary system for this concept is a pool-type and the main characteristics can be found in Figure 2. A peculiarity in this concept is the argon gas lift system for primary coolant circulation to avoid rotating parts (mechanical pumps) immersed in Pb-Bi.

Figure 2. Primary system – main sections

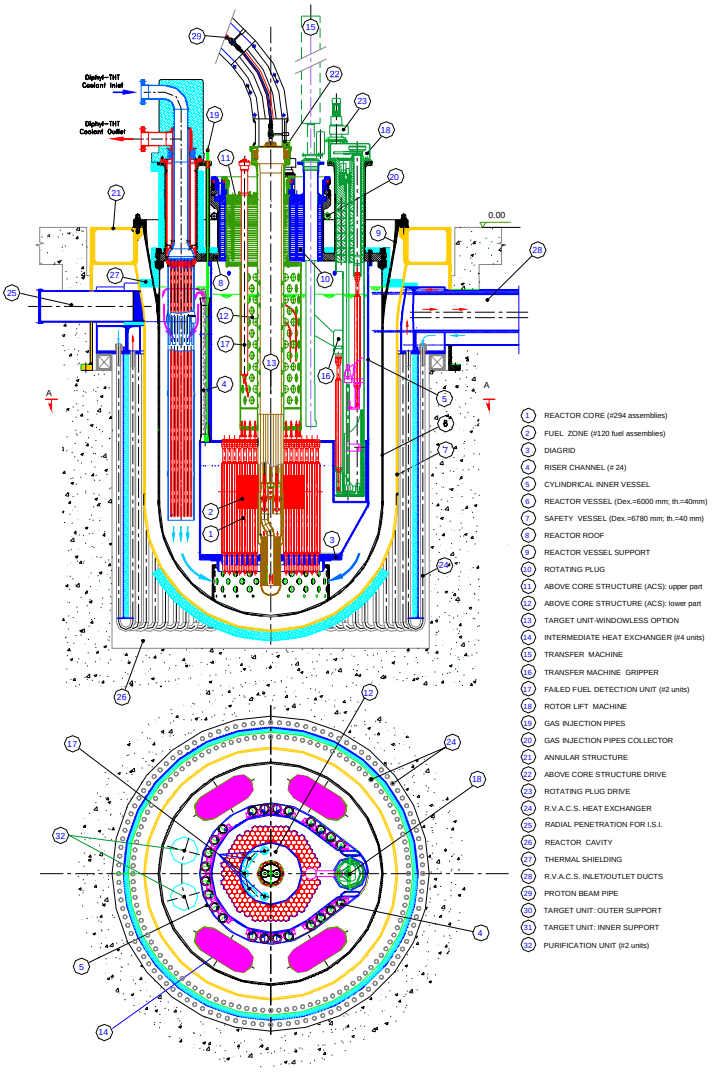

The LBE target containing the spallation products is kept confined within the target unit in order to prevent the contamination of the primary LBE coolant. The target unit is a removable component of slim cylindrical form, positioned co-axially with the reactor vessel which also serves as an inner radial restraint of the core. Its component parts are the proton beam pipe, the heat exchanger and the LBE circulation system, that can be designed with forced or natural circulation, depending on the two design options currently under study: windowless or window.

The core (Figure 3) consists of 120 fuel assemblies arranged in an annular array of five rows. The inner row surrounds the target unit. The assemblies are all alike, each loaded with 90 fuel pins, which have the same cross-section and fuel MOX composition with two different enrichments. The 42 fuel assemblies of the two innermost rows are enriched as the standard Superphénix reload fuel, the remaining 78 fuel assemblies are higher enriched at 28.25% Pu, to set an operational $k_{eff} = 0.97$ at nominal power and BOL.

Figure 3. Core cross-section

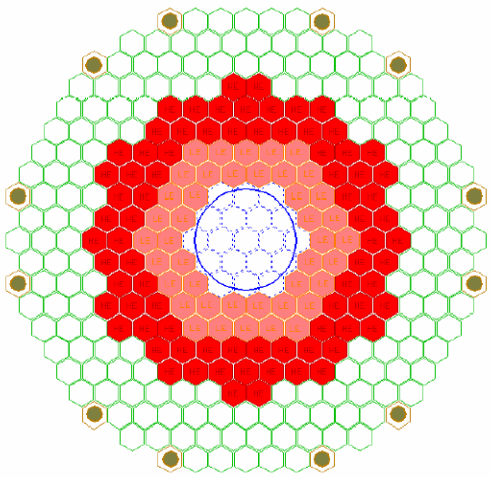

For this concept it is concluded that:

- The LBE-cooled XADS concept has been developed at a sufficient level as to allow the identification of critical issues; for most of them, in any case, suitable solutions have already been identified.

- An operational $k_{eff} = 0.97$ at beginning of cycle and full power guarantees an adequate subcriticality margin under any operational and accident conditions (DBC and DEC) without the need for shutdown or control rods. Compensation of fuel burn-up would be achieved by increasing the 600-MeV proton beam current up to 6 mA max at EOL.

- In spite of the large mass of Pb-Bi of the primary system, the main and safety vessels can resist seismic loads because the reactor assembly rests on horizontal anti-seismic supports.

- The reactor can accommodate either a window or a windowless target unit, both designed as retrievable components. The final choice can be postponed even if the windowless option appears to present more merit in terms of less reactor roof activation, longer lifetime and reduced need of material qualification.

- The low LBE temperature and velocity allow the use of proven stainless or martensitic steels, even if qualification is still necessary.

- Early results of the transient analyses indicate that the design exhibits a large safety margin on account of a combination of very favourable safety characteristics.

- The combination of good heat transfer properties, large thermal inertia and high boiling point of the primary coolant, with the design characteristics of the core, primary system, secondary system and reactor vessel air cooling system, all favourable for the promotion of natural circulation, prevents voiding within the core and fuel clad overheating even under the most severe transient conditions.

MYRRHA, a 50-MW lead-bismuth-eutectic-cooled concept by SCK•CEN

The MYRRHA project is based on the coupling of a proton accelerator with a liquid Pb-Bi windowless spallation target, surrounded by a Pb-Bi-cooled subcritical neutron multiplying medium in a pool-type configuration with a standing vessel (Figure 4). The spallation target circuit is fully immersed in the reactor pool and interlinked with the core but its liquid metal content is separated from the core coolant. This is a consequence of the windowless design presently favoured in order to use low-energy protons on a very compact target at high beam power density in order not to lose on core performance.

Figure 4. MYRRHA 3-D vertical view

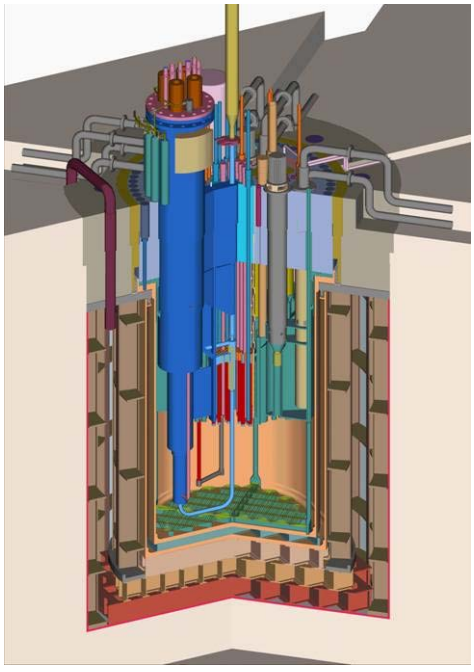

The core pool contains a fast-spectrum subcritical core (Figure 5) cooled with Pb-Bi eutectic (LBE). The core is fuelled with typical fast reactor fuel pins with an active length of 600 mm arranged in hexagonal assemblies. The three central hexagons are left free for housing the spallation module. The core is made of fuel hexagonal assemblies of 85-mm flat-to-flat, composed of MOX typical fast reactor fuel (Superphénix-like fuel rods) with total Pu contents of 30% and 20%.

Figure 5. MYRRHA core layout

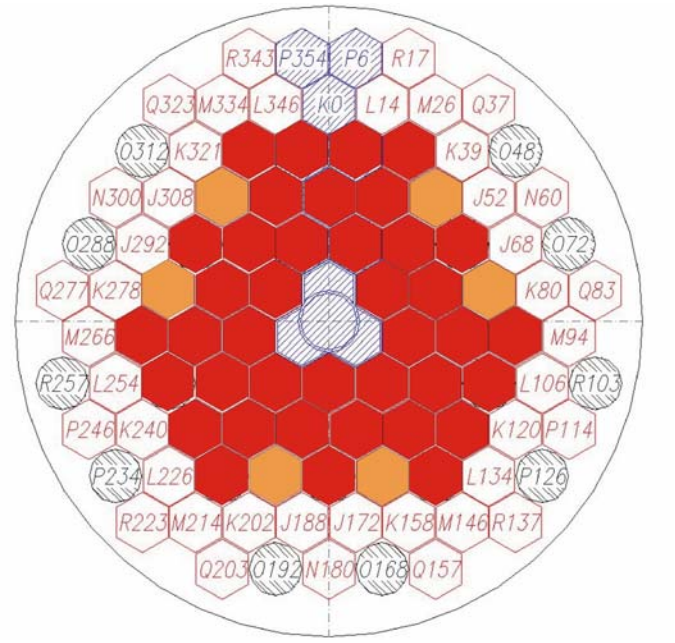

Since access from the top is very restricted and components introduced into the pool will be buoyant due to the high density of the LBE, the loading and unloading of fuel assemblies is foreseen to be carried out by force feedback-controlled robots in remote handling from underneath. The pool also contains the liquid metal primary pumps, the heat exchangers presently using water as a secondary fluid and the two fuel-handling robots based on the well-known rotating plug of fast reactors.

The spallation circuit connects directly to the beam line and ultimately to the accelerator vacuum. It contains a mechanical impeller pump and a LM/LM heat exchanger to the pool coolant (cold end). For regulation of the position of the free surface on which the proton beam impinges (whereby this defines the vacuum boundary of the spallation target), it comprises an auxiliary MHD pump. Further on, it contains services for the establishment of proper vacuum and corrosion-limiting conditions.

By mid-2002, the MYRRHA pre-design file had been submitted to an International Technical Guidance Committee for reviewing the pre-design phase as achieved for the MYRRHA project. This international panel consisted of experts from research reactor designers, reactor safety authorities and spallation target specialists. The conclusions and recommendations of this panel were as follows:

- No show-stoppers are identified in the project.
- More attention should be paid to safety case studies and iterate to the pre-design before entering the detailed engineering phase.
- Address some R&D topics that can lead to timing bottlenecks very soon, such as fuel pin and assembly development and qualification.
- Make a decision on the accelerator option (cyclotron vs. linac) and eventually revisit beam parameters.

MYRRHA responds to the objectives of the XADS facility in terms of demonstration and performance, and also responds by design to some key issues related to the LBE ADS such as:

- The LBE corrosion by leaving the majority of the system at "cold" conditions and limiting the LBE velocity below 2.5 m/s.
- Criticality control during core loading by leaving the spallation target in position and loading from underneath.
- Avoiding spallation target window break by choosing the windowless design.
- Addressing the ISI&R and the O&M from the conceptual design by means of robotics and ultrasonic visualisation.

A 80-MW gas-cooled concept by FRAMATOME ANP

The reference basic features have been fixed by the PDS-XADS project global coherency:

Reactor power	80 MWth
First subcritical core	Classical FBR fuel U-PuO_2 (Pu < 35%)
Accelerator	Linac type
Core and target unit	Designed for E = 600 MeV, I < 6 mA,
Target	Physically separated from the reactor

The main parameters for this gas-cooled design are:

Primary coolant fluid	Pressurised helium at about 6MPa
Primary helium containment	Metallic vessels
Power conversion system	Heat exchanger and circulator

The overall reactor architecture is shown in Figure 6.

The spallation target consists of a 460-mm diameter, 25-mm thick tube submitted to external helium pressure bolted on the roof slab and guided at the core centre. The thimble houses the target unit located at core centre and composed of a vacuum tube, an internal tube for flow arrangement and the liquid lead-bismuth eutectic (LBE) spallation material container. The proton beam enters the beam tube at the upper end of the target unit, penetrates the beam tube window, located just above core centre line and impinges on the upward flowing target LBE below the window (spallation zone). The target LBE is circulated by pumps and cooled by an external heat exchanger located in the target cooling room, outside the reactor vessel. The LBE external circuit option is favourable with respect to both neutronic efficiency and maintenance of target unit and components.

The XADS gas-cooled core is built up from a ring of 90 fuel subassemblies (SAs) surrounding the spallation target which take up the central locations (Figure 7). Surrounding the core are steel reflector SAs in turn surrounded by shield SAs containing boron carbide to limit damage to the RPV. Six absorber rods, located at the core fuel zone periphery, are to be used only during shutdown conditions to bring sufficient reactivity margins mainly with respect to fuel handling error and accidental water ingress in the core. The design of the core has been based largely upon previous fast reactor experience.

Figure 6. Gas-cooled XADS overall architecture

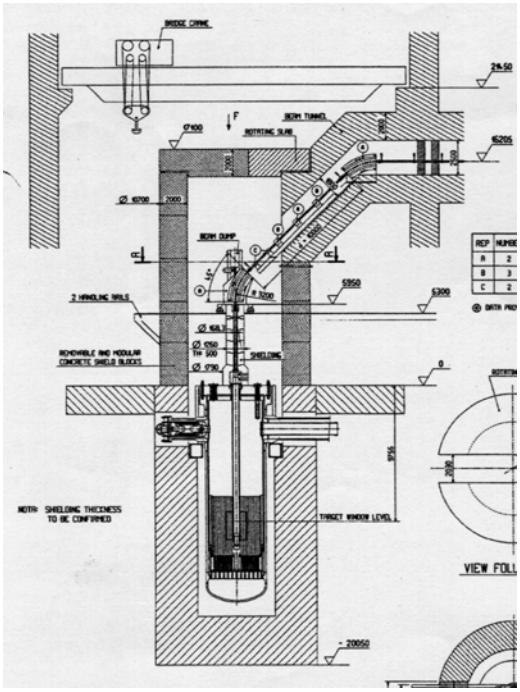

Figure 7. Gas-cooled XADS core layout

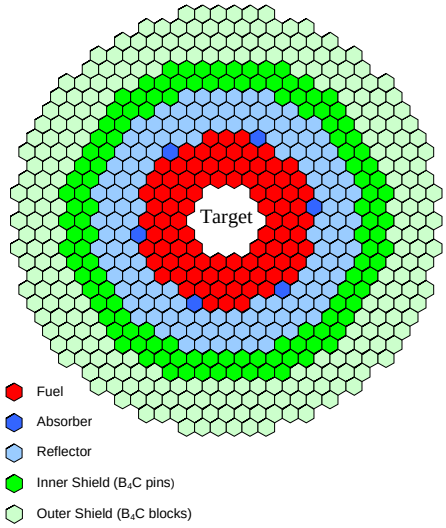

The XADS gas-cooled system has reached the end of the preliminary studies devoted to the definition and the justification of a reference and consistent reactor design. The basic options, sub-systems and components are described and ongoing analysis did not reveal major feasibility issues. Some important features are to be checked further such as:

- Selection of a core reference between single and multi-batch concepts and optimisation of core thermal-hydraulics.

- Confirmation of core subcriticality levels and associated measurement system.

- Reactor transient analysis (accelerator beam trip, transition between nominal and cold shutdown conditions, loss of flow and loss of coolant accidents) and consequences on structural mechanic analysis.

- Feedback on DHR system operating conditions and design.

- Evaluation of mechanical integrity and resulting residence time of beam tube and target unit.

- Confirmation and improvement of radiation dose rates outside and inside the reactor vessel, shielding design and definition of core instrumentation and ISI&R provisions.

- Reactor containment specification and design.

The PDS-XADS reference accelerator

The main technical specifications for the XADS accelerator are summarised in Table 1. These characteristics clearly show that this machine belongs to the category of the so-called high-power proton accelerators (HPPA). HPPA are presently very actively studied (or even under construction) for a rather broad use in fundamental or applied science. The overall performance of the subcritical system will be critically determined by a strict adherence of the XADS accelerator to its specifications. Compared to other HPPA, many requirements are similar, but it is to be noted that the reliability specification, i.e. the number of unwanted "beam trips", is rather specific to the use as driver for an ADS. The reference design had to integrate this stringent requirement from the very beginning, taking into account that this issue could be a potential "show-stopper" for ADS technology in general.

Table 1. XADS proton beam specifications

Max. beam intensity	6 mA CW on target (10 mA rated)
Proton energy	600 MeV (includes 800 MeV upgrade study)
Beam entry	Vertically from above preferred
Beam trip number	Less than five per year (exceeding 1 second)
Beam stability	Energy: −1%, Intensity: −2%, Size: −10%
Beam footprint on target	Gas-cooled XADS: Circular ˘ 160 LBE-cooled XADS: Rectangular 10 · 80 MYRRHA: Circular, "donut" ˘ 72
Intensity modulation	0.2 ms "holes" in CW beam for neutronics measurements, repetition frequency 0.01-1 Hz

The proposed reference design for the XADS accelerator, optimised for reliability, is shown in Figure 8. It is composed of a "classical" proton injector (ECR source + normal conducting RFQ structure). Additional warm IH-DTL or/and superconducting CH-DTL structures are used up to a transition energy. At this point a fully modular superconducting linac accelerates the beam up to the final energy.

Up to the transition energy, fault tolerance is guaranteed by means of a "hot standby" spare. Above this energy, "spoke" and, from 100 MeV on, "elliptical" cavities are used. Beam dynamic calculations for this part have shown that an individual cavity failure can be handled at all stages without loss of the beam. Besides this fault tolerance, another remarkable feature of the concept is its

Figure 8. XADS reference accelerator layout; a doubled injector accelerator is followed by a fully modular spoke and elliptical cavity superconducting linac

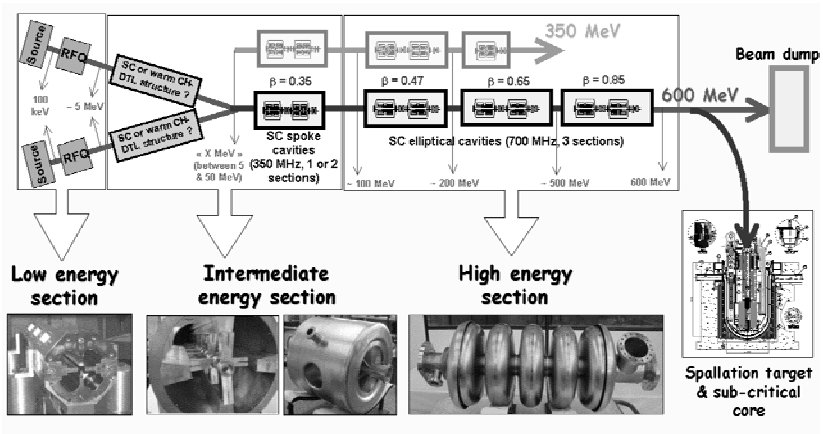

validity for a very different output energy range: 350 MeV for the smaller-scale XADS requires nine cryomodules of $\beta = 0.65$ elliptical cavities; in order to obtain 600 MeV, 10 more cryomodules simply have to be added (seven with $\beta = 0.65$ and three with $\beta = 0.85$) and 12 additional ($\beta = 0.85$) boost the energy to 1 GeV. Therefore, the small-scale XADS accelerator is already fully demonstrative not only of the 600-MeV XADS (and could be converted to it), but even for an industrial machine.

The chosen superconducting cavities are the subject of important R&D programmes presently underway. The performance of the prototypes has been measured to exceed the operational characteristics for the XADS by a very comfortable safety margin that ensures the "over-design" criteria imposed by the reliability strategy.

Within a period of less than two years, it has been possible to develop a generic and robust technical solution for the XADS accelerator and its associated beam line. This solution, based on a superconducting linear accelerator, can fulfil *a priori* the specifications for the XADS. This linac can be used for all different versions of XADS studied within the 5th FP, and it is also representative of an industrial machine.

The proposed machine is reliable through the rigorous implementation of a highly modular system with de-rated components operated in a fault-tolerant manner. The continuation of the vigorous R&D programme presently underway, with a focus on the reliability aspect within the 6th FP, places the XADS accelerator on a roadmap in line with the TWG recommendations.

Conclusion

Within the PDS-XADS project, supported by the European Commission, are performed design studies for the three XADS concepts. The accelerator study has shown that it is possible to develop a generic and robust technical solution for the XADS accelerator and its associated beam line. The PDS-XADS project will be finalised at the end of October 2004.

The first R&D needs resulting from the design studies have been identified and described on specific R&D questions sheets. These sheets have been issued and distributed to the organisations involved in the ADOPT network on P&T activities within the Fifth Framework Programme. The sheets constitute a valuable input for the preparation of the P&T-related projects for the Sixth Framework Programme.

REFERENCES

[1] Rubbia, C., *et al*., *A European Roadmap for Developing Accelerator-driven System (ADS) for Nuclear Waste Incineration*, published by ENEA, ISBN 88-8286-008-6 (2001).

[2] Cinotti, L., *et al*., "Status of the Studies Performed by the European Industry on the LBE-cooled ADS", *InWor proceedings*, ISBN 9076971072.

[3] Aït Abderrahim. H., *et al*., "MYRRHA, A Multi-purpose Accelerator-driven System for R&D State-of-the-art of the Project at Mid-2003", *InWor proceedings*, ISBN 9076971072.

[4] Giraud, B., "Preliminary Design Study of an Experimental Accelerator-driven System, Overall Description of the Gas-cooled System", *InWor proceedings*, ISBN 9076971072.

[5] Mueller, A.C., "The PDS-XADS Reference Accelerator", *InWor proceedings*, ISBN 9076971072.

STATUS OF THE MEGAPIE PROJECT

F. Groeschel[1], A. Cadiou[2], C. Fazio[3], T. Kirchner[2], G. Laffont[4], K. Thomsen[1]
[1]Paul Scherrer Institut, Spallation Neutron Source, Villigen PSI
[2]École des Mines, Laboratoire SUBATECH, Nantes
[3]Forschungszentrum Karlsruhe GmbH, Nukleare Sicherheitsforschung, Eggenstein-Leopoldshafen
[4]CEA/Cadarache, DER/STR/LCET, St. Paul-lez-Durance

Abstract

The MEGAPIE project was started to design, build and operate a liquid metal spallation neutron target as a key experiment on the road to an experimental accelerator-driven system and to improve the neutron flux at the PSI spallation source. The design of the target system has now been completed and manufacturing has started. The target is designed for a beam power of 1 MW and 6 Ah of accumulated current. It will contain about 88 l of LBE serving as target material and primary heat removal fluid. The heat will be removed by forced convection using an in-line electromagnetic pump with a 4 l/sec capacity. The heat will be evacuated from the target through 12 mono-wall cooling pins via an intermediate oil and a water cooling loop. The beam window made of the martensitic steel T91 will be cooled by a jet of cold LBE extracted at the heat exchanger exit by a second EM pump from the LBE main stream.

A preliminary safety analysis has been performed considering normal, off-normal and accident conditions and a corresponding report has been submitted to authorities for licensing. The experience gained up to now shows that MEGAPIE may well be the first liquid metal target to be irradiated under high-power beam conditions.

Introduction

Based on an initiative of PSI, CEA and FZK, the MEGAPIE project was officially started in 2000 to design, build and operate a liquid metal spallation neutron target of 1-MW beam power as a key experiment on the road to an experimental accelerator-driven system [1]. The project is supported by an international group of nine research institutions (Figure 1) and is partially funded by the European Union within the Fifth Framework Programme.

Figure 1. The MEGAPIE partners



Objective of the project

MEGAPIE is an experiment to be carried out in the SINQ target location at the Paul Scherrer Institute and aims at demonstrating the safe operation of a liquid metal spallation target at a beam power in the region of 1 MW. It will be equipped to provide the largest possible amount of scientific and technical information without jeopardising its safe operation. The minimum design service life will be 1 year (6 000 mAh).

Whereas the interest of the partner institutes is driven by the development needs of ADS, PSI is interested in the potential use of a LM target as a SINQ standard target providing a higher neutron flux than the current solid targets. Calculations of the undisturbed thermal neutron flux for the LBE target in comparison to the former zircaloy and current steel-clad solid lead target yield a gain of about 40% at the beam tube entrance positions (25 cm) [2].

Target system and performance

A sketch of the target and its main properties are shown in Figure 2. It is designed to accept a proton current of 1.74 mA, although the probable current in 2005 may not exceed 1.4 mA. The 65-kW thermal energy deposited in the LBE in the bottom part of the target is removed by forced circulation by the main in-line electromagnetic pump through a 12-pin heat exchanger (THX). The heat is evacuated from the THX via an intermediate diathermic oil and an intermediate water cooling loop to the PSI cooling system. The cooled LBE then flows down in the outer annulus. The beam entrance window is especially cooled by a cold LBE jet extracted at the THX outlet and pumped by a second EM pump through a small diameter pipe down to the beam window. The mass transport and temperature distribution is shown in Figure 3. The thermal-hydraulic system behaviour has been modelled with the RELAP5 code for normal and transient operations (beam trips and interrupts). The operating conditions were chosen in such a way to keep the LBE temperatures below 400°C and the maximum flow velocities

Figure 2. Model of the MEGAPIE target and its main characteristics



Dimensions

Length:	5.35 m	Weight:	1.5 t
LBE volume:	88 l	Gas volume:	2 l
Design pressure:	16/10 bar	Operating pressure:	0-3.2 bar
Design temperature:	400°C	Insulation gas:	0.5 bar He

Materials

Lower liquid metal container:	T91
Upper container	316L
Lower target enclosure:	AlMg3

Heat removal and beam window cooling

Deposited heat:	650 kW
Forced convection assisted by buoyancy	
Main pump:	EM in-line pump (4 l/sec)
Bypass pump:	EM in-line pump (0.35 l/sec)

Liquid metal container
Upper container (316L, body of THX)
Lower container with beam entrance window (T91)

LBE flow control
Main flow and bypass flow guide tubes
EMPS with in-line main pump and bypass pump
Target heat exchanger

Temperature control
Central rod with 20 kW heater

Outer enclosure (2nd barrier)
Target head
Upper target enclosure
Lower target enclosure with beam entrance window (AlMg3)

Figure 3. Mass transfer and temperature distribution in the target at normal operation

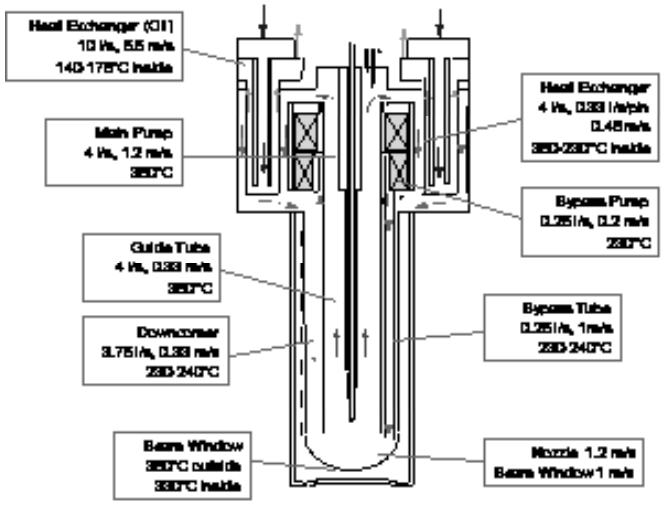

at about 1 m/s. Under these conditions, the corrosion rates in T91 and 316L steel remain low (<0.1 mm/year). This may, however, not be true for the beam entrance window, where interaction with the beam occurs. Specific investigations are therefore undertaken within the design support group to clarify this (LISOR and STIP) as well as the materials' susceptibility to liquid metal embrittlement [3-5].

The target itself is composed of nine subcomponents, which are manufactured separately and then assembled:

- Central rod inserted in the upward LBE flowpath carrying a 22-kW heater and a set of neutron detectors.

- Main flow guide tube separating the hot LBE upflow from the cold downflow in the outer annulus. The heat transfer across the tube wall raises the temperature of the downflowing LBE from 230 to 250°C. The guide tube is equipped with a number of thermocouples to monitor the temperature field in the spallation zone.

- Attached to the top of the tube is the electromagnetic pump system, consisting of the concentrically arranged bypass pump and the in-line main pump on top of it. Both pumps are equipped with electromagnetic, three-coil flow meters respectively. The Institute of Physics (IPUL) in Latvia designed the pumps and has built and tested a prototype of the main pump to demonstrate its proper functioning. While the pump performed according to predictions [6,7], the flow meter did not achieve the accuracy specified and failed during the test. Figure 4 shows a sketch of the pump system and the performance characteristics of the prototype pump.

- The pump system is surrounded by the target heat exchanger (THX), consisting of 12 pins concentrically arranged and 120 cm long. The pins' performance has been experimentally investigated [8] and numerically assessed [9]. Using the diathermic oil Diphyl THT as a cooling medium, it was necessary to implement a spiral in the oil path to increase the contact length. The main problem in the design of the THX was to comply with the complex thermal conditions and to limit the resulting thermo-mechanical stresses. This was accomplished by attaching the pins to the inlet and outlet oil distribution boxes by flexible bellows and inserting thin shrouds as heat shields. The heat is removed from the THX by an intermediate oil loop designed by Ansaldo. An intermediate water cooling loop designed and built by PSI then evacuates the heat from the oil loop. Using this concept, any interaction of LBE with cooling water is eliminated. The pressure in the oil loop is always kept higher than that of the water loop and that in the target. The oil is not significantly affected by interaction with LBE, except for the normal thermal and radioactive decomposition. The loops are also designed to serve during the target testing, which requires special operating conditions (see below). Table 1 provides the characteristic loop parameters. The heat exchanger also forms the upper enclosure of the LBE and the gas expansion tank. The lower enclosure of LBE is formed by the lower liquid metal container.

- The lower liquid metal container is made of the martensitic steel T91. The beam entrance window is hemispherical with a wall thickness tapered from 1.5 mm in the centre to 2 mm at the outer rim. The window is made of a forging and is EB-welded to the tube, which is 2 mm thick in the spallation zone and 4 mm in the upper part. Special attention is paid to the proper control of the temperatures and stresses in the beam window caused by the energy deposited by the proton beam. The current design relies entirely on CFD modelling and FEM calculations. Table 2 shows the amount of energy deposited in the different target components by a 1.74-mA current calculated with the CFX4 and FLUKA codes. The agreement is satisfactory. Different designs of beam window cooling have been investigated, finally leading to the reference design of a bypass jet flow along the long axis of the beam footprint and a 30° slanted guide tube. Figure 5 shows the reference design and the corresponding flow and temperature fields in the LBE as calculated by CFX-4. The design provides sufficiently low temperatures in all the components with respect to corrosion and thermal stresses as shown in Table 3.

Figure 4. Sketch of EMP system and prototype main pump characteristics

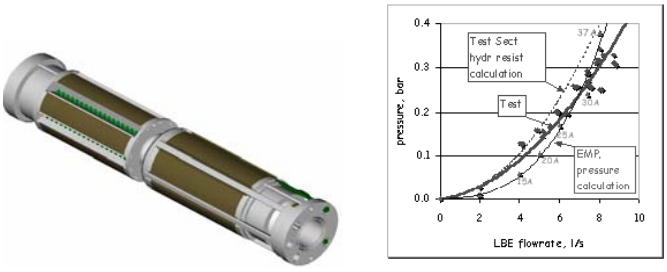

Table 1. Main parameters of the heat removal system

	LBE THX	Oil IHX	H_2O IHX
Inlet temp. [°C]	330	165	40
Outlet temp. [°C]	230	130	59
Oil loop			
Flow rate [kg/s]	9.28	Speed [m/s]	3.5
Pump head [m]	12	P drop [kPa]	626

Table 2. Energy deposited in the target components at 1.74-mA beam current

Material	FLUKA [kW]	CFX-4.3 [kW]
LBE	705.8	709.9
Window T91	5.56	5.28
T91 hull	2.68	1.21
Guide tube	5.55	6.03
Total	719.6	722.4

Figure 5. Temperature distribution in LBE in the spallation zone [11]

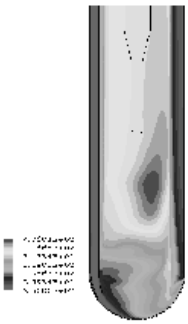

Table 3. Temperature in target components of the reference design as a function of beam current and bypass jet flow direction (parallel or perpendicular major axis of beam footprint)

Beam [mA]	Maj. axis	Peak temperature [°C]			
		LBE	Guide tube	C. rod	Window
1.74	= Bypass	422.7	368.2	386.6	370.2
	⊥ Bypass	424.1	363.1	389.5	360.3
1.4	= Bypass	384.4	339.4	355.7	342.5

Corresponding stress calculations using the above data as input yielded acceptable thermal and overall stresses in the beam window and the guide tube. For the optimum configuration, the maximum stresses in the beam window and the guide tube amount to 55 and 63 MPa, respectively, as shown in Table 4.

Table 4. Maximum temperatures and Mises stresses in the guide tube and beam window as a function of beam orientation to bypass jet flow for the reference design

Beam orient.	LBE weight	Peak temperature [°C]			
		Guide tube	Window	Guide tube	Window
0°	No	367	370	386.6	370.2
0°	Yes	367	370	389.5	360.3
90º	No	362	359	355.7	342.5

The lower liquid metal container, the flange of the guide tube and the heat exchanger constitute the boundary for the LBE, called the hot part. The second boundary is formed by three components, which are separated from the inner part by a gas space filled with either 0.5 bar He or Ar. The gas will stay enclosed during the experiment and only the pressure will be monitored. The components are the:

- Lower target enclosure, a double-walled, D_2O-cooled hull made of AlMg3. The containments of the current targets are made of the same material and experience on its radiation performance exists up to about 10 dpa. The enclosure is designed to contain the LBE in the case of a number of hypothetical accidents, which would lead to the breach of the inner container. Its proper functioning has been assessed by FEM calculations [12]. The enclosure is flanged to the upper target enclosure, formed by a stainless steel tube. This tube is welded to the target head.

- Target head, consisting of the main flange, which positions the target on the support flange of the central tube of the SINQ facility, and the crane hook. All supplies to the target and instrumentation lines are fed through the target head.

- Target top shielding, which connects the hot part to the target head. The LBE-containing part of the target is thus suspended from the target head and allowed to expand with the temperature. The component also contains tungsten to shield the target head area from the intense radiation of the LBE and the noble gases and volatiles collected in the gas expansion tank.

Ancillary systems

While the target is designed by CNRS-SUBATECH, the ancillary systems are designed and provided by PSI, ENEA and Ansaldo. The main components are the:

- Heat removal system already described above.

- Gas handling system for the cover and insulation gas. Although small in quantity (about 8 litres), the gases produced by the spallation process represent a high radioactive source term that must be properly handled to cope with the release limitations imposed under normal and accident conditions. The gases are collected in the target expansion tank and periodically evacuated via filters into a decay tank. The radioactive inventory accumulated in the target is so high that additional filters (active carbon) in the beam transport compartment and the TKE are required to retain all gases (except the noble gases) in case of a severe accident.

- LBE fill and drain (F&D) system. Draining of the active LBE had originally been envisaged and a corresponding engineering concept had been worked out. The installation of the complex and expensive equipment in the TKE (heavily shielded container permanently installed) turned out to be difficult and the operation was judged very risky with respect to radiation protection. Due to a better understanding of the LBE freezing process, it seems feasible to sufficiently control the LBE expansion (roughly 1.5% in the solid state with time) to avoid damage to the structural materials, which would jeopardise PIE. Freezing of the LBE in the target at the end of the experiment was therefore chosen as reference design and a F&D system to handle only un-irradiated LBE is now worked out. Its main purpose is to condition the LBE before filling, fill and drain the target during testing and fill the target in the TKE. The LBE expansion process has been modelled by FEM, showing that the stresses on the containers can be limited, if the LBE is solidified in a special procedure, which allows the LBE to creep [14].

- Beamline adaptations including advanced beam monitoring.

- Handling devices for the target decommissioning, storage, dismantling and disposal.

- Control system with the adaptation of the SINQ infrastructure.

Figure 6 shows the layout of the main ancillary systems. All connections to the target have to pass by the target head. Components handling radioactive products under normal operation are placed in a second containment filled with He at a pressure below ambient. Activity is continuously monitored.

Figure 6. Layout of the ancillary systems with, from left to right: insulation gas system, cover gas system with double containment, fill & drain system and heat removal system

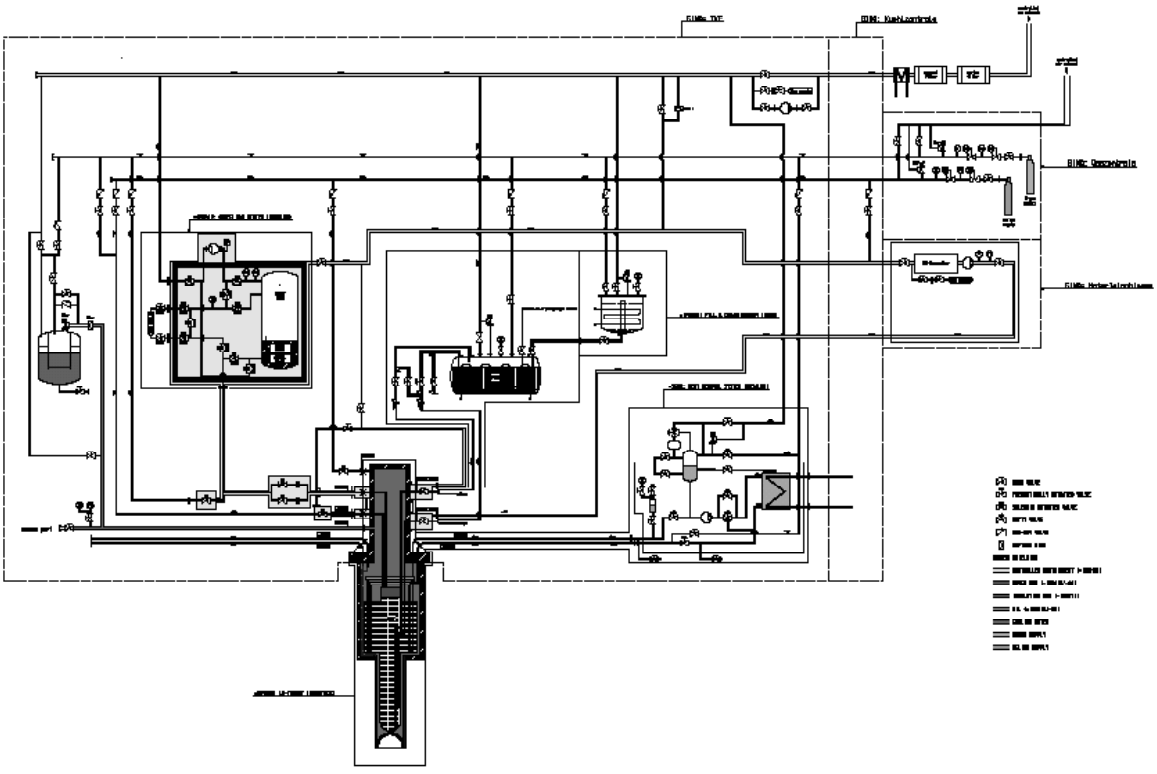

Manufacturing and quality assurance

The target system has been designed and is now manufactured at different sites in Europe. The assurance of the appropriate quality is therefore a key issue. The following modules are currently employed to assure proper quality:

- *Design validation*. Verification of the design and compliance with accepted standards by an independent, second member or group of the project team.

- *Manufacturing quality*. Establishment of a quality plan by the manufacturer, approval by the project QM, surveillance of the tests and assessment of the results by the manufacturer, the project quality manager or a certified body according to the Q-plan.

- *Materials*. Application of referenced materials with Q-certificate.

Safety analysis and licensing process

The safety concept is based on the defence-in-depth approach to contain the LBE, using four barriers for the liquid metal and three barriers for the gas phase. Accident scenarios have been established, analysed and countermeasures have been elaborated considering:

- Internal forces, such as beam focusing, LBE leak, LMC fracture, D_2O leak, gas leak.

- External forces, such as earthquake and airplane crash.

The safety concept must take the operability of the SINQ into account. In this case, we rely on the two inner barriers being part of the target system. The safety concept cannot rely on the integrity of the first barrier alone. The knowledge concerning the interaction of irradiation, LBE and mechanical loads with the structural materials is not sufficiently established (it is one of the goals of the experiment). The possible failure of the first barrier is detected by different sensors, which will trigger the stop of the beam and the transition of the target into a safe condition. The key element for LBE leaks is a sensor placed in the bottom of the target. A leak in the gas phase will be detected by monitoring the radioactivity in the He gas of the second containment. A breach of the first barrier and containment within the second barrier will cause no contamination of the SINQ environment. The target can be extracted and replaced without severe delay.

The two barriers may be breached due to malfunctioning of the proton beam. The target is hit by a fully or partially focused beam, if the target E fails or is bypassed. The peak current density is increased by more than 20-fold. Calculations show that the LMC beam entrance window can only withstand for less than a second [15]. Although the AlMg3 LTE itself supports the high local energy deposition, it will fail soon afterwards when contacted by LBE, if the beam is not switched off. Although devices exist to detect malfunctioning of the beam, two new monitoring devices are under development, given the high risk of such an incident. The beam slit is intended to block those protons bypassing the target E. These protons deviate from the normal path due to their slightly higher energy. The VIMOS device monitors the temperature distribution of the beam footprint on a tungsten grid just ahead of the target. Both devices were installed during the shutdown 2004 and shall prove their functionality before installation of the MEGAPIE target. The perforation of both beam entrance windows will send the LBE down the beam line. The LBE will be collected in a specially designed catcher, but the beam line will be heavily contaminated. The beam line will, however, withstand the pressure increase caused by the LBE/D_2O

interaction as shown in simulations with the MATTINA code [16]. Extraction of the target will require special measures and the operation of the SINQ is interrupted for several years. The reliable detection of beam malfunctioning is therefore a key requirement.

The protection of the public is a major concern. Source term and spreading calculations [15] show that the activity is sufficient to exceed the dose limit imposed by law. It is set at 1 mSv for the public. It had been reduced to this value from 100 mSv with the decision to release PSI from the emergency organisation. Whereas the target is designed to withstand a safety earthquake (probability of 10^{-4}/year) it must be assumed that the target and the beam line will fail during severest accidents. The inventory of the target will spread out in the beam transport channel compartment and the volatile components will be released. Calculations showed that the iodine isotopes, in particular ^{125}I, make the highest contribution to the dose outside PSI, which may reach 230 mSv. Upgrading of the ventilation system with earthquake resistant carbon filters and retention of the iodine brings the dose down to 66 μSv, which is acceptable. A similar upgrading is required for the target head compartment.

Licensing of the experiment by the authorities requires clearance for the following steps before the start of irradiation:

- Operation of the heat removal system.
- Operation of the gas system.
- Inactive operation of the target system.
- Dismantling, transport and waste disposal.
- Active operation of the target system.

Conclusions

The manufacturing of the target has started. Some details, like detectors, still have to be elaborated and the final design has to be validated. The progress on the ancillary systems is according to plan. PSI has managed to complete the installations in the beam line and the piping and cabling during the shutdown 2004. Assessment of the beam monitoring devices is now underway. The start of irradiation in May 2006 is still within reach.

Acknowledgements

The financial support of the European Union under Contract FIKW-CT-2001-00159 and by the Swiss Government under Contract BBW-Nr.01.0298 is acknowledged.

REFERENCES

[1] Bauer, G.S., M. Salvatores, G. Heusener, "MEGAPIE, a 1 MW Pilot Experiment for a Liquid Metal Spallation Target", *J. Nuclear Mat*., 296, 17-35 (2001).

[2] Foucher, Y., *Étude et développement d'une cible spallation*, Doctoral Thesis, Université de Nantes (2002).

[3] Kirchner, T., Y. Bortoli, A. Cadiou, Y. Foucher, J.S. Stutzmann, T. Auger, Y. Dai, S. Dementjev, K. Geissmann, H. Glasbrenner, F. Groeschel, F. Heinrich, K. Kohlik, G. von Holzen, Ch. Perret, D. Viol, "LISOR, a Liquid Metal Loop for Materials Investigation Under Irradiation", *J. Nuclear Mat*., 318, 70-83 (2003).

[4] Dai, Y., F. Groeschel, W. Wagner, "Using SINQ Targets for Materials R&D for Future High-power Spallation Targets", presented at *ICANS-XVI*, Neuss, May 2003.

[5] Kalkhof, D., M. Grosse, "Influence of PbBi Environment on the LCF Behaviour of SNS Target Container Materials", *J. Nuclear Mat*., 318, 143-150 (2003).

[6] Dementjev, S., F. Groeschel, S. Ivanov, E. Platacis, G. von Holzen, A. Zik, *Report on the MEGAPIE EM Pump Prototype Test*, PSI MPR-11-DS34-005/0 (2003).

[7] Stieglitz, R., *MHD-features of the Main Service and Bypass Pump in the MEGAPIE Design*, FZK Report 6826 (2003).

[8] Agostini, P., E. Baicchi, *Observations Resulting from the MEGAPIE Cooling Pin Test in Bradimone*, ENEA Report MP-T-R-001 (2002).

[9] Maciocco, L., L. Sorrentino, *Thermal Fluid Dynamic Analysis of the MEGAPIE Target Heat Exchanger in Steady State and Transient Conditions*, CRS4 Technical Report 03/## (2003).

[10] Stieglitz, R., "Thermohydraulic Investigations for MEGAPIE – The HYTAS, KILOPIE and Heated Jet Experiments", *MEGAPIE TRM*, Paris (2003).

[11] Dury, T., A. Zucchini, "The MEGAPIE Liquid-metal Spallation Target: CFD and SA Design Support at PSI and ENEA", *Proc. ICANS-XVI*, Neuss, May 2003, 1257-1276.

[12] Ni, L., F. Groeschel, "Hypothetical Accident Analyses on the MEGAPIE Lower Target Enclosures", submitted to *J. Nucl. Mat*.

[13] Zucchini, A., *MEGAPIE – Target Stresses Due to LBE Expansion After Solidification*, ENEA Report RT/2002/49/FIS (2002).

[14] Leung, W., *A Report on the Preparations of the MEGAPIE Integral Test*, PSI TM-34-02-09 (2002).

[15] Jacobs, H., *Untersuchung zum Sicherheitskonzept des MEGAPIE-Targets – Druckentwicklung im Strahlrohr im angenommenen Störfall "Bruch der Strahlfenster an Targetbehälter und Sicherheitshülle*, FZK Report 6637 (2002).

[16] Fuchs, A., S.G. Jahn,, A. Janett, *Störfallbetrach-tungen für den MEGAPIE-Betrieb der SINQ*, PSI TM-96-02-08 (2002).

ADS ACCELERATOR RELIABILITY ACTIVITIES IN EUROPE

Paolo Pierini
Istituto Nazionale di Fisica Nucleare, LASA, Via Fratelli Cervi, 201 20090 Segrate (MI), Italy

Luciano Burgazzi
Ente Nazionale Energie Alternative, FIS-NUC, Via Martiri di Monte Sole, 4 40129 Bologna, Italy

Abstract

In this work we report the activities performed in Europe to assess the reliability characteristics for an ADS-class accelerator system. These activities are mainly carried in the context of Working Package 3 ("Accelerator") of the EC programme PDS-XADS (funded by the Fifth Framework Programme, under contract FIKW-CT-2001-00179) aimed at the design of a highly reliable accelerator for an experimental ADS. We review the reliability-oriented guidelines followed to select the reference accelerator design, and present the methodologies used for highlighting the critical areas needing further work and R&D activities in future programmes. Furthermore, we describe the synergies with ongoing high-energy physics programmes aimed at the availability assessment of complex accelerator systems, which may facilitate the compilation of a much-needed reliability database of accelerator components. A rough exploratory "parts count" reliability analysis is then presented and briefly discussed to assess the needed work on the path to obtain more accurate reliability/availability predictions of the ADS accelerator operation.

Introduction

The reliability and availability requirements that an ADS design should fulfil have been mainly derived from the considerations expressed in a European Technical Working Group report [1]. The reference option for the PDS-XADS [2,3] accelerator is discussed in a separate contribution of these proceedings [4], in the internal deliverables issued by the programme [5,6] and in several other publications [7-9]. An important consideration was assumed in the above references concerning the duration of allowed beam trips from the accelerator. The order of magnitude of the allowable duration of the beam trips has been set to 1 second. Beam trips with duration much smaller than the threshold of 1 second lead to insignificant transients in the subcritical system, and no limits on the occurrence of such trips have been set. Regarding the damage to the reactor structures, the spallation target and the fuel, the allowable number of long beam interruptions (> 1 s) depends on the technological details of these equipments (window concept, materials, primary coolant). Nevertheless, in all cases this number is very limited. The order of magnitude is hundreds per year, depending on ADS type and design, assuming the plant is designed for a lifetime of 40-60 years. However, especially considering plant availability, the allowed number of even longer-term beam interruptions (the ones that lead to plant shutdown) is very limited. The PDS-XADS programme set as an objective for the accelerator design the value of few (five) unexpected beam interruptions per year with duration of the order of 1 s or longer.

The current operational experience at accelerator facilities world-wide surely exceeds by a great amount these requirements as regards allowed accelerator faults, but until now none of the existing accelerators has been designed with similarly demanding requirements. The design of an accelerator system can –and should – be devised using reliability-oriented criteria from its early conception stages (bearing in mind that extra costs would be needed for implementing the necessary redundancy and fault tolerance capabilities) and there is a considerable potential for improving the reliability, availability and fault rates from that demonstrated by present accelerators. It is also important to keep in mind that highly available accelerators do exist – the typical operation performance of third-generation light sources shows an overall beam availability well above 98%, but short (from few hours to a day) maintenance periods are scheduled on a frequent basis (typically weekly) and longer maintenance shutdowns are planned on a yearly basis. The impact of these maintenance periods is therefore not accounted for with regard to beam availability for user experiments. However, the accelerator maintenance policy highly influences the capability of reaching high ADS availability and low fault rates. The short maintenance periods scheduled in accelerator facilities are not compatible with the ADS, where the maintenance policy would be based on longer periods (from once every three months to once per year), in order to be compatible with the ADS fuel cycle. Hence, provisions need to be made to guarantee a high availability during the longer operation periods.

Reliability-oriented design considerations

Suitable strategies need to be followed early in the design in order to reach the extremely low fault rates expected from the ADS [6,10]. Compliance with these strategies is standard practice in reliability engineering [11], which is primarily a discipline aiming at the use of technical expertise to assist engineers in preventing or reducing the rates of failures in complex systems. Reliability engineering guidelines are followed for many industrial applications (from military systems and aerospace applications to consumer electronics and the automotive industry), where a precise definition of the reliability and availability goals is set early in the conception phase and reliability practices are used in all stages of the product life cycle, up to the production and service maintenance procedures.

As a starting point of any reliability-oriented design, it is necessary to identify the causes of all possible failures that might occur in the system. Where possible, these causes should be removed (either by a suitable design or operation of the components) and, for those that are impossible to avoid,

strategies for dealing with the corresponding failures should be identified (e.g. by adding redundancies in the system or providing fault tolerance capabilities). The task of reliability engineering is to devise schemes for reliability estimations of new systems through the analysis of the reliability data of its components. The reliability design of a new system is generally an iterative process, which starts from a preliminary technical design (based on existing expertise for similar systems), evaluates its failure modes (with a list of possible causes), highlighting the critical areas, and derives first estimations of the overall reliability. The results of this analysis are then used for modifications in the technical design aimed at improvements in the system reliability and availability.

For most systems, due to the technical complexity of the design, it is not enough to specify and allocate the reliability of components in order to accurately predict the reliability of the system. Several formal mathematical and statistical methods can be applied to measure and assess reliability characteristics, but the associated uncertainties are high, leading to estimates with limited credibility. However, there exist design principles (and valuable tools for analysis) that can help to achieve a reliable system. First of all, since the failure rates of a component are usually strongly dependent on the stresses during its operation, components, where possible, should be operated at less severe stresses than those for which they are rated (part de-rating). Then, the formal mathematical and statistical methods teach us that not only the component specifications contribute to the reliability pattern of a complex system, but also, even more importantly, the logical and functional connections drive the overall system reliability (role of parallelism: different implementations of redundancies and spares, role of “strong design”, i.e. fault tolerance). In other words, proper planning of redundancies allows building reliable systems out of moderately reliable components.

The fact that existing accelerator facilities are not designed and optimised with respect to reliability considerations has a similarity in the historical evolution of other fields; see for instance the aerospace industry, where the reliability improvement has been attained via systematic application of reliability methods in design, and strict adherence to production, qualification tests and acceptance procedures. The same approach could and certainly should be applied to particle accelerators aiming at the ADS goals. A special effort can be dedicated to considerably improving availability by considering all the elements that influence repair times: the fault detection and diagnosis process, the preparation time needed to conduct the repair, the fault correction time itself, the post-repair verification strategies and finally the time to restart the system once the fault is corrected. Time needed to localise the exact cause of a failure can be reduced by proper installation of (redundant) diagnostic tools and the use of a dedicated control system. The time needed for repair also depends on policies concerning spare parts, redundant systems and fast access to failing components. Finally, the components’ mean time between failures can be increased by preventive maintenance, in addition to a strong design and de-rated operation.

The solution based on a superconducting linac represents the simplest solution for the accelerator design. It shows a very high degree of modularity – a repeated pattern of transversely focusing elements alternating with independently phased accelerating cavities – which allows a natural implementation of component de-rating, redundancy capabilities and (at least partially) fault tolerance with respect to radiofrequency failures.

One of the subsystems that will play a crucial role in maintaining a high reliability/availability and a low fault rate during the accelerator operation, and committed to guarantee the necessary fault tolerance, is the machine control system. It is clear that this support infrastructure needs to be based on an entirely new design philosophy with respect to existing accelerator facilities where, usually, the goal is to stop the beam as fast as possible when a component failure is detected, in order to start as soon as possible the procedures necessary for the repair. The control system will need to include strategies for dealing with faulty components, gracefully bringing them off-line while preserving the

beam delivery within nominal target requirements. Given the redundancy intrinsically built into the design, and to avoid the abnormal intervention of the compensative actions due to a "spurious" fault detection, all the main signals should be redundant, and "voting schemes" need to be handled. The implementation of such a system will be strongly related to a number of requirements that still have to be precisely identified for the accelerator operation. For example, to handle the fault tolerance of RF cavities, the control system may intervene first by resetting the phases of adjacent cavities (with pre-defined tabular procedures) in order to guarantee beam transmission without losses, and then gracefully recover the nominal parameters. During this short time, which can be of the order of milliseconds to fractions of a second, the beam may fall outside the stability range set by the beam specifications, but only for this limited time. Presumably, the accelerator control system will also be driven by signals coming from reactivity measurements of the subcritical core, but at the present stage their role and consequences have not yet been addressed in the overall system design, and possibly the choice of different cores and target configurations (e.g. window or windowless for the LBE core design) will lead to different specific operating requirements and constraints. Moreover, there will be constraints provided by safety regulation, especially for what concerns radiation safety and associated interlocks.

Reliability figures of merit and goals: R, A or FR?

We have already introduced the concepts of reliability (R), availability (A) and fault rates (FR). These three quantities characterise different aspect of the operational behaviour of a system, and it is crucial to identify and set the proper requirements and assess relative weights to each one of the three.

The failure rate (FR) is the expected (average) number of failures per unit time of operation. Usually, the failure rate of any device will show a typical "bathtub curve", with increased failure rates at the beginning and end of its lifetime ("childhood diseases" and "ageing"). Typically, a large region of the device lifetime is characterised by a slowly increasing or constant fault rate operation (for a given load condition). The MTBF is the inverse of the steady-state fault rate. The reliability $R(t)$ is the survival probability that the system (perfectly operational at $t = 0$) is still operating at time t. This parameter, evaluated at the duration of the mission time, is of paramount importance in mission-critical operations, for which it is crucial to minimise the occurrence of any system failure during the mission time (e.g. airplanes, satellite instrumentation, etc.). For a system with a uniform fault rate λ, reliability evolves in time according to the exponential law $R(t) = \exp(-\lambda t)$. Finally, availability is the portion of time that, on average, the system is up and functional. For an unrepairable system $A(t) = 1 - R(t)$, whereas in the repairable case one can define the steady-state availability as:

$$A_{\infty} = \frac{MTBF}{MTBF + MTTR}$$

where MTTR is the system mean time to recovery.

The reliability (R) of a series connection between components is merely the product of the reliability of the components. Therefore, complex systems for which many components are in series connection are typically characterised by a low reliability figure, approaching zero as more components are added, and, in order to increase it, parallelism must be provided. No matter how low R may evaluate to, the system availability can approach unity when MTTR << MTBF.

The ADS operation is not a mission-critical operation, where the presence of the beam needs to be guaranteed reliably at any particular instant during the operation time. On the contrary, the specifications ask that, for each operational year, the number of faults should be limited to a few (five), that is, a

requirement of a fault rate of five faults per year. Assuming an operational cycle of three months accelerator operation, followed by a one-month-long stop, this translates to a FR requirement of approximately 8×10^{-4} h^{-1}, i.e. a system MTBF of 1 300 h. In this case the reliability at the end of each cycle would be $R(2\ 190\ h) = 0.19$, even if the operational goal is achieved. Of course, the requirement for the ADS is really to limit the total number of faults while guaranteeing an overall high availability during its mission time. For the example above, a mission availability of approximately 98% can be reached if the MTTR is limited to a day. The precise values to require for the FR and mission availability depend on the assumption of the ADS operational cycle, strictly related to the fuel cycle issues. The above numbers are used to provide a simple, yet effective, numerical example.

In conclusion, *an ADS-class accelerator design is required to aim at a very low fault rate during its mission time* (due to the modest tolerance of the subcritical reactor to unexpected shutdowns), while meeting a mission availability goal that remains to be precisely set on the basis of the minimal transmutation rates assumed as a goal in the design. Too much importance cannot be given to obtaining a high mission reliability goal.

Reliability prediction and analysis methodologies

The reliability/availability estimations generally fall in two broad categories, depending on the approach to the system being analysed. They can be *deductive* if they follow a top-down analysis, starting from a precisely described system layout, considering the contribution of the individual components on the basis of their connection and location in the system, or *inductive* if they follow a bottom-up analysis, starting from the individual components and assessing their role in the system under consideration.

Deductive methods require the most detailed information about the different nature of connections between the system components, in addition to reliability figures for the components themselves (in terms of failure rates or MTBF and MTTR). The most common method is the set-up of reliability block diagrams (RBD), a visual arrangement of the component connections representing a given state of the system (under normal operation, fault conditions, etc.). From these diagrams, and using formal mathematical models, the reliability of the system in the given state can be assessed.

The inductive methods require a less detailed knowledge of the precise system configuration and component connection, and ranges from the “parts count” reliability assessment to the Failure Modes and Effects (Criticality) Analysis (FMEA/FMECA). The FMEA aim is to extensively list all possible component faults, identifying their causes, the possible preventive and corrective actions – and determining the consequences at various levels of the system (and, optionally, deriving a criticality ranking on the basis of expected occurrence or severity of the consequences). In the absence of precise technical information at the system/component level, it is possible to set up a FMEA analysis on the basis of subjective engineering expert judgment. This activity has been performed for the PDS-XADS linac [6,10]. The FMEA assumes a single component fault condition in order to assess its consequences on the system and can then complement with a fault tree analysis, a top-down (deductive) method that examines the “failure space”, where all the basic component and subsystem faults are arranged in a hierarchical tree according to the system event that they lead to. Conditional gate conditions (“AND”, “OR” …) are identified and shown in the fault tree hierarchy in order to assess the minimal conditions of component failures that lead to a system fault (cut-set analysis).

Although the possibility of giving precise estimates for the reliability of the accelerator system is limited both by the present stage of the design and by the uncertainties intrinsically associated to all the methods briefly discussed in the preceding subparagraph, nonetheless, a few guidelines can be followed early in the system design in order to aim at a high reliability/availability. These guidelines

are mostly driven by the use of common sense in the system design stage, looking for simplicity and parallelism, and avoiding excessive stresses in the component operation (de-rating). Also, special effort needs to be directed toward the design of subcomponents, aiming at the design and qualification of objects with low failure rates and short repair times. It is also important to note that the mean time to repair (MTTR) of the system components needs to take into account not only the repair time itself, but also all the time needed for fault detection and identification, any time needed before accessing the component (e.g. radiation decay times), time to bring the spare part into position, and finally the time for system re-start and re-validation. All these times may be longer than the repair time and strongly depend on the whole system layout.

The PDS-XADS linear accelerator has been designed and analysed based on the considerations outlined above: the critical components have been de-rated with respect to the technological limitations (to avoid "load-strength" interferences), and the fault tolerance (resulting from detailed beam dynamics simulation) with respect to the main failures identified by a qualitative FMEA analysis has been assessed [12].

Fault tolerance assessment

A fault tolerant system has the ability to operate - possibly with reduced performances but within its requirements – in the presence of faulty components. Such a system needs to detect and diagnose the component fault, to isolate failing components and avoid fault propagation, and finally to compensate and recover from the fault, possibly with real time reconfiguration capabilities. Redundancy and parallelism are the key characteristics of fault tolerance, but they do not guarantee it automatically. For an ADS fault tolerance needs to be extended to the tight requirement of few beam interruptions per year (with durations of > 1 s). The accelerator must tolerate most components' faults without requiring a beam stop, since the beam start-up procedure would probably exceed this time limit. This is probably the most difficult point to assess in the accelerator design, because it is not only a technical problem, but also has deep interactions with the physics of high power beams and with the role of the accelerator control system. A preliminary assessment of the fault tolerance characteristics of an ADS-class superconducting linac, based on beam physics and modelling, is presented elsewhere in these proceedings [12].

(The need for an) Accelerator component database

The absence of a coherent, credible and validated component database with reliability figures for ADS accelerator components results in huge uncertainties in any reliability/availability assessments that could be performed with standard methodologies. Generally speaking, accelerator components are classified in two main broad categories. The first concerns the "industrial" components which are found mainly in the support systems as cooling systems, vacuum devices (pumps, valves), cryogenic components, or standard accelerator magnets and magnet power supplies, for which failure data are available from a large operating experience or other areas of applications as, for instance, fission and fusion field, medical accelerators, aerospace or cryogenic industry. The second category concerns major *ad hoc* accelerator components (HV sources, RF systems, cavities …) for which reliability parameters are inferred on the basis of either operational data of existing similar facilities (accelerator for high-energy physics or synchrotron radiation user facilities) or from vendors and the practice of "expert judgement". Clearly, many world-wide accelerator facilities have huge databases with many years of operating performances of components which are a useful source of information, but the data organisation in a coherent database has not yet been performed, mainly due to the great differences in data collection and log keeping between laboratories and to the lack of manpower required for such an effort [13].

The limits to the role of the component characteristics

However, it should be kept in mind that the connection (logical or functional) between components usually has a greater role in determining the system reliability/availability as opposed to the component characteristics. The failure of a single redundant component does not generate a failure of the system, and generally the system fails only when all (or most of) the redundant components fail. Obviously, while the parallel redundancy reduces the number of system failures, it increases the number of failing components, and the associated logistics. Furthermore, several options exist for parallel redundancy. The ideal situation, rarely met in reality, is "hot" parallelism, which assumes that the parallel components are statistically independent and the system is able to instantaneously detect the fault. Parallel components also exist in "warm" or "cold" configurations, depending on the failure rate of the standby component (in the warm case the failure rate of the standby component is lower than that of the operating, in the cold case it is zero). In these cases, switching devices triggered by fault detection diagnostics need to be included in the analysis. Moreover, time may be needed for the warm/cold component to provide the functions of the failing component.

As a last comment, when planning parallelism, special attention needs to be paid to common cause failures, which may have a probability of occurrence higher than the failure probability of an individual component, thus completely cancelling any possible reliability gain obtained by parallelism. Common cause failures may be associated with failure in the fault detection and switching systems, or with common support systems (e.g. power supplies, common control system, human errors, etc.). Also, failure of one component may determine an increase in the load conditions of other components, again causing a decrease in reliability due to "next-weakest link" failures. Other more complex arrangements are possible with highly reliable electronic equipments, like the "k out of n" redundancy, and may include voting mechanisms to assist in the detection of the failing component.

Design for high availability of future HEP accelerators

Future high-energy physics (HEP) programmes like the proposal to build a linear collider (LC) with a 500-GeV (extensible to 1 TeV) centre of mass collision energy have the ambitious goal of realising extremely complex and technologically challenging high beam power electron accelerators for fundamental subnuclear physics within the coming decades. The various designs proposed rely on two different and competing technologies: a high-frequency normal-conducting RF accelerator (NLC/GLC) and a moderate frequency RF linac, which pushes the limits of the technology of RF superconductivity with bulk niobium resonators (TESLA). In both cases the linear collider machine complex ranges in length more than 30 km. The successful operation of this technology at the TESLA Test Facility has been the driving motivation for the choice of the same technology for the much more moderate performance goals of the ADS accelerator.

A number of international panels and committees have been set to review and compare the designs, and assess the technical merits of the two proposed technologies. What has clearly emerged is that "if the typical reliability of HEP accelerators is scaled to the size of a 500-GeV c.m. linear collider, then the resulting uptime will be unacceptably low" [14]. This consideration stems from the fact that any reliability estimate starting from the "parts count" will lead to reliability and availability characteristics that would be too low for the realisation of the physics programme, and to huge logistics efforts for system maintenance. As an example, each of the two TESLA main SC linacs has approximately 10 000 cavities powered by slightly less than 300 high-power RF sources feeding 36 cavities each [15]. For all LC designs the main goal is to reach high beam availability at the interaction region to attain a 9-months-per-year operation cycle, measured in terms of total integrated luminosity for the experiments.

The linear collider designs have been reviewed by the ILC-TRC [14], identifying the necessary R&D activities that need to be undertaken to address areas of concern and ranking them in priority. Reliability considerations have been ranked in priority only after the actions needed to address the technical feasibility of the solution. In particular, for the TESLA design, no specific R&D items concerning the technical feasibility rank have been identified, whereas all LC designs have been asked to evaluate the reliability characteristics of critical subcomponents. A US-based panel was formed to prepare a technological comparison between the two competing technological options, and delivered a report in March 2004 [16] that includes a full section dedicated to a preliminary availability analysis of the two technologies. A Monte Carlo program was developed by an expert group in order to model the unavailability budget of the complex LC schemes and make predictions on the required MTBF of several key components of the main subsystems of the accelerator needed in order to guarantee a nominal availability of 85%. The results have been compared with the estimated nominal design MTBF, in order to determine the improvement factors needed and derive a model for costing the additional R&D efforts required to reach the high availability goals.

This excellent and rather sophisticated study, performed in a limited time, is still “a first crude step” [16] in order to determine a full availability model for such a complex machine and many important components have been treated by necessity as “lumped elements”, while the main linear accelerator and damping rings have been modelled to a large extent, including many beam dynamics based considerations in the Monte Carlo simulations. This choice is of course justified by the fact that the study was meant to make a relative comparison of the two different technologies, so the accelerators have been detailed in the areas where they differ most, leaving lumped elements where common technologies or subsystems were used in the two different proposals. Nonetheless, data of many years of operation of particle accelerators have been collected (mainly from SLAC and Fermilab) and reviewed in order to actually feed the simulation with starting values for component MTBF. The study represents a valid source with which to cross-check the component database for an ADS reliability study.

It should be noted, however, that these availability considerations were not raised in the mid-90s, when the first designs of the linear collider were first conceived, and were not even mentioned in the first ILC-TRC report in 1995. To some extent, the availability/reliability design revision is still in a “preliminary phase”, as the availability requirements were set after the first technological design. The proposed schemes for the ADS linear accelerator were outlined early in the conception stage using reliability-oriented design procedures and have much less ambitious technological goals.

An exploratory parts count reliability assessment for an ADS linac

Along the path to provide a better characterisation of the ADS linac, a rough “parts count” reliability estimation has been performed, assuming no fault tolerance is provided in the accelerator, which is modelled effectively as a series connection of all its components, besides a redundant injector. Thus, each component fault leads to a system fault. Obviously in this case, due to the considerations expressed in the preceding paragraphs, the reliability of such a system is practically zero for any practical mission time.

The model was fed with a preliminary set of MTBF data collected mainly from IFMIF or LANSCE experience and complemented with engineering judgement where data was missing. Given the subjectivity at this preliminary stage of the input data, especially in the MTTR data, that do not include logistic and waiting times, the results are only intended as a guideline for the identification of critical areas, and the study will be further iterated in the near future after a cross-check with other component sources, as the one described in the preceding paragraph.

Table 1. Main subsystems used for the "parts count" estimation

Subsystem	Main components	Redundancy	Comments
Ion source	1 lumped unit	2 systems in parallel	
RFQ	1 RF structure 2 RF systems		
Intermediate energy Beta = 0.15 spoke cavity	36 cavities 36 RF systems 36 magnets	None	18 focusing lattices
Intermediate energy Beta = 0.35 spoke cavity	60 cavities 60 RF systems 40 magnets	None	20 focusing lattices
High energy Beta = 0.47 elliptical cavity	28 cavities 28 RF systems 28 magnets	None	14 focusing lattices
High energy Beta = 0.65 elliptical cavity	51 cavities 51 RF sources 34 magnets	None	17 focusing lattices
High energy Beta = 0.85 elliptical cavity	12 cavities 12 RF sources 8 magnets	None	4 focusing lattices

Besides the warnings expressed above on the credibility of the results, this very rude parts count estimation performed for a three-month mission time led to a system MTBF of 28 h with a MTTR of 5 h, resulting in a 85% overall availability. An analysis of the percentage contribution to the overall failure rate is shown in Table 2.

Table 2. Percentage contribution to the overall failure rate from the subsystems

Subsystem	FR contribution (%)
Proton injector	0.6
Intermediate-energy section low beta	19.0
Intermediate-energy section high beta	31.7
High-energy section low beta	14.6
High-energy section intermediate beta	26.2
High-energy section high beta	6.7
High-energy beam transport system	0.1
Beam delivery system	0.1
Cryogenics	0.4
Water system	0.1
Compressed air	0.2
Electrical power	0.3
Total for accelerator	100

Clearly in this extremely oversimplified parts count estimation the critical points are found in the regions with a higher number of components (high beta spoke and intermediate beta elliptical). This is a simple artefact of placing all components in a series connection. Obviously the numerical values of

such a simulation are reported only for illustrative purposes, both for the subjectivity of the input data and for the oversimplification of the model. However, based on the very modular nature of the superconducting linac, on the fact that fault tolerance with respect to many single failure events have been assessed [12], and on the possibility to include redundancies in many subsystems, it does not seem too optimistic to reach a 50 times improvement in the system MTBF in order to reach the goal of 1 400 h, with a more realistic system description and a careful evaluation and validation of the input data to the simulations.

Conclusions

In the practice of reliability engineering it is not enough to specify and allocate the reliability of components in order to accurately predict and control the system reliability, and strategies have to be implemented early in the system design to guarantee the necessary degree of redundancy and fault tolerance. The current work on ADS-class linear accelerators, with a modular design and a high degree of redundancy, suggests that a wide margin exists for the implementation of fault tolerance handling practices in several criticality areas.

The FMEA analysis has been a useful tool to identify the reliability critical areas in the ADS linear accelerator design, and to plan for the fault tolerance strategies. In the analysis of the reliability potential of the linac configuration, no fundamental showstoppers emerged, that could compromise the possibility of reaching the high reliability and availability goals. A preliminary exploratory study on a rough parts count model suggests that the design has the potentials for reaching the extremely low fault rate goal, but more work is needed in developing more realistic reliability models and in the set-up of a meaningful reliability component database. Finally, a large interest is growing in the HEP community for the availability predictions of linear colliders, which is greatly synergic with ADS reliability assessment activities.

Acknowledgements

This work has been partially supported by the PDS-XADS programme, funded by the EC in the 5th Framework Programme, under contract FIKW-CT-2001-00179, and by the INFN TRASCO/ADS, NTA/TTF programmes. The contribution of all PDS-XADS WP3 participants is acknowledged.

REFERENCES

[1] *A European Roadmap for Developing Accelerator Driven Systems for Nuclear Waste Incineration*, ETWG on ADS, April 2001, http://www.enea.it/com/ADS.

[2] Carluec, B., "The European Project PDS-XADS", *InWor for P&T and ADS Workshop*, Mol (2003).

[3] D'hondt, P., "European XADS-PDS", these proceedings.

[4] Vandeplassche, D., *et al*, "The PDS-XADS Reference Accelerator", these proceedings.

[5] *DEL02-009, PDS-XADS: Requirements for the XADS Accelerator & the Technical Answers*, Henri Safa, ed., Contractual Deliverable 9 of PDS-XADS, FIKW-CT-2001-00179.

[6] *DEL03-057, PDS-XADS: Potential for Reliability Improvement and Cost Optimization of Linac and Cyclotron Accelerators*, Paolo Pierini, ed., Contractual Deliverable 57 of PDS-XADS, FIKW-CT-2001-00179.

[7] Mueller, A.C., "The PDS-XADS Reference Accelerator", *InWor for P&T and ADS Workshop*, Mol (2003).

[8] Safa, H., "Design of a XADS Linear Accelerator", *InWor for P&T and ADS Workshop*, Mol (2003).

[9] Junquera, T., "Status and Perspectives of the R&D Programs for the XADS Linear Accelerator", *InWor for P&T and ADS Workshop*, Mol (2003).

[10] Pierini, P., "Reliability Studies of the PDS-XADS Accelerator", *InWor for P&T and ADS Workshop*, Mol (2003).

[11] O'Connor, P.D.T., "Practical Reliability Engineering", J.Wiley & Sons, UK.

[12] Biarrotte, J-L., *et al*., "Beam Dynamics Studies for the Fault Tolerance Assessment of the PDS-XADS Linac Design", these proceedings.

[13] Hardy, L., "Accelerator Reliability – Availability", *Proceedings of EPAC 2002*, Paris, France, 149.

[14] International Linear Collider Technical Review Committee, 2003 Report, available from the site: http://www.slac.stanford.edu/xorg/ilc-org/2002/index.html.

[15] *TESLA Technical Design Report, Part II: The Accelerator*, DESY 2001-011, ECFA 2001-209, TESLA Report 2001-23, TESLA-FEL 2001-05.

[16] *U.S. Linear Collider Technology Options Study*, The U.S. Linear Collider Steering Group Accelerator Sub-committee, Linear Collider Option Task Forces, available from the site: http://www.slac.stanford.edu/xorg/accelopts.

ADS NEUTRONICS

W. Gudowski
RIT, Sweden

No paper was available at the time of publication.

ADS SAFETY

P. Coddington
PSI, Switzerland

No paper was available at the time of publication.

TECHNOLOGICAL ASPECTS AND CHALLENGES FOR HIGH-POWER PROTON ACCELERATOR-DRIVEN SYSTEM APPLICATION

Yanglai Cho
Argonne National Laboratory, Argonne, IL 60439 USA

Abstract

It is a generally accepted fact that construction of a high-power proton accelerator (HPPA) capable of driving a system of nuclear subcritical assembly for nuclear transmutation or energy amplification is feasible theoretically and conceptually. However, there are a number of technological challenges in several areas that need to be solved so ADS can become feasible. In this paper, we discuss the key requirements of ADS, available technologies and extension and/or extrapolation of today's technology to render the ADS practical. ADS technology would necessarily be an extension of the accelerator of the Spallation Neutron Source (SNS), which is under construction at Oak Ridge National Laboratory. A discussion on how to extend SNS technology to ADS technology is also provided. As both accelerator and target/reactor would operate in uncharted regions of performances, extending and integrating today's technology to the ADS realm would require many performance/requirements trade-offs between accelerator and reactor designers. The uncharted regime of performance includes two to three orders of magnitude higher beam power, improving the reliability of the accelerator to that of a similar range of reactor, and improving and controlling accelerator beam loss fraction to the 10^{-6} range in order to facilitate hands-on maintenance of the accelerator system. An opinion on a possible road map to achieve the ADS goals is also provided.

Introduction

Some 70 years ago, the first series of accelerator-based nuclear transmutation experiments were performed at Cavendish Laboratory using a Cockloft and Walton constructed 300-kV high voltage rectifier-accelerator. One of the most famous and important results was the discovery of neutrons by James Chadwick in 1932. Today's proposal for an accelerator-driven system (ADS) to change species of nuclei from one kind to another is a continuation of the work started by the Cavendish Laboratory team under the leadership of Lord Rutherford. The differences between then and now are accelerator energy, beam current and accelerator reliability. Chadwick counted neutrons with his 10 fingers, while ADS attempts to produce neutrons in units of kilogramme per year. To produce such a quantity of neutrons, an ADS accelerator requires a beam energy of 1 GeV or more, beam current of 20 mA to 100 mA, and should be operational for 24 hours a day, seven days per week with 100% reliability. For the purposes of discussion, it is assumed that 20 mA is the desired current.

Today's accelerator meets the energy and current requirements of an ADS system separately and not simultaneously. At a beam energy of 600 MeV or above, the beam current requirement must be improved by one to two orders of magnitude. The average current of 1 mA beam for 800-MeV proton acceleration was demonstrated by the LAMPF linac a few decades ago. A 1.4-mA, 1-GeV accelerator (SNS) is under construction, and an SNS upgrade plan to ~4 MW is proposed. In other words, the beam current goal is within striking distance. However, the question regarding the system reliability/ availability requires fresh thinking by accelerator designers/builders, accelerator users, and accelerator managers. In other words, a paradigm shift is required for all parties interested in the ADS in order to obtain ~100% reliable accelerators.

Other challenges facing ADS include controlling potential beam loss throughout the accelerator system. Beam instability induced by varying beam dynamic conditions of the accelerator can initiate uncontrolled beam losses. Excessive beam loss produces hazardous environmental conditions. Past experience shows that a 1-W/m beam loss is tolerable for hands-on maintenance.

In this paper, a short description of a typical conceptual ADS facility and the technology needed to make the concept viable is presented in the next section, followed by a short introduction to "reliability engineering", which is given in order to explain what is needed to improve the facility reliability. A discussion on beam loss is provided to show the extent of extrapolation from today's practice. One method of extrapolating to the future is to expand the SNS technology to the ADS, and this is described in a section below. Possible R&D and a trade-off study are also described. Loss of one W/m for the SNS corresponds to a fractional loss of $\sim 1 \cdot 10^{-6}$/m. A reliable prediction of such a small fractional number by numerical or analytical computation is very difficult. The fractional loss requirement for an ADS machine is even smaller than that of the SNS. The requirement is smaller by one or two orders of magnitude depending on the required current of the machine.

A typical facility for ADS and available technology

An accelerator of ADS is used to produce ~ kg of free neutrons per year in order to change nuclei of one bulk material to another. Such a quantity free neutrons without fission multiplication can produce a proton beam of an order of 100 MW striking a heavy element target. When the target system is a subcritical assembly, the beam power requirement is reduced by a large factor depending on the criticality condition. Thus one can conjecture an ADS facility should be able to handle a beam power of ~20 MW. Since the SNS has a designed beam power of 1.4 MW, the required beam power of ADS is one order of magnitude higher than the performance today's technology can facilitate.

The SNS uses both room temperature and superconducting radio-frequency (SRF) technology, which supplies 80% of the beam energy. The room temperature portion is used to accelerate the beam to energy of less than 200 MeV, where particle velocity is less than 0.5 of light velocity, and rapidly varying. The SNS chooses to use the room temperature technology in this region purely due to the lack of time to develop. Figure 1 shows a schematic layout of the SNS linac. The linac operates with a beam duty factor of 6%. The changes or improvements required to evolve an SNS-type linac into an ADS linac are discussed later.

Figure 1. Schematic layout of the SNS linac

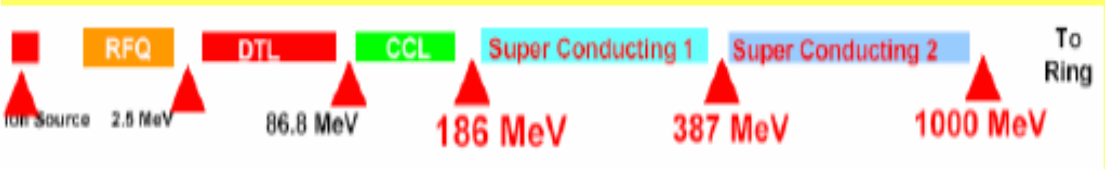

A typical accelerator for ADS would have a beam energy of 0.6 to 1.5 GeV, a beam current of 20 to 100 mA, and a duty factor of 100%. The layout would be similar to Figure 1 except that DTL and CCL could be replaced with cryogenic structures. The DTL could be replaced with an IH structure being developed in Frankfurt, and CCL could be replaced with spoke cavities or elliptical cavities. Current technology meets the required beam energy and current separately and not simultaneously. A challenge is to operate at high energy and high current with infinitesimally small beam loss and closed to 100% reliability. In the past, accelerators were never required to be as reliable as reactors. Improving accelerator reliability requires a different design/construction philosophy.

Reliability engineering

Since the invention of accelerators from the 1930s to the 1950s, almost all accelerators were used for nuclear/particle physics experiments to discover new nuclei, new particles, new phenomena and to measure fundamental numbers. The nuclear/particle physics community in the past would rather have higher-energy particles than higher current or higher-energy particles than high accelerator reliability. There were a number of reasons for these preferences. The probability of a discovery of a new particle or phenomenon is higher at higher energies. Typical particle/nuclear physics experiments run about a week, a few months, or years, and therefore an accelerator availability of 80% or so is acceptable to this community as long as the state of the accelerator has an energy frontier.

On the other hand, over the past 20 years, accelerator builders for spallation neutron sources and synchrotron light sources have implemented a marked improvement in accelerator availability. For example, the Rapid Cycling Synchrotron (RCS) and its associated neutron-generating target system of the Intense Pulsed Neutron Source (IPNS) at Argonne National Laboratory have a 20-year average availability of better than 95%. The availabilities of the Advanced Photon Source (APS) and the European Synchrotron Radiation Facility (ESRF) have achieved 98% over the past several years. A very high availability is required for structural analyses research using neutron scattering or synchrotron radiation. The requirement comes from the following facts: 1) users of such facilities usually prepare samples to be exposed to neutron or photon beams, 2) such sample preparation may take two weeks or more, 3) the sample lifetime with or without beam exposure could be as short as a few hours, and 4) if the sample misses the beam exposure due to machine unavailability, then the user must start the sample preparation over again. The requirement for high availability from scientific users was instrumental in the improvement implemented in light sources and neutron sources. It is reasonable to conjecture accelerator builders of ADS would improve the reliability of the machine.

It may be instructive to review the basics of "reliability engineering" described at the first meeting of this series of workshop held in Mito, Japan [1]. The frequency of system or hardware failure or trip is described with failure rate, λ, which is the inverse of mean time between failure (MTBF). Though the failure rate is constant over a shorter time range, the failure rate increases as the system becomes older. The failure is also higher during a "breaking in" period soon after construction. This time variation of failure rate has the shape of a bathtub, and is known as a failure rate bathtub curve amongst reliability engineering professionals. Figure 2 shows a series of bathtub curves indicating the influence of design stresses, quality control during construction, and preventive maintenance during operations. As for design stress, it is preferable to design with low stresses as long as the budget allows.

Figure 2. Reliability bathtub curves as functions of various conditions

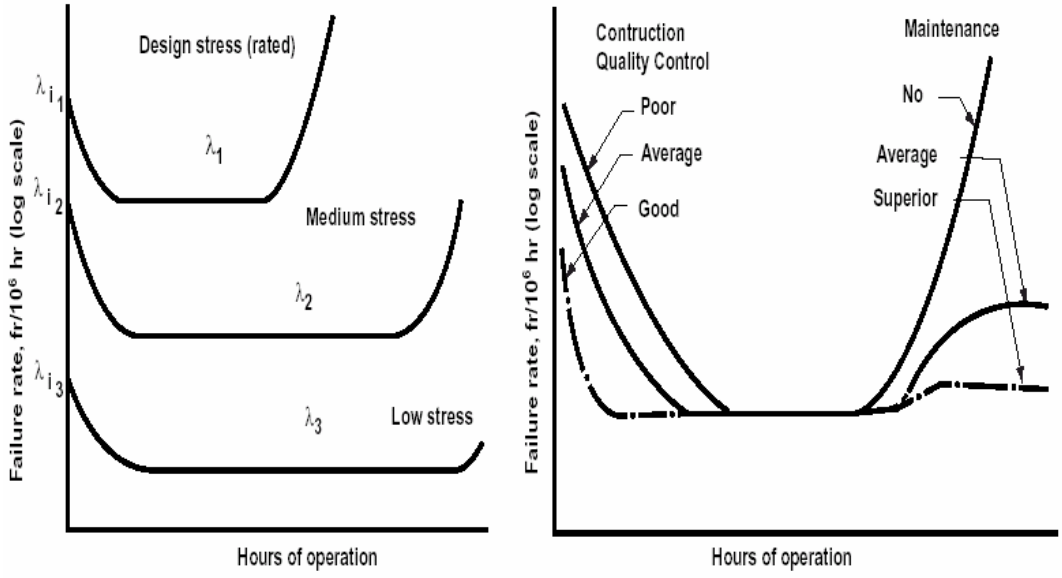

Thus the first task of designing a system is to make the MTBF of an integrated system as long as possible. The second task is to make the time required to repair the failed hardware as short as possible. The usual methods for shortening the repair time are to have redundancies or hot spares for hardware prone to fail and devising "quick connects and disconnects" to install and remove it from the system.

The superconducting portion of the SNS has a special feature of fault tolerance designed into the system in order to eliminate on-line repair time of cavity and its RF power supply failures. There are 81 cavities in the cold section and each cavity is powered by its own klystron. If one or two cavities fail, the linac can be retuned to operate without shutting down. This is a new feature of the SNS linac.

Making an accelerator complex as reliable as a reactor is going to be a challenge.

Beam loss consideration

Excessive uncontrolled beam loss in an accelerator complex brings not only a radiation hazard to personnel and environment but also prevents hands-on maintenance. Beams lost in a controlled fashion (controlled loss) usually collect in a catcher. Experience has shown a loss less than 1 W/m is tolerable for hands-on maintenance. Figure 3 shows calculated and measured residual radiation of accelerator hardware measured at 30 cm from the surface after a 4-hour cooling period following a shutdown under a continual loss of beam at a level of 1 W/m as a function of proton beam kinetic energy. The measured

Figure 3. Residual radiation vs. kinetic energy of proton beam under 1 W/m loss (computed and measured)

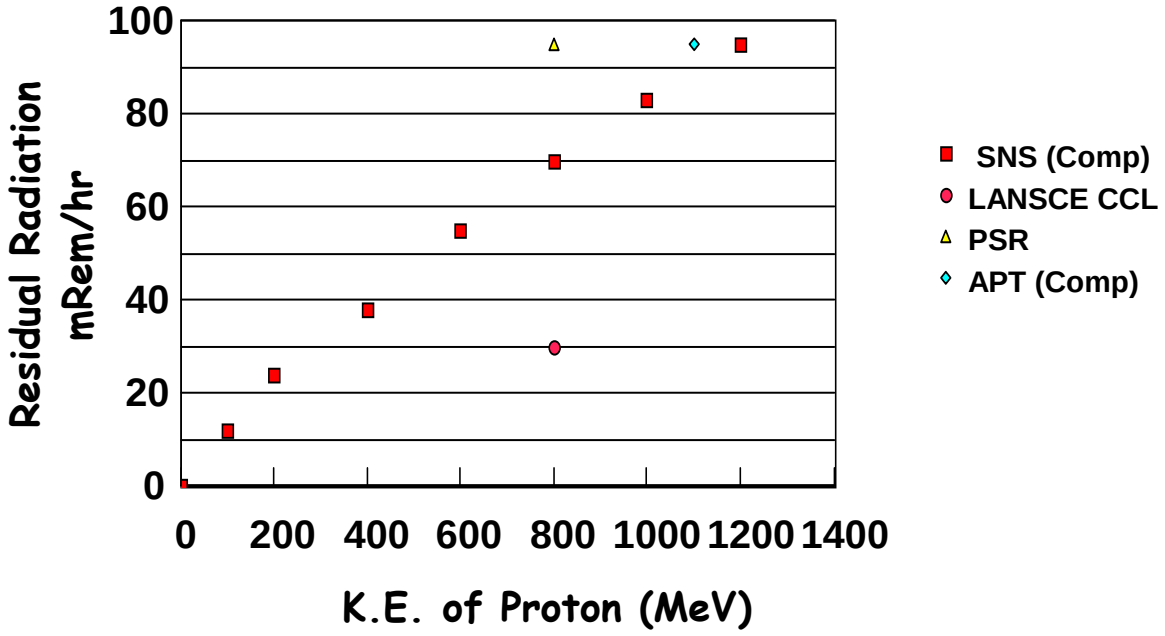

points are from LANSCE linac and PSR ring. The calculated values are from the SNS and APT. It is generally accepted that under a residual radiation of ~100 mRem/hr or less, hands-on maintenance can be performed [2].

The challenge is making uncontrolled beam loss less than 1 W/m throughout the facility. If one takes a 20-MW beam power facility, the allowable fractional loss is $5 \cdot 10^{-8}$ /m. This kind of small loss is hard to predict because of imperfections in numerical calculations as well as incomplete input to the calculation. Accurate prediction and preventive measures are challenges that need to be solved. After construction completion, the measurement of beam losses at the SNS would show how easy it is to obtain required beam loss control at ADS.

From Spallation Neutron Source (SNS) to ADS

It is instructive to compare the SNS accelerator with a 20-MW ADS accelerator. There are many similarities and differences between the two. SNS was a warm machine and the design was changed to a cryogenic machine in 1999 based on available new technologies [3]: Cavity technology came from DESY which was developed in connection with the TESLA proposal and high-power power-coupler from KEK developed in connection with KEK-B-Factory. Figure 4 shows a picture of an Nb cavity and a power coupler. However, there is a remnant of room temperature technology in the SNS linac below 186 MeV as shown in Figure 1. The conversion took place two years after construction started, and the reason why the old technology was kept was lack of time to undertake the R&D necessary for the converting section below 186 MeV in 2000.

The SNS time-averaged beam current is 1.4 mA with a beam duty factor of 6% and RF duty factor of 7%. The peak current of the linac is about 25 mA. If the SNS linac were to operate in CW mode, the beam power becomes about 23 MW, which is an ADS beam power.

Figure 4. SNS niobium cavity (left) and power coupler (right)

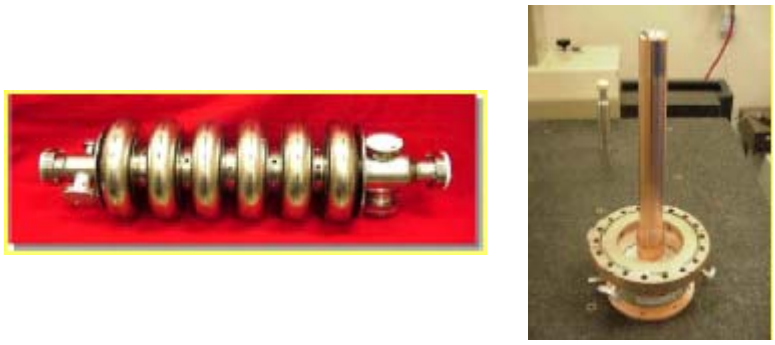

Therefore, what are the changes necessary to build a CW 23 MW machine based on the SNS technology?

It is advisable to eliminate the warm section below 186 MeV. There are a couple of new technologies being developed around the world. One is the so-called spoke cavities being developed at ANL, LANL and Orsay, and the other is the IH structure being developed for GSI by the University of Frankfurt.

Since the idea is only to change the linac duty factor, the peak beam current of the machine does not change. Therefore it is important to note that beam dynamics associated with high current remains the same as that of the SNS. Beam stability criteria remain same.

A major upgrade required would be a cryogenic plant. Due to the change of RF duty factor from 7% to 100%, the dynamic heat load would increase by a factor of 15 from that of the SNS. For a given final energy of a linac, dynamic heat load is proportional to accelerating gradient; therefore a trade-off optimisation between gradient and costs of construction and operation should be performed in order to minimise the costs.

One of the SNS subsystems which would not function properly is the beam diagnostic system. Since the beam is CW rather than pulsed, the frequency response of the diagnostic system should be in the 200 MHz range, which is the bunch frequency of the beam formed at the initial RFQ. The frequency response of the SNS could be much lower because the pulse repetition rate is 60 Hz. An additional complication and intriguing challenge is how to commission or turn on the linac after shutdown.

When an accelerator is turned on for commissioning or after a shutdown, the beam trajectory is unknown because there are too many parameters which influence the trajectory, and these parameters are imperfectly known. A mis-steered beam can destroy the machine and present a hazard to people and the surroundings. To find the trajectory one needs a beam intense enough to provide signals in the diagnostics, and weak enough not produce a radiation hazard or destruction of hardware even if the beam is mis-steered. For a pulsed machine like the SNS, the condition just described is achieved by reducing repetition rate to, say, 1 Hz or less and reducing the beam pulse length from 1 msec to, say, 10 msec while maintaining the pulse peak current. In this example the intensity reduction is 6 000 times less. In a CW machine, these features are not available, and one has to design the commissioning mode from the beginning by either providing a different set of diagnostics or providing pulsed or chopped beam operations.

Perhaps the most difficult extrapolation from the SNS to ADS is that of the beam loss prediction and control. Under the 1 W/m allowable loss criteria, the ADS beam loss has to be 15 times smaller than that of the SNS.

Interface between accelerator and reactor

The presently conceived interface between the ADS linac and the reactor is to insert the horizontal beam from the linac into the reactor vertically using a set of bending magnets situated above the reactor. This bend region would contain elaborate sets of charged beam and neutron diagnostics. The Nb surface of the linac accelerating structure is at a cryogenic temperature of 2 K, while the reactor is at a high temperature due to nuclear reactions and possibly emitting fission product gases. When the Nb surface is contaminated the performance of superconductivity could be degraded.

One of the challenges is to design and construct the bend region such that it can accommodate quick service to the beam transport and the reactor diagnostics. All existing spallation neutron sources except SINQ at PSI, Switzerland have horizontal beam delivery systems. Experience by SINQ on the vertical beam delivery system maintenance, inspection and other services could be helpful in designing future vertical delivery systems. The bending magnets in this area should be made of inorganic materials so that radiation damage to the magnets is minimal.

Another challenge is the windowless vacuum isolation between the accelerator and reactor. It is reasonable to assume that existing materials would not withstand this kind of radiation environment, and it is conjectured that either new technology or new materials are needed for the window and/or isolation. It is noted that there are a number of papers addressing “window” issues in this workshop.

R&D and trade-off

The ADS will advance accelerator and reactor technologies together, interfacing the two toward an uncharted regime. Therefore it can be expected that a number of difficulties will have to be faced. Some of the difficulties could be mitigated jointly by accelerator builders and reactor builders by trading difficulties and complementing each other. This is called “sharing difficulties” or “sharing pains” between subsystems.

Since no high-energy accelerator has been as reliable as a reactor, the question remains as to what kind of reliability the ADS reactor can tolerate. A HPPA can be made as reliable as a reactor with a large sum of additional costs. On the other hand, if a reactor can be designed to tolerate some amount of unreliability of an accelerator, there could be cost savings in accelerator construction. Such R&D efforts should be carried out in an iterative manner between accelerator builders and reactor builders in the “sharing pains” manner.

The diagnostics concerning the beam delivery system and reactor area would be in an uncharted domain. Developing equipment which does not intercept the beam, yet measures the beam profile and/or position, is essential. Furthermore, these instruments are likely to be situated in an area where back-streaming neutrons certainly cause radiation damage to the equipment. Additional requirements include a long MTBF and quick reparability. Redundancies and spares may or may not useful because of the extremely high level neutron radiation in the area. It is a challenge. As the expertise regarding radiation damage resides with reactor designers, this topic would also benefit from a joint effort between accelerator and reactor experts.

Other key R&D and trade-off studies include the isolation issue concerning the “beam window” to isolate the accelerator from the reactor, and vertical beam insertion to the reactor through a beam delivery system.

A road map for a high-power proton accelerator-driven nuclear system

The following is an opinion of the author regarding a possible road map leading to a high-power proton accelerator for an accelerator-driven nuclear system.

The Japan Proton Accelerator Research Complex (J-PARC) R&D plan on ADS work in Japan was presented at this workshop. The plan includes a "transmutation physics part" and a "transmutation engineering part." The facility to carry out the R&D is under construction, and will use a 200-kW beam (600 MeV, 1/3 mA) from J-PARC injector linac. A transmutation physics study planned requires only a 10-W beam.

My opinion is that the plan proposed by J-PARC is prudent, proper and a practical approach toward an ADS system. It is a wise plan to understand and attempt to solve ADS reactor physics and engineering issues with a modest beam power instead of starting with 10 s of MW beam. Since there may be number of unknown difficulties achieving 10 s of MW HPPA based ADS system, a graded approach may be a worthwhile option and should be considered. One natural graded approach is to start with 200 kW to 2 MW to 20 MW machines. In this chain of graded approach, the first two machines would exist within a few years at JAERI and ORNL, respectively.

Under the graded approach concept, every laboratory interested in an ADS system should join the J-PARC effort to learn and to solve reactor problems at 200 kW level internationally. In the same manner that EU-funded collaborative work exists in Europe, it seems natural for Asian countries to form a collaboration with JAERI. Putting resources together and eliminating duplications will expedite the programme with minimum expenditures for each collaborating laboratory. A model for such international collaboration is that of the TESLA Test Facility (TTF). Since 1992 the TESLA collaboration centred at DESY in Hamburg, Germany, consisting of some 50 institutions, has developed very high gradient (~40 MeV/m) superconducting cavities and built an initial linac of 300 MeV, and more recently of 1 000 MeV, using the cavities developed by the collaboration. The initial linac was to demonstrate a self-amplified spontaneous emission (SASE) free electron laser, and the latter linac is the driver for a VUV free electron laser user facility. As noted earlier, the SNS uses technology developed by TESLA.

The uniqueness of the TESLA collaboration is that each collaborator contributed their expertise and in-kind hardware. For example, cavity materials and construction from DESY, some RF power supplies and power couplers from FNAL, cryomodules from INFN, injector from CEA and Orsay, vacuum chambers for FEL from ANL, and so on. The results of these collaborative effort is an approved proposal to build an X-ray FEL at DESY as a European facility and a proposal to build a 500-GeV linear collider, which is under review by the International Committee on Future Accelerators. This model of international collaboration can be used to carry out developmental work for an HPPA-driven ADS. This proposal does not advocate discontinuing national institutional programmes in favour of the collaboration. However, national programmes can be tailored to complement the collaborative effort.

Summary

The technological aspects and challenges of employing a high-power proton accelerator to drive accelerator-driven nuclear system are discussed. There are a couple of requirements which where today's accelerators have not demonstrated. One is achieving a reactor-like reliability and the other is controlling beam losses to an unprecedented level. A trade-off between accelerator and reactor to mitigate these difficulties is proposed. A road map to achieve an ADS facility is also proposed.

If the SNS linac were to run in CW mode without changing the beam peak current as it was designed for the pulsed mode, the beam power would become 23 MW. This level of beam power is a desired level of the ADS system. The technology and performance of the SNS linac would guide the ADS linac design and performance. For example, if one finds the SNS beam loss is 10 times less than conjectured today, then the ADS linac should be able to facilitate hands-on maintenance.

The fault tolerant design implemented in the SNS linac should be tested to its full extent to determine whether such a system can be used to improve the reliability of an ADS linac in order to meet the requirement of only five trips per year.

REFERENCES

[1] Cho, Y., "Reliability and Availability of High Power Proton Accelerator", *Proceedings of the OECD NEA Workshop on Utilisation and Reliability of High Power Accelerators*, Mito, Japan (13-15 Oct. 1998).

[2] *Beam Halos and Scraping*, N. Mokhov and W. Chou, Eds., Fermi National Accelerator Laboratory (1999).

[3] Cho, Y., *et al*., *Preliminary Design Report – Superconducting Radio Frequency Linac for the Spallation Neutron Source*, SNS-SRF-99-101, Oak Ridge National Laboratory (20 Dec. 1999).

TECHNICAL SESSION I

Accelerator Reliability

Chairs: A. Mueller, P. Pierini

THE PDS-XADS REFERENCE ACCELERATOR

Dirk Vandeplassche and Yves Jongen for the PDS-XADS Working Package 3 Collaboration
Ion Beam Applications SA, Chemin du Cyclotron 3, B-1348 Louvain-la-Neuve, Belgium

Abstract

Accelerator-driven systems place very stringent availability requirements on the proton beam led into the subcritical reactor core. This paper describes the technical options chosen by a European collaboration supported by the European Commission in the framework of a Preliminary Design Study of an eXperimental ADS (PDS-XADS). These options are considered a sound basis for the development of an ADS-compatible accelerator. It mainly consists of a superconducting linac fed by an ECR ion source and a four-vane RFQ. The modularity of such an accelerator is a strong advantage, and high availability may be obtained by the proper combination of maximum reliability and of a powerful fault tolerance scheme. The methods to obtain fault tolerance are described, and the upcoming R&D programme is presented. The importance of an adapted construction methods is stressed.

Introduction

The Preliminary Design Study of an eXperimental Accelerator-Driven System (PDS-XADS) is a project is supported by the European Commission within its Fifth R&D Framework Programme under contract number FIKW CT-2001-00179. It has 26 participants, and is co-ordinated by FRAMATOME ANP SAS.

The project is subdivided into Work Packages, among which WP3 has the mission to work out the technical answers concerning accelerator requirements. WP3 is a collaboration among Belgium (IBA), France (CEA, CNRS, FRAMATOME ANP SAS), Germany (Universität Frankfurt, FZ Jülich, FRAMATOME ANP GmbH), Italy (INFN, ENEA, Ansaldo) and Portugal (ITN).

The requirements for the particle beam delivered by the accelerator are defined by WP1, which is responsible for the global coherence of the project. The most relevant ones are listed as follows:

Particle	Protons
Energy	350-600 MeV – 1%
Intensity	0-6 mA – 2% (but 10 mA capable)
RF duty cycle	CW
Beam time structure	200 ms holes at 1 Hz
Beam trips < 1 s	Not accounted for
Beam trips > 1 s	5 per year

Clearly, the last of these requirements is particularly challenging: an availability of this level has never been obtained or demanded of any particle accelerator. However, there is no *a priori* reason to believe that this level of availability is unattainable. It is WP3's task to identify the topics needing further R&D and which will allow us to reach the stated goal.

At the start of the project the design of the accelerator, and even its type, was entirely free. Very soon, however, the need for a reference design was obvious; reliability studies, in particular, cannot be conducted without a reasonably concrete representation of the machine. The reference design will be presented here.

Options and choices

When dealing with the reliability challenge, very early analyses have shown that a general principle must be adopted, underlying the set of fundamental choices to be made for the reference design. This principle is:

> The required level of reliability can only be achieved if a high degree of *fault tolerance* can be implemented.

Indeed, we consider that present-generation storage rings actually do obtain a remarkably high reliability (certainly the highest in the accelerator world), but that this level is definitely below our requirement. Of course, these machines are built with state-of-the-art components in terms of mean time between failure (MTBF), but this is not sufficient; hence the need for an "added principle". It is lucky that, in theory, our ADS application can well accept the fault tolerance principle because short beam interruptions may be tolerated.

Immediate corollaries of fault tolerance are redundancy and modularity. It is clear that our reference design has to be built along these lines of thought.

The type of accelerator

At the start of the project, cyclotron and linac accelerators were considered in parallel. It was soon concluded, though, that the cyclotron's potential for reliability increase is very limited, and that the possibilities of implementing fault tolerance are practically inexistent. Also, extrapolation towards higher performances is hardly conceivable. Hence, the cyclotron is ruled out, and the PDS-XADS reference accelerator will be of the linac type.

Global structure

The first point to be addressed: the design should be based on proven principles and on average performances. The second point: for a CW linear accelerator, it is very appealing to apply RF superconductivity wherever possible. At the same time, superconducting RF cavities naturally appear as the ideal candidates in a scheme where modularity is wanted. They are in agreement with the first point, but the low β application makes a rather new domain for them.

So, globally the linac will have a classical layout in which the main high-energy section is preceded by an intermediate-energy section, itself being fed by an RFQ and, of course, an ion source. The high-energy section will consist of *elliptical* superconducting cavities, the frequency being set to 704 MHz. Fault tolerance will obviously be translated into "missing cavity tolerance", and this property will have to be demonstrated. For the intermediate-energy section, a number of options are open, and they will have to be evaluated individually against our criteria. The low-energy section relies on existing designs, but their reliability will have to be established.

Figure 1. Schematical layout of the XADS linear accelerator

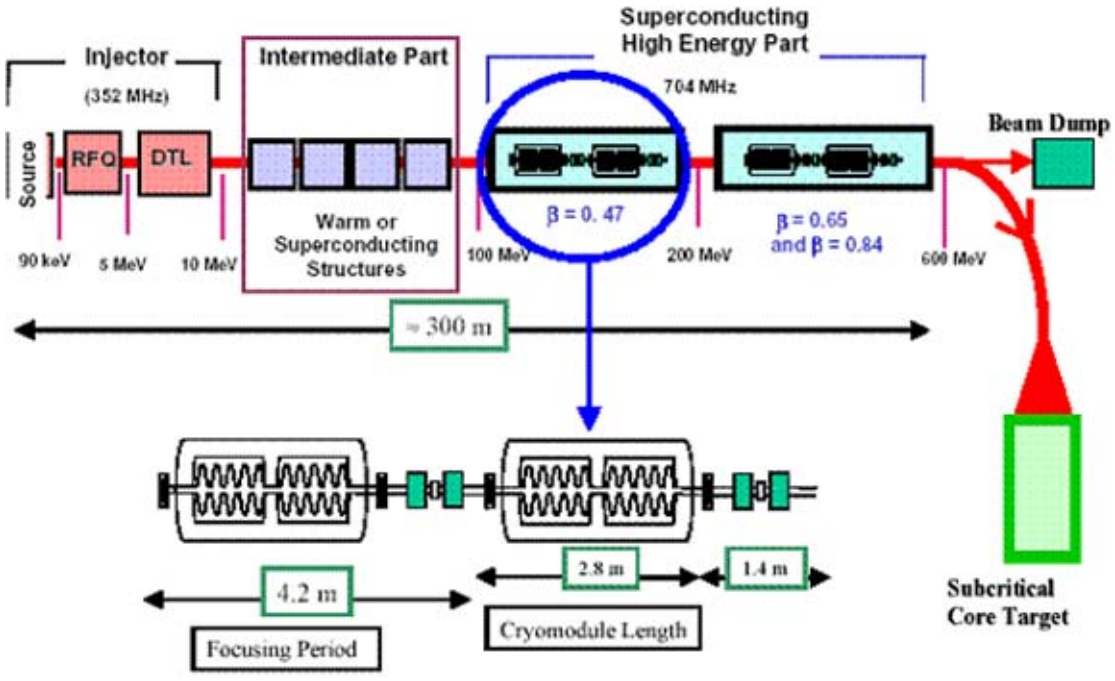

Low-energy section

The low-energy section or injector section consists of an ECR-type ion source feeding into a room temperature RFQ.

The French source SILHI [1] has been designed and built for a proton current of 100 mA in the framework of the IPHI project [2]. Its long-term availability has been shown and improved in several test runs. Its performance in terms of reliability will have to be established in the down-rated situation of XADS during a dedicated test run.

The RFQ is of the four-vane-type at a frequency of 352 MHz. Fully relevant designs, compatible with CW operation, have been made at several laboratories [3-5]. They are typically capable of beam currents around 100 mA and output energies of ‡ 5 MeV. For our XADS application, some design parameters are optimised for reliability and availability, possibly at the cost of an increase in length. On the other hand, it is definitely our goal to limit the output energy of the RFQ as much as possible by an adequate choice of the subsequent accelerating structure.

It should be mentioned that these designs will be optimised to achieve the highest reliability, but that the fault tolerance principle cannot be realised at the level of the beam by a single one of these sections: the failure of any element will cause the beam to disappear. Hence, it appears that explicit redundancy by doubling the low-energy section will be required.

High-energy section

From around 100 MeV onwards the superconducting elliptical cavities at 704 MHz become the most efficient and the most cost-effective choice [6]. In order to span the full range of beam velocities, the high-energy linac is divided into three zones, corresponding to geometrical b values of 0.47, 0.65 and 0.85. Transitions occur around 200 and 490 MeV, and the 0.85 zone could operate up to 2 GeV. A b = 0.47 realisation is shown in Figure 2. For XADS, multi-cell cavities are foreseen, assembling five or six cells per cavity.

Figure 2. Two of the b = 0.47 single-cell cavities built for the Italian TRASCO programme, after fabrication (left) and on the test stand before cryogenic measurements (right)



Transverse focusing is obtained by periodic normal-conducting quadrupole doublets with long drift lengths. These drift lengths are filled with cryomodules; a cryomodule typically houses three cavities.

In this section, modularity is strong, both in cavities and in transverse focusing elements. This will allow the implementation of an adequate fault tolerance scheme, which will cope with the loss of a cavity as well as with the loss of a quadrupole.

Intermediate-energy section

In this section, going from the exit of the RFQ to around 100 MeV, the optimal choices of the accelerating structures are far less clear, and a number of options remain open. It is most probable that our existing design rules, along with the shortest possible RFQ, will impose the use of at least two different structures to span this energy region.

Coming down from 100 MeV, the superconducting two gap *spoke* cavities at 352 MHz are considered very promising candidates [7]. A "β = 0.35" section would allow to accelerate from ~20 MeV to 100 MeV. As with the high-energy superconducting sections, modularity is high, and it can be made fault tolerant against a cavity loss and against a quadrupole loss. A cross-section and a prototype of a "β = 0.35" spoke cavity are shown in Figure 3.

Figure 3. "β = 0.35"spoke cavity

Left – cross-section, right – prototype (IPN Orsay – CERCA)

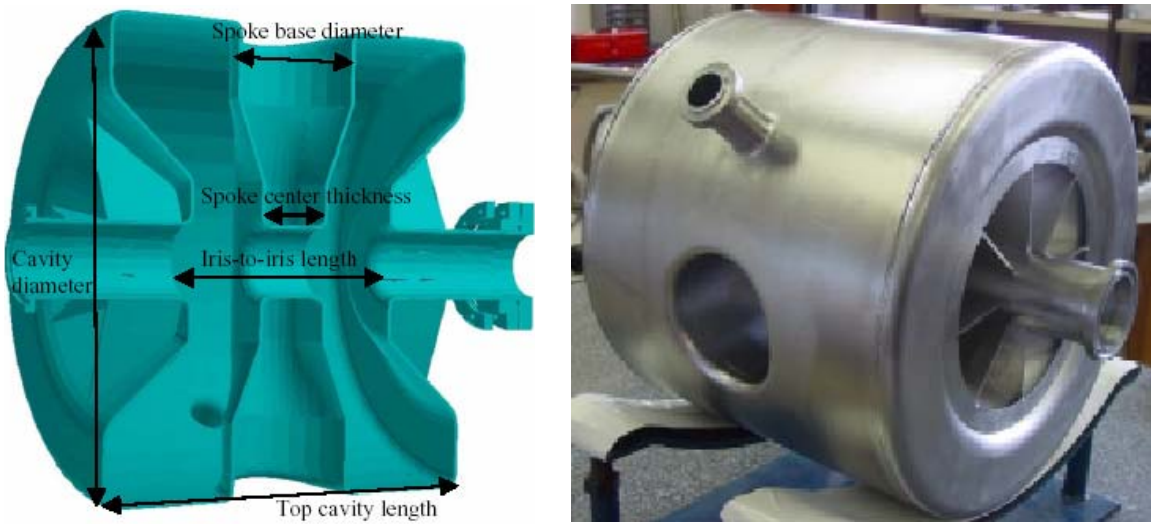

At the low-energy side, exit of the RFQ, the lowest possible injection energy is looked for. Here, the H-type drift tube structures are considered as the most effective. They are combined in multi-cell cavities, and taking advantage of the KONUS focusing scheme [8], which allows for long drift spaces between the quadrupole triplets, the drift tubes can be free of focusing elements.

For room temperature structures, either the IH or the CH configuration may be used, depending on frequency and on beam velocity. They have appealing properties concerning their radial size and their shunt impedance, and their CW capabilities are significantly superior to those of the classical DTL. Nevertheless, they will have to be studied and proven. A promising candidate would be a RT IH structure with a very low β capability (e.g. β = 0.065, 2 MeV injection energy) accelerating up to, say, 20 MeV. Such a structure would very effectively limit the RFQ requirements.

Figure 4. Sectional view of a 350-MHz CH-type DTL cavity

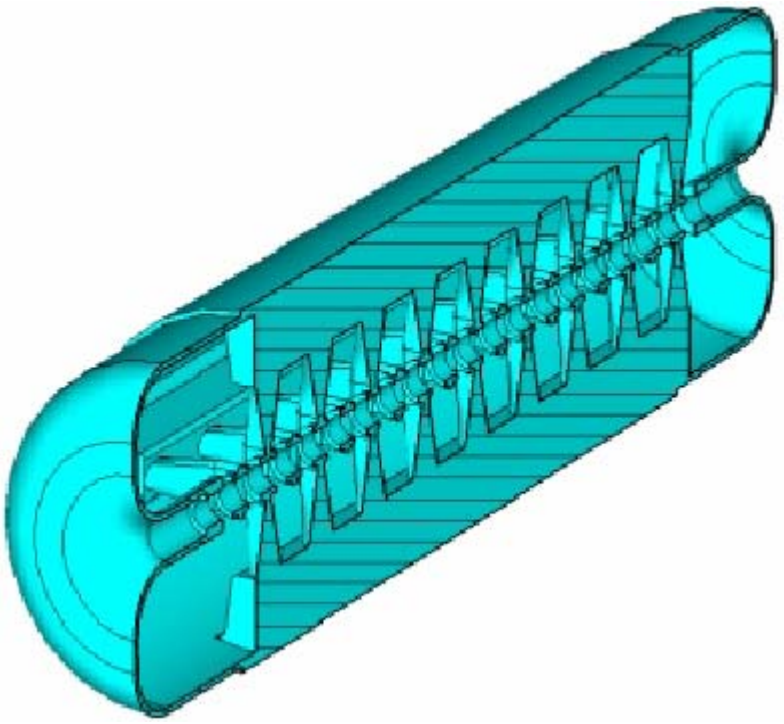

The CH structure may also be considered in a superconducting version [9]. Its mechanical robustness and its very good voltage breakdown properties allow for this. This option is really attractive for XADS, but its very low β capabilities may be limited. A 350-MHz 19-cell prototype for $\beta = 0.1$ is being designed (University of Frankfurt) and will be constructed.

The situation of these multi-cell cavities with respect to our fault tolerance philosophy is equal to that of the low-energy section. Therefore, here again, explicit redundancy by doubling the structures will be required.

Fault tolerant schemes

The capacity of recovering a good quality beam with a failing cavity or with a failing quadrupole is fundamental for the fault tolerance principle to be valid. This capacity has been studied in a spoke cavity section. At present this study is limited to a "before – after" situation, and the actual possibilities of a smooth transition are still unknown. However, certain rules may already be established:

- If a cavity fails and nothing is done, the beam is always completely lost.
- If a cavity fails and an appropriate local compensation is applied, the nominal beam parameters at the target may be restored.
- If a quadrupole fails, the whole doublet is to be switched off. Nominal beam parameters at the target can be restored by readjusting a few surrounding quadrupoles.

The local compensation for a failing cavity typically concerns the four surrounding cavities, which are retuned in amplitude and in phase. When also retuning the quadrupole gradients, an almost perfect re-matching of the beam may be obtained (see Figure 5).

Figure 5. Beam envelopes in the 5-600 MeV XADS reference linac

Left – Nominal case. right – case with failure of spoke cavity #4, after retuning of the field amplitudes and phases of spoke cavities #2, #3, #5 and #6, and adjusting the four nearest quadrupoles. Note the different scales on the phase (bottom) plots.

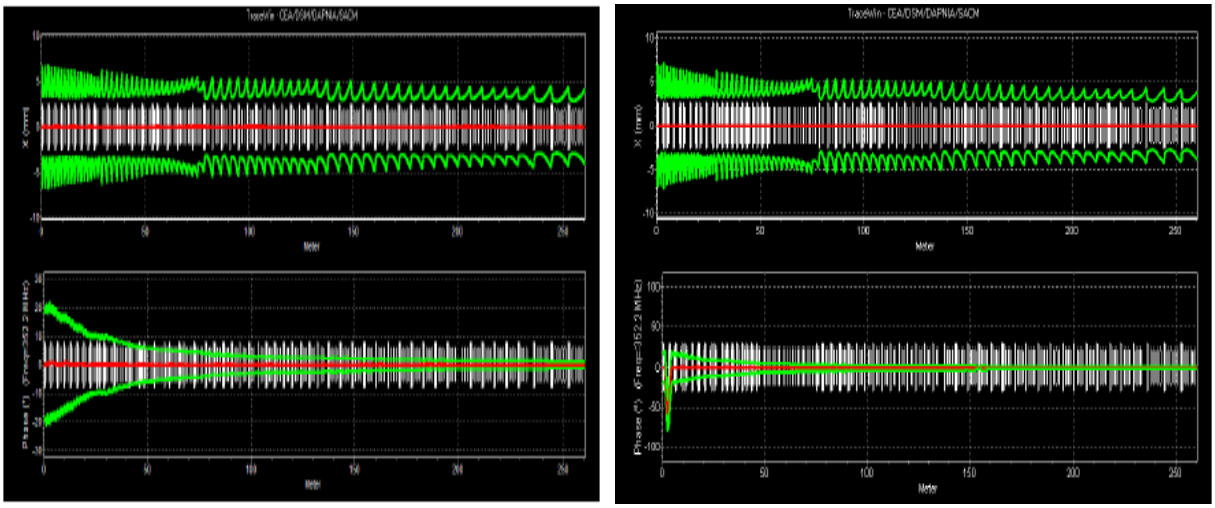

In order to implement such a correction scheme, it is of course required to have adequate margins on the accelerating fields and on the available RF power. Moreover, the low-level RF control system has to cope with these correction schemes, and it will require the development of novel fast digital feedback circuits.

Global overview

In view of the above discussion on reliability and fault tolerance, the XADS reference linac becomes different from the schematic in Figure 1. Let us assume that the spoke cavity section starts at energy X (X will most probably lie in the range 20-40 MeV). The part of the linac below X will not benefit from the "missing cavity correction scheme". Therefore, it is now foreseen to double this part entirely, thereby introducing a permanent hot spare. For recall, it will consist of an ECR ion source, an RFQ and some kind of H-type structure. Figure 6 shows the corresponding schematic.

The layout of the beam line will depend on the relative positioning of the accelerator and the subcritical reactor. In any layout, however, a few properties are recurring:

- The beam line, and especially the 90 vertical bend on top of the reactor, will be achromatic. Transverse beam emittances are small, and therefore it will be possible to use light magnets.

- The small transverse beam emittances allow the distance between the last magnet and the target to be ~16 m.

- A raster scanning system will allow determining the beam footprint on the target according to the needs.

Figure 6. Schematic view of the redundant and fault tolerant XADS linac

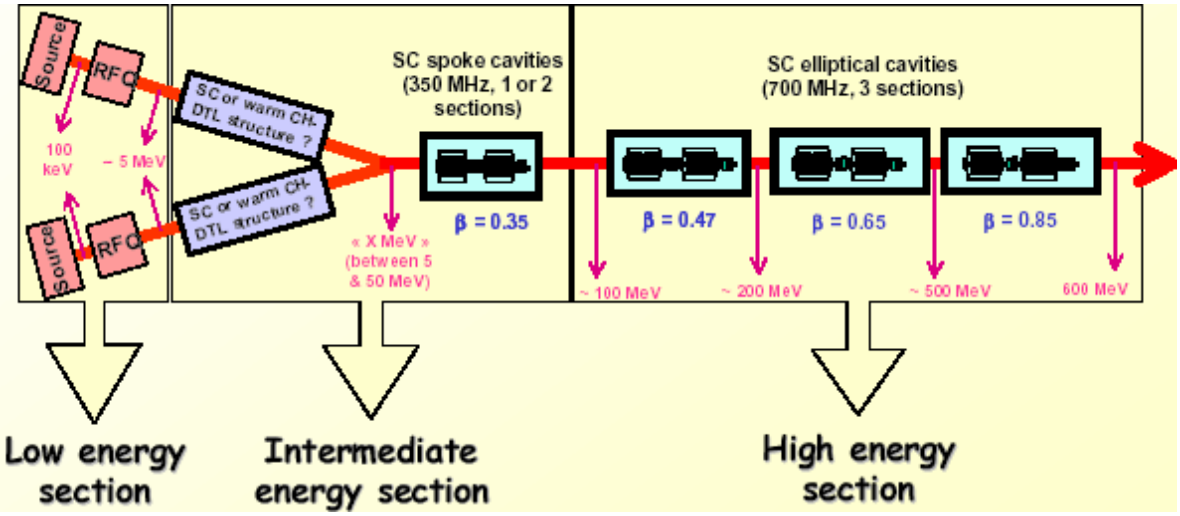

R&D

The upcoming R&D programme has three major goals, and all of them are in view of obtaining the requested overall availability. The R&D items have been distributed among the WP3 partners, and they have been introduced into the European Commission's 6th R&D Framework Programme proposal called EUROTRANS.

1) It must be proven that the required level of reliability of the individual components can be achieved. This needs prototypical elements to be built and tested. In the low-energy section, a long test run is planned with the existing IPHI injector, i.e. the source and the RFQ (3 MeV) (CEA). In the intermediate-energy section, it is foreseen to build a complete spoke resonator, possibly embedded in its cryomodule (CNRS). Finally, in the high-energy section, a complete $\beta = 0.5$ cryomodule with N cavities and their RF-couplers will be built and tested (INFN).

2) The open questions regarding the bridge between the RFQ and the spoke section must be resolved. To that end, it is planned to build a complete superconducting CH accelerating structure on one hand (U. Frankfurt), and a room temperature IH accelerating structure on the other hand (IBA).

3) As the RF low-level control is so vital for the reliability scheme, its development (and mainly of the new fast digital circuits) must be considered as a separate R&D item (CEA). Some remaining questions on the RF power amplifiers have to be resolved (e.g. klystrons vs. IOTs). Finally, a full beam dynamics analysis including transients and fault recovery will be performed.

Design choices and construction methods

The availability of the XADS proton beam can only be brought to a very high level if the fault tolerance scheme, which has been discussed so far only at the level of the global object "accelerator", is generalised to all the lower-lying implementation levels. Therefore, the principles of modularity and/or of redundancy have to be applied as much as possible at all stages of design and development.

This should be considered as a general design guideline that will efficiently lead to the highest main time between failures (MTBF) values. Another guideline for maximising MTBF is the use of down-rated components – note, however, that fault tolerant modularity will usually impose this anyway.

Along with increasing the MTBF, it is equally important to minimise the main time to repair (MTTR), because this is essential for the fault tolerance to express itself in the long run. The lowest MTTR means a very high level of maintainability, which is largely obtained by adequate construction methods. From the largest items (in our case full cryomodules or complete power RF amplifiers) to the smallest power converters, things have to be built for optimal accessibility and easy (= quick) exchange. In the context of an accelerator facility, radioprotection is an important issue, and a two-parallel tunnel building layout seems inevitable. Finally, a maximally pushed application of modularity and of uniformity and standardisation is a good guarantee for fast interventions, but on the strict condition that it is supported by both a performing alarm system and a ditto documentation.

As a final remark, it is of course necessary to safeguard the facility over time through an adequate maintenance plan. The XADS cycle is presently foreseen as a one-month shutdown period after a three-months run. From the accelerator point of view, it is felt that this cycle leaves ample time for a normal four-month maintenance, but that a longer period should be available at a yearly basis.

Extrapolations

The question about the possibilities to extrapolate the given XADS design towards an industrial transmutation application was raised at the outset of the PDS-XADS project, and it is the object of a future deliverable. The feeling with respect to the present linac layout is the following:

- The extension of the energy range is straightforward. The $\beta = 0.85$ section will accelerate up to 2 GeV, whereas transmuter systems would typically only require 1 GeV.

- A significant increase in the beam current is well within the possibilities of the present linac design. We are not touching any fundamental space charge limitation: the ion source is designed to inject 100 mA into the RFQ. After some preliminary discussions, the general feeling is that a 1-GeV, 20-mA beam is within the possibilities of our existing design philosophy. Such a beam would be sufficient to drive a 1-GW thermal power subcritical reactor.

Note that, for safety reasons, it is intended to strictly limit the electrical grid power available to the XADS accelerator, so as to create a physical impossibility to exceed a given beam power.

Conclusion

Accelerator reliability levels that are well beyond the present standards are of vital importance for any ADS project. It is clear, however, that this high reliability will not be achieved at the first go. This is why experimental systems (XADS), i.e. relatively small-scale systems but with all the features of a full-size system, are so important: they allow for the mandatory learning process to take place.

We believe that the reliability goal is achievable if, in the first place, the correct rules and principles are applied at all stages of development. At the design stage, these principles aim at reaching optimal modularity and fault tolerance, and at defining correct specifications. At the manufacturing stage, these principles aim at realising the specifications by a strict quality control, thus assuring the highest MTBF figures. At the commissioning stage, the rules must guarantee that the operational parameters are brought in agreement with the design values, possibly by adjusting the design models.

At this point operation starts, and this is where reliability can gradually be set up, by building on the preceding achievements. Reliability can only be "grown" from high-quality technical building blocks by adding the correct mental attitude. Operation needs a "reliability-minded" crew, who will be able to continuously improve the system and bring it ever closer to the reliability goal. The development of an ADS-compatible accelerator will need to go through this learning process. Placing it in the framework of an XADS project is the most efficient way to go.

REFERENCES

[1] Gobin, R., *et al*., *Proc. EPAC2002*, Paris, France, 1712 (2002).

[2] Beauvais, P-Y., *et al*., *Proc. EPAC2002*, Paris, France, 539 (2002).

[3] Schrage, D., *et al*., *Proc. Linac'98*, Chicago, USA, 679 (1998).

[4] Pisent, A., *et al*., *Proc. Linac2000*, Monterey, USA, 902 (2000).

[5] Ferdinand, R., *et al*., *Proc. Linac2000*, Monterey, USA, 551 (2000).

[6] Biarrotte, J-L., *et al*., *Proc. 9th Workshop on RF Superconductivity*, Santa Fe, USA (1999).

[7] Olry, G., *et al*., *Proc. EPAC2002*, Paris, France, 2271 (2002).

[8] Ratzinger, U., *Habilitationsschrift*, Johann Wolfgang Goethe Univ., Frankfurt, Germany (1998).

[9] Eichhorn, R., U. Ratzinger, *Proc. Linac2000*, Monterey, USA, 926 (2000).

DEVELOPMENT OF A SUPERCONDUCTING PROTON LINAC FOR ADS

Nobuo Ouchi, Nobuo Akaoka, Hiroyuki Asano, Etsuji Chishiro,
Yuya Namekawa, Hiroyuki Suzuki, Tomoaki Ueno
JAERI, Japan

Shuichi Noguchi, Eiji Kako, Norihito Ohuchi, Kenji Saito, Toshio Shishido, Kiyosumi Tsuchiya
KEK, Japan

Kouichi Ohkubo, Masanori Matsuoka, Katsuya Sennyu
MHI, Japan

Takashi Murai, Toshihiro Ohtani, Chihiro Tsukishima
MELCO, Japan

Abstract

ADS require a high-intensity proton accelerator of which energy and beam power are about 1 GeV and 20-30 MW, respectively. JAERI, KEK, MHI and MELCO have conducted a programme for the development of a superconducting proton linac for the ADS since 2002. This programme, which is based on the achievement of the J-PARC design work, consists of two parts, development of a 972-MHz cryomodule and system design of a superconducting proton linac in the energy range between 0.1 and 1.5 GeV. In the development work of the 972-MHz cryomodule, a prototype cryomodule which includes two nine-cell cavities of $\beta = 0.725$, will be developed and the goal is stable operation in the horizontal tests at the surface peak field at 30 MV/m. In the system design work, a preliminary beam dynamics design has been determined with the configuration of a cryomodule with two 972-MHz, nine-cell elliptical cavities, and a room-temperature focusing magnet. This paper provides the present status of the cryomodule development and the system design.

Introduction

JAERI proposes an ADS which consists of superconducting proton linac, spallation target of lead-bismuth eutectic and a subcritical core. In this proposal, the energy and beam power of the superconducting proton linac are 1.5 GeV and 20-30 MW, respectively. JAERI has conducted an R&D programme for the ADS since 2002 in collaboration with national laboratories, universities and companies. This programme includes R&D on a superconducting proton linac, lead-bismuth technology and subcritical core design and technology.

The R&D on the superconducting proton linac, which is based on the achievement of the J-PARC design work, consists of two parts, development of a 972-MHz cryomodule [1] and the system design of a superconducting proton linac in the energy range between 0.1 and 1.5 GeV.

In the development work for the 972-MHz cryomodule, which is conducted by JAERI, KEK and MHI, a prototype cryomodule is currently being assembled. The cryomodule includes two 972-MHz nine-cell cavities of $\beta = 0.725$. The goal of this work is stable operation in the horizontal tests at the surface peak field at 30 MV/m, which corresponds to an accelerating gradient of about 10 MV/m. The cavity development, which includes the vertical tests, is mainly being performed at KEK. The horizontal tests will be performed at JAERI, where a 972-MHz klystron, also utilised for the high-power tests of the power couplers, is in operation.

In the system design work, which is conducted by JAERI, KEK and MELCO, a preliminary beam dynamics design has been established with a configuration of a cryomodule with two 972-MHz, nine-cell elliptical cavities, and a room-temperature focusing magnet. The total number of cryomodules and their length are outlined in this work.

Cryomodule development

Cryomodule design

Figure 1 shows an overview of the cryomodule. Two 972-MHz nine-cell elliptical cavities are installed in the cryomodule, for which the operating temperature is designed to be 2 K. Each cavity is surrounded by a jacket-type liquid helium (LHe) vessel made of titanium. A box-shaped LHe reservoir tank, which is located above the cavities, connects both LHe jackets.

Figure 1. Overview of the prototype cryomodule

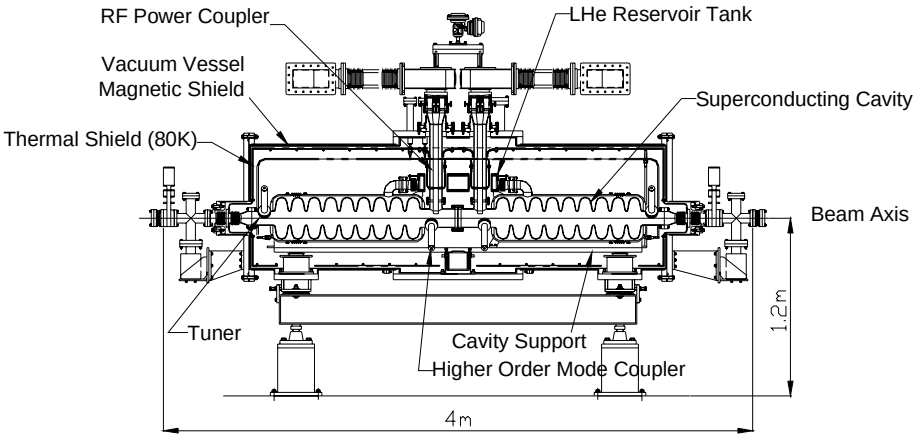

Coaxial-type power couplers, of which the inner and outer diameters are 34.7 mm and 80 mm, respectively, are located at the centre of the cryomodule. KEK-TRISTAN-type disk windows are placed at the room temperature region. Inner conductors of the power couplers and the windows are cooled by water. Cooling of the outer conductors is achieved by thermal intercepts at 5 K and 80 K. A high-power test of the power couplers was carried out successfully with a maximum RF power of 1 MW in pulsed mode operation; the pulse width and repetition rate are 0.6 ms and 25 Hz, respectively. Details of the power coupler design and the test results are presented in Ref. [2]. A higher-order mode (HOM) coupler is attached at both ends of each cavity. The HOM couplers located at the power coupler side are made of niobium and are designed to be cooled by LHe. The HOM couplers located at the outer side are made of copper without any cooling because of the reduced heating. Details of the design for the HOM coupler are presented in Ref. [1].

The tuning system consists of pulse motors and a piezo actuator is located outside the cryomodule. Each LHe jacket includes bellows and tuning force is applied from the tuning system with coaxial rods.

The heat shield at 80 K is installed in the cryomodule and is cooled by liquid nitrogen (LN_2). Thermal intercepts at both 80 K and 5 K, which are cooled by LN_2 and LHe, respectively, are also installed at power couplers, beam pipes and tuning rods. The cavity support is cooled by LN_2 at 80 K and the thermal insulation between the support and the cavity is achieved by GFRP. In order to achieve operation of the cavity at 2 K, a JT valve is installed in the cryomodule. Therefore, the cryomodule has three independent cryogenic flows, LN_2 at 80 K, LHe at 5 K and 2 K. The static heat load for each flow is estimated: 64 W, 16 W and 5 W for 80 K, 5 K and 2 K, respectively. A magnetic shield made of permalloy is installed just on the inner side of the vacuum vessel of the cryomodule.

Superconducting cavity

Figure 2 shows the shape of the 972-MHz, nine-cell cavity of $\beta = 0.725$, which includes the surrounding LHe jacket. The cell length and the total length including beam pipes are 112 mm and 1 397 mm, respectively. The equator and iris diameters are 277 mm and 90 mm, respectively, while the beam pipe diameter at the power coupler side is expanded to 126 mm in order to obtain sufficient external Q of the power coupler of $5 \cdot 10^5$. The RF parameters of this nine-cell cavity are summarised in Table 1 [3]. The wall thickness of this cavity is 3.8 mm, which is thicker than other superconducting elliptical cavities in order to provide the stiffness and to reduce the Lorentz force detuning. As the stiffness of the LHe jacket is also important to reduce the Lorentz force detuning, the shape of the end plates of the jacket was optimised so as to obtain sufficient stiffness. The stationary Lorentz force detuning was calculated to be 130 Hz at the surface peak field of 30 MV/m (i.e. accelerating field of about 10 MV/m).

Figure 2. 972-MHz, nine-cell elliptical cavity of $\beta = 0.725$

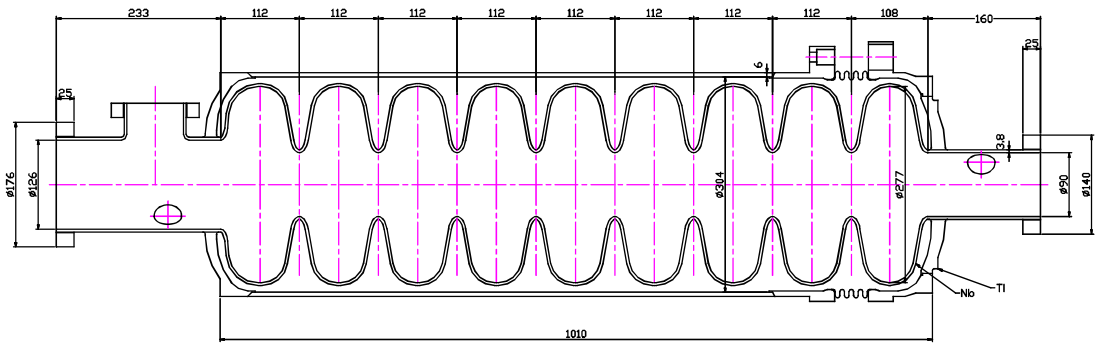

Table 1. RF parameters of the cavity

Esp/Eacc	3.07
Hsp/Eacc	55.4 Oe/(MV/m)
R/Q	478 Ω
Geometrical factor	208 Ω
Cell-to-cell coupling	2.80%

For the fabrication of the cavity, a new approach was applied in deep drawing; the shape of the die was optimised so as to minimise the forming error using a structural analysis and an error of less than 0.3 mm was obtained [4]. Pre-tuning was performed after fabrication of the cavity and field flatness above 98% was obtained for both cavities [5].Vertical tests of the cavities at 2 K were carried out after the surface treatments of barrel polishing and electropolishing. Figure 3 shows the final results of the vertical tests. Surface peak fields of 32 MV/m and 34 MV/m were obtained for two cavities (type-R and type-L cavities), which satisfied our target value of 30 MV/m.

Figure 3. Final results of the vertical tests of the cavities

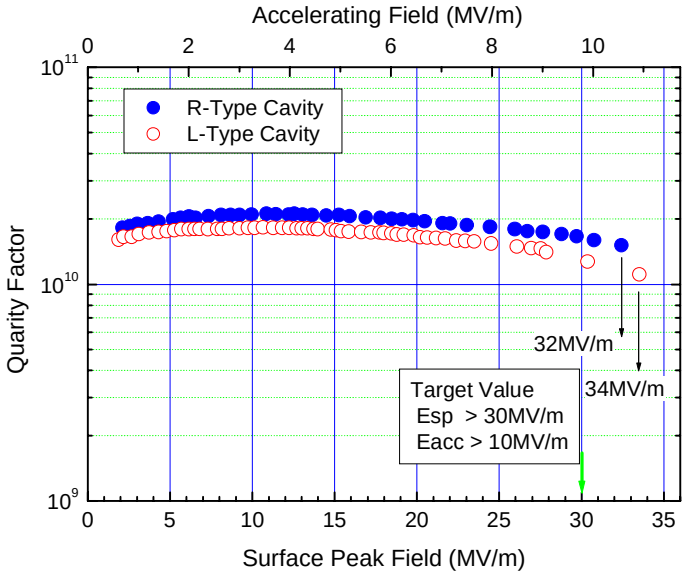

Cryogenic system for horizontal test

As described in the previous section, the cryomodule has three independent cooling lines of LN_2 at 80 K, LHe at 5 K and 2 K. Figure 4 shows a flow diagram of the cryogenic system for the horizontal test. The cryogenic system consists of the cryomodule, the valve box, the joint box, Dewars and other auxiliary components. Refrigerant for each line is fed from portable Dewar individually. The valve box is installed for connection and feed control of the refrigerants to the cryomodule. In the superconducting linac of the ADS plant, a similar valve box will be installed while the refrigerant will be fed directly from a refrigerator. The joint box is installed for the connection between the valve box and the Dewars, which is designed so as to exchange the Dewar during the experiment.

As for the line of LHe at 2 K, the LHe vessel is evacuated to about 4 kPa by a vacuum pump at the room temperature region. A vapour separator and a heat exchanger are equipped in the valve box in order to increase the production efficiency of LHe at 2 K in the cryomodule. The JT valve in the

Figure 4. Flow diagram of the cryogenic system for the horizontal test

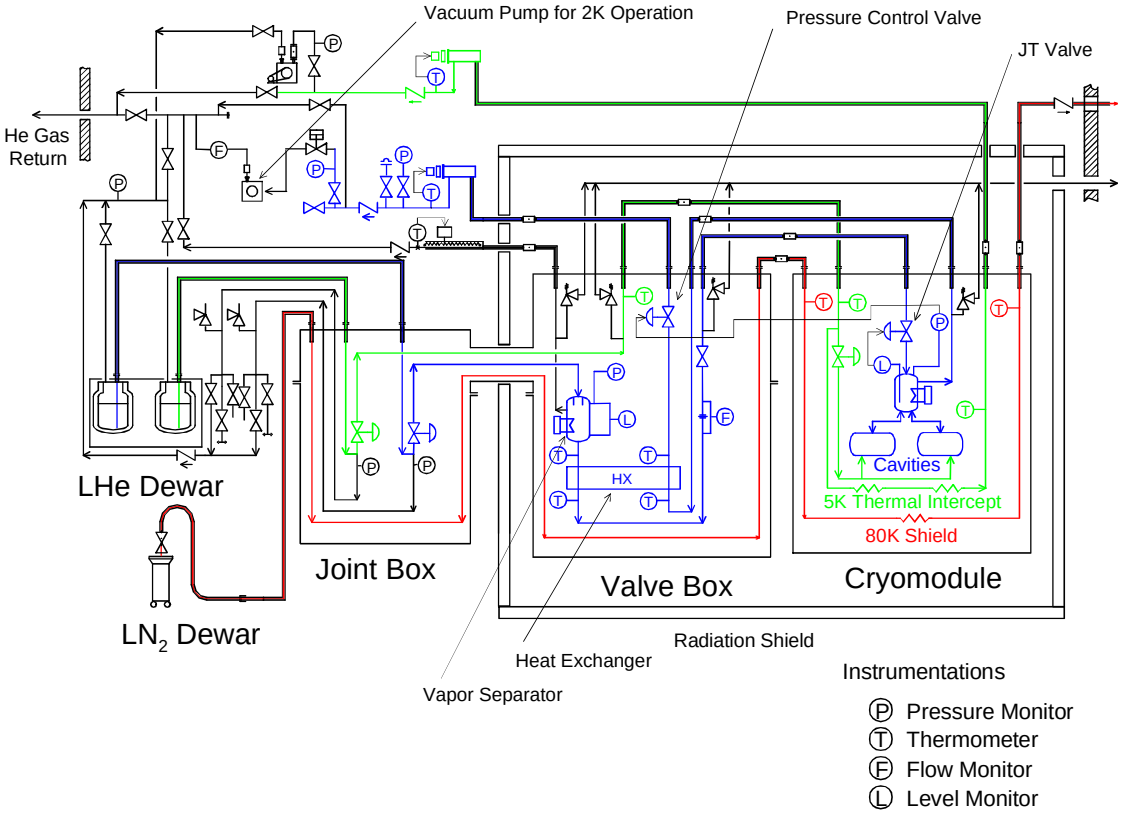

cryomodule produces the superfluid LHe and controls the LHe level in the LHe vessel. A valve placed on the He gas return line in the valve box performs pressure control of the LHe vessel, thus also temperature control of the LHe.

As for the line of LHe at 5 K, a valve in the joint box performs the flow control. In the cryomodule, this line is connected to the LHe vessel, which is used for the cooling down from room temperature to 5 K.

As for the line of LN_2, no control valve is placed in the cryomodule, the valve box and the joint box. The valve at the LN_2 Dewar performs the flow control manually.

Experimental arrangement and schedule of the horizontal test

The experimental arrangement of the horizontal test of the cryomodule is displayed in Figure 5. The cryomodule and the valve box are located in a radiation shield. The joint box, Dewars and the vacuum pump are located outside of the shield. An RF power source, klystron, is located at a lower level. A waveguide system is connected from the klystron and the RF power is divided for two cavities.

Final assemblage will be soon be complete at the JAERI Tokai site. The horizontal test is planned for 2004. In the test, the RF high power test will be performed for the final goal of the surface peak field of 30 MV/m. Additional testing planned includes cryogenic tests and low-level RF tests, including heat leak and temperature distribution measurement, a control test at 2 K operation, measurements of quality factors for the accelerating mode as well as HOMs, tuning tests and so on.

Figure 5. Experimental arrangement of the horizontal test

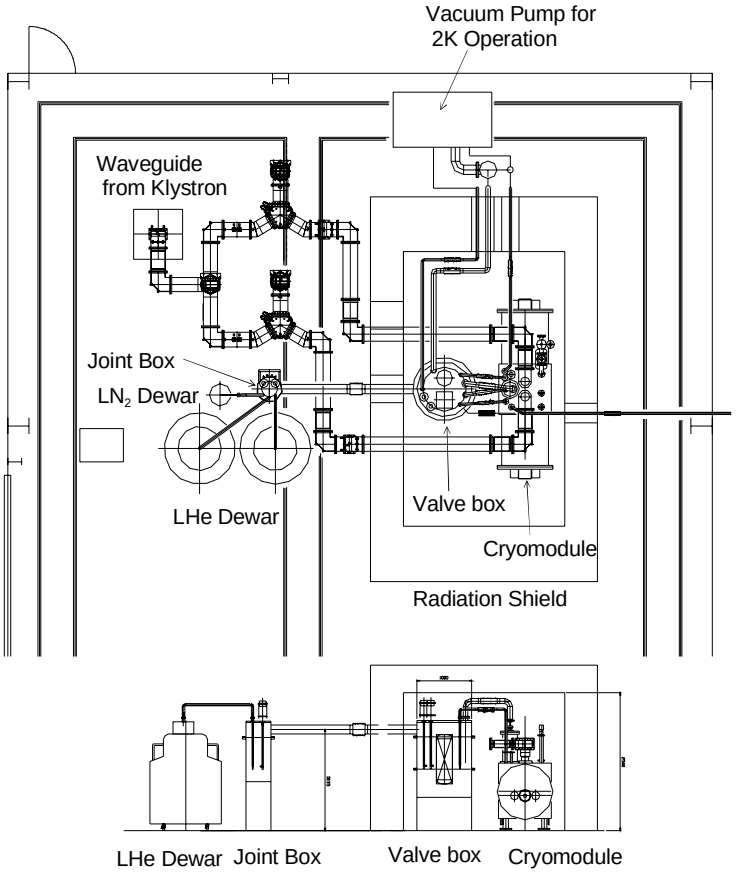

System design of superconducting linac for ADS

In the system design work, a preliminary beam dynamics design of the superconducting proton linac has been established in the energy range between 1 00 MeV to 1.5 GeV.

Basic design parameters

Table 2 shows the basic parameters for the beam dynamics design. In this energy range, the b value changes from 0.428 to 0.923. Parameters of accelerating frequency, number of cells in a cavity, number of cavities in a cryomodule and maximum surface peak field are set to be the same as the parameters of the prototype cryomodule. Phase slip in a cavity, which comes from a mismatch between beam b and cavity cell length, is set to be within −30 in order to obtain smooth bunching, as the synchronous phase angle is set to be -30 . According to this condition, the number of cavity groups is deduced to be 10 in the energy range 100 MeV to 1.5 GeV, which is larger than other superconducting linac designs because of the larger number of cells in a cavity of nine. The focusing magnet is considered to be a quadrupole doublet in a room temperature region between the adjacent cryomodules. The schematic view of the lattice structure is shown in Figure 6. The zero current transverse phase advance is set to be 70 , which is constant in a superconducting linac region. The longitudinal phase advance is obtained from the accelerating field of the cavity, while the maximum longitudinal phase advance is limited to 65 to avoid structural resonance in the beam dynamics.

Table 2. Basic parameters for the beam dynamics design

Energy range	100~1 500 MeV	Beam current	20~30 mA
b range	0.428~0.923	Synchronous phase	-30
Accelerating frequency	972 MHz	Phase slip in a cavity	Within −30
No. of cells in a cavity	9	No. of cavity groups	10
No. of cavities in a cryomodule	2	Focusing magnet	Room temperature
Max. surface peak field	<30 MV/m	Transverse phase advance	70 (I = 0A)

Figure 6. Schematic view of the lattice structure

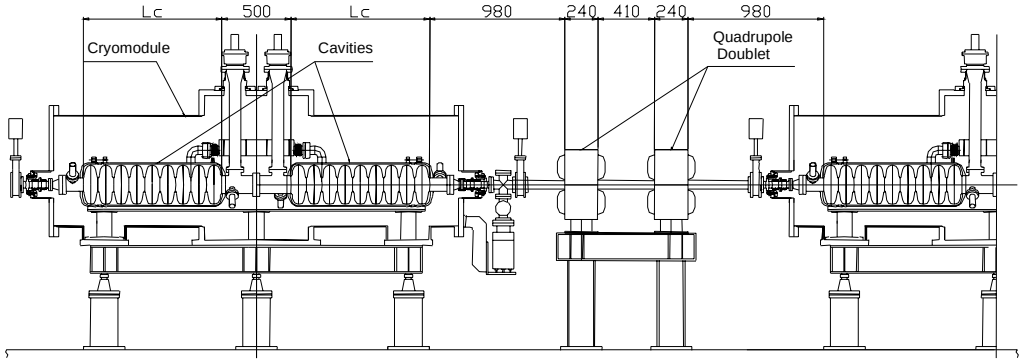

Preliminary superconducting cavity design

Preliminary designs of 10 kinds of superconducting cavities have been established in order to obtain the ratios of the surface peak field to the accelerating field and the transit time factors. Table 3 summarises the RF parameters of the cavities.

Table 3. RF parameters of the cavities

b	Esp/Eacc	Transit time factor	R/Q (W)
0.444	7.40	0.634	87.38
0.480	6.27	0.648	121.23
0.518	5.34	0.662	162.67
0.560	4.70	0.673	215.48
0.604	4.07	0.685	278.75
0.653	3.60	0.695	356.10
0.705	3.16	0.702	443.28
0.761	2.84	0.708	543.37
0.822	2.56	0.715	661.44
0.888	2.30	0.721	749.59

Lattice design

As shown in Figure 6, drift spaces between two cavities in the cryomodule, and between the cavity end and qadrupole magnet are set to be 500 mm and 980 mm, respectively. The effective length of the quadrupole magnet and drift space between the doublet are set to be 240 mm and 410 mm, respectively. These parameters are the same as for the superconducting linac design of the J-PARC project.

Table 4 summarises the structure of the superconducting linac. In this design, 106 cryomodules, i.e. 212 cavities, are necessary in the energy range from 100 to 1 500 MeV and total length is 560 m. As shown in Table 4, the lower-energy part, especially the 100-180 MeV region, is quite inefficient; 21 cryomodules and 100 m are necessary. The main reason for this inefficiency is a higher Esp/Eacc ratio. Optimisation of the lattice design as well as the cavity design is necessary for the final design of the superconducting linac.

Table 4. Basic structure of the superconducting linac

	Cavity b	Beam b	Beam energy (MeV)	No. of cryomodules	Length (m)
1	0.444	0.428~0.462	103.1~122.7	7	32.1
2	0.480	0.462~0.499	122.7~147.3	7	32.8
3	0.518	0.499~0.539	147.3~179.2	7	33.5
4	0.560	0.539~0.582	179.2~220.1	7	34.3
5	0.604	0.582~0.629	220.1~272.6	7	35.2
6	0.653	0.629~0.679	272.6~348.5	8	41.3
7	0.705	0.679~0.733	348.5~443.1	8	42.5
8	0.761	0.733~0.791	443.1~605.2	11	60.1
9	0.822	0.791~0.855	605.2~876.5	15	84.5
10	0.888	0.855~0.923	876.5~1 510	29	168.6
Total				**106**	**564.8**

Beam simulation

Beam simulation of the superconducting linac was performed using the TRACE-3D and modified PARMILA codes. In the simulation, the initial beam emittances are referred from the J-PARC beam design data. As an example of the results, Figure 7 shows the 90% emmittance in both transverse and longitudinal directions. As shown in the figure, emittance growth is not observed in the beam simulation results.

Figure 7. 90% emittance obtained in the beam simulation

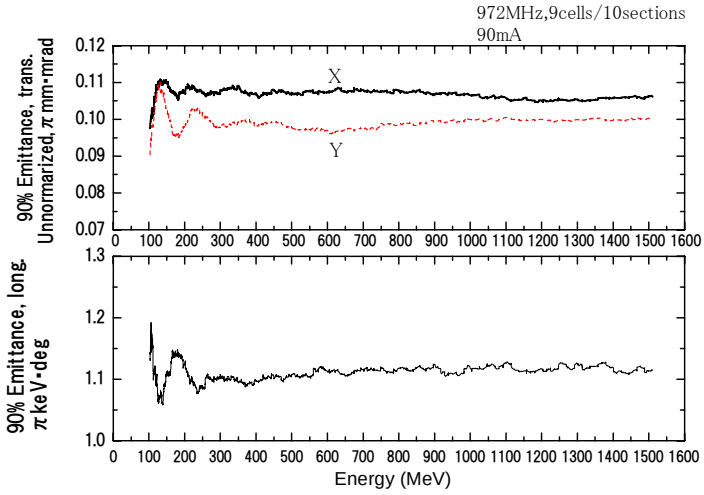

Conclusion

The development of a superconducting proton linac, cryomodule the system design are ongoing. As concerns the cryomodule, fabrication has been completed and final assemblage will soon be finished as well. The horizontal test will be performed in 2004 toward the goal of a maximum surface peak field above 30 MV/m. Regarding the system design, a preliminary beam dynamics design has been determined. The present result, however, provides more cryomodules and a longer total length than expected. Additional optimisation is thus necessary.

REFERENCES

[1] Noguchi, S., *et. al*., "Prototype Cryomodule for the ADS LINAC", *Proc. of the 11th Workshop on RF Superconductivity*, Luebeck/Travemuende, Germany (2003) MoP32, in press.

[2] Kako, E., S. Noguchi and T. Shishido, "Input Couplers for 972 MHz Superconducting Cavities in the High Intensity Proton Linac", *Proc. of the 11th Workshop on RF Superconductivity*, Luebeck/Travemuende, Germany (2003) ThP27, in press.

[3] Kako, E. and S. Noguchi, "RF Design of a 972 MHz Superconducting Cavity for High Intensity Proton Linac", *Proc. of EPAC2002*, Paris, France, pp. 2244.

[4] Saito, K., S. Noguchi and T. Ohta, "Half-cell Die Design for Right Cavity Geometry in High Intensity SC Proton Linac", *Proc. of the 11th Workshop on RF Superconductivity*, Luebeck/Travemuende, Germany (2003) TuP41, in press.

[5] Shishido, T., E. Kako and S. Noguchi, "Development of Pre-tuning System for 972 MHz 9-cell Superconducting Cavities", *Proc. of the 11th Workshop on RF Superconductivity*, Luebeck/ Travemuende, Germany (2003) TuP42, in press.

SPOKE CAVITIES: AN ASSET FOR THE HIGH RELIABILITY OF A SUPERCONDUCTING ACCELERATOR

STUDIES AND TESTS RESULTS OF A β = 0.35, TWO-GAP PROTOTYPE AND ITS POWER COUPLER AT IPN ORSAY

C. Miélot
Institut de Physique Nucléaire
Orsay, France

Abstract

Taking into account the PDS-XADS requirements concerning accelerating field, quality factor and reliability, two spoke-type cavities have been designed at IPN Orsay. One of them has been successfully tested and the second one is currently being fabricated. This paper reports on the excellent performance of the first cavity, substantially exceeding the requirements, which make spoke cavities an attractive solution for a reliable PDS-XADS proton driver.

Introduction

Studies on spoke cavities are in progress at IPN Orsay. Taking into account the requirements defined by deliverable D57 of PDS-XADS [1,2], a $\beta = 0.35$ spoke cavity has been designed. Fabricated by CERCA, the cavity was tested at IPN. A second spoke cavity with $\beta = 0.15$ has been designed and is presently being fabricated. As shown in P. Pierini's contribution to this conference, superconducting spoke cavities seem to be an attractive solution for the low β section of the XADS accelerator. In this paper, subsequent to a short description of the design and fabrication process, we will discuss the results of the tests performed at IPN and demonstrate their good performances with respect to the established requirements. One of the main imperatives for the whole accelerator is reliability, such that the feasibility of producing this system on industrial scale can be shown. The system must be fault tolerant, and the number of beam trips should be less than five per year. The result of the tests will show that using spoke cavities for the low β section is a good strategy for achieving the goal of reliability.

Design and fabrication

These cavities are referred to as "spoke" cavities within the accelerators community because of the "spoke-like" part that goes through the outer wall of the cavity (see Figure 1). This spoke defines two gaps in which the electric field can accelerate the proton beam that goes through the central hole of the spoke. The accelerating field of these resonating cavities is driven by an external RF transmitter linked to the cavity by a coupling port. The cavities are made of bulk niobium (superconducting metal at working temperature 4 K). The $\beta = 0.35$ cavity, named "AMANDA", had been designed with the help of the electromagnetic code MAFIA. The optimisation of E_{pk}/E_{acc} (the ratio of peak electric field on the wall of the cavity and accelerating field) and of B_{pk}/E_{acc} (magnetic peak field out of accelerating field) lead to a diameter D of one-third of the accelerating length: $D = 1/3\ L_{acc}$. The shape of the central spoke has been designed to reduce B_{pk}/E_{acc} (optimisation of the spoke extremities diameter) and to increase the transit time factor T_t, given by $\Delta E = e.V.T_t$, where ΔE is the energy gain, e the proton charge and V the maximum voltage in the gap (see Figure 1). To ensure rigidity and good mechanical performances, stiffeners have been added on the flanges of the cavity as shown in Figure 2.

Fabrication was ensured by CERCA, using specially designed tools. The centre shape of the spoke was made possible by squeezing the cylinder while the rest of the spoke was strictly maintained. Table 1 shows the main characteristics (in mm) of the $\beta = 0.35$ spoke cavities.

Figure 1. Shape of a spoke cavity (CATIA software)

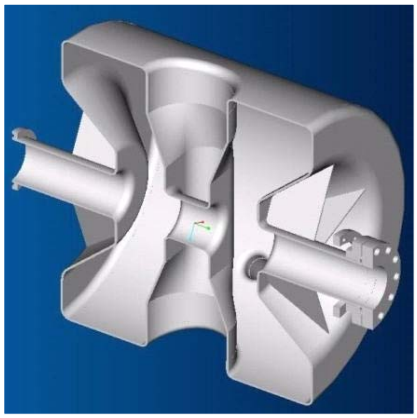

Figure 2. Stiffeners on the cavity flanges (ACORD-CP software)

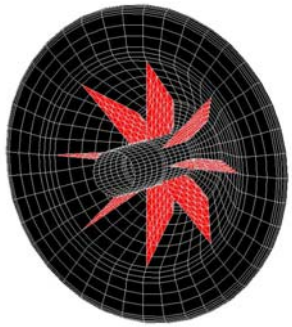

Table 1. Main characteristics of AMANDA (in mm)

Cavity diameter	408
Total length	354
Spoke base diameter	118
Spoke centre thickness	67
Spoke centre width	147
Gap centre to gap centre	150
Iris to iris	200
Beam tube length	150
Beam tube aperture	60

Tests results

Lorentz force coefficient

Measuring the frequency shift with the variation of E_{acc}, we could deduce the value of the Lorentz force coefficient, which is K = -5.6 Hz/(MV/m)^2, shown in Figure 3. The measures have been taken with a stiffening system mounted on the cavity. This value is in good agreement with the predicted value of -8 Hz/(MV/m)^2, given the numerous approximations in the code, meaning that the mechanical behaviour of the cavity is better than the more challenging behaviour of low-ƀ elliptical cavities.

Figure 3. Frequency (MHz) vs. E_{acc}^2 (MV/m)^2

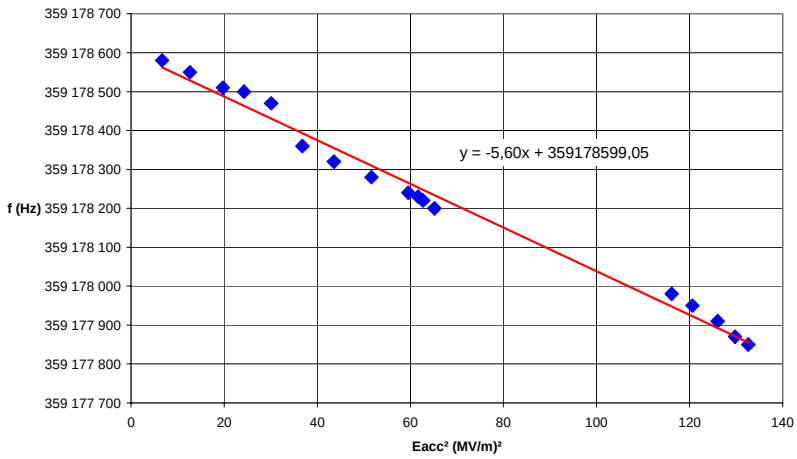

Surface resistance

The first measure of surface resistance [Figure 4, measuring G/Q_0 (diamonds) where G is the given geometrical factor of the cavity, $G = R_s.Q_0$, with the surface resistance R_s and Q_0 the quality factor] gave a value of 10 nΩ for residual resistance. After staying 67 hours at 100 K another measure gave 70 nΩ for residual resistance (squares, Figure 4). The value of residual resistance was found by comparison with empirical formula for surface resistance:

$$R_s = 9.10^{-5}.\frac{1}{T}.f^2.\exp\left(-1.83.\frac{T_c}{T}\right) + R_{res}$$

where T is the temperature, f the frequency and T_c is the critical temperature of niobium (T_c = 9.2 K). This value is appropriated under the condition that the cavity is protected from the 100 K effect; this is an important point that will have to be taken into account for minimising the losses on the cavity walls. Indeed, when left at a temperature around 100 K, the hydrogen that is inside the niobium precipitates into components which in term increase R_s.

Figure 4. Surface resistance of the cavity walls (Ω) vs. 1/Pcav (1/W)

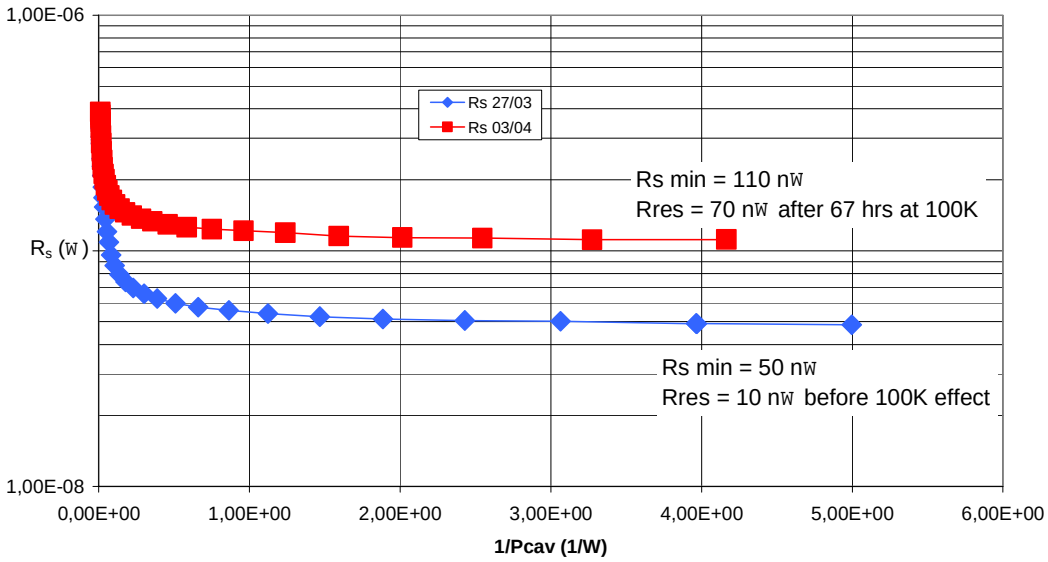

The quality factor Q_0

Measures of Q_0 vs. E_{acc} were performed under various conditions: with and without high pressure rinsing (HPR), with ultra-pure water, with different coupling positions, and with and without helium processing. The main results are given in Figures 5 and 6.

After 67 hours at 100 K the maximum E_{acc} is down to 11.9 MV/m with $Q_0 = 3.10^8$ (see Figure 5). These tests were performed using the beam tube as coupling port. Then it can be noted that HPR is absolutely necessary; as show in Figure 6, this usual processing allows reaching high E_{acc}. The limitation encountered during the first test (without HPR, diamonds in Figure 6) was due to multi-pacting. Multi-pacting is a field-limiting resonant phenomenon due to secondary emitted electrons. Even after HPR – but without He processing – the same multi-pacting barrier was encountered between 1.5 MV/m and 2 MV/m. He processing is another usual process, used in cavity preparation and tests. It consists

Figure 5. Q_0 vs. E_{acc} (MV/m)

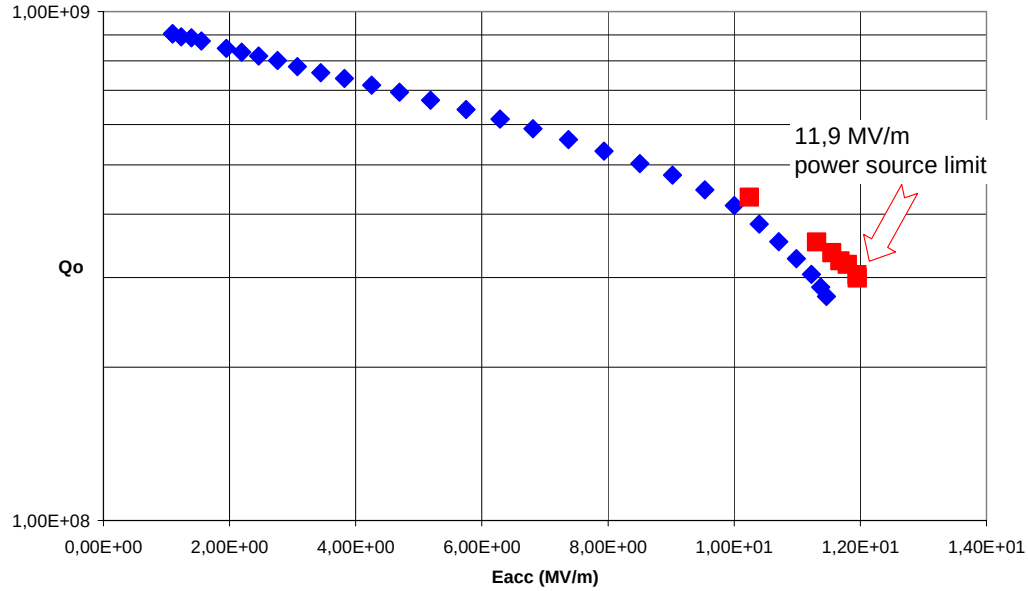

Figure 6. Q_0 vs. E_{acc} without HPR (diamonds), with HPR and without He processing (squares) and with both HPR and He processing (triangles)

The red star indicates the requirements for PDS-XADS: E_{acc} = 7 MV/m with $Q_0 = 5.10^8$.

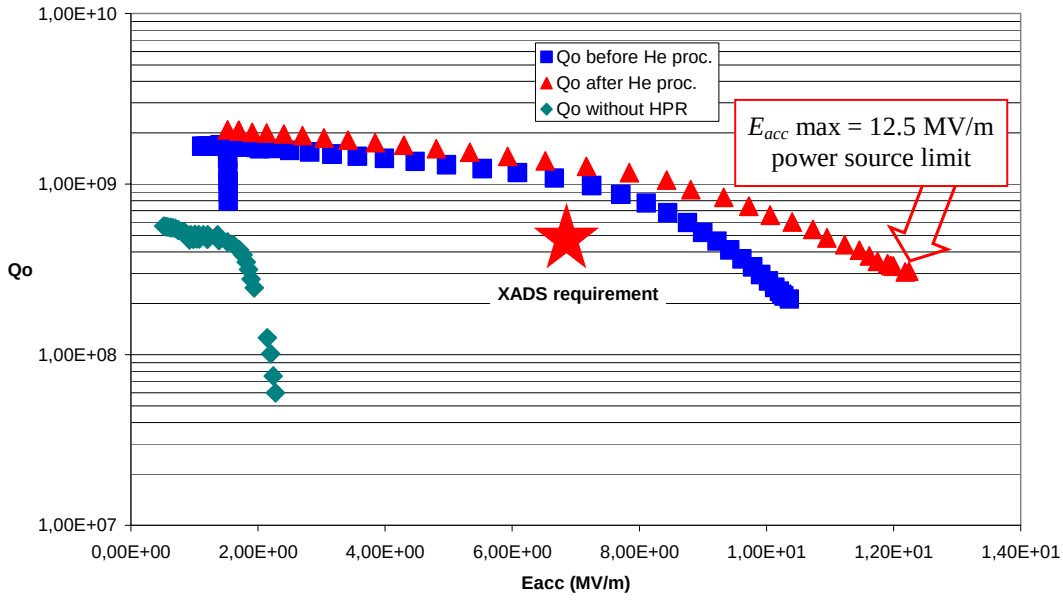

of introducing a low pressure of He (10^{-5} mbars) inside the cavity, and using RF power to produce arcing that destroys electron emitting sites. After two He processings we could achieve E_{acc} = 12.55 MV/m ($Q_0 = 3.10^8$); this maximum is due to source limitation (no quench). Within that test we could also achieve $Q_0 = 2.10^9$ at low field. Regarding the requirements for PDS-XADS, it can be seen that we have achieved a comfortable performance margin that is a very positive point for reliability. Table 2 sums up the results of the tests.

Table 2. Main characteristics of the tests results

Test no.	Rinsing	Coupling	Low field Q_0	E_{acc} max
1 January 2003	No HPR	Coupling port	5.00E+08	2.3 MV/m
2 March 2003	HPR	Beam tube	2.10E+09	12.2 MV/m
3 July 2003	HPR	Coupling port	4.00E+08	12.55 MV/m

Losses on antenna, coupling port position

During the last test we used a variable coupler to feed the RF power through the coupling port. Figure 7 shows the increase of the losses on the antenna when it was moved from a 23-mm position to 11 mm within the port. This meant that the coupling port was set in an area where the magnetic field was rather high, so it was decided to proceed with numerical calculations to choose an optimised location for the coupling port. The calculations were also performed to determine an accurate port diameter in order to avoid multi-pacting problems. The results of the simulations are given in the next section.

Figure 7. Q_0 vs. position of the antenna inside the coupling port (mm)

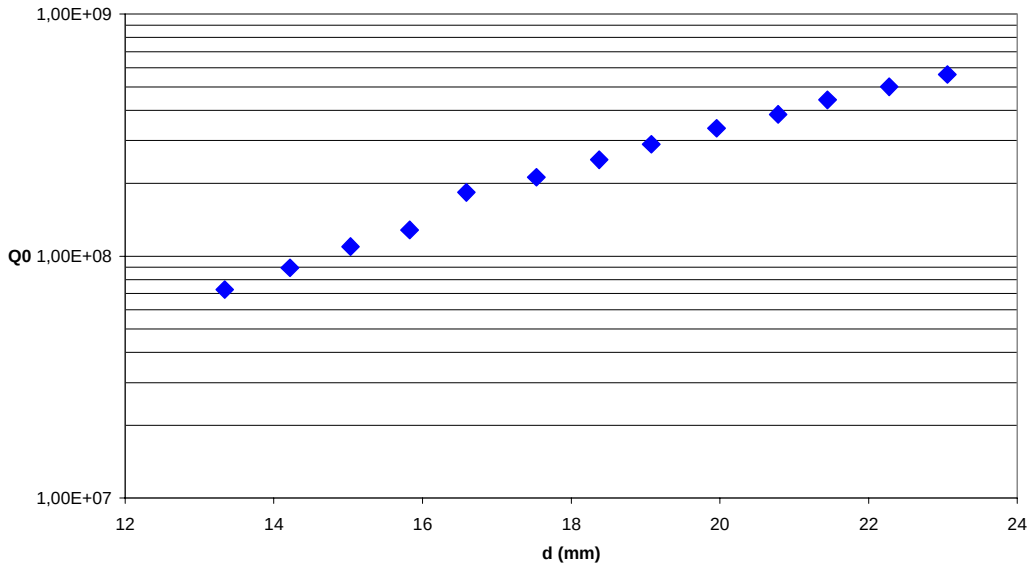

Numerical simulations

Position and diameter of the coupling port

All the numerical simulations are undertaken using the ANSOFT HFSS electromagnetic code. Regarding multi-pacting occurrences and compromising with mechanical limitations, we chose a port diameter F = 53 mm. Table 3 shows the RF threshold power multi-pacting barrier (in kW) for different port diameters and for orders 1 to 10. The lower the order, the more often this multi-pacting barrier can occur. Since 20 kW must be fed to the cavity, the diameter chosen must allow to sustain such a power without a multi-pacting barrier. It is reasonable to avoid multi-pacting until order 3 regarding the low

probability of a higher order barrier to occur. In Table 3, the threshold powers that can be overcome with no multi-pacting regarding the 20 kW power to be carried through the line are shaded in grey. This means, for example, that with the choice of F_{port} = 50 mm, an order 2 multi-pacting barrier occurs at P = 16.38 kW. As the power in the line is 20 kW, this multi-pacting order is reached. As this order is low enough to be dangerous, we want to avoid it. With a F_{port} = 56 mm, this order requires 25.77 kW to start, thus limiting the power to 20 kW will eliminate such a possiblity.

Table 3. Multi-pacting barriers for order 1 to 10 for different port diameters. The diameter of the antenna is given for line impedance of 50 Ω.

Multi-pacting order	F_{port} (mm)	30	50	56	60	70	100
	F_{ant} (mm)	13.03	21.72	24.32	26.06	30.4	43.43
1		3.07	23.7	37.3	49.15	91.06	379.26
2		2.12	16.38	25.77	33.96	62.92	262.05
3		1.2	9.41	14.81	19.52	36.16	150.61
4		0.72	5.56	8.76	11.54	21.38	89.04
5		0.45	3.46	5.44	7.17	13.28	55.33
6		1.29	2.28	3.59	4.73	8.76	36.47
7		0.21	1.61	2.53	3.34	6.19	25.79
8		0.16	1.24	1.95	2.57	4.76	19.82
9		0.13	1.04	1.63	2.15	3.99	16.63
10		0.12	0.95	1.49	1.96	3.64	15.16

Once the diameter was determined, the numerical simulation concerning the port position was undertaken. The position is given by the angle of the port with the spoke. The initial position is given by φ = 45° in Figure 8.

Figure 8. Start situation: port angle = 45

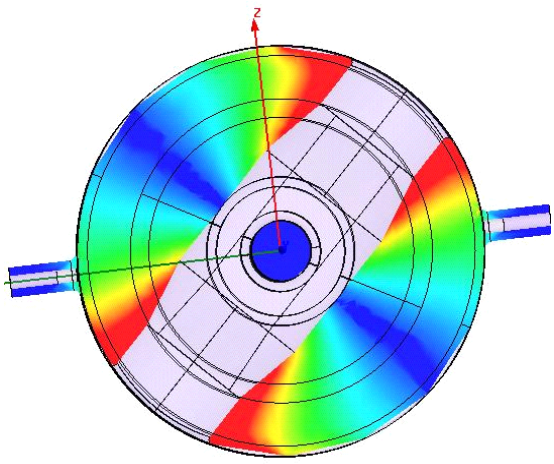

The normalised losses decrease a φ increase from 45° to 90°. Figure 10 shows the integrated squared magnetic field on the antenna surface that is actually in contact with the field for the AMANDA cavity. It was therefore decided that the next cavity would be fabricated with a 90° angle, as shown in Figure 9.

Figure 9. Final situation: port angle = 90

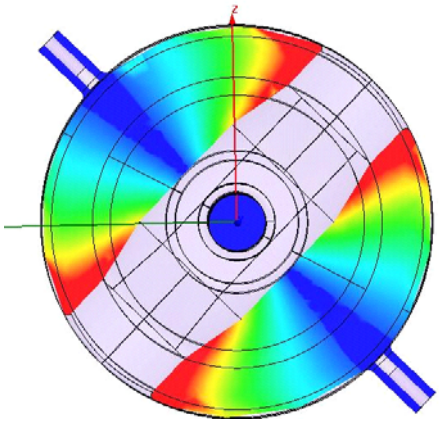

Figure 10. Normalised integral of squared magnetic field on antenna surface vs. angle of the port with the spoke

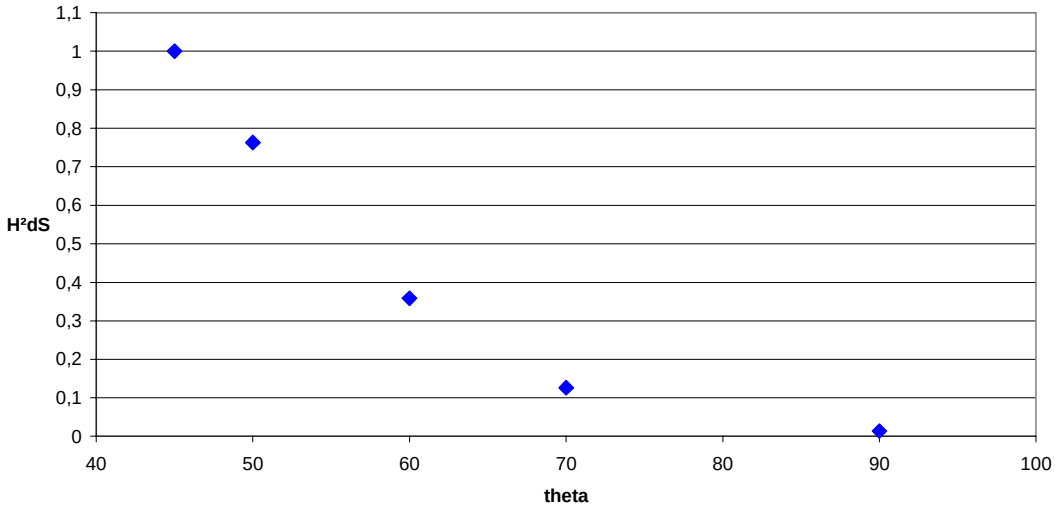

Coupling with angle φ = 90°, antenna position

The results of the simulations show that the requirements for the coupling factor (regarding the intensity of the beam and the corresponding power to be provided) can be easily reached with the new port position. The position of the antenna is given on the axis of the port. Figures 11and 12 show the simulations results for a β = 0.35 cavity and for a β = 0.15 cavity.

Studies in progress on power coupler

In addition to the developments on the spoke cavities, the associated power coupler is also under study. The main work, at this moment, concerns the ceramic window. Many window shapes have already been investigated to choose the accurate one. Table 4 shows the main parameters that will determinate which window to choose for the spoke cavity. From these results it can be inferred that the cylindrical type of window, shown in Figure 13, is the most appropriated for spoke coupler.

Figure 11. Q_i vs. antenna position (mm)

On the left of the vertical line, inside the cavity, on the right, inside coupling port for AMANDA (β = 0.35)

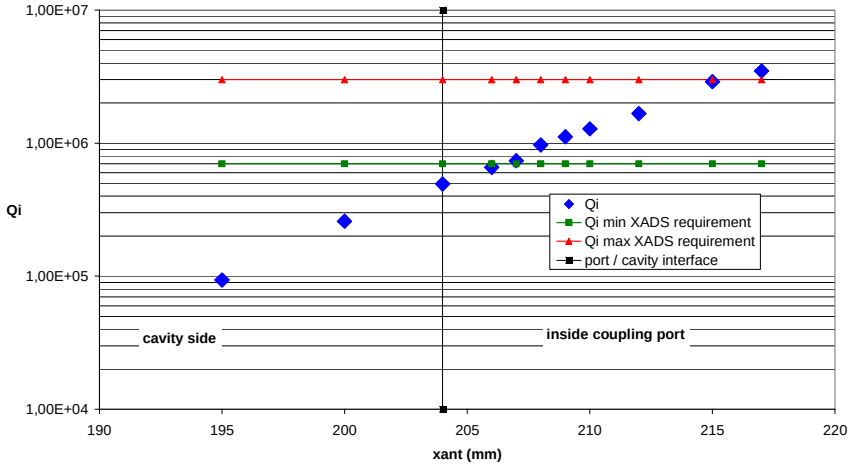

Figure 12. Q_i vs. antenna position (mm) for β = 0.15 spoke cavity

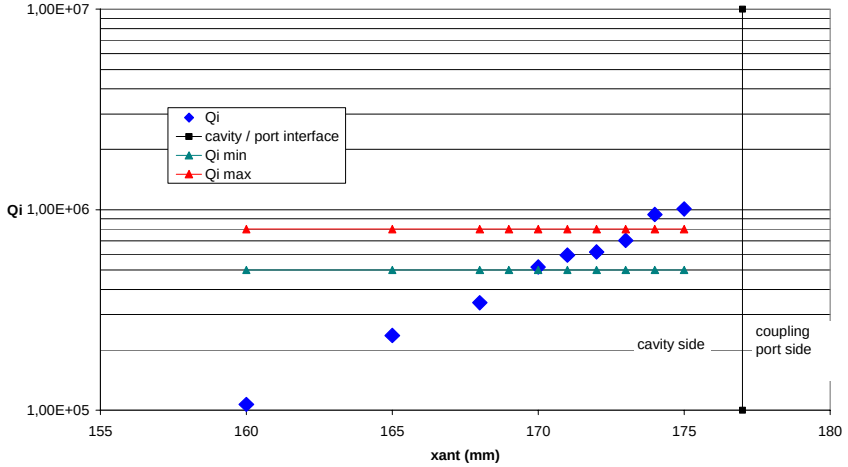

Table 4. Main parameters of different window shapes for spoke power coupler

	Window type				
	Disc with chokes	**Disc (no chokes)**	**Cylindrical**	**Waveguide/ coax**	**Disc with chokes**
S11 at 352 MHz (dB)	-55.4	-58	-45.17	-60	-40.2
Bandwidth (MHz)	>1 000	760	410	6	8
Esurf max (V/m)	9.88E+04	1.24E+05	1.50E+04	1.24E+04	2.30E+04
Losses inside the window (W)	60	71.75	68.2	147	33
% Pinc	0.30%	0.36%	0.34%	0.74%	0.17%
Window volume (cubic mm)	2.86E+04	1.65E+04	8.11E+04	1.61E+06	1.37E+05
Volumic losses (W/mm^3)	2.10E-03	4.34E-03	8.41E-04	9.14E-05	2.41E-04

Figure 13. Cylindrical window simulation model

Darker shading (orange) – conductors, lighter shading (green) – ceramic window

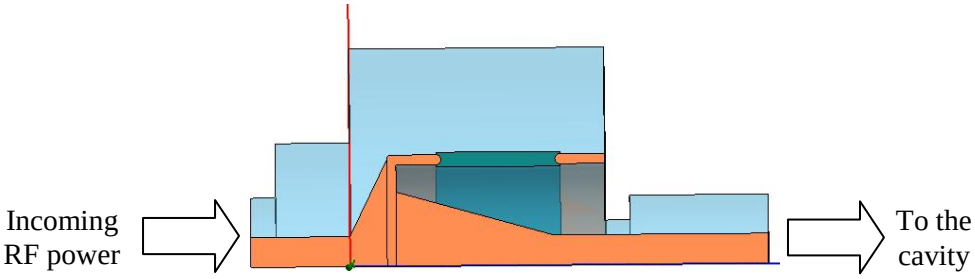

Conclusion

The overall design achieved concerning AMANDA and its mechanical stability show that this cavity is a very good component for a fault tolerant linac for PDS-XADS. Indeed, the good performances (E_{acc} max = 12.5 MV/m and $Q_0 = 1.5 \cdot 10^9$ at E_{acc} = 7MV/m) are much higher than the established requirements (E_{acc} = 7 MV/m with $Q_0 = 7 \cdot 10^5$) and allow de-rated mode operation that is an *a priori* asset for reliability.

Acknowledgements

The author would like to thank Alex C. Mueller and the team working on spoke cavities at IPN Orsay for their help.

REFERENCES

[1] Pierini, P., “ADS Reliability Activities in Europe”, these proceedings.

[2] Vandeplassche, D., *et al*., “The PDS-XADS Reference Accelerator”, these proceedings.

CHINESE STATUS OF HPPA DEVELOPMENT

X.L. Guan, S.N. Fu*, B.C. Cui, H.F. Ouyang*, Z.H. Zhang*, W.W. Xu*, T.G. Xu*
China Institute of Atomic Energy, P.O. Box 275, 102413 Beijing, China
*Institute of High Energy Physics, P.O. Box 918, 100039 Beijing, China

Abstract

A 3.5-MeV RFQ accelerator for a Chinese accelerator-driven subcritical reactor system (ADS) has been under construction in China over the past two years. It is is a 75-keV/3.5-MeV, 352.2-Hz, 50-mA four-vane type RFQ. In this paper the characteristics of the machine are described, including its physical parameters, RF characteristics, thermal and structural analyses, cold model measurements, RF power system and its fabrication test of technology model. The microwave ion source and the LEBT also are described.

Introduction

The R&D activities of HPPA technology are of key importance for the development of the accelerator-driven subcritical system (ADS), which is an entirely new approach toward the exploitation of next-generation nuclear energy [1].

According to present technical and budget status in China, a multi-purpose verification system is under consideration [2,3], which consists of a low-energy accelerator (150-MeV/3-mA proton linac) and a swimming pool light water subcritical reactor.

The China Institute of Atomic Energy (CIAE), the Institute of High Energy Physics (IHEP) and the Institute of Heavy Ion Physics at Peking University (PKU-IHIP) have been collaborating on the R&D necessary for the proposed accelerator since 2000.

Since then, various aspects of their R&D work, such as ECR high-current ion source, RFQ design and technology study, superconducting cavity study, the conceptual design of a 150-MeV/3-mA proton linac, and the preliminary design of a 1-GeV, 20-mA linac and intense-beam physics, have been proceeded with.

Two ECR proton sources have been built. As a first step toward a CW beam, a high duty factor RFQ is now being built at IHEP. Some R&D activities have been performed to pave the way for the final fabrication of the RFQ accelerator. The formal RFQ cavity is now under construction. Over the past few years, close co-operation with LNL, INFN, KAERI, KEK and CERN have been of extremely helpful regarding our HPPA work.

ECR ion source

An electron cyclotron resonance (ECR) ion source [4] is selected for the source of our verification facility system. A microwave power of 2.45 GHz is adopted. The 1-kW microwave power is coupled to the plasma chamber by a rectangular-to-ridged wave guide through a microwave window. The plasma chamber is a 100-mm long cylinder with a diameter of 100 mm. An accelerating and decelerating three-electrode extraction structure is adopted. The beam is anticipated to have a normalised rms emittance of 0.129 pmm mrad. The discharging chamber is designed to withstand a potential voltage of up to 75 kV.

A multi-slit and single-thread emittance measuring unit has been installed and measurements have been carried out.

The measurement result of beam emittance for this ion source with 60 mA and 60 keV is shown in Figure 1, as is the configuration of the ECR ion source.

Various efforts have been made to optimise the reliability [5]. A reliability test operating for more than 120 hours at 65 mA/75 keV is shown in Figure 2. Over the entire operation period, there are only three trips, and the mean time of recovery is 3 minutes; the longest uninterrupted period reached is up to 110 hours. The reliability of this kind of source can attain 99.9%.

High-current RFQ

A first step toward a CW beam, a high duty-factor RFQ, is now being built at IHEP, financially supported by a national programme of the MOST. Some R&D activities have been performed to pave the way for the final fabrication of the RFQ accelerator. The formal RFQ cavity is now being constructed.

Figure 1

The measurement result of beam emittance
(W = 60 keV, I = 60 mA, $\varepsilon_{(norm.\ rms)}$ = 0.129 πmm-mrad)

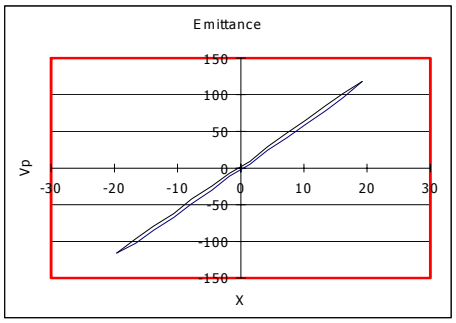

The configuration of the ECR ion source

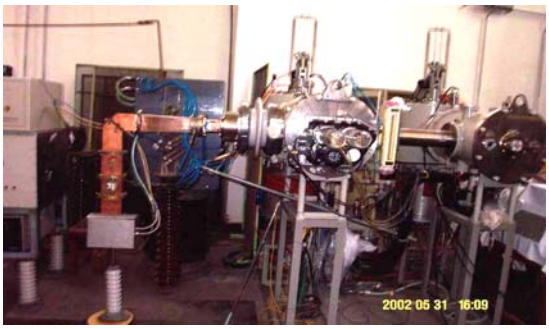

Figure 2. Reliability test – operation for more than 120 hours at 65 mA/75 keV

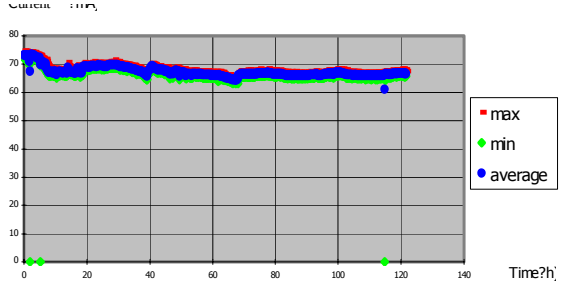

120 hours reliability test run

The RFQ structure is a four-vane type designed to accelerate a 50-mA peak current proton beam with an input energy of 75 kV. The structure was divided into four sections: the radial matching section (RMS), the shaper (SH), the gentle bunch (GB) and the accelerating section. The RFQ is 5.5 times longer than the RF wavelength. The longer the RFQ, the less stable it is against perturbations. In order to overcome this problem, the resonant coupling concept is applied, as is the case at LANL. The RFQ is longitudinally divided into two pieces separated by a coupling cell where electrodes belonging to two different RFQ pieces are facing one other. The parameters of the RFQ beam dynamics are determined. The cell design and beam dynamics simulation are provided by PARI and PARMTEQM, which decide the cell parameters used for machining the vane modulation as shown in Figure 3 [6]. The exact location of the segment gap is determined by LIDOS.RFQ [7] for zero-field crossing the gap ($\cos(kdz + j_S) = 0$), as shown in Figure 4.

The RF cavity is designed with the 3-D EM code for under-cut, coupling cell and vacuum port. Thermal deformation of the cavity is simulated with the ANSYS code and the water cooling channels have been designed as shown in Figure 5 [8].

R&D of the technological model

The fabrication of the RFQ copper model will be performed by a company situated in Shanghai, China. Some tests for development the mechanical technology must be undertaken [9]. The purpose of the mechanical technology mode is to test the brazing technology for assembling the four vanes together with required mechanical tolerance, for the characteristics of melting filler, for the structure surface and

Figure 3. The results of PARMTEQM to give the main parameters and envelopment

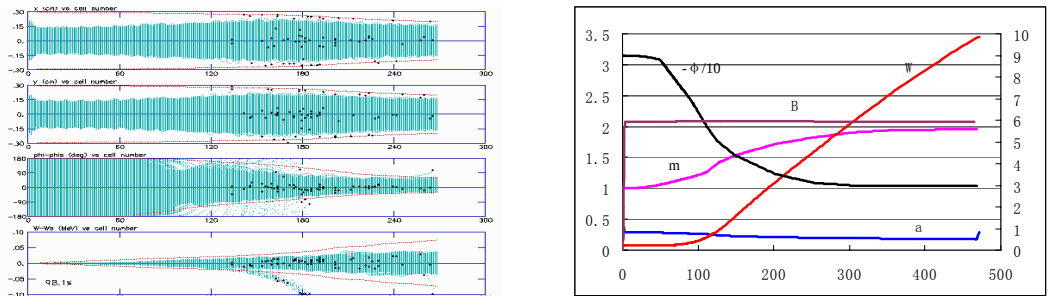

Figure 4. The results of LIDOS.RFQ to determine the exact location of segment gap

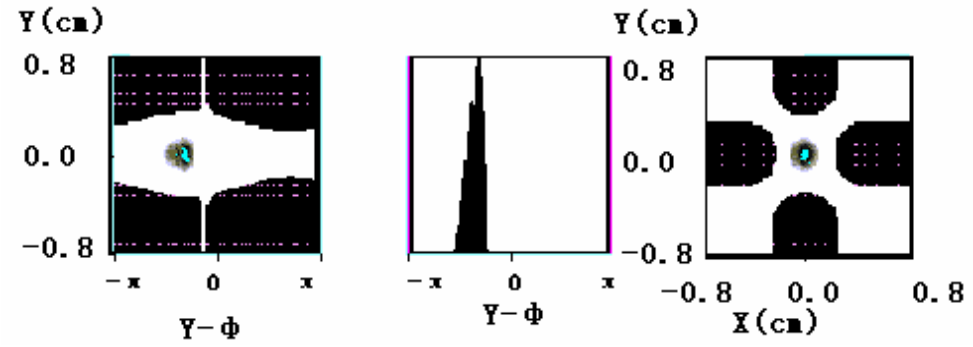

Figure 5. The results of MAFIA to design the RF characteristics of the RFQ

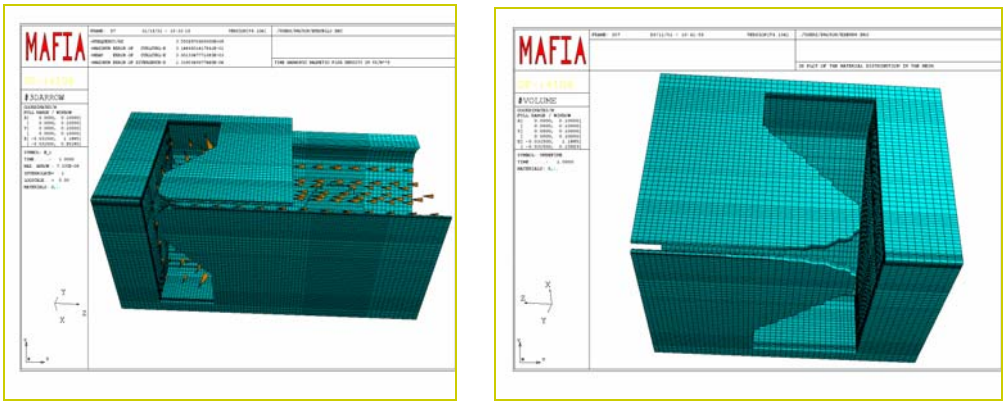

the vacuum leak, to test drill the coolant hole through the 1.2-meter RFQ cavity (12 mm in diameter), and to test the precision machining for the vane electrodes on the numerical controlled mill. At first, a short OFEC copper RFQ section 0.42 m in length was fabricated with fine machining, as shown in Figure 6. The machining tolerance reaches −20 ㎜ on the vane tip and cavity wall measured on a CMM.

Three-step braze: 1) The water cooling channel was covered by brazing plugs before the semi-fine machining. 2) The four vane wall pieces were brazed to form the cavity, and then the end-flange step was machined. 3) All the flanges, i.e. end flanges, vacuum port flanges and tuner flanges, as well as all cooling-water pipes were brazed. A bead-pull measurement was performed for the field distribution analysis of the short model with aluminium undercut ends.

Figure 6. A 0.42-m short OFEC copper section test mode



Two Lab-VIEW codes were applied during the measurements. One was used to control the measurement process and data acquisition via a GPIB-ENET/100 box. The measurement results indicate that there is a little frequency downshift after the second brazing, but a little up-shift after the third brazing. Dipole field distribution along the cavity after final brazing shows about 3% component as shown in Figure 7.

Table 1. The frequency shift after brazing

Brazing step	f_Q(MHz)	df_Q
Before 2nd brazing	351.232	
After 2nd brazing	350.955	-0.277
After 3rd brazing	351.119	+0.171
3-D simulation	351.345	-0.226

Figure 7. Dipole mode

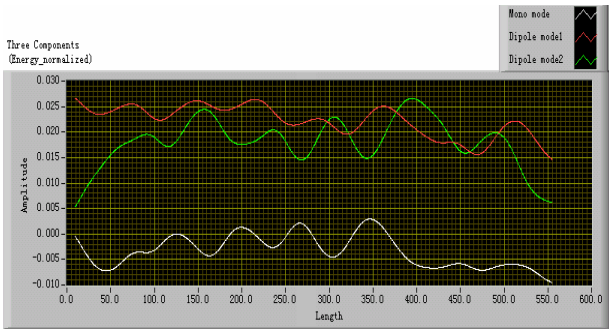

In order to grasp the machining and welding technology, and to examine the creditability of the simulation code, one full-size (1.2-m) section of RFQ cold model was fabricated. There are 16 tuners and four vacuum ports on the cavity, the same number as the real RFQ. However, the electrode is not modulated. A full-length brazing cavity was made for drilling long and small holes for cooling water and brazing a full-volume cavity with all flanges. The vane wall shape was machined after drilling the cooling water channels, and then the holes for vacuum and tuner ports were made. The channels were covered with plugs by brazing. The four pieces were brazed to form the cavity, and the vacuum leakage rate was $1.5 \cdot 10^{-9}$ torr l/s. All ports and the end flanges were then brazed, and leakage was found. After repairing the braze, the leakage rate reached $1.9 \cdot 10^{-9}$ torr l/s. Following the R&D experiences in these technological models, fabrication of the formal cavities has started. The semi-fine machining has been finished. Figure 8 shows a photo of a 1.2-meter full-size section.

Figure 8. Full-size (1.2-m) section of RFQ cold model, fabricated and brazed

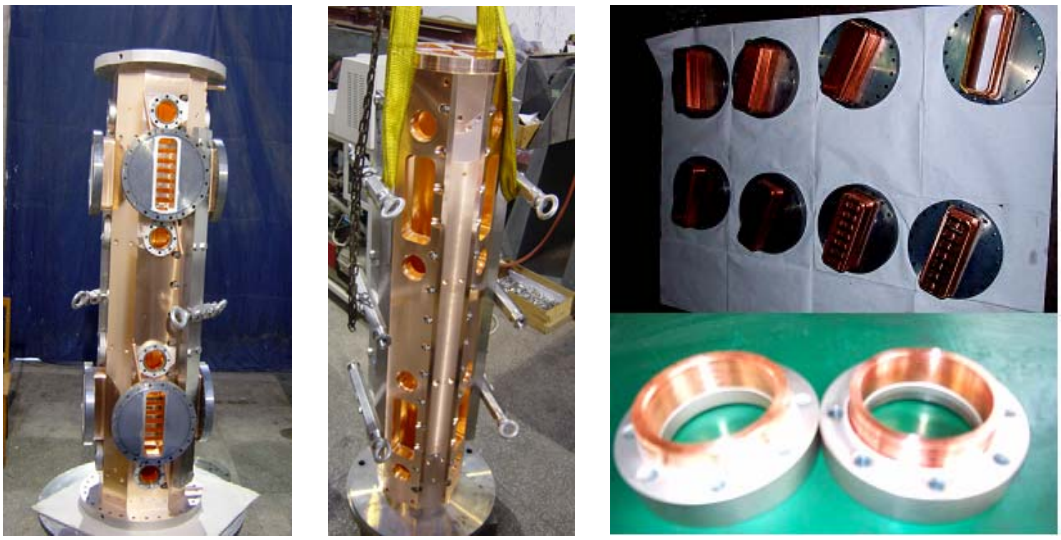

With the tuners, tuning and measuring of RFQ are carried out. With all tuners flush with the inside surface of the cavity, frequencies of the operating mode and the dipole modes are measured [10]. Figure 9 shows a photo of the dipole rods and the measurement result.

Figure 9. The measured dipole-rod effect on quadrupole and dipole modes

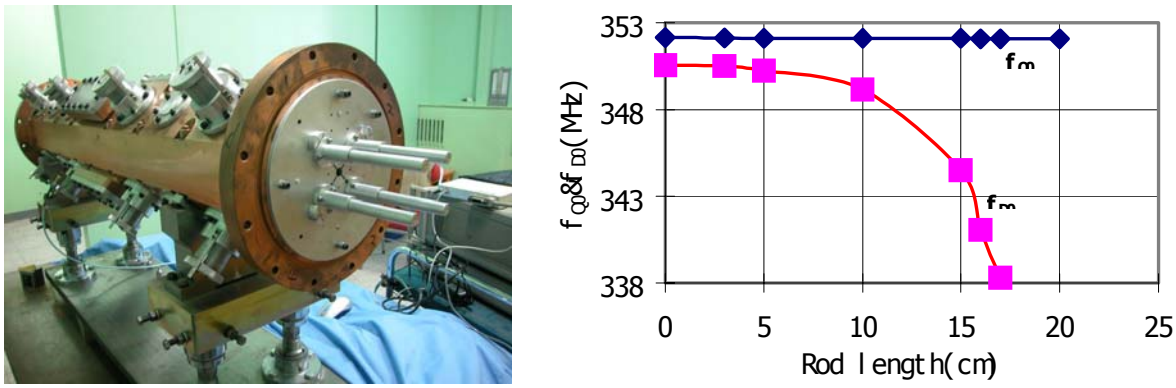

Table 2. The measured and simulated frequency for the quadruple and dipole modes in the case without/with rods

	Rod length	
	0 (cm)	**15 (cm)**
Meas. freq. of TE_{210} (MHz)	350.85	351.15
Simul. freq. of TE_{210} (MHz)	351.15	351.15
Meas. freq. of D_{13} (MHz)	344.82	338.68
Simul. freq. of D_{13} (MHz)	347.81	341.93
Meas. freq. of D_{24} (MHz)	348.50	342.49
Simul. freq. of D_{24} (MHz)	347.81	341.93

The RF power source

CERN kindly provided IHEP with some RF power source equipment for our RFQ .The equipment has been installed at IHEP as shown in Figure 10. It is a CW RF power source of 352.2 MHz/1.2 MW, decommissioned from LEPII. We reconnected the cables of the control rack, which were cut during transportation from CERN.

Figure 10. The RF power source for the RFQ been installed at IHEP



During the preliminary research phase, the 352.2-MHz RF system will be operated in pulse mode. Because the given RF system was previously used for CW operation at CERN, some modifications and improvements are necessary in order to apply them to our pulse mode operation. We have made some indispensable assemblies, and also did some tests and commissioning of every subsystem. At present, we have completed the 100-kV power supply test and long pulse floating desk hard tube modulator test. Furthermore, the initial high-power conditioning of the klystron is being carried out, and output power can reach up to 334 kW in CW mode and 402 kW in pulse mode [11].

Acknowledgements

Much thanks are due to the members of the RFQ team in LNL, INFN, Italy, especially Dr. A. Pisent. The authors would also like to thank the personnel of KAERI, Korea, particularly Dr. B-H. Choi. We wish to thank Professor K. Hubner and Professor Nans from CERN, who were of great help as concerns the experiments of the RF power supply. This work has been supported by the China Ministry of Science and Technology (MOST) and partly by CNSF.

REFERENCES

[1] Shouxian, F., *et al*., CNIC-01468 CNNC-0002, pp. 95-107, May 2000.

[2] Dazhao, D., *Proceedings of the 3rd Workshop on Neutron Science Project*, 17-18 March 1998, pp. 132-140, JAERI-conf.99-003.

[3] Xialing, G., *et al*., CNIC-01468 CNNC-0002, pp. 79-91, May 2000.

[4] Cui, B., *et al*., *Proceedings of APAC01*, Beijing, China, 17-21 September 2001.

[5] Cui, B., *et al*., *Science and Technology of Atomic Energy*, Vol. 36, No. 6, p. 486, Nov. 2002.

[6] Xialing, G., *et al*., *Pramana-Journal Physics*, Vol. 59, No. 5, pp. 951-955, Nov. 2002, New Deli, India.

[7] Bondarev, B.I., *et al*., *Proceedings LINAC'2000*, pp. 830-832.

[8] Ouyang, H., *et al*., *Proceedings of APAC01*, Beijing, China, 17-21 September 2001.

[9] Shinian, F., *et al*., *Proceedings of APAC04*.

[10] Huafu, O., *et al*., *Proceedings of APAC04*.

[11] Zonghua, Z., ed al, *et al*., *Proceedings of APAC04*.

BEAM DYNAMICS STUDIES FOR THE FAULT TOLERANCE ASSESSMENT OF THE PDS-XADS LINAC

J.L. Biarrotte[1], **M. Novati**[2], **P. Pierini**[2], **H. Safa**[3], **D. Uriot**[3]
[1]IPN/IN2P3 Saclay, France
[2]INFN Milano LASA, Italy
[3]CEA Saclay, France

Abstract

In order to meet the high availability/reliability required by the PDS-XADS design, the accelerator needs to implement, to the maximum possible extent, a fault tolerance strategy that would allow beam operation in the presence of most of the envisaged faults that could occur in its beam line components. In this work we report the results of beam dynamics simulations performed to characterise the effects of the faults of the main linac components (cavities, focusing magnets...) on the beam parameters. The outcome of this activity is the definition of the possible corrective and preventive actions that could be conceived (and implemented in the system) in order to guarantee the fault tolerance characteristics of the accelerator. The PDS-XADS programme is funded by the EC 5th Framework Programme, under contract FIKW-CT-2001-00179.

Introduction

In current high-power accelerators, specific diagnostics are usually connected to all major accelerator components, continuously sending status information. Typically, when a component fails (i.e. its information status suddenly switches from "normal" to "faulty"), the beam is immediately shut down. Action is then taken to repair the faulty component, eventually leading to replacement of the hardware. After the maintenance, when accelerator operation is ready to resume, the procedure followed is the same for a new re-start, slowly ramping up in beam power. For most accelerators, the number of beam interruptions rapidly decreases with the trip duration time, thus maintaining an overall good level of availability. For most applications, despite the high number of short-duration breakdowns, the operation is not greatly affected, as a sufficiently high availability is preserved.

For an ADS application, however, any beam trip lasting more than a second will be considered as a major accelerator failure, leading to the reactor core shutdown. Thus, the philosophy prevailing on current machines to cope with component failures must be reconsidered, taking into account that requirement. In particular, for each failure analysis, the design should look at the ability to either maintain the beam under safe conditions, or to recover the beam through, in less than one second. This is a new feature, not required for any other accelerator application, which is quite specific to ADS linacs. In this paper*, we will develop this "fault tolerance" concept, and try to assess its practical implementation through beam dynamics calculations.

The PDS-XADS reference accelerator and the reliability requirement

Consecutive to the work of the European Technical Working Group on Accelerator Driven Systems [1], the Preliminary Design Study of an Experimental ADS (PDS-XADS) was launched in 2001. A large European collaboration supported by the EU within the Fifth Framework Programme performs these studies [2,3]. Five work packages (WP) cover the relevant issues; the WP3† is dedicated to the design of the high-intensity proton accelerator providing the neutron flux to the subcritical reactor via a spallation target [4,5]. The main specifications for this XADS accelerator system are summarised in Table 1.

Table 1. PDS-XADS proton beam specifications

Max. beam intensity	6 mA CW on target (10 mA rated)
Proton energy	600 MeV (includes 800 MeV upgrade study)
Beam entry	Vertically from above preferred
Beam trip number	Less than five per year (exceeding 1 second)
Beam stability	Energy: –1%, intensity: –2%, size: –10%
Beam footprint on target	Gas-cooled XADS: circular ⌣ 160 LBE-cooled XADS: rectangular 10 · 80 MYRRHA: circular, "donut" ⌣ 72

* This paper relies on the studies performed within the PDS-XADS programme, and on the corresponding internal reports: D9 (*Requirements for the XADS Accelerator & the Technical Answers*), D47 (*Accelerator: Feedback Systems, Safety Grade Shutdown & Power Limitation*), D48 (*Accelerator: Radiation Safety & Maintenance*), D57 (*Potential for Reliability Improvement & Cost Optimisation of Linac and Cyclotron Accelerators*) and D63 (*Definition of the XADS-class Reference Accelerator Concept & Needed R&D*).

† The following institutions collaborating within the WP3 are: ANSALDO (Italy), CEA (France), CNRS-IN2P3 (France, co-ordinator), ENEA (Italy), FRAMATOME ANP (France), FRAMATOME GmbH (Germany), FZ Jülich (Germany), IBA (Belgium), INFN (Italy), ITN (Portugal), University of Frankfürt (Germany).

Table 1 notably highlights that a continuous beam operation with only a few (of the order of five per year) beam stops longer than approximately one second is considered to be mandatory for the successful demonstration of the ADS coupling. Given the state-of-the-art in the field of accelerator reliability [6], this requirement appears to be highly challenging.

From this extremely high reliability requirement, WP3 has assessed the corresponding technical answers [7], and a reference solution based on a linear superconducting accelerator with its associated doubly achromatic beam line has been worked out to some level of detail. No potential showstopper on the path for achieving an extremely reliable accelerator has yet emerged from the analyses performed [8,9]. From the reliability and availability specifications, it is clear that suitable design strategies had to be followed early in the conception stage of the XADS accelerator. The main guidelines that have been highlighted to drive the design are: a strong design (which makes extensive use of component de-rating and proper redundancy) and a high degree of fault tolerance (i.e. the capability to maintain beam operation within nominal conditions under a wide variety of accelerator component faults).

This fault tolerance concept is a crucial point in the design of the overall XADS accelerator in order to guarantee the few number of beam stops per year dictated by the target requirements. The state of the art in RF system technology is indeed not reliable enough to envisage an operation of the XADS accelerator during several months without any beam trip. At least a few tens of failures per year can be foreseen, due only to these RF systems, based on parts count reliability estimates. Therefore, even if a great effort can be directed at improving the MTBF of RF systems, it seems difficult to reach the reliability requirements without implementing any fault tolerance philosophy for the linac design.

The proposed reference design for the XADS accelerator, optimised for reliability, is shown in Figure 1. The injection section is composed of a “classical” proton injector (ECR source plus normal-conducting RFQ structure), followed by additional warm IH-DTL and/or superconducting CH-DTL up to a transition energy still to be defined (between 5 and 50 MeV). In this part, fault tolerance is guaranteed by means of a “hot stand-by” spare.

Figure 1. XADS reference accelerator layout: a doubled injector accelerator is followed by a fully modular spoke and elliptical cavity superconducting linac; the 350 MeV option corresponds to a smaller-scale XADS (MYRRHA project). Photos of typical cavity prototypes are shown in the lower part. From left to right: RFQ, CH structure, spoke, elliptical five-cell.

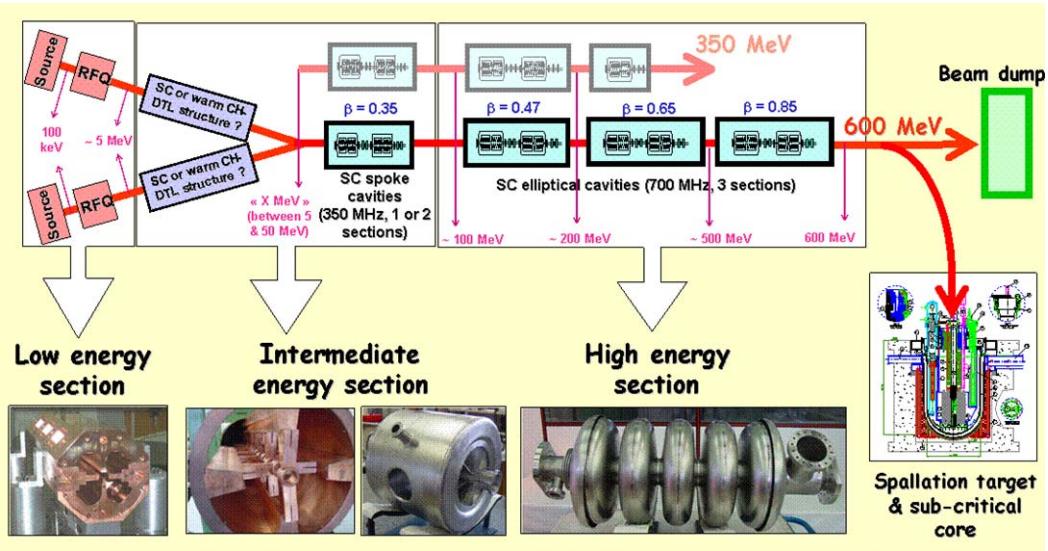

Above this transition energy, a fully modular superconducting linac brings the beam up to the final energy, using spoke and elliptical cavities. This section is designed to be intrinsically fault tolerant, meaning that an individual cavity failure can be handled at all stages without loss of the beam. This characteristic relies on the use of highly "de-rated" and independently-powered accelerating components, associated with a fast digital feedback system and adequate diagnostics.

In the following, the fault tolerance principle of this modular superconducting linac will be analysed by means of beam dynamics simulations. These calculations are performed using the TraceWin and PARTRAN codes developed in Saclay [10], and on the basis of the 5 MeV-600 MeV XADS reference linac layout presented in Table 2. In all cases, a 10-mA proton beam is considered, and the normalised rms emittance values at the input are assumed to be 0.27 π.mm.mrad in the transverse planes, and 0.39 π.mm.mrad in the longitudinal plane. Multi-particle calculations are performed using at least 10 000 particles and considering a Gaussian (truncated at 4σ) phase-space distribution.

Table 2. Layout of the 5 MeV-600 MeV XADS reference linac. Focusing is ensured by warm quadrupole doublets.

Accelerating sections	Frequency	No. of gaps per cavity	No. of cavities per lattice	Input energy	Output energy	No. of cavities
Spoke β = 0.15	352.2 MHz	2	2	5.0 MeV	16.7 MeV	36
Spoke β = 0.35	352.2 MHz	2	3	16.7 MeV	90.5 MeV	63
Elliptical β = 0.47	704.4 MHz	5	2	90.5 MeV	191.7 MeV	28
Elliptical β = 0.65	704.4 MHz	5	3	191.7 MeV	498.1 MeV	51
Elliptical β = 0.85	704.4 MHz	6	4	498.1 MeV	614.7 MeV	12

Consequences of the failure of a RF cavity

Let us assume in this section that the RF system fails to power a cavity somewhere in the linac, and that this cavity is immediately detuned to avoid any beam loading effect. This results in a loss of the energy gain provided by the failed cavity, and then in a beam longitudinal (phase-energy) mismatch at the entrance of the following cavity. Because we deal with a non-relativistic proton beam, this energy loss will imply a phase slip along the linac equal to $\delta\phi = 2\pi(\delta z/\lambda)(\delta\beta/\beta^2)$, increasing with the distance δz from the faulty cavity; β is the beam velocity (normalised to c), λ the RF wavelength and $\delta\beta$ the velocity loss (compared to the reference beam velocity) at δz [11].

Of course, the consequences of such a failure strongly depend on the position of the cavity in the linac, and on its operating conditions. The problem is more serious when the velocity of the particle is low, but also when the accelerating field and the operating frequency of the cavity are high. Figure 2 shows, for each cavity of the XADS reference linac, the phase slip induced at the entrance of the subsequent cavity if a cavity fails. It rapidly appears from this graph that the most critical sections of the accelerator towards the fault tolerance problem are the first β = 0.15 spoke section and the first β = 0.47 elliptical section.

Another important parameter to be taken into account in the analysis is the longitudinal acceptance of the linac. The lower this acceptance (i.e. the higher the synchronous phase compared with the longitudinal size of the beam), the faster the fault-induced phase slip will offset the beam towards the phase instability region. One way to avoid the problem could thus be to lower both the synchronous phase (near the -90 bunching value) and the accelerating gain per cavity all along the linac, but this would lead to an unacceptable increase in linac length and cost.

Figure 2. Beam phase slip induced at the subsequent cavity as a function of the position of the faulty cavity in the linac. This phase slip is of course larger for a faulty cavity located at the end of a lattice.

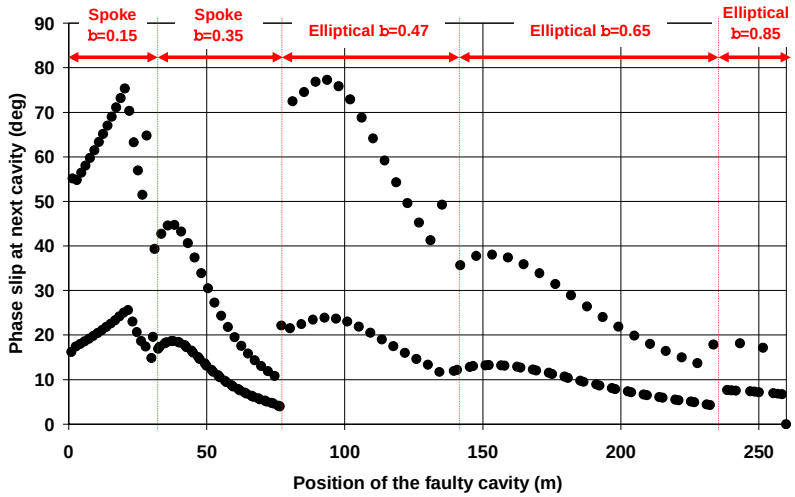

In the XADS reference linac, where conservative but realistic synchronous phase and accelerating field values are used, simulations show that in almost every case, the fault of a cavity induces a sufficient phase slip to rapidly drop the beam out of the phase stability region. The beam can not then be correctly handled longitudinally in the subsequent cavities, and it is finally completely lost later in the linac (see example in Figure 3). This kind of behaviour with a final 100% beam loss is encountered for any cavity fault in the linac, except in the specific case of the first spoke cavity's failure (where only 40% of the beam is lost thanks to the low synchronous phase and the very low accelerating field used in this first cavity) and in the case of the last elliptical cavities' failure, at the very end of the linac, where the induced beam phase slip has no further consequences.

Figure 3. Beam envelopes (x-transverse, phase) in the 5 MeV-600 MeV XADS reference linac if spoke cavity #62 (40 MeV, 50 m) is lost and no compensation action is performed

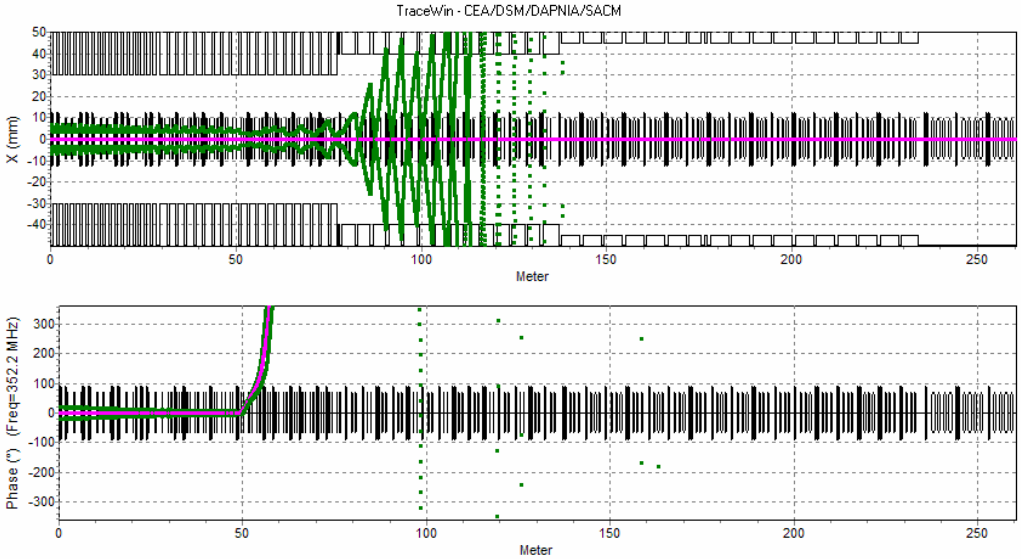

Linac retuning after the failure of a RF cavity

From this first analysis, it is clear that in case of a cavity failure, some kind of retuning has to be performed. The aim of this retuning is to recover the nominal beam characteristics at the end of the linac, and in particular its energy, while ensuring the same level of transmission (and of emittance growth) as for the reference linac case.

To achieve this compensation, the general philosophy is here to re-adjust the accelerating fields and phases of the linac cavities to recover the required longitudinal behaviour of the beam. One simple way to achieve such a retuning is to compensate locally using the accelerating cavities neighbouring the failing one. This method especially has the advantage of involving a small number of elements, simplifying the retuning procedures and limiting the possible induced errors. This is illustrated in Figure 4: if cavity #n is faulty, the four surrounding cavities (#n-2, #n-1, #n+1, #n+2) are retuned to recover the nominal beam energy and phase at the end of the following lattice (point M). This can of course be performed with more (or fewer) cavities if necessary. Practically, the retuning of the cavities is undertaken acting only on their accelerating field amplitude and/or phase. On the transverse beam dynamics side, the gradients of the four focusing quadrupoles located inside the retuned lattices can also be adjusted if needed. Here again, more quadrupoles can be used if necessary.

This retuning must, of course, be performed properly in order to reach a reasonable compromise between the three following goals:

1) *Reaching the nominal energy and phase at point M (and consequently at the target).* In principle, this can be done simply by raising the accelerating field in the surrounding cavities (this is possible because the compensation is made both before and after the failed cavity; this is thus not true for the two first cavities of the linac). This method leads to a very acceptable situation (even at very low energies, see Figure 5), but of course, with such a basic retuning, some beam mismatch often appears both in the longitudinal and transverse planes, inducing emittance growth and halo creation.

2) *Avoiding any beam loss to ensure a 100% transmission, and keeping the emittance growth as low as possible*. This is undertaken first by trying to keep phase advances as smooth as possible, but also by limiting as much as possible the longitudinal size of the beam around the faulty cavity area, so as to maintain the whole bunch inside the phase stability region [this is mainly true in the low-energy sections, see Figure 5(b)]. To achieve all this, an adjustment of the RF phases in the retuned cavities and of a few quadrupole gradients is mandatory.

3) *Ensuring that the accelerating field of the retuned cavities (and the corresponding needed RF power) will not have to be increased too much compared with the nominal operation point*. We chose in the study not to exceed a +30% field increase in the cavities that leads to maximum allowed peak fields of E_{pk} =33 MV/m for the spoke sections (nominal "de-rated" operation point: 25 MV/m), and of B_{pk} = 65 mT for the elliptical sections (nominal "de-rated" operation point: 50 mT). Of course, the more cavities used for the retuning procedure, the more this field increase can be limited. Note that this requirement has been relaxed at the beginning of the linac where cavities are working at the very low peak field required by the nominal operation.

A reasonable compromise between these three requirements is not always easy to reach, especially in the very low velocity section (spoke β = 0.15) where the beam is "debunching" very rapidly at the fault cavity position, leading to halo creation and beam losses if a refined retuning is not carried out. In this case, a strong longitudinal focusing (i.e. high field increase, more than +30%) has to be performed in the retuned cavities to compensate for this effect, though not too much so as to maintain a good longitudinal matching.

Figure 4. Principle of local compensation to recover the beam energy and phase

Of course, in the case of the failure of cavity #1, cavities #2, #3, #4, #5 are used, and in the case of the failure of the last cavity, the four preceding cavities are used.

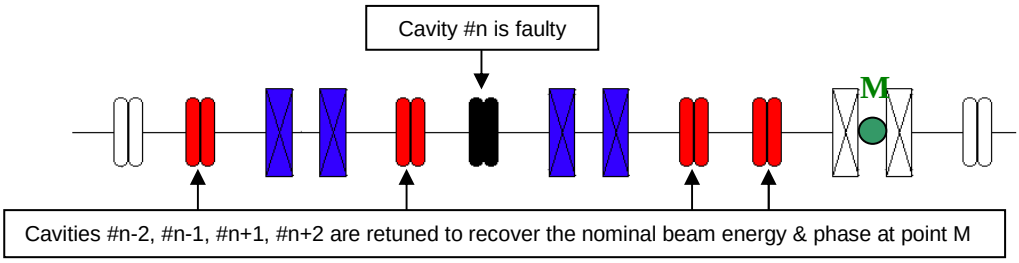

Figure 5. Multi-particle beam envelopes (x-transverse, phase) in the 5 MeV-600 MeV XADS reference linac if spoke cavity #4 (5.5 MeV, 3 m) is lost and compensation is achieved by: raising the field only in the four surrounding cavities (left), or applying the optimal tuning as reported in Table 3 (right).

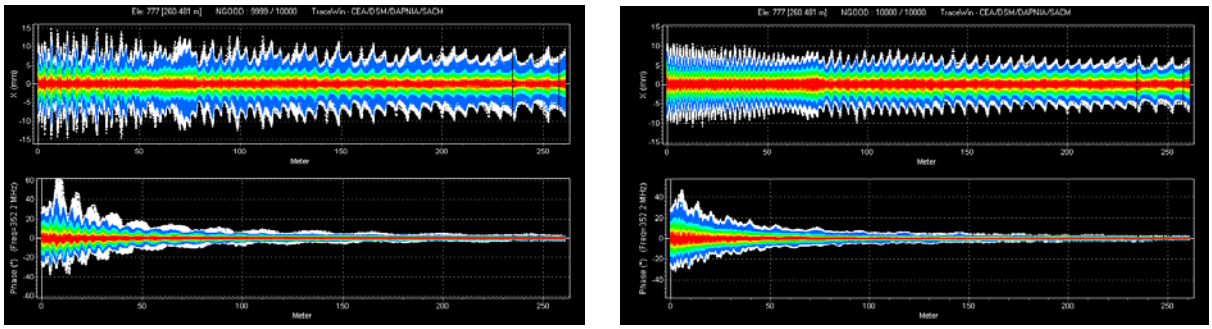

Above 10 MeV, the situation becomes much easier. It is then always possible to recover the beam within the nominal parameters at the end of the accelerator without exceeding a +30% field rise, even if this limitation can be quite difficult to manage in the case where the number of cavities per lattice is small. The levels of emittance growth are always very low, and even meet the nominal values in the elliptical sections (see Table 3). Note that the situation is a bit more complicated when the faulty cavity is located at the transition between two sections (especially at the frequency change).

Based on these considerations, a systematic study of the XADS linac fault tolerance has been performed, optimising the retuned values to be applied for local compensation in the case of the failure of most of the linac cavities. Table 3 reports some of the obtained results. The conclusion of the study is that *in every case, with an appropriate retuning, the beam can be transported up to the high-energy end without any beam loss (100% transmission, reasonable emittance growth), and within the nominal target parameters.*

Case of a quadrupole failure

Calculations have also been performed to analyse the consequences of a quadrupole failure on the beam dynamics in the XADS reference linac. Here again, the consequences of such a failure depend on the position of the failed quadrupole. The situation is more critical in the sections where the safety ratio between the beam tube aperture and the beam size is smaller (see Table 4): the failure of one of the very first quadrupoles of the $\beta = 0.15$ spoke section leads to a beam loss of about 30%, the same

Table 3. Optimised retuning parameters and corresponding beam dynamics behaviour for a few cavity fault conditions. In all cases, the transmission is 100%. Note that the optimisation level can be different depending on the cases.

No. of faulty cavity	Section	Final energy	Emittance growth (%)		Number of retuned cavities (before + after)	Max DEacc (%)	Max E_{pk} (SP) or B_{pk} (EL)	Max Dpower (%)	No. of retuned quads (bef + aft)
			Transv.	Long.					
0	–	Nominal	+5%	0%	–	–	–	–	–
1	SP 0.15	Nominal	+7%	+4%	0 + 4	+67%	19 MV/m	+67%	0 + 4
2	SP 0.15	Nominal	+9%	+12%	1 + 3	+90%	19 MV/m	+68%	0 + 4
3	SP 0.15	Nominal	+10%	+12%	2 + 3	+94%	21 MV/m	+56%	4 + 2
4	SP 0.15	Nominal	+9%	+4%	3 + 3	+46%	15 MV/m	+35%	2 + 4
19	SP 0.15	Nominal	+6%	+6%	2 + 3	+38%	24 MV/m	+48%	2 + 2
20	SP 0.15	Nominal	+9%	+4%	3 + 2	+37%	26 MV/m	+58%	2 + 2
35	SP 0.15	Nominal	+6%	0%	2 + 3	+20%	32 MV/m	+27%	2 + 2
36	SP 0.15	Nominal	+7%	+4%	3 + 3	+22%	34 MV/m*	+32%	2 + 2
37	SP 0.35	Nominal	+6%	0%	3 + 2	+22%	35 MV/m*	+34%	2 + 2
38	SP 0.35	Nominal	+7%	+6%	3 + 4	+29%	31 MV/m	+26%	2 + 2
39	SP 0.35	Nominal	+5%	+5%	4 + 2	+24%	36 MV/m*	+35%	4 + 2
61	SP 0.35	Nominal	+6%	+2%	2 + 3	+25%	31 MV/m	+26%	2 + 2
62	SP 0.35	Nominal	+6%	0%	2 + 2	+26%	31 MV/m	+28%	2 + 2
63	SP 0.35	Nominal	+5%	+1%	3 + 2	+25%	31 MV/m	+27%	2 + 2
94	SP 0.35	Nominal	+6%	+2%	3 + 3	+16%	29 MV/m	+18%	4 + 2
95	SP 0.35	Nominal	+7%	-1%	3 + 3	+22%	31 MV/m	+29%	4 + 2
96	SP 0.35	Nominal	+5%	+1%	4 + 2	+21%	30 MV/m	+25%	4 + 2
97	EL 0.47	Nominal	+6%	0%	3 + 3	+18%	59 mT	+27%	4 + 2
98	EL 0.47	Nominal	+6%	0%	3 + 2	+23%	62 mT	+31%	4 + 2
109	EL 0.47	Nominal	+6%	0%	3 + 3	+20%	60 mT	+28%	4 + 2
110	EL 0.47	Nominal	+6%	0%	3 + 2	+20%	60 mT	+29%	2 + 2
123	EL 0.47	Nominal	+6%	0%	2 + 4	+20%	60 mT	+26%	4 + 2
124	EL 0.47	Nominal	+6%	0%	3 + 3	+19%	60 mT	+28%	4 + 2
125	EL 0.65	Nominal	+5%	0%	2 + 3	+18%	59 mT	+27%	4 + 2
126	EL 0.65	Nominal	+5%	0%	3 + 4	+21%	61 mT	+20%	4 + 2
127	EL 0.65	Nominal	+5%	0%	3 + 3	+21%	61 mT	+25%	4 + 2
146	EL 0.65	Nominal	+5%	0%	3 + 3	+18%	59 mT	+22%	4 + 2
147	EL 0.65	Nominal	+6%	-1%	3 + 4	+19%	60 mT	+22%	4 + 2
148	EL 0.65	Nominal	+6%	-1%	3 + 3	+20%	60 mT	+22%	4 + 2
173	EL 0.65	Nominal	+5%	0%	3 + 4	+17%	59 mT	+19%	4 + 2
174	EL 0.65	Nominal	+5%	0%	3 + 3	+18%	59 mT	+22%	4 + 2
175	EL 0.65	Nominal	+5%	0%	4 + 4	+17%	59 mT	+18%	4 + 2
176	EL 0.85	Nominal	+5%	0%	3 + 5	+18%	59 mT	+22%	4 + 2
177	EL 0.85	Nominal	+5%	0%	4 + 4	+18%	59 mT	+20%	4 + 2
178	EL 0.85	Nominal	+5%	0%	5 + 4	+18%	59 mT	+19%	4 + 2
179	EL 0.85	Nominal	+5%	0%	6 + 4	+17%	59 mT	+16%	4 + 2
184	EL 0.85	Nominal	+5%	0%	4 + 3	+17%	59 mT	+29%	2 + 2
185	EL 0.85	Nominal	+6%	0%	5 + 2	+19%	60 mT	+30%	2 + 2
186	EL 0.85	Nominal	+7%	0%	6 + 1	+21%	61 mT	+33%	2 + 2
187	EL 0.85	Nominal	+6%	0%	7 + 0	+25%	63 mT	+37%	2 + 2

* These values exceed the 33 MV/m maximum allowed value because the tuning acts on a cavity (#38) that is already working at 29 MV/m nominal conditions (this cavity is used for the transition matching between the two spoke sections).

Table 4. Beam losses for a quadrupole failure and for a doublet failure, and possible solutions to recover the beam

		Beam losses		After retuning (case of doublet failure)			
No. faulty quadrupole	**Section**	**Quadrupole failure**	**Doublet failure**	**No. of retuned quadrupole doublets**	**Beam losses**	**Transversal emittance growth**	**Longitudinal emittance growth**
1	Spoke 0.15	28%	0.33%	0 + 7	0.33%	More than 100%	More than 100%
2	Spoke 0.15	26%					
17	Spoke 0.15	18%	0.16%	3 + 3	0.02%	100%	10%
18	Spoke 0.15	22%					
35	Spoke 0.15	9.5%	0%	3 + 3	0%	20%*	-10%*
36	Spoke 0.15	12%					
37	Spoke 0.35	24%	0%	2 + 2	0%	66%*	-12%*
38	Spoke 0.35	22%					
55	Spoke 0.35	12%	0%	2 + 2 or 3 + 3	0%	12%	0%
56	Spoke 0.35	9%					
75	Spoke 0.35	7.5%	0%	2 + 2	0%	5%	0%
76	Spoke 0.35	6%					
77	Ellipt 0.47	0.3%	0%	3 + 3	0%	11%*	-2%*
78	Ellipt 0.47	1%					
89	Ellipt 0.47	3.5%	0%	2 + 2 or 3 + 3	0%	20%*	-10%*
90	Ellipt 0.47	3%					
103	Ellipt 0.47	0.6%	0%	2 + 2	0%	5%	0%
104	Ellipt 0.47	0.5%					
105	Ellipt 0.65	1%	0%	2 + 2	0%	7%	0%
106	Ellipt 0.65	1%					
121	Ellipt 0.65	0.5%	0%	2 + 2	0%	5%	0%
122	Ellipt 0.65	0.5%					
137	Ellipt 0.65	0%	0%	2 + 2	0%	5%	0%
138	Ellipt 0.65	0%					
139	Ellipt 0.85	0%	0%	3 + 1	0%	5%	0%
140	Ellipt 0.85	0%					
143	Ellipt 0.85	0%	0%	4 + 0	0%	5%	0%
144	Ellipt 0.85	0%					

* Emittance exchange in planes to coupling resonances.

failure in the middle of the $\beta = 0.35$ spoke section only leads to a beam loss of about 10%, while the beam loss induced by a quadrupole failure in the elliptical sections is always lower than 5%. Of course, in every case, the beam is strongly mismatched in the transverse planes from the failure position up to the linac end, but the induced longitudinal mismatch is very small, as expected.

The second interesting conclusion is that in the case of a quadrupole failure, the situation is clearly better if the other quadrupole of the doublet is also switched off (see Figure 6). As a matter of fact, the induced mismatching in that case is better balanced between the two transverse planes than if nothing is done. *It is thus recommended to switch off the whole doublet if one quadrupole fails*.

Finally, with an adequate retuning of surrounding quadrupole doublets, it is possible to rematch the beam to the linac and obtain beam envelopes very similar to those of the nominal case. The situation is a bit more complicated in the very low energy section where we did not succeed in recovering a 100% transmission; the situation should probably be improved by including the MEBT quadrupoles (not modelled in the present study) in the matching procedure.

Figure 6. Beam envelopes in the 5 MeV-600 MeV XADS linac

Upper left – failure of quadrupole #75 (no correction), upper right – whole doublet is off (no correction), lower left – the four surrounding doublets are retuned

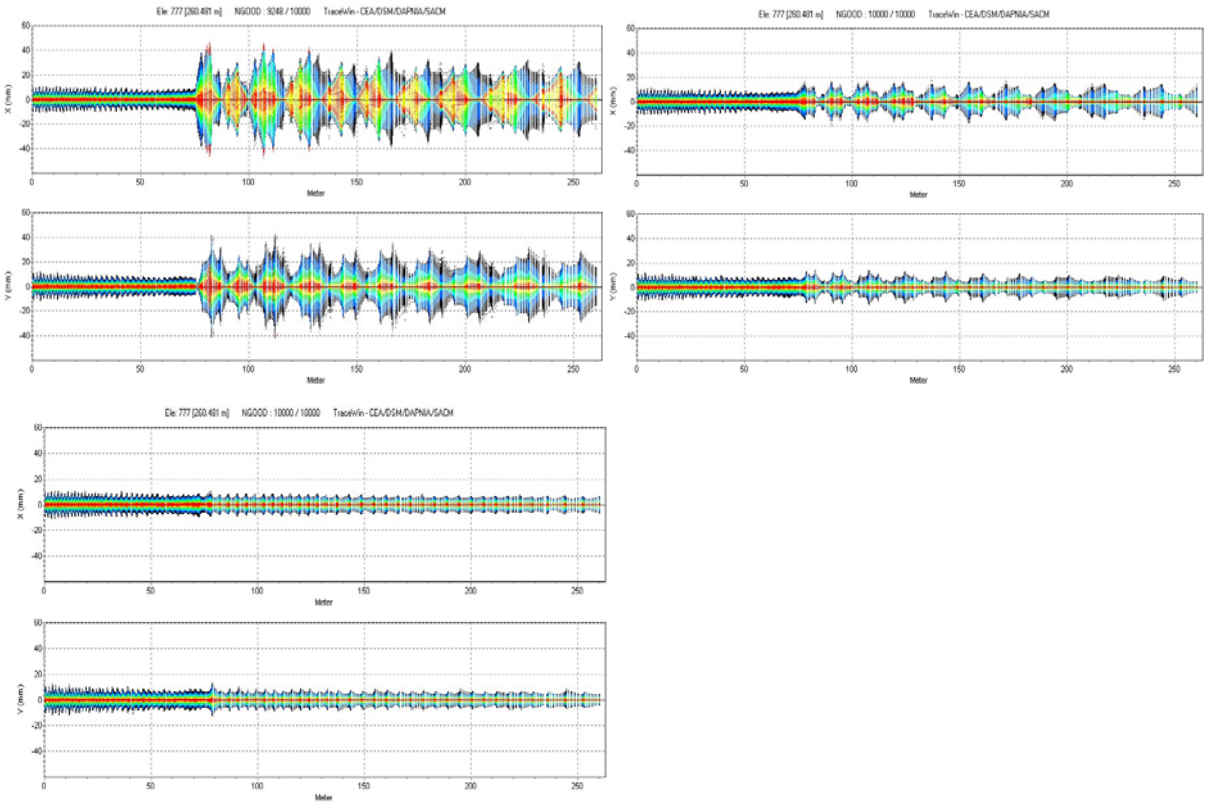

Conclusion and preliminary considerations for a full transient analysis of the problem

The systematic analysis performed to evaluate the fault tolerance capability of the XADS superconducting linac leads to the following conclusions:

- If a cavity fails and if nothing is done, the beam is (almost) always completely lost.
- If a cavity fails and if an appropriately rapid local compensation is done (retuning of a few surrounding cavities field and phase plus adjustment of a few quadrupoles gradients if needed), the nominal beam parameters at the target can be restored.
- If a quadrupole fails, it is advisable to switch off the whole doublet to limit the beam losses along the accelerator. For power supply failures it is thus convenient to power both quadrupoles in the doublet by a single power supply. The nominal beam parameters at the target can generally be restored by readjusting a few surrounding quadrupole gradients.
- The situation is substantially more difficult in the low-energy section of the linac (< 10 MeV).

This analysis is anyway not complete because it only takes into account the beam behaviour before the failure, and in the steady state after the local compensation. The remaining part of the problem consists now in the analysis of the transient state, assuming the beam is not switched off at

the source during the fault compensation procedure, and in optimising the way the retuning procedure is carried out in order to minimise the possible integrated beam losses during these transients. In particular, this study will have to establish if, in case of a cavity fault, both RF and beam have to be switched off before re-starting (approach no. 1), or if RF has to be maintained while micro-switching the beam (approach no. 2).

Full analysis of the problem will really start in the 6th Framework Programme with the development of a new simulation code coupling both beam dynamics and RF feedback loop calculations. A first approach of such a "transient analysis" tool is summarised in Figure 7. R&D activities concerning superconducting cavities, to definitely demonstrate performances that ensure the "over-design" criteria necessitated by the reliability requirement, and on the development of adequate digital LLRF systems are also foreseen [12].

Figure 7. Proposed approach for a full transient analysis of the local compensation procedure

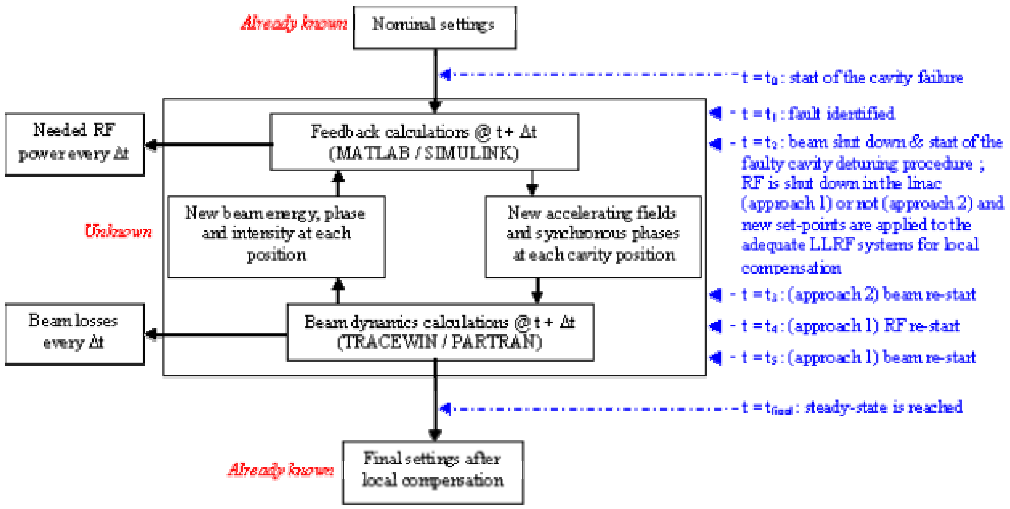

REFERENCES

[1] Rubbia, C., *et al.*, A *European Roadmap for Developing Accelerator Driven Systems (ADS) for Nuclear Waste Incineration*, published by ENEA, ISBN 88-8286-008-6, Rome (2001).

[2] Carluec, B., "The European Project PDS-XADS", *InWor for P&T and ADS Workshop*, Mol, (2003).

[3] D'hondt, P., "European XADS-PDS", these proceedings.

[4] Mueller, A.C., "The PDS-XADS Reference Accelerator", *InWor for P&T and ADS Workshop*, Mol (2003).

[5] Van de Plassche, D., *et al.*, "The PDS-XADS Reference Accelerator", these proceedings.

[6] Safa, H., “Design of a XADS Linear Accelerator”, *InWor for P&T and ADS Workshop*, Mol (2003).

[7] Pierini, P., “Reliability Studies of the PDS-XADS Accelerator”, *InWor for P&T and ADS Workshop*, Mol (2003).

[8] Pierini, P., “ADS Reliability Activities in Europe”, these proceedings.

[9] See, e.g. Nicolas Pichoff and Didier Uriot, “New Implement in TraceWin/PARTRAN Codes: Integration in External Field Map”, *PAC’2003*, Portland (2003).

[10] Pichoff, N., H. Safa, “Reliability of Superconducting Cavities in a High-power Proton Linac”, *EPAC’2000*, Vienna (2000).

[11] Junquera, T., “Status and Perspectives of the R&D Programs for the XADS Linear Accelerator”, *InWor for P&T and ADS Workshop*, Mol (2003).

HIGH-ENERGY BEAT TRANSPORT LINES AND DELIVERY SYSTEM FOR INTENSE PROTON BEAMS

P.A. Schmelzbach
PSI, Switzerland

No paper was available at the time of publication.

CONSTRUCTION OF A FFAG COMPLEX FOR ADS RESEARCH IN KURRI

Minoru Tanigaki, Kaichiro Mishima, Seiji Shiroya
RRI, Kyoto University, Kumatori, Osaka 590-0494, Japan

Yoshihiro Ishi, Shintaro Fukumoto
Mitsubishi Electric Corporation, Kobe, 652-8555, Japan

Shinji Machida, Yoshiharu Mori
KEK, Tsukuba, Ibaragi 305-0801, Japan

Makoto Inoue
SLLS, Ritsumeikan University, Kusatsu, Shiga 525-8577, Japan

Abstract

The Kumatori Accelerator-driven Reactor Test project (KART) was undertaken at Kyoto University Research Reactor Institute (KURRI) as of fiscal year 2002, with the aim to demonstrate the basic feasibility of ADS and to develop a 150-MeV proton Fixed-field Alternating Gradient (FFAG) accelerator complex as a neutron production driver. This FFAG complex will be connected with the Kyoto University Critical Assembly (KUCA) for basic ADS experiments by the end of March 2006.

Introduction

As a substitute for the 5-MW reactor at Kyoto University (KUR), a neutron source based on the ADS concept was proposed in 1996 [1]. The conceptual design study on ADSR using the MCNPX code clarified the lack of reliable effective multiplication factor k_{eff} in the proton energy region between 20 MeV and 150 MeV. Since the experimental studies in our institute were performed using KUCA and a 300-keV Cockcroft-Walton accelerator [2,3], a proton beam source which covers between 20 MeV and 150 MeV is required to extend our study on ADS.

The requirements towards proton sources for ADS are: 1) high beam intensity, 2) highly efficient power consumption and 3) high stability during operation. The FFAG accelerator, originally proposed by Ohkawa 40 years ago [4], is regarded as a good candidate as the proton driver for ADS. Because of its fixed magnetic field, the high repetition rate of beam acceleration and the greatly reduced power consumption in the accelerator engendered by the introduction of a superconducting magnet are expected. Despite such attractive features, no FFAG with RF has yet been realised until recently, except electron models, due to technical difficulties such as the production of a wide-band high-voltage RF cavity or the lack of long straight sections for beam injection and extraction. Recently, Mori, *et al*. developed a wide-band RF cavity with FINEMET [5] and succeeded in the first acceleration of proton with a 500-keV PoP FFAG synchrotron [6]. They have now developed a "return-yoke free" magnet for the 150-MeV FFAG synchrotron [7] in which they try to extract the beam from the FFAG for the first time.

On the basis of our study and the technical developments concerning FFAG, the KART project was approved and commenced as of fiscal year 2002. In this project, the basic feasibility of ADS and the multiplication factor k_{eff} in the energy region of $E_p = 20 \sim 150$ MeV will be studied. Another important aim in this project is to develop a practical FFAG accelerator as a proton driver for ADS.

FFAG accelerator complex

In the KART project, a FFAG accelerator complex is now under construction as the proton source for ADS study. This complex consists of one FFAG with an induction unit for acceleration as the injector and two FFAGs with RF as the booster and main accelerators, respectively. All of these accelerators will be in pulse operation at the repetition rate of 120 Hz. A schematic diagram of our FFAG complex is shown in Figure 1. Basic specifications for this FFAG complex are summarised in Table 1. The layout of these FFAG accelerators in the accelerator room is shown in Figure 2.

Figure 1. Schematic diagram of FFAG complex at KURRI

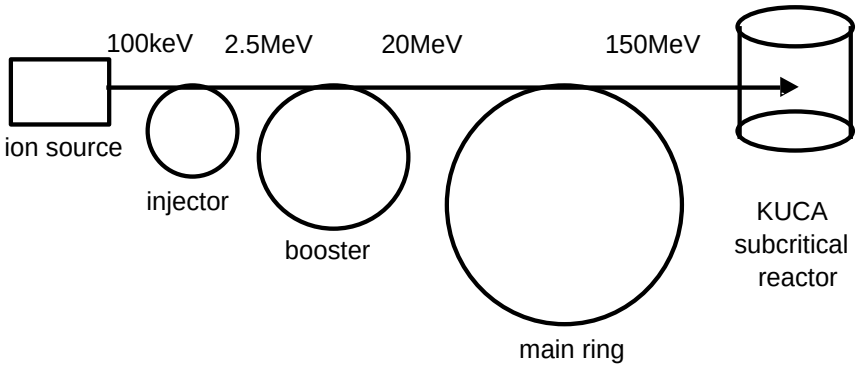

Table 1. Specifications of the FFAG complex

	Injector	Booster	Main
Focusing	Spiral	Radial	Radial
Acceleration	Induction	RF	RF
k	2.5	4.5	7.6
E_{inj}	100 keV	2.5 MeV	20 MeV
E_{ext}	2.5 MeV	20 MeV	150 MeV
p_{inj}/p_{ext}	5.00	2.84	2.83
r_{inj}	0.60 m	1.42 m	4.54 m
r_{ext}	0.99 m	1.71 m	5.12 m

Figure 2. FFAG complex at KURRI

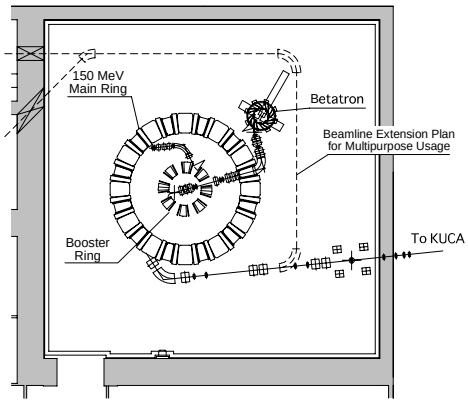

Figure 3. The schematic diagram of the FFAG complex at KURRI

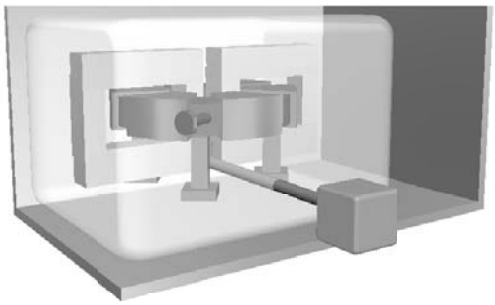

H^+ ions are produced in a typical multi-cusp type ion source, then extracted and accelerated to 100 keV. Since all of the FFAG complexes are operated in pulse mode, the beam is bunched by an electrostatic beam chopper in the transport line.

In the present FFAG complex, a 2.5-MeV FFAG with an induction unit for acceleration is used as the injector. This FFAG has 12 sprial sector magnets with a spiral angle of 42°. A typical pattern of induced acceleration voltage is shown in Figure 4. In this operation pattern, the compression of injected beam pulse is achieved by the abrupt increase of induced electric field. In the current plan, the beam pulse ejected from the injector is compressed to 5 μs; it was originally 50 μs.

Figure 4. Acceleration pattern of the FFAG injector

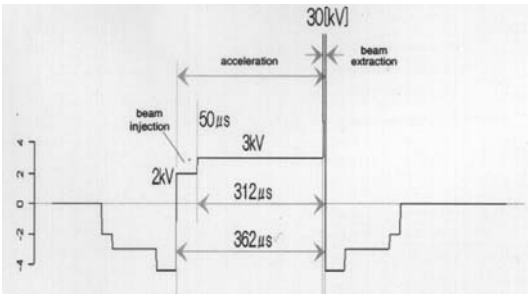

The beam from the FFAG injector at the energy of 2.5 MeV is then accelerated up to 20 MeV in this booster ring. This FFAG synchrotron is the radial sector type, consisting of eight cells of DFD magnets. The lattice structure of this booster ring is shown in Figure 5. These magnets are "return-yoke free" magnets with a flat pole face, and each magnet has 22 trim coils placed along the r direction to produce the magnetic field following the function of $B = B_0 (r/r_0)^k$. The advantage of using trim coils is that one can easily change k by choosing a proper current set to trim coils, which is an important characteristic for the variable-energy FFAG accelerators. A 2-D simulation of a FFAG magnetic field calculated by POISSON is shown in Figure 6.

Figure 5. Lattice structure of the booster ring

Green and blue lines are the beam orbits corresponding to r_{inj} and r_{ext} , respectively

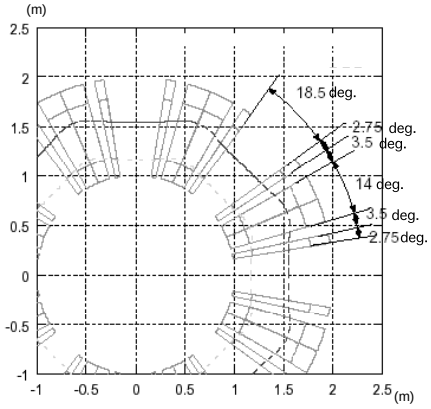

Figure 6. A typical 2-D simulation of magnetic field for the magnet in the booster ring

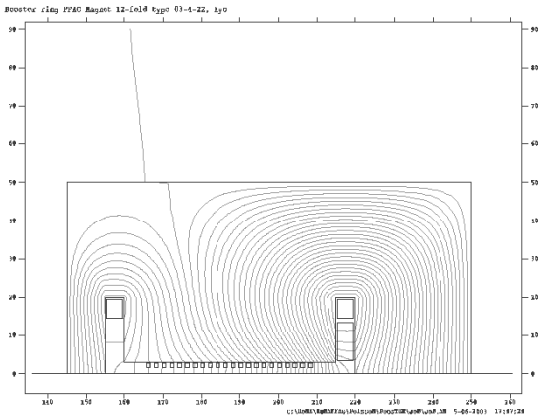

The main accelerator is identical to the 150-MeV FFAG synchrotron which is now being tested at KEK [7], with the exception of some modifications to achieve the high repetition rate in the acceleration in the current FFAG complex. Two RF cavities are placed in the main ring to compensate the low acceleration voltage (~10 kV) from the wideband RF cavity. This is because we must complete the acceleration of the injected beam bunch from the booster within each repetition period of ~100 μs. Another difference is in the magnets, i.e. the cross-section of return yoke and the purity of iron are increased to accept a high magnetic flux required for 200-MeV acceleration, expecting a beam energy upgrade through the reinforcement of power supplies in the near future.

Beam injection and extraction

The advantage of the FFAG accelerator is its fast acceleration and high repetition rate due to its fixed magnetic fields. Therefore, a beam injection and extraction fast enough to follow up such a high repetition rate is required in the practical FFAG accelerator. Detailed discussion on the beam injection and extraction for the 150-MeV FFAG synchrotron has already been made by Aiba, *et al*. [8], and the fast beam extraction with kicker and septum magnets will be employed both in the booster and main accelerators. In the case of FFAG betatron, kicking out of the beam is achieved by producing an abrupt increase in the magnetic field at the induction core.

Such RF signals can easily be produced by a signal generator (SG) based on DSP, in which the waveform itself can be programmed as much as the memory in the SG allows. A typical example of a RF signal generated by Tektronix AWG420 is shown in Figure 7.

Figure 7. a) A typical RF sweep pattern of the booster and main rings in the current FFAG complex. b) An example of RF outputs from Tektronix AWG420 programmed to follow the RF sweep pattern shown in a).

In b), blue and violet waves are the RF signals and the yellow gate signal shows the desired in-phase timing. In this case, both RF signals are programmed to have the same phase of 0° on a desired timing.

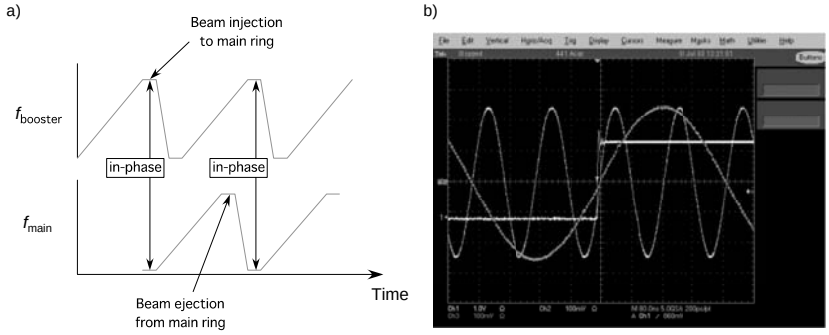

Current status and future prospects

The construction of the building for the FFAG complex, designated as the “Innovation Research Laboratory” will be completed at the end of March 2004. This building is designed not only for the FFAG accelerator complex, but also for multi-purpose usage of the beam from the FFAG complex, including nuclear physics, chemistry, material science and cancer therapy.

The FFAG complex itself will be constructed in the fall of 2004. The first beam from this FFAG complex is expected by the end of March 2005. Basic studies on ADS will be employed just after the beam line between the FFAG complex and KUCA will be ready, expected by the end of March 2006.

REFERENCES

[1] Kawase, K. and M. Inoue, "Neutron Factory Project at KURRI", *APAC 1998*, Tsukuba, Japan, p. 104.

[2] Shiroya, S., H. Unesaki, *et al*., "Neutronics of Future Neutron Source Based on Accelerator Driven Subcritical Reactor Concept in Kyoto University Research Reactor Institute (KURRI)", *Int. Seminar on Advanced Nucl. Energy Systems Toward Zero Release of Radioactive Wastes, 2nd Fujiwara Int. Seminar*, 6-9 Nov. 2000, Shizuoka, Japan, *Abstracts*, p. 58.

[3] Shiroya, S., H. Unesaki, *et al*., *Trans. Am. Nucl. Soc., 2001 Annual Mtg*., 17-21 June 2001, Milwaukee, Wisconsin, p. 78.

[4] Mori, Y., *et al*., "A New Type of RF Cavity for High Intensity Proton Synchrotron Using High Permeability Magnetic Alloy", *EPAC 1998*, p. 299.

[5] Aiba, M., *et al*., "Development of a FFAG Proton Synchrotron", *EPAC 2000*, Vienna, Austria, p. 581.

[6] Adachi, T., *et al*., "A 150 MeV FFAG Synchrotron with "Return-yoke Free" Magnet" *PAC 2001*, Chicago, IL, USA, p. 3254.

[7] Aiba, *et al*., "Beam Injection and Extraction in 150 MeV FFAG", *EPAC 2002*, Paris, France, p. 1076.

IMPROVEMENT OF RELIABILITY OF THE TRASCO INTENSE PROTON SOURCE (TRIPS) AT INFN-LNS

G. Ciavola, L. Celona, S. Gammino, L. Andò, M. Presti,
A. Galatà, F. Chines, S. Passarello, XZh. Zhang
Istituto Nazionale di Fisica Nucleare – Laboratori Nazionali del Sud, Italy

M. Winkler
GSI, Germany

R. Gobin, R. Ferdinand
CEA/Saclay, France

J. Sherman
LANL, USA

Abstract

Over the past two years, INFN-LNS has undertaken to improve the source reliability for high-power proton accelerators. A full set of magnetic field measurements has been carried out to define a different design of the TRIPS magnetic system, based on permanent magnets, in order to increase the reliability of the source devoted to the ADS. The OPERA-3D package was used to design the new magnetic system as a combination of three rings of NdFeB magnets and soft iron in between. The description of the magnetic measurements and the comparison with the simulations are presented, along with the design of a new version of the source, called PM-TRIPS. Finally the new low-energy beam transfer line (LEBT) will be described, with particular regard to the improvement of accelerator availability, which can be obtained with the installation of two PM-TRIPS sources or more on a switching magnet.

The TRIPS proton source

The *TRA*smutazione *SCO*rie (TRASCO) project is an R&D programme whose goal is the design of an accelerator-driven system (ADS) for nuclear waste transmutation. The high-current CW proton linear accelerator will drive a subcritical system devoted to the transmutation of nuclear wastes [1]. The scheme of the whole accelerator is shown in Figure 1; it consists of a high-intensity proton source that provides the beam to a high-energy linac made up of an RFQ [2], and medium and high accelerator sections. The final goal is the complete a conceptual design of the linac up to energies greater than 1 GeV for a nominal proton current of 30 mA [3]. The accelerator design is carried out by different INFN laboratories and the LNS is in charge of the source design and construction.

Figure 1. The TRASCO accelerator scheme

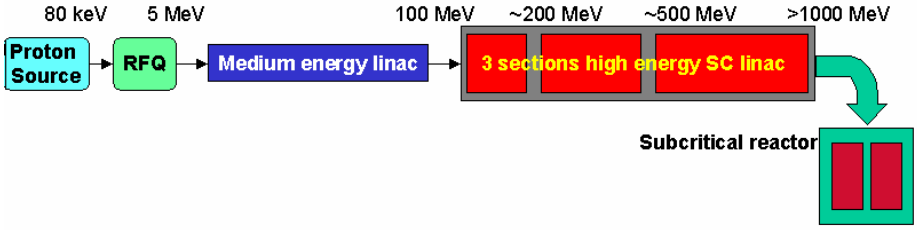

The *TR*asco *I*ntense *P*roton *S*ource (TRIPS) is a high-intensity microwave source whose goal is the injection of a maximum proton current of 35 mA in the following RFQ, with a RMS normalised emittance lower than 0.2 p mm mrad; the operating voltage is 80 kV.

With respect to other sources for high-intensity applications, some new features have been added, according to the experience gained by the LNS Ion Source R&D Team with the high-intensity SILHI [4] source and with the high-efficiency MIDAS source [5]. The microwave matching system has been improved, an on-line movable coils system has been realised, and the extraction system has been optimised with the aim to increase the source availability and reliability in order to meet the requirements of the ADS driver.

The final design of TRIPS is shown in Figure 2, along with a photo of TRIPS on the 100-kV platform. The plasma is created by a 2.45-GHz, 2-kW magnetron coupled to the cylindrical water-cooled OFHC copper plasma chamber (100 mm long and 90 mm in diameter) through a circulator, a four-stub automatic tuning unit and a maximally flat matching transformer [6]. The transformer optimises the coupling between the microwave generator and the plasma chamber. It realises a progressive matching between the waveguide impedance and the plasma impedance, thus concentrating the electric field at the centre of the plasma chamber and increasing the proton fraction and the current density, which arrives up to 200 mA/cm^2, i.e. near the Child-Langmuir limit. A detailed description of TRIPS is given in Ref. [7]. The experimental set-up consisted at the beginning of a straight low-energy beam transfer line (LEBT) and only in 2003 did we installed a bending magnet in order to have a H^+ beam without contaminants.

Measurements of the beam emittance and space-charge compensation have been carried out with an emittance measuring unit (EMU) and a four-grid analyser (FGA) kindly provided by CEA, Saclay.

The measurements confirmed the computer code simulations, showing that the typical emittance of the source is between 0.07 p and 0.2 p mm mrad for currents between 30 and 50 mA (6-mm extraction hole). Our efforts were focused on the optimisation of the beam transport through the 30° dipole magnet, by changing some key parameters such as the puller voltage, the solenoid current and the RF power in order to minimise the beam aberrations and the space-charge effect.

Figure 2. The TRIPS ion source design and a photo of the source

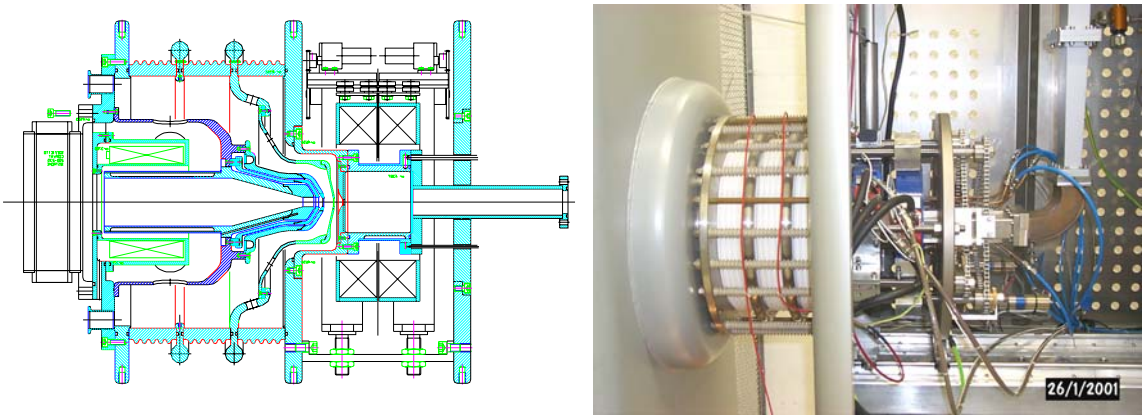

Finally, we also checked the influence of beam line pressure on the space-charge compensation by using both the FGA and the EMU and injecting a controlled amount of nitrogen into the beam line, as had already been done with the SILHI source for different gases [8].

Figures 3 and 4 show the experimental set-up used in the measurements reported on here, with the EMU on the 0° branch and 30° branch, respectively. In the latter case we investigated both horizontal and vertical emittance (Figure 5). The section of the LEBT before the 30° dipole magnet consists of a direct-current current transformer (DCCT 1), a focusing solenoid, a four-sector ring to measure beam misalignments and a second current transformer (DCCT 2).

Figure 5 shows that the emittance does not change significantly in absolute values in the three situations, remaining around 0.14 p mm mrad for a 30-mA beam.

The normalised emittance decreases by putting the N_2 gas in the beam line, as shown in Figure 6; in fact we measured 0.148 p mm mrad with the N_2 and 0.185 mm mrad without N_2.

Figure 3. The low-energy beam transfer line with the emittance measurement unit on the 0° line

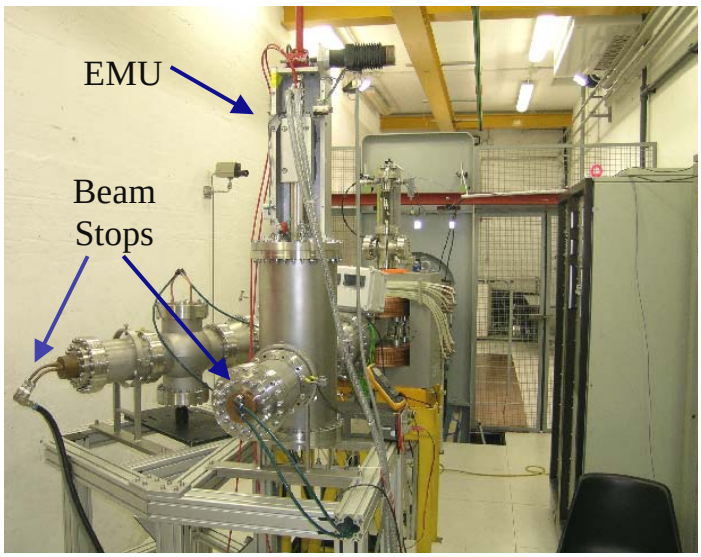

Figure 4. Emittance measurement unit on the 30 line (vertical and horizontal position)

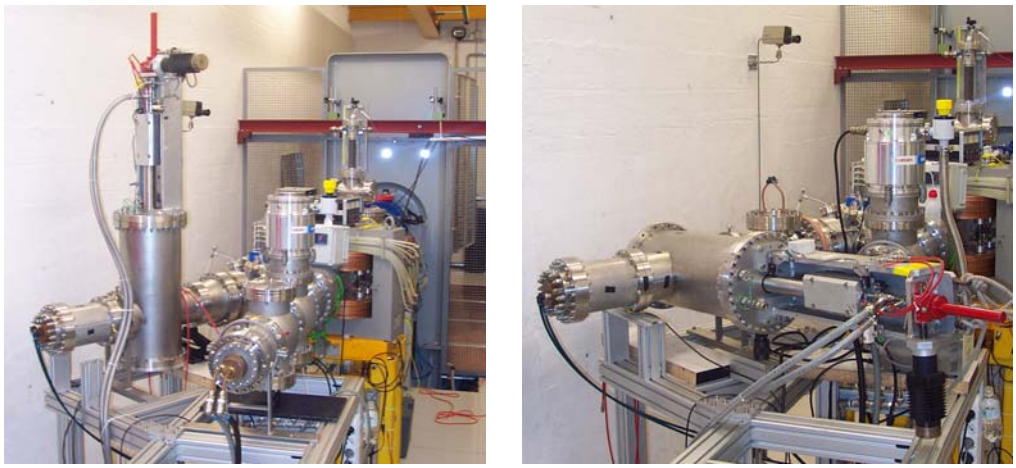

Figure 5. The proton beam emittance measured with: V_{extr} = 80 kV, I_{beam} = 30 mA respectively (from the left) on the 0° line, on the 30° line horizontally and vertically (e_{rms} » 0.14 p mm mrad)

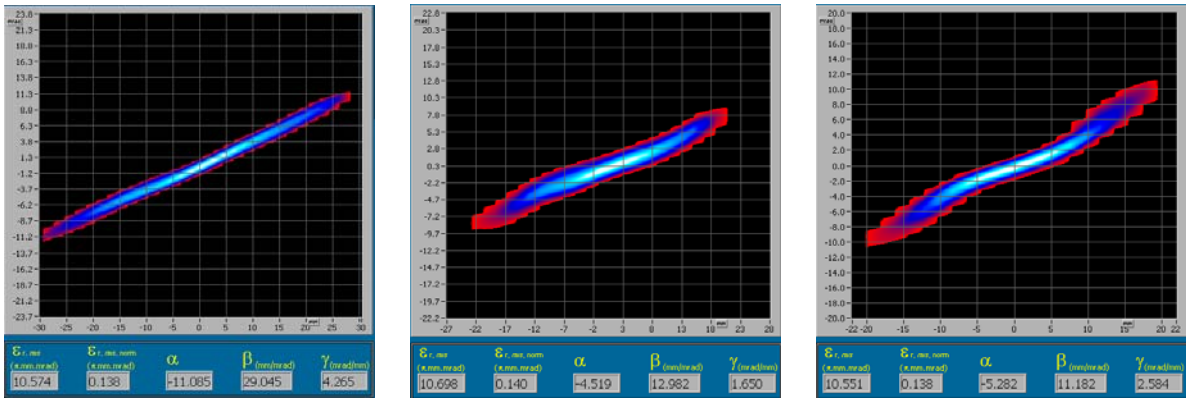

Figure 6. The RMS normalised emittance with and without N_2 in the 30° line with the EMU in horizontal position for beam current of 35 mA

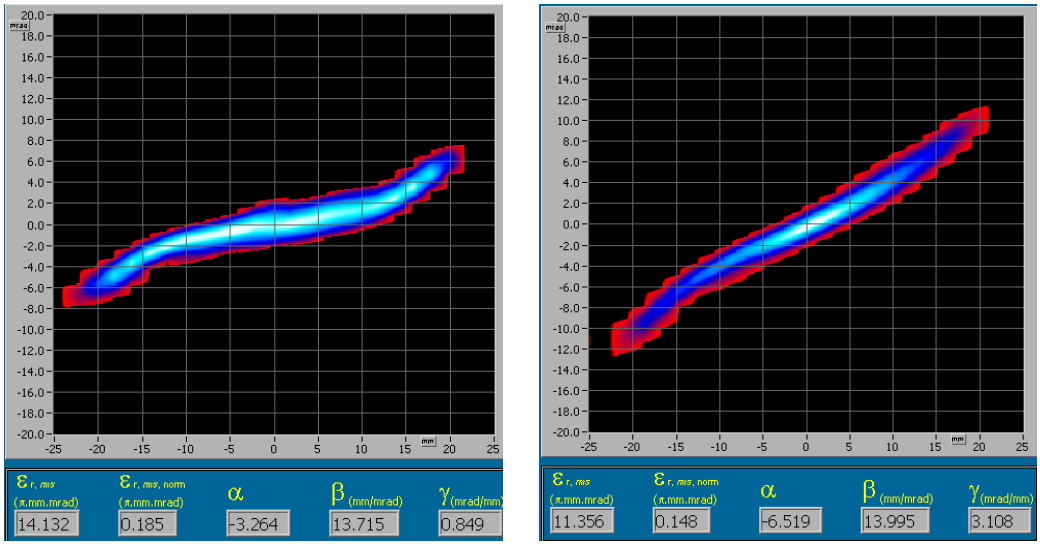

Comparing our measurements with those reported in [9], we also observed a little growth of the emittance because of the longer LEBT; in fact we passed from 0.138 p mm mrad to 0.156 p mm mrad with the RF power at 550 W and I_{sol} = 260 A.

The beam compensation was also measured, and it is always above 90% except for the case of a narrow beam close to the FGA, which was observed for a small range of solenoidal field between 240 and 260 A over 500 A. The measurements of proton fraction also provided satisfactory results, with values above 70% for beam power above 700 W (Figure 7).

Figure 7. The proton fraction vs. the RF power for a 80-keV, 35-mA proton beam

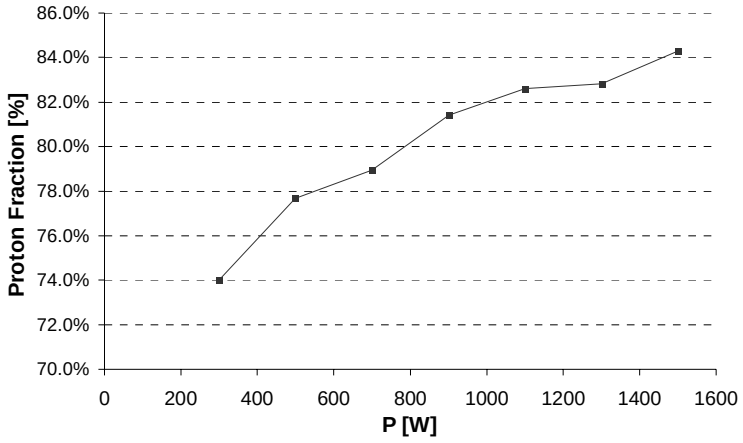

TRIPS reliability

The reliability is so crucial for the ADS driver that stringent requirements were demanded of the injector. In fact, beam availability close to 100% for long-term operations is mandatory for ADS purposes.

Such a value has not yet been achieved, but an encouraging value of 99.8% has been achieved on a long run test lasting over 142 h (see Figure 8). During the test two types of sparks were recorded:

- Sparks that caused the interruption of source operations and required about two minutes to manually recover the beam at full intensity. Automatic recovery is under development.

- Sparks that are immediately recovered by the automatic procedures already implemented (the down-time is practically absent).

Two sparks of the first type and four sparks of the second type occurred, for a total of 99.8% reliability. The source did not require any particular tuning operations, except for slight variations of the hydrogen pressure in the plasma chamber. This parameter has a strong influence on the beam current stability, along with the discharge power. For this reason, feedback procedures have been implemented in the new control system and they are in the debugging phase.

Other than the high-voltage column and gas feedback, no other critical component was observed, with the exception of the microwave window, which may be changed once per 3 000 or 5 000 hours in order to prevent a vacuum breakdown which may stop the source for 24-48 hours.

Figure 8. The reliability test over 142 hours (reliability was 99.8%)

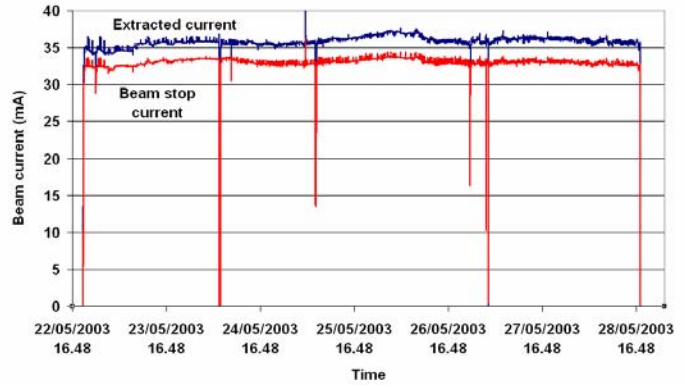

The optimum magnetic field and the PM-TRIPS design

In order to simplify the source and to increase the reliability of the injector, the construction of an optimised source called PM-TRIPS has been carried out.

The main modifications concern a simplification of the extraction geometry and of the extraction column, along with the replacement of the movable coils and power supplies with permanent magnets. This permits to avoid the use of a high voltage platform and of the insulation transformer, as the gas pipe and the microwave line will be insulated on their own. All the devices will be at ground potential except for the plasma chamber and the permanent magnets, which will make easier and more reliable the computer control of the source itself.

Figure 9 shows the design of PM-TRIPS compared with that of TRIPS. The plasma chamber and the microwave line are equal to the one used on TRIPS. The overall source dimensions are smaller due to a compact extraction system.

Figure 9. Comparison between TRIPS (left) and PM-TRIPS (right)

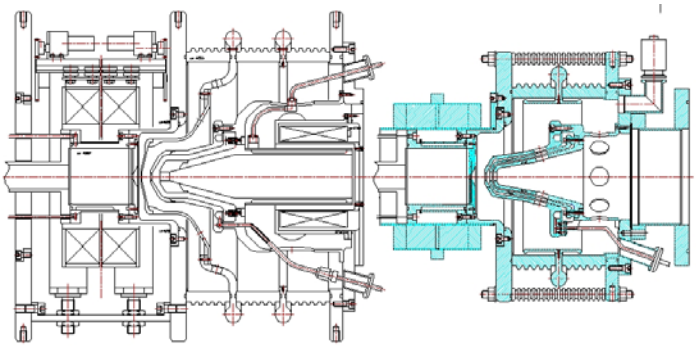

The extraction geometry was studied with the AXCEL code; with respect to the TRIPS source the extraction system was simplified by employing only four electrodes instead of five.

The five-electrode topology was chosen for TRIPS as it allows the on-line optimisation of the extracted beam and it is certainly important if the same source should work at a different current value. However, for a source designed to work continuously around a fixed current value, such flexibility can be sacrificed without a loss in terms of beam emittance.

The four-electrode system consists of a plasma electrode, made of molybdenum, two water-cooled grounded electrodes made of copper and a negatively-biased screening electrode, also made of copper, inserted between the two grounded electrodes, in order to avoid secondary electrons due to residual gas ionisation, going backwards. The shape, the extraction holes and the gap widths were recalculated with a special care to further reducing the extraction zone length, where the beam is not compensated. The RMS normalised emittance calculated 10 cm from the extraction electrode is 0.05 p mm mrad, which is almost the same as that calculated at the same position for the five-electrode configuration. Figure 10 shows a trajectory plot assuming a beam current of 40 mA (90% proton, 10% H^{2+}) with a space-charge compensation of 98% after the second grounded electrode.

Figure 10. Trajectory plot of the PM-TRIPS extraction system (units in cm)

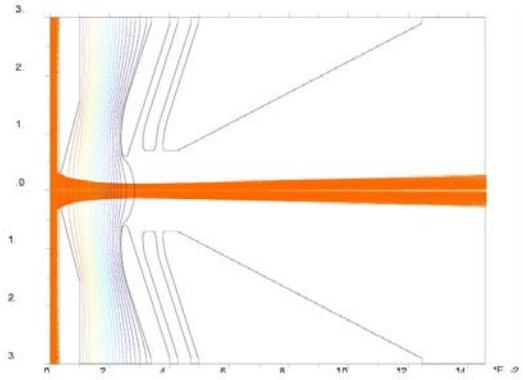

The other improvement consists of the optimisation of the permanent magnet system executing systematic measurements to obtain the best magnetic field profile for the TRIPS source by changing the coil positions and currents.

Figure 11 shows the beam current for different values of the coil current and position. From these measurements we concluded the following:

- The source is more sensible to variations of the extraction coil rather then to variations of the injection coil.
- The best performances are clearly obtained when the two ECR zones are located exactly on the BN disks, i.e. at the two ends of the plasma chamber.

Figure 11. The extracted current for different values of current and position of the two coils (the best operating point is represented by the dot)

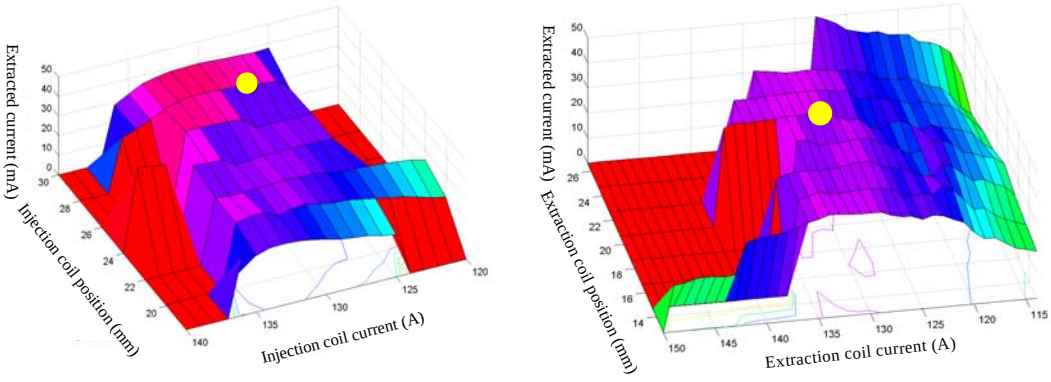

We modelled the PM-TRIPS magnetic system with the aim to reproduce such an optimum field by using soft iron and permanent magnets. The magnetic system consists of a set of three VACODYM 745 HR permanent magnets, packaged together with two soft iron spacers and supported by a stainless steel tube. A good agreement has been found between the ideal TRIPS magnetic field and the expected magnetic profile produced by the permanent magnets, as shown in Ref. [9], where a full description of the magnetic measurements is available and the TOSCA modelling is reported.

The PM-TRIPS and preliminary results

The magnets were delivered in April 2004 and were prepared for installation over the platform, in order to review the standard operation in the usual TRIPS environment before implementing a full HV insulation.

The magnetic field measurements were carried out with a special regard to the stray field over the extraction region which may generate a Penning discharge. The concern for the absolute values of the magnetic field inside the chamber was not so great; the plateau in Figure 11 shows that a change of few tens of Gauss may change the peak current only slightly.

A good agreement has been found between the experimental PM-TRIPS magnetic field profile and the field calculated with the OPERA code (Figure 12).

Figure 12. Comparison of optimised PM-TRIPS measured field with that calculated using OPERA

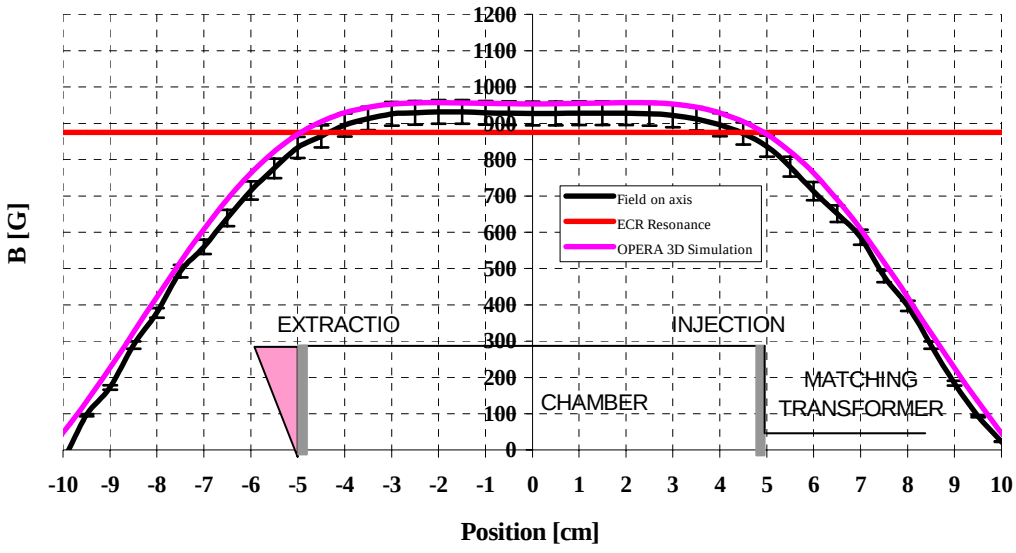

The plasma was easily ignited without high voltage for the beam extraction, and the vacuum featured regular behaviour; but as soon as the high voltage was set on, a Penning discharge occurred in the extraction column. Because of this, we decided to stop the source tests until an effective shielding of the stray field in the extraction region is obtained. A study with the TOSCA code was begun and the preliminary calculations show that an existing spare VACODYM ring with an additional iron ring may dump the unwanted field down to acceptable values. Our goal is to decrease the stray field below the value that was obtained with the coil system (a few hundred Gauss). Figure 13 shows the PM-TRIPS temporary test bench.

Figure 13. The PM-TRIPS source installed over the TRIPS platform

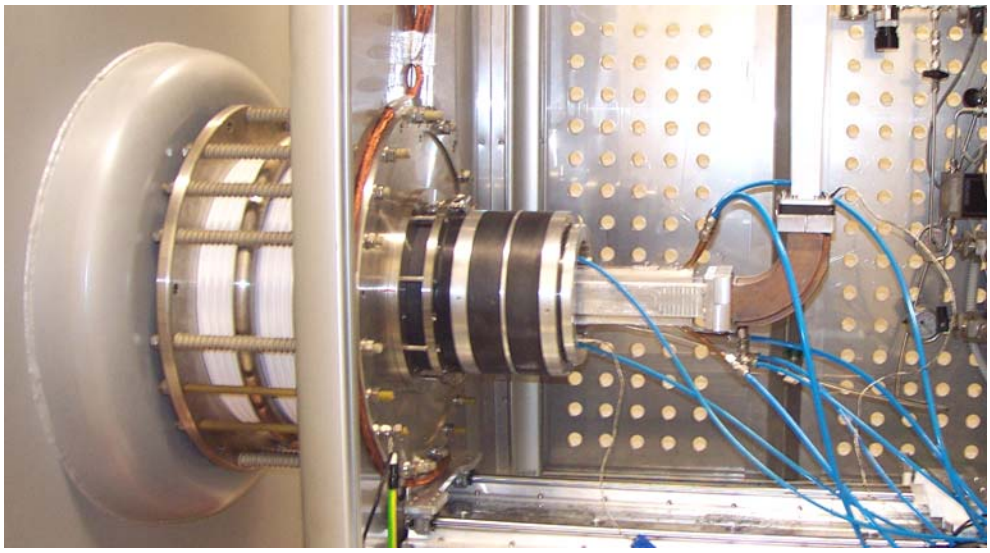

Low-energy beam transfer line (LEBT)

An important point for a further increase of the reliability in ADS plants is the redundancy of the sources. In fact, as the investment in the source is negligible with respect to the cost of the whole accelerator, the design of an injector with two sources working at the same time was considered, as shown in Figure 14. When a beam trip occurs the system would switch from one source to the other. This could be the solution to unexpected failures of the source in ADS plants. Such an operating mode could allow to schedule different periods of maintenance for each source while the other is working, thus permitting to provide the proton beam to the accelerator without interruption. Finally, the use of two sources in ADS plants is mandatory to maximise the mean time between failures (MTBF) and minimise the mean time to repair (MTTR).

Figure 14. The proposed injection scheme for ADS plants

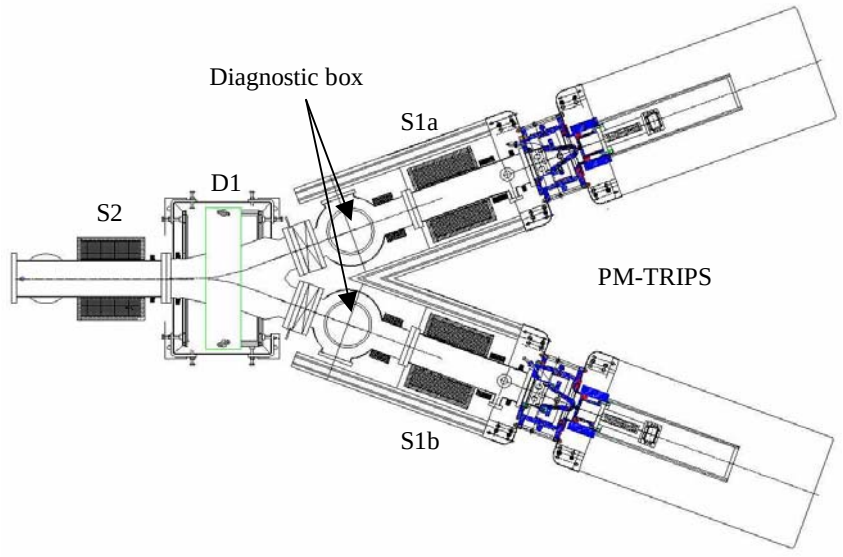

The system consists of two solenoids before and after a 20° dipole magnet. The length of the solenoids is 300 mm, but could be shortened, since in all calculations the magnetic field stayed well below 0.5 T. The dipole magnet was assumed to be rectangular; the beam enters the magnet under an angle of 20 , thus two sources can be coupled to the magnet. The overall length of the system is approximately 2.7 m.

Ion optical calculations were performed using the computer codes GICO and TRANSPORT. The initial phase space of the beam was assumed to be $x_0 = y_0 = -3$ mm and $a_0 = b_0 = -30$ mrad. Calculations were done for an H^+ beam, which is extracted with 80 kV voltage leading to a magnetic rigidity of approximately 0.041 Tm of the beam. Figure 15 shows the first-order beam envelopes in the x- and y-direction for a fully compensated beam (0-mA trace) and for a 35-mA proton beam with 85% of compensation (5-mA trace). It can be observed that an almost parallel transport is guaranteed for a relevant part of the LEBT and losses should be maintained low in such a manner. The separation between H^+ and H_2^+ is much larger than the dimensions of the two beams even in the presence of space-charge forces.

In both cases it is feasible to refocus the beam to a size of $x_{fin} \approx y_{fin} \approx -4$mm.

Figure 15. Layout of the PM-TRIPS beam transport line. First-order beam envelopes are drawn for an assumed uncompensated beam current of 0 mA (dashed lines) and 5 mA (solid lines), respectively.

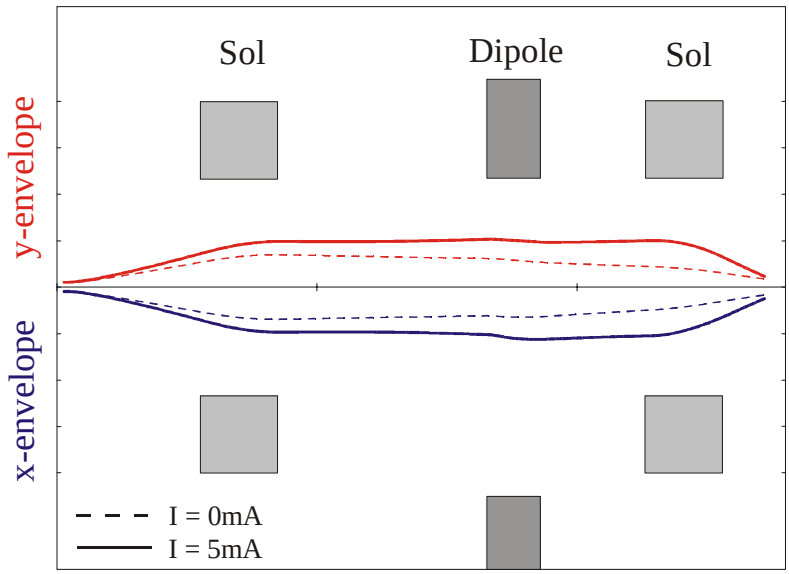

Mid-term perspectives

The TRIPS source fulfilled all the requirements of the TRASCO/ADS project in terms of beam intensity, reproducibility, emittance and stability except for the high requested reliability at 80 kV.

The new configuration with a bending magnet permits easier operation of the facility and will improve the overall reliability. Higher-order calculations will soon be carried out to investigate the appealing possibility offered by two, simultaneously available compact sources.

We plan to solve the stray field problem of PM-TRIPS by June 2004, and then start to characterise the source over the HV platform. Afterwards, a full characterisation in the new environment (with insulated waveguide and gas pipe) will be performed.

Extensive reliability tests will be undertaken before the displacement of PM-TRIPS to the Laboratori Nazionali di Legnaro of INFN, where the source will be installed in 2005.

REFERENCES

[1] Carminati, F., *et al*., CERN Report No. CERN/AT/93-47.

[2] Ciavola, G., *et al*., *Proc. 21st Int. Conf. on Linear Accelerators*, Korea (2002).

[3] *Status of the High Current Proton Accelerator for the TRASCO Program*, The TRASCO-AC Group, Report No. INFN/TC-00/23.

[4] Gobin, R., *et al*., *Rev. Sci. Instrum*., 75(5) (2004).

[5] Celona, L., *et al*., *Proc. of 7th Eur. Part. Acc. Conf*., Wien, 1601 (2000).

[6] Celona, L., *et al*., *Rev. Sci. Instr*., 69(2), 1113 (1998).

[7] Ciavola, G., *et al*., *Rev. Sci. Instr*., 73(2), 1030 (2002).

[8] Beauvais, P-Y., *et al*., *Rev. Sci. Instr*., 71(3), 1413 (2000).

[9] Celona, L, *et. al*, *Rev. Sci. Instrum*., 75(5) (2004).

AN IMPROVED SUPERCONDUCTING ADS DRIVER LINAC DESIGN

R.W. Garnett, F.L. Krawczyk, G.H. Neuschaefer
Los Alamos National Laboratory, Los Alamos, New Mexico

Abstract

In this paper we discuss recent work to further improve our superconducting (SC) ADS driver linac design. Our design assumes use of the 6.7-MeV LEDA RFQ as an injector to the SC driver linac. We have examined the feasibility of accelerating a 20-mA CW beam to 600 MeV using only 350-MHz SC multi-spoke resonator cavities operating at 4 K. Replacing the 2 K, 700-MHz SC elliptical cavity sections with spoke resonators has several advantages, including reduced cryo-plant operating cost and an improved real-estate accelerating gradient due to the longer active lengths of the 350-MHz cavities. We discuss the details of the new design layout and beam dynamics simulations, including effects due to operational and alignment errors. Preliminary cavity modelling results for the proposed five-gap spoke resonators are also discussed. This accelerator design would be appropriate as a driver linac for applications such as waste transmutation, fusion materials testing, etc.

Introduction

In this paper we discuss the results of a feasibility study to design an ADS driver linac to accelerate a 20-mA CW beam to 600 MeV using only 350-MHz superconducting (SC) spoke resonator cavities operating at 4 K. This design work is primarily an extension of the final all-SC design completed for the Accelerator Production of Tritium (APT) Project [1] which was initially based on other previous work for APT/AAA [2,3]. Replacing the 2 K, 700-MHz SC elliptical cavity sections with spoke resonators has several advantages including reduced cryo-plant operating cost and an improved real-estate accelerating gradient due to the longer active lengths of the 350-MHz cavities. We discuss the details of the new design layout and beam dynamics simulations, including beam matching, and effects due to operational and alignment errors. Preliminary cavity modelling results for the five-gap resonators to be used in the high-energy section of the linac are also discussed.

Design details

Our superconducting (SC) linac design is based on the APT design discussed in Ref. [1] with the replacement of the $\beta = 0.48$ and $\beta = 0.64$ elliptical SC cavities with five-gap (four-spoke) spoke resonator cavities. The $\beta = 0.82$ section of the linac has been eliminated due to the reduced final beam energy of 600 MeV. In this example design we have used SC solenoids inside each cryomodule for transverse focusing instead of transitioning to room-temperature doublets at high energy as was done for APT. Table 1 gives the linac parameters for this design. Figure 1 shows schematic layouts of the cryomodules for each section along with the present RF configuration. A detailed layout of the cryomodule was completed in an earlier study [4]. The cryomodule parameters determined from that study are assumed here also.

Specific phase and accelerating gradient ramps are used to adiabatically capture the Low-energy Demonstration Accelerator (LEDA) RFQ beam [5] and to make the transitions from section-to-section as current insensitive as possible. These ramps have been modified from our previous design in order to match between the newly introduced spoke cavity sections. As can be seen in Figure 1, in Section 1 it has been assumed that each cavity is driven by a separate RF generator. In the other sections, two or three cavities will be driven per RF generator. For these sections it is assumed that the phases can be set individually for each cavity, however, each set of cavities driven by a single RF generator must receive the same power (split equally).

Just as in our previous design, it is assumed that Sections 1 and 2 will be powered by commercially available inductive output tubes (IOTs). However, the power required per cavity in Sections 3 and 4, assuming 20-mA operation and the selected accelerating gradients, exceeds the operating limits of all presently available IOTs. As a result, klystrons will be used to provide RF power to these cavities. The maximum power required for a cryomodule is 408 kW for Section 3 and 560 kW for Section 4. Figure 1 presently shows a three-way split between cavities in these cryomodules. This is naturally based on the total number of cavities in each section being divisible by three. However, a four-way split could save substantial RF system costs (25-33%) and still allow a conservative operating margin for the klystrons [6].

Figure 2 shows the synchronous phase ramping used in our design. Figures 3 and 4 show the transit-time factor and E_0T, respectively, as a function of beam energy along the linac. Figures 5 and 6 show the transverse and longitudinal zero-current phase advances per period and per unit length for this design.

Table 1. SC linac design parameters

	Section 1	Section 2	Section 3	Section 4	Total
Structure type	Two-gap spoke	Three-gap spoke	Five-gap spoke	Five-gap spoke	
Frequency (MHz)	350	350	350	350	
Cavity geometric beta	0.175	0.34	0.48	0.64	
Cavity bore radius (cm)	2.5	3.0	3.0	3.0	
L-cavity (active) (m)	0.100	0.333	0.826	1.100	
L-cavity (physical) (m)	0.200	0.433	1.101	1.371	
L-magnet-to-cavity (m)	0.300	0.300	0.300	0.300	
L-magnet (m)	0.150	0.150	0.250	0.400	
L-warm-to-cold-1 (m)	0.394	0.394	0.394	0.394	
L-warm-to-cold-2 (m)	0.419	0.419	0.419	0.419	
L-warm-space (m)	0.300	0.300	1.413	1.413	
L-cryomodule (m)	4.226	6.624	5.266	6.226	
L-cryoperiod (m)	4.526	6.924	6.679	7.639	
L-focusing period (m)	2.263	3.462	6.679	7.639	
Cav/cryomodule	4	6	3	3	
Cav/section	80	36	21	39	176
No. of cryomodules	20	6	7	13	46
DW/cav (MeV)	0.08-0.64	0.48-2.11	4.20-6.81	8.81-9.33	
Synchronous phase ( )	-45 to -32	-32 to -28.4	-28	-28	
E_0T (MV/m)	1.13-7.51	1.71-7.50	4.63-7.50	7.28-7.71	
Win, section (MeV)	6.70	43.12	112.01	239.30	
Wout, section (MeV)	43.12	112.01	239.30	600.03	
DW/section (MeV)	36.42	68.89	127.29	360.73	
Section length (m)	90.52	41.54	46.75	96.31	278.12
Max. coupler power @ 20 mA (kW)	12.7	42.9	136.0	187.0	
No. of cavities/RF generator	1	2	3	3	
No. RF generators/ section	80	18	21	39	158
Magnet type	SC solenoid	SC solenoid	SC solenoid	SC solenoid	
Magnet field	1.55-3.32 T	3.84-4.36 T	3.96-4.84 T	4.16-5.88 T	
Average RE gradient (MV/m)	0.40	1.66	2.72	3.63	2.13

Figure 1. Schematic cryomodule layouts for each superconducting linac section

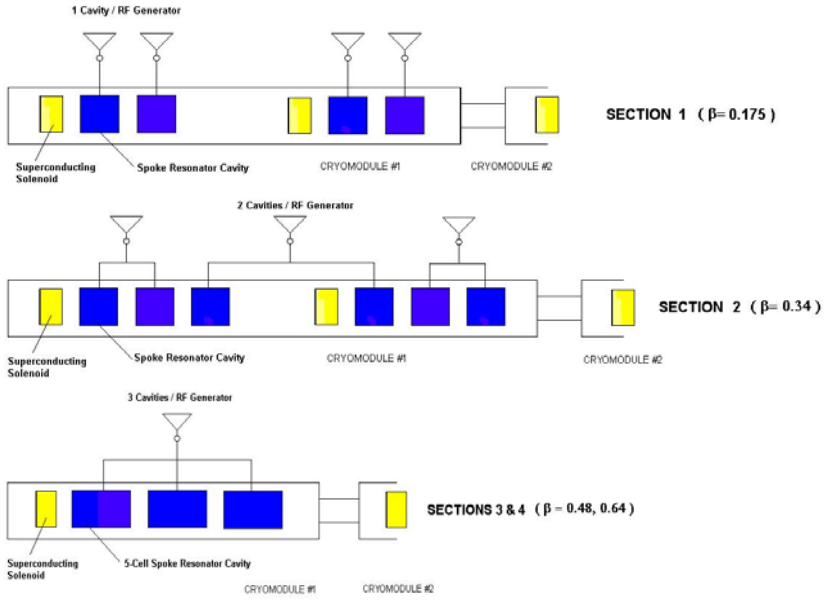

Figure 2. Synchronous phase as a function of beam energy along the linac

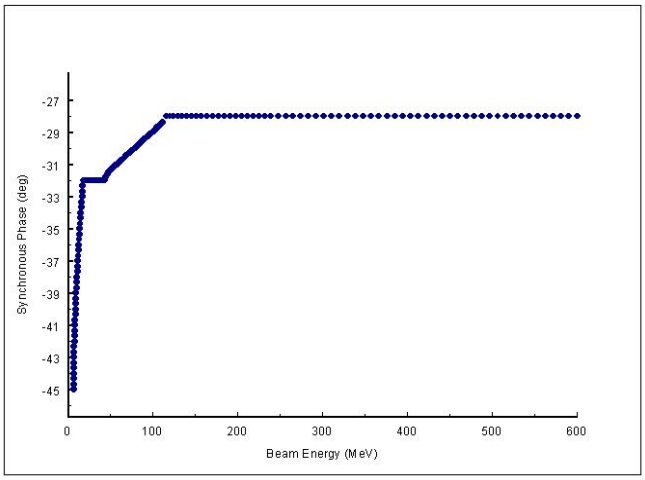

Figure 3. Transit time factor as a function of beam energy along the linac

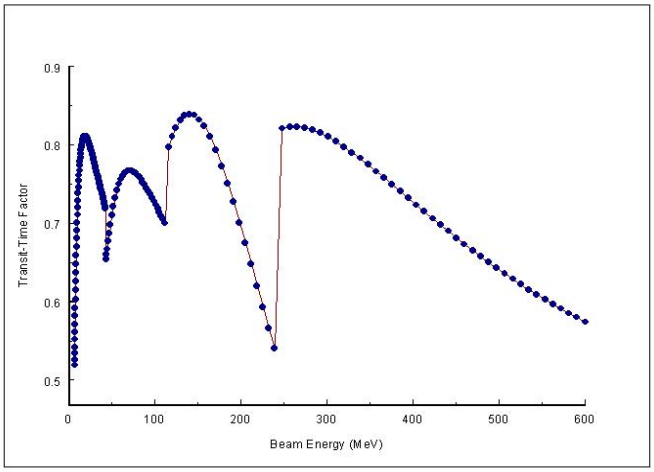

Figure 4. E_0T as a function of beam energy along the linac

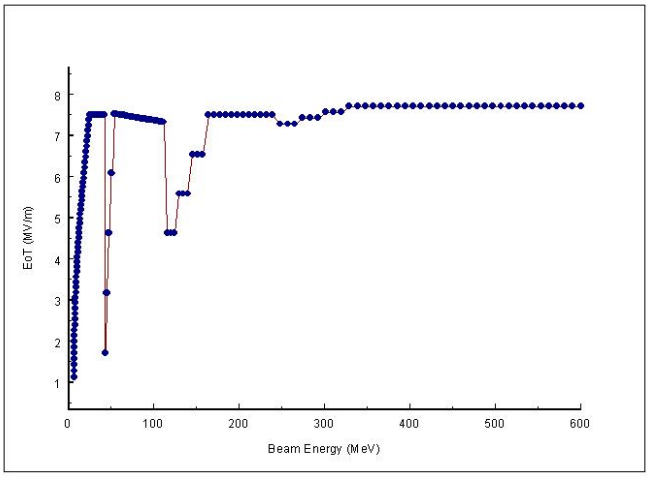

Figure 5. Zero-current phase advances per period as a function of beam energy along the linac

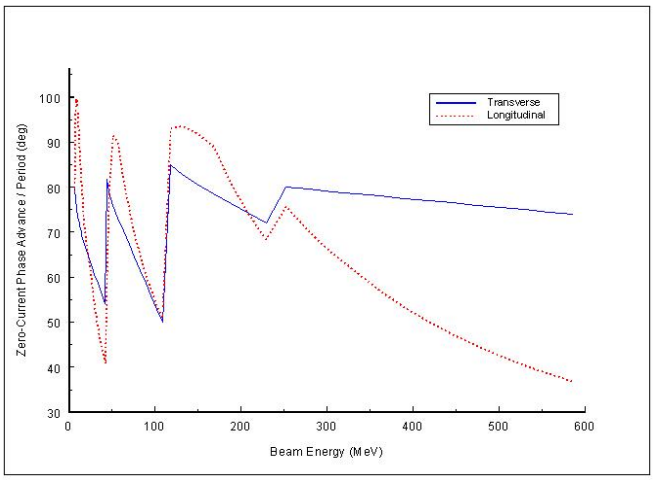

Figure 6. Zero-current phase advances per unit length as a function of beam energy along the linac

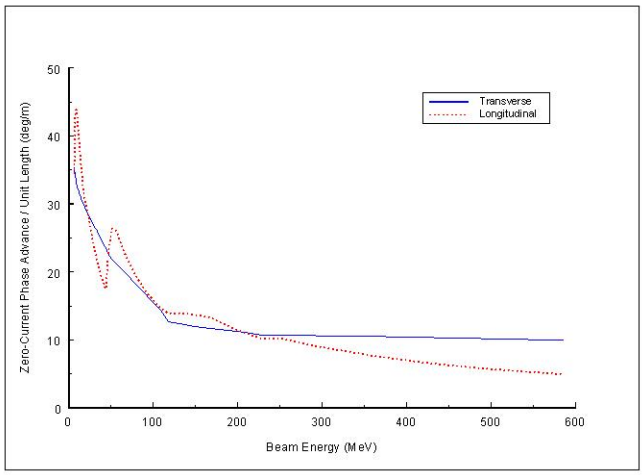

Examination of Table 1 shows that the use of five-gap spoke resonator cavities in the higher-energy sections of the linac significantly increases the real-estate accelerating gradient. An improvement of a factor of approximately 2.4 in the 112-600 MeV sections of the linac is observed as compared to previous designs using 700-MHz elliptical cavities. This is primarily due to the increased active cavity length at the lower operating frequency.

The expected performance of the $\beta = 0.175$, two-gap cavities has already been well-documented based on both calculations and measurements of a prototype cavity [7,8]. Performance of the $\beta = 0.34$, three-gap cavities has been estimated based on these results [9]. The details of the five-gap cavity design are discussed later in this paper. The maximum accelerating gradient used in this design is 7.7 MV/m, which seems reasonable based on the measurement results for the two-gap cavities.

An integrated mechanical and RF design for a power coupler was completed for the $\beta = 0.175$, two-gap spoke resonator cavities [10]. The power will be coupled electrically into the cavities using a coaxial-type coupler design. The direct coupling of the RF power into the cavity reduces the RF losses

and thereby maintains the overall RF efficiency of the spoke resonator cavities. The use of a single power coupler per cavity is the preferred approach based on preliminary estimates that indicate that the introduction of a second coupler significantly degrades the performance of the cavity. The maximum CW power per coupler is expected to be approximately 190 kW in Sections 3 and 4, where the five-gap cavities are used. At this power level, additional power coupler development may be necessary to meet the requirements for this design.

For our study we examined two schemes to match the LEDA RFQ beam into the SC linac at 6.7 MeV. The first scheme uses a more conventional approach and does not require any modification of the LEDA RFQ. It uses six magnetic quadrupoles and two RF bunching cavities to transform the RFQ output beam. Therefore, eight parameters must be varied and properly set to achieve the matching conditions. However, this scheme was found to be not very effective.

The second scheme requires modification of the last section of the LEDA RFQ to produce a round beam at the exit. This is desirable since the matched beam into a solenoid focusing system is round. The exit section of the RFQ must be increased from 6 cm in length to approximately 30 cm to achieve this. To maintain the present overall RFQ tank length and therefore minimise the required RFQ modifications, the increase in exit section length is achieved by removing a few accelerating cells in the last section of the RFQ. New RFQ vanes would need to be manufactured for the last section.

Removal of a few accelerating cells will reduce the RFQ output energy from 6.7 MeV to 6.5 MeV. If necessary, this 0.2 MeV energy difference can easily be compensated for in the high-energy end of the SC linac to recover the final desired 600-MeV linac output energy. This scheme uses two RF bunching cavities, a matching solenoid, and the first solenoid of the SC linac to achieve the matching conditions. This solution requires control or variation of only four parameters to perform matching.

The cryomodule layouts shown in Figure 1 were determined primarily by mechanical engineering constraints. Because of the relatively long focusing periods that result as a consequence, it will probably not be possible to design a completely current-insensitive matching section between the RFQ and the SC linac. The LEDA RFQ has both strong transverse and longitudinal focusing. The transverse focusing strength (zero-current transverse phase advance) per unit length in this RFQ is approximately 1.96 /cm. The focusing strength per unit length at the front-end of the SC linac is approximately 0.336 /cm, a factor of 5.8 weaker. Either weaker focusing in the RFQ or stronger focusing in the SC linac would be required to allow a nearly current insensitive matching section to be designed. Weakening the RFQ focusing will tend to destroy the beam quality and may not be desirable. We studied the effect of reducing the longitudinal focusing at the RFQ exit and found no improvement in the ease of matching or beam capture at high beam currents. It appears that stronger longitudinal focusing per unit length in the SC linac is required to allow operation at high beam currents as discussed in our previous report [1].

Simulation results

All beam dynamics simulations were carried out using 10 000 macroparticles. The PARMTEQM code was used to perform the RFQ simulations. A matched input beam distribution was generated in the code. The beam was then propagated through the RFQ and the desired matching section configuration. The PARMTEQM output beam distribution was then read into the LINAC code. This code was used to simulate the SC linac. Simulations for the ideal linac, with no errors, were performed along with cases including the full range of alignment and RF errors as previously specified for the APT project. LEDA injector data was used to determine the RFQ input emittances to be used in the simulations [11]. Table 2 shows the LEDA beam emittances for various currents.

Table 2. RFQ input and output emittances

Current (mA)	In (p-cm-mrad)	Out-ϵ_x (p-cm-mrad)	Out-ϵ_y (p-cm-mrad)	Out-ϵ_L (deg-MeV)
0	0.0060	0.01324	0.01390	0.2866
20	0.0072	0.01778	0.01778	0.1860
100	0.0122	0.03036	0.03050	0.2115

Simulations were carried out for the ideal linac for 0 mA, 20 mA, and 100 mA to check the current insensitivity of the matching scheme and the performance of the linac, including beam losses. The matching section parameters were set to the 20-mA matched beam settings. Beam losses were observed for the 100-mA case, however, the linac performance is acceptable for 20 mA.

Simulations with alignment and RF errors were performed for 20 mA only. A set of twenty 10 000-macroparticle simulations, each having a different set of random errors, was run. The magnitudes of the errors were assumed to be identical to those used for the baseline APT design and are shown in Table 3. Solenoid fringe fields extending out to a distance equal to the solenoid aperture radius were also included. Figure 7 shows the maximum beam amplitude as a function of beam energy including the full set of alignment and RF errors. All 20 simulation runs are plotted so that the spread in values can be observed. Only 15% of the runs exhibited beam loss. Of those runs, all had losses of 10^{-4}, all occurring in Section 1 of the linac. The RF errors were found to cause the observed beam loss. Reducing the magnitudes of the RF errors somewhat did not eliminate the losses. Section 1 of the linac will need improvement to further minimise or eliminate the beam loss and to allow a sufficient operating margin with achievable operational errors. Additionally, the transverse emittance of the beam was found to be well-behaved in spite of the small longitudinal beam losses; due to random errors, it grew approximately 30% during the simulations. The effects of component failures in the linac were not studied. Such a study, including compensation methods, could be carried out after additional design optimisation has been completed.

Table 3. Random errors used in the superconducting linac simulations

Description of error	Random error value (–)
Solenoid transverse displacement (x and y)	0.25 mm
Solenoid tilt	0.16 mrad
Solenoid field strength	0.25%
Cavity transverse displacement (x and y)	0.75 mm
Klystron amplitude (static error)	2.0%
Klystron phase error (static error)	2.0
Cavity amplitude error (static error)	5.0%
Cavity phase error (static error)	5.0
Klystron amplitude (dynamic error)	1.0%
Klystron phase (dynamic error)	1.0
Cavity amplitude (dynamic error)	5.0%
Cavity phase (dynamic error)	5.0

Figure 7. Maximum beam amplitude as a function of beam energy along the linac for 20 mA and all errors

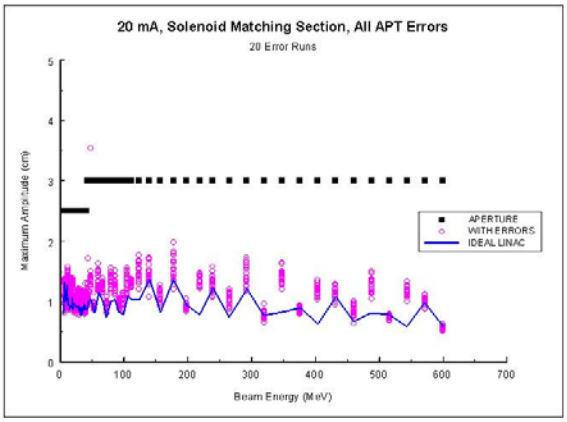

Preliminary five-gap multi-spoke resonator design

The possibility of replacing five-cell elliptical resonators at $\beta = 0.48$ and $\beta = 0.64$ with spoke resonators having the same number of cells has been investigated. A preliminary design and optimisation of candidate spoke geometries was done with Microwave Studio (MWS). The results of this study were used to provide transit time factor data for the design and the beam dynamics simulations presented earlier. The active lengths of the five-gap spoke resonators were found to be approximately 60% longer than the equivalent elliptical cavities at 700 MHz.

Some cavity optimisation was attempted. The spoke cross-section was optimised using a mid-cell and appropriate boundary conditions for the π-mode. The optimised spokes were then used to assemble a full five-gap (four-spoke) resonator. Figure 8 shows the full $\beta = 0.48$ geometry. Note that the end-cells are approximately half the length of the inner cells. This is required to produce flat fields along the structure, as also shown in Figure 8. These same techniques have been fully demonstrated for the $\beta = 0.175$ spoke resonator we built and tested in 2002 [12]. A parameter study was also done to simultaneously minimise peak electric and peak magnetic fields. Each geometric change also changed the frequency of the structure. To compare structures with the correct frequency, MWS was allowed to automatically re-tune the frequency close to 350 MHz by correcting the cavity radius. The parameters varied in the study were the radius of the spoke base, the width of the racetrack and the thickness of the racetrack. Table 4 gives the RF-parameters of the five-gap cavities after some optimisation.

Figure 8. Full five-cell model of the $\beta = 0.48$ spoke resonator. The on-axis electric field is also shown.

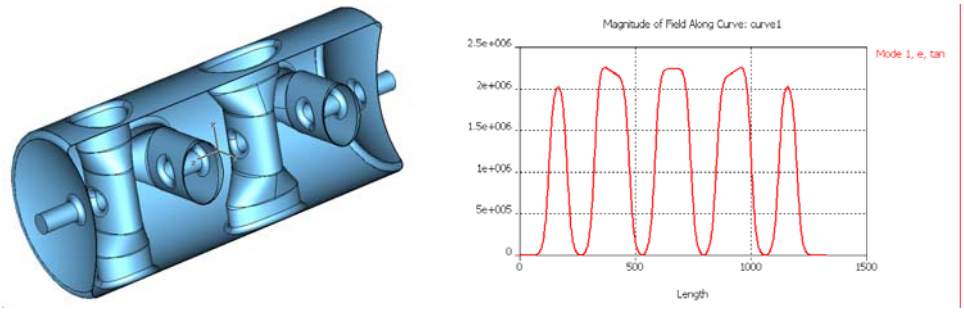

Table 4. RF-parameters for the β = 0.48 and 0.64, five-gap spoke resonators

	β = 0.48	**β = 0.64**
Frequency	350 MHz	350 MHz
R_s	4.893 mΩ	4.846 mΩ
Q_0 (RT)	18 200	19 430
Q_0 (4 K, 60 nΩ)	1.484E+09	1.584E+09
G	89.07 Ω	94 Ω
P_{cav} (4 K, 60 nΩ)	1.51 W	1.40 W
U	0.5 J	0.5 J
Active length	0.833 m	1.0871 m
Length (flange-to-flange)	1.109 m	1.303 m
Voltage	1.501 MV	1.52874 MV
E_0T	1.8019 MV/m	1.4063 MV/m
Transit-time factor	0.818	0.817
E_p/E_0T	3.49	3.74
B_p/E_0T	11.62 mT/MV/m	11.56 mT/MV/m
B_p/E_p	3.33	3.09
E_p/E_{0Ave}	2.86	3.06

In order to further improve on our preliminary cavity design, we will need to examine and take advantage of approaches used by other groups [13] that might ameliorate the performance of the multi-gap spoke resonators. We have already taken advantage of the dish-shaped end walls such as those used in the ANL designs [14]. We have also used different spoke shapes at the ends and middle of the resonator to tailor the spoke shapes to better accommodate the magnetic field pattern along the structure. Other methods of improvement, such as using a rectangular cavity body as proposed by FZ Jülich [15] (making more room for the magnetic field around the spoke base), should also be examined.

Summary

A design for an all-SC linac using only spoke resonator cavities to accelerate a 20-mA beam to 600 MeV for ADS applications has been completed. Our study has shown that replacing the 700-MHz elliptical cavities with 350-MHz, five-gap spoke resonator cavities offers many significant improvements to our previous design, the most important of which is the improved real-estate accelerating gradient resulting from a shorter overall linac length. Operational cost savings should also be realised by the elimination of the 2 K elliptical cavities and their associated cryo-plant. A particular beam dynamics and operational advantage is the larger longitudinal acceptance that is maintained throughout the linac by operating only at 350 MHz and thereby reducing the effects of RF errors.

Some additional design optimisation is desired, however. We continue to observe beam losses in the lowest-energy section of the SC linac when random alignment and operational errors are included. To further improve this section of the linac, we will examine an alternative RFQ design optimised for 20-mA operation and consider the possibility of using other, more compact SC structures in the first section. Additionally, the choice of geometric-β for the five-gap cavities should be re-evaluated to see if further improvements in the transit time factors are possible. Testing of a prototype five-gap cavity would also be desirable.

REFERENCES

[1] Garnett, R. and G. Neuschaefer, *APT SC Linac Design and Beam Dynamics*, Los Alamos National Laboratory Memorandum, LANSCE-1:01-075, 13 September 2001.

[2] Garnett, R., *ADTF Superconducting Design*, Los Alamos National Laboratory Memorandum, LANSCE-1:01-047, 1 May 2001.

[3] Garnett, R., *ADTF Superconducting Linac Design – Viability of Reducing Number of Spoke Sections*, Los Alamos National Laboratory Memorandum, LANSCE-1:01-049, 4 May 2001.

[4] Garnett, R., *ADTF Cryomodule Layout Clarification*, Los Alamos National Laboratory Memorandum, LANSCE-1:01-063, 16 July 2001.

[5] *Summary on LEDA RFQ Performance*, Accelerator Production of Tritium Project Technical Note, LA-UR-01-2670, July 2001.

[6] Rees, D., private communication.

[7] Krawczyk, F.L., *et al*., *Design of a Low-β, 2-Gap Spoke Resonator for the AAA Project*, Los Alamos National Laboratory Report, LA-UR-01-3218, 2001.

[8] Tajima, T., *et al*., "Results of Two LANL $\beta = 0.175$, 350-MHz, 2-Gap Spoke Cavities", *Proceedings of the 2003 Particle Accelerator Conference*, Portland, Oregon, 12-16 May 2003.

[9] Krawczyk, F.L., *RF Design of Spoke Resonators for the AAA Project*, Los Alamos National Laboratory Report, LA-UR-02-6872, Workshop on the Advanced Design of Spoke Resonators, Los Alamos, NM, USA (2002).

[10] Krawcyzk, F.L., *et al*., "An Integrated Design for a Beta = 0.175 Spoke Resonator and Associated Power Coupler", *Proceedings of the 8th European Particle Accelerator Conference*, Paris, France, 3-7 June 2002.

[11] Wangler, T., private communication.

[12] Krawcyzk, F.L., *et al*., "Design of a $\beta = 0.175$ 2-Gap Spoke Resonator", *Proceedings of the 10th Workshop on RF Superconductivity*, Tsukuba, Japan, September 2001.

[13] Shepard, K.W., P.N. Ostroumov and J.R. Delayen, "High-energy Ion Linacs Based on Superconducting Spoke Cavities", *Phys. Rev. ST – Accel. and Beams*, Vol. 6, 080101 (2003).

[14] Fuerst, J.D., *et al*., "Superconducting 345 MHz Two-Spoke Cavity for RIA", *Proceedings of the 2003 Particle Accelerator Conference*, Portland, Oregon, 12-16 May 2003.

[15] Zaplatain, E., *et al*., "Low-beta SC Cavity for ESS", *Proceedings of the 8th European Particle Accelerator Conference*, Paris, France, 3-7 June 2002.

METHODS AND CODES FOR ESTIMATION OF TOLERANCE IN RELIABLE RADIATION-FREE HIGH-POWER LINAC

A.P. Durkin, I.V. Shumakov, S.V. Vinogradov
Moscow Radiotechnical Institute RAS
Russia, 117519, Warshawskoe shosse, 132
E-mail: lidos@aha.ru

Abstract

Successful development of a reliable and normal hands-on maintainable high-power linac requires minimisation of beam losses along the accelerator. The high sensitivity of the high-power linac focusing channel to random perturbation encourages designers to concentrate their attention on the tolerance estimation problem. The degradation of beam parameters, including transverse size and emittance growth, is caused by channel and beam parameter perturbations. The calculation of channel sensitivity permits to estimate the influence of each perturbing factor on the beam parameters and to determine the main source of perturbation, to find perturbing factors compensation possibilities and to determine the factors required to guarantee beam passage throughout the real channel without losses. Methods for the estimation of tolerance in high-power linac accelerating-focusing channels are considered in the present paper. The realisation of these methods in the LIDOS code package is presented. Monte Carlo simulation results for various types of accelerating channels are discussed.

Introduction

It is generally acknowledged that the main source of particle losses in the extended linac channel is the Coulomb field of space-charge-dominated beam. However, there are the non-Coulomb effects concerned with external field perturbations (external perturbations) and their influence on beam dynamics is comparable with the action of space charge.

It is convenient to split external perturbations into two groups: constructive (regular) perturbations caused by the distinction of a real structure from an ideal one and perturbations caused by random parameter deviations within given tolerances. In the latter case only the probability that the beam size will be no more than a given value can be found. In connection with the strict requirement for channel transparency and also with the complex procedure for channel retuning and readjustment, the confidence level chosen must be sufficiently large.

The calculation of the accelerating/focusing channel is always based on the specific mathematical model involving a description of the external accelerating and focusing forces.

In this model as a rule, the focusing field linear dependence on transverse co-ordinates and accelerating field axis distribution is used. The channel based on such models will be called ideal. Of course, there are no unprojected losses in the ideal channel.

The degradation of output beam parameters, including transverse size and emittance growth, is caused by channel and beam parameter perturbations (not always small). The influence of perturbations upon the beam output parameters is determined by quantity, which has come to be known as the channel sensitivity. The goals of beam dynamics investigations are:

- Knowledge concerning channel sensitivity – each perturbing factor influences output beam parameters.
- The possibilities of compensating for perturbing factors.
- Redundant factor determination guaranteeing beam passage throughout the real channel without losses.

The cardinal problem is to choose the channel with minimum sensitivity in order to minimise the beam losses during the process of accelerating.

Below we consider the main sources of perturbations, perturbation field characteristics and their influence on output beam parameters.

Main perturbations in different channels

RFQ linac

Random errors independently arising in each cell are the most dangerous. In this case there is a possibility of unfavourable realisation with each subsequent cell amplifying the disturbances of all previous ones.

Let us consider possible types of random perturbation, disturbed field characteristics, their influence on initial beam parameters, and the possibility of theoretical and numerical investigations of the different factors.

- *Electrode modulation deviation.* Main effect – changes in accelerating field amplitude, leading to coherent longitudinal oscillations and longitudinal repulsion. Result – longitudinal phase volume increase at the output of accelerator. Weak effect – Changes in focusing field and transverse effective emittance increase produced by these changes.

- *Aperture radius deviation.* Main effect – changes in focusing field gradient, deviation of accelerator axis from ideal line (axis may be presented as polygonal line), quadrupole symmetry violation. Result – transverse beam mismatching, coherent beam oscillations about real accelerator axis and transverse phase volume increase produced. Weak effect – appearance of new random non-linear field harmonics, changes in accelerating field.

Linac with focusing by quadrupole magnet lenses

- *Lens end displacements regarding linac axis.* These perturbations turn up as a result of errors in lens settings as well as a result of errors during lens manufacturing. Main effect – beam coherent oscillations regarding linac axis and effective emittance growth.

- *Deviations of focusing field gradient in lenses.* Main effect – beam gradually mismatching and growth of transverse oscillation amplitude. In this case beam emittance is retained but effective emittance grows.

- *Median plane rotations of quadrupole lens.* Main effect – beam gradually mismatching and growth of tranverse oscillation amplitude. In this case relations between X-oscillations and Y-oscillations turn up, leading to beam emittance growth. The effective emittance also grows.

- *Distinction of vane shape from hyperbole shape.* Linear focusing fields are possible only in the case when vanes have hyperbole form. In practice focusing fields contain non-linear components. There are non-linear components connected with the vane real shape. These components are the same for all lenses and they will be designated as constructive non-linearity. Other non-linear components can be designated as random non-linearity and they are connected with errors during vane manufacturing. Main effect – a coupling between X- and Y-oscillations leading to phase trajectory deformations and effective emittance growth. If the ratio of transverse oscillation period length to focusing period length is near to integer then resonance events can take place. In the non-resonant case maximal amplitude of transverse oscillations does not increase with growth of focusing period number. Random non-linearity also leads to effective emittance growth along with growth of focusing period number.

Linac with focusing by solenoid lenses

- *Lens end displacements regarding linac axis*. Both effects and methods of study are the same as for quadrupole lenses.

- *Deviations of solenoid field induction.* Effects and methods of study are the same as for deviations of focusing field gradient in quadrupole lenses.

Channel sensitivity definition

The mathematical foundation and main treatments are given in the Refs. [1-5], as are the tolerance estimations for various types of focusing and accelerating channels. Below, we investigate the parameters determining the sensitivity of the long channel to external perturbations.

Let us consider as an example the motion of particles in the focusing channel with random errors in focusing field gradients:

$$x'' + \tilde{G}(z)\, x = 0$$

Let us consider $\tilde{G}(z)$ as $\tilde{G}(z) = G(z)\,(1 + a(z))$, where $G(z)$ is non-perturbed field gradient and $a(z)$ is a function for perturbation description.

As shown in the above-cited works, it is necessary to transform the variables x, dx/dz to phase variables r,h. The variable r^2 is quadric in x,dx/dz, describing the ellipses matched with the ideal periodical channel. The variable h is an addition due to external perturbations. As a result, the main equation takes the form:

$$\begin{cases} r' = r\, a\, G\, r^2 \sin^2(mz + h + y) \\ h' = a\, G\, r^2 \cos^2(mz + h + y) \end{cases}$$

where m is phase advance, and r is the beam envelope with an emittance of unity in the ideal channel.

The right part of the second equation does not depend on r, so it can be solved separately. If $h(z)$ is the solution of the second equation, then the solution of the first equation has the following form:

$$\frac{r(z)}{r_0} = q(z) = \exp\left(\int_0^z aGr^2 \sin(mt + h + y)\cos(mt + h + y)dt \right) = \exp(F(z))$$

It can be seen from the obtained relation that distribution of the random value $q(z)$ is determined by distribution of random value $F(z)$.

If the focusing channel contains N periods, then $F(z)$ can be presented as the sum of the statistical independent components adequate to corresponding periods L_k:

$$F(N) = \sum_{k=1}^{N} F_k = \sum_{k=1}^{N} \int_{L_k} aGr^2 \sin(mt + h + y)\cos(mt + h + y)dt$$

Using an approximate solution of the second equation:

$$h(N) = j_0 + \int_0^N aGr^2 \cos^2(mt + j_0 + y)dt = j_0 + \sum_{k=1}^{N} h_k = j_0 + \sum_{k=1}^{N} \int_{L_k} aGr^2 \cos^2(mt + j_0 + y)dt$$

we obtain with an accuracy of a^3:

$$F_k = \int_{L_k} aGr^2 \left(\tfrac{1}{2}\sin^2(mt + j_0 + y) - \cos^2(mt + j_0 + y) \sum_{i=1}^{k} h_k \right) dt$$

Suppose $a(z)$ is piecewise constant function that is equal to the relative error of the field gradient inside any element of the channel. In this case, the integral is calculated only along the part of the period containing the perturbation. If σ^2 is the mean square value of the field gradient tolerance, then using statistical independence of errors for different focusing periods and averaged over oscillations we obtain relations for the mean value and dispersion of $F(N)$:

$$M[F(N)] = D[F(N)] = \frac{\sigma^2}{8}\sum_{k=1}^{N}\left|\overline{Gr^2}\right|_k^2 = \frac{\sigma^2}{8}\sum_{k=1}^{N} S_k$$

As shown in Ref. [4], if σ^2 is the mean square value of the focusing field gradient relative error then the probability that effective emittance growth would be no more than x is determined by the function $P(x) = 1 - e^{-(\ln x)^2/D^2}$, where $D^2 = \frac{\sigma^2}{4}\sum_{k=1}^{N} S_k$. If σ^2 is the error of axis transverse displacement then the probability that the centre of the output beam displacement would be no more than x is determined by the function $P(x) = 1 - e^{-x^2/D^2}$, where $D^2 = \sigma^2\sum_{k=1}^{N} S_k$. We can give the definition of S_k as the sensitivity of a period numbered k. Then total sensitivity of the channel will be the sum of period sensitivities $S = \sum_{k=1}^{N} S_k$.

The regions of stability diagrams for RFQ and some types of quadrupole channels are shown in Figures 1-4. In these regions the isolines of transverse oscillation frequency μ and sensitivity $S = \left|\overline{Qr^2}\right|^2$ are plotted. We use traditional co-ordinates: focusing parameter $B = \frac{eU}{m_0c^2}\kappa\left(\frac{\lambda}{a}\right)^2$ and de-focusing parameter $A = \frac{\pi^2 eU\sigma}{4W_s}\left|\sin\mu_s\right|$ for the RFQ diagram. For the quadrupole channels we use focusing parameter $Q = \frac{eGL^2}{m_0c\beta\gamma}$, where G is the focusing field gradient, L is the length of the focusing period, and de-focusing parameter $A = \frac{\pi eE_m L^2}{m_0c^2(\beta\gamma)^3\lambda}\left|\sin\mu_s\right|$, where E_m is the accelerating wave amplitude and λ is the RF field wave length. In Figures 1-4 μ-isolines correspond to the values (from bottom to top) $\mu = 0$, $\mu = \pi/3$, $\mu = \pi/2$, $\mu = 2\pi/3$, $\mu = \pi$.

Figure 1. Sensitivity *S* of RFQ channel

1 – 40, 2 – 50, 3 – 60, 4 – 70, 5 – 80 (from left to right)

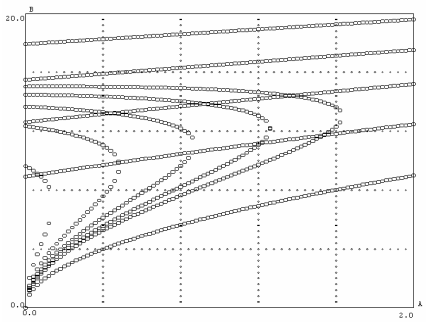

Figure 2. Sensitivity *S* of FODO channel

1 – 30, 2 – 35, 3 – 40, 4 – 45, 5 – 60 (from left to right; Gap/Period = 0.5)

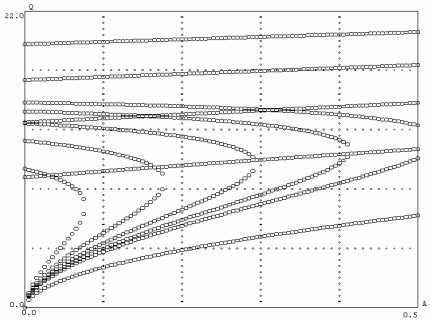

Figure 3. Sensitivity *S* of FDO channel

1 – 70, 2 – 85, 3 – 100, 4 – 115, 5 – 130 (from left to right; Gap/Period = 0.8)

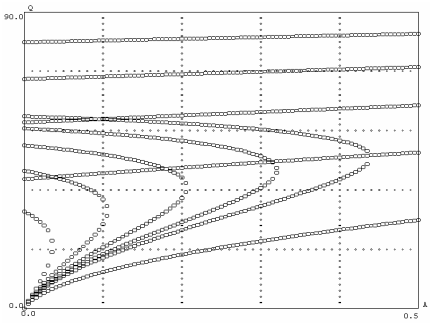

Figure 4. Sensitivity *S* of FDO channel

1 – 100, 2 – 130, 3 – 160, 4 – 190, 5 – 220 (from left to right; Gap/Period = 0.9)

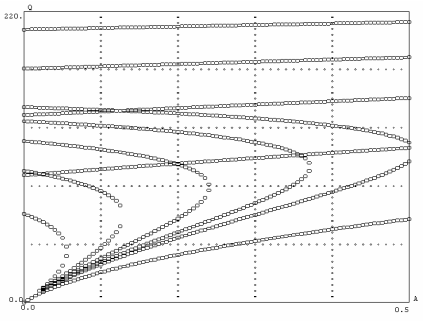

As is seen from these diagrams, even within the boundaries of the operating region of stability diagram the channel sensitivity can be varied two times by value. So for choice and calculation parameters of the long linac channel the reported results must be taken into account.

Numerical estimations of perturbation influence

Extensive studies of different types of perturbations are being carried out in support of the analytical estimations cited above. Numerical results are in reasonably good agreement with analytical ones. This allows establishing the analytical estimations as good for beam transverse size and emittance growths under perturbations.

Below, we consider several focusing channels as examples and compare their sensitivity as regards random perturbation action.

RFQ channel

Let us consider as an example an RFQ channel operating at 352 MHz and accelerating protons from 0.1 to 5 MeV. The channel length is 8 m, vane voltage was changed from 100 to 123 KV, and bore radius changes along the channel from 4.1 to 3.6 mm (matching section not included). Statistical simulation of beam dynamics was performed in order to estimate variations of output beam parameters due to possible deviations of accelerating and focusing field inside cells. The change of the average radius position for each cell was considered as a perturbation factor. It was assumed that the average radius inside the cell varies linearly. The random value distributed uniformly inside [-dr, dr] was added to the top value of cell average radius. Random values for different cells were chosen independently. Beam simulations were performed for dr =10 mm and dr =25 mm. Beam energy losses, phase width, momentum spread, transverse size, beam centre displacement, beam RMS and total emittances were calculated as integral characteristics. The values were integrated over all particles within one RF period.

Calculations were performed by LIDOS.RFQ.Designer. In order to reduce computation time they were carried out in ideal RF fields. An "ideal" result (dr = 0) was also obtained in ideal RF fields. The number of random realisations was 50 for each type of error.

In general, it can be stated that dr = 10 mm is acceptable whereas dr = 25mm is dangerous, as a probability exists that beam size growth will be large and will be lead to additional beam losses. Thus with dr = 25 mm summary power dissipated on channel walls reaches 2.5 KW with a probability of 0.8.

Figure 5. Lost particle total power

In ideal channel lost particle total power equals 0.134 kW

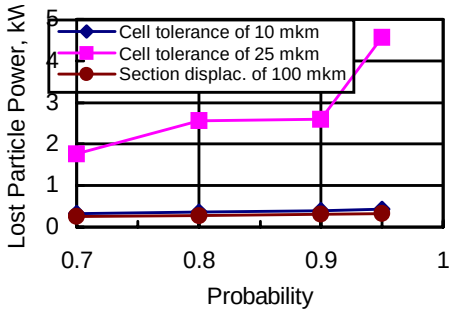

Figure 6. Beam transverse sizes R/R_0

Ideal value equals 1.00

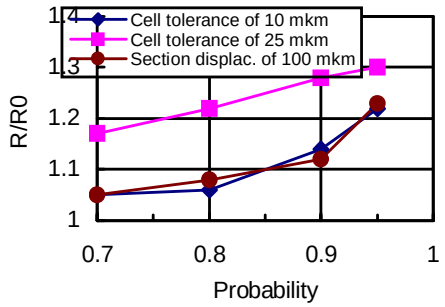

Focusing channel with magnet quadrupole lenses

Let us consider an FDO channel with 300 focusing periods. Suppose that the lens takes 0.1 of the period. For σ = 0.05 mm we obtain a confidence level for a beam oscillation amplitude, which is no more than 3 mm, of only 0.3.

If we want the same limitation of 3 mm to take place with a probability 0.9, then the necessary RMS value of primary error must be 0.018 mm.

If in the above FDO channel the RMS value of the magnetic field tolerance is equal to 0.5%, the probability of beam transverse size increasing by a factor of no more than 1.2 is equal to 0.2. This probability is equal to 0.9 when the same tolerance RMS value is 0.17%.

Taking into account the lens rotation influence for the considered case we determine that with a probability of 0.9 the beam size increasing factor is no more than 1.3 when the RMS value for the lens rotation angle is equal to $\sqrt{\overline{\gamma^2}} = 0.2$.

Solenoid lenses focusing

If we consider the same period as in the previous examples, where lens length takes 0.1 of period length, then for a quadrupole and solenoid channel sensitivity comparison we obtain the approximate relations $Q_{quad} \approx 4Q_{sol}$ and $\rho^2_{quad} \approx 1.7\rho^2_{sol}$. From these relations we determine that with the same RMS displacement of the lens ends we obtain approximately the same statistics as with beam centre displacement. In order to receive with the same probability uniform growth of effective emittance, we must have an RMS value of $\sigma_{\Delta H/H}$ 2.5 times bigger then $\sigma_{\Delta B/B}$. All of these elements, along with a missing of rotation error for the solenoid lens, render the solenoid channel much less sensitive to perturbations than the quadrupole one.

The relations and examples cited above show that in an extended focusing channel, external perturbations are of considerable importance for the understanding of effective emittance growth. Ignoring external perturbations can lead to intolerable losses.

Compensation of external perturbations

Compensation of focusing channel axis displacements

The basic sources of axis displacements are inexact channel adjustment and lens magnetic axis displacements. For the partial correction of the first source the adjustment method with maximum correlation between lens displacement must be used. In this case the linac axis may be presented as a smooth curve which is superposed by a random component. A smooth curve does not cause coherent amplitude growth, and the total perturbation effect will decrease.

The magnetic axe displacement cannot be compensated. In order to suppress coherent oscillation amplitude, sections for beam transverse position correction are inserted. In an ideal case, at the output of the correction section the beam runs axially. Correction methods and algorithms were considered in Ref. [5].

Compensation of magnetic field gradient deviations

This perturbation effect may be depressed by establishing a correlation between deviations of adjacent lens magnetic fields. It can be done if there are electromagnetic quadrupoles. The correlation takes place when the lens groups are energised from one power supply. The number of independent error sources reduces and the perturbation effect depresses.

Compensation of quadrupole lens rotations

In this case, the correlation cannot be introduced and this is the reason why requirements concerning the lens rotation tolerance must be strict. In order to eliminate these perturbations, the quadrupole lenses should be replaced by solenoidal ones.

Monte Carlo simulation module for LIDOS.RFQ.Designer code

To choose RFQ channel optimal parameters, random perturbation influences have to be taken into account and an estimation of tolerances must be given. The goal of the LIDOS.RFQ.Designer package [6-11] development is to help the user to solve this problem.

The new version of the package contains the module “Statistics”. Random realisations of a channel taking into account deviations of vanes from their ideal positions are generated. From cell to cell the random deviations are statistically independent. To compute the vane surface position we base our calculations on the following parameters: r is the distance from axis to cell beginning, m is the vane modulation and L is the cell length. With perturbations the parameter r is changed over a random value Δ. For a cell numbered k we use $\tilde{r}_k = r_k + \Delta_k$. In turn the deviations of any vane inside the cell are also statistically independent.

If the channel is divided into sections the other source of perturbation is the independent deviation of section vane ends.

The code simulates beam dynamics for every version of the channel. To decrease the time taken to calculate the statistics, the visualisation of the current version can be switched off. Because it takes the calculation of many random versions to obtain a sufficient statistic (as a rule no less than 50), this procedure is very time consuming, so it is possible to stop calculations and to continue at any time with the previous version.

The “Advisor” module offers supplementary visual information for tolerance estimation. Above, we define parameter S as sensitivity of period to perturbations. In this case the relation determining this parameter is as follows:

$$S = \left(B \int_0^1 \rho(t) \cos 2\pi t \, dt \right)^2$$

where B is a focusing parameter, ρ is the envelope of matched beam with the emittance of unity in the ideal channel.

The visual information presents the plot of sensitivity versus number of cells as well as statistic estimation concerning effective emittance growth and beam centre transverse displacement. The error integrals are calculated in accordance with the relations given above: if σ^2 is the mean square value of

the focusing field gradient relative error then the probability that effective emittance growth would be no more than x is determined by the function $P(x) = 1 - e^{-(\ln x)^2/\sigma^2}$, where $\sigma^2 = \frac{s^2}{4}\sum_{k=1}^{N} S_k$. If s^2 is the error of axis transverse displacement then the probability that the centre of output beam displacement would be no more than x is determined by the function $P(x) = 1 - e^{-x^2/\sigma^2}$, where $\sigma^2 = s^2\sum_{k=1}^{N} S_k$. For both cases S_k is the sensitivity of cell numbered k and N is the total number of cells.

Examples of output pictures from the "Statistics" module are shown in Figures 7-10. An RFQ channel with a frequency of 175 MHz and accelerating protons with energies ranging from 0.05 MeV to 2 MeV have been used as an example. The statistics were calculated for two values of tolerance: 10 mm (Figures 7 and 9) and 25 mm (Figures 8 and 10).

Figure 8. Statistics of *RMS-Emittance XX'*

Mean – 0.28, sigma – 0.01, ideal – 0.28

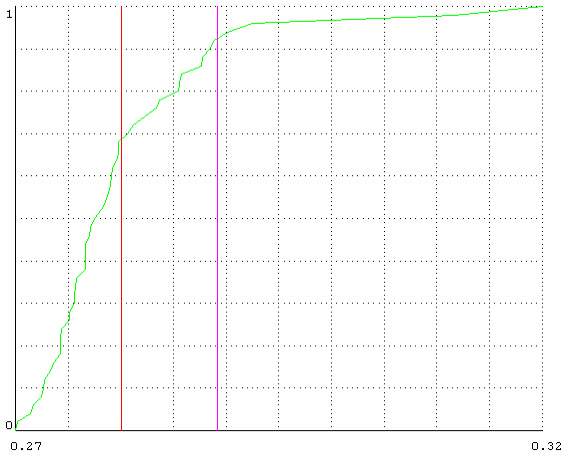

Figure 9. Statistics of *RMS-Emittance XX'*

Mean – 0.34, sigma – 0.05, ideal – 0.28

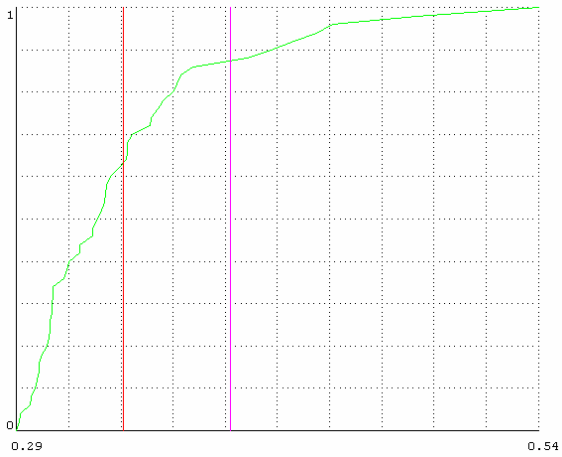

Figure 10. Statistics of *Total Emittance XX'*

Mean – 2.63, sigma – 0.06, ideal – 2.60

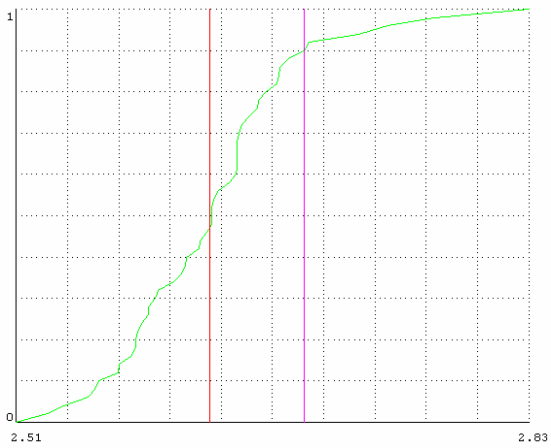

Figure 11. Statistics of *Total Emittance XX'*

Mean – 3.08, sigma – 0.18, ideal – 2.60

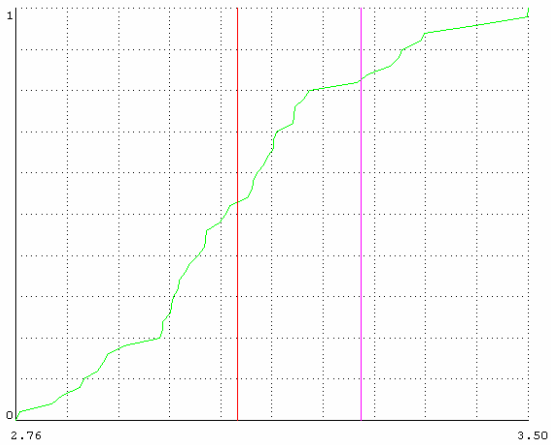

REFERENCES

[1] Bondarev, B.I., A.P. Durkin, B.P. Murin, L.Yu. Soloviev, "Random Perturbation of the Transverse Motion of Protons in a Linear Accelerator and Their Correction", *Particle Accelerators*, Vol. 6, No. 1, pp. 27-40 (1974).

[2] Bondarev, B.I., A.P. Durkin, **"**Non-Coulomb Perturbations Influence on Beam Dynamics in Extended Accelerating/Focusing Channels", *Proceedings of 2003 Particle Accelerator Conference*, Portland, Oregon, USA, 12-16 May 2003, pp. 3002-3004.

[3] Bondarev, B.I., A.P. Durkin, L.Yu. Soloviev, "Influence of Focusing Fields Errors on the Particles Motion in Linac", *Journal of Technical Physics*, Vol. 49, No. 8, pp. 1662-1672 (1979) (in Russian).

[4] Murin, B.P., B.I. Bondarev, A.P. Durkin, "An Approach to the Design of a Robust Focusing Channel", *Proceedings of 1992 Linear Accelerator Conference*, Ottawa, Ontario, Canada, 24-28 August 1992, Vol. 2, pp. 731-733.

[5] Murin, B.P., B.I. Bondarev, A.P. Durkin, L.G. Lomize, L.Yu. Soloviev, "Some Aspects of Simultaneous Acceleration of Proton and H^- Beams in a Linac", *Particle Accelerators*, Vol. 6, No. 3, pp. 133-139 (1975).

[6] Murin, B.P., B.I. Bondarev, A.P. Durkin, *et al*., "A Computing Optimization System for Ion Linac Accelerating/Focusing Channels", *Proceedings of 1992 Linear Accelerator Conference*, Ottawa, Ontario, Canada, 24-28 August 1992, AECL-10728, Vol. 2, pp. 734-736.

[7] Bondarev, B.I., A.P. Durkin, *et al*., "LIDOS – Unconventional Helper for Linac Beam Designing", *Computational Accelerator Physics Conference, AIP Conference Proceedings 297*, Los Alamos, NM, pp. 377-384 (1993).

[8] Bondarev, B.I., A.P. Durkin, G.H. Gillespie, "Beamline Parameter Optimization in the Framework of the LIDOS.Advisor", *Proceedings 2nd International Workshop Beam on Dynamics & Optimization*, St. Petersburg, Russia, 4-8 July 1995, pp. 61-64.

[9] Bondarev, B.I., A.P. Durkin, S.V. Vinogradov, J-M. Lagniel, R. Ferdinand, "CW RFQ Designing Using the LIDOS.RFQ Codes", *Proceedings XIX International Linac Conference*, LINAC'98, Chicago, Illinois, USA, 23-28 August 1998, pp. 502-504.

[10] Bondarev, B.I., A.P. Durkin, S.V. Vinogradov, I.V. Shumakov, "New Tasks and New Codes for RFQ Beam Simulation", *Proceedings XX International LINAC Conference*, Monterey, California, 21-25 August 2000, pp. 830-832.

[11] Shumakov, I.V., B.I. Bondarev, A.P. Durkin, Yu.D. Ivanov, S.V. Vinogradov. "Monte Carlo Simulation Module for LIDOS.RFQ.Designer Code", *Proceedings 2003 Particle Accelerator Conference*, Portland, Oregon, USA, 12-16 May 2003, pp. 3530-3532.

STATUS OF THE SPALLATION NEUTRON SOURCE ACCELERATOR COMPLEX*

Stuart Henderson
Spallation Neutron Source Project, Oak Ridge National Laboratory, USA

Abstract

The Spallation Neutron Source accelerator system will provide a 1-GeV, 1.44-MW proton beam to a liquid mercury target for neutron production. The accelerator complex consists of an H^- injector capable of producing a 38-mA peak current, a 1-GeV linear accelerator, an accumulator ring and associated transport lines. The linear accelerator consists of a drift-tube linac, a coupled-cavity linac and a superconducting linac which provide a 1.5-mA average current to the accumulator ring. The design of the accelerator systems is complete; installation of the accelerator components is in progress; and staged beam commissioning is proceeding as installation progresses. The installation and final commissioning of the project is on schedule for completion in early 2006. The status of the project design, installation and commissioning will be presented.

* SNS is managed by UT-Battelle, LLC, under contract DE-AC05-00OR22725 for the US Department of Energy. SNS is a partnership of six national laboratories: Argonne, Brookhaven, Jefferson, Lawrence Berkeley, Los Alamos and Oak Ridge.

Introduction

The Spallation Neutron Source (SNS) is a short-pulse neutron scattering facility under construction at Oak Ridge National Laboratory by the US Department of Energy. At 1.44 MW of proton beam power on target, the SNS will operate at powers a factor of 7 beyond that achieved at what is now the most intense short-pulse neutron source, the ISIS facility at Rutherford Appleton Laboratory in the UK [1]. The SNS is a partnership of six US DOE national laboratories, each of which is designing and manufacturing a portion of the facility. The project is now in a construction phase, with transition to operations expected in 2006.

The SNS accelerator complex [2] is composed of a 2.5-MeV H^- injector [3], a 1-GeV linear accelerator [4], an accumulator ring and associated beam transport lines [5]. The SNS baseline parameters are summarised in Table 1. The injector (also called the front-end systems) consists of an H^- volume ion-source with a 50-mA peak current capability, a radio-frequency quadrupole and a medium-energy beam transport line for chopping and matching the 2.5-MeV beam to the linac. The linear accelerator consists of a drift-tube linac (DTL) with an output energy of 87 MeV, a coupled-cavity linac (CCL) with an output energy of 187 MeV, and a superconducting RF linac (SCL) with 1-GeV output energy. The linac produces a 1-msec long, 38-mA peak, chopped beam pulse at 60 Hz for accumulation in the ring. The linac beam is transported via the high-energy beam transport (HEBT) line to the injection point in the accumulator ring, where the 1-msec long pulse is compressed to less than 1 microsecond by charge-exchange multi-turn injection. In baseline operation, beam is accumulated in the ring over 1 060 turns reaching an intensity of $1.5 \cdot 10^{14}$ protons per pulse. When accumulation is complete the extraction kicker fires during the 250-nsec gap to remove the accumulated beam in a single turn and direct it into the ring-to-target beam transport (RTBT) line, which takes the beam to a liquid-mercury target.

Table 1. SNS baseline parameters

Beam power on target	1.44 MW
Beam energy	1 000 MeV
Linac beam macropulse duty factor	6.0%
Beam pulse length	1.0 msec
Repetition rate	60 Hz
Chopper beam-on duty factor	68%
Peak macropulse H^- current	38 mA
Average linac H^- current	1.6 mA
Ring accumulation time	1 060 turns
Ring bunch intensity	$1.6 \cdot 10^{14}$
Ring space-charge tune spread	0.15
Beam pulse length on target	695 nsec

Staged commissioning of the accelerator complex is proceeding as installation progresses. At this point, construction of all accelerator tunnels and enclosures is complete. The final project construction effort is focused on the target and the central laboratory and office buildings. To date, the front-end systems and half the drift-tube linac have been beam commissioned. Table 2 summarises the main commissioning results, comparing beam measurements with design goals.

Table 2. Beam commissioning performance to date

	Baseline design or goal	Achieved in commissioning
DTL1 peak current [mA]	38	40
DTL1-3 peak current [mA]	38	38
DTL1 beam pulse length [msec]	1.0	1.0
DTL1 average current [mA]	1.6	1.05
DTL1 horizontal emittance [p mm mrad (RMS, norm.)]	0.3	0.30 (fit), 0.40 (RMS)
DTL1 vertical emittance [p mm mrad (RMS, norm.)]	0.3	0.21 (fit), 0.31 (RMS)
DTL1 duty factor	6.0%	4.0%
MEBT beam energy [MeV]	2.5	2.45 – 0.010
DTL2 output energy [MeV]	22.89	22.94 – 0.11

Front-end status

The front-end systems were designed and built by Lawrence Berkeley National Laboratory (LBNL), commissioned at LBNL in May 2002, and reassembled and recommissioned at ORNL in late 2002. The front end consists of a volume H^- ion source with a 50-mA peak current, 6% duty factor and an electrostatic low-energy beam transport (LEBT) line to provide a properly matched, 65-keV beam for injection into the RFQ. Pre-chopping is performed by the LEBT chopper which deflects 32% of the beam onto the front face of the RFQ with a rise/fall time of 40 nsec. The RFQ is designed for a 38-mA peak output current, operates at 402.5 MHz and provides a 2.5-MeV output beam energy. The medium-energy beam is transported to the drift-tube linac via the MEBT, which contains four RF rebuncher cavities to properly match the beam longitudinally, a set of matching quadrupoles, and a fast chopper system with 10 nsec rise/fall time to remove the "partially chopped" beam from the LEBT chopper and further reduce the beam extinction ratio to below 10^{-4}.

A peak MEBT output current of 50 mA was demonstrated, surpassing the design goal of 38 mA. In subsequent DTL commissioning, the front-end systems have operated at full 1 msec pulse length, and provided a 1-mA average current (4% duty factor) beam for injection into the DTL. The MEBT output beam emittances were measured and found to be in the range of 0.25-0.30 p mm-mrad (RMS, normalised) which meets the specification. Additionally, the MEBT output energy was measured and found to be 2.45 – 0.01 MeV, compared with the 2.5-MeV nominal, design energy.

The MEBT contains a number of beam diagnostic devices which are, or will be, important for characterising the beam parameters prior to injection into the linac. In addition to beam position monitors and wire scanners, a diagnostics box is being commissioned with an in-line slit/harp emittance measurement station, a 3-D beam profile system based on a mode-locked laser, and a fast-faraday cup for measurement of the longitudinal beam profile.

Linac status

The linac consists of three sections: the DTL, the CCL and the SCL. The DTL, CCL as well as all the high-power RF systems for the linac were designed and procured by Los Alamos National Laboratory (LANL).

DTL status and commissioning results

The drift-tube linac consists of six accelerating tanks with a final output energy of 87 MeV. The DTL operates at 402.5 MHz, the same bunch frequency as the RFQ. Tanks are individually powered with klystrons of 2.5-MW peak power and 8% duty factor capability. The transverse focusing is arranged in a FFODDO lattice utilising permanent-magnet quadrupoles. Some empty drift tubes contain beam position monitors and dipole correctors. The inter-tank sections contain toroidal beam current monitors, wire scanners and energy degrader/faraday cups.

To date, the entire DTL has been RF-tuned and installed in the linac tunnel. DTL tank tuning has resulted in longitudinal fields within the specification of −1% of design. The first three DTL tanks have been commissioned with beam.

The first three of six DTL tanks have been commissioned with beam in two separate runs. In the first run, DTL tank 1 (output energy 7.5 MeV) was commissioned into a dedicated diagnostics system (the "D-plate") equipped with a full-power beam stop. In the second commissioning run, DTL tanks 1-3 (output energy 40 MeV) were commissioned into a low-power beam stop. The goals of the commissioning runs have been to demonstrate full system functionality, demonstrate beam acceleration with design beam parameters to the limits of the available beam stop, test and validate beam commissioning algorithms, and commission the installed diagnostic devices.

The basic procedure for setting the RF phase and amplitude of the DTL tanks relies on installed energy degrader/faraday cups (ED/FC) after each tank. A thin carbon absorber with thickness chosen to absorb low-energy beam particles is placed in front of a faraday cup (FC), and the FC signal is recorded as a function of the tank phase and amplitude. The phase is obtained by maximising the transmitted (on-energy) beam current, while the amplitude is determined by comparing the measured phase-width of the transmitted current with simulation predictions.

For the DTL1 beam commissioning run, a dedicated diagnostics system with energy degrader/ faraday cups, wire scanners, beam position monitors, slit/harp emittance system and a bunch-shape monitor was installed following the tank to enable detailed characterisation of the output beam parameters. Following this short diagnostics beam line was a full beam-power beam stop.

Table 2 summarises the DTL commissioning results. The design peak current of 38 mA was readily achieved. A 1-msec long beam pulse was generated at a 20-mA average current during the pulse (at low duty factor). Finally, a 1-mA average current beam was accelerated in DTL1 with 100% beam transmission. For this demonstration, a beam pulse of 26-mA peak current, 650-microsecond pulse length at 60 Hz (7.5-kW beam power) was achieved. Figure 1 shows an overlay of beam current monitor signals in the MEBT and DTL1 during this high-power operation.

Extensive DTL1 output beam emittance measurements were performed. Figure 2 shows a vertical emittance measurement at a 38-mA peak current. The data are analysed in two ways. First, a Gaussian fit is performed to the two-dimensional beam distribution in position-angle space to obtain an emittance that is representative of the beam core. Values obtained in this way are 0.21 π mm mrad (RMS, normalised) in the vertical plane and 0.30 π mm mrad in the horizontal plane. In a second analysis, the RMS of the beam distribution is calculated with a 1% threshold (relative to the peak beam intensity) to remove spurious noise. Values obtained in this way are somewhat larger than the core emittances: 0.31 π mm mrad, and 0.40 π mm mrad in the vertical and horizontal, respectively. Further analysis of the large set of emittance data is in process.

DTL tanks 1-3, with output energies of 40 MeV, were recently beam commissioned. Again, peak currents of 38 mA transported through all three tanks with 100% transmission were demonstrated. The beam stop limited beam pulse lengths to less than 50 microseconds, and repetition rates to 1 Hz.

Figure 1. Overlay of beam current monitors after the RFQ, MEBT, DTL1 and at the beam stop, respectively. The data were recorded during the 1-mA average current, high-power run.

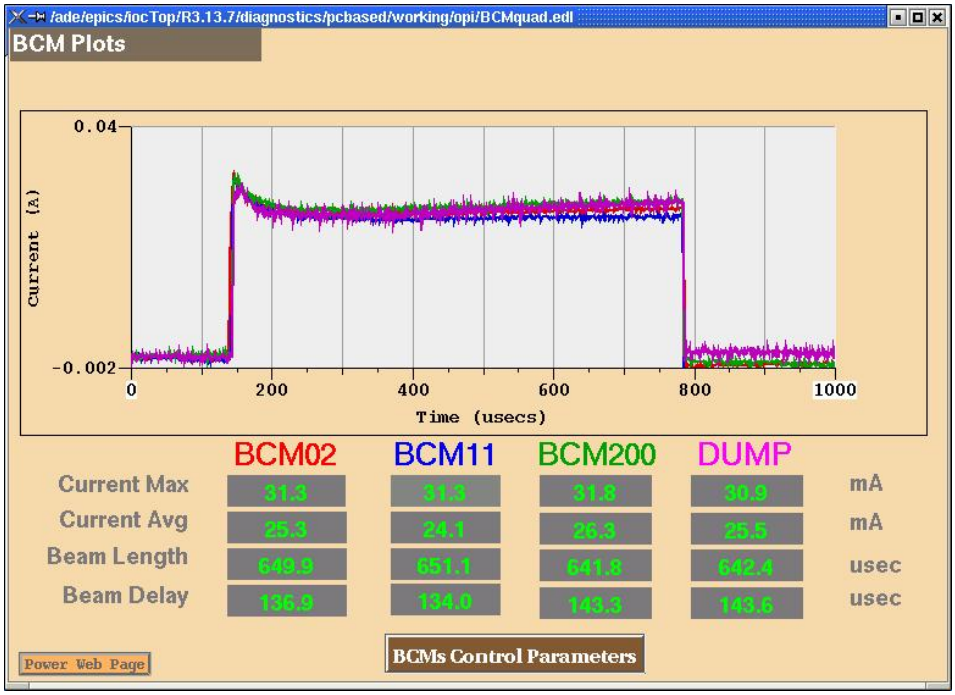

Figure 2. DTL tank 1 vertical output emittance at 38-mA peak current. Angle (mrad) is plotting vs. position (mm).

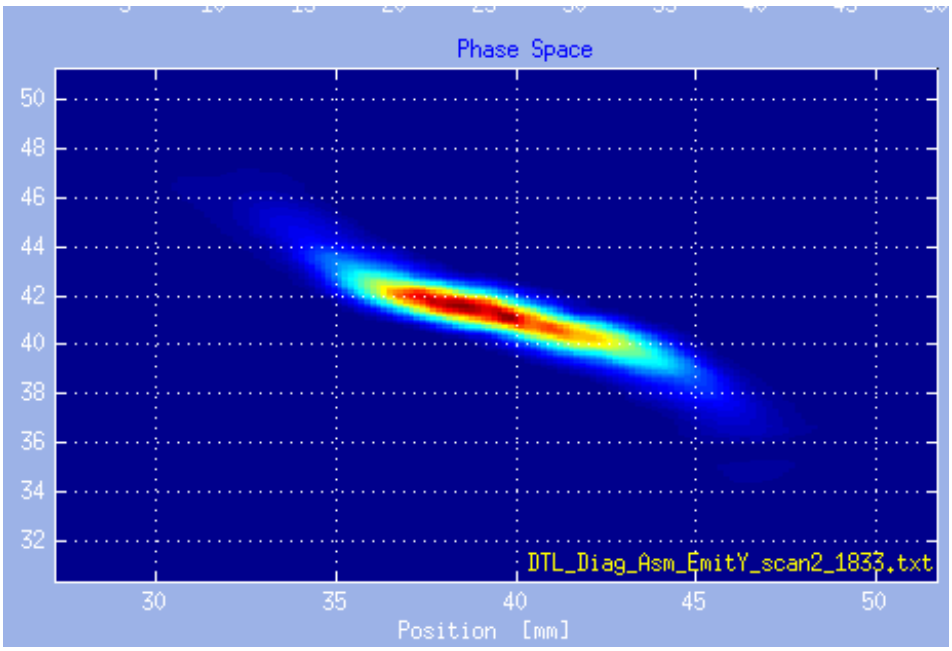

Coupled-cavity linac status

The CCL consists of four modules, each containing 12 segments (coupled by bridge couplers) driven in the p/2 mode. The CCL operates at 805 MHz, double the frequency of the upstream linac components. Each module is powered in two locations with a single 5-MW peak power klystron. The inter-segment spaces contain quadrupoles, dipole correctors and a suite of diagnostic devices, including beam position monitors, wire scanners, and bunch-shape monitors for measuring the longitudinal beam profile.

The coupled-cavity linac modules have been manufactured, delivered and installed in the tunnel. The first two modules have been RF-tuned, and the last two modules are being tuned. CCL module 1 was RF-processed up to the design accelerating field in approximately two days. Installation of the remaining CCL beam line hardware is in progress. The complete DTL and CCL linacs will be commissioned in August 2004.

Superconducting linac status

The superconducting linac is being built by the Thomas Jefferson National Accelerator Facility. The SCL utilises six-cell elliptical p-mode superconducting niobium accelerating cavities. Two structures, one with matched velocity b = 0.61 (the medium-beta cavity), and another with matched b = 0.81 (the high-beta cavity) are used in the SCL. The medium-beta portion of the SCL consists of 33 cavities in 11 cryomodules, and the high-beta portion consists of 48 cavities in 12 cryomodules. The peak surface field in the medium-beta cavities is 27 MV/m, giving an accelerating gradient of 10.2 MV/m for the matched particle. In the high-beta cavities, the nominal peak surface fields are 35 MV/m, giving 15.6 MV/m accelerating gradient. The quality factor is greater than $5 \cdot 10^9$. The transverse focusing is accomplished with a doublet focusing lattice located in the warm sections between cryomodules. Each RF cavity in the SCL is independently powered by a single 550-kW klystron. This powering scheme maximises the flexibility of the SCL, providing the ability to drive well-performing cavities harder, and "tune-around" cavities that may be unpowered. In addition to beam position monitors, a laser-based beam profile system is being utilised [6].

To date, all medium-beta cryomodules have been constructed, and eight have been installed in the tunnel on the SNS site. All cavities have exceeded the specified accelerating gradient and quality factor. The high-beta cryomodules are in full production. Recently, 4.5 K liquid He was made in the central helium liquifier (CHL). CHL commissioning is underway and it is expected that the first cryomodule will be cooled down in late summer 2004. Testing of cryomodules in the linac tunnel will proceed through late 2004, with beam commissioning of the SCL scheduled for March 2005.

Ring and transport lines status

The ring and transport line systems were designed by Brookhaven National Laboratory (BNL). The H^- beam from the linac is transported to the ring in the high-energy beam transport (HEBT) line. Before the 90 bend in the HEBT is a tuning beam dump (the linac dump) which will be used for linac commissioning and linac tune-up during operations. The HEBT delivers the beam to the stripping foil for charge-exchange injection into the accumulator ring. Un-stripped H^- and partially stripped (H^0) beams are fully stripped in a second foil and transported to the injection dump via the injection dump line. The injection dump is designed to handle 10% of the design beam power (150 kW) that can be expected from the combination of stripping inefficiency and linac beam that misses the foil. Also included in the HEBT are transverse and longitudinal collimation systems which remove the beam halo and deposit those particles in fixed absorbers.

The ring is a four-fold symmetric lattice with long straight sections each with a dedicated function. The injection systems are contained in one straight section, fixed collimators are located in another, the extraction systems populate the third, and the RF systems are contained in the fourth section. The 1-msec long beam pulse from the linac is accumulated over 1 060 turns in the ring by charge-exchange multi-turn injection. Phase-space painting is utilised in all three dimensions. In the transverse, sets of horizontal and vertical injection kickers are used to ramp the closed orbit away from the injection foil during accumulation. Longitudinal painting is accomplished with an energy spreader cavity. The beam is captured in a single h = 1 RF bucket of 40-kV amplitude with a dual-harmonic (h = 2) amplitude of 20 kV to increase the bunch factor.

Central to achieving low loss in the ring is adequate vacuum chamber aperture and an efficient collimation system [7]. The uncontrolled beam loss criteria for the ring is 1 W/m, which amounts to about 10^{-4} fractional uncontrolled beam loss. The vacuum chamber aperture is everywhere at least 480 p mm mrad, with the exception of the fixed collimators, which provide limiting horizontal and vertical apertures of 300 p mm mrad in heavily shielded and water-cooled collimator assemblies. Phase-space painting is performed in all three dimensions to a resulting transverse emittance of about 200 p mm mrad. The collimation system is "two-stage" in the sense that beam halo particles first strike a fixed scraper, placed at about 240 p mm mrad, propelling these particles to large amplitude, so that they are removed at the fixed collimators. Simulations show that about 10^{-3} of the beam particles strike the primary scraper, and about 90% of those are absorbed in the fixed collimators, with the other 10% giving rise to uncontrolled beam loss at a level of 10^{-4} of the beam.

Once accumulation is complete, a set of single-turn kickers are fired to deflect the accumulated beam into the ring-to-target beam (RTBT) transport line which takes the beam to the liquid mercury target. Located midway along the RTBT is another tuning beam dump (the extraction dump) with a 7.5-kW beam power capability.

The HEBT beam line is almost completely installed and the straight portion is under vacuum. The ring arcs are delivered in "half-cell" assemblies which contain one dipole, one quadrupole and associated correctors and their beam pipes. Twenty-five (25) of the 32 half-cells have been delivered and installed in the tunnel. Ring power supply production is in full swing and power supply delivery has commenced. Ring high-power RF systems have been built and the first has been delivered to ORNL. The injection magnet systems are built and an assembly test is underway. The collimation systems are being delivered to ORNL. Ring beam commissioning up to the extraction beam dump is scheduled for June-November 2005. Commissioning of the final portion of the RTBT and the liquid mercury target itself is scheduled for February 2006 in order to declare project construction completion in March 2006.

REFERENCES

[1] Prior, C., *et al*., *Proc. Part. Acc. Conf. 2003*, p. 1527.

[2] Holtkamp, N., *Proc. Part. Acc. Conf. 2003*, p. 11.

[3] Aleksandrov, A., *Proc. Part. Acc. Conf. 2003*, p. 65.

[4] Jeon, D., *Proc. Part. Acc. Conf. 2003*, p. 107.

[5] Wei, J., *Proc. Part. Acc. Conf. 2003*, p. 571.

[6] Assadi, S., *Proc. Part. Acc. Conf. 2003*, p. 2706.

[7] Cousineau, S., *et. al*., *Proc. Eur. Part. Acc. Conf. 2002*.

TECHNICAL SESSION II

Target, Window and Coolant Technology

Chairs: X. Cheng, T-Y. Song

RESEARCH AND DEVELOPMENT ON LEAD-BISMUTH TECHNOLOGY FOR ACCELERATOR-DRIVEN TRANSMUTATION SYSTEM AT JAERI

Yuji Kurata[1], **Kenji Kikuchi**[1], **Shigeru Saito**[1],
Kinya Kamata[2], **Teruaki Kitano**[2], **Hiroyuki Oigawa**[1]
[1]Japan Atomic Energy Research Institute, Japan
[2]Mitsui Engineering & Shipbuilding Co., Ltd., Japan

Abstract

R&D on lead-bismuth technology have been conducted for an accelerator-driven system. From the test results of 316SS using JLBL-1 for 3 000 h without active oxygen control, mass transfer from high temperature to low temperature parts was observed. It was found that deposition of Pb/Bi and Fe-Cr grains in the annular channel of the electro-magnetic pump caused plugging and decrease in flow rate. The modification of the loop system brought about a good effect on operation. Significant erosion/ corrosion was not observed in the experiment using the MES loop for 1 000 h under 10^{-5} wt.% oxygen conditions. The results of static corrosion tests showed the following: corrosion depth decreased at 450 C with increasing Cr content in steels while corrosion depth of JPCA and 316SS became larger due to ferritisation caused by dissolution of Ni and Cr at 550 C. Si-added steel exhibited good corrosion resistance at 550 C.

Introduction

The management of high-level radioactive wastes (HLW) is one of the most important issues for the utilisation of nuclear fission energy. The accelerator-driven transmutation system (ADS) is an attractive system which enables to incinerate long-lived nuclear wastes such as minor actinides by combining a proton accelerator, spallation target and subcritical core [1,2]. Therefore, research and development (R&D) concerning the ADS have been carried out in recent years.

Liquid Pb-Bi eutectic (LBE) is a potential candidate of the target and coolant for the ADS. The LBE has the advantage of a low melting point, low vapour pressure, good neutron yield, low neutron absorption and chemical stability in comparison with sodium. However, LBE technologies have not yet been fully established for nuclear systems. In particular, corrosion of structural materials is a concern due to the high solubility of the main elements of the structural materials in LBE.

In order to realise the ADS, JAERI has started a wide range of R&D activities: design study of a large-scale ADS, superconducting linear accelerator, LBE and subcritical reactor physics technologies. In the LBE technologies, four main fields are being studied: 1) corrosion of structural materials, 2) thermal-hydraulics of LBE, 3) behaviour of radioactive impurities, and 4) irradiation damage of materials by protons and neutrons. R&D activities on corrosion of structural materials are reviewed in this paper.

Liquid metal loops are often used to estimate the actual corrosion behaviour in LBE since velocity effect, erosion and mass transfer caused by solution at high-temperature parts and precipitation at low-temperature parts are involved in the ADS plant. The LBE loop for material corrosion (JLBL-1) was installed at JAERI in January 2001 and corrosion tests have been conducted [3,4]. Furthermore, material corrosion loop tests are underway at Mitsui Engineering & Shipbuilding Co., Ltd. (MES) as a joint research to accumulate a materials database for the ADS. Static corrosion tests are also useful for understanding corrosion mechanisms and screening various materials. The purpose of this paper is to describe the status and results of LBE loop tests and static corrosion tests. First, the design of a large-scale ADS will be shortly introduced. After results of material corrosion tests using JLBL-1 are described, the results obtained in an oxygen-controlled LBE using the MES loop are discussed. In addition, static corrosion test results are presented focusing on the effects of temperature and alloying elements in steels on corrosion behaviour.

Design of a large-scale ADS

The ADS proposed by JAERI is an 800 MWth, LBE-cooled, tank-type subcritical reactor with a spallation target of LBE. Figure 1 shows a conceptual drawing of the 800 MWth LBE-cooled ADS. Two criteria were set regarding the thermal-hydraulics and the beam window: 1) the flow rate of LBE should not exceed 2 m/sec and 2) the outer surface temperature of the beam window should not exceed 520 C. As a result of some design modifications, the coolant inlet temperature and outlet temperature were 300 C and 410 C, respectively. Figure 2 shows the results of thermal-hydraulics and temperature analyses for the LBE target and beam window.

Corrosion tests using JLBL-1

Figure 3 shows an initial flow diagram of JAERI materials testing of the Pb-Bi loop (JLBL-1). This loop consists of an electro-magnetic pump, a heater, a test section, a cooler, an expansion tank, an electro-magnetic flow meter and a dump tank. The electro-magnetic pump is a linear inductive type with

Figure 1. Concept drawing of 800 MWth ADS

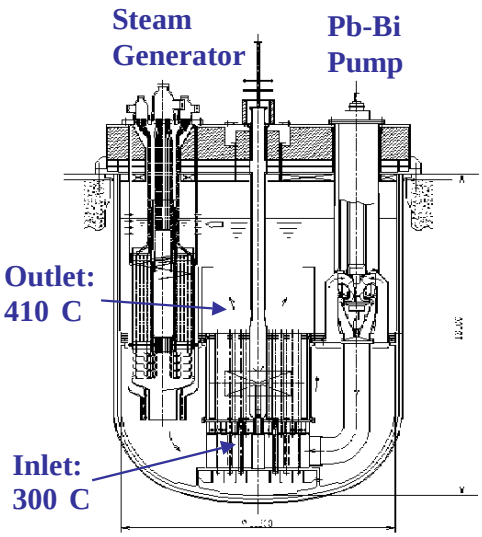

Figure 2. Results of (a) hydraulic and (b) temperature analysis for LBE target and beam window

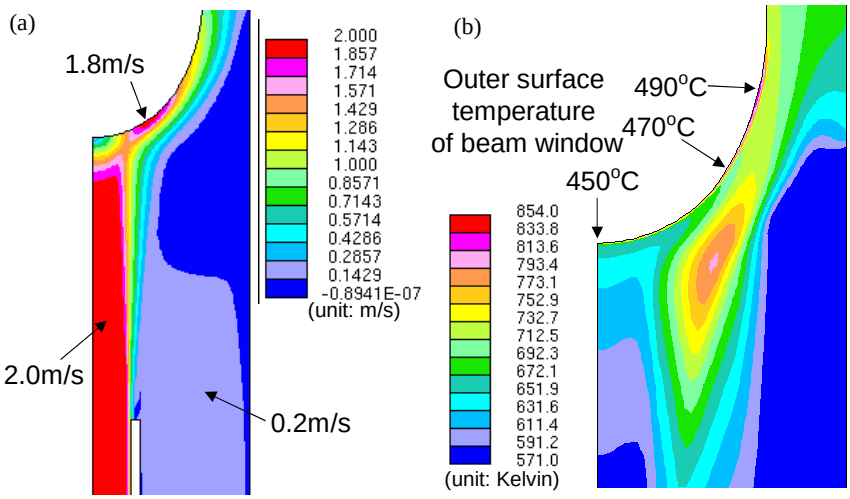

Figure 3. Flow diagram of materials testing Pb-Bi loop (JLBL-1)

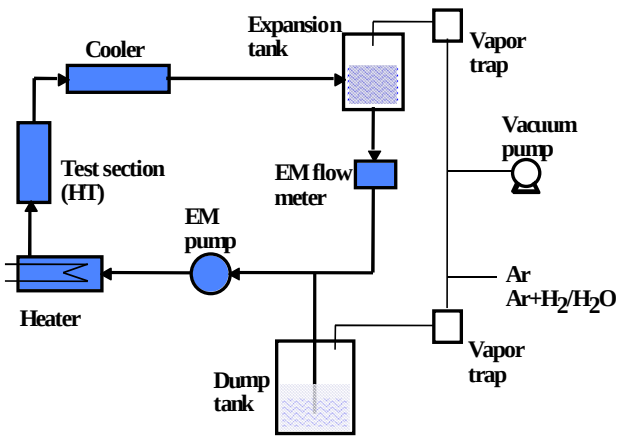

an annular channel. The test section is a specimen tube with an inner diameter of 9.8 mm and a tube thickness of 2 mm. All of the materials for the piping and tanks in contact with LBE were type 316SS. In the first and second tests, type 316SS was used as a specimen tube. During the first test, the maximum temperature, the temperature difference and the flow velocity at the test section were 450 C, 50 C and about 1 m/s, respectively. Initially the electro-magnetic flow meter was calibrated. The calibration curve was obtained from the correlation between the EMF output and the flow rate measured from the time in a constant level change in the expansion tank during the drainage. Figure 4 shows a schematic diagram of the electro-magnetic flow meter and the calibration curve obtained at 400 C. Electrodes of the electro-magnetic flow meter contact with flowing Pb-Bi in the flow channel. As shown in Figure 4, a linear relationship between the output and the flow rate was obtained. An argon gas of 99.95% purity covered the expansion tank during the operation. Oxygen in LBE was not controlled actively. Thin floating oxide was observed on the surface of LBE in the expansion tank through the observing window. It was thus considered that the oxygen concentration under operation was the saturation concentration, $3.2 \cdot 10^{-4}$ wt.%.

Figure 4. Schematic diagram of an electromagnetic flow meter and the relationship between flow rate and the output of the flow meter. The temperature of liquid Pb-Bi was 400 C.

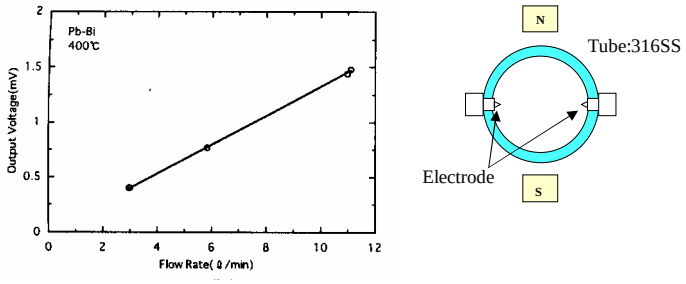

The first test result of JLBL-1 is described hereafter. After the first test of about 3 000 h (3 126 h), a specimen, circulation tubes and an electro-magnetic pump channel were cut and inspected. Figure 5 shows the axial cross-section of type 316SS specimen tube after the corrosion test. As can be seen in this figure, pits and hollows are observed and a grain boundary fissure is also recognised. The final treatment of the type 316SS specimen tube was cleaning with hot acid. Since this treatment produced deeply dug grain boundaries, it is considered that the rough surface with deeply dug grain boundaries accelerated corrosion/erosion by flowing Pb-Bi. The corrosion depth of type 316SS at the high-temperature part is estimated to be about 100 ㎜/3 000 h.

Figure 5. Corrosion of type 316SS tube specimen after the first corrosion test in liquid Pb-Bi using JLBL-1

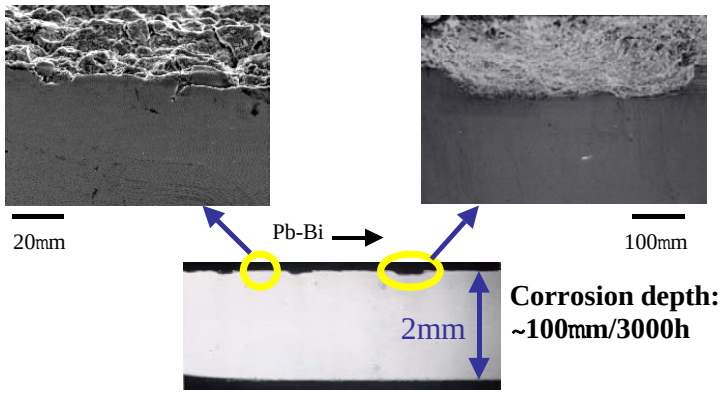

A decrease in the flow rate with increasing operation time was experienced during the first test. It was remarkable when the corrosion test was restarted after draining of Pb-Bi on account of a stoppage of electric supply. In order to examine the cause of the decrease in flow rate, not only a specimen but also circulation tubes and an electro-magnetic pump channel were inspected. Figure 6 shows an appearance of the shaft of the electro-magnetic pump and the analysis of the deposits in a channel. It was found that grey, thick deposits formed in the narrow channel causing plugging and the decrease in flow rate. As shown in Figure 10, the deposits consist of Pb/Bi and grains of Fe-Cr ferrite. Precipitation of these grains consisting of Fe-Cr (Fe:Cr = 9:1) was widely found on the circulation tubes at 400 C [3]. The considered process of dissolution and precipitation is the following: Fe, Cr and Ni are dissolved into Pb-Bi from type 316SS at the high-temperature parts and Fe-Cr grains precipitate at the low-temperature parts according to the difference in solubility.

Figure 6. Analysis of deposits in a narrow channel of the electro-magnetic system: EDX analysis of cross-section of deposits

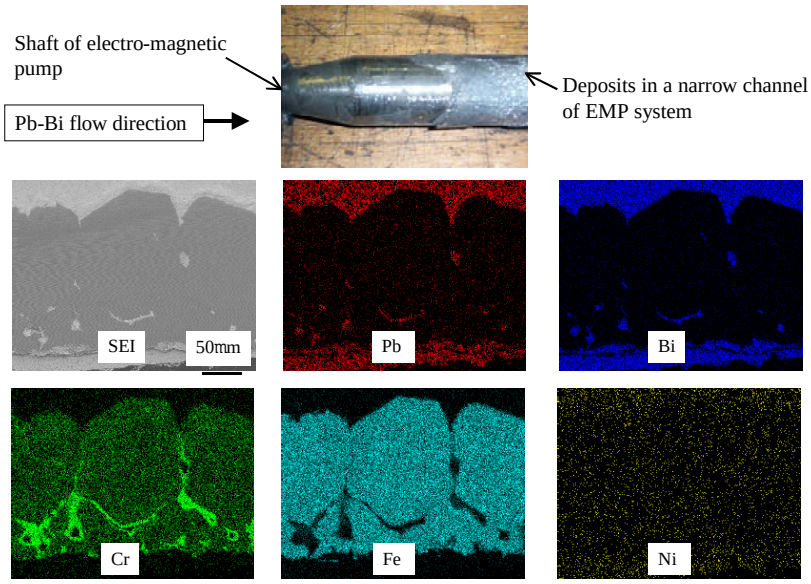

In the second corrosion test, modification of JLBL-1 and the tube specimen was carried out. Three metallic filters were set and the channel of liquid Pb-Bi in the EMP system was made wider in JLBL-1. Although an oxygen control system and an oxygen sensor were also set in the loop, they were not used in the second corrosion test. The inner surface of type 316SS tube specimen was mechanically polished before testing. Other experimental conditions in the second corrosion test were the same as those in the first one. Decrease in Pb-Bi flow was not observed up to 3 000 h in the second test. It is considered that addition of metallic filters to JLBL-1 and modification of the EMP system had a positive effect on the operation of the Pb-Bi loop system. Furthermore, the corrosion depth of type 316SS was reduced to about 20 ㎜ in the second loop test.

Corrosion tests using MES loop

A material corrosion test was conducted using an MES loop to accumulate a wide range of corrosion data in LBE. Figure 7 shows a flow diagram of the MES loop. The loop consists of an electro-magnetic pump, an electro-magnetic flow meter, an economiser, a heater, a test section, an air cooler, an expansion tank, oxygen sensors, an oxygen control system, filters and a dump tank. Oxygen sensors produced by MES were set in the loop. Yttria-stabilised zirconia (YSZ) solid electrolyte and a

Figure 7. Flow diagram of the Mitsui Engineering and Shipbuilding Co., Ltd (MES) loop

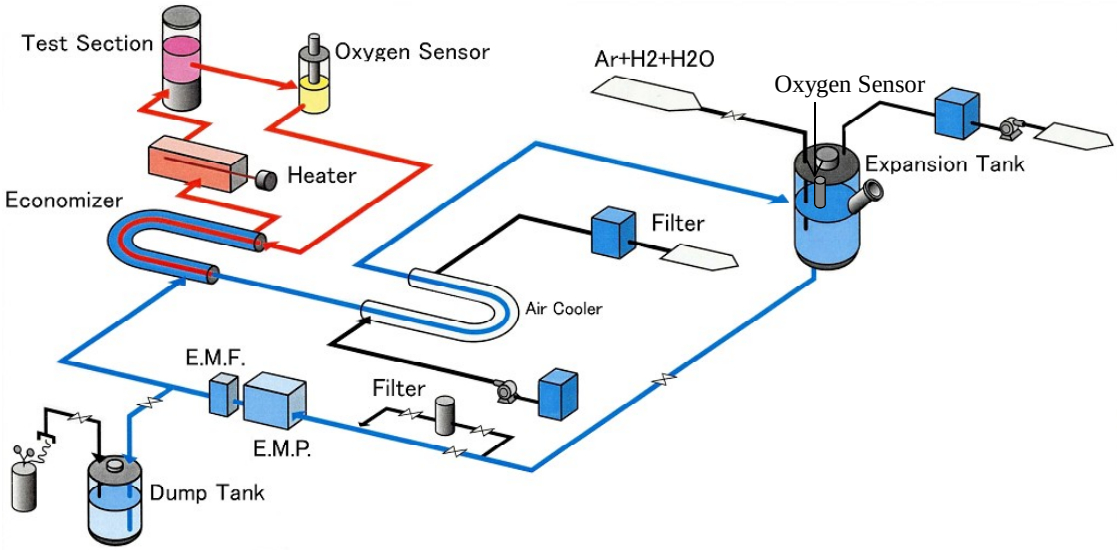

Bi/Bi_2O_3 reference electrode were used in the oxygen sensor. Bubbling of Ar-H_2 gas and Ar-H_2/H_2O gas was used for the control of oxygen concentration in LBE. Figure 8 shows the arrangement of specimens and Pb-Bi flow direction at the test section in MES loop. The relationship between the specimen and the Pb-Bi flow simulated that between the beam duct and Pb-Bi flow in the conceptual drawing of the ADS. The liquid Pb-Bi collides the tip of specimens and flows up the side of specimens axially. The specimen was rod-type with a diameter of 8 mm and a length of 130 mm. JPCA (15Cr-15Ni-2Mo) and F82H (8Cr-2W) steels were used as specimens. During the test using the MES loop, the maximum temperature, temperature difference and flow velocity at the test section inlet were 450 C, 100 C and 0.4~0.6 m/s, respectively. Oxygen concentration in LBE was controlled to $1 \cdot 10^{-5}$ wt%. The test time was 1 000 h.

Figure 8. Schematic drawing of test section in the MES loop and rod-type corrosion specimens

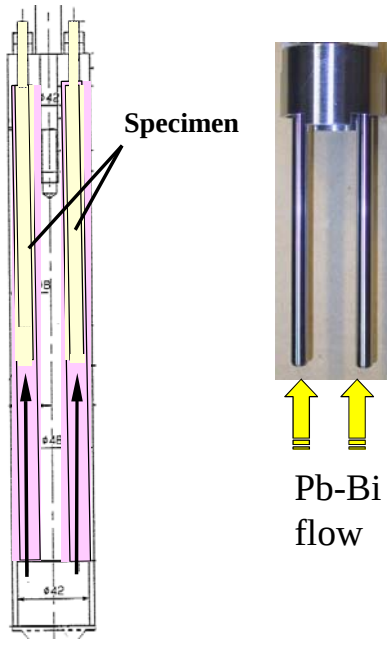

Figure 9 shows a cross-section of the F82H specimen after corrosion for 1 000 h. Significant corrosion/erosion was not observed at either the tip or side parts at 450 C for 1 000 h. Uniform oxide films were formed on the surface of all parts including the tip. From electron-probe micro analysis and X-ray diffraction results, the oxide films consist of outer magnetite, Fe_3O_4 and inner spinel Fe-Cr oxide. The thickness of the oxide films was from 6 to 8 mm. The thickness of the oxides formed on F82H in this study was below half that formed on 2.25Cr-1Mo steel tested under similar conditions at the Institute for Physics and Power Engineering (IPPE) loop. As seen in Figure 10, no significant corrosion/erosion was observed for the JPCA specimen, although there were small hollows with a depth of 1~2 mm near the corner of the tip. A hole with a depth of 8~10 mm was also observed near the corner of JPCA (Figure 11). The oxide film was not detected on the surface of the JPCA specimen by usual methods. A corrosion test with a maximum temperature of 500 C is underway using the MES loop. Corrosion tests with longer times are also scheduled.

Figure 9. Cross-section of F82H specimen after corrosion test for 1 000 h using the MES loop

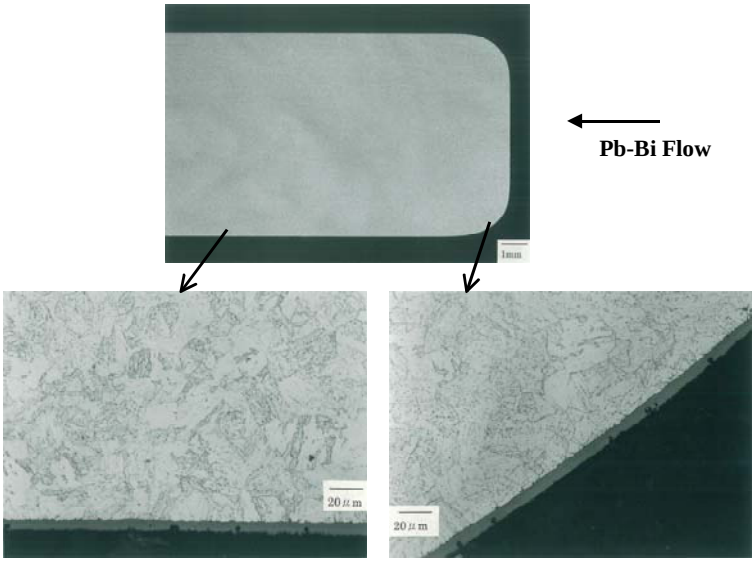

Figure 10. Cross-section of JPCA specimen after corrosion test for 1 000 h using the MES loop

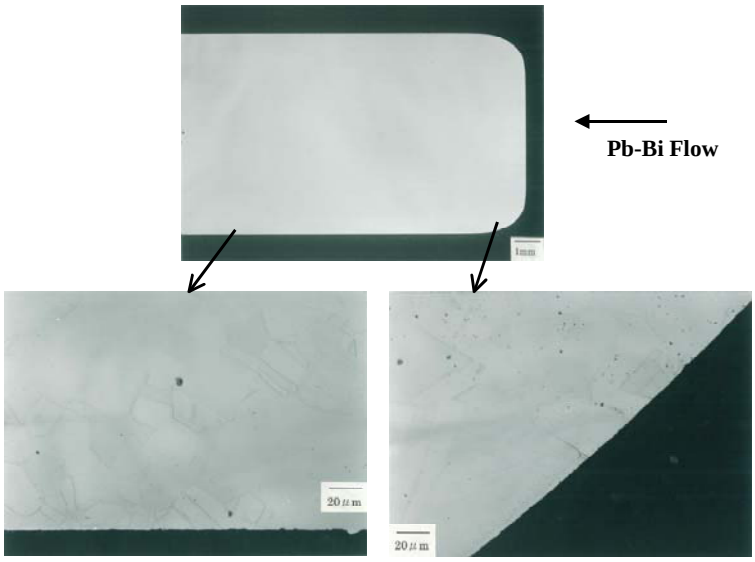

Figure 11. A hole with a depth of 8~10㎛m observed on the corner at JPCA specimen after corrosion test

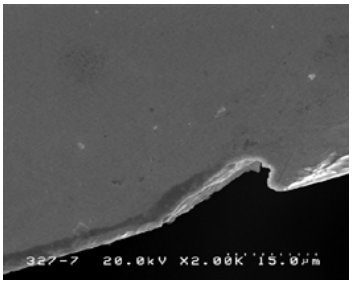

Static corrosion tests

Static corrosion tests of various steels were conducted in oxygen-saturated liquid Pb-Bi at 450 C and 550 C for 3 000 h to study the effects of temperature and alloying elements on corrosion behaviour. Materials used in the experiment were F82H (8Cr-2W), Mod.9Cr-1Mo (9Cr-1Mo), 410SS (12Cr), 430SS (16Cr), 2.25Cr-1Mo, Fe, JPCA (15Cr-15Ni), 316SS (17Cr-11Ni) steels and Si-added steel, SX (18Cr-19Ni-5Si). The size of corrosion specimens was 15 mm · 30 mm · 2 mm, and a hole 7.2 mm in diameter was made at the top of the specimen for installation. Figure 12 shows a schematic drawing of static corrosion equipment. Components contacting liquid Pb-Bi were made of quartz in the corrosion equipment. Fresh eutectic Pb-Bi (45Pb-55Bi) of 7 kg was used in the test. The Pb-Bi was melted in a pot under an argon gas environment. Argon gas of 99.9999% purity was used as a cover gas over the liquid Pb-Bi. Corrosion tests were conducted at 450 C and 550 C for 3 000 h. A thin PbO film was formed on the surface of the liquid Pb-Bi and corrosion tests were made in oxygen-saturated liquid Pb-Bi. Oxygen saturation concentration was estimated to be $3.2 \cdot 10^{-4}$ wt.% at 450 C and $1.2 \cdot 10^{-3}$ wt.% at 550 C using the equation in the literature [5].

Figure 12. Schematic drawing of static corrosion equipment in liquid Pb-Bi

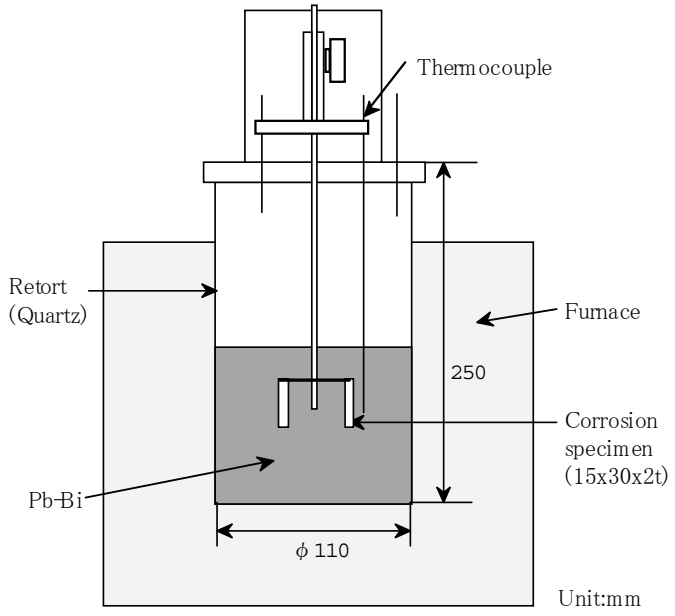

Figure 13 shows the relationship between corrosion depth and Cr content in steels with some scanning electron microscope (SEM) images after corrosion at 450 C. Corrosion depth decreased at 450 C with increasing Cr content in the steels regardless of ferritic/martensitic steels or austenitic steels. The corrosion depth of Si-added steel, SX, was very small. The corrosion films of the steels, except for SX, were oxides of Fe and Cr. A decrease in Cr, Ni and Fe concentrations was not observed near the surface region from the results of EDX analysis for JPCA and 316SS specimens after corrosion at 450 C; it is considered that appreciable dissolution of these elements has not occurred under these conditions.

Figure 13. Results of static corrosion test at 450 C for 3 000 h

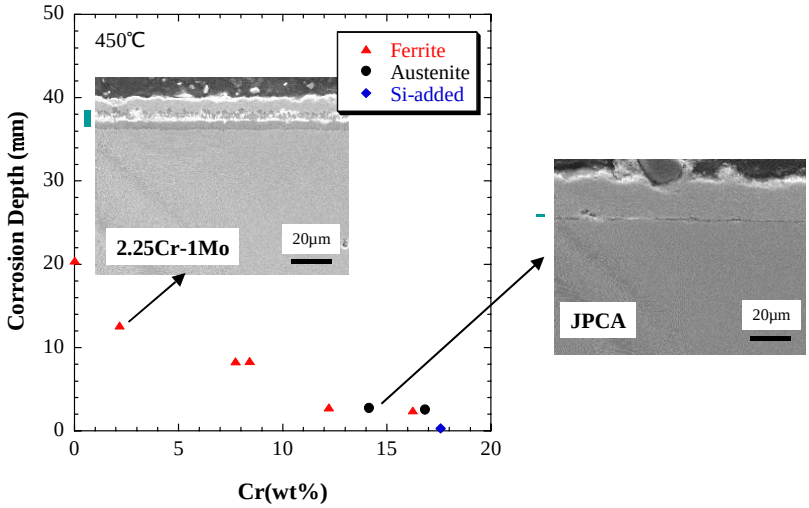

On the other hand, the thick ferrite layer produced by dissolution of Ni and Cr was formed on the surface of JPCA and type 316SS with low Si contents. Pb and Bi penetrated into the formed ferrite layer. Figure 14 shows the relationship between corrosion depth and Cr content in steels with some SEM images after corrosion at 550 C. The corrosion depth of ferritic/martensitic steels, which is shown as a triangle in the figure, also decreases at 550 C with increasing Cr content in the steels while corrosion depth of austenitic steels, JPCA and 316SS, becomes large because of the formation of the ferrite layer at 550 C.

Figure 14. Results of static corrosion test at 550 C for 3 000 h

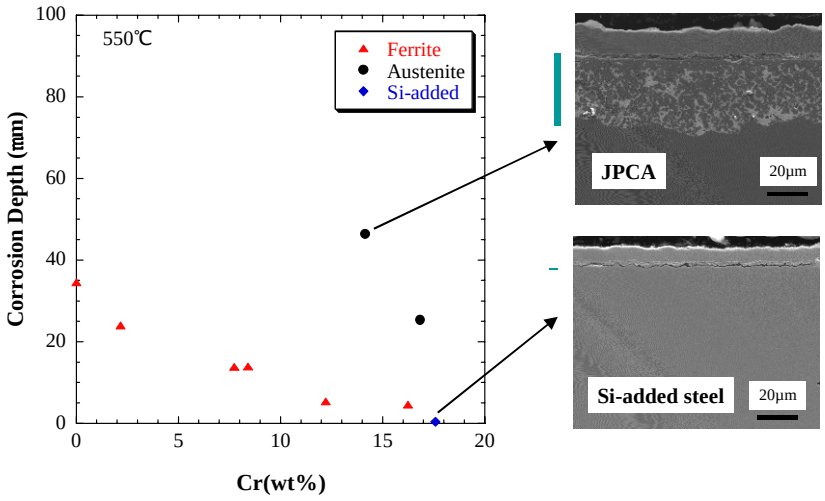

The corrosion depth of SX is very small at 550 C in spite of the austenitic steel. A protective oxide film composed of Si and O is formed on the surface of SX containing 4.8% Si during corrosion in liquid Pb-Bi at 550 C. The thin oxide film prevents dissolution of Ni and Cr into Pb-Bi and the steel containing Si shows excellent corrosion resistance in LBE [6]. Martensitic steels containing Si were developed for nuclear use in Russia [7]. Russian martensitic steel with 1.8% Si exhibited good corrosion resistance in flowing liquid Pb-Bi [8,9]. Some Al surface-alloyed steels also showed good corrosion resistance in flowing liquid Pb-Bi [10]. It is considered that SX steel exhibited good corrosion resistance in LBE because of its high Si content, about 5%.

Conclusions

Research and development on lead-bismuth technology for ADS have been conducted at JAERI and MES as a joint research programme with progress of design study of a large-scale ADS. The main results are as follows:

- From the first test result of JLBL-1, mass transfer from high-temperature to low-temperature parts was observed. Grains of Fe-Cr precipitated at the low-temperature parts. The corrosion depth of type 316SS at the high-temperature part was estimated to be about 100 ㎜/3 000 h. From experience of operating JLBL-1, it was found that deposition of Pb-Bi and Fe-Cr grains in the annular channel of the electro-magnetic pump caused plugging and decrease in flow rate. The modification of the loop system such as adoption of metallic filters and a wide channel, and the use of an inner-polished 316SS tube brought about a good effect.

- The corrosion test using the MES loop was conducted under the condition where the liquid Pb-Bi collides with the tip of rod-type specimens under oxygen-controlled conditions. Significant corrosion/erosion was also not observed for F82H and JPCA specimens in the experiment for 1 000 h under 10^{-5} wt.% oxygen condition. Oxygen control techniques in LBE were obtained through operating the MES loop.

- The results of static corrosion tests under oxygen-saturated conditions showed effects of temperature and alloying elements in steels on corrosion behaviour. Corrosion depth decreased at 450 C with increasing Cr content in steels regardless of ferritic/martensitic steels or austenitic steels. The corrosion depth of ferritic/martensitic steels also decreased at 550 C with increasing Cr content in steels, whereas the corrosion depth of austenitic steels, JPCA and 316SS became larger due to ferritisation caused by dissolution of Ni and Cr at 550 C than that of ferritic/ martensitic steels. An austenitic stainless steel containing about 5% Si exhibited fine corrosion resistance at 550 C because the protective Si oxide film was formed.

Acknowledgements

This work was partly funded by the Ministry of Education, Culture, Sports, Science and Technology (MEXT) as one of the R&D programmes for innovative nuclear systems. The authors are grateful to Drs. Tsujimoro, Sasa and Nishihara of JAERI, Dr. Iwata of Mitsubisi Heavy Industries Ltd and Dr. Ono of Mitsui Engineering & Shipbuilding Co., Ltd.

REFERENCES

[1] Takano, H., K. Nishihara, K. Tsujimoto, T. Sasa, H. Oigawa and T. Takizuka, *Progress in Nuclear Energy*, 37, 371 (2001).

[2] Mukaiyama, T., T. Takizuka, M. Mizumoto, Y. Ikeda, T. Ogawa, A. Hasegawa, H. Takada and H. Takano, *Progress in Nuclear Energy*, 38, 107 (2001).

[3] Kikuchi, K., Y. Kurata, S. Saito, M. Futakawa, T. Sasa, H. Oigawa, E. Wakai, K. Miura, *J. Nucl. Mater*., 308, 348 (2003).

[4] Kurata, Y., M. Futakawa, K. Kikuchi, S. Saito, T. Osugi, *J. Nucl. Mater*., 301, 28 (2002).

[5] Gromov, B.F., Y.I. Orlov, P.N. Martynov and V.A. Gulevsky, *Proceedings of Heavy Liquid Metal Coolants in Nuclear Technology, HLMC'98*, 5-9 October 1998, Obninsk, Russia, p. 87 (1999).

[6] Kurata, Y., M. Futakawa, *J. Nucl. Mater*., 325, 217 (2004).

[7] Yachmenyov, G.S., A.Ye. Rusanov, B.F. Gromov, Yu.S. Belomytsev, N.S. Skvortsov and A.P. Demishonkov, *Proceedings of Heavy Liquid Metal Coolants in Nuclear Technology, HLMC'98*, 5-9 October 1998, Obninsk, Russia, p. 133 (1999).

[8] Barbier, F., A. Rusanov, *J. Nucl. Mater*., 296, 231 (2001).

[9] Benamati, G., C. Fazio, H. Piankova, A. Rusanov, *J. Nucl. Mater*., 301, 23 (2002).

[10] Mueller, G., A. Heinzel, J. Konys, G. Schumacher, A. Weisenburger, F. Zimmermann V. Engeliko, A. Rusanov, V. Markov, *J. Nucl. Mater*., 301, 40 (2002).

VACUUM GAS DYNAMICS INVESTIGATION AND EXPERIMENTAL RESULTS ON THE TRASCO ADS WINDOWLESS INTERFACE

P. Michelato, E. Bari, E. Cavaliere, L. Monaco, D. Sertore
INFN Milano, LASA, Italy

A. Bonucci, R. Giannantonio
SAES Getters S.p.A., Italy

L. Cinotti
Ansaldo, Italy

P. Turroni
ENEA Bologna, Italy

Abstract

TRASCO ADS is a programme aiming at the design of an accelerator-driven subcritical system in which INFN, ENEA and Italian firms work on the preliminary study and design of the high-intensity proton linac accelerator and on the windowless interface between the accelerator and the reactor.

The accelerator UHV and the spallation target vacuum are divided only by a suitable pumping and trapping system for the gases and the vapours emerging from the molten LBE. In order to design a pumping system for the accelerator-reactor interface region, vacuum gas dynamics theoretical considerations and experimental evaluations are needed to understand the behaviour of the vapours and gases in the target region. For the same purpose the literature data and experimental results on the radioactive gases and vapours, produced by the spallation process, must be investigated.

From the vacuum gas dynamics point of view, a numerical method based on angular coefficients has been validated to estimate the net flux of the LBE vapours and the gases coming from the spallation process, the oxidation control and the tube outgassing.

From the safety point of view, preliminary experiments are under way for an estimation of the net flux of high-activity gases such as mercury and polonium (using tellurium as a polonium simulator) with the purpose to evaluate the radioactivity in the beam tube.

All these data, compared with those from literature and the experimental results, give an improvement towards a suitable design of the pumping system for an ADS windowless interface according to technological and nuclear safety constrains.

Introduction

The vacuum system specifications and performances for the windowless interface of an ADS are critical due to many factors. The vacuum system has to ensure the proper vacuum conditions both in the linac and in the interface region. Moreover, it absolutely must ensure the proper control of the radioactive compounds that are produced inside the target during machine operation. Vacuum system characteristics must cope with the difficult environmental conditions, along with the safety and reliability rules typical for nuclear plants.

During the analysis of these factors, we have investigated, both from theoretical and experimental points of view, the vacuum dynamics of vapours and gases, the chemistry and physics of evaporation and some radioactivity aspects.

Further preliminary considerations on technological and engineering issues are also discussed. Specific results are related to the Ansaldo XADS reactor layout (80 MWth, LBE-cooled) [1,2] but they are valid for different configurations through appropriate scale laws.

The windowless interface vacuum system design

The evaluation of the source terms is an essential requirement for defining the vacuum system. They depend on different parameters such as the beam current, the physical properties of the target (composition, temperature, vapour pressure), the properties of the other materials exposed to vacuum, the amount of leaks, the throughput of gases used for the control of the oxidation of steels, etc.

The conductance of the beam pipe is the other boundary condition which is a function of the temperature and molecular mass of the gas or vapour considered. The conductance C gives the upper limit for the pumping speed available in the interaction region.

The well known relationship between the equilibrium pressure P_{eq} and the mass throughput Q_s (the source term) is:

$$P_{eq} = \frac{Q_s}{S_{eff}}$$

in which the term S_{eff}, the effective pumping speed, must include the conductance C and the presence of a distributed pumping surfaces.

We can individuate three different species of gases and vapours that represent the source terms:

- LBE vapours.
- Hydrogen and its isotopes and inert gases coming from spallation process.
- High-activity vapours such as mercury and polonium.

LBE vapours

LBE is the main component in the target loop exposed to vacuum. We have studied in depth the LBE evaporation phenomena in vacuum, the vapour condensation on cold surfaces, the vapour phase composition and the vapour dynamics [3,4].

A direct measure of the LBE vapour pressure is not practical due to condensation processes that may affect the manometer operation. For this reason, we undertook flux measurements to validate a proper numerical model that allows to estimate both the LBE evaporation rate at different temperatures and the sticking probability of LBE vapours on a stainless steel surface [4,5].

Data relative to our measured specific evaporation rates at different temperatures are shown in Figure 1 (compared with the Raoult Law), where "new data" have been measured under Knudsen conditions, in a new experimental apparatus.

Figure 1. Measured and calculated LBE evaporation rate as a function of 1/T

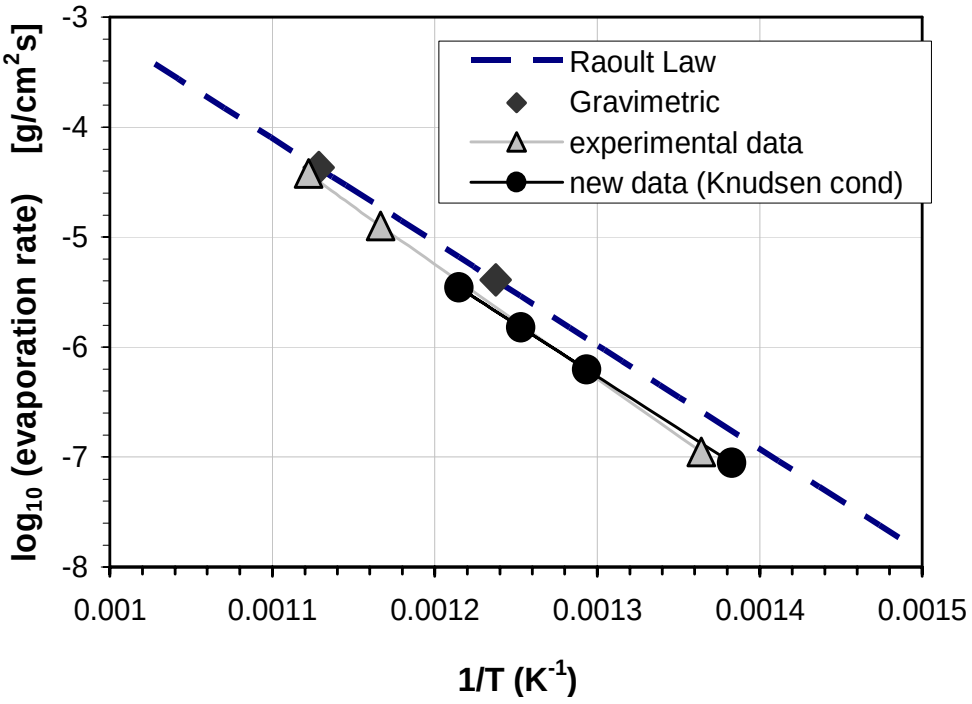

Actually, once the beam pipe geometry and the temperature of the LBE surface are fixed, using the numerical model and the measured data (evaporation rate and sticking probability), we can now describe the vapour fluxes of LBE inside the beam line. This allows evaluating, for instance, the amount of LBE emerging from the target and the evaporation/condensation distribution along the beam tube.

Concerning the Ansaldo design of the XADS, the LBE evaporating surface measures 60 cm^2 (12 cm · 5 cm). The first 7 m of the beam tube, starting from the LBE surface, is tapered and operates at about 400 C. Its cross-section varies from 12 cm · 5 cm at the source to 4 cm · 5 cm at the end. The remaining part of the beam tube has a constant rectangular cross-section (4 cm · 5 cm) with a temperature gradient going from 400 C to room temperature at the vessel roof. This means that the condensation phenomena of LBE vapours take place in this second section of the beam line.

The LBE surface temperature foreseen in the Ansaldo design is about 435 C. The temperature of the tapered part of the beam line is determined by the primary LBE temperature. For a conservative approach, our evaluation has been made assuming a LBE target temperature of 460 C. Data relative to LBE evaporation are shown in Table 1. These results highlight that both in the interaction point and at the reactor exit the LBE amount and flux should not influence the proton beam.

An estimation of the partial pressure of the LBE vapours can be obtained using our numerical model. Data are listed for different temperatures in Table 1. The partial pressure of the LBE vapour does not constitute a serious problem from the point of view of the vacuum technology due to the "condensation" pump effect of the tube walls.

Table 1. LBE evaporation data

LBE temperature (C)	Evaporation rate (g $cm^{-2}s^{-1}$)	Mass evap. at the tapered tube inlet (g/y)	Massive flux at the beam tube outlet (reactor exit) (mg/y)	Estimated pressure at the interaction point (mbar)
435	$4.7 \cdot 10^{-8}$	89	8.5	$1.3 \cdot 10^{-6}$
460	$1.1 \cdot 10^{-7}$	212	20	$3.3 \cdot 10^{-6}$
550*	$4.7 \cdot 10^{-6}$	8 890	845	$1.6 \cdot 10^{-4}$

* Data at 550 C are relative to the fault condition with only one propeller pump working [1,2].

We have also examined the vapour phase composition of LBE and found a different composition with respect to the liquid one. In fact, the vapour phase is enriched by bismuth that is the more volatile element: its concentration goes from 55% of the liquid LBE to a percentage between 65% and 80% in the vapour, depending on the LBE temperature. This fact has no strong vacuum implication but may play a significant role as concerns the nuclear safety: radioactive isotope 210 of Bi will decay to Po that will be then distributed all along the beam pipe.

Hydrogen isotopes and inert gases originating from spallation process

In this section we discuss the source terms relative to the so-called non-condensable gases.

Hydrogen and its isotopes

Hydrogen and its isotopes are mainly produced in ADS by a spallation process. A further hydrogen source (not tritium) comes from thermal desorption: hydrogen is diluted in metal as LBE and stainless steel (for instance 316LN may contain hydrogen up to 0.12 normal l/kg) [6].

Nevertheless the contribution of the thermal desorption from metals does not significantly increase the source terms and it will contribute only during the start-up operation of the reactor [7].

Table 2 shows the source data for hydrogen isotopes, generated only by spallation process, related to a proton beam of 5 mA, 600 MeV [8,9] and the production yield, the total activity, the beam pipe conductance and calculated equilibrium pressure.

For hydrogen isotopes Eq. (1) can be applied and the conductance calculation, also for complex vacuum systems, can be easily done using a standard approach. The pressure indicated in Table 2 is the minimum achievable partial pressure for hydrogen isotopes in the interaction region.

Noble gases resulting from spallation process

The spallation process also produces noble gases for which it is possible to apply Eq. (1) for the equilibrium pressure calculation. Table 3 shows the source terms and conductances as in Table 2. The calculations show that the contribution of noble gases to the equilibrium pressure is at least one order of magnitude lower than those of hydrogen isotopes.

Table 2. Amount of gases produced with a 5-mA beam, E_P = 600 MeV

Isotope	Yield: atoms/proton	Production in 1 yearG (normal l)	Q (mbar l/s)	Beam pipe conductance (l/s)	Pressure S_{pump} = ¥ (mbar)	Activity in 3 years (Bq)
H_2	1.75	64.2	$2.0 \cdot 10^{-3}$	16.0	$1.3 \cdot 10^{-4}$	
D_2	$3.2 \cdot 10^{-1}$	11.6	$3.7 \cdot 10^{-4}$	11.4	$3.2 \cdot 10^{-5}$	
T_2	$9.6 \cdot 10^{-2}$	3.5	$1.1 \cdot 10^{-4}$	9.3	$1.2 \cdot 10^{-5}$	$5.2 \cdot 10^{15}$
Total		**79.3**	**$2.5 \cdot 10^{-3}$**		**$1.7 \cdot 10^{-4}$**	**$5.2 \cdot 10^{15}$**

Table 3. Amount of noble gases produced with a 6-mA beam E_P = 600 MeV [1,2]

Isotope	Production in 1 year G (normal l)	Q (mbar l/s)	Conductance (l/s)	Pressure S_{pump}= ¥ (mbar)	Activity in 3 years (Bq)
He	9.6	$3.1 \cdot 10^{-4}$	11.4	$2.7 \cdot 10^{-5}$	0
Ar	0.023	$7.2 \cdot 10^{-7}$	3.8	$1.9 \cdot 10^{-7}$	$3.2 \cdot 10^{12}$
Kr	0.5	$1.7 \cdot 10^{-5}$	2.6	$6.6 \cdot 10^{-6}$	$7.7 \cdot 10^{13}$
Xe	0.21	$6.7 \cdot 10^{-6}$	2.1	$3.3 \cdot 10^{-6}$	$2.6 \cdot 10^{13}$
Total	**10.4**	**$3.4 \cdot 10^{-4}$**		**$3.6 \cdot 10^{-5}$**	**$1.1 \cdot 10^{14}$**

* Activities data are relative to a 5-mA beam [8,9].

The vacuum pumps for non-condensable gases

For non-condensable gases, we have analysed different pumping solutions: cryogenic, ion getter, turbomolecular, diffusion and non-evaporable getter (NEG) pumps. Table 4 shows the compatibility and efficiency of the different pumps relative to the gas to be pumped.

Table 4. Compatibility and efficiency of the different pumping systems relative to the gases to be pumped

Y – satisfactory, N – can not be used, P – poor pumping efficiency

Gas to be pumped	Refrigerator-cooled cryopump	Liquid-He-cooled cryopump	Ion getter pump	Turbomole cularpump	Diffusion pump	Non-evaporable getter (NEG) pump
H_2,D_2, T_2	Y	Y	Y	Y	Y	Y
He	P	Y	P	Y	Y	N
Noble gases	Y	Y	P	Y	Y	N

- *Refrigerator-cooled cryopump*. They use a closed-cycle refrigerator with a typical power of a few W at 10 K. They can pump all the gases but He (it can be pumped in small quantities with bad equilibrium pressure). The pump capacity is large but not infinite (it is a sorption pump: the hydrogen capacity is of the order of tens of normal litres). If the pump stops, all the condensed and confined gases are released in the system. Typical lifetime is some tens of thousands of hours in a non-radioactive area. The pumping of radioactive compounds forces to evaluate both the lifetime reduction, due to radiation damage, and the heat induced by the radioactive decay that can overload the refrigerator. They are commercial products.

- *Liquid-helium-cooled cryopump*. They are not commercial products and the use of LHe may overcome some limitations in pumping and sorption capacity with respect to other cryopumps. In any case, if the pump is warmed up, all the sorbed gases will be released. This choice forces the use of cryogenic transfer line, cryogenic storage system and helium liquefier.

- *Ion pump*. All the reactive gases can be efficiently pumped, while noble gases can be confined with low efficiency and with very low sorption capacity. In case of power failure these pumps do not release any gases. The sorption capacity is limited. Operating life at 10-6 mbar is about 50 000 h and the pump can also properly work in a radioactive environment. The pump has no mechanical moving parts. The typical application is UHV systems where the pump lifetime and efficiency is high. This is the pump that usually is used all along the accelerator beam lines.

- *Turbomolecular pump*. They are transfer pumps and their capacity is infinite. They use a high speed turbine (typically 60 000 rpm) and they can pump all gases. Reliability is high (MTBF is typically 20 000 h) in a non-radioactive environment. There are some experiences for the use of these pumps for tritium [10] but, from what we know, not for pumping other highly radioactive gases. They require a constantly-running fore-vacuum pump. These pumps are commercial products.

- *Diffusion pumps*. They use a high-speed oil vapour jet for transferring gas molecules to the fore-vacuum pump. The pumping efficiency is high for all gases. Drawbacks come from the presence of oils in the pump that may contaminate the vacuum system. The pumping of high-activity gases and tritium should be investigated. These pumps are commercial products.

- *Non-evaporable getter pumps*. They are based on chemisorption and physisorption properties of particular alloys. They pump only reactive gases; hydrogen isotopes are temporarily diluted in the alloy and they can be released by heating the getter at high temperature. Other gases, such as oxygen and carbon monoxide, are permanently confined. The sorption capacity for hydrogen is high (about 20 scc for each gram of gettering alloy) and the equilibrium pressure is very low. For instance, a pump with 1 kg of alloy may adsorb about 30 normal litres of hydrogen before saturation. There is no pumping capacity for noble gases. The pumps have no moving parts and do not need, after the first activation, any power supply for hydrogen pumping. They are available as commercial products and can be designed in dedicated configurations for special applications.

These analyses provide the opportunity to make a preliminary evaluation concerning the compatibility of the different pumping techniques with the ADS interface application.

- NEG pumps appear to be the best choice for pumping hydrogen isotopes (also for tritium) that are strongly confined in the metal alloy [11]. The large hydrogen throughput forces the use of a large amount of NEG.

- For high-activity gases that can not be pumped using NEG, turbomolecular pumps are a possible alternative; they are reliable but their use in nuclear and radioactive environments must be carefully tested.

- The use of cryogenic pumps, at least those refrigerator-cooled, appears to be critical due to the handling of the large thermal power resulting from the decay of the pumped radioactive products.

- Ion getter pumps are the best choice for the beam line, where the contribution of non-condensable gases has been reduced by many orders of magnitude.

- A diffusion pump appears to be critical due to the presence of oil.

High-activity vapours: Polonium and mercury

Among the radioactive spallation products, it is necessary to investigate the evaporating behaviour of Hg and Po. While the vacuum performances are not affected since the amount of these vapours is negligible related to the LBE mass, it is relevant to their contribution to the total activity in the vapour/condensed phase along the beam line.

Polonium

^{210}Po is an a emitter with $T_{1/2}$ = 138.4 d and specific activity of $1.67 \cdot 10^{14}$ Bq/g. Elemental polonium exhibits a vapour pressure many orders of magnitude higher than that of LBE.

$$\log P_{Po}\,[torr] = -\frac{5377.8}{T\,[K]} + 7.2345 \quad [12,13]$$

In addition, some discordance concerning the vapour pressure trends of this element can be found in literature [14].

Literature data about the composition of the vapour phase of LBE with Po impurities can be found only in Ref. [15]. This paper indicates that, as specifically concerns polonium, the vapour phase is mainly composed of PbPo (99.8%) and only by 0.2% of pure polonium. These data are not relative to an evaporation process in vacuum where, in our opinion, the behaviour of the evaporation process can be very different. As a consequence, this estimation of the evaporation rate can not be directly extrapolated for the purposes of the XADS project.

Difficulties to produce, handle and measure polonium properties force us to find a polonium simulator. We have chosen tellurium as a polonium simulator for the following reasons:

- They are both in the chalcogens group.

- Similar elemental vaporisation enthalpies (103 kJ/mol for Po [13] 104.6 kJ/mol for Te).

- Similar oxidation states (+4 main state).

- Similar electronic affinities.

Analogous vaporisation enthalpies are confirmed by small variations of the ratio between the vapour pressure of the two elements over a wide temperature range (400 C-600 C) [12,13,16-18].

Therefore, we set up a suitable apparatus to measure the evaporation rate of Te impurities diluted in LBE under vacuum condition.

Tellurium experiments

Figure 2 shows a sketch of the apparatus used for our evaporation experiments. In all our experiments, we have diluted, in 1 kg of LBE, 100 mg of Te (100 ppm in mass).

Figure 2. Experimental apparatus for the measure of the evaporation rate of Te impurities in LBE

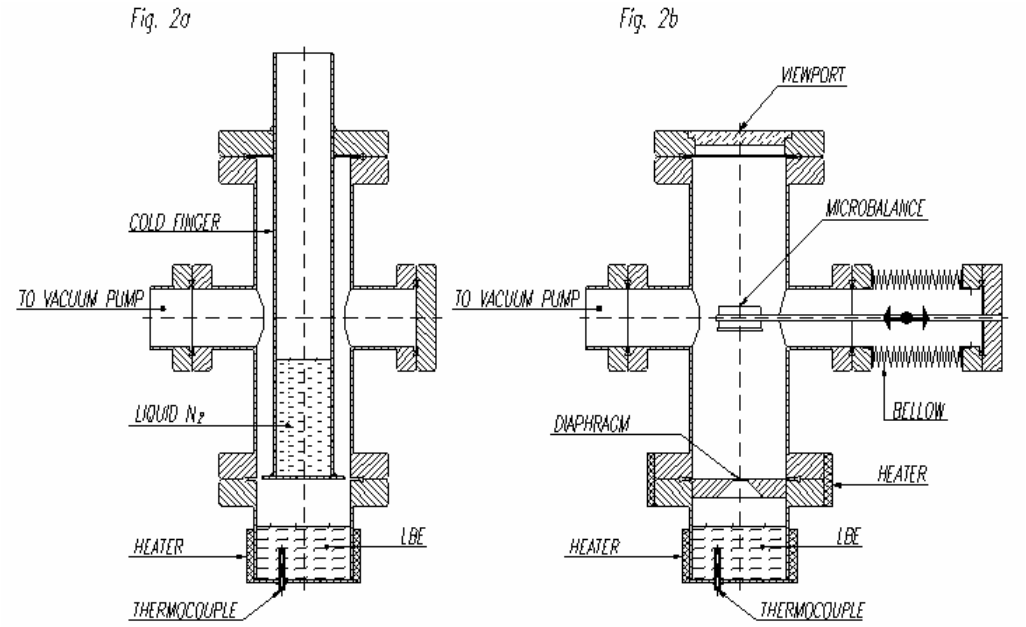

Two different techniques have been applied: the first one [see Figure 2(a)] foresees a cold finger that condensates the vapours, whose composition and mass are determined using chemical analysis [Inductive Coupled Plasma (ICP)]. The second technique foresees the use of a quartz thickness monitor [Figure 2 (b)] and a diaphragm that allows measuring both the instantaneous evaporation rate vs. time and the integral amount of evaporated material (using ICP analysis of the deposited film) under Knudsen conditions.

Results have been analysed with the same numerical approach used for the determination of the LBE evaporation rate. In the first run we used the set-up with the cold finger. The chemical analysis of the condensed material, after one hour at 400 C, is shown in Table 3.

Table 3. Chemical analysis of the first deposited layer. Source temperature is 400 C.

Temp. = 400 C	Pb (mg)	Bi (mg)	Te (mg)
Deposited material	192	216	852

In the first hour, less than 1% of Te is evaporated from the melt, while the LBE vapour phase has a composition similar to the one described earlier.

Further investigations have been undertaken to characterise the evaporation process using the second experimental set-up, with the vapour source under Knudsen flow conditions [Figure 2(b)] and using the microbalance to record the thickness of the deposited layer. Figure 3 shows the data measured with the melt at 400 C.

Figure 3. Measure of the tellurium impurities' evaporation from LBE in steady state

LBE temperature is 400 C, Te concentration is 100 ppm

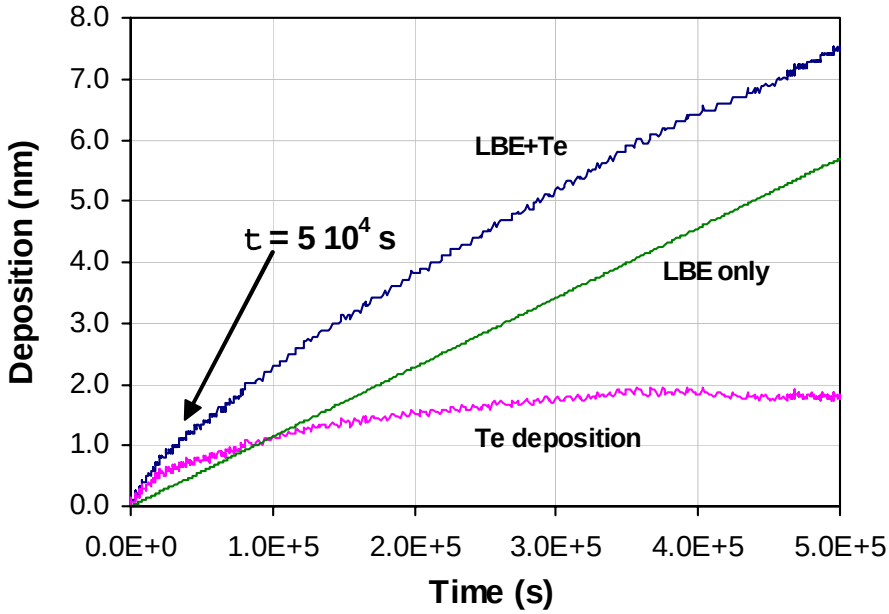

The amount of Te evaporated from the melt is calculated subtracting the known pure LBE data (estimated before) from the total measured deposition (LBE+Te).

Analysing the data relative to tellurium, its behaviour can be fitted with an exponential function:

$$d = d_0 \left(1 - e^{-t/\tau}\right) \; ; \quad d_0 = 1.9, \; \tau = 5 \; 10^4 \, \mathrm{s}$$

where d is the thickness of the deposited layer, d_0 is the asymptotic thickness and τ is the time constant. This corresponds to a source term, calculated with a simplified view factor method as discussed below, whose integral is less than 1 mg of Te (assuming a Te sticking probability similar to LBE). The tellurium evaporation is then limited to a few mg. Further heating at 500 C, in the same run, shows no more tellurium build-up on the microbalance. This confirms the hypothesis of diffusion limited behaviour or a possible chemical interaction between Te and LBE. At 500 C we observed a linear deposition rate lower than the theoretical one for pure LBE. This can be explained by residual oxides or tellurium compounds (PbTe and Bi_2Te_3 are lighter than LBE) floating on the surface. If substantially all Te would react with LBE, the new compounds (PbTe or Bi_2Te_3) could generate some tens of mm thick film on the melt surface acting as a diffusion and evaporation barrier.

Figure 3 refers to the apparatus working at the final constant temperature. Figure 4, on the other hand, shows the tellurium deposition during the transient towards the final temperature. The net Te deposition suggests that there were a few tellurium grains floating on the melt, which evaporated independently from LBE. We estimate this quantity of tellurium to be about 1 mg.

The comparison of the results obtained with the cold finger (Table 3) and microbalance set-up (Figure 3) shows that in the first case the contribution from the transient part during the temperature ramping, as discussed above, is the main term hiding the effective evaporation once the final temperature is reached.

Figure 4. Tellurium deposition during temperature ramp

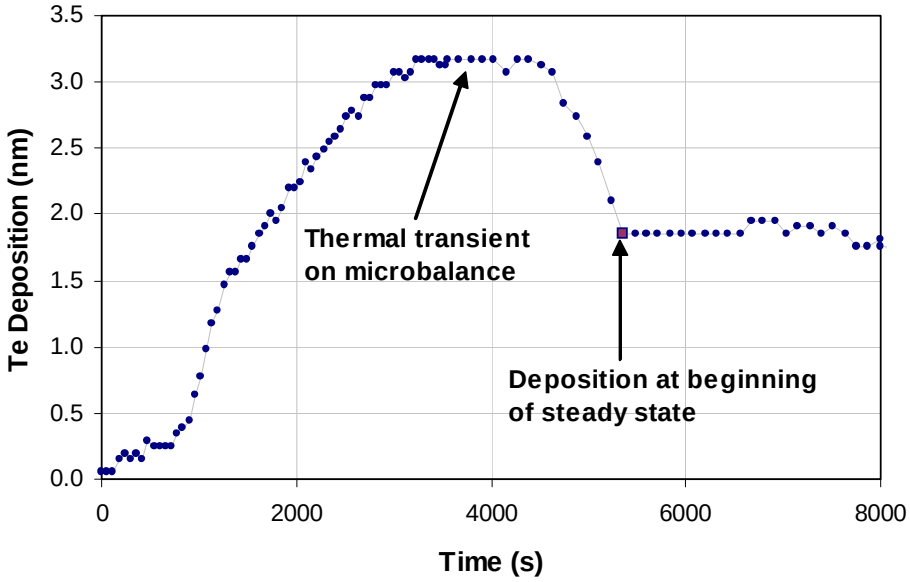

It must be remarked that surface cleanliness of the melt, even during the Knudsen flow state, is a critical factor because the initial hydrogen diluted in the LBE and in the steel of the vacuum tubes helps to maintain the cleanliness of the melt surface only once. Experiments done with non-controlled surface conditions, i.e. re-heating of the same melt after cooling down, even maintaining the vacuum, gave contradictory and useless results.

An experiment at 450 C with a “fresh” melt using the Knudsen experimental set-up delivers substantially similar results (Figure 5).

Figure 5. Tellurium deposition at a constant temperature of 450 C

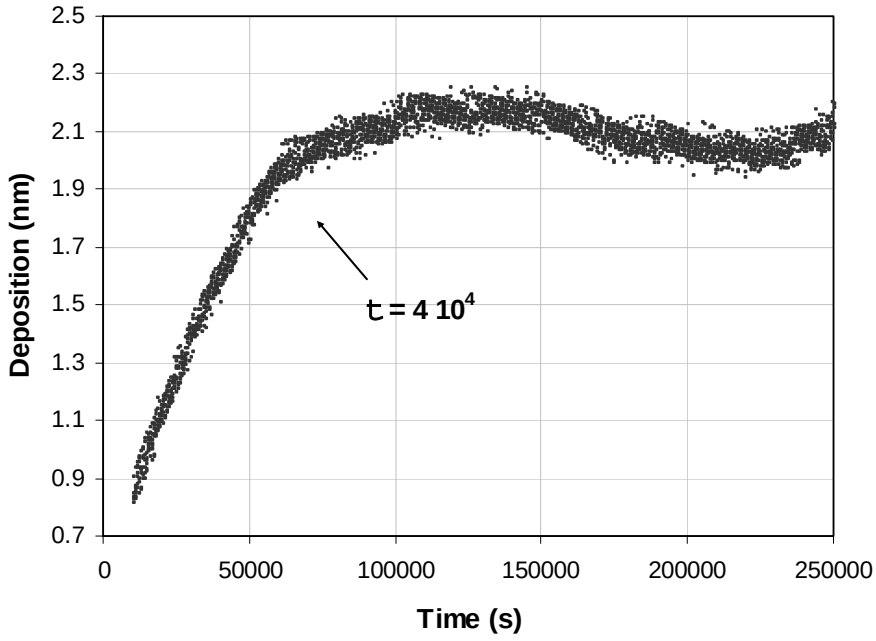

For the estimation of the amount of tellurium that left the melt during these experiments we use the view factor model to correlate the thickness of the deposed layer with the source term by means of a factor. These data are in reasonable accord with the chemical analysis performed on the microbalance quartz at the end of the measure. In this case the asymptotic deposition value of 2 ÷ 2.1 nm corresponds to about 0.8 mg of Te to be compared with 0.65 mg (ICP analysis on the microbalance quartz).

It is interesting to note that measured time constant τ and asymptotic deposition d_0 do not vary significantly in dependence of the melt temperature (see Figures 3 and 5).

If we now apply the results thus far obtained with tellurium to polonium, in the target operative conditions (i.e. 435 C) we could say that no more than 1 ÷ 1.5% of the total amount of generated polonium will leave the target. The total amount of Po [8,9] that evaporates during three years of continuous running is about 1 g.

To validate our assumptions of similar behaviour between Te and Po, further experiments are needed. In particular, the use of Po as a tracer impurity would allow validating the results so far obtained and the setting of proper scaling laws.

Mercury

The other highly volatile spallation product that can cause problems similar to those of polonium is mercury, which exhibits isotopes with short half-lives and extremely high specific activity (10^{18} Bq/g).

Experiments to analyse vacuum dynamics of mercury vapours are planned in the near future.

Conclusions

In this paper, we have investigated the general rules for a preliminary evaluation of the vacuum system of a windowless interface for an ADS.

The vapour and gas source terms have been discussed and data have been applied to a given beam line geometry.

Concerning LBE vapours we are able to describe vapour distribution and fluxes in the beam tube. Our model can be transferred to every other geometry, also complex. Net flux at the reactor exit and LBE partial pressures are negligible.

Non-condensable gases as hydrogen isotopes and helium are the main problem for the vacuum point of view; simplified calculations and indications about the different pumping technologies that can be used have been discussed.

The evaporation process and the gas dynamics of high-activity vapours such as Hg and Po, not problematic from the vacuum point of view, are crucial for radioprotection and nuclear issues. Evaporation experiments using LBE with Te traces, as a polonium simulator, have been done and extrapolated results would indicate that only 1% of the Te diluted in the LBE will evaporate.

REFERENCES

[1] Cinotti, L., *et al*., "XADS Cooled By Pb-Bi System Description", *Proceedings of the International Workshop on P&T and ADS Development*, Mol, Belgium, October 2003.

[2] Cinotti, L., *et al*., "Design of a Windowless Target Unit for the XADS Lead-bismuth Cooled System", *Proceedings of the International Workshop on P&T and ADS Development*, Mol, Belgium, October 2003.

[3] Michelato, P., *et al*., "Theoretical and Experimental Evaluation of the Windowless Interface for the TRASCO-ADS Project", *Journal of Vacuum Science and Technology*, in print (2004).

[4] Bonucci, A., *et al*., "The Method of Angular Coefficient a Powerful Tool to Address Complex Vacuum Gas Dynamics Problems", *XVI AIV Conference*, Catania (2002).

[5] Saksaganskji, G.L., Molecular Flow in Complex Vacuum Systems, Gordon and Breach Science.

[6] Acciaierie Valbruna, Italy, private communication.

[7] Calder, R. and G. Lewin, *British Journal of Applied Physics*, Vol. 18, pp. 1459-1472 (1967).

[8] Petrovich, C., *Radiation Transport Responses in the Windowless Target*, PDS-XADS Deliverable 60.1 (2003).

[9] Petrovich, C., *Evaluation of Spallation Products in Pb-Bi Cooling Systems of ADS-DF*, Final Report Tecla Deliverable 5, ENEA FIS – P130 – 001 (2002).

[10] Pearce, R., *et al*., EFDA Vacuum Pumping Developments on the JET Tokamak.

[11] Saes-Getters S.p.A, *NEG Pumps Catalogs.*

[12] Brooks, L.S., *J. Am. Chem. Soc*., 77, 3211 (1955).

[13] Moyer, H., *et al*., *Polonium*, US AEC Report, TID 5221 (1956).

[14] Eichler, B., *Die Flüchtigkeitseigenschaften des Poloniums*, PSI Bericht Nr. 02-12, Juni 2002, ISSN 1019-0643.

[15] Los Alamos National Laboratory, internal report LA-UR 98-1995.

[16] "CRC Handbook of Chemistry and Physics", 52nd ed. (1971-1972).

[17] Brooks, L.S., *J. Am. Chem. Soc*., 5 Jan. 1952.

[18] Smithells, "Metals Reference Handbook", Butterworths (1978).

CORROSION TESTS IN THE STATIC CONDITION AND INSTALLATION OF CORROSION LOOP AT KAERI FOR LEAD-BISMUTH EUTECTIC

J-E. Cha, C-H. Cho, T-Y. Song
Korea Atomic Energy Research Institute, Korea

Abstract

Lead-bismuth eutectic (LBE) corrosion has been considered as an important design factor to limit the temperature and velocity of the accelerator-driven transmutation system. For the corrosion study, KAERI finished the set-up of the LBE static corrosion facility and also finished the preliminary design of a dynamic corrosion loop and started a set-up process to construct the loop by the fall of 2004. In this paper, we describe the results of the preliminary static test during 500 hrs under a reduced condition to check the performance of the static facility. We also describe a design concept of corrosion loop and the state of the art for its installation at KAERI, as well as the results of EM pump preliminary testing.

Introduction

ADS has been widely studied over the past few years, as it has the possibility to transmute minor actinides and long-lived fission products in nuclear spent fuel. Since 1997, KAERI has also conducted systematic studies to develop the ADS system, called HYPER [1]. HYPER is a 1 000 MWth fast spectrum reactor with $k_{eff} = 0.98$ that has been designed to transmute TRU, ^{99}Tc and ^{129}I. LBE is preferred as the target material due to its high production rate of neutrons and effective heat removal. Recently, LBE has been widely studied as a core coolant and target material of ADS in various countries. However, LBE and lead are more corrosive than sodium because the solubility of Ni, Cr and Fe is high. Thus, LBE corrosion has been considered as an important design factor to limit the temperature and velocity of the ADS system [2-4].

In designing HYPER, it was taken into consideration that the average temperatures of LBE at the inlet and outlet are 340 C and 490 C, respectively. The maximum temperature of the cladding is estimated at around 575 C. In the case of the beam window, the LBE corrosion effect can be combined with radiation damage to produce more severe damage. The maximum temperature of the beam window contacted with LBE is designed not to exceed 500 C.

Several methods have been considered to prevent the corrosion problem in LBE. In the research on LBE technology, it has been made clear that the corrosion behaviour is controlled by the oxygen concentration in the liquid LBE. Thus, one method is to form a stable oxide layer on the material surface through an oxygen level control in LBE. Another is to modify the material compositions or the surface of the material. If an appropriate method to prevent corrosion cannot be found, the design should be modified so that the maximum temperature decreases.

Static corrosion tests are useful to investigate the corrosion properties and modes of various kinds of materials to develop corrosion-resistant materials for liquid LBE. KAERI recently finished the set-up of the LBE static corrosion facility and began a static test and systematic research to develop the measuring techniques for the control of the oxygen concentration.

Corrosion tests using a liquid-metal loop are also necessary to estimate the corrosion and erosion behaviour in the LBE flow. KAERI recently finished the preliminary design of a dynamic corrosion loop and started a set-up process to construct the loop by the fall of 2004. We also have a long-term plan to build a proton irradiation test loop since it is essential to estimate the effects for irradiation of high-energy protons and neutrons on the beam window materials. In this paper, we described the results of the preliminary static test with SUS316 and HT9 during 500 hrs under a reduced condition to check the performance of the static facility. For the corrosion loop, we describe a general design concept and the state of the art for the installation at KAERI.

Test in static corrosion facility

Figure 1 shows the schematics of the static corrosion facility recently installed at KAERI. It is mainly composed of tube furnaces, a gas supply system and a glove box. The glove box was installed to control the gas concentration during the treatment of test samples. A wall of the glove box is connected to a flange of the furnace to install and draw out the test samples for the static corrosion experiment; bottom of the glove box is also connected with a flange of the test section of the dynamic corrosion loop.

The gas control of the glove box is conducted with an argon gas or a mixture gas of argon and hydrogen. The furnace has three independent heaters to reduce the temperature difference along the quartz test tube (70 mm in inner diameter and 700 mm in length). The gas concentration of the furnace

Figure 1. Schematics of static corrosion facility

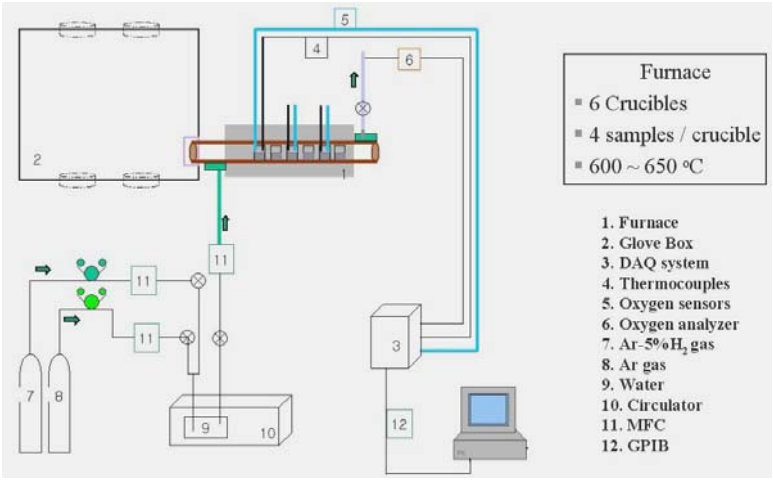

is monitored at the inlet and outlet position with the oxygen analysing system of ZIROX SMGT 1.6 up to oxygen partial pressure $O_2(10^{-1})$ ppm. The temperature of liquid LBE is measured by a K-type sheathed thermocouple in each crucible. The mass flow of gas is controlled with the mass flow controllers (MFC), the pressure regulators and the needle valves.

A total of six crucibles are installed in the test tube of the furnace and a total of four samples are mounted in each crucible. The LBE mass in a ceramic crucible was around a total of 55 g LBE for the corrosion test, which was calculated by considering the solubility, the volume of LBE and the contact surface between the samples and the LBE. The test samples in Table 1 were prepared by annealing for one hour at 1 050 C. The heat treatment was conducted at 750 C for two hours for the HT9 after annealing. Its dimensions are: 10 mm in width, 18 mm in height and 2 mm in thickness. The experiment was conducted at a temperature of 650 C during 500 hours. The oxygen concentration was controlled with the mixture ratio of H_2 and H_2O vapour.

Table 1. Chemical composition of specimens (wt.%)

Material	C	Si	Mn	Ni	Cr	Mo	V	Nb	W	P	S	N
HT9	0.19	0.36	0.59	0.53	11.79	0.99	0.31	0.02	0.49	0.019	0.006	< 0.01
316L	0.02	0.35	1.8	12.1	17.3	2.31	–	–	–			

Figure 2 shows the EPMA results of the 316L and HT9 exposed to LBE at 650 C with a reduced condition for 500 hours. The oxygen meter shows that the oxygen content in the flowing gas is less than 10^{-8} wt.%. Table 2 explains the EPMA data results of Figure 2. In spite of the well-known serious corrosion attack for 316L, no dissolution attack was shown and the oxygen layer was not detected. It is necessary for us to investigate the test conditions, which should include the oxygen concentration and the surface of the specimens.

Corrosion loop

Figure 3 shows the schematic diagram of the dynamic corrosion loop to be installed at KAERI. The LBE loop is an isothermal loop. The flow velocity in the test section was designed to be around 2 m/s in the range of 400-550 C and the charging volume of the LBE is around 0.03 m^3 in the circulation loop.

Figure 2. SUS 316L, HT9 at 650 C with oxygen content <10^{-8} wt.%(500 hrs)

a) 316L *b) HT9*

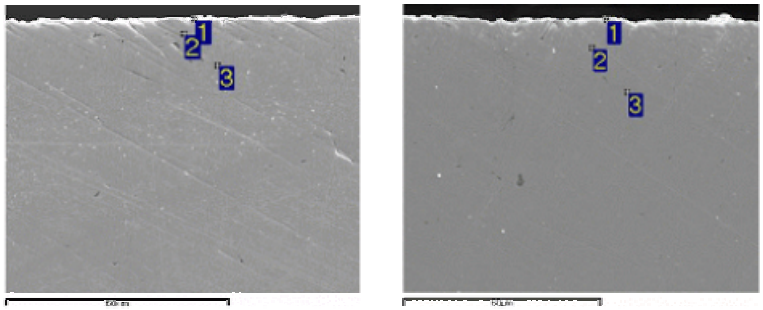

Table 2. The EPMA results of 316L, HT-9 at 650 C

Location	316L						HT9					
	Fe	Cr	Ni	Pb	Bi	O	Fe	Cr	Ni	Pb	Bi	O
1	67.43	21.13	9.98	0.25	0	1.20	93.27	3.87	0	0	1.33	1.54
2	70.76	17.48	10.62	0	0.42	0.72	91.27	6.26	0.16	0	1.56	0.75
3	70.08	17.25	10.83	0	0.95	0.88	85.12	12.15	0.51	0	1.42	0.81
Original	70.6	17.3	12.1				87.68	11.79	0.53			

Figure 3. Three-dimensional schematics of corrosion loop

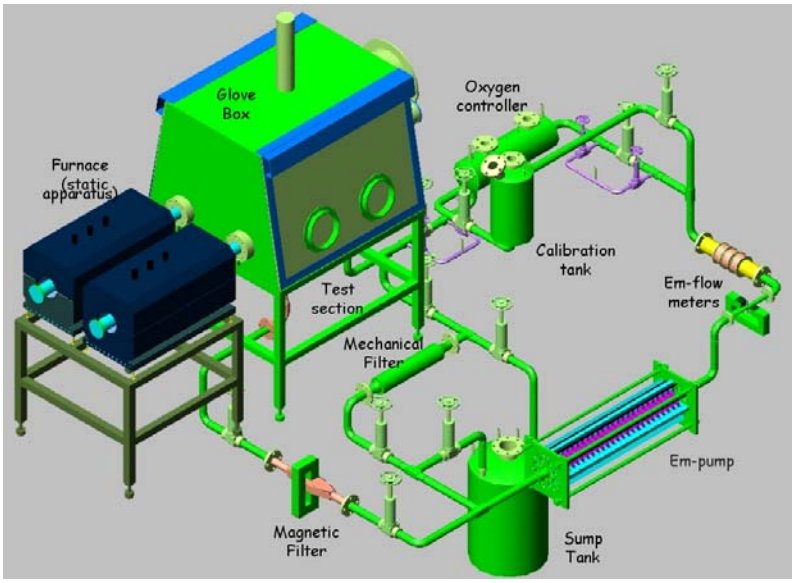

The LBE loop is mainly composed of a main test loop, a bypass loop for filtering LBE and a mixture gas supplying system. The liquid metal in the main test loop circulates in the following order: EM pump fi EM flow meter fi oxygen controller fi test section fi magnetic filter fi EM pump. The major specifications of KAERI's loop are summarised in Table 3.

Since LBE is a heavy liquid metal and has a higher viscosity than water or sodium, the forced convection loop should be designed to reduce the pressure drop to be as small as possible and adopt a pump with a high pumping head. From the analysis of the pressure drop, the specification of the piping

Table 3. Major specification of corrosion loop

Operation temperature	400 C ~ 550 C (max. 600 C)
Liquid metal volume	Pb 44.5%, Bi 55.5%, 0.08 m^3
Test section	3/4 inch, Sch. 40, SUS 316 seamless pipe, V_{mean} = 2 m/s (at 45 lpm)
Sample specification	f 8 mm, thickness 2 mm, height 5 mm
Piping system	1.5 inch, Schedule 40, SUS 316 pipe
Flow measurement	EM flow meters
Liquid metal pumping	EM pump (60 lpm, 4 bar, 40 kVA)
Oxygen control	H_2/H_2O partial pressure (10^{-5} wt.% ~ 10^{-7} wt.%)
Purification	Magnetic filter, mechanical filter

system was determined as 1.5-inch pipe to reduce the pressure drop by a high mean fluid velocity. The pressure drop of the main test loop was estimated at around 3 bar (3 m head in LBE) with a flow rate of 60 lpm.

The LBE is circulated with an electromagnetic pump (60 lpm, 4 bar, 40 kVA), which is a kind of annular linear induction pump designed by an equivalent electric-circuit method. By considering the uncertainty, the pump head was conservatively determined as 4 bar under a maximum flow rate to overcome the pressure loss of the LBE flow.

The flow rate is measured with electromagnetic flow meters based on Faraday's induction law [5]. In the present study, several types of electromagnetic flow meters will be serially installed to investigate the effects such as contact impedance due to wall oxidation and others. The performance of every EM flow meter can be calibrated with a calibration tank in the loop.

A total of 0.08 m^3 of LBE is stored in the sump tank before charging into the test loop. Most parts of the piping system are made of stainless steel pipe 1.5 inches in inner diameter (SUS 316, 1.5 inch schedule 40) and are connected by welding for the prevention of leakage of the LBE.

The oxygen concentration of the range of 10^{-7} wt.% ~ 10^{-5} wt.% is controlled by a chemical equilibrium between the mixture gas of hydrogen-argon and the water vapour. At present, the oxygen concentration in the LBE and mixture gas is measured with an oxygen sensor made of a yttria-stabilised zirconia as a solid electrolyte cell and Pt/air as a reference system. The electric potential between the LBE flow and the reference electrode is measured by a voltmeter with a high input impedance to maintain the difference of the oxygen concentration. The oxygen partial pressure is determined by Nernst's equation.

The oxygen controller is used to control the level of the oxygen concentration in the loop and expand the liquid LBE during the test. Direct control of the oxygen concentration is not easy since the required oxygen level is very low. However, the oxygen partial pressure P_{O2} can be chemically controlled with the ratio of the other gases involved, e.g. the $H_2/O_2/H_2O$. In order to control the oxygen level in the loop, a mixture gas of argon, hydrogen and water vapour is continuously injected into the LBE flow in the oxygen controller.

$$C_O = C_{O,S}\left(\frac{P_{O_2}}{P_{O_2,s}}\right)^2 \quad [\text{wt\%}] \tag{1}$$

$$P_{O_2} = \left(\frac{P_{H_2O}}{P_{H_2}} \right)^2 \exp\left(\frac{2\Delta G^{o}_{H_2O}}{RT} \right) \quad [\text{bar}] \tag{2}$$

where C_O is the oxygen concentration, $C_{O,S}$ is the solubility of oxygen in the LBE and P_{H2O} and P_{H2} are the partial pressure of H_2O and H_2, respectively and $\Delta G^{o}_{H_2O}$ is the oxygen potential of water vapor.

Test samples are installed in the test section with an annular cross-section. In order to treat the test samples in a regulated oxygen environment, the upper part of the test section is installed inside the glove box. The test section is made of a seamless pipe (SUS 316, 3/4 inch, Schedule 40). Most LBE flows in the test section have to be turbulence due to a high density. Test samples are mounted from a distance of 15~20 D_h (hydraulic diameter of test section). In fact, the disance of the entrance zone is longer than this distance. However, we determined the distance as small as possible by considering the pressure drop, the static head and the height of set-up space. Test samples in Table 4 will be firstly prepared from the static test and have the dimension of 8 mm in outer diameter, 2 mm in thickness and 5 mm in height.

Table 4. Compositions of test samples (composition, wt.%)

	C	Si	Mn	Ni	Cr	Mo	V	Nb	W	P	S	N
HT9	0.19	0.36	0.59	0.53	11.79	0.99	0.31	0.02	0.49	0.019	0.006	0.01
HT9M	0.145	0.1	0.45	0.46	9.79	1.23	0.2	0.18	–	<0.003	<0.003	0.02
HT9MN	0.15	0.072	0.49	0.05	10.0	1.28	0.205	0.204	–	0.002	0.004	>0.02
T91	0.105	0.43	0.38	0.13	8.26	0.95	0.20	0.075	–	0.009	0.003	0.055
9Cr-1Mo	0.099	0.32	0.42	0.10	9.03	0.96	0.22	0.094	–	<0.003	0.003	0.032
316LN	0.022	0.53	0.87	10.6	17.69	2.61	–	–	–	0.02	0.001	>316ss
AISI 316L	0.02	0.35	1.8	12.1	17.3	2.31	–	–	–			
9Cr-2WVTa	0.11	0.21	0.44	<0.01	8.90	0.01	0.23	–	2.01	0.015	0.008	0.0215

Generally, an EM pump has been employed to circulate electrically conductive liquids like molten metals by Lorentz force ($J \cdot B$) generated from the surrounding magnetic field and its perpendicular current. We adopted an EM pump as the pumping device in the test loop by considering corrosion. In the present design, the EM pump of an annular linear induction type with a flow rate of 60 lpm and a head of 4 bar is designed by using the electrical equivalent circuit method that is applied to linear induction machines for the circulation of the liquid LBE. In an annular-type pump, the developing force is generated by a cross product of the azimuthally-induced current (J) at the liquid metal and the radial magnetic field (B) form the outer core. The maximum velocity was 1.5 m/s in the annular channel of the EM pump.

Figure 4 shows the cross-section of the annular linear induction EM pump to be designed. It is divided into the electromagnet made of the inner and outer cores with a high magnetic permeability and exciting conductor coils, and ducts with a narrow annular channel gap for the liquid-metal flow. The EM pump with designed variables by the equivalent circuit method is operated for the corrosive LBE circulation under a high temperature around 500 C. Therefore, the material of the EM pump should be compatible with those operation conditions. A silicon-iron sheet (0.35 mm) with a high magnetic permeability is selected as the core material to keep the magnetic property under a high temperature. The outer and inner cores are fabricated by the stacking of thin silicon-iron plates to reduce the Joule's heat losses by the eddy current. Moreover, cores are arranged radially so that the stacked direction of the inner core is consistent with that of the outer core for directing the strong magnetic field towards

Figure 4. Schematics of annular linear induction EM pump

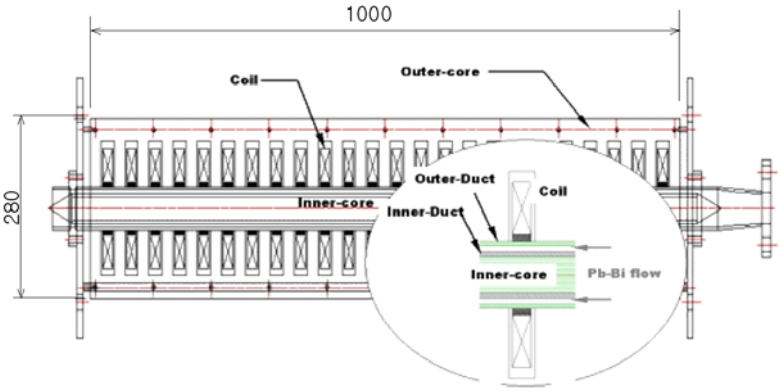

the radial direction. As coil conductors, an alumina-dispersed, strengthened copper band (GLIDCOP, AL-15, 1.0 mm) is employed taking into account the mechanical and electrical properties under a high temperature, which are a small volume expansion coefficient and a sufficient electrical conductivity compared with the other conductors in the operation environment. The mica-silicon insulator (1.0 mm, SR864G) that has flexibility in the coil curvature and durability under high temperatures is inserted between the coils to prevent an electrical short circuit. On the other hand, to prevent the distortion of the magnetic field at the narrow flow channel, the ducts are made of austenitic stainless steel with non-ferromagnetic material.

Figure 5 shows an EM pump system manufactured for the corrosion loop and a measuring system to investigate its performance. The performance of the EM pump was measured using a one-component dynamometer and strain amplifier after calibration with the known weight. For the verification of the magnetic field, we used a three-component Gauss meter and a transverse and an axial-type probe. The EM pump and dynamometer were installed on the accurate stone table to prevent vibration and deformation. A stainless steel pipe was inserted into the annular space as an LEB simulator and several thermocouples were attached to check the temperature of the EM pump.

Figure 5. EM pump system and the measuring system of its performance

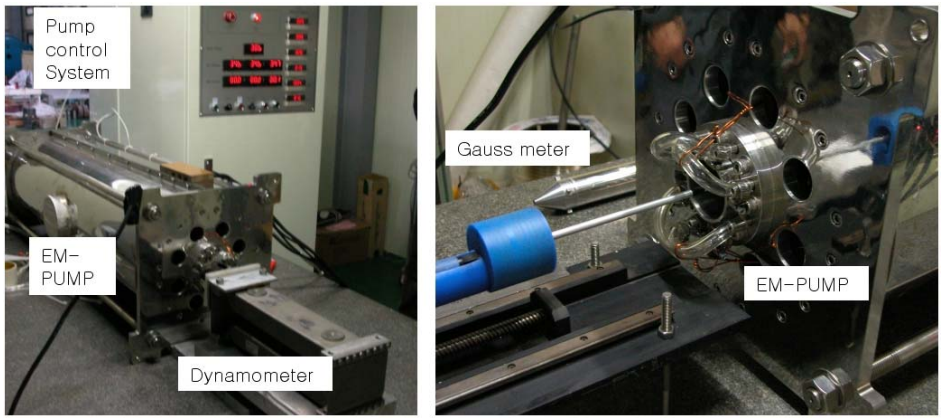

Figure 6 shows the performance of the EM pump. We calculated the pressure head from the measuring force by dividing the area of annular space between the outer duct and inner duct. The pressure head of the initial design was not enough to pump the LBE in the loop and thus we checked the magnetic field of annular space with the Gauss meter. The pressure head of the revised pump was

Figure 6. Pumping power of EM pump with current input

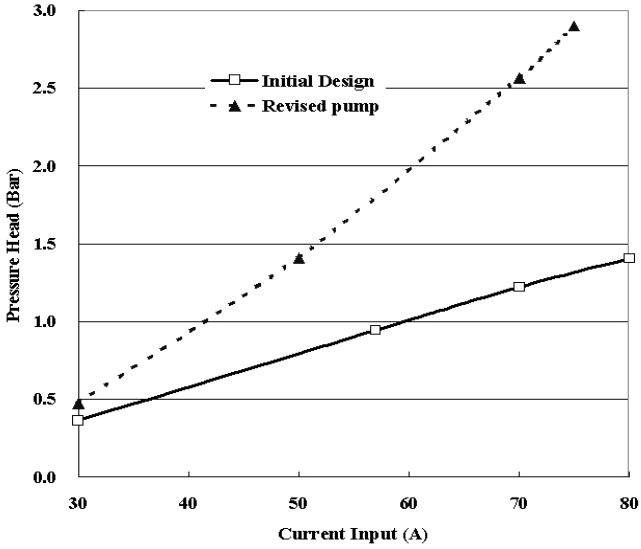

largely enhanced after changing the structure of the inner core and the inter-core gap between the inner core and outer core. From this test, we confirmed that the prototype EM pump could operate more than around 500 C and pumped the LBE more than 2.5 bar.

Figure 7 shows the schematics of the corrosion loop and its main components. Most of the components to be installed on the loop have already been manufactured, and a set-up process will be completed by the fall of 2004. The valve was specially manufactured for the LBE environment, which was considered for the temperature of seal and did not include any bellows.

Figure 7. State of the art of KAERI's corrosion loop installation

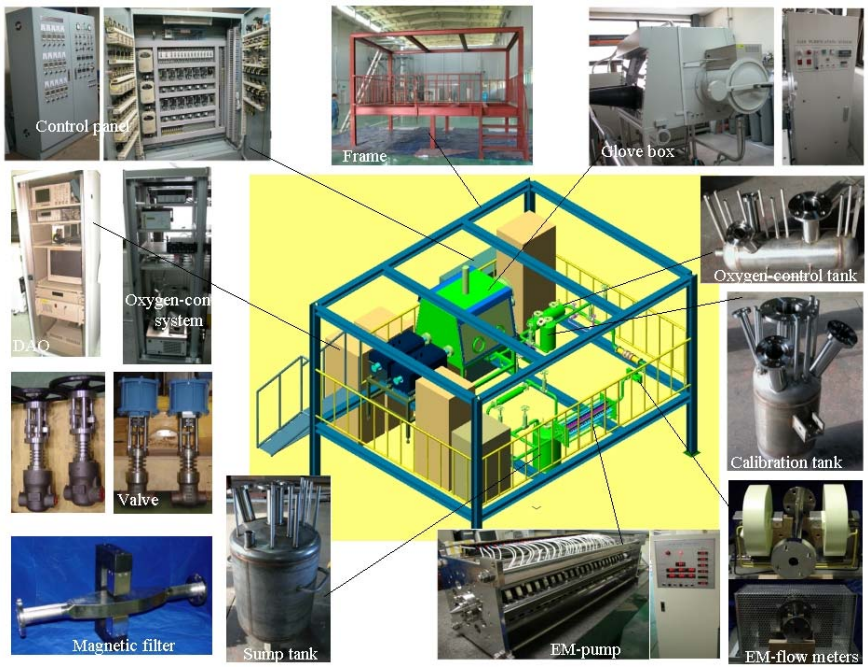

Conclusions

KAERI finished the set-up of the LBE static corrosion facility and started a static test for material screening and a systematic research to develop the measuring techniques for the control of oxygen concentration. KAERI completed the preliminary design of a dynamic corrosion loop on the basis of thermal and hydraulic experience of the sodium test and started a set-up process to construct the loop by the fall of 2004. From the EM pump test, we confirmed that the prototype EM pump could operate at more than around 500 C and the LBE pumped at a rate of more than 2.5 bar.

REFERENCES

[1] Park, W-S., *et al*., *Development of Nuclear Transmutation Technology*, KAERI report, KAERI/RR-1702/96 (1996).

[2] Lai, G.Y., "High Temperature Corrosion of Engineering Alloys", ASM Int., Materials Park, OH 44073 (1990).

[3] Orlov, Y.I., *et al*., "The Problems of Technology of the Heavy Liquid Metal Coolants (Lead-Bismuth, Lead)", *Proc. of the Heavy Liquid Metal Coolants in Nuclear Technology*, Obninsk (1998).

[4] Mueller, G., *et al*., "Investigation on Oxygen Controlled Liquid Lead Corrosion of Surface Treated Steels", *J. of Nuclear Materials*, 278, 85-95 (2000).

[5] Shercliff, J.A., "The Theory of Electromagnetic Flow Measurement", Cambridge University Press (1962).

THE VACUUM INTERFACE COMPATIBILITY EXPERIMENT (VICE) SUPPORTING THE MYRRHA WINDOWLESS TARGET DESIGN

P. Schuurmans, P. Kupschus, A. Verstrepen, J. Cools, H. Aït Abderrahim
SCK•CEN, Mol, Belgium

Abstract

The MYRRHA accelerator-driven system (ADS) is being developed in Mol, Belgium incorporating a windowless spallation target, as this is the only option within the constraints of the envisaged neutron source performance. In this paper the research programme and experimental set-up required for the R&D effort towards the conditioning of Pb-Bi eutectic for use in a *windowless* liquid-metal spallation target are presented. The experiences acquired commissioning the set-up, the current status of the experiment and first results are discussed.

Introduction

Lead-bismuth eutectic (LBE) has interesting properties as a target material for high-power spallation sources. It is sufficiently heavy to provide an adequate yield in the spallation reaction, rather transparent for fast neutrons and has a quite low melting point of LBE (123 C) so the forced convection method to remove heat deposited in the target by the proton beam by circulating the liquid LBE can be used at modest temperatures. However, "off the shelf" LBE is not necessarily suited for use in a spallation loop because possible insoluble contaminations might accumulate at particular positions in the loop (e.g. at ridges), thus giving rise to an increased pressure drop, diminished flow and possibly complete blocking. Thus, a cleaning procedure is required. In addition, LBE is quite corrosive as regards stainless steel due to the high solubility of Fe and Ni. The process can be kept under control by establishing a dynamic equilibrium between the oxygen in the LBE and that on the surface of the vessel. This implies a control of the oxygen level in the LBE to the level of about 10^{-6} wt.% [1], whereas untreated LBE is almost saturated with oxygen; here also, a conditioning procedure is needed.

For MYRRHA [2] a windowless spallation target design was chosen because of the space permitted in the high-performance subcritical core to accommodate the spallation loop. The 120 mm central hole limits the proton beam to about a 70 mm diameter since a minimal lateral target volume is needed for an efficient spallation reaction. A 350-MeV, 5-mA proton beam was chosen for reasons of geometry and the performance requirements of the subcritical core. The resulting current density runs up to about 150-200 $\mu A/cm^2$ due to beam profile shaping. This value exceeds other attempts for a window design for spallation sources that are already at the cutting edge of present-day technology by more than a factor three, and thus a window between target and beam line is not feasible in MYRRHA. This fact raises a third item in the preparation of LBE for use as spallation target material. The common vacuum between target and beam line allows the beam to interact with the gas above the target coming from initial outgassing, liquid-metal evaporation and later emanations of volatile spallation products from the target surface. The proton beam will trigger an ionisation cascade by generating secondary electrons from the gas and thus cause the formation of secondary plasma that may transfer a part of the megawatt beam power to the beam line walls. In turn, the plasma causes sputtering on the inner beam line walls and an increase in desorption and evaporation since both electrons and ions in the plasma will have enough energy to drive out atoms from the walls. Eventually a plasma formation runaway could take place, leading to beam tube damage and eventually to beam clogging.

The plasma problems can be solved if a sufficiently high vacuum above the target ($<10^{-3}$ mbar) can be achieved. The vacuum pumping speed (ref: H_2) in the direct area of the target surface, however, is limited to about 100 l/s due to space constraints in the subcritical core. With these values, the highest acceptable emanation rate is around 10^{-1} mbar l/s. This represents 1 g of H_2 per day being emanated from close to 5 000 kg of LBE in the spallation loop. Since the amount of plasma formation critically depends on the competition between the pumping capacity and the outgassing/evaporation rate, both should be investigated in a realistic situation where quantitative data are obtained to establish and/or confirm design criteria for the spallation loop. It is indeed not *a priori* clear to which level volatile elements are removed in the conditioning process of the LBE before operation of the target. In any case, the problem is too complex to be dealt with reliably on the basis of theoretical model calculations alone.

Other issues to be investigated that are closely related to the outgassing problem are the dynamical behaviour of volatile spallation elements like Hg and Po: to what is the emanation rate from the free surface and how do molecules propagate towards the vacuum system. Obviously, this has direct implications on radioactive waste management and operational control of the spallation source.

Experimental programme

As MYRRHA is the first ADS project to clearly adopt a windowless design, it is necessary to obtain a quantitative experimental compatibility assessment of the free LBE target surface with the beam tube vacuum. To investigate the items raised above an experimental set-up was built combining two vessels, in each of which a part of the experimental programme will be carried out. In the barrel-shaped preconditioning vessel (PCV) the procedures for the initial cleaning, oxygen level control and coarse outgassing of the LBE will be studied. The second vessel, built to perform the vacuum interface compatibility experiment (VICE), is largely a one-to-one ultra-high vacuum (UHV) model that mimics the lower part of the beam line connecting to a liquid-metal target in the centre of the subcritical core. The large scale avoids the need to extrapolate the results from small-thimble experiments, which would not necessarily scale in all respects. In the device we will study metal evaporation, emanation of volatile spallation products and the initial and long-term outgassing of the target material. Possible compound formation and the gas transport properties of the beam line will also be studied. The main detector is a high-resolution quadrupole mass spectrometer placed near the top of the vessel. Data will be taken as a function of pressure and temperature. The measured flow rates will be calibrated by comparison with known externally introduced mass flow rates using the mass spectrometer as the differential detector. It may be noted that related work is being undertaken in the framework of TRASCO-ADS [3]. In the next sections, both experimental vessels, the equipment and operational procedures that will be used in the gas experiments and the present status are described [4].

As a first step in the programme the emanation of all types of spallation products and liquid-metal evaporation was estimated [5] (Figure 1) using a deterministic model of the vacuum pumping scheme of the lower end of the spallation loop and beam line. Instant release of all products and zero sticking coefficients were assumed, representing, at least from a vacuum point of view, a worst-case scenario. It was found that this contribution to the atmosphere above the target can easily be tolerated if the particle emanation of the free surface is less than the equivalent emission occurring when the full surface is at 500-600 C. This indicates the importance of the limited acceptability of hot-spots.

Figure 1. Estimated emanation of spallation products and liquid-metal evaporation in the MYRRHA spallation source as a function of temperature

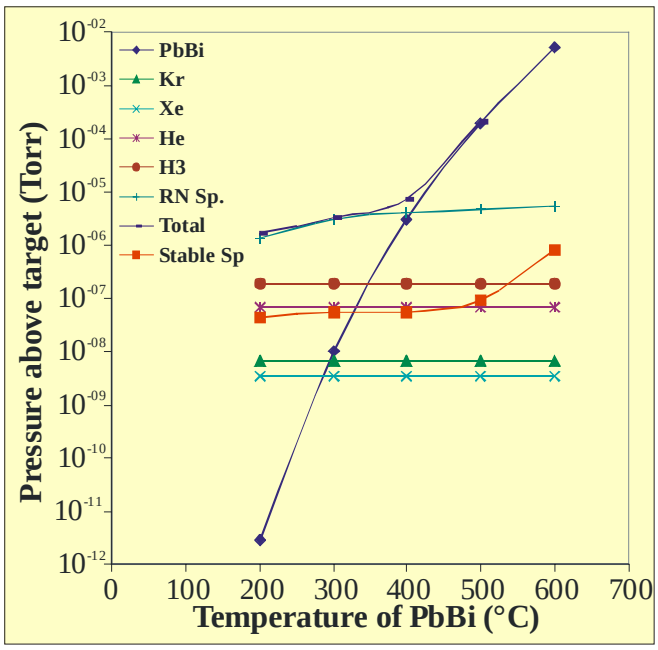

The preconditioning vessel

A scheme of the precondition vessel (PCV) is shown in Figure 2. It is a 68.5 l barrel-shaped 10 bar pressure UHV vessel for temperatures up to 500 C. The ultra-high vacuum (UHV) preparation includes inner surface cleaning and electro-polishing to avoid any contamination of the LBE material, thus ensuring clean experimental conditions. The vessel can simply be cleaned and re-polished to return it to its initial state should any damage occur. This also makes the PCV suited to simulate and study possible oxygen ingress and the subsequent reconditioning of the vessel and the LBE. Its main use, however, is in the initial conditioning procedure of the LBE. For this, 100.00(1) kg (9.6 l) of LBE was molten in the PCV (Figure 3) at a pressure of 10^{-7} mbar. Temperatures are measured by K-type thermocouples and controlled by a Labview® based data-acquisition and control program (DAC) that also monitors the status of other sensors (pressure, oxygen control). During commissioning a bake-out sequence of 5 h at 200 C, 11 h at 330 C and 6 h at 400 C was used. It was shown that the vessel can be heated homogeneously to 2% and temperatures can be kept stable to within 1 C.

After the LBE melt, the liquid surface is inspected visually via two 67-mm quartz windows on top of the vessel that can withstand an interior pressure of up to 10 bar. A double set of helicoflex-type metal seals are used to allow window temperatures up to 450 C. An internal shutter system is foreseen since the windows become opaque after a few weeks at 400 C due to LBE vapour deposits. When surface contamination of the liquid metal is too severe – which may occur since most insoluble impurities will be lighter than the LBE and thus float – a first coarse cleaning can take place by opening the vessel under an inert gas flow and skimming the surface. Subsequently, excess PbO must

Figure 2. A schematic overview of the preconditioning vessel

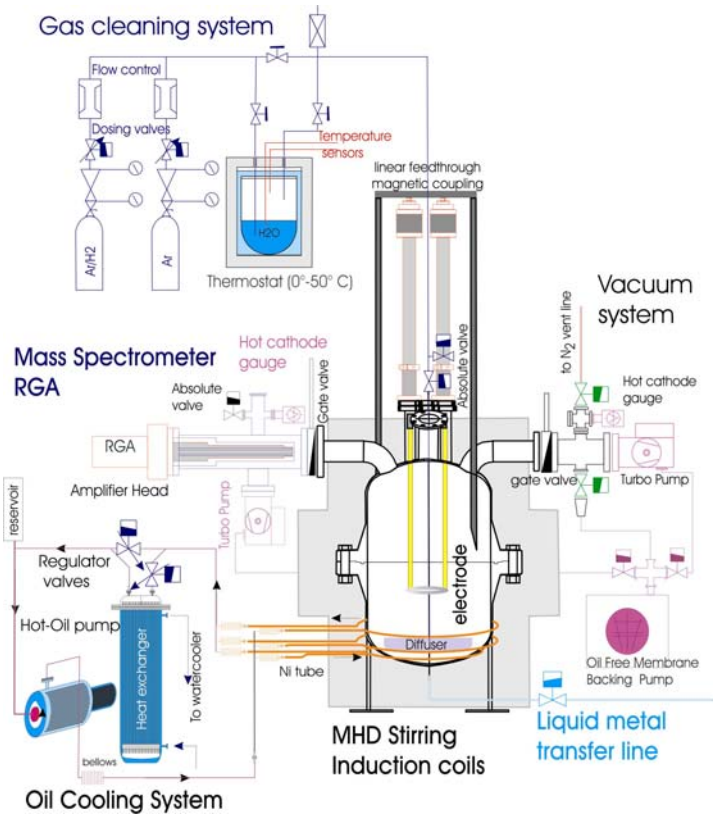

Figure 3. The bottom shell of the PCV being loaded with LBE bars. In the top right corner the connections to the Ni coils are seen.

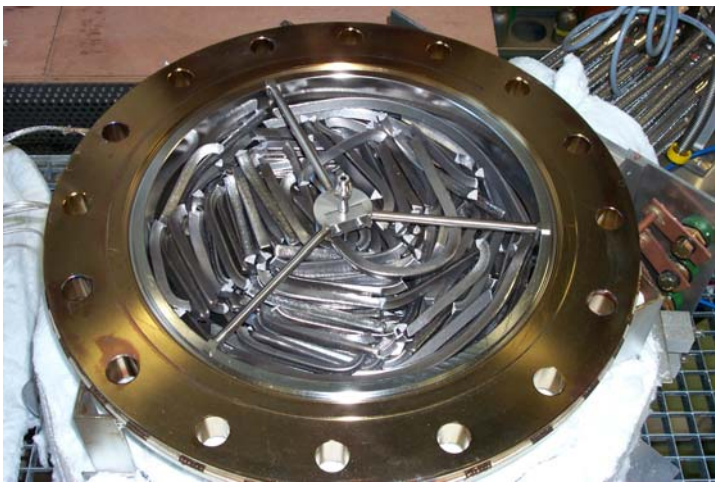

be removed by lowering the oxygen content in the liquid LBE. For this purpose the PCV is equipped with a gas cleaning system where water vapour is added to a 5% H_2/Ar mixture by bubbling it through water that can be set at any stable temperature between 0 and 50 C. By tuning the gas flow and the water temperature the H_2/H_2O ratio that governs the oxygen potential is set to the desired level. The gas mixture is then spread out in the liquid metal via a stainless steel diffuser. At the exit, the water content of the gas is verified using a chilled-mirror dew point meter. A solid zirconium-oxide electrolytic cell with a Pt/air reference system monitors the oxygen content in the vessel while probes with Ni/NiO and Bi/Bi_2O_3 references are dipped into the LBE melt. After the gas cleaning, most insoluble material will have been removed. Yet, for the small amount of debris that may still be present on the face of the melt, electrical glow discharge cleaning is foreseen (Figure 4). A Cr-coated electrode is mounted on a magnetically coupled linear motion feed-through. After the chamber is evacuated, an appropriate reducing gas, e.g. deuterium, is injected to create a background pressure of 10^{-4}-10^{-2} mbar. A bias voltage on the electrode in the gas creates plasma that bombards the surface of the liquid metal and the walls of the vessel, thereby reducing and removing outer layers. This material is then eliminated from the vessel by the pumping system.

Figure 4. The inside of the upper lid of the PCV showing from left to centre: internal thermocouples, glow discharge electrode, inspection window and inlet tube for gas treatment

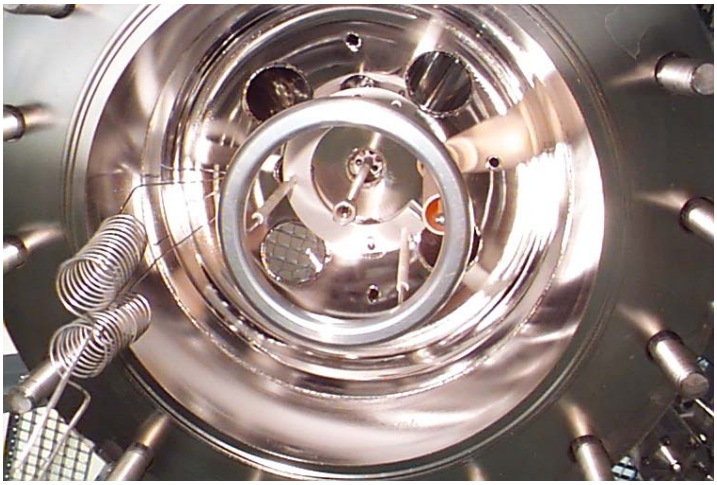

The liquid metal contained in the PCV is stagnant, although the experiments discussed here are to represent a moving free surface in a liquid-metal loop. Thus, it is essential to be able to renew the surface of the melt. Also, for most cleaning processes that only work efficiently on good contact of the gas with the LBE, surface renewal is important. To achieve this, magneto-hydrodynamic (MHD)–driven stirring is installed using three sets of Ni-tube coils, put around the vessel. Each set is connected to one of the three phases of a special 50-Hz mains transformer that delivers up to 600 A RMS current in each phase. The low frequency assures a penetration depth of the AC magnetic field of a few cm. Finite-element calculations have shown that, e.g. at 2 cm from the inside wall of the vessel, a magnetic field of up to 10 mT can be reached. With the viscosity and density of the molten LBE given, this suffices to create a recurrent flow in the crucible going up (down) along the walls and down (up) through the centre of a few cm/s.

The UHV in the PCV is generated by a small 60 l/s turbopump with greased bearings backed by a diaphragm pump. The system yields a minimal hydrocarbon contamination in the vacuum vessel without using a turbopump with full magnetic bearings. It has an end-vacuum capability for leak testing down to mass spectrometer conditions below 10^{-7} mbar and can cope with the expected emanations. Pressure readout from a full range Bayert-Alpert (BA) ionisation/pirani gauge ($5\ 10^{-10}$-1 000 mbar) is stored by the DAC system. The vacuum pump and gauge are separated from the main vessel by a 63-mm UHV gate valve. Opposite to this, a 100-mm UHV gate valve allows the installation of a rest gas analyser (RGA) based on a triple-quadrupole mass spectrometer. A more detailed description of the RGA will be given in the next section.

Before and after each cleaning step in the conditioning of the LBE, the overall outgassing and evaporation flow rate will be assessed by measuring the pressure reached in the vessel against a known pumping speed and by observing the time evolution of the pressure rise in the closed-off vessel. Also, the qualitative appearance of the eutectic mirror will act as an important guide in the cleaning process. In the development of the cleaning procedure, these data will be taken after repeated exposures to air and following application of the various cleaning methods. Once the process is complete, the liquid LBE is shifted to the VICE vessel. A 6-mm stainless steel transfer tube connects the bottom of the PCV with the inlet port in VICE. On both ends, a diaphragm valve allowing a temperature of up to 260 C terminates the line. To be able to transport the LBE mainly by gravity, the PCV is positioned on a platform such that the bottom of the vessel is about 2 cm above the level of the inlet port in VICE. However, the possibility exists to pressurise the PCV during the move with an inert gas that is eventually used at the end of the transfer procedure to purge the transfer line.

The VICE vessel

The VICE vessel is a 5-m high elongated UHV chamber resembling the lower part of the proton beam line near the liquid-metal target. A schematic drawing of the device is shown in Figure 5. At the bottom of the column the LBE, coming as pre-treated from the PCV, is stored in a 900-mm high crucible. The entry point of the transfer line is at the lowest port above the surface level of the melt. The line itself continues below the surface level to ensure that any material added later on (e.g. tracer Hg or Te) is deposited into the melt. In its top part, the VICE vessel holds a ca 3-m long baffle system that gives VICE a conduction rate limitation for the assessment of flow rates and to possibly limit (retard) the migration of condensable metal vapours to the top. It consists of 36 truncated cones with a base diameter of 240 mm and an 80-mm free bore. Thermocouples are installed on the baffle that can be cooled or heated separate from the vessel by circulation liquid of the correct temperature through a built-in circuit. A quartz oscillator microbalance is foreseen to be mounted to assess the evaporation and outgassing rate of condensable materials in the free bore. Also, dismountable surface elements on the baffle will permit post-mortem study of deposits on test areas. At the very top, a single window is

Figure 5. An overview of the technical layout of the VICE experimental vessel

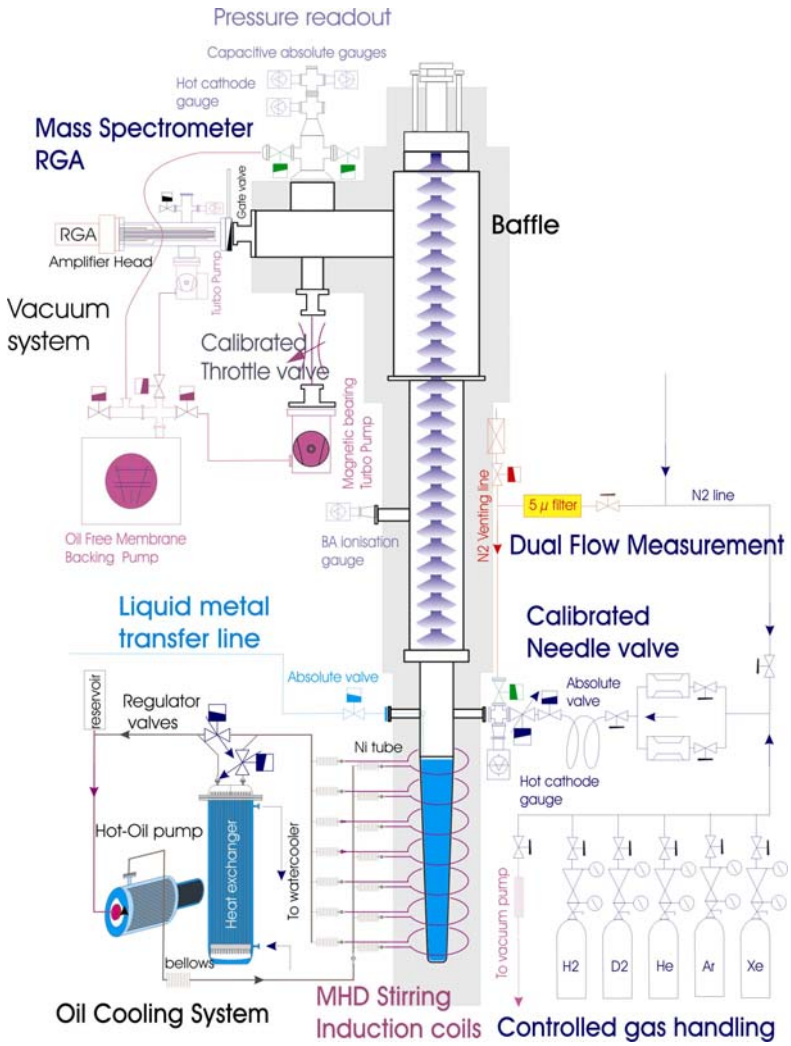

placed, similar to the ones on the PCV. Besides visual inspection of the melt surface, it allows experiments concerning laser-based level detection (LIDAR) that could possibly be carried out in VICE in preparation for the real level monitor to be employed on MYRRHA. As before, the inner surface of VICE is electro-polished and cleaned to UHV requirements. However, because of the specific geometry of the vessel, reconfiguration of the surface finish after extended damage has occurred is not easy. The full VICE vessel can be baked to 500 C, for which purpose a 7-kW heating and temperature control system, similar in design and operation to the one on the PCV, is installed. The MHD stirring device is also similar as before, though here 12 coils are installed because of the elongated shape of the crucible. Each of these is connected alternately to one of the three phases of the 600-A mains transformer. A glow discharge cleaning electrode can also be installed in the VICE vessel, albeit in a fixed position. It will solely be used for minor corrections since the bulk of the conditioning should already have taken place in the PCV.

At the top of the vessel a 400-l/s magnetic bearings turbopump with an integral Holweck stage, able to discharge against 10 mbar and backed by a 3-m^3/h membrane pump, is placed. To ensure that the total pumping speed is dominated by the dimensions of the vessel and not by the pump, it is oversized relative to the geometrical pumping speed of the vessel of less than 100 l/s (H_2 value). The

vacuum system in VICE is completely oil-free, thus preventing any hydrocarbons from entering the vacuum. Still, the pump is able to provide the vessel with initial clean UHV conditions reaching a base pressure below 10^{-8} mbar. At the entrance of the turbopump the pumping speed can be throttled over nearly four orders of magnitude to almost zero by a calibrated variable conduction valve. This device is implemented for flow rate measurements and to obtain a means of changing the pressure over a reasonable range independently of the flow rate in the system in a stable manner. The valve can also be fully closed so that it acts as a shut-off valve (albeit with internal Viton seal). The entire VICE-PCV vacuum system is metal-sealed to the outside atmosphere to achieve absolute He leak-tightness ($<10^{-9}$ mbar.l/s for components, $<10^{-8}$ mbar.l/s for the system) and a maximum bake-out temperature.

The vacuum gauges that provide pressure readout are not merely process control devices but form an integral part of the data-collecting equipment. During the outgassing and evaporation experiments the pressure over the full vessel must be known as accurately as possible. To this end, two hot-cathode/ pirani full range gauges ($2\ 10^{-6}$-1 000 mbar) are placed, one just above the liquid-metal surface and one at the top end of the column. In the centre of the vessel a Bayert-Alpert (BA) ionisation/pirani full range gauge ($5\ 10^{-10}$-1 000 mbar) is mounted and a pair of absolute capacity pressure gauges providing a total range of 10^{-4}-110 mbar is put at the top of the set-up. All vacuum gauge readings are registered in the DAC computer. A known drawback of a hot-cathode gauge is its long-term drift that limits its accuracy to about 30%. In our set-up, they can be calibrated against the BA gauge and the capacitive gauges in the low- and high-pressure ranges respectively. The latter two types have an accuracy of about 5% and 0.15% over their respective useful ranges. The (re-)calibration is practically done by gradually changing the pressure via the calibrated throttle valve or by slowly venting the vessel through the needle valve after the pumps have been closed off. It is foreseen to calibrate the gauges for a particular type of gas using one of the species available in the controlled gas handling system.

The rest gas analyser (RGA) is the most important diagnostic tool in the liquid-metal outgassing and evaporation experiments discussed here. The apparatus is based on a Hiden triple-quadrupole mass spectrometer. In combination with a dedicated 0-50 amu RF generator, the RGA reaches a mass resolution $\mathrm{D}m/m > 2\ 000$ in the 0-50 amu range. Although mass calibration of the spectrometer is relatively straightforward, an absolute signal calibration is not possible since it depends on the efficiency of the ion source and the detector, which may drift for various reasons. Thus, differential calibration against a known gas flow is necessary. The spectrometer itself is housed in its own small vacuum chamber that has a turbopump and a full range hot-cathode vacuum gauge. At the entrance of the RGA chamber an additional variable aperture is introduced. This makes it possible to match the required vacuum for the RGA to the experimental vacuum that is to be changed as matter of the experiments, by differential pumping. The chamber also acts as a protection for the fragile quadrupole structure and makes is relatively easy to move the RGA to either one of the PCV or VICE vacuum vessels.

A gas-inlet port is placed just above the level of the liquid metal to allow gas flow calibration. The flow is controlled by an all-metal regulating needle valve with a minimal flow of 10^{-10} mbar l/s for pure gasses. A shut-off diaphragm valve is placed in series. The mass flow is measured by a set of two parallel mounted differential heat transfer type flow meters giving a total measurement range of almost four orders of magnitude down to 10^{-2} mbar l/s with a relative accuracy of 1%. For lower flow rates, the needle valve calibration will be used. In the gas-handling system H_2, D_2, He, Ar and Xe are presently foreseen as calibration gases. N_2 is also available, although it is taken from a supply of liquid nitrogen at hand in the laboratory. The calibration gases are not limited to the species mentioned here since in principle, any known gas can be used. Once a known gas flow is allowed into the vessel, its signal can be measured by the mass spectrometer. However, the transport properties of the gas through the VICE column (and through the beam tube in reality) will depend on the pressure and temperature and thus the calibration must be done all temperature and pressure regimes used in the real experiment. They should also be repeated in close time-wise proximity before and after the actual measurements.

When the calibration is established, mass flow rates of emanated gases and vapours measured in the RGA in given circumstances can be linked to an evaporation or outgassing rate. The composition of the gas flow will be resolved using the mass characteristics of the gas as measured by the quadrupole spectrometer. In this way the emanated species can be identified. In these conditions the eventual experiment can be performed measuring the mass flow rates of material outgassing or evaporating from the liquid melt. These values are expected to lie between 10^{-6} and 10^{-1} mbar l/s. The data will be taken as a function of the pressure in the vessel, the liquid melt temperature, the stirring rate and the baffle temperature. The experimental data will serve as input into the modelling of the interaction of the proton beam with the emanated gasses and vapours in order to eventually assess the plasma formation problem described in the introduction.

In a second stage, stable isotopes resembling the spallation products like, e.g. Hg and Te, may be added to the LBE via the liquid-metal transfer line. By using the MHD stirring device the materials should be adequately mixed such that in effect the outgassing of spallation products is simulated. Subsequently, the mass flow of the spallation product will be measured as a function of time at a given temperature and pressure. In this way the measurement will yield information on the dynamical gas transport properties of the beam line and the time-integrated signal will give data on the emanation probability of spallation products produced in the target. Of course, because of the time dependence, the tracer material will have to be inserted in a pulsed mode.

At present, the commissioning and testing stage of the VICE vacuum vessel and instrumentation is well underway while the commissioning of the PCV is finished. The vessel has been loaded with 100 kg of LBE and the initial coarse outgassing tests have taken place. The characteristic spikes in the vacuum pressure readout due to the release of gaseous inclusions in the LBE ingots during melt were observed. After 24 h of pumping with the LBE at 150 C a base pressure of $1\ 10^{-6}$ mbar was reached. However, it was found that even after several days, stirring of the melt induced additional gas emanation to a sufficient level to increase the pressure to 10^{-3} mbar. This shows the importance of stirring the melt during the outgassing process. When heating the LBE to 400 C, the bulk of the outgassing appeared to start only above 320 C (Figure 6), with the development of bubbles yielding pressure spikes. With the LBE at 400 C, a pressure of $4\ 10^{-6}$ mbar was eventually achieved after seven days of pumping. These values are two orders of magnitude below the minimal requirements mentioned in the introduction. However, the presence of a PbO layer on the liquid LBE possibly inhibits gas emanations from the surface and thus these preliminary results do not show the intrinsic vacuum compatibility of the windowless target design. To check this issue, the vessel was opened with the melt at 150 C and exposed to air for 24 h without stirring. Prior to re-closing the vessel, the surface of the LBE was mechanically skimmed. After subsequent reheating and pumping, a pressure below 10^{-6} mbar was reached within 24 h after reheating the melt to 400 C. This indicates that initial outgassing only needs to be done once as long as the melt is kept stagnant when a cover gas is used.

The next step is the (time consuming) development of the cleaning and oxygen control process. In the first instance a gas diffuser with a sintered stainless steel surface was employed to distribute the H_2/Ar gas in the melt in very fine bubbles. However, the sintered material turned out not to be able to withstand immersion in LBE for extended periods of time. This is probably due to wetting of the LBE on the large surface of the sintered part. At present, tests are undertaken with a much coarser diffuser using thick-walled stainless steel tubing with 2-mm holes.

During the outgassing and conditioning experiments, a layer of “black dust” was formed on the quartz viewport windows. The study of this layer is relevant since the nature of the deposit will not only have implications on the instrumentation in the vacuum of the spallation loop but also on that in the gas plenum above the main LBE pool [2]. Chemical analyses have shown that the deposit consists

Figure 6. Initial outgassing of LBE at 400 C

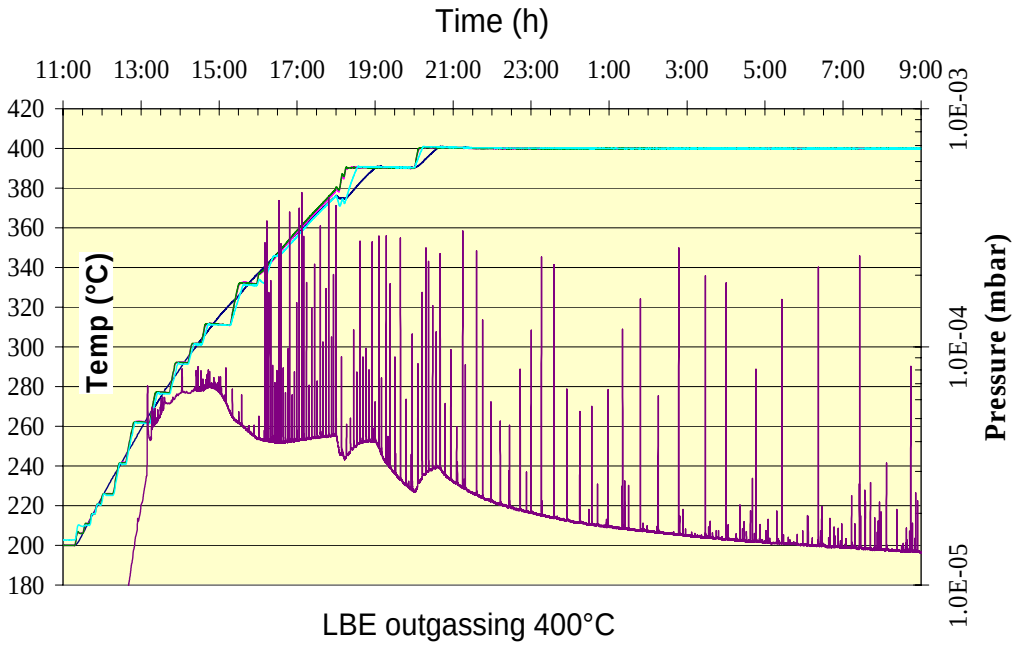

of 69% Bi and 31% Pb with other detectable elements (Zn and Sn) only present at the ppm level. Comparing this to the composition of the LBE in the vessel (54.3 wt.% Bi and 45.7 wt.% Pb by analyses) we see that there is a small preference for Bi deposition and thus there is no indication that the "black dust" should be mainly PbO. On electron microscope images of the layer it can be seen that the layer is built up from small 500-nm droplets. It is not clear whether these are formed by surface tension when Pb and Bi vapour condenses on the quartz windows or that the droplets are formed as an aerosol during the gas treatment phase of the conditioning process. This question will only be resolved when the analyses of a "black dust" layer deposited in clean UHV conditions is complete.

Figure 7. Electron microscope images of LBE deposited on quartz windows. In the background SiO_2 fragments of the substrate are seen. The bulk of the substrate is seen on the bottom left.

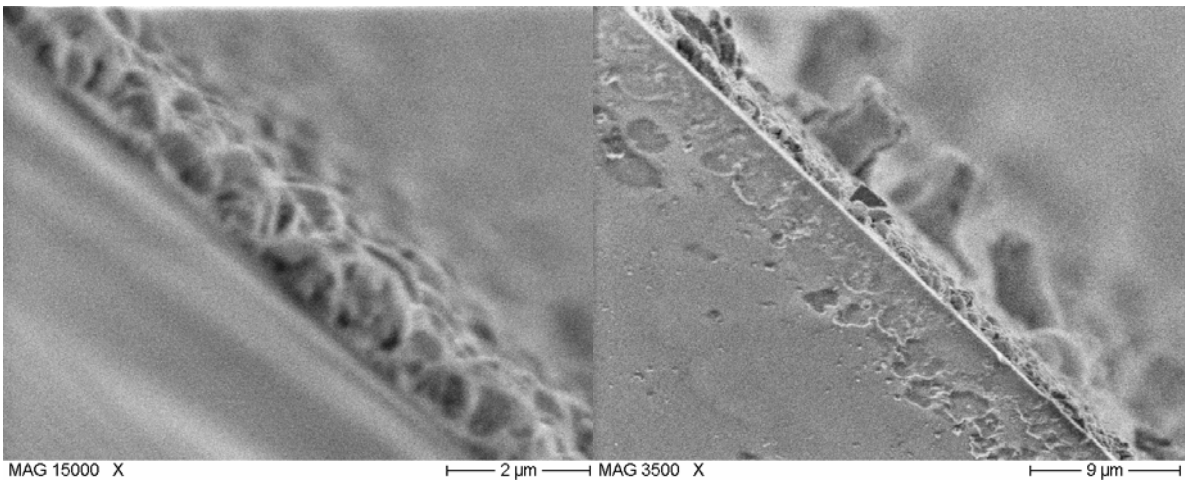

REFERENCES

[1] Muller, G., G Schumacher, F. Zimmermann, *J. Nucl. Mater*., 278, 85-91 (2000).

[2] Aït Abderrahim, H., *et al*., "MYRRHA: A Multi-purpose Accelerator Driven System for Research and Development", *Nucl. Inst. and Meth. in Phys. Res*., A463, 487-494 (2001); see also from the same author, "MYRRHA: A Multi-purpose Accelerator Driven System for R&D State of the Art Mid-2003", *Proceedings of the International Workshop on P&T and ADS Development*, Mol, Belgium, 6-8 October 2003, ISBN 9076971072.

[3] Michelato, P., *et al*., "TRASCO-ADS Project Windowless Interface: Theoretical and Experimental Evaluation", *Proceedings of the International Workshop on P&T and ADS Development*, Mol, Belgium, 6-8 October 2003, ISBN 9076971072; see also from the same author, these proceedings.

[4] Schuurmans, P., P. Kupschus, A. Verstrepen, J. Cools, H. Aït Abderrahim, "VICE: R&D Support for a Windowless Liquid Metal Spallation Target in MYRRHA", *Proceedings of the International Workshop on P&T and ADS Development*, Mol, Belgium, 6-8 October 2003, ISBN 9076971072.

[5] Vermeersch, F., *et al*., *Calculation of the Pressure Distribution in the MYRRHA Spallation Target Vacuum System*, SCK•CEN internal report, Nuclear Studies IDPBW/NS/Fve/01 (2002).

INTRODUCTION OF A DUAL INJECTION TUBE FOR THE DESIGN OF A 20 MW LEAD-BISMUTH TARGET SYSTEM

Chung-Ho Cho, Yonghee Kim, Tae-Yung Song
Korea Atomic Energy Research Institute
150 Duckjin-Dong, Yuseong, Daejeon, 305-353 Korea

Abstract

A spallation target system is a key component in the development of an accelerator-driven system (ADS). It is known that a 15-25 MW spallation target is required for a practical 1 000 MWth ADS. The design of a 20 MW spallation target is very challenging because more than 60% of the beam power is deposited as heat in a small volume of the target system. In the present work, a numerical design study was performed to obtain the optimal design parameters of a 20 MW spallation target for a 1 000 MWth ADS. A dual injection tube was proposed for the reduction of the LBE flow rate at the target channel. The results of the present study show that a 30-cm wide proton beam with a uniform beam distribution should be adopted for the spallation target of a 20 MW power. When the dual LBE injection tube is employed, the LBE flow rate is reduced by a factor of four without reducing the maximum allowable beam current.

Introduction

In an ADS a high-energy proton beam is impinged on a heavy metal target to produce spallation neutrons that are multiplied in a subcritical blanket. Therefore, the spallation target is one of the most important units of an ADS. Lead-bismuth eutectic (LBE) is preferred as the target material due to its high neutron production rate, effective heat removal and a very small amount of radiation damage properties. In addition, it can be used simultaneously as a reactor coolant.

The key issue in the target design is how to design an appropriate beam window and LBE flow so that the system can sustain thermal and mechanical loads as well as radiation damage. Recently, there have been some intensive studies on the design of LBE spallation targets [1,2]. It is well known that a proton beam power of 15-25 MW is required for a practically sized (~1 000 MWth power) ADS [3]. The design of a 20 MW spallation target is very challenging because more than 60% of the beam power is deposited as heat on the window and in a small volume of the target system [4].

Due to the difficulties of designing high-power targets, a three-beam target system was proposed by Forschungszentrum Karlsruhe; the target designs without beam windows are also considered in the MYRRHA project and the X-ADS design [5,6,7]. Although these proposals have some preferable characteristics for high-power targets, they still have some difficulties in other aspects when compared to the more typical LBE target designs (i.e. a single beam with a solid window).

The main objective of the present paper is to show the possibility of designing a 20 MW LBE spallation target with a beam window. In a previous study, we designed a 20 MW LBE target for HYPER [8]. However, it was found that the LBE flow rate was too high at almost 10% of the total coolant flow rate, and the average LBE temperature rise in the target outlet was too low compared to the LBE heat-up in the core. These problems result in an increased pumping power of the coolant, potential thermal striping of the core upper structures and a decrease in the thermal efficiency of the system. Thus, it is essential to reduce the LBE flow rate in the target channel without hampering the target performance.

For this purpose, we introduce a dual LBE injection tube (DIT), which controls the LBE velocity distribution at the target inlet. Sensitivity studies for the DIT have been performed for the HYPER target system and the results are provided in this paper.

Target system

The Korea Atomic Energy Research Institute (KAERI) has been developing an ADS called HYPER [10]. HYPER is a 1 000 MWth fast spectrum reactor with $k_{eff} = 0.98$ and is designed to transmute the TRU, Tc-99 and I-129 coming from PWRs. HYPER is expected to need a 19 mA proton beam of 1 GeV to sustain the 1 000 MWth power level.

LBE is the target material and the target coolant. The beam window material is 9Cr-2WVTa. It is advanced ferritic-martensitic steel that is known to be more resistant to LBE corrosion than austenitic steels and does not show a ductile-to-brittle transition temperature (DBTT) problem while being resistant to radiation damage [11].

The cylindrical beam tube and hemi-spherical beam window are adopted in the basic target design of HYPER. Although hexagonal fuel assemblies surround the LBE flow channel, the target channel is assumed to have a cylindrical shape for the thermal-hydraulic calculation of the target channel. Figure 1 shows the reference target system schematically. The beam window diameter (D_w) and the beam window thickness are 35 cm and 2.0 mm, respectively. The target channel diameter (D_t)

is set at 66 cm. The beam diameter (D_b) should be as large as possible since a larger beam diameter means a smaller beam current density, which makes the peak temperature lower. There should be a minimum distance between the beam tube and the beam. But, since the proton beam may shift from its original axis, the minimum distance between the beam tube and the beam is 0.5 cm larger than a proton beam shift distance, or $D_w - D_b = 5$ cm. Two alternative radial distributions of the proton beam current density (uniform and parabolic distributions) are considered in the thermal-hydraulic analysis.

The LBE inlet temperature (T) is the same as the inlet temperature of the core coolant, 340°C. The pressure load, which is applied to the beam tube located 10 cm above the junction point of the beam tube and the beam window, is assumed to be 16 atm. LBE inlet velocity (V) can be adjusted locally by using orifices, although the flow is connected to the core coolant LBE.

The first criteria are the maximum allowable velocity and the temperature of the LBE. The erosion and corrosion rates of the structural material are increased as the LBE velocity and temperature increase. Therefore, the velocity of the LBE is fixed at 500°C and 2 m/s [12]. The second set of criteria are the maximum allowable temperature and the stress of the beam window. Steels are usually degraded significantly if the temperature is too high. Therefore, 600°C is chosen as the maximum allowable temperature for the beam window. The stress intensity of the beam window is not allowed to exceed 1/3 of the yield strength of 9Cr-2WVTa [13]. The yield strength of 9Cr-2WVTa is 480 MPa at 600°C, which means the maximum allowable stress is 160 MPa [14].

Figure 1. The reference target system

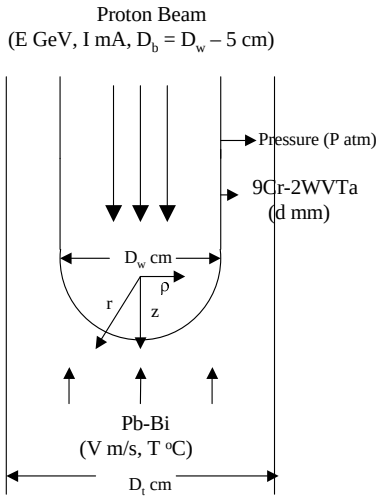

Numerical simulation

The material data for the calculation are listed in Table 1. The data used for the LBE and 9Cr-2WVTa are values at 450°C and 500°C, respectively. Since the data used for 9Cr-2WVTa are not available, the data of 9Cr-MoVNb except for yield strength are used. Due to the two being ferritic 9Cr steels, the thermal expansion coefficient, density and thermal conductivity are not very different.

Table 1. Material data used for calculations

LBE (450°C)	Density (10.2 g/cm^3) Thermal conductivity (14.2 W/m·K) Thermal expansion coeff. (1.2×10^{-4} K^{-1}) Viscosity (1.39 centipoise)	9Cr-2WVTa (500°C)	Density (7.6 g/cm^3) Thermal conductivity (30 W/m·K) Thermal expansion coeff. (1.23×10^{-5} K^{-1})

The heat generation inside the beam window and the LBE is calculated using the LCS 2.7 (LAHET code system) [15]. The thermal-hydraulic analyses of the target system are performed using the CFX 4.4 code. In the thermal-hydraulic analyses, all the calculations were performed using the standard k-ε turbulence model to predict the turbulent flow characteristics, and the logarithmic law of the wall to predict the near-wall characteristics. Sufficient mesh refinement is used in each case to obtain y+ values between 30 and 200 in the heated regions, indicating that the turbulence model can provide reasonable predictions in these regions. The calculation is performed as a steady state simulation using the SIMPLEC solution algorithm and upwind differencing scheme. Also, the thermal-hydraulic behaviour is evaluated using an axi-symmetric model. The maximal uniform inlet velocity of the LBE is decided based on the criterion that the LBE velocity at the target system does not exceed 2 m/s. Figure 2 contains a schematic of the computational domain and the adopted boundary conditions.

Figure 2. The computational domain and the BC

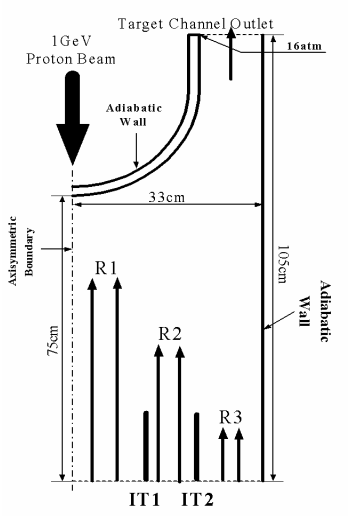

Heat generation

The heat generation inside the beam window and LBE is calculated using the LCS 2.7 for the two types of proton beam distributions – uniform and parabolic distributions. The results of the LCS are fitted to obtain the current density functions, which express the heat generation rates with a variable proton beam current.

1. A parabolic distribution is as follows:

$$Q = C\frac{2I}{\pi R_b^4}(R_b^2 - \rho^2) \qquad \text{unit: W/cm}^3 \tag{1}$$

2. A uniform distribution is as follows:

$$Q = CI \qquad \text{unit: W/cm}^3 \qquad (2)$$

where I = proton beam current (mA), R_b = beam radius (cm), ρ = distance from the centre (cm) and C = fitted coefficient.

First, thermal-hydraulic analyses of the reference target system were performed to compare the two beam profiles, uniform and parabolic, under the same calculation conditions. The LBE inlet velocity was 1.31 m/s and the beam current was 20.0 mA. The peak temperatures of the LBE with a parabolic and uniform beam distribution were 654°C and 505°C, respectively. In addition, the peak temperatures of the beam window with the parabolic and the uniform distribution were 736°C and 547°C, respectively. Clearly, the uniform beam distribution provides a lower peak temperature. In the same case, the allowable beam currents satisfying the design criteria with a parabolic and a uniform distribution were calculated to be 10.1 mA and 19.3 mA, respectively. All the cases show that the allowable beam current is constrained by the peak temperature of the LBE, 500°C, not by the peak temperature of the beam window, 600°C. In the case of the uniform beam distribution, the allowable beam currents were 19.3 mA, which is about twice that of the parabolic beam profile case.

Consequently, the uniform beam target system was adopted for HYPER. However, this target system has two unfavourable features: 1) LBE flow rate (4 562 kg/s) is almost 10% of that of the active core (45 506.26 kg/s) and 2) average LBE exit temperature (356°C) is too low when compared to the core average coolant temperature of 490°C. The large flow rate in the target channel increases the pumping power and the temperature difference between the target coolant and the core coolant may cause the so-called thermal striping behaviour. Thus, it is highly desirable that the LBE flow rate be minimised, while keeping the maximum proton beam.

For a comparison, we analysed the target with an LBE flow rate reduced by 50%. In this case, the maximum beam currents satisfying the design criteria with parabolic and uniform distributions were calculated to be 5.4 mA and 10.1 mA, respectively. The target system with a reduced flow rate does not offer a sufficient beam current to sustain the 1 000 MWth power level of the HYPER.

Effect of single injection tube

The lesser the flow rate of the target channel, the lesser the allowable beam current; thus, it is difficult for the present target system to reduce the flow rate with a sufficient beam current to sustain the 1 000 MWth power level of HYPER. As a result, a cylindrical injection tube (IT), which is located in the centre of a target channel, was introduced to reduce the flow rate in the target system.

In order to investigate the effect of the single injection tube (SIT), thermal-hydraulic analyses were performed with the two types of proton beam distributions with a beam current of 20 mA. The SIT diameter and the SIT height were 31 cm and 10 cm, respectively, and the thickness of the IT was 2 mm. Due to the proton beam diameter being 30 cm, the SIT diameter was wider than that of the proton beam to avoid any direct irradiation of the proton beam at the SIT. The LBE inlet velocity at the target channel without SIT was 0.655 m/s. The LBE inlet velocities of R1 and R2 (+R3) were 1.5 m/s and 0.417 m/s, respectively.

Figure 3 shows the temperature distributions of the wetted surface at the beam window with/without the SIT. Without the SIT, the peak temperature of the wetted surface at the beam window is 928°C for the parabolic beam and 657°C for the uniform beam. With the SIT, the peak temperature of the wetted surface at the beam window is 652°C with the parabolic beam and 515°C with the uniform beam. With the SIT, the peak temperature of the wetted surface at the beam window is significantly reduced.

Figure 3. Temperature distributions of the wetted surface at the beam window

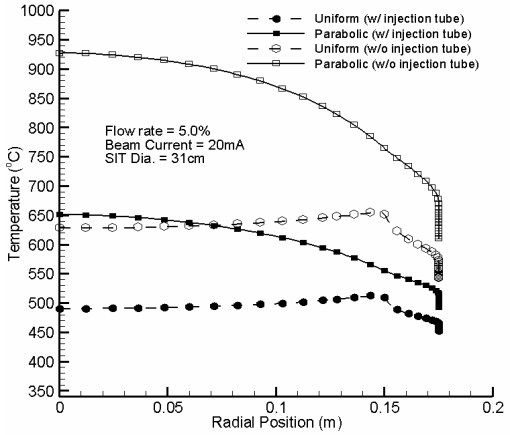

For the SIT concept, thermal-hydraulic analyses were performed to determine the maximum beam current satisfying the design criteria. The LBE inlet velocities of R1 and R2 (+R3) were 1.635 m/s and 0.378 m/s, respectively. The maximum beam currents satisfying the design criteria with the parabolic and the uniform beam distributions were calculated to be 10.3 mA and 19.6 mA, respectively. The results show that the introduction of an SIT is a good counterproposal to reduce the flow rate of the target system with a sufficient beam current to sustain the 1 000 MWth power level of the ADS.

In order to investigate the effect of a variation in the SIT diameter, thermal-hydraulic analyses were performed. The diameter of the SIT was varied from 10 cm to 35 cm and the SIT height was fixed at 10 cm. The LBE inlet velocity of R1 was fixed at 1.5 m/s and the LBE inlet velocity of R2 (+R3) was decided based on the flow rate of the target system not exceeding 5.0% of that of the active core. The proton beam current was 20 mA. Figure 4 shows the temperature distributions of the wetted surface at the beam window with the SIT diameter variation. In the case of the uniform beam, the wider the diameter of the SIT, the greater the cooling effect at the beam window. In the case of the parabolic beam, the narrower the diameter of the SIT, the greater the cooling effect at the beam window.

In order to investigate the changes of temperature and velocity distribution in the target system with flow rate variations, thermal-hydraulic analyses were performed. The SIT diameter and height were fixed at 10 cm. Beam currents of the parabolic and uniform beams were 12.3 mA and 19.6 mA, respectively. While the LBE inlet velocity of R1 was fixed at 1.95 m/s, the flow rate of R2 (+R3) was reduced little by little. The flow rate of R1 was 156 kg/s, or 0.34% of that of the active core.

The peak temperature at the beam window and the LBE with the flow rate variation is shown in Table 2. The temperature distributions of the wetted surface at the beam window are shown in Figure 5. Although the total flow rate of the target channel was reduced to 2.8% of that of the active core, in the case of the parabolic beam, the changes of the peak temperature were very small. But, in the case of the uniform beam, the changes of the peak temperature with the flow rate variation were larger than that of the parabolic beam. When the LBE inlet velocity of R2 (+R3) was 0.62 m/s, the peak temperature of the LBE of the wetted surface at the beam window met the design criterion. In the

case of the parabolic beam, the peak temperature of the wetted surface at the beam window gradually shifted outwards from the centre of the beam window along the beam window surface, which was contrary to the typical temperature distribution at the beam window surface with a parabolic beam. In the case of the uniform beam, the peak temperature of the beam window occurred near the intersection of the proton beam boundary with the beam window and increased with the flow rate reductions.

Figure 4. Temperature distributions of the wetted surface at the beam window with the SIT diameter variation

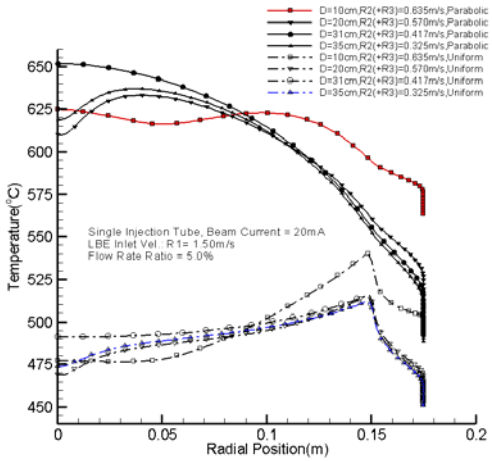

Table 2. Peak temperature of the beam window and the LBE with flow rate reduction

LBE inlet velocity of R2 (+R3) (m/s)		0.62	0.5	0.4	0.3	0.25
Total flow rate ratio of target channel (%)		5.0	4.07	3.33	2.57	2.21
Parabolic	Peak temp.(beam window, inner surface, °C)	529	528	527	526	525
	Peak temp.(beam window, wetted surface, °C)	479	478	478	481	483
Uniform	Peak temp.(beam window, inner surface, °C)	540	544	550	558	562
	Peak temp.(beam window, wetted surface, °C)	500	505	511	518	523

Figure 5. Temperature distribution of the wetted surface at the beam window with the flow rate reduction

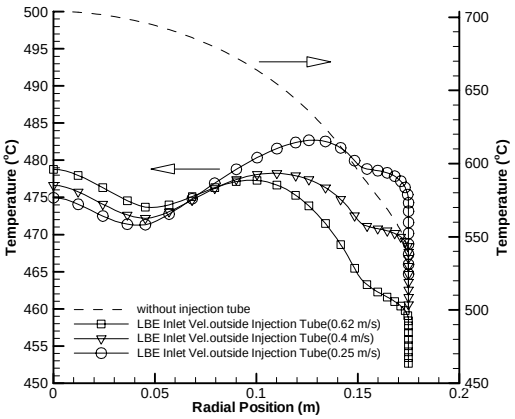

(a) Parabolic beam

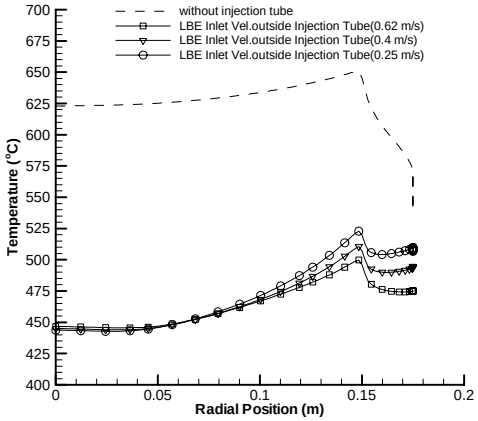

(b) Uniform beam

Figure 6. The velocity and temperature distribution in the target channel with flow rate variations

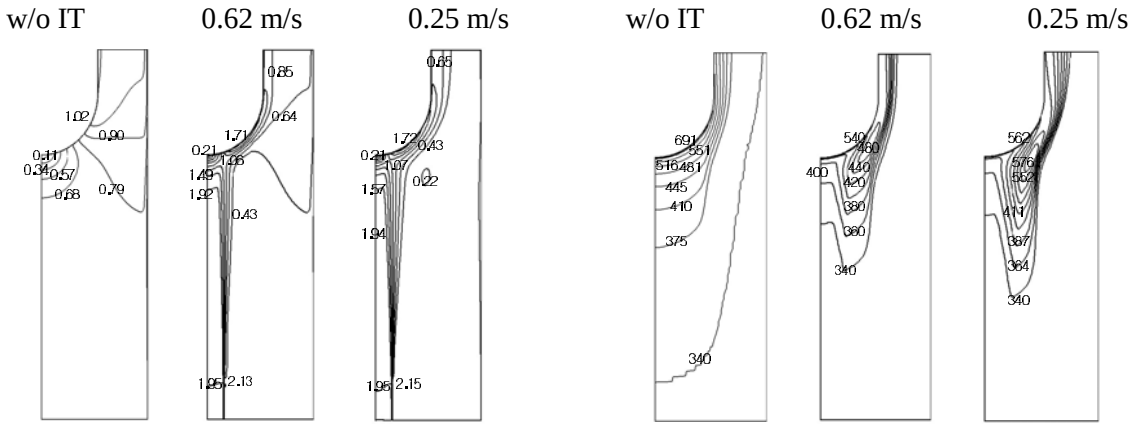

Figure 6 shows the velocity and the temperature distribution in the target system with the flow rate reduction of R2 (+R3). Due to the relatively high velocity of the LBE of R1, the flow stagnation region existing below the beam window centre was substantially decreased. But, with the injection tube, another flow stagnation region developed below 45° from the beam window centre when the flow rate of R2 (+R3) was reduced substantially. It caused a temperature increase of the LBE near the intersection of the proton beam boundary with the beam window, and the peak temperature of the LBE occurred at the thermal island in the flow field of the LBE.

Effect of dual injection tube

It is clear that the target system with an SIT offers not only a more allowable beam current but also a significantly reduced flow rate at the target channel. However, when an SIT is employed, a new flow stagnation region develops below the beam window with the flow rate reductions. It causes a temperature increase of the LBE near the intersection of the proton beam boundary with the beam window. In addition, with the SIT concept, the LBE flow rate could not be further reduced without reducing the maximum allowable beam current. Therefore, we introduced a dual injection tube (DIT), which provides a greater degree of freedom in the LBE flow field control.

Table 4. Parameter sets of DIT

Case 1	Case 2	Case 3	Case 4
D1 = 10 cm, D2 = 30 cm	D1 = 10 cm, D2 = 35 cm	D1 = 20 cm, D2 = 30 cm	D1 = 20 cm, D2 = 35 cm

In order to investigate the effect of DIT, thermal-hydraulic analyses were performed with a fixed flow rate of the target system, 5% of that of the active core, and the results are shown in Figure 7. There are four kinds of DIT as shown in Table 4. The LBE inlet velocities of R1 and R2 were 1.95 m/s and 1.0 m/s, respectively. The beam currents of the parabolic beam and the uniform beam were 12.3 mA and 19.6 mA, respectively.

In Figure 7, in all cases except Case 1, a drop in temperature occurred at the beam window centre. In the case of the uniform beam, the wider the diameter of the inner IT (IT1), the greater the cooling effect at the beam window. In the case of the parabolic beam, the smaller the diameter of the inner IT

(IT1), the greater the cooling effect at the beam window. The results showed that Case 1 with the parabolic beam and Case 3 with the uniform beam would be the optimum parameter set from the viewpoint of the peak temperature at the beam window.

Figure 7. Temperature distributions of the wetted surface at the beam window with DIT diameter variations

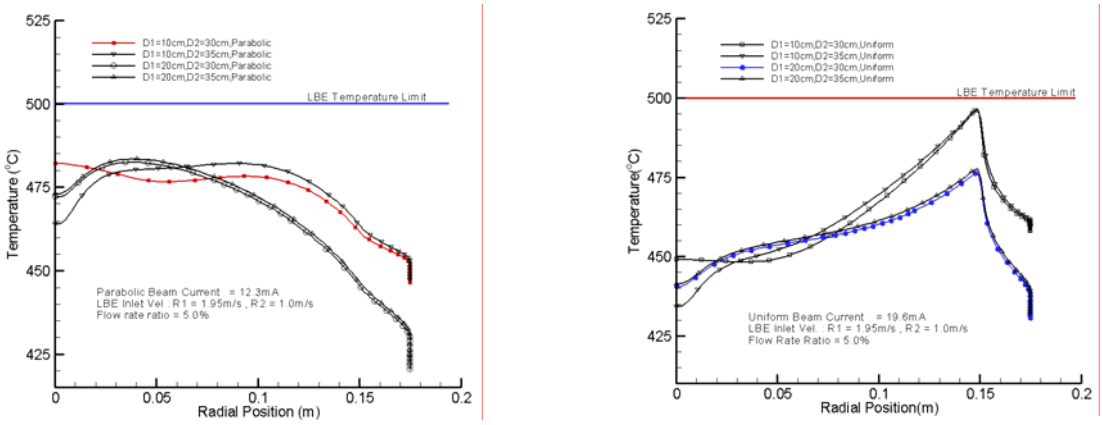

(a) Parabolic (b) Uniform

In order to investigate the changes of the temperature distribution at the beam window with the flow rate variations, thermal-hydraulic analyses were performed with Case 1 and Case 3 (results are shown in Figures 8 and 9). The beam currents of the parabolic and the uniform beam profile were 12.3 mA and 19.6 mA, respectively. The LBE inlet velocities of R1 for Case 1 and Case 3 were 1.95 m/s and 1.80 m/s, respectively. While the LBE inlet velocity of R3 was fixed at 0.2 m/s, the flow rate of R2 was reduced little by little.

Figure 8. The temperature distributions of the wetted surface at the beam window with the parabolic beam

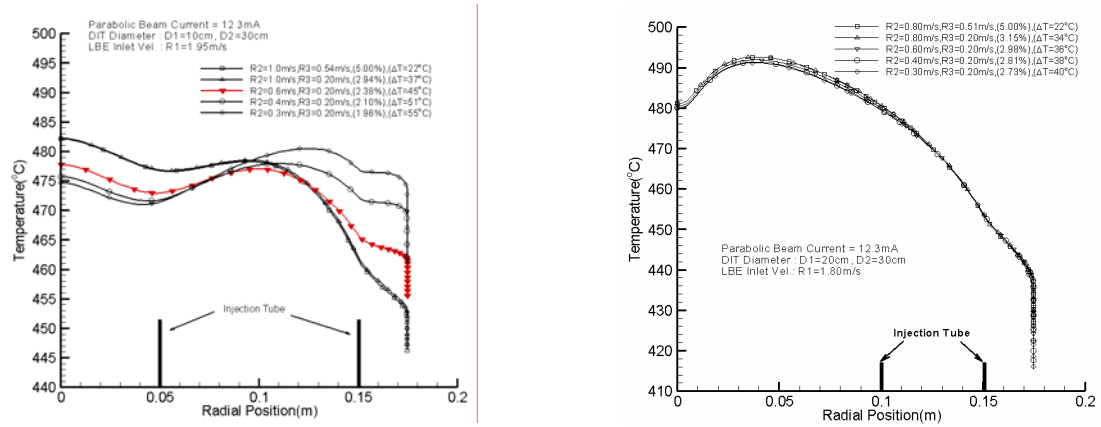

(a) Case 1 (b) Case 3

In Figure 8, Case 1 was more effective for beam window cooling than Case 3. In the case of R2 = 0.3m/s, the LBE flow rate of the target channel could be reduced by a factor of five with an increased allowable maximum beam current (14.0 mA) and an average LBE exit temperature (395°C). In the case of R2 = 0.6 m/s, which would be the optimum case from the viewpoint of the peak temperature at the beam window, the allowable maximum beam current was 14.28 mA.

As shown in Figure 9, Case 3 was more effective for the beam window cooling than Case 1. Also, the temperature increases of the wetted surface at the beam window with the flow rate reductions were smaller than with Case 1 or the SIT. The results showed that a new flow stagnation region, which developed below the beam window, was very well controlled by the DIT. In the case of R2 = 0.3 m/s, the LBE flow rate of the target channel could be reduced by a factor of four with an increased allowable maximum beam current of 21.27 mA and an average LBE exit temperature of 398°C.

Figure 9. Temperature distributions of the wetted surface at the beam window with the uniform beam

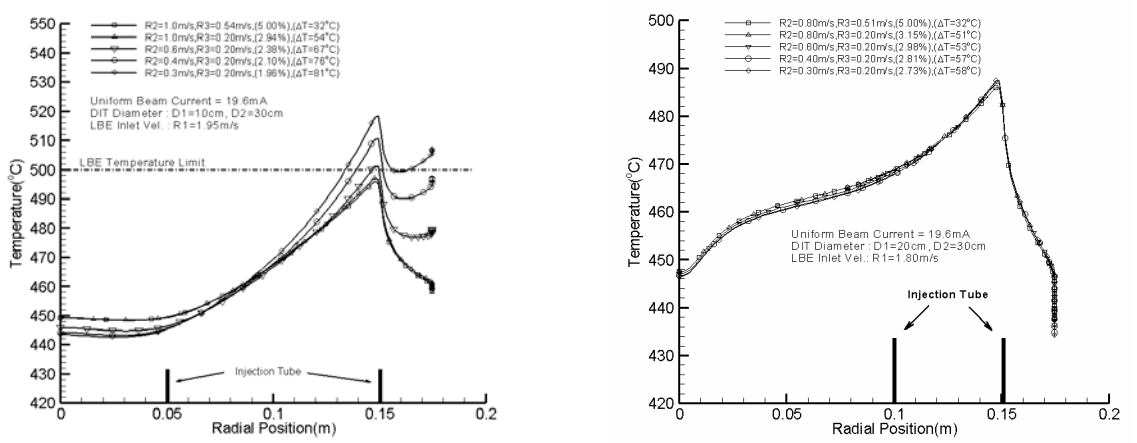

(a) Case 1 (b) Case 3

Conclusions

In this paper, a cylindrical injection tube, which is located in the centre of a target channel, was introduced to reduce the flow rate at the target system.

With a dual injection tube having a 10 cm inner tube diameter and a 30 cm outer tube diameter, the allowable maximum beam current was 14.0 mA for a parabolic beam, which was ~159% higher than that of the target system without an injection tube. In addition, with a dual injection tube having a 20 cm inner tube diameter and a 30 cm outer tube diameter, the allowable maximum beam current was 21.27 mA for a uniform beam, which was ~111% higher than that of the target system without an injection tube. From the viewpoint of thermal-hydraulics, the results show that a smaller diameter of the inner injection tube would be appropriate for the parabolic beam and a wider diameter of the inner injection tube would be appropriate for the uniform beam.

The results indicated that the target system with a dual injection tube offers not only a higher allowable beam current but also a significantly reduced flow rate at the target channel. If the inlet velocity of R3 was further reduced, the LBE flow rate could be decreased without reducing the maximum allowable beam current (currently being tested in a related study).

Acknowledgements

The Korean Ministry of Science and Technology (MOST) provided support for this work.

REFERENCES

[1] Buono, S., *et al*., "Numerical Studies Related to the Design of the Beam Target of the Energy Amplifier Prototype", Heavy Liquid Metal Conference 1998, Vol. 1, pp. 249 (1998).

[2] Cheng, X., I. Slessarev, "Thermal-hydraulic Investigations on Liquid Metal Target System", *Nuclear Engineering and Design*, 202, 297-310 (2000).

[3] Kim, Y.H., *et al*., "Optimisation of Height-to-diameter Ratio for an Accelerator-driven System", *Nuclear Science and Engineering*, Vol. 143, pp. 141-157 (2003).

[4] Tak, N.I., *et al*., "Numerical Studies on Thermal Hydraulics of HYPER Target", AccApp & ADTTA '01, Reno, Nevada, 11-15 November 2001.

[5] Cheng, X., *et al*., "Thermal Hydraulic Design of an ADS with Three Spallation Targets", *Proceedings of ADTTA '99*, Prague, Czech Republic (1999).

[6] Tichelen, K.V., *et al*., "MYRRHA Project, a Windowless ADS Design", *Proceedings of ADTTA '99*, Prague, Czech Republic (1999).

[7] Ansaldo, "XADS Pb-Bi Cooled Experimental Accelerator Driven System Reference Configuration", Summary Report (2001).

[8] Cho, C.H., T.Y. Song, N.I. Tak, "Numerical Design of a 20 MW Lead–Bismuth Spallation Target for an Accelerator-driven System", *Nuclear Engineering and Design*, Vol. 229, pp. 317-327 (2004).

[9] Park, W.S., *et al*., Development of Nuclear Transmutation Technology, KAERI/RR-1702/96 (1997).

[10] Dai, Y., "Martensitic/ferritic Steels as Container Materials for Liquid Mercury Target of ESS", *Proceedings of the International Workshop on the Technology and Thermal Hydraulics of Heavy Liquid Metal*, 6.27-6.39 (1996).

[11] Yachmenyov, G.S., *et al*., "Problems of Structural Materials' Corrosion in Lead-Bismuth Coolant", *Proceedings of Heavy Liquid Metal Coolants in Nuclear Technology*, Vol. 1, pp. 133-140 (1999).

[12] Rust, J.H., *Nuclear Power Plant Engineering*, Haralson Publishing Company, pp. 385 (1979).

[13] Klueh, R.L., "Experience with Ferritic/Martensitic Steels for Fusion Application", *Proceedings of International Workshop on Spallation Materials*, 3.3-3.26 (1996).

[14] Prael, R.E., *et al*., *User Guide to LCS: The LAHET Code System*, LA-UR-89-3014, Los Alamos National Lab (1989).

DESIGN STUDY AROUND BEAM WINDOW OF ADS

Hiroyuki Oigawa, Kazufumi Tsujimoto, Kenji Kikuchi, Yuji Kurata, Toshinobu Sasa, Makoto Umeno, Kenji Nishihara, Shigeru Saito, Motoharu Mizumoto, Hideki Takano
Japan Atomic Energy Research Institute, Japan

Kimikazu Nakai, Azuma Iwata
Mitsubishi Heavy Industries, Ltd., Japan

Abstract

The Japan Atomic Energy Research Institute (JAERI) is conducting the research and development (R&D) on the accelerator-driven subcritical system (ADS) for the effective transmutation of minor actinides (MAs). The ADS proposed by JAERI is an 800 MWth, Pb-Bi cooled, tank-type subcritical reactor loaded with nitride fuel (MA+Pu). Pb-Bi is also used as the spallation target. In this study, the feasibility of the ADS was discussed by focusing on the design around the beam window. The partition wall was placed between the target region and the ductless-type fuel assemblies to keep the good cooling performance for the hot-spot fuel pin. The flow control nozzle was installed to cool the beam window effectively. The thermal-hydraulic analysis showed that the maximum temperature at the outer surface of the beam window could be repressed below 500 C even in the case of maximum beam power (30 MW). The stress caused by the external pressure and the temperature distribution of the beam window was below the allowable limit.

Introduction

To realise the effective transmutation of minor actinides (MA) by an accelerator-driven subcritical system (ADS), a high-power spallation target should be installed at the centre of the core. In the case of JAERI's reference ADS, the proton beam power of ~30 MW is necessary to keep the thermal power of the subcritical core at 800 MWth. Such a high-power spallation target is believed to be achievable only by a liquid heavy metal target such as lead-bismuth eutectic (LBE).

In the design study of ADSs worldwide, two types of spallation targets are proposed – a window type and a windowless type. JAERI has been conducting the design study of the ADS with the beam window, accounting for the difficulty in the stable control of the free surface of the LBE target by the windowless type. Nevertheless, various difficulties arose in the design of the beam window for the high-power spallation target: appropriate cooling, corrosion, structural stress, irradiation damage, etc. In this report, the present status of the design study around the beam window is presented and its feasibility is discussed.

Description of system specification

The subcritical reactor was an 800 MWth, LBE-cooled, tank-type reactor as shown in Figure 1, where LBE was also used as the spallation target. Two primary pumps and four steam generators were contained inside the reactor vessel.

The subcritical core is composed of MA nitride fuel, where plutonium is added at the initial loading of the first cycle to reduce the burn-up swing reactivity. In the reference core design, two-zone fuel loading is adopted to mitigate the high-power peaking factor [1]. The proton energy is set at 1.5 GeV, though it should be optimised in the future considering the trade-off between the cost of the accelerator for higher energy and the engineering difficulty for higher current.

Figure 1. Concept of 800 MWth, LBE-cooled, tank-type ADS

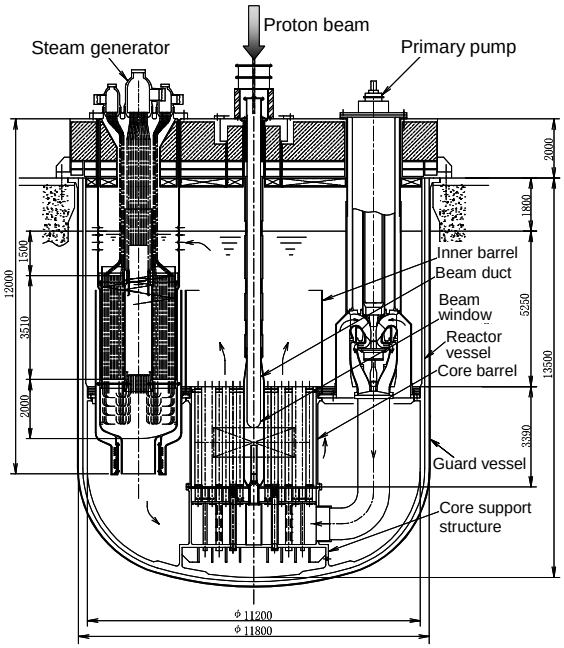

All the fuel in the core was simultaneously unloaded every 600 effective full-power days (EFPD). The unloaded fuel was reprocessed by the pyrochemical method (dry process) to remove the fission products. After the reprocessing, the new nitride fuel was refabricated by adding 250 kg of MA. Figure 2 shows an example of the change of the effective multiplication factor, k_{eff}, according to the fuel burn-up. The maximum value of k_{eff} was set at 0.97, considering reactivity insertion during accidental situations. The plutonium contents in the initial loading fuel were adjusted to 30% and 48% for inner and outer cores, respectively, so that the reactivity swing was minimised. Nevertheless, the minimum k_{eff} of ~0.94 was found at the EOC of the second cycle, which means that the burn-up swing reactivity was ~3% Dk. The proton beam current, which kept the thermal power at 800 MW, is shown in Figure 2 where the proton energy was fixed at 1.5 GeV. The maximum beam current of ~18 mA (i.e. 27 MW) was necessary at the minimum k_{eff}. During the equilibrium cycles, the beam current was adjusted from 8 to 12 mA (i.e. 12 to 18 MW).

Figure 2. Burn-up reactivity change and required beam current to keep thermal power

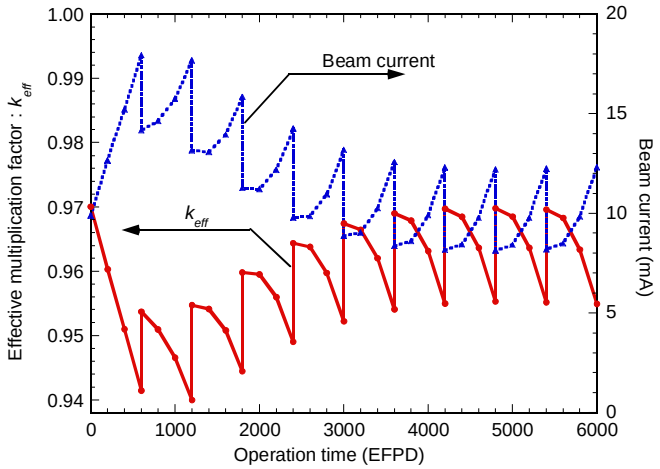

Considering the above-mentioned conditions, we will discuss the feasibility of accepting a 30 MW proton beam. It should be noted that we could reduce the maximum beam current if the temporary low-power operation is acceptable. For example, when we set the limit of the beam current at 15 mA (22.5 MW), the thermal power at the minimum k_{eff} would be ~670 MW, which does not seem so serious a deterioration of the system performance.

Preliminary design around beam window

In JAERI's reference design of the ADS, ductless-type fuel assemblies were adopted to reduce the core size, the amount of the waste and neutron capture reactions, and to enhance the cooling capability. In the design around the beam window and the core, LBE was distributed to the target region and the core region at the bottom of the core. In the preliminary design without any wall between the target region and the fuel region, the thermal-hydraulic analysis showed that the cross flow of LBE between these regions occurred as shown in Figure 3 (where the inlet flow speed for each fuel assembly and the target region was determined according to the power density of each region). The observed cross flow deteriorated the flow speed of LBE around the innermost fuel and hence the cooling performance of the hot-spot fuel pins was seriously affected. In addition, the temperature of the beam window became more than 700 C in the case of a sharply peaked proton beam with Gaussian distribution.

Figure 3. Hydraulic analysis for preliminary design without partition wall and inlet nozzle

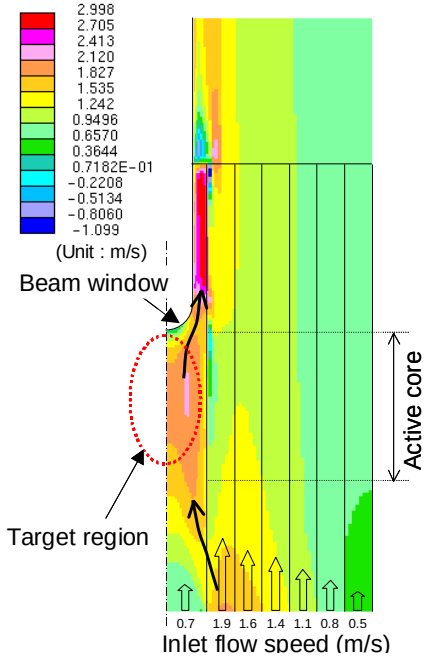

From this preliminary analysis, the following strategies were considered to find the solution: 1) a partition wall between the target region and the fuel region is necessary to keep the good cooling performance for the fuel pin, 2) the flow distribution among the fuel assemblies is not easy when the ductless-type configuration is adopted, 3) a flow control nozzle is necessary to cool the beam window effectively and 4) other parameters such as the coolant inlet temperature, beam duct diameter and the size of the target region should be optimised. The current design around the beam window derived from the above considerations is shown in the next section.

Modification of design around beam window

The inlet LBE temperature for both the target and the core coolant was reduced to 300 C, while 330 C was adopted in the former design. Although this reduction in temperature may have a negative effect on the power generation efficiency, it is still considered in the acceptable range. The diameter of the beam duct was also expanded from 40 cm to 45 cm to reduce the peak power of the proton beam, though this expansion of the target region deteriorates the neutron economy.

The flow speed of LBE in the core region was set at 2 m/s uniformly to avoid cross flow. But, the erosion and corrosion of fuel claddings by LBE at this flow speed should be examined experimentally. The flow speed of LBE in the flow control nozzle for the target inlet was also set at 2 m/s.

The resultant concept of the spallation target and the core regions is shown in Figure 4. The detail of the design around the beam window is shown in Figure 5. The minimum and maximum gap distances between the beam duct and the partition wall were 1.1 cm and 9.5 cm, respectively. The detailed description of the beam window shape is shown in Figure 6. The thickness of the beam window is 2.0 mm at the centre part and 4.0 mm at the waist part. These two parts should be smoothly connected so as to avoid stress concentration. The thickness of the beam duct is 10 mm.

Figure 4. Design concept of the spallation target and core regions

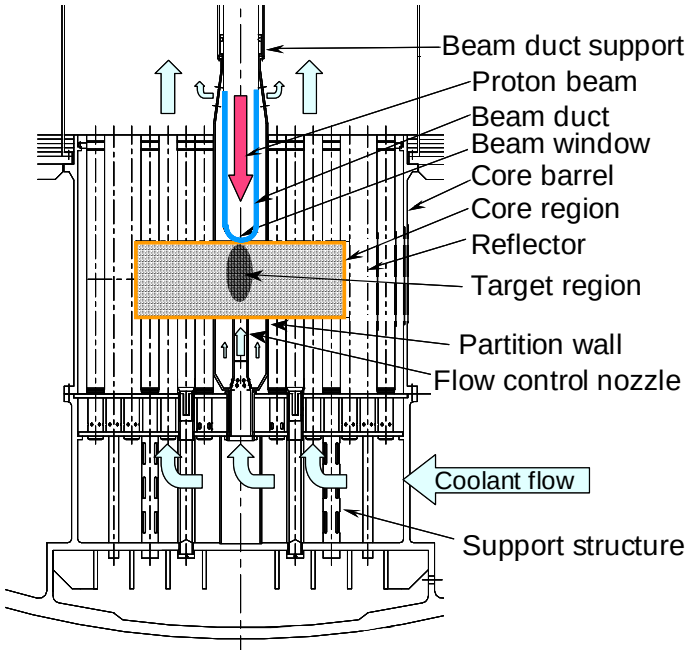

Figure 5. Current design around beam window

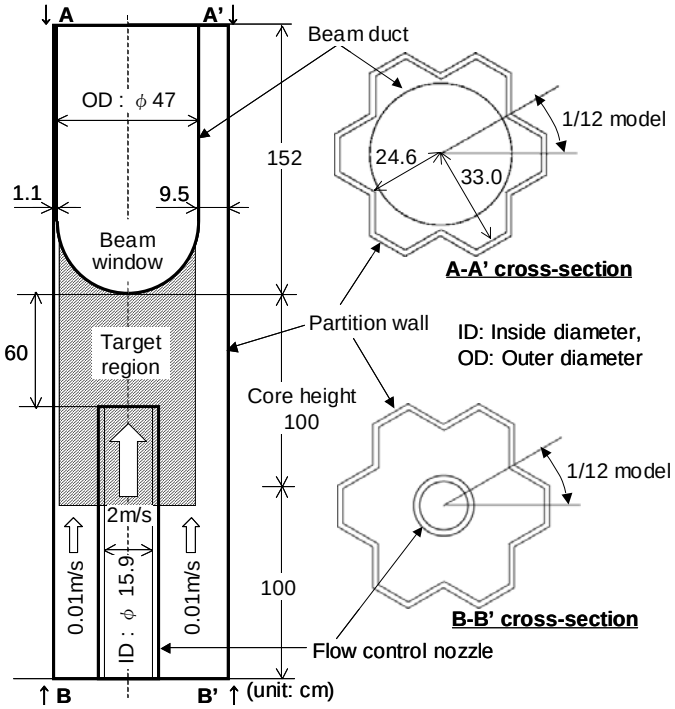

Figure 6. Detailed description of beam window design

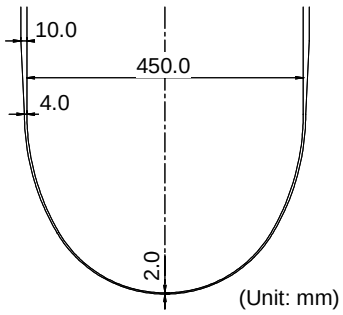

The selection of material to be used for the beam window may be one of the toughest issues in the design of the ADS because many factors should be taken into consideration: compatibility with LBE, irradiation effect, strength in high temperature, creep rapture strength, workability, etc. Two candidates were chosen in the meantime – HCM12A and F82H. Characteristics of these materials are summarised in Table 1. The material properties of HCM12A were used in the analysis described below.

Table 1. Characteristics of material chosen temporarily as candidates for beam window (at 550 C)

	HCM12A (Ferritic steel)	**F82H (Martensitic steel)**
Composition Fe/Cr/W (%)	86/12/2	90/8/2
Tensile strength (MPa)	397	408
Yield stress (MPa)	333	348
Young's modulus (MPa)	$16.6 \cdot 10^4$	$18.3 \cdot 10^4$
Poisson's ratio (–)	0.31	0.30
Thermal expansion coefficient (/K)	$13.4 \cdot 10^{-6}$	$12.2 \cdot 10^{-6}$
Heat conductivity (W/m/K)	29.5	32.2

Thermal-hydraulic analysis of target region

To validate the effect of the above-mentioned design modification, thermal-hydraulic analysis was carried out for the target region. The input beam was 1.5 GeV · 20 mA = 30 MW with Gaussian distribution. The deposited heat generation by the beam was calculated as 15.7 MW. The maximum beam density at the centre of the beam window was 30 mA/cm^2, which caused the heat deposit density of ~700 W/cm^3 in the structural material of the beam window.

Figure 7 shows the results of the hydraulic analysis while Figure 8 shows the temperature analysis. The flow control nozzle is beneficial for effective cooling of the beam window as shown in Figure 7. It should be noted that there will be a stagnant zone at the centre of the beam window when the axially symmetric design is adopted as the present design. Figure 8, however, shows the good cooling performance by such a symmetric design; the outer surface temperature at the centre of the beam window was ~450 C. The maximum temperature at the outer surface of the beam window was found at the peripheral region of the window, instead of at the centre, and its value was ~490 C. It is said that the corrosion of steel alloy by LBE becomes serious above 500 C, though this tendency largely depends on the composition and the surface conditions of the materials and the temperature, as well as on the flow speed and the oxygen concentration of LBE. The present design, therefore, can be regarded as feasible in terms of material corrosion.

Figure 7. Result of hydraulic analysis for beam window

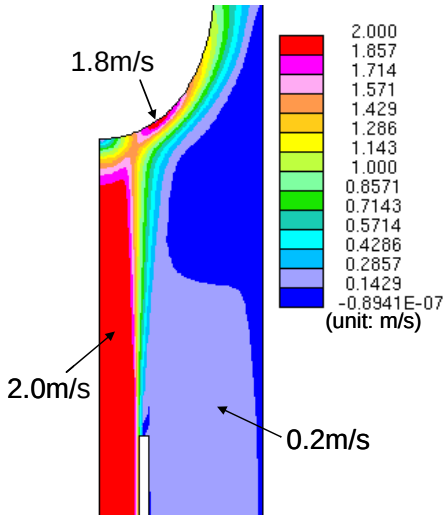

Figure 8. Result of temperature analysis for LBE target and beam window

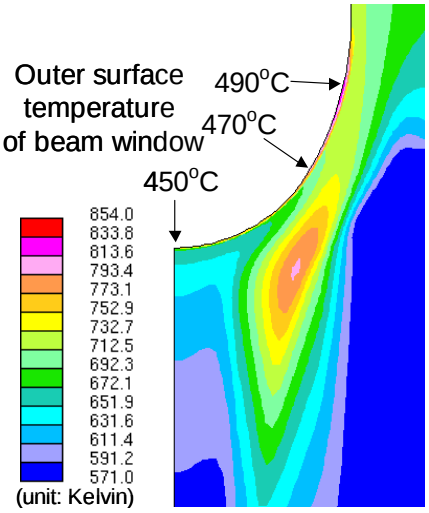

Structural analysis of beam window

The beam window was under stress by several forces such as: external pressure caused by the hydraulic head of LBE (~680 kPa), cover gas (~100 kPa) and kinetic force of LBE flow (~20 kPa), and thermal stress mainly caused by the temperature difference between the inner and outer surfaces of the beam window. Figure 9 shows the calculated temperature distributions at the inner and outer surfaces of the beam window and the coolant LBE. The maximum temperature difference between the inner and outer surfaces (~50 C) was found at the centre of the beam window. The thermal stress caused by this temperature difference was compressive stress at the inner surface and tensile stress at the outer surface. Since the external pressure caused the compressive stress on both surfaces, the total stress became larger on the inner surface. The resultant Mises stress distributes as shown in Figure 10. The maximum value (~106 MPa) was found at the centre of the beam window. This stress is well below 1/3 of tensile strength shown in Table 1 and therefore the beam window can be judged as feasible from the viewpoint of stress.

Figure 9. Position-dependent temperature of beam window and coolant LBE

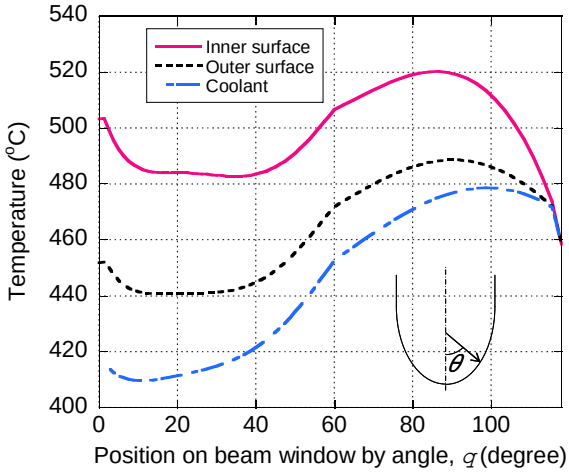

Figure 10. Position-dependent stress caused by temperature difference and external pressure

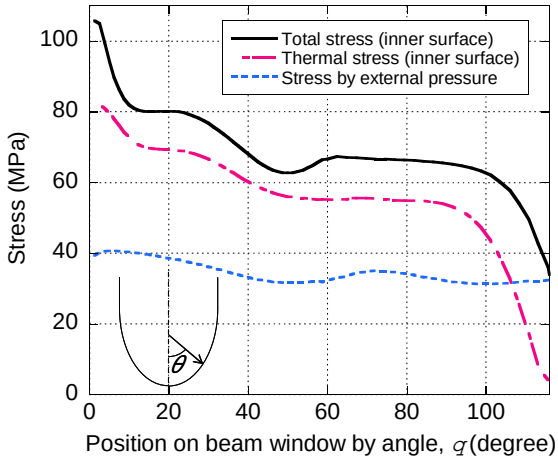

In addition to this analysis, compression buckling was also analysed. The results showed that compression buckling would result from external pressure of 3.8 MPa, which is more than four times the expected external pressure (0.8 MPa). As for creep, ~0.03% of creep strain was expected even for the 10 000 hours of 120 MPa stress at 520 C. These analyses show that the feasibility of the beam window can be established if the material properties are not seriously deteriorated by the irradiation damage caused by neutrons and protons.

Consideration of other factors

The beam window is heavily exposed by protons and neutrons. The irradiation damage of the beam window was calculated as ~72 DPA (displacement per atom) by neutrons and 6 DPA by protons for a 300-EFPD operation. The helium production was calculated as ~0.15 at.% for the same operation period. To validate the feasibility of the material, therefore, it is essential to accumulate the irradiation data for candidate materials. It should be noted that the combination of neutron irradiation in fast neutron reactors and proton irradiation in the spallation condition is necessary to understand the duplicated effect of heavy irradiation and helium accumulation. The beam window would be exchanged

every one or two years. The partition wall and flow control nozzle would also be exchanged periodically because they too suffer from heavy irradiation. Thus, further study in order to estimate the lifetime of the beam window is a necessary next step.

In the hydraulic analysis described in the previous section, it was assumed appropriate to set the flow rate of the target LBE at the given value. In the design of the whole system, however, how to distribute the flow rate for the core and target regions is one of the technical issues to be developed. A preliminary concept for the target region is shown in Figure 11. Orifices are placed to control the flow rate of the LBE. In the present design where the primary pumps are commonly used for both the core coolant and the target, it is not possible to adjust the flow rate of the target by the pump power (though the beam power should be changed to control the core thermal power during the operation). Experimental validation of the flow control mechanism is considered necessary because the LBE may erode the orifices and change its dimension during the operation.

In the present design concept, contamination of the primary circulation system by spallation products is a concern. This issue remains to be solved in a further study in connection with the development of the polonium management technique.

Figure 11. Concept of flow control mechanism for LBE target

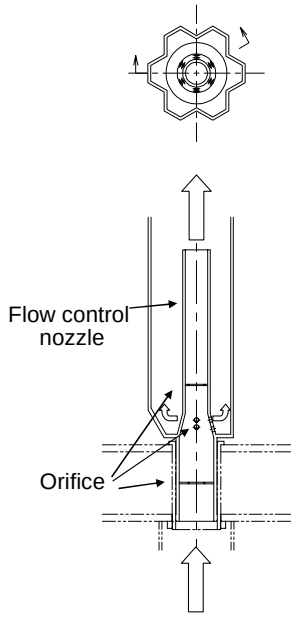

Conclusion

The present conceptual design of an 800 MWth ADS with LBE target/coolant was described and its feasibility was discussed by focusing on the design of the beam window. The partition wall was placed between the target region and the ductless-type fuel assemblies to keep the good cooling performance for the hot-spot fuel pin. A flow control nozzle was installed to effectively cool the beam window. The thermal-hydraulic analysis showed that the maximum temperature at the outer surface of the beam window would be lower than 500 C even in the case of maximum beam power of 30 MW. The stress caused by external pressure and temperature distribution of the beam window was calculated as 106 MPa, which was below 1/3 of the tensile strength of the material.

Further study, including experimental validation, is considered necessary for some technical issues such as: irradiation damage to the beam window, the flow control mechanism for the core and the target regions, and management of spallation products and polonium.

Acknowledgements

This work was funded by the Ministry of Education, Culture, Sports, Science and Technology (MEXT) as one of the R&D programmes for innovative nuclear systems.

REFERENCE

[1] Tsujimoto, K., *et al*., "Neutronics Design for Lead-bismuth Cooled Accelerator-driven System for Transmutation of Minor Actinide", *J. Nucl. Sci. Technol*., 41, 21 (2004).

PRIMARY ISOTOPIC YIELDS FOR MSDM CALCULATIONS OF SPALLATION REACTIONS ON ^{208}Pb WITH PROTON ENERGY OF 1 GeV

Sheng Fan[1,2,3], **Wenyun Luo**[2], **Fang Yan**[1], **Hongzhou Zhang**[1,4], **Zhixiang Zhao**[1]
[1]China Institute of Atomic Energy, Beijing, 102413 China
[2]Shanghai Applied Radiation Institute, Shanghai University, Shanghai, 201800 China
[3]Physics Department, Hunan City University, Yiyang, 413000 China
[4]Physics Department, Northwest University, Xi'an, 710006 China

Introduction

Spallation reactions have recently attracted considerable attention due to their importance in technical applications and fundamental physics. For example, they can act as intense neutron sources for accelerator-driven radiologically clean nuclear systems (ADS) [1,2] for energy generation and nuclear waste transmutation. In this system, lead constitutes an ideal spallation target since its neutron yield is high and it is very transparent to neutrons of energies below 1 MeV. Isotopic production data from proton-induced reactions with energies up to 5 GeV are of great importance for understanding the reaction mechanisms of intermediate nuclear reactions. Recently, precise and numerous measurements of elements produced from proton-induced spallation reactions with energy ranges from 10 MeV to 5 GeV using several target materials were carried out [3-5] due to the interest in a spallation neutron source and ADS. More than 15 000 experimental data points have been obtained. R. Michel [3-5], *et al*., systematically investigated the data in order to provide a database for model calculations while Yu. E. Titarenko [6] measured the yields of residual product for proton energies from 100 to 2 600 MeV to compare theoretical codes. The target elements were chosen according to their relevance in cosmo chemistry and cosmo physics applications in which the production of cosmogenic nuclides in extraterrestrial matter, the target elements with atomic numbers < 29 and a few high-Z, such as Rb, Sr, Y, Zr, Te, Ba, Nb, etc. are needed. Heavy elements such as Ta, W, Hg, Pb, Bi, Tu and U are under discussion as spallation target materials for spallation neutron source and ADS applications.

However, while these experiments showed the isotopic cross-section of heavy residuals, light residuals were not given. Heavy residual production cross-section relied on mass spectrometry [3-5] and radiochemical methods [7], which only give cumulative yields due to long-lived residuals resulting from short-lived beta decay of primary reaction products. Development of precise spallation reaction models suffered due to lack of primary experimental data. It is hard to systematically compare model calculations with available measured data to investigate the physical reasons for shortcomings of theoretical models. When T. Enqvist [8]/GSI used inverse kinematics by bombarding a liquid hydrogen target with relativistic heavy ions, cross-sections of produced primary residuals from manganese to lead were obtained.

Some theoretical codes (i.e. LAHET [9], quantum molecular dynamics (QMD) [10]) and the semi-empirical method (i.e. Silberberg's YIELDX [11]) can be used to study the isotopic product data from proton-induced spallation reactions with intermediate energies. However, general experience has shown that these models and codes do not satisfy the accuracy requirements of engineering needs for isotopic production [3,6]. S. FAN, one of the authors, introduced a fission model into QMD [12,13] to investigate the mass and charge distribution of residual nuclear fragments from proton-induced reactions with incident energies up to several GeV. The simulation results using QMD plus a fission model were in good agreement with the experimental data; however, the fission model in QMD is only a semi-empirical model. Recently, the cascade exciton model (CEM) was developed to investigate intermediate energy reactions with fission processes and shell corrections introduced into the model [14-18]. The CEM code includes an old cascade code by Toneev and Gudima [19], which models inelastic nucleon/pion nucleus collisions at energies from tens of MeV to 5 GeV, and an exciton/evaporation model, which models the stage following the cascade.

In the present work, the many stage dynamical model (MSDM) [19-21] developed by Russian scientists was adapted to investigate the primary isotopic product cross-section of proton-induced spallation on ^{208}Pb with the energy of 1 GeV. The simple Fermi-gas level density was replaced by the Ignatyuk formula in MSDM to improve the simulations.

MSDM code

The MSDM [19-21] code has been under development since the 1970s by Russian scientists to study intermediate energy nuclear reactions based on well-known Russia nuclear models (e.g. Dubna cascade model, cascade exciton model). MSDM was extended to calculate hadron-induced spallation.

MSDM simulated in an exclusive approach both hadron-nucleus and nucleus-nucleus interactions at energies up to 1 TeV. MSDM was modelled as a three-step process. The first step (the intra-nuclear cascade stage of the reaction below 600 MeV) was treated according to the Dubna cascade model. In this step, the nucleon-nucleon collisions inside the nucleus induced the loss of a few nucleons and led to the formation of an excited pre-fragment. Above 10 GeV, the independent quark-gluon string model (QGSM) [22] was used. In the intermediate area (600 MeV to 10 GeV), an extension QGSM was adopted. A self-consisted description of the cascade stage was provided over a whole energy range of primary hadrons up to 1 TeV. Evolution of the excited residual nucleus to an equilibrium state was described in terms of the pre-equilibrium model based on a Monte Carlo solution of the corresponding master equation (this is the second stage). In the third step of the process, the excited nucleus was de-excited by evaporation of light particles or by fission. Equilibrium de-excitation of the residual nucleus included several mechanisms. For light nuclei (A < 16), the modified Fermi break-up model [23] was used. Medium and heavy nuclei at moderate excitations (E < 2 MeV/nucleon) underwent evaporation, including fission competition for heavy nuclei. Highly excited nuclei (E > 2 MeV/nucleon) could decay into several excited fragments according to the statistical model of multi-fragmentation with consequent particle emission. The equilibrium de-excitation stage completed the run of the MSDM generator.

In the MSDM code, the level density adopted the simple Fermi-gas formula [20]:

$$\rho\left(E^*\right) \sim \exp 2\sqrt{aE^*}$$

with the level density parameter a = (0.1 to 0.14) AMeV^{-1}.

To take into account shell effects on level densities and their decrease with increasing excitation energy, the Ignatyuk formula [24] of the level density parameters was adopted:

$$a\left(Z,N,E^*\right) = \bar{a}(A)\left\{1 + \delta W_{gs}\left(Z,N\right)\frac{f\left(E^* - \Delta\right)}{E^* - \Delta}\right.$$

$$f(E^*) = 1 - \exp\left(-\gamma E^*\right)$$

where $\bar{a}\,(A) = \gamma_1 A + \gamma_2 A^{2/3}$ B_s is the asymptotic Fermi-gas values of the level density parameter at high excitation energies, B_s is the parameter about the surface area of the deformed nucleus. As an approximation, B_s is related to the excitation energy of nuclei in the surface area and can be written as:

$$B_s \propto \frac{E^*}{A} \times A^{2/3} = E^* \times A^{-1/3}$$

and where the parameters γ_1, γ_2 and γ can be taken as $\gamma_1 = 0.072$, $\gamma_2 = 0.257$ and $\gamma = 0.052$ MeV^{-1}.

Figure 1. Comparisons of the MSDM simulations with the Fermi-gas level density (dot lines) and Ignatyuk formula (solid lines)

The formation cross-sections of the mass and charge distribution; the fission and spallation products of the residuals are shown at the p + ^{208}Pb reaction with proton energy of 1 GeV. The squares and dots denote the experimental data by T. Enqvist of GSI [8].

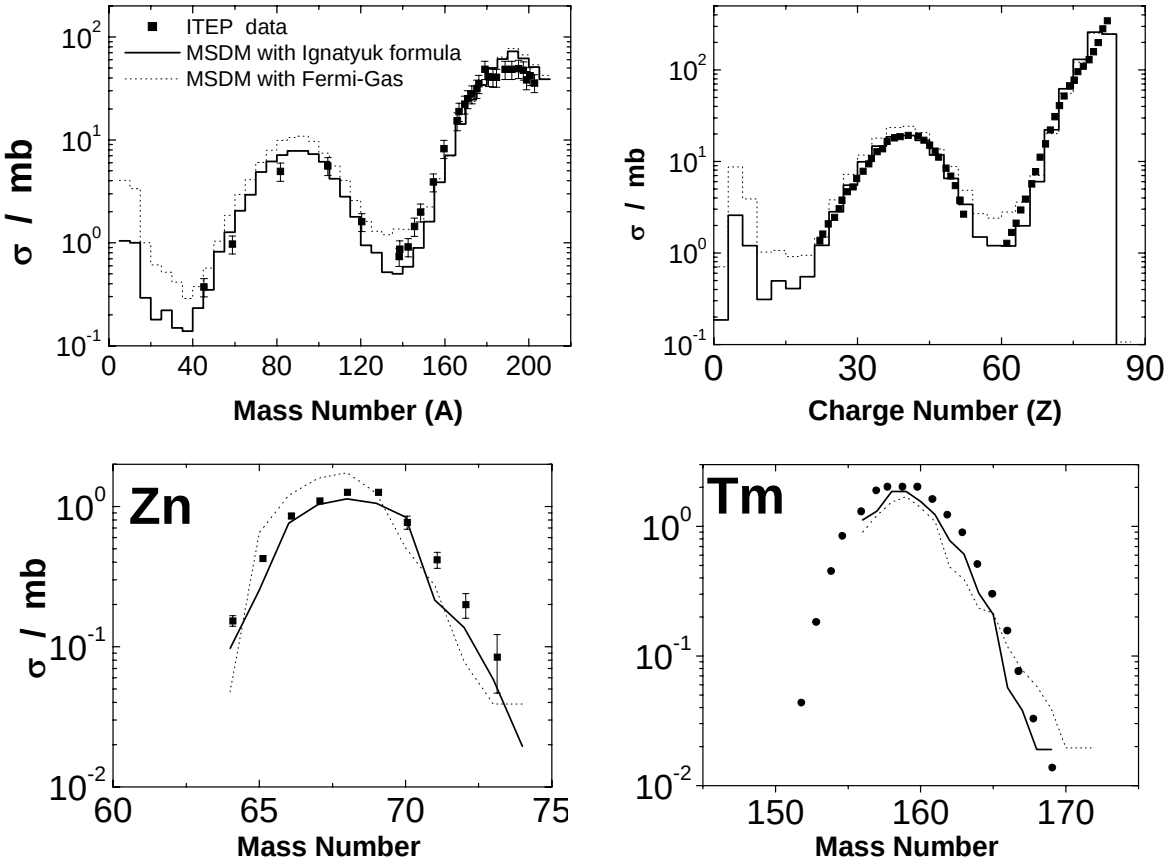

Calculation results

Figure 1 shows the calculation results by using the MSDM code with the Fermi-gas level density (dot lines) and Ignatyuk formula (solid lines) for the formation cross-section of the mass and charge distributions at fission (Zn – Figure 1) and spallation (Tm – Figure 1) products. The dots represent experimental data [8] of a proton-induced reaction on ^{208}Pb with energy of 1 GeV. The simulations of MSDM with Fermi-gas level density were: 50% larger than the experimental data at the fission peak, lower at the spallation part and two times larger at the regions of $50 \le Z \le 70$ and $120 \le A \le 160$. The same conditions were seen in the isotopic production cross-sections of the fission (Zn) and spallation (Tm) products. It is clear that simulations by MSDM with Ignatyuk formula level density were in good agreement with experimental data, more so than by MSDM code with Fermi-gas level density.

Figure 2 gives the formation cross-section of residue charge and mass distribution for ^{208}Pb with proton energy of 1 GeV. Good agreement was achieved for both charge and mass spectra for MSDM simulations with experimental data [6,8]. Two components can be found in Fig. 2: a fragmentation peak (collecting the heavy residuals left after evaporation of remnant products close to targets, Z~80 and A~200) and a broad fission peak (centred around Z~40 and A~100, half the target mass number). The

MSDM calculations showed a left peak around A~4 since the MSDM simulations included light particles (such as p, d, t, ^{3}He, ^{4}He emission), which were not present in the measured data. Calculations performed using the INCL4+KHSv3p model, the LAHET code (v2.7) and YIELDX (Silberberg's semi-empirical method) are shown together with the present work in Figure 2. Fission fragments of the residual products simulated by LAHET are much lower than the experimental data in fission distribution and are in good agreement with the fragmentation peak. YIELDX results show large deviation from experimental data.

Figure 2. Residual charge (left) and mass (right) production cross-sections for ^{208}Pb with incident proton energy of 1 GeV

The squares represent experimental data by Yu. E Titarenko at ITEP [6], the dash line denotes the GSI experimental data [8]. The predictions of the INCL4+KHSv3p model [25] for charge distribution are given by the dot/dash line, the simulations of the LAHET and YIELDX codes are shown by the open circles and dot lines, respectively. The vertical step lines show the simulations of the MSDM code with the Ignatyuk formula.

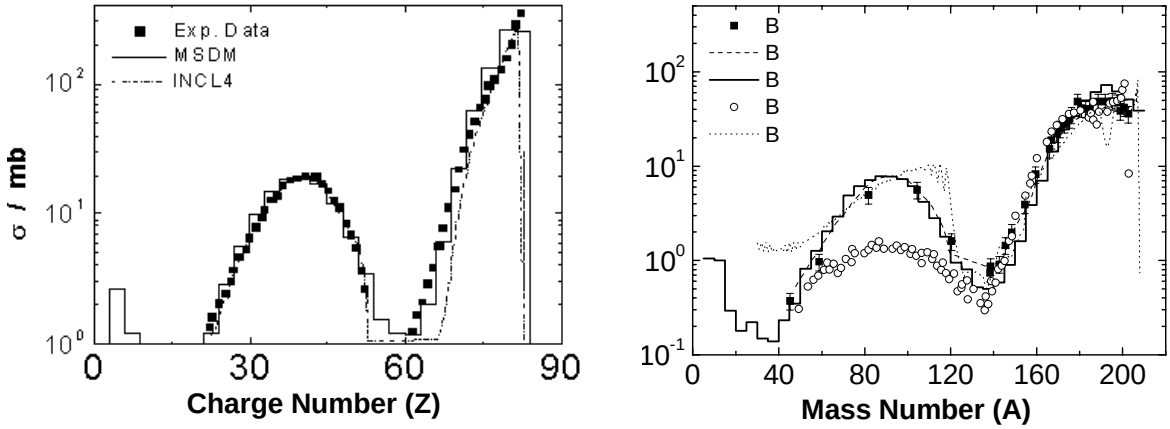

Summary

In the present work, the Ignatyuk formula of the level density was adopted to replace the Fermi-gas level density in the MSDM code in order to take into account the shell effects on level densities and their decrease with increasing excitation energy. With this change, the calculation results of MSDM (for the formation cross-section of charge and mass distribution of proton-induced spallation reactions on ^{208}Pb with an energy of 1 GeV) were in good agreement with the experimental data.

Acknowledgements

S. Fan, one of the authors, would like to thank Professor S. N. Wang for her input. This work was supported by the National Natural Science Foundation of China under contract No. 10305021. Furthermore, the work was supported by the National Key Item of Foundation Research and Development Project of China under contract G1999022600.

REFERENCES

[1] Bowman, C.D., E.D. Arthur, *et al*., *Nucl. Instr. Meth*., A320, 336 (1992).

[2] Rubbia, C., J.A. Rubio, *et al*., CERN/AT/95-45(ET), CERN (1995).

[3] Michel, R., R. Bodemann, *et al*., *Nucl. Instr. Meth*., B129, 153 (1997).

[4] Gloris, M., R. Michel, *et al*., *Nucl. Instr. Meth*., A463, 593 (2001).

[5] Gloris, M., R. Michel, *et al*., *Nucl. Instr. Meth*., B113, 429 (1996).

[6] Titarenko, Yu.E., V.F. Batyaev, *et al*., INDC(CCP)-434, Vienna (2002).

[7] Suemmerer, K., W. Bruechle, *et al*., *Phys. Rev*., C42, 2546 (1990).

[8] Enqvist, T., W. Wlazlo, *et al*., *Nucl. Phys*., A686, 481~524 (2001).

[9] Prael, R.E., H. Lichtenstein, LANL Report No. LA-UR-89-3014, Los Alamos (1989).

[10] http://www-xdiv.lanl.gov/XTM/LSC/lahet-doc.html.

[11] Aichelin, J., G. Peilert, *et al*., *Phys. Rev*., C37, 2451 (1988).

[12] Silberberg, R., C.H. Tsao, *Phys. Reports*, 191, No. 6, 351~408 (1990).

[13] Fan, S., Z. Li, *et al*., *Nucl. Sci. and Eng*., 137, 89 (2001).

[14] Sheng, F., Zhuxia, L., *et al*., *Eur. Phys. J*., A4, 61 (1999).

[15] Mashnik, S., *et al*., *J. of Nucl. Sci. and Tech*., Supplement 2, 785~788 (2002).

[16] Mashnik, S., *et al*., *J of Nucl. Sci. and Tech*., Supplement 2, 720~725 (2002).

[17] Sierk, A., *et al*., LANL Report LA-UR-98-5998 (1998).

[18] Peterson, R.J., *et al*., *Eur. Phys. J*., A10, 69-71 (2001).

[19] Prokofiev, A.V., *et al*., *Nucl. Sci. and Eng*., 131, 78-95 (1999).

[20] Gudima, K.K., S.G. Mashnik, *et al*., *Nucl. Phys*., A401, 329 (1983).

[21] Botvina, A.S., A.S. Iljinov, *et al*., *Nucl. Phys*., A475, 663~686 (1987).

[22] Dementyev, A., V. Gurentsov, *et al*., *Nucl. Phys*., B (Proc. Suppl.) 70, 486 (1999).

[23] Toneev, D., N.S. Amelin, K.K. Gudima, *The Independent Quark-gluon String Model for Heavy Ion Collisions at Ultrarelativistic Energies,* Preprint GSI-89-52, Darmstadt, 1989; Yadern Fizika, 51, 1730 (1990).

[24] Fermi, E., *Prog. Theor. Phys*., 5 1570 (1950).

[25] Ignatyuk, A.V., G.N. Smirenkin, *et al*., Yad. Fiz., 21, 1185 (1975).

[26] Boudard, A., J. Cugnon, *et al*., *Phys. Rev*., C66, 044615 (2002).

CFD ANALYSIS ON THE ACTIVE PART OF WINDOW TARGET UNIT FOR LBE-COOLED XADS

Nam-il Tak, Hans-Joachim Neitzel, Xu Cheng
Forschungszentrum Karlsruhe
E-mail: Namil.Tak@iket.fzk.de

Abstract

The window target unit for an LBE-cooled primary core is one of the basic options considered in the framework of the preliminary design study of an experimental accelerator-driven system (PDS-XADS). In the present work, a numerical design study using the computational fluid dynamics (CFD) code CFX 5.6 was performed for the active part of this option with special attention to the coolability of the window. Steady-state as well as beam trip behaviours under normal operating conditions were investigated with the advanced turbulence model combined with the advanced wall treatment available in the new CFX 5 version. Based on the results of CFX 5.6 calculations, the window thickness was reduced to 2 mm in the centre from the initial proposal of 3 mm in order to satisfy the thermal design limit. The maximum temperature change rate of the window under beam trips is predicted to be as high as 412 C/s at 0.1 s after the beam interrupt. It is clear that beam trips with a beam interrupt duration less than 1 s could also be crucial to the integrity of the window.

Introduction

Transmutation of long-lived radionuclides using an accelerator-driven system (ADS) is a promising solution for reducing the long-term radiotoxicity of nuclear wastes. The practicability of ADS on an industrial scale requires the operation of a small-scale experimental ADS. One of the key milestones in the European ADS roadmap [1] is the design and construction of the European experimental ADS (XADS). At the present stage, European research institutions including Forschungszentrum Karlsruhe (FZK), industrial partners and universities are working together on the PDS-XADS project. The main objectives of the PDS-XADS project are to select the most promising technical options, to address the critical points of the entire ADS system (i.e. accelerator, spallation target unit and subcritical core), to identify further research and development (R&D) needs, to define safety and licensing issues, to preliminarily assess the cost of the installation and to consolidate the roadmap of the development of a European XADS. In addition, the studies will allow for the maintenance of a high level of nuclear technology expertise in Europe.

Three different reactor core concepts were taken into consideration, i.e. a small core (~20-40 MW) cooled by lead-bismuth eutectic (LBE), a large (~80 MW) LBE-cooled concept and a large (~80 MW) gas-cooled concept. Regarding the large core concepts, three different designs (mainly) of a spallation target were investigated [2]. These were the window target in the LBE-cooled core, the window target in the gas-cooled core and the windowless target in the LBE-cooled core. There were some advantages and disadvantages in the window target compared to the windowless one. Due to very high-energy protons and neutrons, the high irradiation damage rate of the window material was quite a critical issue vis-à-vis the window target.

From a thermal-hydraulic point of view, however, the main issue of the window target was the cooling capability of the window. The window is a thin physical barrier that separates the vacuum from the LBE, and high thermal loads as well as irradiation loads exist due to spallation reactions. Therefore, special attention must be paid to cool down the window for the thermal-hydraulic design of the window target.

This paper presents numerical studies using CFD technology and the main results achieved on the lower part of the window target in the LBE-cooled XADS. The CFX 5.6 code [3] was used, which provided the possibility to use various advanced turbulence models combined with an advanced wall treatment [e.g. the shear stress transport (SST) turbulence model with automatic wall treatment]. Selection of an appropriate turbulence model for the prediction of window temperature was very important because flow stagnation occurs just below the window centre where the largest thermal load exists. It was reported in the validation study by Vieser, *et al.* [4], that the SST turbulence model performs better than the k-ϵ and the k-ω turbulence models on the prediction of stagnation heat transfer. The automatic wall treatment is useful from a practical perspective since it allows for the use of coarser meshes near walls than with typical low Reynolds number treatments.

Physical model

The target unit in the centre of the XADS core was composed of an evacuated central beam tube inside the target shell, which acted as a physical boundary between the spallation material (LBE) and the reactor coolant. The proton beam entered the beam tube at the upper end, penetrated the beam window and impinged on the upward flowing LBE. This produced a large heat deposition in the LBE as well as in the window. With 600 MeV of beam energy, ~70-80% of the beam energy was deposited as heat in the lower part of the target (the so-called active part). The deposited heat was removed in a heat exchanger at the upper end inside the target unit and LBE flow was driven by buoyancy force

without pumps. Therefore, sufficient height and small pressure loss were required to guarantee efficient, natural circulation. The total height of the target unit was 7.8 m. But, the present work focused on the lower part of the target unit (shown in Figure 1) for a detailed CFD analysis. The 5-mm thick guide tube was placed to separate the downward cold LBE and the upward hot LBE. The lower end of the guide tube is referred to as the funnel. A careful design of the funnel was important because it affects the natural circulation flow in the target and the injection flow to the window. In the initial stage of target design the thickness of the window was chosen as 3 mm. One of the challenging issues of the window target is the selection of the window material. The reference material for the present work was T91.

Figure 1. Geometry of the lower part of the XADS target

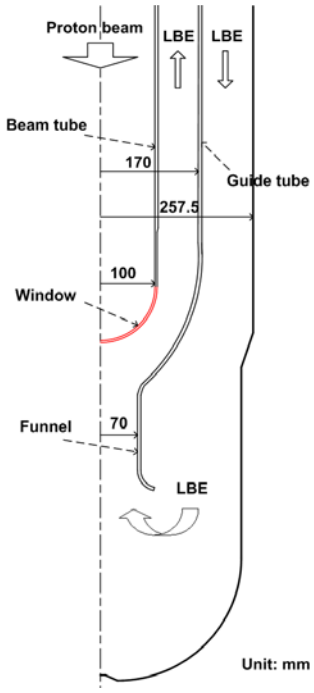

Spallation heat

The current density of the proton beam with a radius of 8 cm follows an elliptical radial distribution, which can be written as:

$$F(r) = \frac{3I_0}{2\pi r_0^2}\left[1 - \left(\frac{r}{r_0}\right)^2\right]^{1/2} \quad (1)$$

where I_0 is the total proton beam current, r_0 is the radius of the beam and r is the radial distance from the axis of the beam. The heat deposition profile in the target unit was evaluated by neutronic analysis using the MCNPX 2.4.0 code and the results [5,6] were used as the heat source in the CFD analysis. Fine meshes were adopted near the window to satisfy the CFD requirements on the MCNPX calculation. Figure 2 shows a typical heat deposition in the target unit. The maximum heat deposition density, 0.15 kW/cm^3/mA, was located ~2 cm below the window centre. In the window, the maximum heat deposition density reached 0.14 kW/cm^3/mA on the centre of its outer surface where flow stagnation was expected. The influence of the reactor core on the heat deposition near the window was found to be negligibly small.

Figure 2. Typical heat deposition in the XADS target (kW/cm^3/mA) [5]

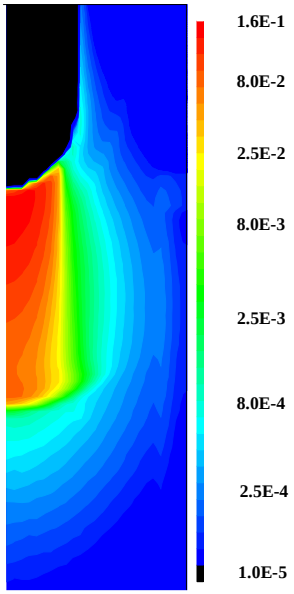

The magnitude of the beam current is increased with fuel burn-up. In the present work, the maximum beam current (6 mA) from the XADS accelerator was considered as the reference value. With a beam current of 6 mA, total heat deposition in the target and the window were 2.8 MW and 39 kW, respectively.

Numerical approach

For the present CFD analysis, the lower part of the target (i.e. from the bottom to an elevation of 1 m above the window) was considered (see Figure 1). An axi-symmetrical 2-D computational domain was chosen due to symmetric conditions. The geometry for the computation was generated by revolving a 2-D surface three degrees; hexahedral grids were made. In symmetric axes, prisms were placed. The total number of grids including prisms was 119 012. The SST turbulence model with automatic wall treatment was selected and fine meshes were applied to regions close to walls, particularly around the window. Figure 3 shows the y+ distribution along the outer surface of the window for the reference meshes. The grid sensitivity study confirmed that the grid size used for the present calculations was appropriately fine. The second order advection scheme was adopted and the second order backward Euler scheme, which is an implicit timestepping scheme with second order accuracy, was applied for transient simulations.

Since the target is cooled by natural circulation, thermal-hydraulic conditions of incoming flow to the computational domain must be calculated in advance. The results of the one-dimensional code HERETA [7] developed by FZK were used for these conditions. In addition, the wall temperature of the outer target shell determined by HERETA was applied for the thermal boundary conditions for the reactor core. With the reference design parameters under steady-states conditions, the LBE flow rate and the inlet LBE temperature were calculated as 192 kg/s and 233 C, respectively. The predicted wall temperature of the outer target shell was in the range of ~256-275 C.

Figure 3. Y+ plot along the outer surface of the window

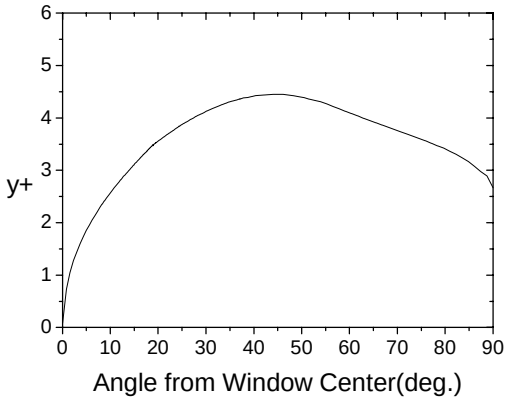

Results and discussions

Steady-state results

Results of initial design

CFX 5.6 calculations were performed for the initial design with a 3-mm thick window. Figure 4 shows the predicted velocity contour in the lower part of the target. As expected, flow stagnation near the centre of the window can be seen clearly in this figure. Flow separation occurred both in the downcomer and in the riser. In the downcomer, flow separation started earlier than expected. Additional CFX 5.6 calculations neglecting the buoyancy effect showed that this earlier separation resulted from the buoyancy effect. The predicted maximum LBE velocity was 1.282 m/s, which is considerably below the design limit of 2 m/s.

Figure 4. Velocity contour of initial design

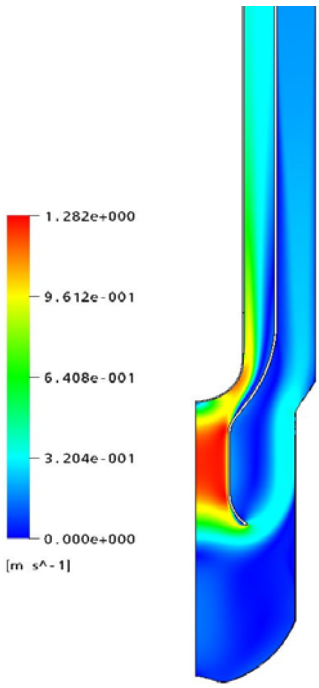

The corresponding window temperature is provided in Figure 5. The maximum window temperature occurred in the centre of the window and was as high as 596 C. The maximum temperature drop across the window thickness was 123 C. The maximum temperature of the guide tube was 450 C, which was much lower than that of the window. However, it should be noted that this value exactly corresponds to the thermal design limit of the guide tube specified in the technical specifications [8]. Since the predicted maximum window temperature exceeded the design limit (525 C), modification of the initial design was necessary.

Figure 5. Window temperature of initial design

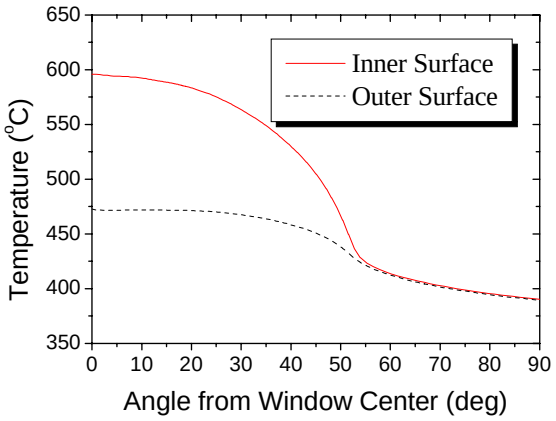

Results of modified design

One of the proposals for the modification of the initial design was to reduce the window thickness. Figure 6 shows the CFX 5.6 results with a reduced window thickness. The definition of d is shown in Figure 7. The window thickness was gradually reduced in the direction to the window centre without changing the thickness of the cylindrical part of the beam tube. By reducing the window thickness to 2 mm in the centre, the maximum window temperature was reduced by 86 C and kept below the design limit. The preliminary structural analysis [9] confirmed that the maximum stress for this modified window design was in the allowable range. Therefore, all the remaining calculations in this paper were made based on the modified window design with 2 mm thickness in the centre.

Figure 6. Effect of window thickness on maximum window temperature

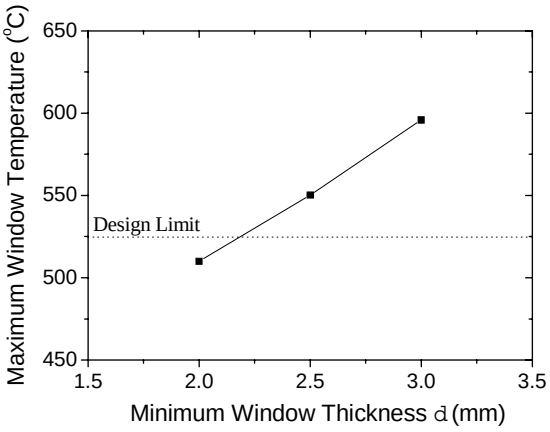

Figure 7. Definition of d for window thickness variation

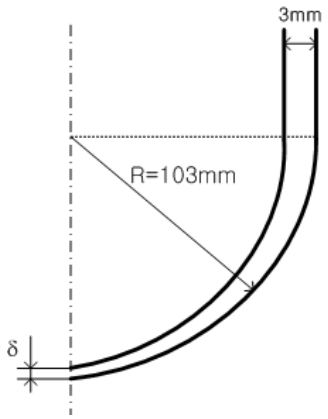

Effects of funnel size

A series of HERETA calculations showed that the size of the funnel is the most important design parameter affecting the natural circulation flow around the target. As shown in Figure 8, when the funnel is wider, the LBE flow rate is increased due to the small flow resistance while the injection speed to the window is decreased due to the increase of flow area. Both effects contribute oppositely to the window cooling. Therefore, detailed simulations are necessary to get an optimum size of the funnel. Figure 8 shows the results of the CFX 5.6 calculations for three different funnel sizes. When the funnel size was reduced by 20 mm from the reference funnel size (140 mm), the maximum window temperature was reduced by 7 C. However, the temperature of the guide tube increased dramatically because heat generation rate in the guide tube was larger than that of the original design. Furthermore, it was deduced from a sensitivity study that a reduction in the guide tube thickness cannot reduce the maximum guide tube temperature down to the design limit. When the funnel size was increased by 20 mm, the maximum window temperature was increased by 21 C (beyond the design limit). Based on the above results, the reference funnel size was therefore considered as the optimum value.

Figure 8. Effects of funnel size on mass flow rate and average LBE speed in funnel

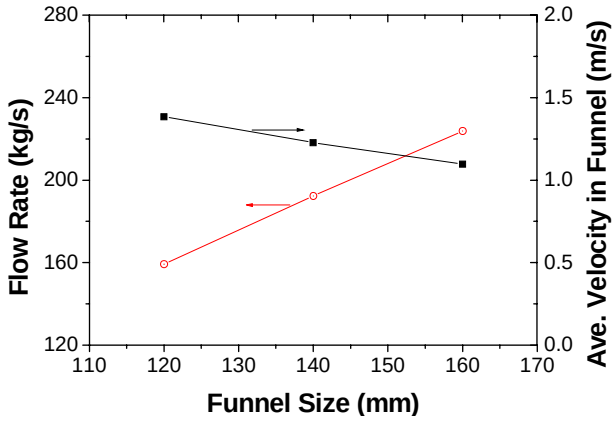

Figure 9. Effects of funnel size on maximum temperatures of the window and the guide tube

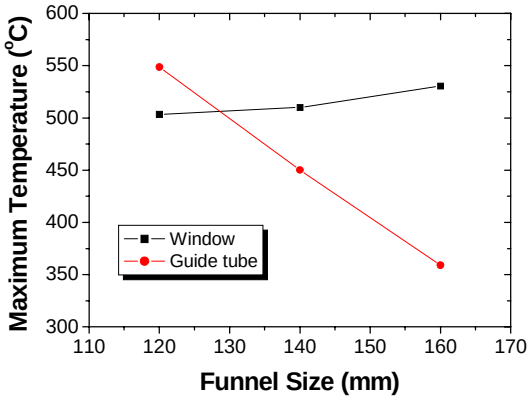

Effects of burn-up

During the XADS operation, the beam current is increased with the burn-up to compensate the subcriticality of the reactor core. Temperature profiles vary accordingly with the beam current. The preliminary neutronic calculation in Ref. 6 shows that the beam current is varied from 2.47 mA at BOC (k_{eff} » 0.97) to 5.1 mA at EOC (k_{eff} » 0.94). The results of CFX 5.6 calculations performed for both BOC and EOC conditions with corresponding beam currents are shown in Figure 10. It can be seen that the maximum window temperature was far below the design limit during the entire fuel cycle (~3 years).

Figure 10. Temperature profile of the inner surface of the window in BOC and EOC conditions

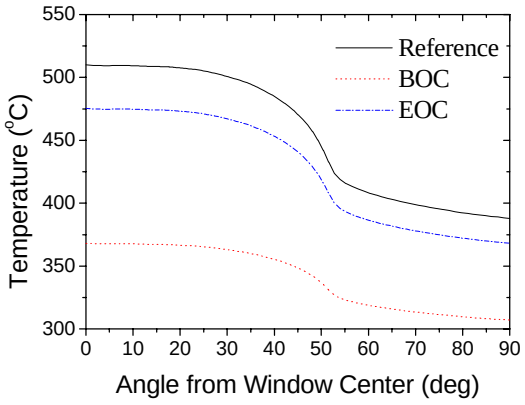

Beam trips

Experience with existing accelerators has shown that beam trips occur very frequently. Moreover, beam trip is an important design criterion since a frequent beam trip produces thermal cycle and leads to additional loads to the window. In the technical specifications of the accelerator of XADS [10], the frequency of beam trips with a time duration longer than one second must be kept below five times per year. No special requirements are defined for the beam trips with a beam interrupt duration shorter than one second. In the present work, beam trips with interrupt durations of 0.1, 0.3, 0.5 and 1 second were analysed. In the case of beam trips with a longer interrupt duration, reactor shutdown was expected.

The HERETA calculations showed that the mass flow rate of LBE and the inlet LBE temperature are hardly changed under short beam trips. In the case of a 1 s beam trip, the change of the mass flow rate of LBE is less than 2% and the change of the exit LBE temperature from the heat exchanger is less than 1 C. Figure 11 shows the predicted temperatures at the central points of both window surfaces under various beam trip conditions. For better understanding, the case of beam shut off was also simulated and presented in Figure 11.

Figure 11. Temperature behaviours of the window under beam trips

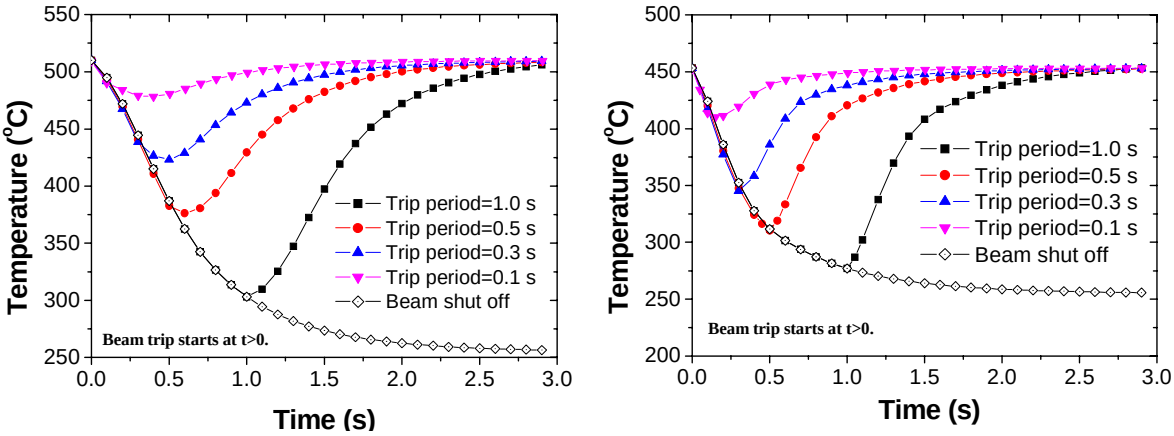

(a) Centre of inner surface (b) Centre of outer surface

In Figure 11, the beam interrupt starts at time point 0 s, and the beam power recovers after corresponding trip periods (i.e. beam interrupt durations). Temperature drop and temperature recovery in the window can be clearly seen in Figure 11. As expected, beam trips with a smaller trip period resulted in a smaller temperature drop. The window underwent a temperature drop up to 207 C for the trip period of 1 s, whereas the maximum temperature drop was 32 C for the trip period 0.1 s. Figure 11 also shows that the steepest slope is located between 0 and 0.5 s after the beam interrupt, regardless of the investigated trip periods. Thus, additional CFX 5.6 calculations were performed with a much finer timestep for the first 0.5 s after the beam interrupt to evaluate more accurately the maximum temperature change rate. Results are presented in Figure 12. The predicted maximum temperature change rate, which was as high as 412 C/s at the centre of the outer surface of the window,

Figure 12. Temperature change rate of the window after beam interrupt

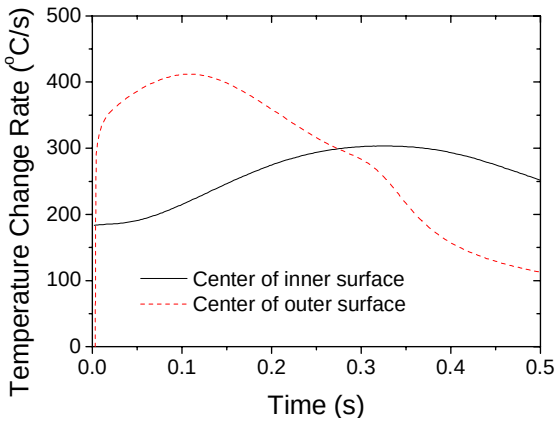

occurred ~0.1 s after the beam interrupt. It was clear that beam trips with a trip period shorter than 1 s could also be crucial events affecting the integrity of the window, although no attention was paid to these trips in the technical specifications of the XADS accelerator. Moreover, expectations indicated that beam trips with a trip period shorter than 0.1 s do not have enough time to reach the maximum temperature change rate of 412 C/s. It was concluded that related to both maximum temperature drop and temperature change rate, beam trips with a trip period shorter than 0.1 s are less critical than those with a trip period longer than 0.1 s, and thus were not further analysed in this paper. Furthermore, it was shown that the numerical timestep for the CFX simulation must be much smaller than 0.1 s to accurately capture the temperature change rate.

Conclusions

Among the proposed spallation target designs in the PDS-XADS project, the window target unit for the LBE-cooled primary core is one of the basic options for XADS. In the present work, steady-state as well as beam trip behaviours under normal operating conditions were investigated using the CFX 5.6 code for the active part of this target, focusing on the cooling capability of the window. Based on the results of the CFX 5.6 calculations, the following conclusions are made:

- The predicted maximum LBE velocity in the active part of the target is 1.282 m/s, which is considerably below the design limit. Stagnant flow exists near the centre of the window where the largest thermal load occurs.

- The maximum temperature of the initially proposed 3-mm thick window exceeds the design limit by 71 C. Therefore, design modification is necessary.

- By a reduction in window thickness to 2 mm in the centre, the maximum window temperature can be kept below the design limit.

- The reference funnel size (140 mm) is proven as an optimum value in terms of the cooling capability of the window and the guide tube.

- During the entire fuel cycle (~3 years) the maximum window temperature for the modified design (2-mm thick window in the centre) is far below the design limit.

- The temperature drop under the beam trip with 1 s trip period is predicted up to 207 C. The beam trips with smaller trip periods result in smaller temperature drops.

- For all beam trip conditions analysed, the predicted maximum temperature change rate is as high as 412 C/s, which occurs about 0.1 s after the beam interrupt.

- Beam trips with a trip period less than 1 s could also be crucial events affecting the integrity of the window, and, therefore, need to be considered in the design of the XADS accelerator.

Nowadays, due to the fast development of computer hardware as well as software, more and more applications of CFD codes to nuclear engineering and designs are envisaged. Although a CFD code is believed to be the best tool for the design and analysis of spallation targets, it should be noted that the validation of CFD codes is still not complete, particularly in areas such as turbulent heat transfer in liquid metals.

Acknowledgements

This work has been carried out in the framework of the PDS-XADS project partially financed by the 5th Framework Programme of the European Commission (contract number FIKW-CT2001-00179).

REFERENCES

[1] *A European Roadmap for Developing Accelerator-driven Systems (ADS) for Nuclear Waste Incineration*, Report of the European Technical Working Group on ADS, April 2001.

[2] Coors, D., *et al*., "Target Units for XADS Primary System", *EURADWASTE 04*, Luxembourg, 29-31 March 2004.

[3] *CFX 5.6 Manuals*, ANSYS Incorporated (2003).

[4] Vieser, W., *et al*., *Heat Transfer Predictions using Advanced Two Equation Turbulence Models*, CFX Technical Memorandum, CFX-VAL10/0602 (2002).

[5] Travleev, A., C.H.M. Broeders, Private Communication, September (2003).

[6] Batta, A., *et al*., "Window Target Unit for the XADS Lead-bismuth Cooled Primary System", *Proceedings of the International Workshop on P&T and ADS Development 2003*, Belgium, 6-8 October 2003.

[7] Neitzel, H-J., J.U. Knebel, *Auslegung eines geschlossenen 4 MW-targetmoduls mit Wärmeabfuhrsystem für eine ADS-anordnung*, Forschungszentrum Karlsruhe, Report No. FZKA 6687, February 2002.

[8] Cinotti, L., *et al*., Private Communication, July 2002.

[9] Zucchni, A., Private Communication, January 2004.

[10] Richard, P., *et al*., Private Communication, July 2002.

OPTIMISATION OF A CODE TO IMPROVE SPALLATION YIELD PREDICTIONS IN AN ADS TARGET SYSTEM

Tetsuo Sawada, Manabu Orito, Hiroshi Kobayashi,
Toshinobu Sasa*, Vladimir Artisyuk**
Research Laboratory for Nuclear Reactors
Tokyo Institute of Technology
2-12-1 O-okayama, Meguro-ku, Tokyo 152-8550, Japan
Tel: 03 5734 3062; Fax: 03 5734 2959
E-mail: tetsuo@nr.titech.ac.jp
**Doctorate student from JAERI*
***Currently with INPE, Obninsk, Russia*

Abstract

In an accelerator-driven system (ADS), a target system is incorporated. The main purpose of the target system is to produce excess neutrons, which brings the subcritical reactor core in an ADS to critical condition. Critical condition allows for operation as a reactor system specifically to fulfil transmutation capability as well as electricity generation. From a safety point of view, the target system is quite a new component and potentially provides a novel radiotoxic burden to the environment and to humans. It is generally understood that there is still unknown physics involved in the operation of a target system, in particular, regarding nuclear spallation. Moreover, we have not yet developed the related engineering to cope with so-called “spallation products.” As a primary step towards better comprehension, this paper describes how we can have a better computational tool to predict the yields of spallation products in a proposed target system.

Introduction

Spallation neutron source is made with an intense beam of high-energy particles hitting a thick target made of heavy nuclei in an accelerator-driven nuclear transmutation system. As a by-product of this process, a lot of spallation isotopes are produced. The produced spallation isotopes show extensive distribution regarding mass number and lifetime. It is understood that there are some spallation products that have radioactivity comparable with Po, which is considered hazardous to humans and is followed attentively in the case of a Pb-Bi cooling system. In this regard, the amount of spallation yield must be evaluated with accuracy.

We developed a code to search a set of optimum parameters that is incorporated in the evaluation code to be compared with experiments. This optimisation code was combined with the evaluation code in order to increase accuracy of prediction of spallation yields.

We will show that the optimisation system combined with the particle and heavy ion transport code system (PHITS) [evaluation code] improved the accuracy of prediction of spallation product yields.

Computational simulation of spallation experiments by PHITS code

We used NMTC series code for the transportation of high-energy particles (including the spallation process) and we introduced the ATRAS code system. In ATRAS, NMTC/JAERI97 [1] was incorporated: the evaluations of total cross-sections below 100 MeV and elastic cross-sections are improved, ISOBAR model including the pre-equilibrium process for the intra-nuclear cascade model is introduced, and the function of level density is improved. Then, the jet AA microscopic transportation model, by which we calculate the hadron cascade process, was introduced into NMTC/JAERI97 (called NMTC/JAM). One of the crucial improvements for NMTC/JAM was the incorporation of the general evaporation model (GEM) [2] that can simulate the evaporation and fission processes in order to model particle injection from excited target nuclei. This has been acknowledged to be quite effective for the evaluation of spallation with much improved precision. For NMTC/JAM, the following improvements were incorporated into the PHITS code: the transportation of heavy irons, the quantum molecular dynamic model and the transportation of low-energy particles.

The recent development of the PHITS code has been focused mainly on heavy ion transportation and the effects of magnetic fields and gravity. Thus, the comparison between code predictions and experimental measurements was not performed for the intra-nuclear cascade ~1 GeV, particle evaporation in the pre-equilibrium process and from the equilibrium excited state, and the fission model, which are our major interests for the evaluation of spallation products in the ADS target system.

Our primary objective of the current study was to optimise the parameters prepared in PHITS and to reproduce the experimental data that were recently generated by GSI [3].

To measure the discrepancy between calculated predictions and experimental data, we employed the so-called “F-value”, which is defined below:

$$F = 10^{\sqrt{\langle f \rangle}} \qquad \text{and} \qquad f = \log(\sigma_{cal,i} / \sigma_{\exp,i})^2$$

where σ_i is the production cross-section of the ith nuclide produced by spallations in the target. The suffixes “exp” and “cal” mean experimental measurement and calculated value, respectively. In the PHITS code, there are variations in applied intra-nuclear cascade models, evaporation models and the energy level for the intra-nuclear cascade model as well as the intermittent use of the Coulomb

diffusion model. Thus, there were numerous sets for the associated input parameters. We needed to choose a technique to find the optimum sets of input parameters in order to obtain the overall most preferable production cross-sections. For this purpose, we used the method of *maximal likelihood function*. The maximal likelihood function is defined as follows:

$$L(\vec{q}; \sigma_{phits}, d) = \frac{1}{(2\pi d^2)^{n/2}} \exp[-\frac{(\vec{\sigma}_{ex} - \vec{\sigma}_{phts}(\vec{q}))^2}{2d^2}]$$

where d is the experimental error matrix, which will be a diagonal matrix when there is no correlation among errors, and $\vec{q}$ is a vector of input parameters. This likelihood function signifies the probability that the calculated production cross-sections agree with the experimental measurements. In order to determine the maximum of the function, we use the logarithmic maximal likelihood function defined by:

$$M(\vec{q}) \equiv \log L(\vec{q}; \sigma_{phits}, d).$$

The adopted parameters to optimise are: the parameter for the calculation model choice of 14, which takes the discrete values, and the five continuous parameters. Degree of freedom was 256 for the 276 experimental data that we used.

Global optimisation method

We used the maximal likelihood method to optimise these parameters, utilising the likelihood function made of the production cross-section for each isotope produced by spallation. In order to search global maxima for the likelihood function, the DIRECT algorithm [4] was used, which is known to be a very efficient method for optimisation. In this algorithm, we can find the maxima with better accuracy by automatically dividing the parameter space to trap the point of the maximal value. Figure 1 shows the schematic image of narrowing down the space to the subspace where we can find the maximal point. Among the provided experimental data, we used selected data of isotopes produced with high production cross-sections. This data was chosen because the calculated statistical error grows for isotopes produced with small production cross-sections. For each element, we centred the isotope with the largest yield. Then, for comparison with the experiments, we weighed the isotopes by a Gaussian distribution having the width of neutron numbers with statistical accuracies of greater than 0.1 under the same conditions. By this method, we performed the optimisation for all nuclides with mass numbers from 40 to 200. There are two ways of optimisation – one is global optimisation over all elements and the other is local optimisation for a specific element.

Figure 2 shows the results obtained for $_{60}$Nd, which is one of the rare earth elements of interest to us. This case is optimised specifically to Nd. As the figure indicates, the experimental measurements were very well-reproduced. However, the overall χ^2 value was 659, which means it is a less preferable reproduction of the experimental measurements as a whole.

Figure 1. Schematic image of dividing the parameter space through the DIRECT algorithm

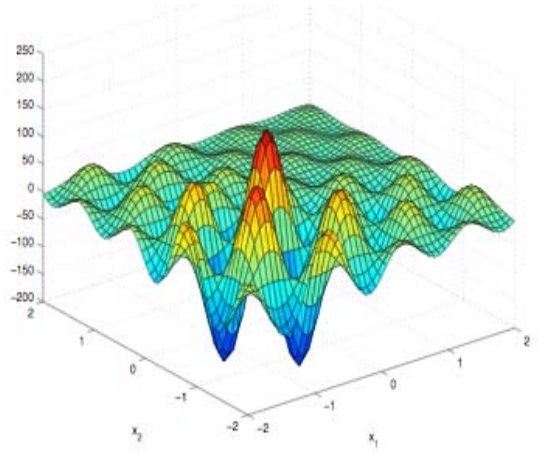

Figure 2. Production cross-section of $_{60}$Nd in the reaction ^{208}Pb + p (1 GeV) obtained through experiments and simulations

(a) CASCADE code simulation, (b) PHITS code simulation without optimisation and (c) PHITS code simulation with optimisation

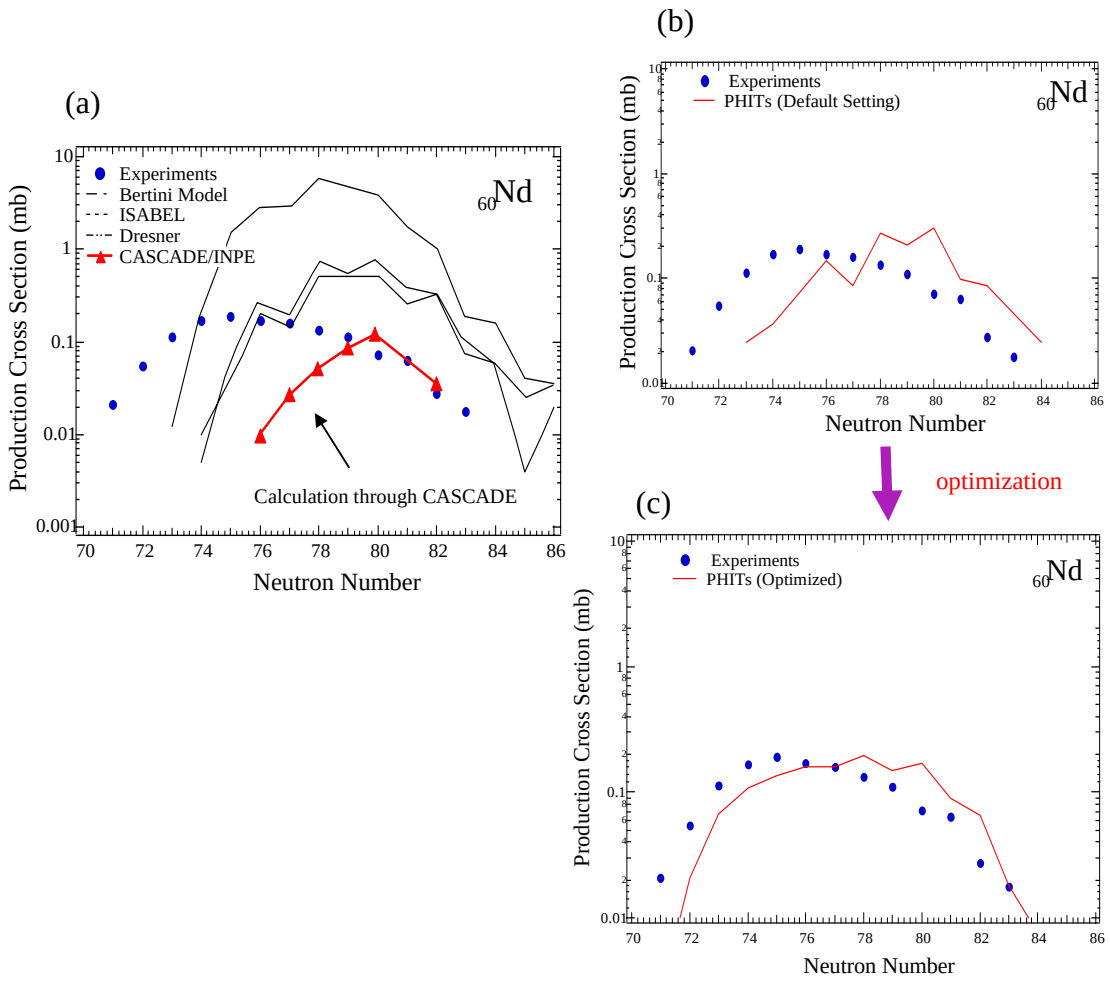

Figure 3 shows the results of global optimisation with the c^2 value of 397. As shown, the reproduction capability for nuclides with atomic numbers from 30 to 50 was very well-improved. However, when the atomic number was greater than 60, the production cross-sections for isotopes with excess protons were badly underestimated. It can be understood that injection of neutrons during the evaporation process seems to be underestimated in the experiment because it occurs in evaporation under an equilibrium state. For this study, intra-nuclear cascade calculations using the molecular dynamics model were not performed. This was due to the very long CPU time required and the division of parameter space not being precise enough to produce satisfactory results. In any case, we think that our work has shown that the neutron emission model during evaporation should be improved.

Figure 3. Production cross-section in the reaction ^{208}Pb + p (1 GeV). Results of the PHITS code simulation with global optimisation.

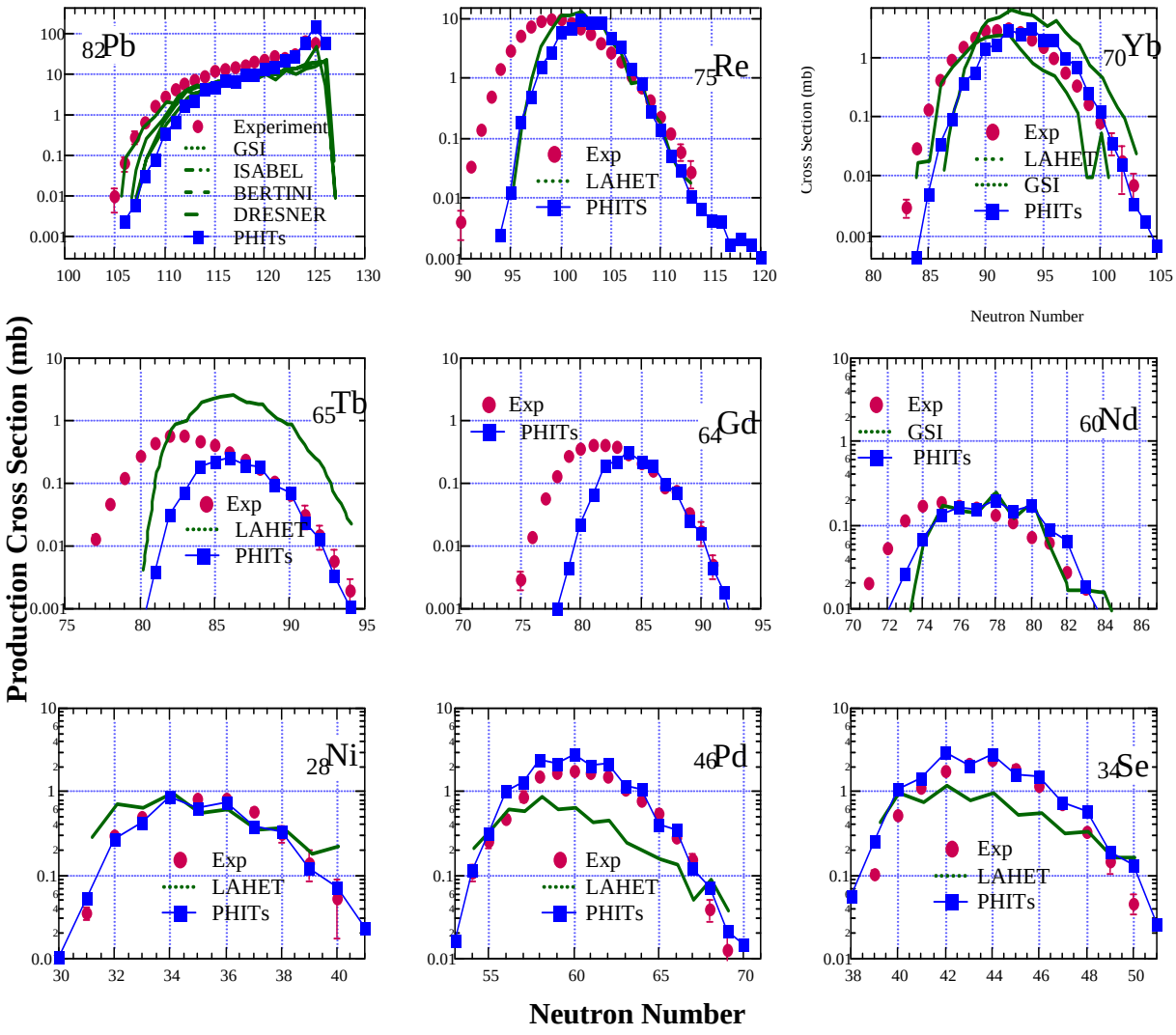

Figure 4 shows the comparison between calculations and experiments over all mass numbers. For this figure, we integrated the production cross-sections over all the produced isotopes with the same mass number. Here we found some problematic discrepancies for the rare earth region and elements with mass numbers less than 80.

Figure 4. Production cross-sections integrated over all produced isotopes with the same mass number and obtained through a PHITS code simulation with global optimisation (red line) and experiments (filled red circles)

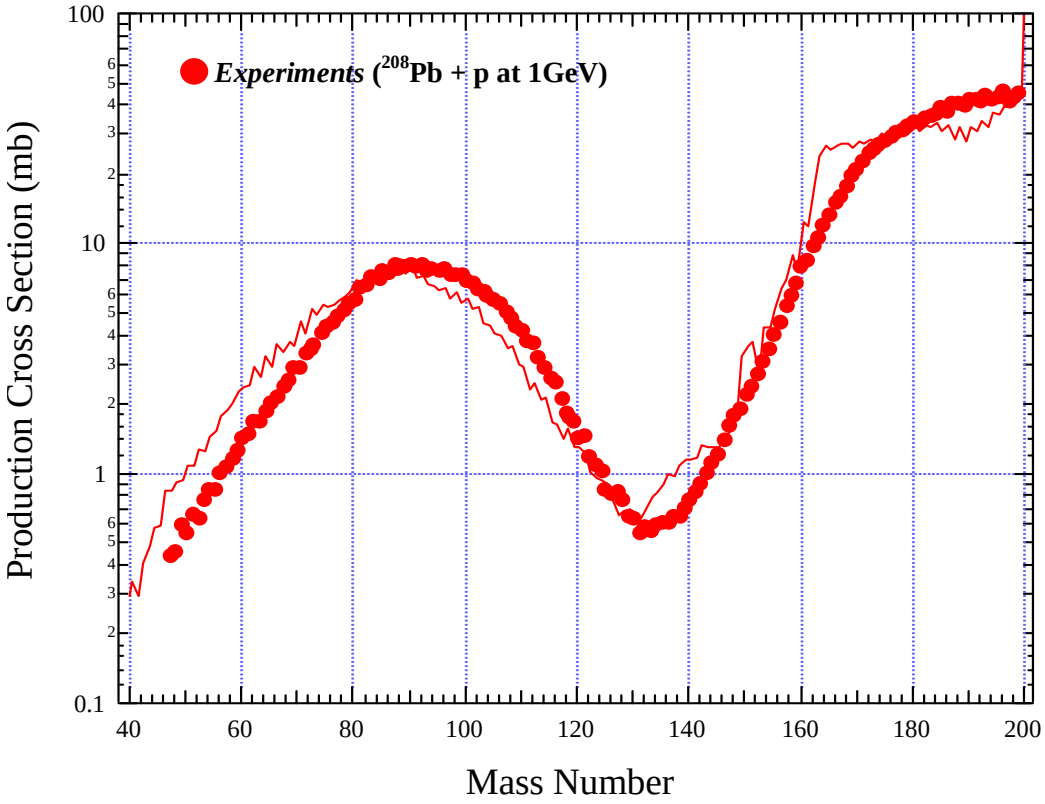

Discussion

As seen in Figure 3, for elements with an atomic number larger than 60, the calculated results were rather shifted to the isotopes of larger mass numbers, so that the production cross-sections of excess proton isotopes were underestimated. This simply means that the neutron emission from residual nuclei was smaller compared with the experiments. If we consider that almost all neutrons are emitted during the evaporation process, we can guess the following reasons for the discrepancy.

The simplest reason may be that the excited energy for the transition to the evaporation process is too low, such that the condition of the emission of neutrons during evaporation is not well-developed. In order to resolve this issue, we need to incorporate the pre-equilibrium process and leave enough excited energy to promote neutron emission during evaporation. Raising the excited energy at the final stage of the cascade process would also be effective. This can be done by setting a smaller value for the energy cut-off parameter in the cascade process. In fact, we confirmed that this is effective in increasing the production of proton-excess isotopes. Unfortunately, energy cut-off was not an input parameter for PHITS code but a built-in one, and thus not included in the global optimisation procedure.

The other possibility is that the discrepancy may be improved by considering neutron emission in the transition to fission, with the formation of multiple fragments of residual nuclei in the range of excited energy ~4 to 5 MeV. It should be noted that we must re-evaluate physical parameters used in the evaporation model if we modify the models preceding the evaporation process. The fact that in Figure 4 we observe a discrepancy between experiments and calculations for nuclides where the mass number was less than 80 indicates the drawback in the evaluation of the fission process.

Figure 1 shows the comparison of experiments and predicted production cross-sections of PHITS with optimum parameters.

Summary

Via the above-described optimisation method, we obtained better prediction capability using the PHITS code for overall yields of spallation products generated and accumulated in an ADS target system. In particular, the predicted cross-sections for the low mass isotopes were in good agreement with experiment data. On the other hand, the discrepancy for high mass isotopes was relatively large. From this study, we found that the predicted cross-sections were sensitive to the parameters that determine the energy at which the adopted intra-nuclear cascade model was changed or at which the evaporation model was to be adopted. For even better prediction capability, we need to further improve excited energy for the evaporation process, which is currently underestimated, and the model for the fission process.

Acknowledgement

This study was performed under contract with JAERI, which is financially supported by MEXT.

We could not have launched this study without the great amount of research effort and related fruitful results by Professor Masaki Saito and his research group of the Tokyo Institute of Technology, which preceded our work.

REFERENCES

[1] Iwase, H., K. Niita, T. Nakamura, *J. Nucl. Sci. Techn.*, 39, 1142 (2002).

[2] Furihata, S., *et al*., JAETI-DATA-CODE-2001-015.

[3] Enqvist, T., *et al*., *Nucl. Phys*., A686, 481 (2001).

[4] Jones, D.R., *Encyclopedia of Optimization*, Vol. 1, 431 (2000).

TECHNICAL SESSION III

Subcritical System Design and ADS Simulations

Chairs: W. Gudowski, H. Oigawa

RESEARCH ON THE ACCELERATOR-DRIVEN SUBCRITICAL REACTOR AT THE KYOTO UNIVERSITY CRITICAL ASSEMBLY (KUCA) WITH AN FFAG PROTON ACCELERATOR

Tsuyoshi Misawa, Hironobu Unesaki, Cheol Ho Pyeon, Chihiro Ichihara, Seiji Shiroya
Research Reactor Institute, Kyoto University, Kumatori, Osaka 590-0494, Japan

Abstract

At the Kyoto University Research Reactor Institute (KURRI), a new project for research on the accelerator-driven subcritical reactor (ADS) was started in 2002. For this project, a new ring-type accelerator based on the up-to-date FFAG (fixed field alternating gradient) technology will be under construction through 2005. With this new accelerator, a proton beam having arbitrary energy from 2.5 to 150 MeV will be generated and the proton beam from this accelerator will be introduced into a core at the Kyoto University Critical Assembly (KUCA) in order to generate high-energy neutrons via collision with heavy metal (e.g. tungsten). Before starting this new experiment, basic research on ADS was performed at KUCA, combining a KUCA core with an accelerator to generate 14 MeV neutrons via a D-T reaction and to investigate the nuclear characteristics of a subcritical reactor with an external neutron source.

Introduction

Accelerator-driven subcritical reactors (ADS) have attracted worldwide attention in recent years. ADS have been developed for the purposes of producing energy and transmuting minor actinides and long-lived fission products, as a result of their superior safety characteristics and potential for burning plutonium and other nuclear wastes. It is well-known that the advantage of ADS is the rare chance of energetic reactivity accidents due to its subcritical operation.

At the Kyoto University Research Reactor Institute (KURRI), a new project for research on ADS was started in 2002. For this project, a new ring-type accelerator based on up-to-date FFAG (fixed field alternating gradient) technology will be constructed, which can produce a proton beam of ~1 microampere current with arbitrary energy from 2.5 to 150 MeV. The proton beam from this accelerator will be introduced into the core of the Kyoto University Critical Assembly (KUCA) to induce high-energy neutrons generated by bombarding a heavy metal (e.g. tungsten). This new accelerator system is now under construction and new experiments at KUCA with the FFAG accelerator will begin in 2005 [1-3].

Before beginning the new ADS experiment using an FFAG accelerator, basic research on ADS was performed at KUCA. This involved combining KUCA with a Cockcroft-Walton type accelerator that was already equipped at KUCA. The present study discusses the results of experiments and calculations performed at the KUCA core for the preliminary study on ADS using the present D-T accelerator.

Core configuration

The KUCA A-core, which is a solid moderated core with highly enriched uranium fuels and a polyethylene moderator among the three cores (A, B and C) of KUCA, was combined with a pulsed neutron generator of the Cockcroft-Walton type installed at KUCA. A polyethylene-moderated and reflected core loaded with highly enriched uranium-aluminium (U-Al) alloy fuel was assembled at the A-core position as shown in Figure 1. All the ADS experiments were carried out at this core. As shown in Figure 2, the fuel rod consisted of polyethylene and U-Al plates with upper and lower polyethylene reflectors of more than 50 cm. The active height of the core was ~40 cm. The neutron spectrum of the core could be changed by adjusting the combination of 1.6-mm (1/16-inch) thick U-Al plates and 3.1-mm (1/8-inch) thick polyethylene plates that were piled up in the fuel rod [5].

A pulsed neutron generator run by a Cockcroft-Walton type accelerator was installed at KUCA to accelerate a deuteron beam up to ~300 keV and to make collisions with a tritium target located outside the core (see Figure 2) generate 14 MeV pulsed neutrons via D-T reaction. The pulse frequency could be changed up to 1 kHz depending on the purpose of the experiment. These pulsed neutrons were injected through a layer of the polyethylene reflector into the assembly, which was maintained at subcritical state.

The following experiments have been carried out thus far for the ADS study: (1) subcriticality measurement via the pulsed neutron method or modified source multiplication method, (2) neutron flux distribution measurement using optical fibre detectors or the foil and wire activation method in the subcritical core, (3) neutron spectrum measurement via the irradiated foil unfolding method, (4) neutron noise analysis such as the new variance-to-mean ratio method with pulsed neutron source to measure subcriticality or core properties, and so on. The results of the experiments were analysed with a deterministic method using an SN transport code and Monte Carlo code (e.g. MCNP [4]).

Figure 1. Structure of the KUCA core

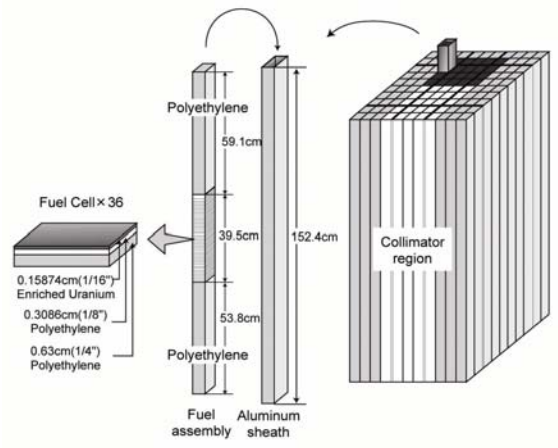

Figure 2. Horizontal core configuration

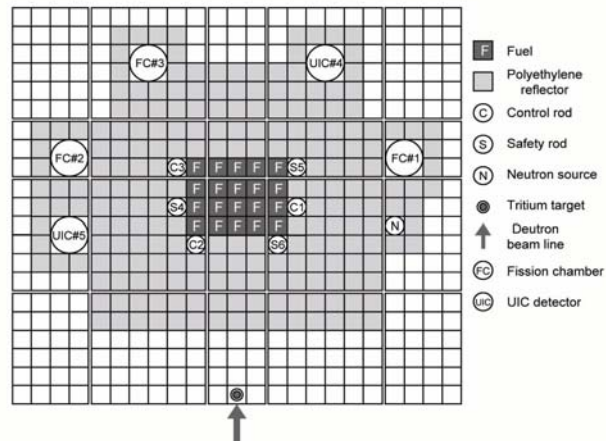

Design of neutron beam collimator

The numerical experiments were carried out at the KUCA combined with the accelerator that generates 14 MeV high-energy neutrons. First, the neutron collimator to introduce high-energy neutrons effectively into the core was designed. The collimators were provided in the polyethylene reflector region, towards the core from the target and at the centre region in the axial direction. As shown in Figure 3, several kinds of assemblies with a beam tube inside were adopted to make up the collimator region – polyethylene, polyethylene with mixture of ^{10}B (to shield thermal neutrons) and iron metal (to shield fast neutrons). These materials were used to moderate the fast neutrons or to absorb the additional neutrons that were moderated around the target region. The installation patterns of collimators in the reflector region are shown in Figure 4. For the numerical simulations using MCNP, attention was paid to neutron multiplication in the core and neutron flux distribution along the neutron guide passage as well as to when collimators were installed in the polyethylene reflector region.

From these analyses, it was concluded that the Figure 3/Case 4 installation pattern of collimators was the best pattern to effectively introduce fast neutrons into the core and to reduce the thermal neutrons that were moderated by the wall of the beam transport tube in the collimator region.

Figure 3. Collimator patterns in the reflector region

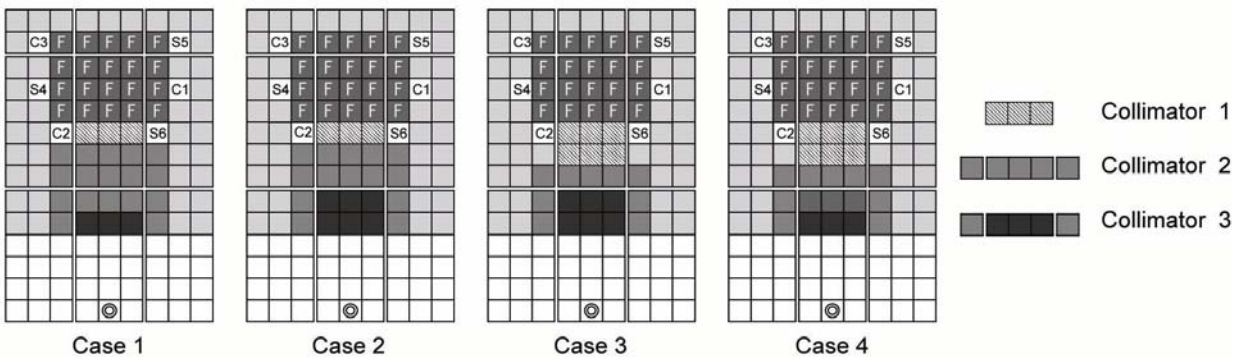

Measurement of reaction rate distribution

Since the study of neutron flux distribution in subcritical systems is one of the important topics in ADS design, flux distribution measurements were carried out at the KUCA core with the accelerator. At the KUCA core, gold foils were used for this purpose. However, in a subcritical state, it is difficult to measure the reaction because the reactor power is determined by subcriticality accelerator power and its value is much lower than that of a core in a critical state. To overcome this difficulty, indium (In) wire [measures neutron flux by ^{115}In (n, gamma)^{116m} In reactions] was used in the experiments for the present study. Indium wire of 1.5-mm diameter was set in vertical direction (see Figure 1) along the collimator and the accelerator was operated about three hours to irradiate the wire. Note that the subcriticality of the core was adjusted by the position of control rods, which was about -1% dk/k. After irradiation, the wire was cut into small pieces and the emitted gamma-rays were measured by a pure Ge detector. Figure 4 shows the indium reaction rate distribution with and without the collimator (Figure 3/Case 4) together with the calculated results from the MCNP code. It was found that the reaction rate was accurately measured by this method even in a subcritical state and that the present collimator acted as transporter of neutrons into the fuel region (due to increasing the reaction rate in the fuel region). The calculated results from MCNP agreed well with the measured ones.

Figure 4. Measured reaction rate distribution by indium wire in vertical direction with and without collimator together with calculated results by MCNP

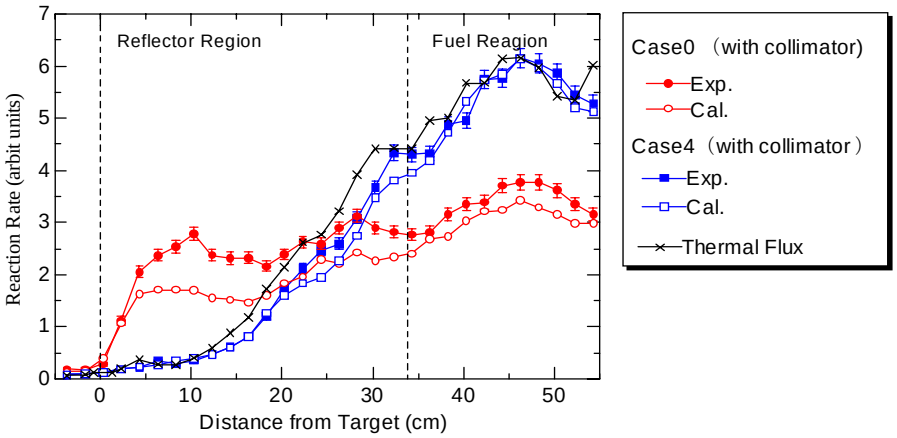

Measurement of reaction rate by fast neutrons

Fast neutrons in the subcritical core were measured by the activation method using threshold detector foils that react with neutrons of higher than threshold energy. Table 1 shows the reaction types used in the present experiments, where 10 threshold reactions were adopted to measure fast neutron reaction. In the experiments, foils were set in the fuel region and in front of the tritium target. They were irradiated about six hours and the emitted gamma-rays were measured by a pure Ge detector. Table 1 shows the results of each reaction rate with and without a collimator (Figure 3/Case 4). It was found that each reaction rate was measured within 10% accuracy by this method even in a subcritical state.

Table 1. Reaction rate of threshold irradiation foils

Reaction Type	Threshold [MeV]	Reaction Rate [s^{-1}] $\times 10^2$ with Collimator		Reaction Rate [s^{-1}] $\times 10^2$ without Collimator	
		Fuel	Target	Fuel	Target
$^{115}In(n,n')^{115m}In$	0.5	3.40	2.20	2.32	2.45
$^{58}Ni(n,p)^{58}Co$	1.9	8.51	10.2	1.79	22.8
$^{64}Zn(n,p)^{64}Cu$	2	9.86	13.0	4.22	11.9
$^{56}Fe(n,p)^{56}Mn$	4.9	5.08	7.40	3.12	8.34
$^{27}Al(n,\alpha)^{24}Na$	4.9	1.40	1.18	0.707	5.54
$^{24}Mg(n,p)^{24}Na$	6	0.505	1.03	0.35	1.24
$^{200}Hg(n,2n)^{199m}Hg$	8.1	0.129	0.300	0.0676	0.323
$^{127}I(n,2n)^{126}I$	9.3	3.21	10.6	1.05	10.7
$^{63}Cu(n,2n)^{62}Cu$	11.9	7.28	26.8	3.23	35.3
$^{58}Ni(n,2n)^{57}Ni$	13	0.567	0.626	0	0.744

Measurement of neutron noise of ADS

For the safe operation of ADS, it is important to detect subcriticality in real-time, and the neutron noise analysis method is one of the appropriate methods for this purpose. A new noise data acquisition system has been developed [6] and was used for these experiments. With the ADS system, neutron counts are fluctuated not only by the effect of chain reaction that is observed in a critical reactor, but also by periodic operation of an external neutron source from the accelerator. Including these effects, a new formulation based on the variance-to-mean ratio method (Feynman-alpha method) was developed.

Figure 5 shows results of measured data by the pulsed neutron method and the variance-to-mean ratio method (Feynman-alpha method) when the repletion period was 0.01 seconds. It was found that measured Y-values agreed well with theoretical values that were obtained by fitting the experimental data. Furthermore, Table 2 shows the results of measured prompt neutron decay constants (alpha values) by these different analysis methods that agreed well. From these results, it was found that subcriticality of the system, which was obtained from the prompt neutron decay constant (alpha value), could be observed in real-time when neutron noise data was obtained during the operation of the ADS.

Figure 5. Measured neutron decay after neutron injection from accelerator (right) and measured Y-values (circles) and fitted lines by Feynman-alpha method (left)

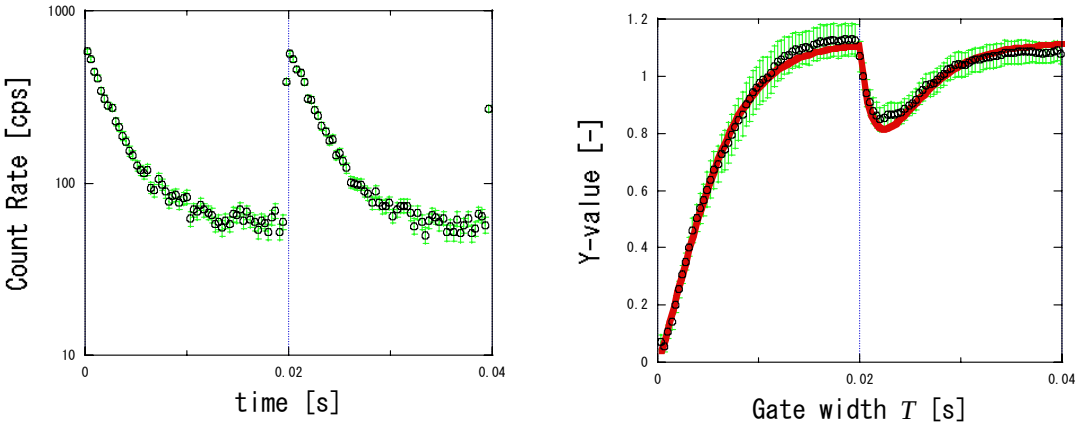

Table 2. Results of measured prompt neutron decay constants (alpha values) by pulsed neutron method and variance-to-mean ratio method

Pulsed neutron method (Area-ratio method)		V-to-variable-M method	Comparison of α -value
$-\rho$ [$]	α_0 [1/s]	α [1/s]	$(\alpha-\alpha_0)/\alpha_0$
1.597 ± 0.012	357.8 ± 0.9	359 ± 16	0.005 ± 0.045

Conclusion

Several experiments were carried out where the KUCA core was combined with a D-T neutron generation accelerator in order to examine the neutron characteristics of an ADS. In the KUCA core, the neutron transport beam collimators were designed and installed in the polyethylene reflector region, towards the core from the target. Using this system, reaction rate measurements in a subcritical system with an accelerator were carried out by the foil activation method, and the results agreed well with the calculated ones. Moreover, to detect the subcriticality of the ADS, a new neutron noise analysis method based on the variance-to-mean ratio method was developed.

Acknowledgements

The authors wish to thank Dr. Y. Kitamura of Nagoya University and Mr. Y. Hirano of Kyoto University for their generous help throughout the present study.

REFERENCES

[1] Mori, Y., "Multi-orbit Synchrotron with FFAG Focusing for an ADS", *Genshikaku Kenkyu*, 47, 3 (1998).

[2] Shiroya, S., H. Unesaki, T. Misawa, "Accelerator-driven Subcritical Reactors in Japanese Universities: Experimental Study Using the Kyoto University Critical Assembly", *Trans. Am. Nucl. Soc*., 2001 Annual Meeting, Milwaukee, Wisconsin, 17-21 June, pp. 78-79 (2001).

[3] Shiroya, S., *et al*., "Experimental Study on Accelerator-driven Subcritical Reactor using the Kyoto University Critical Assembly (KUCA)", *Proceedings of the Int. Conf. on New Frontiers of Nucl. Technol.: Reactor Physics, Safety and High-performance Computing* (PHYSOR2002), Seoul, Korea, 7-10 October, 7C-01 (2002).

[4] Briesmeister, J.F., ed., "MCNP – A General Monte Carlo N-Particle Transport Code, Version 4C", LANL Report LA-13709-M, Los Alamos National Laboratory (2000).

[5] Misawa, T., S. Shiroya, K. Kanda, "Study on Reactivity Worth of Beryllium by (n, 2n) and (ɣ, n) Reactions", *Nucl. Technol.*, 116, 11 (1996).

[6] Kitamura, Y., *et al*., "Reactor Noise Experiments by Using Acquisition System for Time Series Data of Pulse Train", *J. Nucl. Sci. Technol*., 36, 653 (1999).

IMPROVEMENT OF BURN-UP SWING FOR AN ACCELERATOR-DRIVEN SYSTEM

Kenji Nishihara, Kazufumi Tsujimoto, Hiroyuki Oigawa
Japan Atomic Energy Research Inst., Japan

Abstract

JAERI has developed an accelerator-driven subcritical system (ADS) to transmute minor actinides (MA). The key parameter of the ADS is criticality (k_{eff}). Ideally, k_{eff} should be a high constant value during burn-up so as not to be critical. To flatten the burn-up swing, two methods were investigated – adjustment of fuel composition and introduction of burn-up control rods. As a result of these two improvements, burn-up swing decreased below 1% Dk and it was shown that the swing could be approximately zero. Other good results such as the flattening of accelerator power and peaking factor were observed.

Introduction

JAERI has been developing the accelerator-driven subcritical system (ADS) for the transmutation of minor actinides (MA). Since an MA transmuter must support various MA compositions, and MA fuel has small β_{eff}, the ADS is superior to conventional critical reactors as an MA transmuter from the viewpoint of super-criticality accidents. The key parameter of ADS is criticality (k_{eff}), which is normally set to 0.95-0.98. A higher k_{eff} has some benefits such as lower power of the proton accelerator, less damage to the beam window and lower power peak in the MA fuel region. Since the peak position is in the centre of the core and the gradient of power distribution is closely related to criticality, k_{eff} close to critical is appropriate to decrease peaking. Another way to decrease the peaking factor is by dividing the core into regions with different fuel ratios [1,2]. Generally, the decrease of peaking results in the decrease of source effectiveness. This is because the decrease of peaking is achieved by decreasing the neutron worth in the central peaking region.

A higher k_{eff} can adversely affect safety. Thus, ideally, k_{eff} should be a high constant value during all of burn-up as to not be critical. Without any device, k_{eff} swings greatly during burn-up and between some burn-up cycles. To decrease the burn-up swing of k_{eff} near the maximum k_{eff} during all cycles, ADS can adopt two methods – adjustment of fuel composition and introduction of burn-up control rods. In the present study, k_{eff} at the beginning of each cycle was set to constant by adjustment of the ZrN volume ratio in the fuel at each cycle. Then, burn-up control rods were introduced to compensate the reactivity drop caused by burn-up.

The power variation of the ADS is normally controlled by the power of the accelerator. However, this method must be compared with the method of using burn-up control rods. The present work aims to show the ADS design with the burn-up control rods and the effects on the accelerator and the core.

Accelerator-driven system

The reference design of the ADS was a tank-type reactor cooled by a lead-bismuth eutectic (LBE). The main parameters are shown in Table 1. The proton energy was 1.5 GeV and the power was 15 to 40 MW. The fuel consisted of MA nitride (MAN), plutonium nitride (PuN) and zirconium nitride (ZrN). Although PuN is not preferable from the viewpoint of MA transmutation, it was necessary only in the first cycle in order to elevate k_{eff} in the early cycles. ZrN played a role in the dilution of actinide fuel, i.e. to decrease k_{eff} without resizing the core. Parameters adjusted in the present study were the PuN ratio in the first cycle and the ZrN ratio in each cycle.

The maximum value of k_{eff} was determined from safety analysis. The value was set to 0.97 [1]. The breakdown of margin to critical (3.0% Δk) was system cool down (0.193% Δk), beam tube filled with coolant (0.316% Δk), uncertainties for measurement (0.50% Δk), uncertainties for calculation (1.00% Δk) and safety margin (0.75% Δk). Since the majority of the items were uncertainties and margin, it must be continuously investigated.

Table 1. Core characteristics of the ADS

Thermal power	800 MW
Maximum k-effective	0.97
Coolant material	Lead-bismuth
No. of core region	Single
Core height	1 000 mm
Core diameter	1 250 mm1
Pin diameter	7.5 mm
Pin pitch/diameter	1.5
Fuel	Nitride (^{15}N enriched)
MA composition	Spent fuel from FBR
Inert matrix	ZrN (volume ratio: 50-60%)
Initial actinide loading	4-5 ton
Cycle length	600 full power day
Transmutation of actinide	250 kg/y
Proton energy	1.5 GeV
Proton power	15-40 MW
Target	Lead-bismuth

Figure 1 shows the burn-up swing of k_{eff} and proton beam power during 10 cycles of the reference ADS. The result was obtained using a code system consisting of: NMTC/JAERI97 [3] for the transport of protons and high-energy neutrons above 10 MeV, SRAC [4] with JENDL-3.2 nuclear data for effective micro cross-sections, DANT-SYS [5] for the transport of low-energy neutrons below 10 MeV and ORIGEN2.1 [6] for calculating fuel burn-up.

Figure 1. Original variation of k_{eff} and beam power

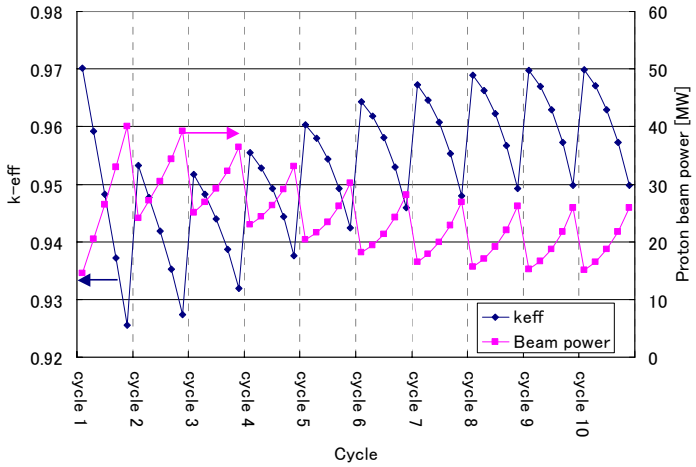

As shown in the figure, k_{eff} reaches a state of equilibrium at the ninth cycle. The variation of k_{eff} was above 4% Dk during the 10 cycles. The burn-up drop of k_{eff} was ~2% Dk except for the first and second cycles. The variation of proton beam power was 15 to 40 MW. If k_{eff} does not vary from 0.97, the power of the proton accelerator can be reduced one-third and spent electricity for the accelerator decreased by 40%. Another advantage would be the decrease of peaking. As shown in Figure 2, the peaking factor of power density (the ratio of maximum power density to that averaged over the fuel region) is closely related to k_{eff}.

Figure 2. Original variation of peaking factor of power density

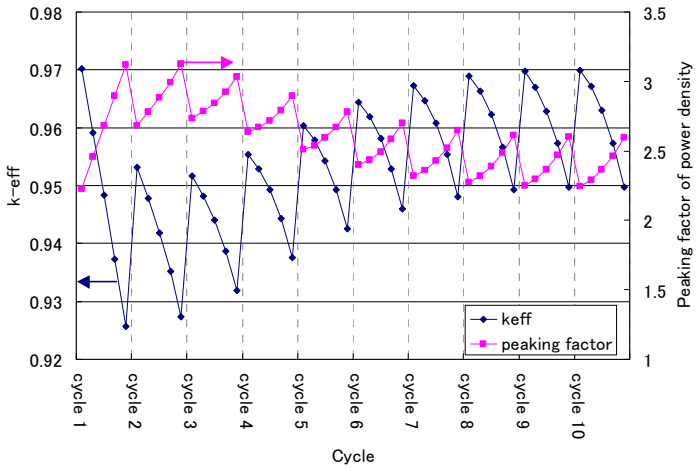

Improvement of k_{eff} at the beginning of each cycle (BOC improvement)

As shown in Figure 1, k_{eff} at the beginning of the cycle (BOC) is different, especially in the early cycles. Since low k_{eff} at BOC demands high beam power during the cycle, it is important to set k_{eff} to 0.97 at BOC. For this purpose, two parameters can be adjusted – PuN and ZrN densities. In the reference design, PuN was added only to the first cycle so as to set k_{eff} at first cycle/BOC to 0.97, and the density of ZrN was constant during whole cycles. The constant value was decided such that k_{eff} at equilibrium cycle/BOC was 0.97.

Essentially, the addition of PuN led to defective transmutation performance of the ADS. Since the goal of the ADS is to transmute MA, the addition of PuN to MAN meant an increase in the transmutation target materials. However, and only for the first cycle, the addition of PuN was necessary because k_{eff} was too small. Figure 3 shows the ZrN volume ratio versus the burn-up drop of k_{eff} and the PuN ratio at the first cycle. A ZrN ratio less than 55% led to a rise in k_{eff} during burn-up. The ZrN ratio in the first cycle was decided so that the drop became zero. PuN in the first cycle was decided according to the ZrN density (55%).

Figure 3. ZrN volume ratio and burn-up drop of k_{eff} at the first cycle, keeping k_{eff} at 0.97

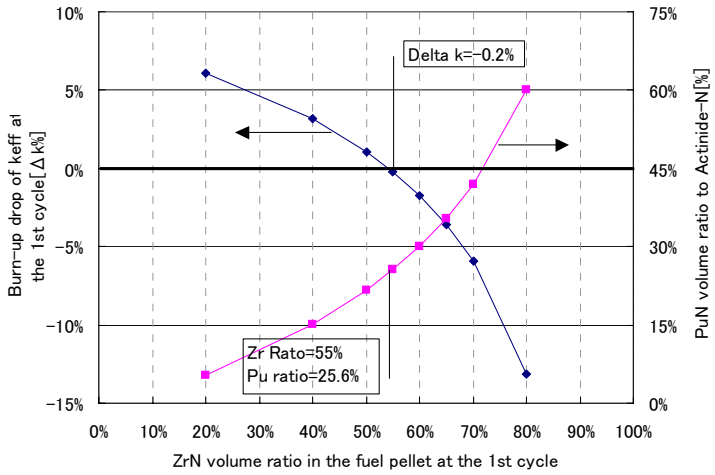

After the second cycle, the PuN addition was not necessary. The ZrN density was altered to maintain k_{eff} at 0.97. However, without any restriction on the change, oscillation of the ZrN density occurred as shown in Figure 4. The mechanism of instability is such that if k_{eff} at EOC of some cycle is small, the volume ratio of the inert matrix in the next cycle becomes lower and the new MA fuel (containing much fertile material) is added to the next cycle. Then, in EOC of the next cycle, k_{eff} is large, the inert matrix becomes large and a small amount of the MA fuel is loaded to the subsequent cycles. One of the methods to restrain oscillation is restriction of the ZrN variation from the previous cycle. Figure 5 shows the result with the restriction (0.5%) of the change in ZrN volume ratio after the fourth cycle. Although k_{eff} of each BOC was not strictly 0.97, oscillation was acceptably restrained.

Figure 4. Adjustment of ZrN volume ratio at each cycle without any restriction

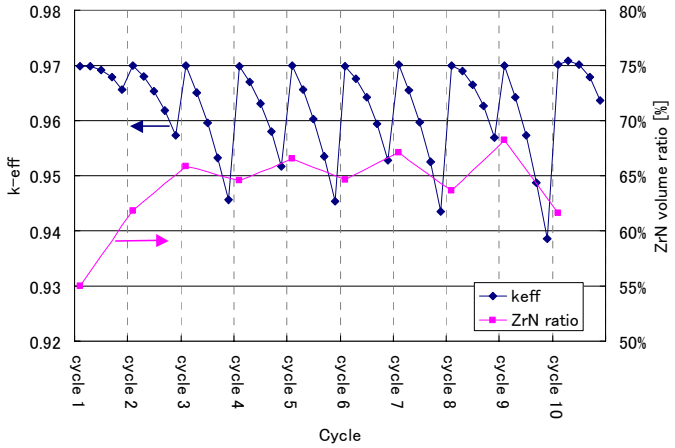

Improvement of k_{eff} during burn-up in each cycle (EOC improvement)

Next, the compensation of burn-up reactivity was investigated using burn-up control rods consisting of 95% ^{10}B-enriched B_4C. The rods were fully loaded into the core at BOC and then drawn up and out of the core during burn-up. The velocity of drawing could be slow and the compensated reactivity was small compared with critical reactors. Since k_{eff} drops about 2% Dk after burn-up as shown in Figure 5, the total reactivity worth of the rods is required to be 2% Dk.

Figure 5. Adjustment of the Zrn volume ratio with restriction of variation from the previous cycle to 0.5%

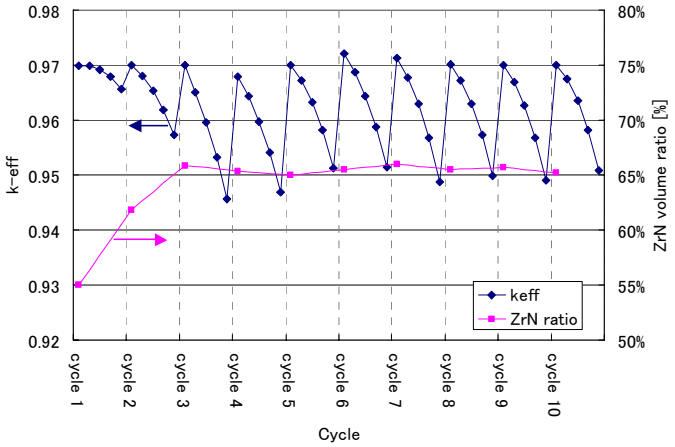

Figure 6 shows the assembly configuration of the core. The possible position of the rods was R = 3 to 9. The reactivity worth of the rods at each position at BOC of the first cycle is shown in Figure 7. The goal of the reactivity worth, 2.0% Dk, could be achieved at the position R = 3 to 7. Table 2 shows the necessary number of rods and related core parameters. For the inner position of the rods, the radial peaking improved, however, source effectiveness worsened due to the decreased worth of the spallation neutron source. Since the radial peaking factor at the R = 7 position was larger than R = 6, and in spite of the source effectiveness being almost same, the positions of R = 3 to 6 were appropriate. The factors effecting the decision regarding the position were:

- Peaking factor in connection with limits of generated heat in clad pin and temperature.
- Source effectiveness in connection with performance and cost of the accelerator and damage to the target window.
- Reactivity worth of single rod in connection with critical safety.
- Structures of the upper core.

Figure 6. Assembly configuration (R = 6)

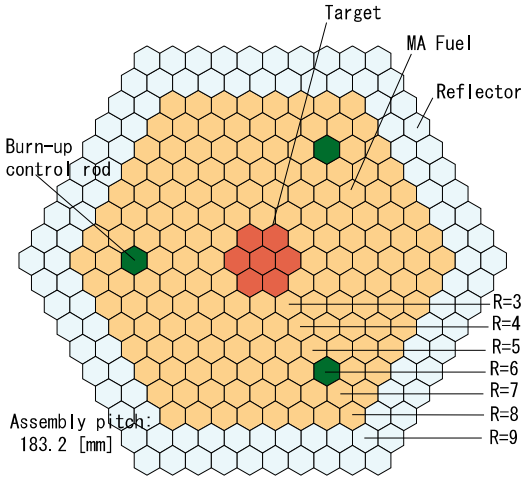

Figure 7. Reactivity worth of the burn-up control rod at BOC of the first cycle

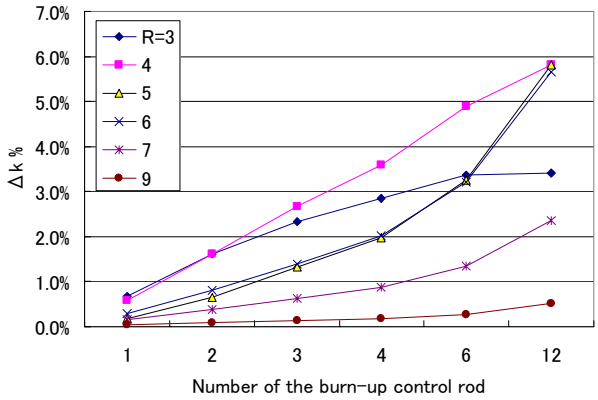

In the present study, the R = 6 position was chosen, taking priority over source effectiveness and ease of attaching the mechanism that drives the rods at the top of the core.

Table 2. Core parameters at each position of the burn-up control rods

R	Number of rods	PuN volume ratio	Reactivity worth [Dk%]	Dk%/ single rod	Radial peaking factor	Source effectiveness (φ*)
Reference	0	22.09%	--	--	1.88	0.681
3	3	24.34%	2.50%	0.83%	1.71	0.463
4	3	24.64%	2.87%	0.96%	1.90	0.604
5	4	25.16%	2.15%	0.54%	2.12	0.744
6	4	24.00%	2.13%	0.53%	2.16	0.760
7	12	24.48%	2.52%	0.21%	2.40	0.770
9	48	22.93%	1.32%	0.027%	2.01	0.732

Result

Figure 8 shows the results of the two improvements to the reference ADS. For the EOC improvement, the three rods were attached at position R = 6 because the reactivity of the four rods increased from 2.13 to 2.5% Dk at the equilibrium cycle (to which the change of flux spectrum led). The burn-up rods were kept out of the core during the first cycle because the reactivity drop was sufficiently small. At the second cycle, the rods were pulled up halfway during the cycle. After the third cycle, the rods were fully used.

Figure 8. Burn-up swing of k_{eff} (original, BOC improvement and EOC improvement)

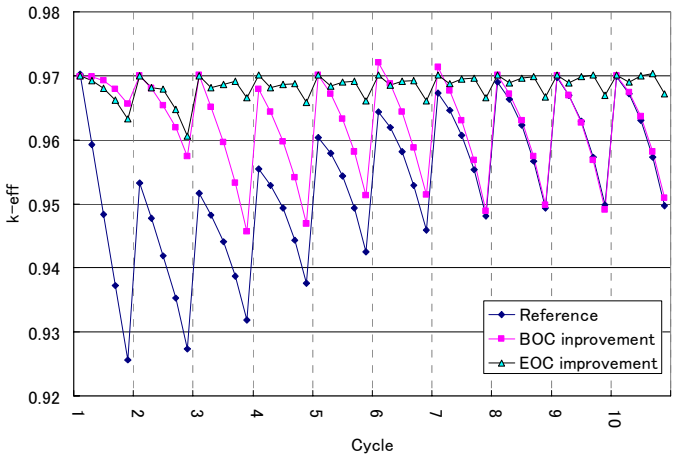

The reactivity swing of k_{eff} improved from 4.5% Dk for the reference design to 2.6% Dk for BOC improvement and to 1.0% Dk for EOC improvement. The swing could be zero if a suitable number of rods and operation method were adopted. Figure 9 shows the necessary accelerator power. The maximum power and electricity consumption of the accelerator decreased under the two improvements.

One of the demerits of rod introduction was increase of actinide inventory in the core, especially in the early cycles (shown in Figure 10). Capacity of the dry reprocessing plant was required to be 12% larger. Figure 11 shows the improvement in the local power peaking. The peaking at BOC of the later cycles was larger with burn-up control rods; however, the peaking factor was improved as a whole.

Figure 9. Improvement of proton power

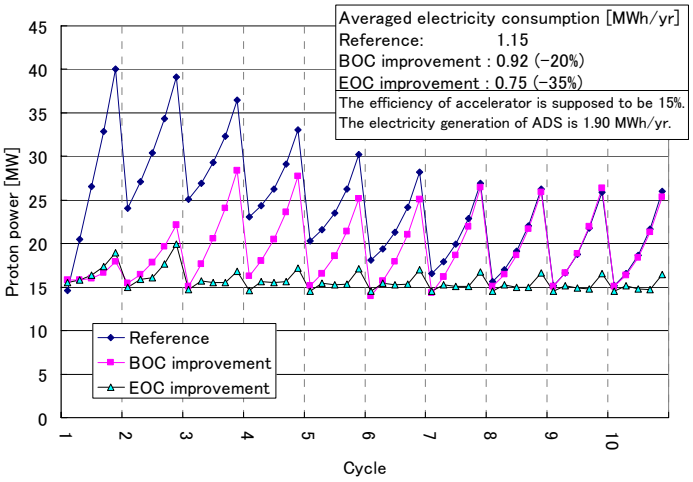

Figure 10. Corruption of heavy metal inventory in the core

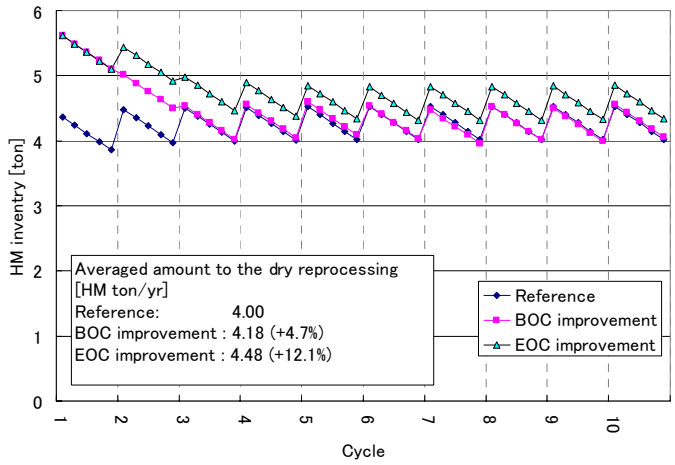

Figure 11. Improvement of local power peaking

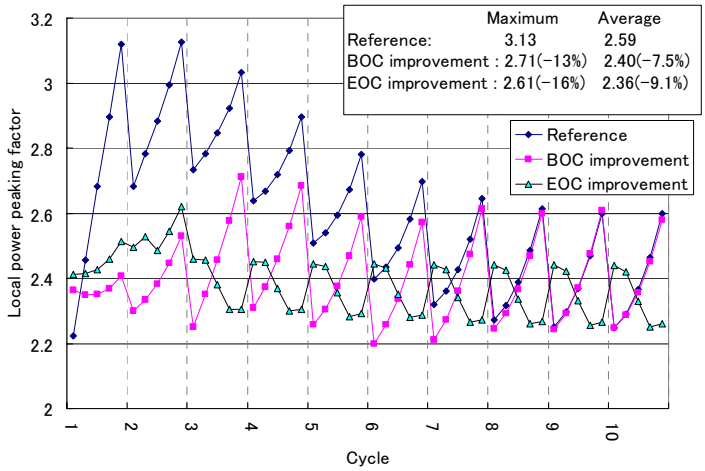

Conclusion

One of the most important parameters for the ADS is k_{eff}, which affects the accelerator, core power peaking and widow damage. Thus, the decrease of the k_{eff} burn-up swing is a major problem for the ADS. Two methods were investigated to improve the burn-up swing – adjustment of fuel composition and introduction of burn-up control rods. As a result of the two improvements, burn-up swing decreased to 1% Dk and it was shown that the swing could be zero. The effect on the accelerator was the decrease of maximum power from 40 MWb to 20 MWb (possibly 15 MWb) and of electricity consumption by 35% (possibly 40%). The power peaking improved by 16%. A disadvantage of the improvements was the 12% increase in the required capacity of the reprocessing plant.

In the future, the negative influence of the introduction of burn-up control rods to the core should be investigated, e.g. complication of the upper structure, thermal stripe near the control rod channel and critical safety with operational error of a single rod. The decrease of window damage should also be calculated. Based on this additional information, ADS with reactivity control should be compared with the reference ADS controlled by the power of the accelerator.

Acknowledgements

This work was funded by the Ministry of Education, Culture, Sports, Science and Technology (MEXT) as one of the R&D programs for innovative nuclear systems.

REFERENCES

[1] Tsujimoto, K., *et al*., "Neutronics Design for Lead–bismuth Cooled Accelerator-driven System for Transmutation of Minor Actinide", *Journal of Nucl. Scie. Technol*., 41, 1, pp. 21 (2004).

[2] Kim. Y., *et al*., "Core Design Characteristics of the HYPER System", *Proceedings of the 7th Information Exchange Meeting on Actinide and Fission Product Partitioning and Transmutation*, Jeju, Korea, OECD (2002).

[3] Takada, H., *et al*., "An Upgrade Version of the Nucleon Meson Transport Code", from the JAERI-Data/Code 98-005, Japan Atomic Energy Institute (1998).

[4] Okumura, K., *et al*., *SRAC95; General Purpose Neutronics Code System*, JAERI-Data/Code 96-015, Japan Atomic Energy Institute (1995) [in Japanese].

[5] Alcouffe, R.E., *et al*., *Users Guide for TWODANT: A Code Package for Two-dimensional, Diffusion-accelerated, Neutral-particle Transport*, LA-10049-M, Los Alamos Scientific Laboratory of the University of California (1990).

[6] Croff, A., *ORIGEN2 – A Revised and Updated Version of the Oak Ridge Isotope Generation and Depletion Code*, ORNL-5621, Oak Ridge National Laboratory (1980).

STATUS OF THE CONCEPTUAL DESIGN OF AN ACCELERATOR AND BEAM TRANSPORT LINE FOR TRADE

S. Monti, L. Picardi, C. Ronsivalle, C. Rubbia, F. Troiani
ENEA, Lungotevere Thaon di Revel, 00196 Rome, ITALY
Tel. +39 06 9400 5774, E-mail: picardi@frascati.enea.it

Abstract

The TRADE (TRIGA accelerator-driven experiment) experiment, which is to be performed in the TRIGA reactor of the ENEA/Casaccia centre, involves the coupling of a 140 MeV, 0.3 mA beam that is produced by a cyclotron to a target hosted in the central thimble of the reactor scrammed to subcriticality. A 25-m long beam line was designed to transfer the beam by injecting it from the pool top, taking special care to have very low losses in the TRIGA reactor building where limited shielding of the beam line is possible. The beam transfer line is composed of a matching section (MS), which matches the beam to the following section, and a final bending section (FB), which shapes and directs the beam onto the target. Attention was paid to reduce the number and size of elements of the FB that were immersed in the pool water. Shielding calculations show that a sustainable radiation level is possible with the foreseen beam losses. The paper presents a description of the beam line at the present stage of the project.

Introduction

The TRADE (TRIGA accelerator-driven experiment) experiment, which is to be performed in the TRIGA water reactor of the ENEA/Casaccia centre, involves the coupling of a 140 MeV, 0.3 mA beam that is produced by a cyclotron to a target hosted in the central thimble of the reactor scrammed to subcriticality [1,2].

The final layout of the TRADE experiment is shown in Figures 1 and 2. It is characterised by having the cyclotron in a shielded area, as small as possible, located nearby the TRIGA building. The cyclotron is mounted on concrete columns and steel supports so that the beam output is at the same level as the top of the TRIGA pool. Cyclotron injection occurs from the bottom so that maintenance and modifications to the injection line of H- ions are easy. The cyclotron output beam is transferred from one building to the other via a section of the transfer line that is shielded by a massive shielded tunnel. This is a long straight line, with a number of quadrupoles that match the beam to the final bending system. The two-dipole, three-quadrupole achromat bends the beam 90 from horizontal to vertical direction. It is partially immersed in the pool's water for shielding reasons. The target is ~4 m down the last dipole. The quadrupoles preceding the final bending achromat can be used to change the spot size and shape on the target. The best effort was made in the design to restrict the beam losses in the TRIGA building, where the shielding should be limited due to space and weight constraints.

Two beams outputs, 180 apart, are foreseen on the cyclotron. The first beam output is for the TRADE experiment, while the second is for the commissioning phase in testing the TRADE optics and the target. The second beam output will also be used for other cyclotron applications when the TRADE experiment is completed.

The following illustrates the preliminary design of the beam transport line (BTL) of the TRADE experiment. The report will cover the design criteria of the BTL, the optics calculations and a preliminary error study on beam line elements.

Accelerator characteristics

The chosen cyclotron was an H- cyclotron with stripping extraction. This cyclotron was selected because it is considered the most affordable solution when taking into account the constraints related to the cost and the relatively short time scale for the implementation of the TRADE experiment. Moreover, the room temperature H- cyclotron relies on a well-proven technology and can be regarded as an evolution of typical H- machines for radioisotope production (Ep ~30-60 MeV). It should be noted, however, that the performance both in terms of energy and intensity for the TRADE accelerator is significantly higher with respect to commercially available units at the present time.

One of the most relevant features of the accelerator is the need for flawless continuity of the beam to be injected in the subcritical subassembly. Therefore, all active components of the accelerator and the beam transport must ensure the utmost reliability during operation. The simple cyclotron chosen in our design is characterised by an extremely small number of active, very reliable components as compared to the number of elements and size of a LINAC accelerator with equivalent performance.

An indicative list of parameters for the TRADE cyclotron is given in Table 1. The particular cyclotron elements that will impact the TRADE beam transport line, apart from general characteristics, are injection and extraction (as with most accelerators). An external H- ion source will operate below the cyclotron. Injection will be performed from the bottom via an injection vertical line equipped with focusing items. A magnetic inflector will bend the beam horizontally into the cyclotron mid plane. At

the operational currents (below 500 mA), space charge effects, which are important mainly in the injection line, are expected to be controlled. A modest, tolerable degradation of the beam characteristics is expected from the extraction H- strippers, similar to those reliably used in existing and commercial cyclotrons. Therefore, a clean beam with small emittance (1-4 p mm mrad, normalised) is expected out of the cyclotron. In order to improve the brilliance performances of the output beam, a pre-bunching and/or chopper section can be used to limit the emittance degradation during acceleration of the cyclotron. The output beam is expected to be characterised by even better performances than required in terms of stability. It will be shown in the following that energy spread and emittance are considered not as limits but as reachable, comfortable values that can make the BTL tuning easy. In Figure 1, a sketch of the cyclotron can be seen. It has been done not for imposing a construction strategy to the supplier but for the sake of elaborating a realistic TRADE layout.

Figure 1. Section of the cyclotron and TRIGA buildings

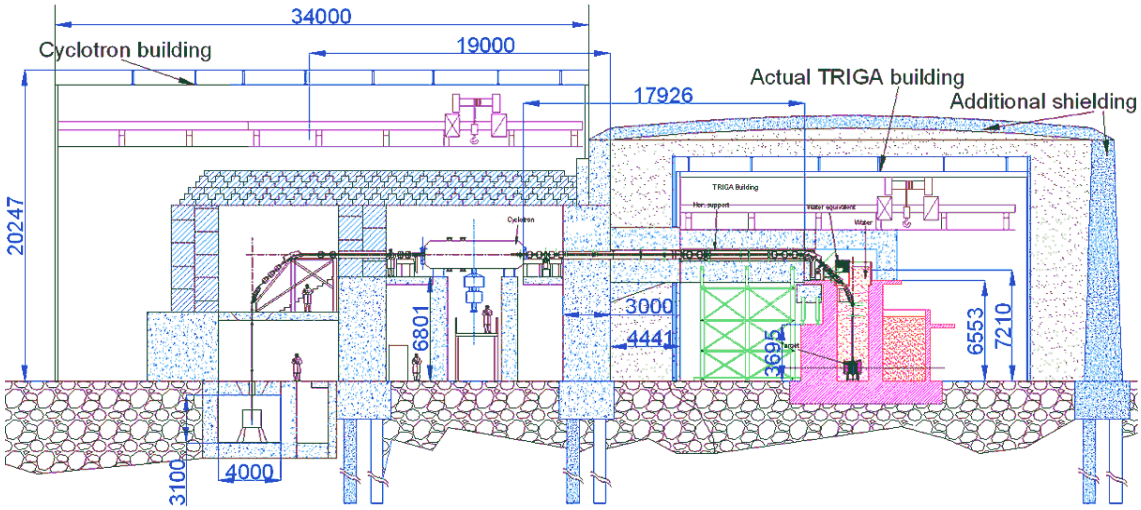

Figure 2. Layout of the TRADE complex

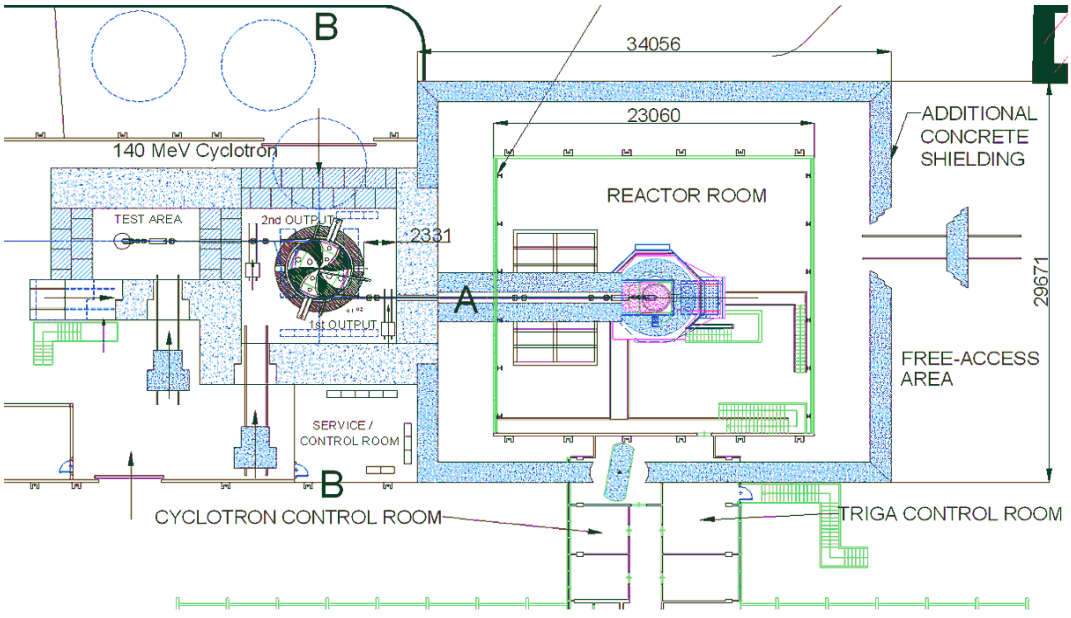

Table 1. Parameters of the TRADE cyclotron

Parameter reference	Value
Output energy	140 MeV
Abs. max. current	500 mA
Normalised transverse emittance at 2s	< 4 p mm mrad
Energy spread	< 1 MeV (90% beam)
Energy precision	< 1 MeV
Beam dimensions	= 7 mm (FWHM in both planes)
Beam temporal distribution	CW; Pulsed (30-1 500 msec), 0-10 Hz
Injected particles	H-
Number of sectors	4
Extraction radius	2.2 m
Cyclotron outside diameter	6.5 m
Total weight	300-400 tons
Extraction	Stripping (carbon foil 70 mg/cm^2)
Beam losses internal to the cyclotron	= 4%

Target characteristics

The target body is described in another paper presented at this workshop. It is machined from massive tantalum. The target has a conical shape, with an input diameter of 49 mm and a useful length of 38 cm. The target thickness in the active zone has been defined in order to stop as much as possible the protons inside the target material. The upper part of the target body is connected to the beam line. The target is surrounded by flow guides that aim to direct the water flow around the body in order to assure an efficient and effective cooling of this critical component. The maximum power manageable by this target is 30-40 kW.

The neutron distribution in the TRIGA core generated by source protons, as well as the power distribution along the target itself, are dependent on the beam shape/dimensions and must comply with requirements of the neutronics for the TRIGA core. Therefore, a certain commitment is made on the beam transport line and diagnostics in terms of beam centroid precision (– 2 mm) and beam dimensions (s = 8.8 – 2 mm). The beam shape is supposed to be Gaussian in simulations, although the real beam distribution is obviously unknown at the moment.

A backup solution of the target is under study with the aim of relaxing the precision requirements and target tolerances.

Beam transport line description

The beam transport line has two main purposes: 1) to rotate the beam direction from horizontal to vertical (90); 2) to match the beam emittance from the cyclotron to the precisely circular shape of the size required by the subsequent target.

The beam transport has been drastically simplified with respect to previous designs [3], reducing integrated bending power to the minimal 90 required by the difference in orientation of the horizontal accelerator and the vertical access tube to the spallation target. The actual version of the TRADE beam line design (Figure 3) includes 12 quadrupoles and two magnets. In particular, the design is comprised of three main sections: a matching section (MS) composed of four quadrupoles for matching the

cyclotron beam to the rest of the BTL, a straight transfer line section (STL) composed of five quadrupoles and a final bending section (FB) that bends the beam 90 downward and is composed of a couple of 45 dipoles with three quadrupoles in between.

Figure 3. Layout of the TRADE BTL

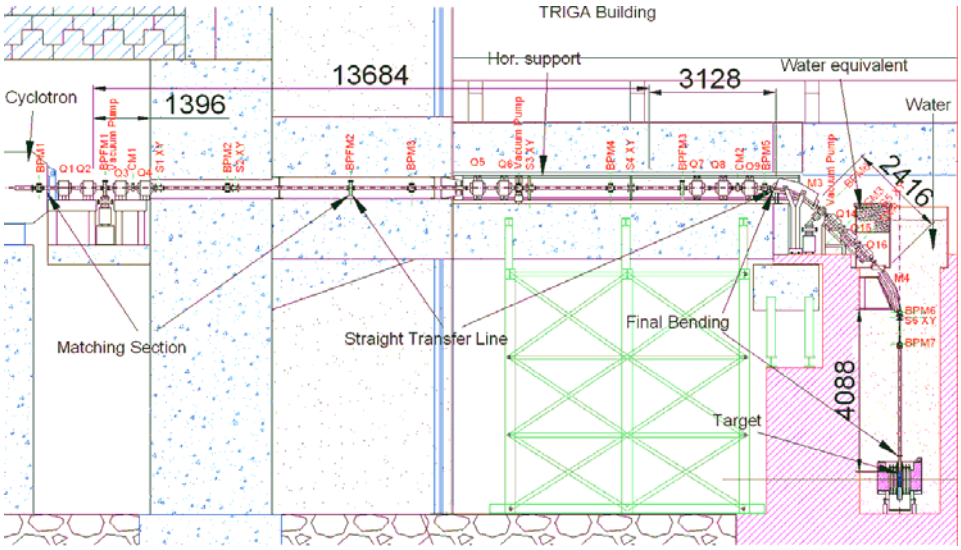

Beam line optics were designed using the TRACE3D code [4]. For beam dynamics calculations, TURTLE [5] and TRACEWIN codes [6] were used. The actual output beam characteristics, namely emittances and other Twiss parameters in both planes, are dependent on actual performance of the accelerator and cannot be entirely defined at design stage. As previously mentioned, they are primarily related to the ion source and injection line performances and to spread due to scattering in the 70 mm carbon stripper foil. A conservative estimate for such a normalised emittance is in the interval between 1-4 p mm mrad (Table 2). The corresponding actual emittances for 140 MeV are in the range of 1.8 to 7.2 p mm mrad. Since the stripper foil gradually deteriorates over time and periodically needs to be replaced, the precise value of vertical and horizontal emittances may vary slightly during operation. On the other hand, the spot size of beam at the target must be very stable and precise at all times. The beam transport must therefore be capable of tracking and continuously adjusting with high precision the relation between the beam emittances in each of the two planes and the size of the final spot.

Table 2. Beam transport line data

Energy	140 MeV	
Normalised emittance, p mm mrad	1	4
Transverse emittance; unnormalised, = 4 ϵ_{rmsun}, p mm mrad	1.8	7.2
ax, ay	-9.7, -9.7	-2.2, -2.2
bx, by mm/mrad	27.2, 27.2	6.8
xmax, ymax, mm	7, 7	
xpmax, ypmax, mrad	2.5, 2.5	
Longitudinal emittance, deg-keV	4 700	
aw	0	
bw, deg/KeV	0.022	
Bunch half-width (RF at 70 MHz)	10	
Energy spread half-width (keV)	470	
Momentum spread half-width	0.179%	

The design criteria for the final part of the BTL were as follows:

- Achieve a circular spot of nominally 40 mm in diameter at the target spot.
- Double achromatic final bending (i.e. D = D'= 0 at output).
- Point-to-point transport between the centres of M3 and M4.
- Minimize the beam sizes at the centre of dipoles M3 and M4 in order to reduce the size and, therefore, the beam losses in the gaps.
- Symmetric expansion in the final drift.
- The two dipoles, each of 45 , have been chosen with a relatively conservative magnetic field of 1.3 Tesla, corresponding to a curvature radius of ~1.36 m.

Additional constraints came from the difficulty of placing magnetic elements in the tiny concrete tunnel through the walls of the cyclotron building. As a result, quadrupoles are present in the cyclotron vault and in the TRIGA building. Here the beam transport must occur at very low losses. The beam line elements are mounted on a support leant on the cyclotron building at one end and on top of the TRIGA pool at the other. The shielding elements are mechanically independent, weighing on a separated structure. This arrangement is considered the best solution for alignments.

Another aim of the BTL design was to include as few elements as possible but, at the same time, to generate an envelope through the BTL. This envelope should be as little as possible depending on the emittance value in the foreseen range of emittances (1-4 p mm mrad), especially in the part of the BTL that extends in the TRIGA building (STL). This task was exploited by optimising the final bending, which includes an achromatic 90 deviation module (composed of two 45 dipoles and three quadrupoles Q14, Q15 and Q16 inserted in the drift section between the two dipoles to control the beam envelopes and to cancel the dispersion function), and by trying to adjust the remaining part of the BTL. Some trials with only six QP in a straight line (two at the cyclotron output, two before the FB and two in between) were encouraging but not fully satisfactory as the beam size increased just in the STL when the emittance was close to or larger than 4 p. [See Figure 4(a) where the 2s beam envelope is drawn along the whole BTL in the two cases of 1, 4 and 6 s mm mrad.]

Increasing the number of quadrupoles from six to nine in the region preceding the FB resulted in a better envelope with less envelope variation in the emittance range. This solution, slightly more expensive, foresees four quadrupoles at the cyclotron output that generate a round beam and double waist in P_o [Figure 4(b)], and five quadrupoles in the STL right before the first FB dipole. As shown in Figure 4(b), the beam envelope shows no significant degradation in the explored emittance range.

The six quads solution was indeed considered a source of possible concern as the beam size increases from 1 to 4 p mm mrad, the beam clearance reduces and the envelope shape becomes less regular. The beam pipe radius, which needed to be at a safe value for minimising losses, is considered above six sigmas, and a beam pipe of 63 mm inner diameter is considered a good value for the quadrupole apertures (and consequently weight) as well as for the other items (steerers, BPMs, etc). The solution with nine quadrupoles in absence of errors gives a beam clearance of ± 6 sigmas in the 1-4 p mm mrad emittance range.

Figure 4. TRACE3D code outputs: envelope (2s) along the BTL tuned for 1, 4, 6 p mm mrad

(a) BTL with six quadrupoles before FB; (b) BTL with nine quadrupoles before FB

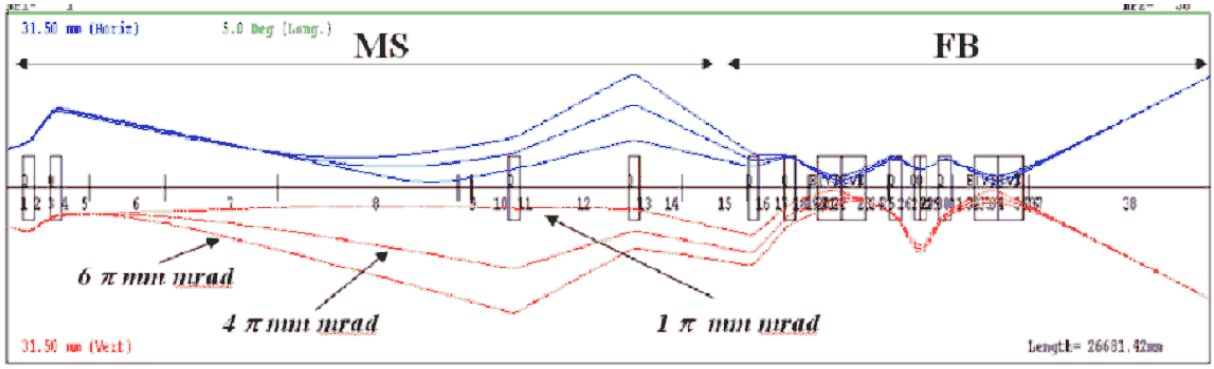

(a)

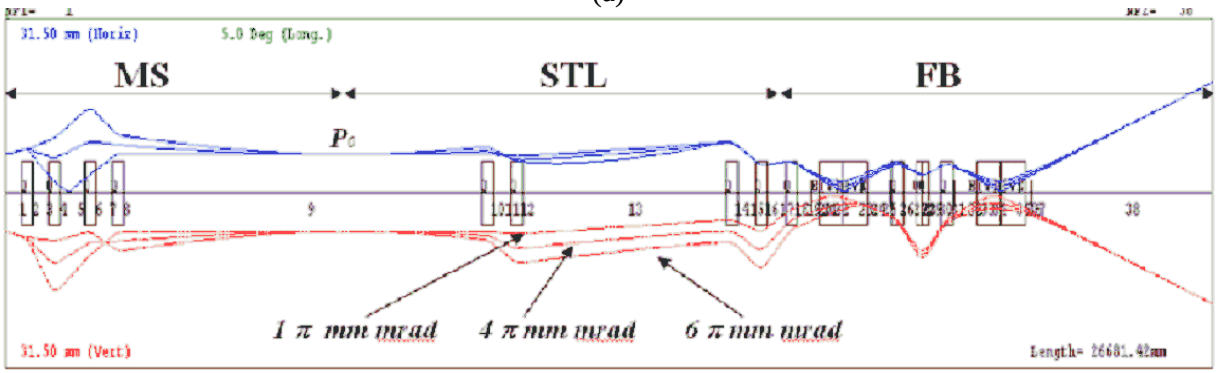

(b)

In the whole range of emittance values, the spot diameter dimension of 40 mm in the middle of the target is obtained only by adjusting the gradients in the MS and STL quadrupoles while keeping the same values in the elements of the FB section (Figure 5).

For a given value of emittance, different input beam transverse phase space characteristics can be matched by adjusting only the four quadrupoles in the MS.

At the point in the BTL where MS ends and STL begins, the beam is round with a diameter of ~14 mm (at 90% beam). There, a profile monitor is placed to check the setting of matching quadrupoles.

The quadrupoles length is 250 mm for the first nine quadrupoles and 300 mm for the three quadrupoles placed between the two dipoles of the FB section. Tuning capability of the BTL was also studied for different values of input beam size and maximum angular divergence. In particular, the case of a round input beam with a diameter of 14 mm was studied with a range of maximum angular divergence of 2.5-5 mrad and compared with an elliptical beam of the same area. In the whole range of input beam parameters, the maximum gradient is below 12 T/m for the first nine quadrupoles and below 15 T/m for the three quadrupoles placed between the two dipoles in FB (maximum value in Q15).

The two dipoles, each of 45 , were chosen with a relatively conservative magnetic field of 1.3 Tesla, corresponding to a curvature radius of ~1.3 m.

Figure 5. Quadrupoles gradient values along the BTL tuned for 1, 4, 6 p mm mrad

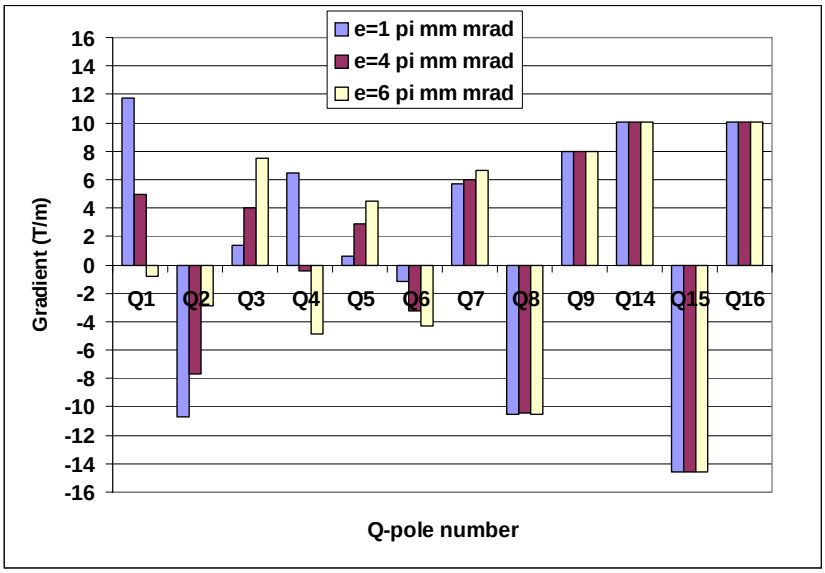

The second dipole M4 (see Figure 3) is immersed in the water pool of TRIGA in order to shield the neutron back-streaming from the core through the beam pipe (50 mm diameter) by ~2 meters of water. In the present layout, in order to limit the elements exposed to insulation problems due to water in the reactor pool, a special cup has been introduced to keep the quadrupole triplet Q14-Q15-Q16 from being immersed. However, the replacement (locally) of water with an equivalent radiation-absorbing material (possibly polyethylene) is foreseen.

In addition, the BTL has a full "zoom" capability for a wide variety of beam configurations, always keeping a round beam shape at the target. More precisely, this is achieved by setting the values in the quadrupoles Q1-Q9, while the values of the final bending elements have been kept constant, pre-set such as to produce a "point-to-point" transport between the centres of M1 and M2 and a minimum in the beam dimension at the centre of the two dipoles M1 and M2. The final size of the ratio a/b is kept constant for both transverse phase planes.

In order to elucidate the method, three possible geometries are shown in Figure 6, all for a normalised emittance of 1 p mm mrad. The magnifying effect at the position of the target is quite evident over very large changes in the parameters.

Figure 6. BTL "zoom" capability with variation 1:2:4 in the final spot size at the target for an input normalised emittance of 1 p mm mrad. The resulting spot sizes are respectively 1, 2, 4 cm.

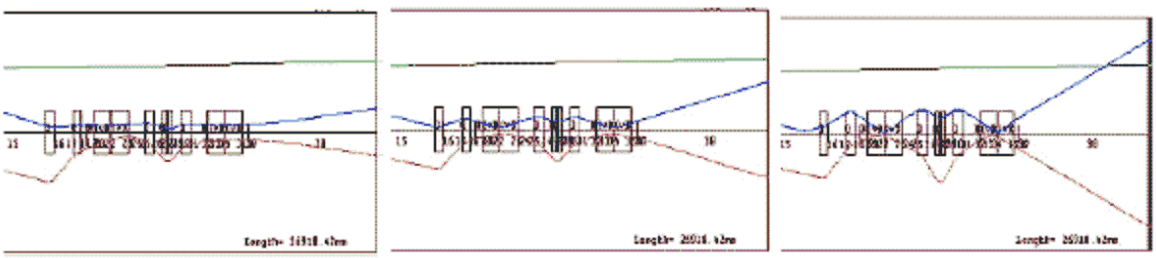

To check for beam losses, a beam dynamics calculation was performed with TURTLE using as input a Gaussian distribution truncated at 4ѕ. We found zero losses for a perfectly tuned beam line without misalignment errors for an internal diameter of the beam pipe equal to 63 mm and a gap equal to 27 mm in the first FB dipole and 21 mm in the second FB dipole.

In order to take into account beam line errors, a preliminary study using the TRACEWIN code was performed. This study was used for designing and checking the correction scheme (steerers and beam position monitors). The diagnostics were based, as is usually the case for beam transport lines, on beam position monitors for the centroid detection, on current transformers for beam current/losses checks, and on beam profile monitors for beam size checking at strategical points. In Figure 3, the precise location of the beam line diagnostic elements and of the steering coils is shown. Three beam profile monitors were used (for tuning the BTL with the cyclotron in pulsed mode at low duty factor): the first one after the first two quadrupoles, the second one at the end of MS where a 14 mm diameter round parallel beam must be found, and the third one just before the last triplet of quadrupoles in STL.

In the calculations, an amplitude error for the alignment of the magnetic elements (quadrupoles and dipoles) of −0.5 mm and a BPM accuracy of 0.1 mm was assumed. A correction set constituted by 6 XY steerers coupled to beam position monitors that measure the centre in both planes was effective to correct element misalignments by providing centroid stability at target of −1 mm (Figure 7).

Figure 7. RMS envelopes computed by TRACEWIN with corrections off and on. Dx = Dy = + 0.5 mm on all the magnetic elements. The BPMs are indicated in red.

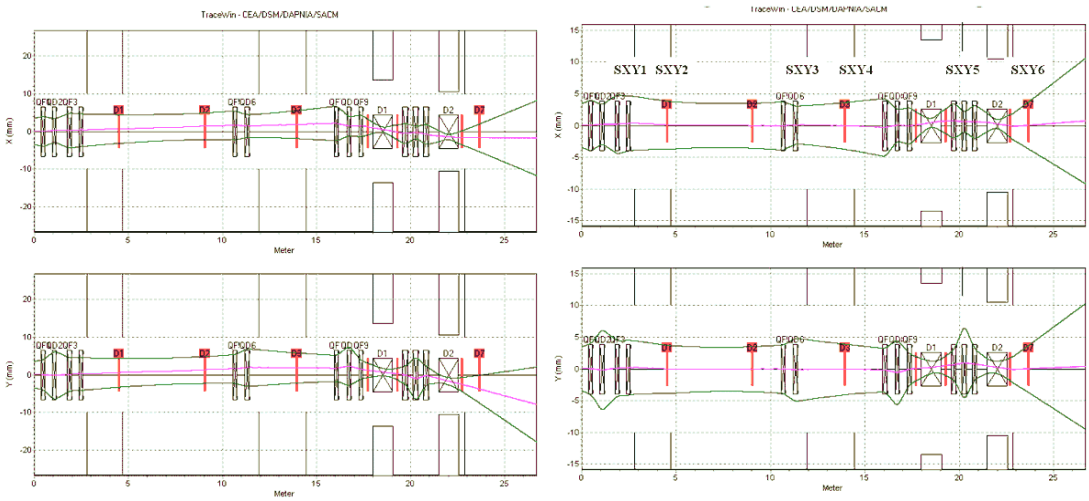

The RMS value of the residual orbit along the BTL is plotted in Figure 8. The figure is the result of statistics over 100 beam lines where the magnetic element errors have an equivalent probability to be between -0.5 mm and +0.5 mm. We note that the RMS jitter centroid position at target was below 1 mm and 2.7 mm in Q15. These are completely reasonable values, which are within the specifications.

Checking the centroid position at target will not be an easy task in the experiment. The last dipole and the following diagnostics and steering elements are immersed in the TRIGA pool. A specific design of the elements in course will be required. The last BPM will be placed about 1 m after the last dipole. Specifically designed diagnostics will be needed for checking the beam footprint on the target. For this task, the possibility to “see” the target via an infrared camera and a suitable arrangement of mirrors is under investigation. By these diagnostics, a measure of the beam distribution could be obtained and, once calibrated, a crude measure of the net current as well.

Figure 8. Residual orbit RMS value along the BTL

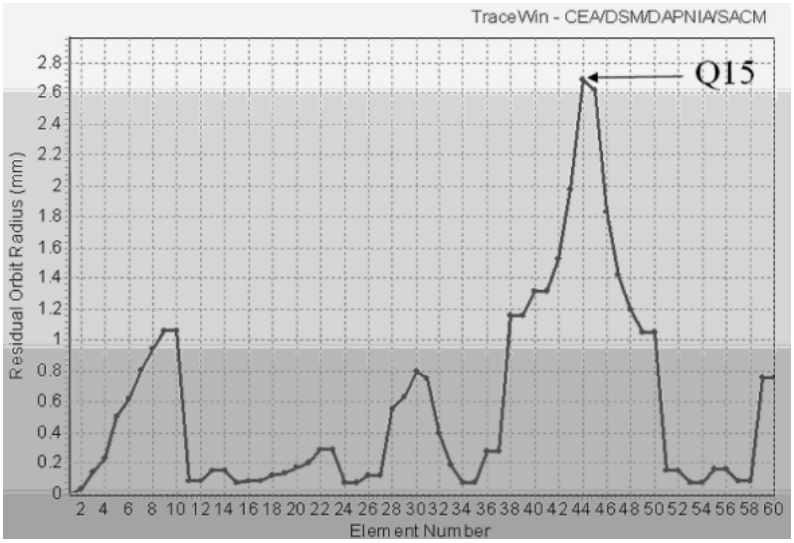

Conclusions

A beam transport line for the TRADE experiment has been designed and defined in its final configuration. It is sufficiently flexible for accepting 1 to 6 p mm mrad beams and for focusing the beam on a target with a zoom capability between 1 and 4 cm or more in diameter. A diagnostics/ correction scheme was studied, with satisfactory performances. Problems still to be solved are the design of beam line elements that are immersed in the TRIGA pool and the diagnostics needed to monitor the footprint of the beam on the target.

REFERENCES

[1] Rubbia, C., *et al*., *TRADE: General Lay-out of the Experimental Facility*, TRADE Technical report, March 2004.

[2] Monti, S., *et al*., "Status of the TRADE Experiment", this workshop.

[3] Picardi, L., *et al*., "Design of the Proton Beam Line for the TRADE Experiment", *Proceedings of AccApp2003*, San Diego, California, June 2003.

[4] Crandall, K.R., D.P. Rushtoi, *TRACE3D Documentation*, LA-UR-97-886.

[5] Brown, K.L., Ch. Iselin, D.C. Carey, *Decay Turtle*, CERN 74-2 (1974).

[6] Duperrier, R., N. Pichoff, D. Uriot, "CEA Saclay Codes Review", ICCS Conference, Amsterdam (2002).

ESTIMATION OF SOME CHARACTERISTICS OF THE CASCADE SUBCRITICAL MOLTEN SALT REACTOR (CSMSR)

A.M. Degtyarev, A.K. Kalugin, L.I. Ponomarev
Russian Research Center – Kurchatov Institute, Russia

Abstract

Characteristics of an ADS burner of minor actinides (MA) were estimated, taking into account the following initial assumptions: 10 MW proton accelerator-driver (1 GeV, 10 mA), two-zone cascade subcritical reactor with $\Delta k_{eff} = 0.05$, central zone of neutron multiplication and transmutation zone on the basis of NaF-ZrF_4 molten salt. Such a scheme reduced by three times the power of the accelerator-driver at the same blanket power. Reactor power was obtained equal to 800 MWth; its burning effectiveness was ~50 kg MA per year or the MA production of five thermal rectors of equal power. The main neutron physics characteristics of the reactor were calculated, including power distribution, reactivity effects, actinides burn-up, thermo-hydraulics of zones, etc.

Introduction

In the last decade, ADS burners have been considered as one of the possible candidates for the transmutation of minor actinides (MA). The natural requirements for such a burner are high efficiency and adjustment to the nuclear fuel cycle. The first requirement needs a high neutron flux and a high unit power of the ADS burner. The power of the proton accelerator-driver (W_a) is related to the blanket power (W_b), with subcriticality Δk by the equation:

$$W_a \approx 0.6\Delta k \cdot W_b \text{, i.e. } W_a \approx 30 \text{ MW at } W_b = 1 \text{ GW.}$$

To reduce W_a it was suggested to use the cascade scheme of the neutron flux amplification [1], which is based on the idea of a two-core reactor with unilateral thermal neutron flux [2].

Cascade amplification factor A is equal to [3]:

$$A = 1 + \frac{k_{21} - \delta}{\Delta k + 2\delta}$$

$$\delta = (k_{21} \cdot k_{12})^{1/2}$$

$$\Delta k = \frac{\Delta k_1 + \Delta k_2}{2} - \sqrt{\frac{(\Delta k_1 - \Delta k_2)^2}{4} + \delta^2}$$

where $\Delta k = 1 - k_{eff}$, $\Delta k_1 = 1 - k_{11}$ and $\Delta k_2 = 1 - k_{22}$ are the subcriticalities of a reactor and C-1 and C-2 cores, respectively, while k_{21} and k_{12} are the probabilities of the forward and back neutron flow between C-1 and C-2 cores (see Figure 1).

Figure 1. The cascade scheme of neutron flux amplification

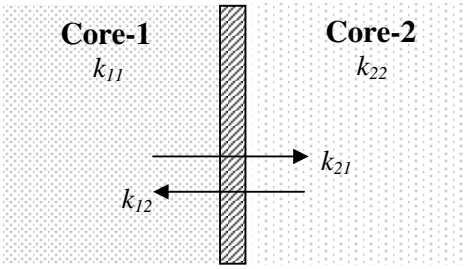

At $\Delta k_1 \approx \Delta k_2$ and $k_{12} << \Delta k << 1$, $\Delta k \approx \Delta k_1 - \delta$ and $A \approx 1 + \frac{k_{21}}{\Delta k}$ necessary accelerator power is reduced in A where $W_a \rightarrow W_a/A$.

The experimental and theoretical justification of the cascade principle was performed in the framework of the ISTC Project #1 486 [4].

The second requirement for ADS burners is adjustment to existing nuclear fuel cycles. At the moment, there is no technology for the fabrication of fuel elements with high concentrations of MA and thus it is natural to use the idea/experience of the molten salt reactor [5]. Preliminary studies of this approach have been reported in several publications [6].

In the text to follow we will present the design of an ADS burner, which combines two ideas – the cascade scheme of neutron flux amplification and molten salt fuel enriched by MA. The main characteristics of this ADS burner will be considered, in particular: ***neutronics, thermo-hydraulics, molten salt fuel and technological restrictions*.**

Main physical assumptions and reactor composition

The ADS burner under consideration consisted of the proton accelerator of power W_a = 10 MW (energy E_a = 1 GeV, current I_a = 10 mA) and the two cores subcritical reactor (blanket) with subcriticality $\Delta k = 1 - k_{eff} = 0.05$. Blanket consisted of two cores (see Figure 2), the first being Core-1 (C-1, zone of cascade amplification, ZCA), which was the neutron production target (three units). The second core was Core-2 (C-2, transmutation zone, TZ), which consisted of molten salt NaF-ZrF_4 with the melting point T_{mel} = 510°C. In comparison with traditional MSR salt LiF-BeF_2, the salt NaF-ZrF_4 has higher solubility of MA and Pu [4]. The zone of cascade amplification C-1 was filled by the Pb-Bi eutectic and had a two-layer structure (Figure 3) – an internal layer consisting of Pu fuel rods with ^{237}Np ends and an outer layer consisting of ^{237}Np (Figure 4). The central region formed by Pu fuel rods had k_∞ = 2.4 and a fast neutron spectrum. ^{237}Np fuel rods around a Pu layer multiplied the fast neutron flux and blocked the decelerated neutron backflow from the transmutation zone C-2 to the neutron generation zone C-1.

Both layers (Pu and ^{237}Np) were divided from the transmutation zone C-2 by the Pb-Bi eutectic, which decelerated neutrons moving from C-2 to C-1. In the C-1 structure, the Pb-Bi eutectic was used simultaneously as the neutron production target, coolant and deceleration ventile between C-2 and C-1.

The geometry of C-1 was optimised: Pu layer radius was 15 cm, ^{237}Np layer radius was 20 cm and Pb-Bi ventile zone radius was 37 cm. Transmutation zone C-2 had a radius of 170 cm and a height of 230 cm. It consisted of homogenous molten salt NaF (53%)/ZrF_4 (47%) with the fissile nuclides Pu (2.9 mol. %) and Np + MA (1 mol. %). This fuel content differed slightly from the MA/Pu ratio of the spent fuel composition presented in Table 1 – VVER spent fuel irradiated up to 40 GW d/t cooled 30 years and PWR spent fuel irradiated up to 33 GW d/t cooled 10 years. To increase the burn-up of MA, we enriched the MA fraction in the start fuel from 16% (in irradiated VVER fuel) to 25%. We considered two options for feeding the ADS burner during operation – 1) VVER irradiated fuel and 2) fuel composition with MA fraction increased 2× (ratio Pu/MA/Np was 73.5/22/4.5).

Table 1. Composition of VVER and PWR irradiated and cooled fuel

Nuclide	Relative concentration %	
	VVER	PWR [10]
^{237}NP	5.2	5.2
^{238}PU	1.4	1.4
^{239}PU	54.7	51.5
^{240}PU	20.0	23.8
^{241}PU	3.0	7.9
^{242}PU	4.5	4.8
^{241}AM	9.9	5.2
^{243}AM	0.9	0.9
^{243}CM	<0.01	0.0
^{244}CM	0.1	0.0
^{245}CM	0.02	0.0

Figure 2. CSMSR structure: 1 – reflector; 2 – TZ hull; 3 – TZ; 4 – ZCA unit

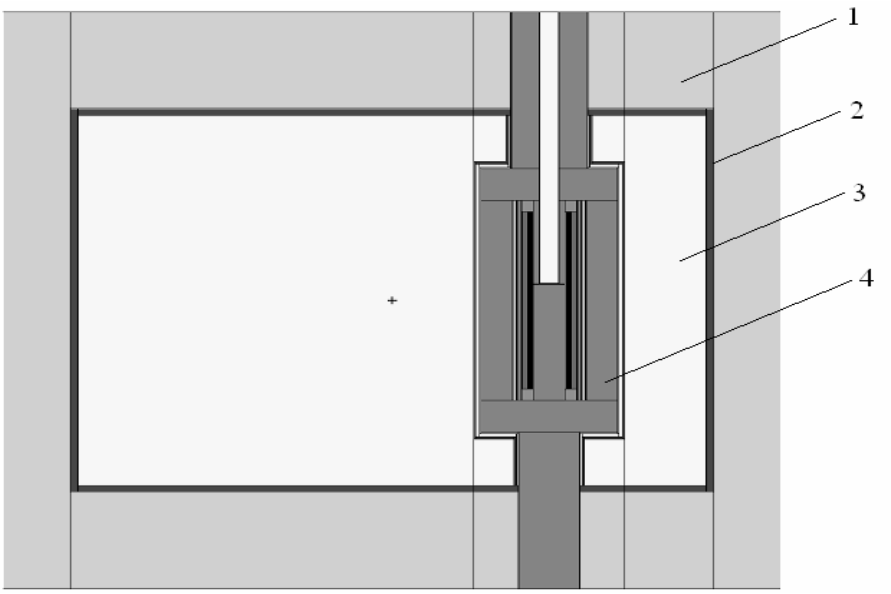

(a) Vertical section

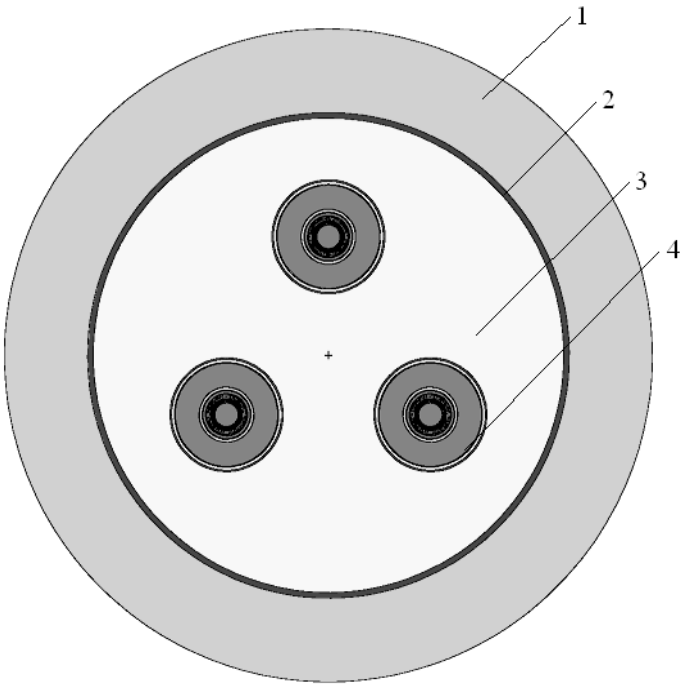

(b) Horizontal section

Figure 3. ZCA structure

1 – proton tube; 2 – Pu zone; 3 – Np zone; 4 – Pu fuel rods ending with Np;
5 – Pb-Bi eutectic; 6 – ZCA cladding; 7 – outlet and inlet tube for Pb-Bi eutectic

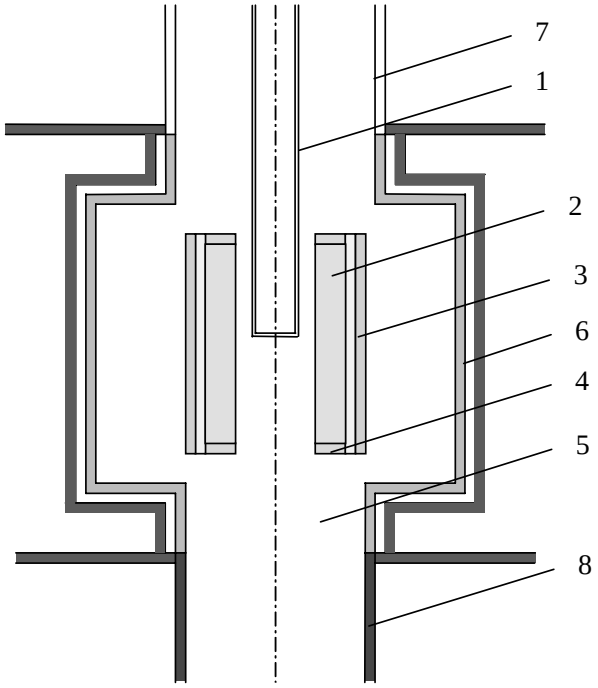

Figure 4. Structure of ZCA fuel rod zone

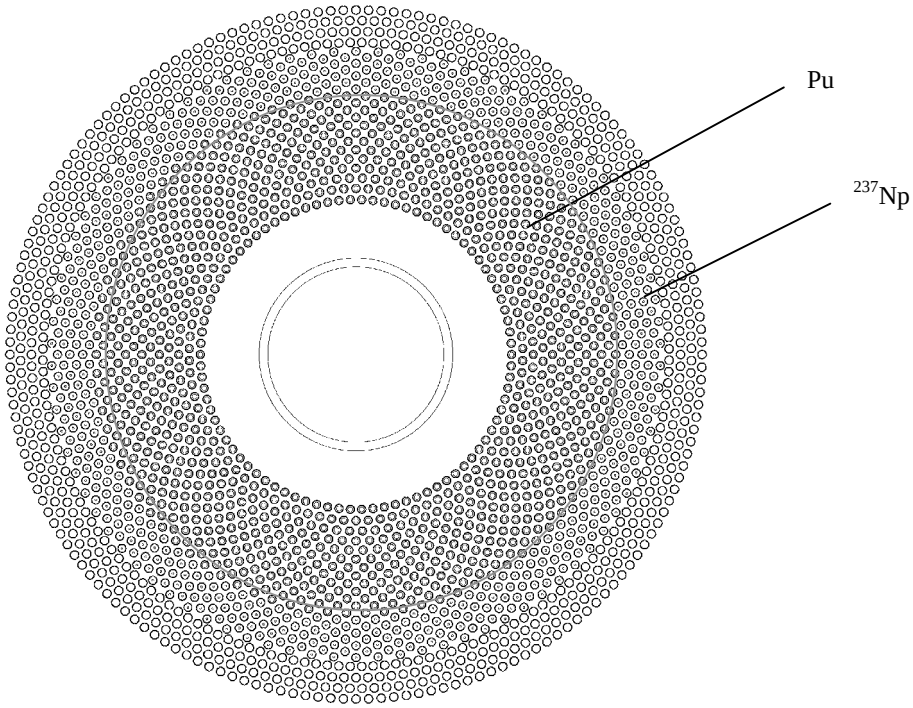

Results of calculations

Calculations were performed using MCNP [7] code coupled with burn-up module ORIGEN [8] and MCU [9] code. The initial calculation data are presented in Table 2.

Table 2. Initial data for calculations

Parameter	Value
Core volume	17.88 m^3
Primary circuit volume	21.83 m^3
TZ power	645.6 MWth
Average overall circuit power density	29.6 Wth/cm^3
Neutron flux	5×10^{14} n/(cm^2s)
Actinide losses during reprocessing	0.1%
Core reprocessing period	1 200 days
Annual load	300 days

Effectiveness of MA incineration during operation period was defined as: (initial MA loading content + MA feeding during operation) – (final MA amount). We accepted a 50-year operation period.

The calculations were carried out for two options of the feeding fuel noted above. Table 3 presents our results in comparison with incineration characteristics of homogenous critical burner SPHINX [10] in an equilibrium regime.

Table 3. Incineration CSMSR characteristics compared to SPHINX

Parameter	CSMSR		SPHINX
	VVER spent fuel Np/Pu/MA:5.2/84/11	VVER spent fuel with increased MA fraction Np/Pu/MA:4.5/73.5/22	
Molar concentration of actinides in salt* (%)	6	7	0.75
Mass of actinides in primary circuit* (kg)	9 851	11 868	3 600
Specific mass of actinides in primary circuit* (kg/MWth)	12.3	14.8	3.0
Actinides composition U/Np/Pu/Am/Cu* (%)	1.7/2.1/83.3/9.5/3.4	2.1/2.1/79.6/13.0/3.3	0.4/1.5/72.5/7.5/18
Incineration capacity Pu/MA/Np** (kg/year)	147/26/20	123.4/51/19.3	~323.3/25.7/16
Specific incineration capacity Pu/MA/Np** (kg/TWhth)	25.6/4.5/3.5	21.3/8.9/3.4	~37.3/2.9/1.8

**End of CSMSR operation*
***Evaluations for SPHINX are from the data presented in [10]*

According to the results of the calculations, CSMSR requires larger specific fuel loading, which arises mainly from the homogeneous structure of the core and the rather low specific reactor power. However, CSMSR does have advantages in MA incineration. VVER irradiated fuel 30 years cooled contains 32.4 kg MA and 15.2 kg Np. Thus, one CSMSR of 800 MWth can support up to 1.6 VVER of 1 GWe, i.e. approximately five thermal reactors of equal power.

Neutronics and thermo-hydraulic characteristics

- A 10 mA accelerator-driver with power W_a = 10 MW can feed an ADS burner with power W_b = 800 MWth. (For comparison, an ABC reactor [11] with power W_b = 711 MWth needs accelerator power W_a = 20 MW).
- Average neutron flux in transmutation zone is 5×10^{14} n/cm^{2}s.
- Cascade amplification factor is $A \approx 3$.
- Power distribution ZCA/TZ is 19/81.
- Specific power releases in ZCA and TZ are $q_v \approx 490$ kW/litre and $q_v \approx 30$ kW/litre, respectively.
- Non-uniformity of TZ power distribution is Kz = 1.5 (axial) and Kr = 1.9 (radial).
- Reactivity effects of ZCA are similar to fast neutron reactors having advantages due to the strong negative void effect.
- Reactivity effects of TZ are also favourable. Positive reactivity effect takes place only at salt freezing, but even in this case with ADS subcriticality of $\Delta k_{eff} = 0.026$.
- Burn-up 9% of ZCA is achieved in 0.8 years between ZCA reloading and can be compensated.

Conclusions

There are several conclusions from the performed calculations.

- A CSMR burner with the power of 800 MWth can incinerate ~50 kg of minor actinides per year, i.e. the MA produced by approximately five thermal reactors of equal power.
- Cascade scheme can reduce by several times the power of an accelerator-driver. ADS power W_b = 800 MWth can be achieved at accelerator power W_a = 10 MW.
- Restriction $\Delta k_{eff} = 0.05$ should be analysed more carefully to enhance the effectiveness of the ADS burner.
- A disadvantage of CSMSR is the intermediate neutron spectrum in TZ and as a consequence the high ratio of Pu/MA = 4/1.
- To enhance the effectiveness of an ADS burner it is necessary first of all to enhance the cascade amplification factor A and to reduce the ratio Pu/MA.

REFERENCES

[1] Kolesov, V.F., S.K. Shtarev, V.Kh. Khoruzhiy, *et al*., "Transmutation Efficiency Calculation in the Blanket on Melted Salts with Central Neptunium Target", International Conference on Accelerator-driven Transmutation Technologies and Application, *AIP Conference Proceedings*, 346, Las Vegas, NV, 1994, Woodbury, New York, 1995, pp. 569-574.

[2] Borst, L., "The Convergatron, a Neutron Amplifier", *Phys. Rev*., v107, No. 3, pp. 905-907 (1957).

[3] Kolesov, V.F., *Aperiodical Impulse Reactors*, RFNC-VNIIEF, Sarov (1999) [In Russian].

[4] *Experimental and Theoretical Justification of the Cascade Scheme of the Subcritical Molten-Salt Reactor for Transmutation of Long-lived Radioactive Wastes of the Nuclear Fuel Cycle*, ISTC Project #1486, Final report (2004).

[5] MacPherson, H., "The Molten Salt Reactor Adventure", *Nuclear Science Engineering*, 90(4), pp. 374-380 (1980).

[6] Vasiliev, A.V., P.N. Alekseev, A.A. Dudnikov, *et al*., "Features of Cascade Subcritical Molten Salt Reactor-Burner of Long-lived Radioactive Wastes", Int. Conf. GLOBAL 2001, Paris, France, 9-13 September 2001.

[7] Vasiliev, A.V., P.N. Alekseev, A.A. Dudnikov, *et al*., "Conceptual Development of Molten-Salt Reactor-Burner of Minor Actinides", *Proceedings of the International Conference on the New Frontier of Nuclear Technology: Reactor Physics, Safety and High-performance Computing*, PHYSOR 2002, 7-10 October 2002, Seoul, Korea.

[8] *MCNP – A General Monte Carlo N-Particle Transport Code, Version 4B*, J. Briesmeister, ed.

[9] *ORIGEN 2.1 – Isotope Generation and Depletion Code – Matrix Exponential Method*, ORNL, RSIC Computer Code Collection, CCC-371, August 1996.

[10] The MCU/REA Code with Data Library DLC\MCUDAT-2.2, *Voprosy Atomnoy Nauki i Techniki*, Ser. FYaR., Issue 3, c. 55-62 (2001) [In Russian].

[11] Szieberth, M., J. Kophazi, B. Yamaji, *et al*., MOST-WP2&3 Reactor Physics Study, Design Review and Nominal Operating Condition, Non-proliferation Issues (2003).

[12] Cowell, B.S., R.A. Krakowski, C.A. Beard, J.J. Buksa, J.W. Davidson, M.H. Fontana, W.C. Sailor, M.A. Williamson, *Accelerator-based Conversion (ABC) of Weapons Plutonium: Plant Layout Study and Related Design Issues*, LA-UR-95-1096, March (1995).

CFD ANALYSIS OF THE HEAVY LIQUID METAL FLOW FIELD IN THE MYRRHA POOL

Ferry Roelofs, Ed Komen
NRG, Westerduinweg 3, PO Box 25, 1755 ZG Petten, The Netherlands

Katrien Van Tichelen, Peter Kupschus, Hamid Aït Abderrahim
SCK•CEN, Boeretang 200, 2400 Mol, Belgium, myrrha@sckcen.be

Abstract

SCK•CEN, the Belgian Nuclear Research Centre, is designing an accelerator-driven system (ADS), MYRRHA, which aims to serve as a basis for the European experimental ADS and to provide protons and neutrons for various R&D applications. It consists of a proton accelerator that delivers a 350 MeV, 5 mA proton beam to a liquid lead-bismuth eutectic (LBE) spallation target, which in turn couples to an LBE-cooled, subcritical fast-spectrum core in a pool-type configuration. The liquid metal flow pattern in the lower part of the MYRRHA pool vessel needs to be investigated in order to assess the details of recirculation and stagnant zones for adequate coolant flow and sufficient physico-chemical mixing as well as to judge the scaling of flow down to a model that can be handled experimentally. To this end, three-dimensional (3-D) computational fluid dynamics calculations were performed by NRG in collaboration with the MYRRHA team.

Introduction

The subcritical core of the MYRRHA ADS is submerged in a pool filled with LBE, which serves as a coolant and neutron reflector medium (see Figure 1 [1]). The ~60 m^3 of LBE fills a vessel of roughly 4 m inner diameter and 6 m height. Under full operational conditions, the LBE is "cold" at ~200 C in the lower part and flows through the central core upwards being heated to ~350°C on average. This "hot" zone is separated by a diaphragm from the "cold" zone. Four eccentrically positioned pumps force the circulating flow downwards through heat exchangers and provide the pressure head for core cooling.

Since the cold zone or lower pool is spacious enough to permit the loading of the core and the exchange of fuel, it is necessary to gain knowledge about the behaviour of the flow pattern in the lower part of the pool with emphasis on the occurrence of recirculation and stagnant zones. Such features could influence the cooling or the physico-chemistry of the LBE that is corrosive to the steel used. The latter will be protected by proper dynamic oxygen control of the LBE whose concentration may not be controllable if sufficient mixing is not allowed. The objective of the present analyses is to evaluate the basic isothermal flow pattern in the lower part of the vessel in order to assess the presence of recirculation and stagnant zones for the full-size device in normal and abnormal operating conditions. The CFD analyses will be extended later on to cases where hot injection takes place and finally the full thermal cycle may be modelled.

Although the CFD results will be used as a guideline, experiments are still necessary but are not economically possible at the scale of the foreseen device. Therefore, the lower part of the MYRRHA pool vessel needs to be scaled down by a linear factor of up to 10, which would allow for the building of a model containing 60 l instead of 60 m^3 of LBE. The second objective of the present analysis is to evaluate the influence on flow topology of the downscaling of the MYRRHA pool by a factor of up to 10. To this end, a scaling method preserving the relevant flow features should be defined.

Figure 1. The MYRRHA ADS and its lower pool model

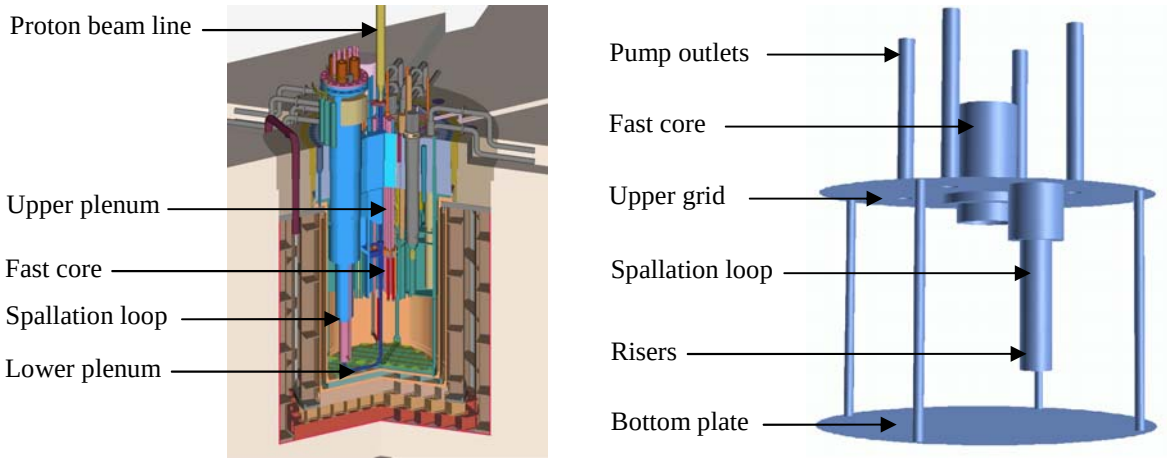

Geometry of the lower MYRRHA pool

The lower pool space of MYRRHA to be modelled is a cylindrical space of 4 m inner diameter and height of ~2 m (see Figure 1). The bottom surface is covered by a unit that provides electrical heating and process gas injection for oxygen control. Neither of the functions is relevant here but the

surface roughness of this structure was taken into account. The same is true for the top boundary, which consists of a grid to prevent detached objects from floating into trapping spaces of the diaphragm. The lower pool unit hangs from the diaphragm, and the four support stanchions for pump and heat exchanger units are to be modelled in case they present obstacles to azimuthally developing flow by virtue of pump imbalances. A further asymmetric obstacle is introduced by the spallation loop. The coupling between the spallation loop and the lower pool through the spallation loop heat exchanger was not modelled. The inlet mass flow rate of the injecting pumps was taken as 350 kg/s for each injecting pump through a nozzle of 200 mm in diameter.

Scaling methods

The turbulent jets leaving the four pump units determine the flow pattern. Three different scaling methods were considered based on varying importance of the physical parameters characterising a jet:

- The turbulent jet is characterised by the Reynolds number with the pool diameter at characteristic length. In this case, the jets emerging from the down-scaled nozzles were equivalent to the jets emerging from the original nozzle when the velocity is increased (*Reynolds number*).

- The time a jet needs to reach the bottom of the MYRRHA pool is considered characteristic for the jet. The inlet velocity was scaled by the same factor as the geometry (*characteristic time*).

- The velocity of the jet at the pump outlet characterises the jet. At the same time, the volume throughput time was kept constant (*inlet velocity*).

The three methods are summarised in Table 1. The correct choice for the scaling method is not obvious and depends on the phenomena investigated. In the case of physico-chemistry effects, timescales are most important and emphasis will be put on the correct representation of residence times.

Table 1. Scaling methods (geometric scaling factor f)

Scaling method	Inlet diameter [m]	Pool diameter [m]	Inlet area [m²]	Pool volume [m³]	Volume flow [m³/s]	Inlet velocity [m/s]	Through-put time [s]	Reynolds number
Reynolds	1/f	1/f	$1/f^2$	$1/f^3$	1/f	f	$1/f^2$	1
Characteristic time	1/f	1/f	$1/f^2$	$1/f^3$	$1/f^3$	1/f	1	$1/f^2$
Inlet velocity	$1/f^{3/2}$	1/f	$1/f^3$	$1/f^3$	$1/f^3$	1	1	1/f

In order to compare results obtained with various scaling methods, a dimensionless velocity and a dimensionless residence time are defined. The dimensionless velocity (v') was obtained by dividing the velocity (v) by the inlet velocity (v_{inlet}):

$$v' = \frac{v}{v_{inlet}}.$$

The inlet velocity was obtained from the specified mass flow rate at the pump outlets, the pump outlet area and the density of the applied fluid. The dimensionless residence time (t'_{res}) was obtained by dividing the residence time (t_{res}) by a characteristic time:

$$t'_{res} = \frac{t_{res}}{D_{pool} / \left(C \frac{\dot{V}}{A_{pool}} \right)}$$

where D_{pool} is the diameter of the pool, $\dot{V}$ is the volume flow and A_{pool} is the area of a horizontal cut-plane of the pool. C equals:

$$C = \frac{A_{pool,\,fullscale}}{A_{inlet,\,fullscale}}$$

where $A_{pool,\,full\,scale}$ is the area of the full-scale pool and $A_{inlet,\,full\,scale}$ is the area of a full scale inlet.

Cases

The flow topology was analysed for various scenarios, with special emphasis on the presence of stagnant zones. In the Base Case scenario, all four pumps had equal performance. For Cases 1a through 1f, one or two pumps were stopped with no throughput permitted; the other pumps had equal performances per pump as compared to the Base Case. This is operationally not correct since the flow rates of the operating pumps would be increased. However, these results will provide the design team with useful information about the residence times for each scenario.

The main dimensions of the pool were scaled down by a factor of five for the Cases 2a, 2b and 2c. Scaling was based on the Reynolds number, characteristic time and velocity, respectively. The model was scaled down by a factor of 10 for Case 3. In this analysis, scaling based on characteristic time was used. The cases are summarised in Table 2.

Table 2. Cases

Case	Case description
Base	No pump tripping and no scaling
1a	Full scale, 1 pump close to the spallation loop tripped
1b	Full scale, 1 pump opposite the spallation loop tripped
1c	Full scale, 2 pumps close to the spallation loop tripped
1d	Full scale, 2 pumps opposite the spallation loop tripped
1e	Full scale, 1 pump close to the spallation loop and 1 pump opposite the spallation loop, but close to the first pump, tripped
1f	Full scale, 1 pump close to the spallation loop and 1 pump opposite the spallation loop, but diagonally opposite to the first pump, tripped
2a	Scaled down by a factor of 5, scaling based on Reynolds number
2b	Scaled down by a factor of 5, scaling based on characteristic time
2c	Scaled down by a factor of 5, scaling based on velocity
3	Scaled down by a factor of 10, scaling based on characteristic time

CFD calculations

CFD model

Computer code

The computations were performed using the widely used commercial CFD code, CFX5.5 [1].

Mesh

The mesh for the lower MYRRHA pool model consisted of 911 000 hexahedral computational cells. The k-ε turbulence model in combination with scalable wall functions as implemented in CFX5 was selected for the current analyses. Therefore, the mesh refinement near the walls should ideally be such that the non-dimensionless distance y^+ is larger than 12 in order to model the boundary layers. However, the wall friction was predicted with sufficient accuracy for this application, even for lower values of y^+ [1]. For the full-scale model, the values of y^+ were in the range of 20 to 200. For the scaled-down model, the values of y^+ were in the range of 4 to 20.

Main fluid dynamics model

The main fluid dynamics model describes a single phase steady-state time-averaged incompressible turbulent flow. The k-ε turbulence model in combination with scalable wall functions as implemented in CFX5 [2] was selected to model turbulence. The MYRRHA core was modelled by a porous medium, such that the pressure drop over the core is in accordance with the actual pressure drop of 3 bar [4] although this may cause a non-physical velocity profile at the core entrance, which must be considered with some prudence. The influence is negligible, however, of the velocity profile at the core entrance for the location where the maximum residence time occurs.

Properties

For the density and the dynamic viscosity of liquid lead-bismuth, constant properties were used at a temperature of 200 C as obtained from [1].

Boundary conditions

At the outlets of the pump sections, the mass flow rate (350 kg/s per pump), the turbulence intensity (5%) and the turbulent length scale (0.02 m) were specified. Based on user experience, it was concluded that the selection of the latter two quantities has no effect on the computed flow field. At the outlet of the MYRRHA core, the static pressure was prescribed, whereas zero normal gradients were used for all remaining flow variables.

In the full-scale model, at the lower and upper plates of the lower MYRRHA pool, no-slip boundary conditions were specified with a wall roughness of 10 mm (for the full-scale model). For the lower plate, this roughness takes into account the presence of electrical heating and process gas injection for oxygen control. For the upper plate, it takes into account the presence of the grid, which prevents detached objects from floating into trapping spaces of the diaphragm. All other walls are considered as smooth walls with no-slip boundary conditions.

Results

Base Case and influence of stopped pumps

The flow field in the Base Case, with all pumps functioning, is shown in Figure 2. This figure also shows iso-surfaces of residence times. The residence time is the time the fluid needs to reach a certain point starting from the inlet. The flow field shows clearly the jets emerging from the pump outlets, reaching as far as the bottom plate.

Figure 2. Flow field [(a), (b)] and iso-surfaces [(c), (d)] of residence times for the Base Case

The contours in Figure 2(a) indicate the velocity. The contours in Figure 2(b) indicate the residence time. The residence time equals 170 s in Figure 2(c) and 270 s in Figure 2(d).

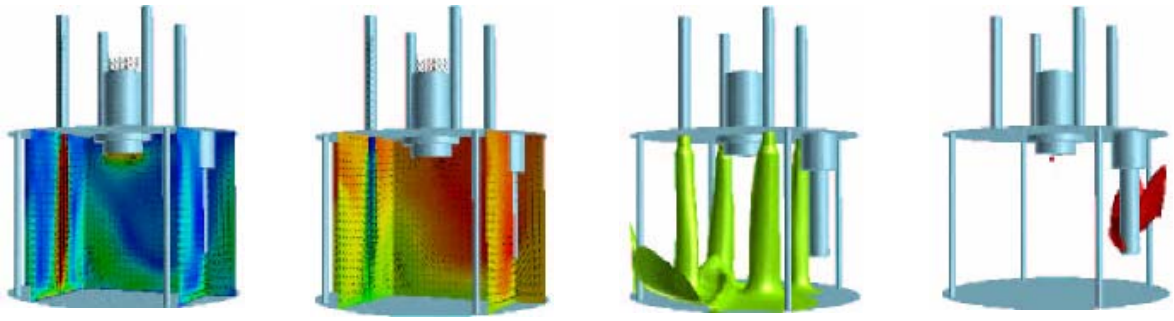

(a) (b) (c) (d)

The maximum residence times of LBE in the MYRRHA pool as observed in the analyses are presented in Table 3. The maximum residence times increased with the number of stopped pumps. For the Base Case where all pumps are functioning, the maximum residence time was 280 s (as compared to the nominal value of 190 s, which is calculated by dividing the exchange volume of ~25 m^3 by the throughput of all four pumps of 1 400 kg/s). For one stopped pump, the maximum residence time increased to approximately 430 s; whereas for two stopped pumps, the maximum residence time increased to ~600 s. This increase of residence time with the number of stopped pumps was caused by the decreased total mass flow rate since each stopped pump causes the total mass flow rate to decrease by 350 kg/s. The comparison of Cases 1a and 1b on one hand, and Cases 1c through 1f on the other hand, showed that the variation of the maximum residence time as a result of the mass flow rate distribution was ~15%. The occurrence of physico-chemical effects and precipitation had a typical timescale of several days. In comparison, the maximum residence times resulting from the analyses were lower by more than a factor of 100.

Table 3. Maximum residence times for the Base Case and Cases 1a through 1f

Case	Maximum residence time [s]
Base	280
1a	430
1b	360
1c	590
1d	560
1e	630
1f	600

Iso-surfaces of residence times are presented in Figure 3 for Cases 1a, 1c and 1e. Figures 3(a), 3(b) and 3(c) indicate which pumps are functioning and which are not functioning. Figures 3(d), 3(e) and 3(f) indicate the locations in the pool where the maximum residence times occur. Typically, the largest residence time occurs in the upper corners of the pool, where the side walls meet the upper grid and near the upper grid and target loop. The latter might change for the better if the spallation loop heat exchanger were modelled because that flow represents some 7% of the total throughput.

Figure 3. Iso-surfaces of residence times: (a) Case 1a, 250 s; (b) Case 1c, 370 s; (c) Case 1e, 370 s; (d) Case 1a, 380 s; (e) Case 1c, 580s; (f) Case 1e, 590 s

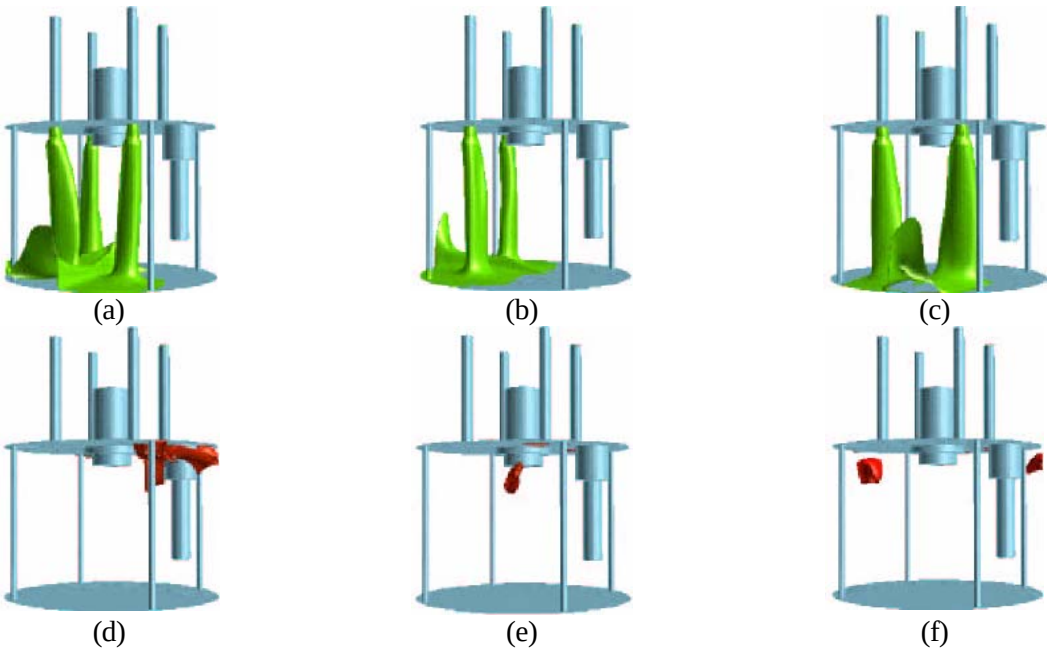

Different scaling methods

The maximum dimensionless residence times of lead-bismuth as observed in the MYRRHA pool are presented in Table 4. All dimensionless residence times were of the same order of magnitude. Where the characteristic time-based scaling (Case 2b) led to practically equal maximum residence times compared to the Base Case, the maximum residence time for the Reynolds number-based scaling (Case 2a) exceeded the maximum residence time of the Base Case by ~22% and the maximum residence time for the velocity-based scaling (Case 2c) exceeded the maximum residence time of the Base Case by ~7%. However, the occurrence of physico-chemical effects and precipitation had a typical timescale of several days. In comparison, even the residence times resulting from the Reynolds number-based scaling were lower by more than a factor 100.

Table 4. Maximum dimensionless residence times for the Base Case and Cases 2a, 2b and 2c

Case	Maximum dimensionless residence time [-]
Base	73
2a	89
2b	72
2c	78

The contours of dimensionless velocity of the flow fields for Cases 2a, 2b and 2c are presented in Figure 4(a), 4(b) and 4(c). The flow fields of the Base Case and Case 2b were quite similar. The flow fields of the Base Case and Cases 2a en 2c were comparable, though less similar than the aforementioned. Iso-surfaces of dimensionless residence times are presented in Figure 4(e), 4(f) and 4(g). The residence time was chosen such that the figure indicates the locations of the largest residence times. The figure shows that the locations of maximum residence time are quite similar for the Base Case and Case 2b. Compared to this, there is less similarity between the locations of maximum residence times for the Base Case and Cases 2a en 2c.

Figure 4. Flow fields (dimensionless velocity) for Cases 2a (a), 2b (b), 2c (c) and 3 (d). Iso-surfaces of dimensionless residence times for Cases 2a (e), 2b (f), 2c (g) and 3 (h).

The dimensionless residence time in (e) equals 83.0, in (f) equals 68.0, in (g) equals 77.0 and in (h) equals 75.0.

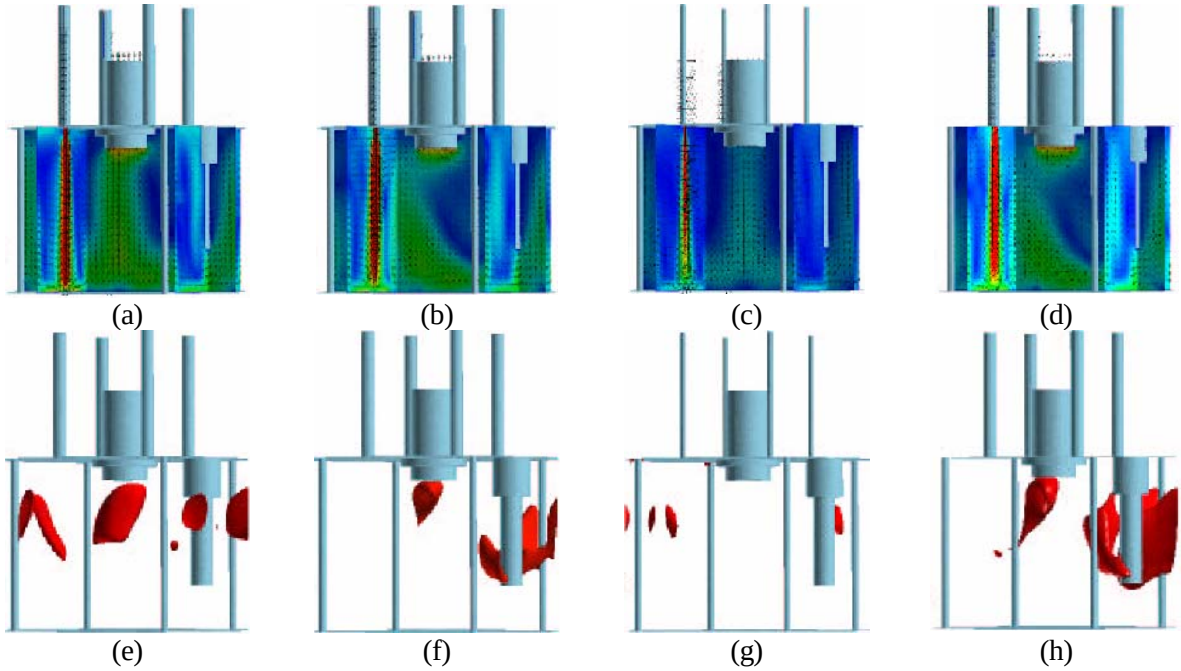

Different scaling factors

From the assessment of the different scaling methods, it was concluded that applying scaling based on characteristic time leads to a very similar flow topology compared to the Base Case. Therefore, the scaling is based on characteristic time (even for the analyses where different geometric scaling factors were applied).

The maximum dimensionless residence times of lead-bismuth in the lower MYRRHA pool as observed in the analyses are presented in Table 5. The maximum dimensionless residence times of the Base Case, Case 2b (scaling factor of five) and Case 3 (scaling factor of 10) are of the same order of magnitude. Both analyses of the scaled-down pool showed nearly equal maximum residence times compared to the Base Case. The maximum residence time of the scaled-down pool exceeded the maximum residence time of the full-scale pool with 11% maximum. Compared to the timescales of physico-chemical effects, both scaling factors resulted in a maximum residence time much lower than a factor of 100.

Table 5. Maximum dimensionless residence time for the Base Case and Cases 2b and 3

Case	Maximum dimensionless residence time [-]
Base	73
2b	72
3	81

The flow fields for Case 2b and Case 3 are presented in Figure 4(b) and 4(d). The analysed flow fields, with the scaling factor applied varying from zero to 10, were all very similar. Iso-surfaces of dimensionless residence times are presented in Figure 4(f) and 4(h). The figures show that the locations of maximum residence times were quite similar for scaling factors applied from zero to 10.

Conclusions and outlook

Based on the isothermal calculations performed in the lower part of the MYRRHA pool vessel, the following are concluded:

- The flow pattern behaves well, even in abnormal operational conditions with two pumps failing. The flow does not contain recirculation zones that result in large residence times or stagnant zones that could influence the cooling or physico-chemistry of the LBE.

- Applying a geometric scaling factor of five hardly changes the flow topology and the maximum residence times with respect to timescales for physico-chemical effects for all three considered scaling methods. Applying a geometric scaling factor of 10 marginally changes the flow topology and the maximum residence times. The scaling factor for a “small”-sized experiment of about eight can be seen as optimal from the point of view of flow similarity and volume reduction.

In the future, CFD analyses will be extended to cases where hot injection takes place and finally the full thermal cycle may be modelled.

REFERENCES

[1] Aït Abderrahim, H., P. Kupschus, Ph. Benoit, E. Malambu, V. Sobolev, Th. Aoust, K. Van Tichelen, B. Arien, F. Vermeersch, D. De Bruyn, D. Maes, W. Haeck, “MYRRHA, A Multipurpose Accelerator Driven System for R&D. State-of-the-art Mid 2003”, *Proceedings of the International Workshop on P&T and ADS Development*, SCK•CEN, BLG-959, ISBN 9076971072, Mol, Belgium (2003).

[2] *CFX5 User Guide*, AEA Technology, Harwell, UK (1999).

[3] Vieser, W., T. Esh, F. Menter, *Heat Transfer Predictions using Advanced Two-equation Turbulence Models*, CFX Validation Report CFX-VAL10/0602 (2002).

[4] Kupschus, P, Vessel Layout c/w/ Spallation, E-mail sent on 11 April 2003.

[5] Van Tichelen, K., Lead-bismuth Properties Database, SCK•CEN Report Number RF&M/KVT/kvt/32.B043000/85/01-47, Mol, Belgium (2001).

RESULTS OF THE SECOND PHASE OF CALCULATIONS RELEVANT TO THE WPPT BENCHMARK ON BEAM INTERRUPTIONS

A. D'Angelo
ENEA/Casaccia, PO Box 2400, 00100 Rome, Italy

B. Arien, V. Sobolev, G. Van den Eynde, H. Aït Abderrahim
SCK•CEN Boeretang 200, Mol 2400, Belgium

F. Gabrielli
Politecnico di Torino, Dipartimento di Energetica, Corso Duca degli Abruzzi 24, 10129 Torino, Italy

On behalf of all the benchmark participants

Abstract

Temperature transients induced by beam interruptions of different durations in MOX-fuelled and lead-bismuth cooled experimental ADS are investigated as a WPPT benchmark computational problem. The final report of the second phase of calculations will be published shortly by the NEA. This second phase of calculations aimed to investigate the impact of different fuel power density conditions on the transient results and uncertainties. Temperature variations are investigated assuming fresh fuel conditions, four different fuel power densities and two interruption durations. The main results obtained by the nine participants are presented and compared in this paper. Moreover, their uncertainty component due to the assumptions on models and data recommended in the benchmark specifications is evaluated by means of sensitivity studies carried out by some participants as a further contribution.

Introduction

The final report of the second phase of benchmark calculations relevant to beam interruptions in a *lead-bismuth cooled and MOX-fuelled accelerator-driven system* will be published shortly by the NEA [1]. Some of the main results of the second phase of benchmark calculations are presented, compared and analysed in this paper. As a reminder, the first phase of calculations [2], mainly devoted to the comparative assessment of different computational methods, was successful because the results obtained by different codes agreed with each other within ~3%.

This second phase of calculations aimed mainly to investigate the transient results and their uncertainties under different fuel power density conditions. To this end, proposed transient calculations are not only relevant to an XADS-type average fuel pin, but also to the case of the XADS-type hottest fuel pin and to the average and hottest pin cases of the MYRRHA-type experimental ADS. Benchmark participants calculated four sets of beam interruption solutions, called "reference results", by assuming models and data recommended in the benchmark specifications [1] for the following four cases:

A) Ansaldo-XADS system-type average fuel pin (~80 W/cm).

B) Ansaldo-XADS system-type hottest fuel pin (~115 W/cm).

C) MYRRHA-XADS system-type average fuel pin (~220 W/cm).

D) MYRRHA-XADS system-type hottest fuel pin (~320 W/cm).

To evaluate the uncertainty of the results, the benchmark calculations were extended to "sensitivity analyses" on assumptions (regarding models and data) that were different from those recommended in the benchmark specifications. The participants also evaluated the impact of any assumption they thought to be a valid alternative or an improvement on the recommendations given in the benchmark specifications. As in the first phase of calculations, the benchmark specification simplifications were designed to have minimum impact on the temperature variations either in the Ansaldo-type or in the MYRRHA-type XADS charged with fresh fuel. The purpose was to enable benchmark results to evaluate, in beginning of life (BOL) fuel conditions, the average and hottest pin initial temperature distributions, temperature variations induced by accelerator beam interruptions with different durations (1 s and 6 s) and corresponding uncertainties.

Concerning the layout of this paper, after an introduction and a short section devoted to the participants and the list of codes used, the third section compares the reference results obtained by the different participants. Owing to the need for succinctness, this paper contains only the results of case B (fuel power density ~115 W/cm) and case D (~320 W/cm). The complete set of results is reported in Ref. [1]. The first part is mainly devoted to results of initial steady state axial temperature distributions (common to all the considered beam interruption transients). A synthesis of the outlet coolant temperature sensitivity analyses performed by different participants is also included to explain why outlet coolant temperatures are particularly precise and independent of fuel power density conditions.

The fourth section is devoted to the main results concerning sensitivity analyses of both the steady state and transient fuel temperatures. Namely, we report the impact on reference results (cases B and D) of assumptions (regarding models and data) that the participants thought to be valid alternatives or improvements on the recommendations given in the benchmark specifications. The aim of this investigation is to evaluate the reference results' uncertainty due to benchmark recommendations on models and data. The general coherence of the different benchmark results is underlined in the fifth section. Concluding remarks are found at the end of the paper.

Benchmark participants and codes used

Table 1. Participant and code lists

Participant	From	Code used
Antonio D'Angelo, F. Gabrielli	ENEA/Casaccia, Italy	TIESTE-MINOSSE
Gert Van den Eynde, Baudouin Arien	SCK•CEN, Mol, Belgium	SITHER-PKS
Kazafumi Tsujimoto	JAERI, Tokai, Japan	EXCURS-M
Marcus Eriksson	Royal Institute of Technology, Stockholm, Sweden	SASSYS/SAS4A
Michael Schikorr	FZK, Karlsruhe, Germany	SIM-ADS
Paul Coddington, Konstantin Mikityuk – 1	PSI, Switzerland	TRAC-M/AAA
Paul Coddington, Konstantin Mikityuk – 2	PSI, Switzerland	LOOP2
Pieter Wakker, Jim Kuijper	NRG, Petten/Arnhem, The Netherlands	TRAC MOD
Ron Dagan, Cornelis Broeders	FZK, Karlsruhe, Germany	SAS4-ADS
Yonghee Kim	KAERI, Daejon, Republic of Korea	DESINUR

Table 1 reports the names of the nine participants for this second phase of benchmark calculations and the codes used. Owing to the fact that PSI solved the benchmark problems by using two different calculation tools, there are a total of ten sets of contributions.

Specifications for the second phase of the benchmark concerned single fuel channel thermal-hydraulics coupled with the point kinetics model of average and hottest fuel pins relevant to two lead-bismuth cooled and MOX-fuelled XADS. In particular, the model refers to the "fresh fuel" assumption corresponding to the BOL fuel condition. Irradiated fuel conditions will be investigated in the near future.

Reference results

As mentioned above, the reference results were obtained by the participants by assuming models and data as close as possible to those recommended in the benchmark specifications. The definition of models and data recommended in the specification is complete. This means that in principle the benchmark problem should not have any degree of freedom and that only the numerical solution of the same equations could induce differences in participant solutions. However, this is not exactly the case. Different codes can often be forced by the users to adopt models and data as close as possible to those recommended in the benchmark specification. The benchmark's first phase of calculations demonstrated that the effect of different codes (and thus slightly different assumptions) on the calculated temperature transients induced by beam interruptions of different durations is not significant for calculations relevant to case A (Ansaldo-XADS average pin), which is characterised by a low fuel power density level. The second phase of calculations aimed to extend the reference result investigation to higher values of fuel power density.

Initial steady state axial temperature distributions

The second phase of benchmark calculations showed that, as expected, higher fuel power density cases are characterised by higher fuel temperatures. Moreover, despite the general agreement on temperature results, larger relative dispersions of the fuel temperatures calculated by the different participants resulted in higher fuel power levels (i.e. for higher heat fluxes through the fuel pin materials and interfaces). In particular, the relative dispersion of the 10 temperature results calculated by different participants (in Kelvin degrees at fuel midplane) increased from case A to D, from a quite

insignificant 1.8% to 3.0%, 5.0% and 5.6%, respectively. This trend of dispersions growing with the fuel linear power will be revisited in the next section and discussed together with the sensitivity to models and data assumed in the calculations.

Transient (time-dependent) results

Fuel temperatures

Figure 1 and Figure 2 show the 10 sets of time-dependent results relevant to the fuel centreline temperature at the fuel zone midplane calculated by different participants for cases B and D. As expected, the reduction in the fuel centreline temperature (just before beam recovery) induced by beam interruption was dependent on the case considered. As reported in Tables I and III, the fuel centreline temperature variation induced by a beam interruption of 1 s was ~90 K in case B and ~260 K in case D.

The relative dispersions among the fuel temperatures (K) obtained by the different participants looked to be largely independent of the time in both the considered beam interruptions (1 s and 6 s). For this reason, the relative dispersion of the temperature variations remained of the same order of magnitude during the whole transient; the relative dispersion of the fuel centreline temperature results increased (by a factor of about two) going from XADS-type to MYRRHA-type cases. Moreover, it appeared to remain close to the 1.8%, 3.0%, 5.0% and 5.6% values mentioned above for the steady state (initial) condition for cases A, B, C and D. This consideration was clearly significant in simplifying the resultant uncertainties and was confirmed by the sensitivity study of fuel temperature results for models and data assumed in calculations (see the next section).

Figure 1. XADS hottest pin fuel centreline temperature transients induced by beam interruptions of different durations (1 s and 6 s)

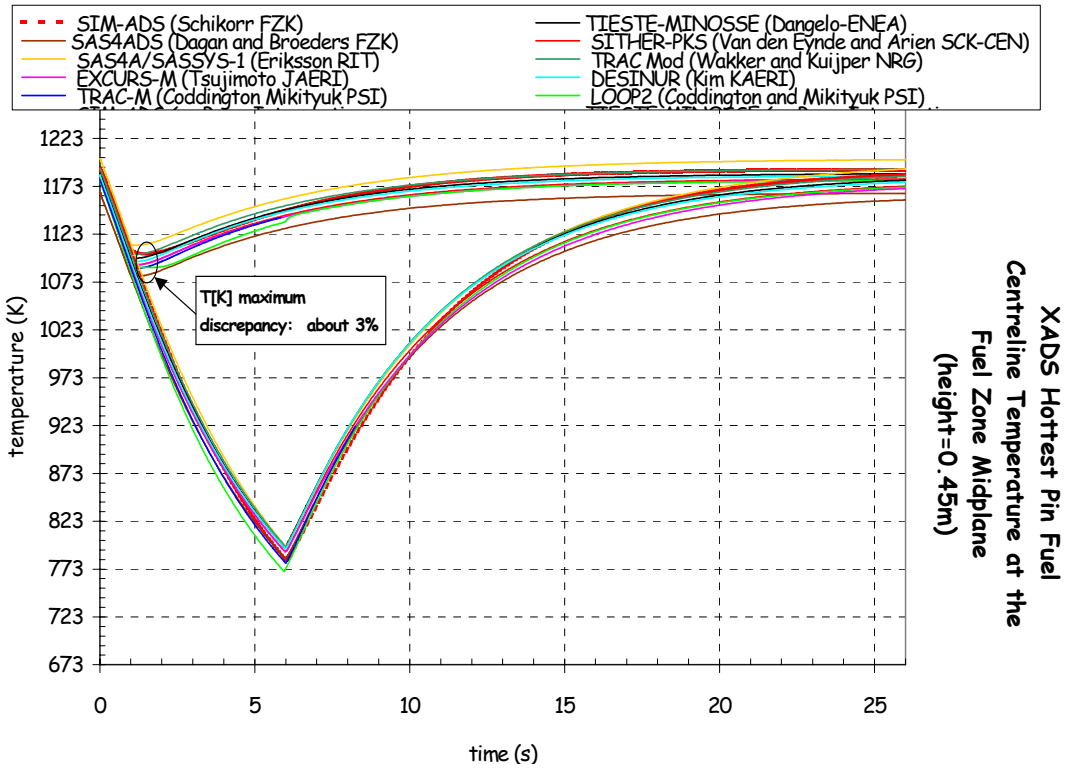

Figure 2. MYRRHA hottest pin fuel centreline temperature transients induced by beam interruptions of different durations (1 s and 6 s)

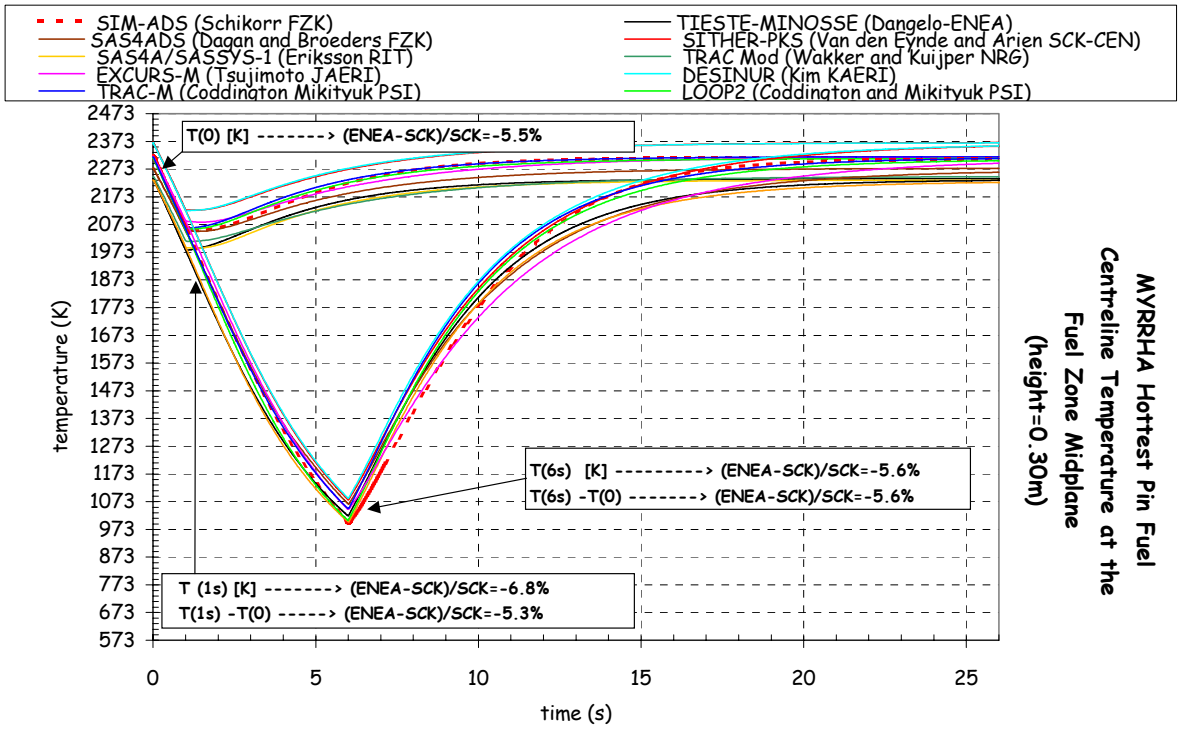

Outlet coolant temperatures

Outlet coolant temperature variations induced by beam interruptions in XADS are of interest to evaluate possible thermal stresses to the above core structure and to intermediate heat exchangers. As reported among the results in Tables II and IV, the outlet coolant temperature reduction induced by 6 s beam interruptions was ~80 K in case B and ~140 K in case D.

Contrary to what we mentioned above for fuel temperatures, the calculated coolant temperatures always appeared to be extremely precise. The steady state and transient coolant temperature results of different participants did not show significant relative dispersions (~1% only) in the considered Ansaldo and MYRRHA-XADS cases.

Sensitivity analyses performed by some participants confirmed that coolant temperature results must be quite precise. Thus, effects should be negligible of slightly different model and data assumptions that participants unintentionally brought about by utilising their codes for reference calculations.

Fuel temperature sensitivity results

Case B: PDS-XADS type hottest fuel pin

On the contrary, sensitivities of fuel temperature results to recommendations given in the benchmark specifications on models and data could be significant. Moreover, fuel temperature sensitivities calculated by benchmark participants generally grew when higher fuel power density cases were considered (i.e. higher heat fluxes through the fuel pin materials and interfaces). The benchmark specifications stressed the opportunity for participants to concentrate efforts on sensitivity studies

(optional contributions), pointing out the most significant perturbations involving the calculation assumptions (impact greater than 5%). For this reason, benchmark participants investigated the sensitivities of the results obtained in case D more than the results obtained in cases characterised by lower fuel power densities (e.g. case B).

Figure 3 shows four sensitivity studies, three by SCK•CEN (SITHER-PKS code) and one by ENEA (TIESTE-MINOSSE code), on different assumptions to calculate the fuel centreline temperature distributions relevant to the PDS-XADS type hottest fuel pin (case B).

Figure 3. Impact of different assumptions on the XADS hottest pin fuel centreline temperature axial distribution

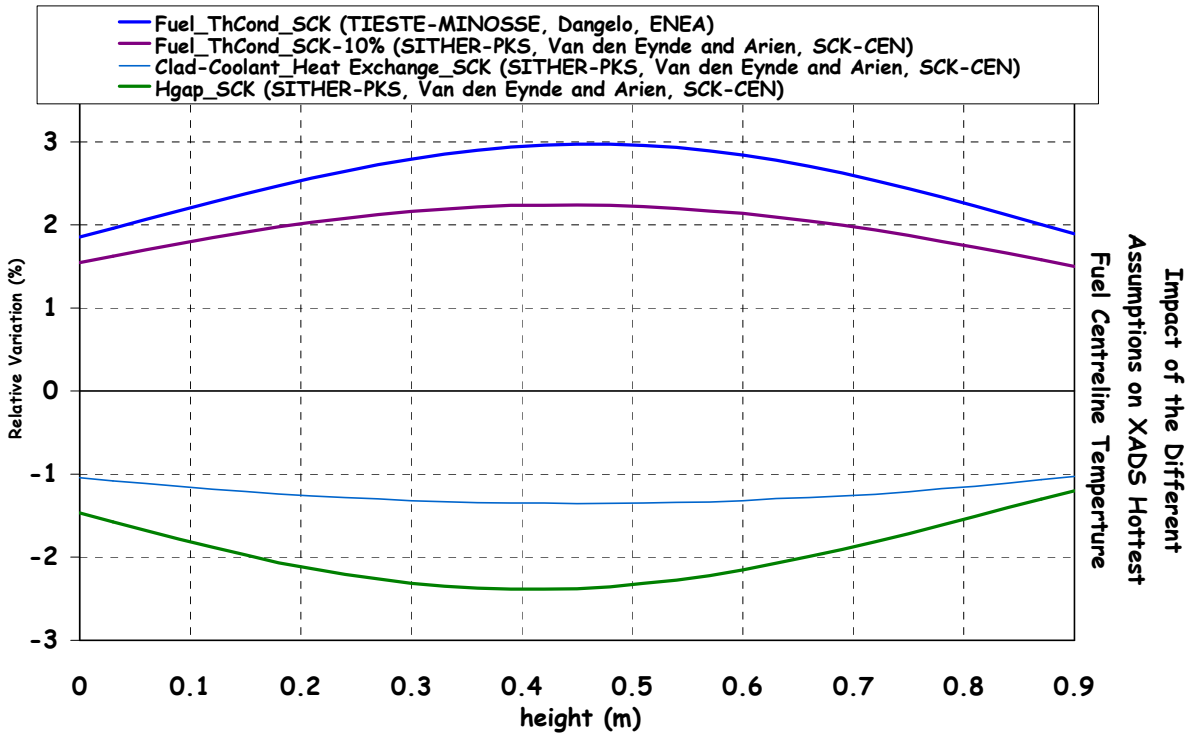

Mox fuel thermal conductivity

Two studies concerned the fuel temperature relative variation due to the use of a different MOX fuel thermal conductivity evaluation. For one, SCK•CEN evaluated the impact on fuel temperatures of MOX fuel conductivity, which was 10% lower than that from the modified Martin model recommended by ENEA [3]. In turn, ENEA evaluated the impact of assuming the MOX fuel conductivity recommended in the benchmark specifications for MYRRHA cases. The MOX fuel thermal conductivity recommended by SCK•CEN in the MYRRHA cases (see second annex of phase II benchmark specifications) came from Daniel Baron's evaluation [4]. This MOX fuel thermal conductivity was ~0.6 $Wm^{-1}K^{-1}$ lower at $T < 1\,800$ K than that recommended by ENEA in the PDS-XADS cases. Considering that different reductions of the fuel thermal conductivities (10% or ~15%) have been investigated, the sensitivity leading to the two effects on the fuel temperatures could be determined. Both results indicated that Baron's MOX fuel thermal conductivity increased by ~3% the fuel temperature in the hottest pin midplane.

In Ref. [3], Daniel Baron evaluated the standard deviation (SD) of experimental data on the UO_2, PuO_2 and MOX fuel thermal conductivity to be of the same order (~0.6 $Wm^{-1}K^{-1}$). Therefore, the value of ~3%, which was evaluated by ENEA as the impact of the assumption of Baron's MOX fuel thermal conductivity, was also the fuel temperature uncertainty due to uncertainty surrounding the fuel thermal conductivity data themselves. Moreover, Daniel Baron indicated as a "central prediction" his fuel thermal conductivity formulation (close to the formulation recommended by SCK•CEN) [5].

Time-dependent results showed a particularly low dependence on time of sensitivities during the transient induced by a 1 s beam interruption.

Finally, by considering both the standard deviation and the probable systematic in comparison with central values, the uncertainty for the PDS-XADS type average fuel temperature (K) and temperature variation was evaluated to be ~4-5%.

Clad-coolant heat exchange model

Figure 3 shows the SCK•CEN result concerning the impact on fuel temperatures of a different assumption for the clad-coolant heat exchange model. The clad-coolant heat exchange correlation recommended for the MYRRHA calculations would lead to slightly lower PDS-XADS fuel temperatures (within ~1%). No uncertainty contribution will be associated to the model assumption on the clad-coolant heat exchange.

Fuel-to-clad gap model

Moreover, Figure 3 shows SCK•CEN results concerning the impact of the temperature-dependent gap thickness model (recommended for the MYRRHA cases) instead of the constant (at room temperature) thickness simplified model recommended for the PDS-XADS calculations. The temperature-dependent gap thickness model would lead to slightly lower fuel temperatures (within less than 2.5%). No uncertainty contribution will be associated with the PDS-XADS reference calculations for this model assumption that is significantly conservative.

Total uncertainty of the calculated fuel temperatures

The uncertainty due to the fuel thermal conductivity recommendation was the only significant uncertainty component that could be evaluated in the case of the PDS-XADS average pin calculations. Thus, a total uncertainty of ~4.5% (at one SD) was evaluated for the PDS-XADS hottest pin fuel temperature (K).

Case D: MYRRHA-type hottest fuel pin

Figure 4 shows a large number of sensitivity studies carried out by ENEA (TIESTE-MINOSSE code), by SCK•CEN (SITHER-PKS code), by PSI (LOOP2 code) and by FZK (SIM-ADS code). Time-dependent investigations demonstrated the low time dependence of the investigated sensitivities (as with the previous case).

Figure 4. Impact of different assumptions on the MYRRHA hottest pin fuel centreline temperature axial distribution

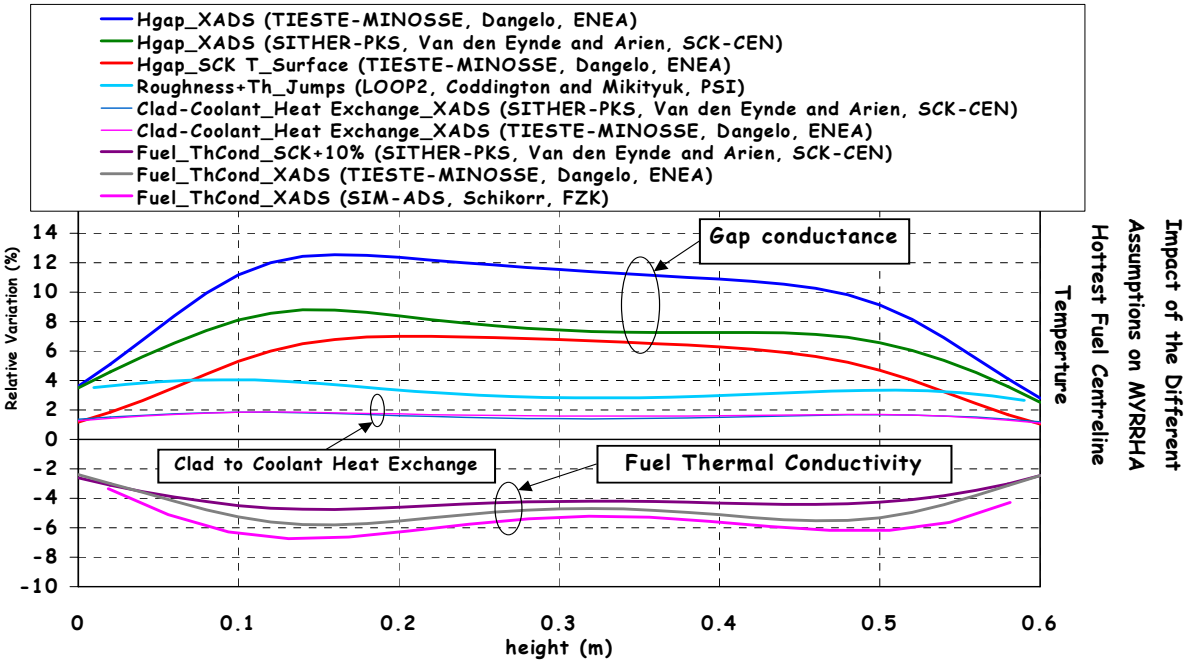

Mox fuel thermal conductivity

Figure 4 shows the excellent agreement between the ENEA, FZK and SCK•CEN results concerning the impact of the fuel thermal conductivity recommended for XADS cases. As previously mentioned for case B, Daniel Baron indicated as a "central prediction" his fuel thermal conductivity prediction, which is close to the thermal conductivity formulation recommended by SCK•CEN for the MYRRHA cases [5]. Moreover, he evaluated the standard deviation of this central evaluation to be of the same order of magnitude (~0.6 $Wm^{-1}K^{-1}$) of the difference between ENEA and SCK•CEN recommendations. Therefore, we can say that the ~6% of fuel temperature variation calculated by ENEA and FZK as an impact of the ENEA recommended fuel thermal conductivity is of the same order of magnitude of uncertainty regarding fuel thermal conductivity.

Clad-coolant heat exchange model

Figure 4 shows the very good agreement between the ENEA and the SCK•CEN sensitivity studies concerning the clad-coolant heat exchange correlation. The use of the correlation assumed for PDS-XADS cases would lead to not much higher fuel temperatures (within ~2%). One per cent (1%) of one SD uncertainty will be taken into account for the slightly non-conservative model on the clad-coolant heat exchange used in the MYRRHA calculations.

Fuel-to-clad gap model

Concerning a possible approximation by the constant thickness (at room temperature) gap conductivity model (recommended for the PDS-XADS cases), Figure 4 shows two impact evaluations – one from ENEA and another from SCK•CEN. In this case, it also appeared that the

simplified model led to too largely conservative temperature evaluations in the MYRRHA conditions of higher fuel power densities. The agreement on the corresponding fuel temperature increases was less good than for the other evaluations. Nevertheless, both evaluations confirmed again the opportunity of the temperature-dependent gap thickness assumption in the MYRRHA heat flux conditions. Figure 4 also illustrates an ENEA investigation on the uncertainty associated to the temperature-dependent gap thickness model. As in the previous MYRRHA average case, ENEA tested the uncertainty induced by the definition of an extreme fuel temperature to evaluate the fuel surface linear expansion (strain) during the transients. ENEA also calculated for this case the impact of assuming the fuel surface temperature to be driving the linear expansion. Figure 4 shows that this extreme choice induced fuel temperature increases that may be significant. An uncertainty of 4% (one SD) could be conservatively retained for the degree of freedom in choosing the temperature driving the fuel surface expansion during a transient.

Figure 4 shows the results of a further sensitivity study performed by PSI on the fuel and clad (internal) surface roughness and its impact on the gap thickness evaluation. Namely, the Ross-Stoute model [6,7] for gap conductance (a_g) was used in the LOOP2 code calculation by PSI, and a two-micron roughness was pessimistically assumed for both the fuel and the clad surfaces [1]. The Ross-Stoute extra thickness of the gap could lead to a variation of ~3% on the initial fuel centreline temperature at the core midplane (see the steady state PSI evaluation in Figure 4).

Finally, in the case of the hottest MYRRHA, 2% uncertainty can be conservatively retained as contributor to fuel gap internal surface roughness, which was not defined in the benchmark specification.

Mox fuel specific heat

The uncertainty of UO_2 specific heat can be evaluated to equal 0.7% up to 2 000 K and 6% for a higher temperature range (from 2 000 to melting point) [8]. For PuO_2 specific heat, the uncertainty can be evaluated to equal 2% from 298 K up to 1 800 K and 13% from 1 800 to melting point [9]. The uncertainty of the MOX fuel (20.5 wt. % PuO_2) specific heat was only 1% below 1 800 K, but increased to ~7.5% above 2 000 K. In the case of the MYRRHA hottest fuel pin, this important increasing of uncertainty above 1 800 K can induce a significant uncertainty component. If we evaluate conservatively that the hottest fuel pin temperatures can be higher than 1 800 , 2 000 K in 25% of its fuel volume, an average uncertainty of ~3% can be conservatively associated to the corresponding heat capacity.

Fuel specific heat has no impact on the initial (steady state) fuel temperatures, but only on fuel temperatures during the transient. This means that, as a peculiarity of this parameter, specific heat can easily induce significant effects on the calculated values of the fuel temperature decreases induced by beam interruptions. Namely, using the impact evaluated by SCK•CEN on the fuel temperature absolute value, it is has been shown that a 10% lower fuel specific heat can induce ~9% larger fuel temperature decreases induced by a 1 s beam interruption. Therefore, the ~3% uncertainty (one SD) of the MYRRHA hottest fuel specific heat can lead to a ~2.7% uncertainty component on the fuel temperature decreases induced by the considered beam interruptions.

Total uncertainty of the calculated fuel temperatures

Combining the 6%, 1%, 4%, 2% and 2.7% components conservatively evaluated as effects of the fuel thermal conductivity, the clad-coolant heat exchange model, the gap model, the Ross-Stoute gap extra width and the fuel heat capacity uncertainties, respectively, 8% of total uncertainty can be

evaluated for the MYRRHA hottest pin fuel temperature variations induced by 1 s beam interruptions. In principle, owing to the lack of the uncertainty component relevant to heat capacity, uncertainty on both the initial and the asymptotic absolute temperatures (K) would come in slightly lower (~7.5% at one SD). Moreover, the uncertainty for the Ross-Stoute gap extra width will be solved in the future by defining the gap surface roughness conditions. But for the sake of simplicity, 8% uncertainty can be assumed at the present time and conservatively extended to the absolute fuel temperatures.

General coherence of the benchmark different results

The sensitivity analysis clearly points out that outlet coolant temperature results are independent of calculation assumptions. This appears coherent with the very precise outlet coolant temperature reference results that were obtained by the different participants using different codes – always within ~1% and independent of the fuel power density condition relevant to the four considered cases.

On the contrary, the fuel temperatures are clearly dependent on some calculation assumptions. In particular, calculated fuel temperature depends mainly on the fuel thermal conductivity data and the fuel-to-clad heat transfer model. The corresponding sensitivities increase for larger fuel power density cases. Consequently, the uncertainties of the fuel temperatures (K) and of their variations also increase for larger fuel power density cases – 3%, 4.5%, 7% and 8% for case A, B, C and D, respectively.

In addition, this sensitivity trend appears coherent with the dispersion of the reference results concerning the fuel temperatures that clearly increase for larger fuel power density cases – 1.8%, 3%, 5% and 5.6% for cases A, B, C and D, respectively. This coherence seems to indicate that the dispersion of reference results is due only to the effects of slightly different assumptions on models or data, which were unintentional (participants tried to reproduce as well as possible the benchmark recommendations).

Concluding remarks

Beam interruptions were investigated in the frame of a second phase of calculations for the OECD/NEA/WPPT computational benchmark. Two lead-bismuth cooled and MOX-fuelled experimental accelerator-driven systems, which are characterised by two different fuel power densities, were considered – PDS and MYRRHA-XADS. Initial temperatures and transients induced by beam interruptions of different durations were calculated either for the average or for the hottest fuel pin case. The 10 benchmark sets of coolant and fuel temperature results, calculated by the nine participants, were compared and the corresponding dispersions were evaluated. The benchmark's second phase of calculations also aimed to analyse the sensitivity to models and data assumed in the calculations. To this end, the benchmark was successful – sensitivities calculated by the different participants were compared and used to evaluate the reference result uncertainties. Resulting temperature variations induced by 1 s or 6 s beam interruptions are reported in Tables I to IV along with their uncertainties. Finally, the general coherence among reference result dispersions and sensitivity results was underlined.

Possible further developments of this beam interruption benchmark are proposed by the participants and will be discussed at the beginning of the next WPPT mandate.

Table I. Fuel temperature variations in PDS-XADS (cases A and B)

Beam interruption (s)	Maximum fuel temperature variations (K)	
	Average pin	Hottest pin
1	*~63 – 2*	*~89 – 4*
6	~270 – 8	~390 – 18

Table II. Coolant temperature variations in PDS-XADS (cases A and B)

Beam interruption (s)	Maximum outlet coolant temperature variations (K)	
	Average pin	Hottest pin
1	~12	~20
6	*~58*	*~80*

Table III. Fuel temperature variations in MYRRHA (cases C and D)

Beam interruption (s)	Maximum fuel temperature variations (K)	
	Average pin	Hottest pin
1	*~190 – 13*	*~260 – 21*
6	~825 – 58	~1 220 – 98

Table IV. Coolant temperature variations in MYRRHA (cases C and D)

Beam interruption (s)	Maximum outlet coolant temperature variations (K)	
	Average pin	Hottest pin
1	~31	~50
6	*~92*	*~140*

REFERENCES

[1] D'Angelo, A., B. Arien, V. Sobolev, G. Van Den Eynde, F. Gabrielli, *Benchmark on Beam Interruptions in an Accelerator-driven System – Final Report on Phase II Calculations*, OECD/NEA/NSD, Paris, France (2004) [To be published].

[2] D'Angelo, A., F. Gabrielli, *Benchmark on Beam Interruptions in an Accelerator-driven System – Final Report on Phase I Calculations*, OECD, Paris, France, NEA/NSC/DOC(2003)17, ISBN 92-64-02138-8 (2003); See also A. D'Angelo, F. Gabrielli, "Benchmark on Beam Interruptions in a Lead-bismuth Cooled and MOX Fuelled Accelerator-driven System", *Proceedings of GLOBAL 2003 Atoms for Prosperity: Updating Eisenhower's Global Vision for Nuclear Energy*, American Nuclear Society and European Nuclear Society (ANS/ENS) International Winter Meeting Embedded Topical Meeting, New Orleans, Louisiana, 16-20 November, pp. 661-666 (2003).

[3] Bellucci, V., S. Buono, G. Fotia, L. Maciocco, V. Moreau, M. Mulas, G. Siddi, L. Sorrentino, *Thermalhydraulic Design of the Fuel Element of the Energy Amplifier Prototype*, CRS4 Technical Report, CRS4 TECH-REP-98/37, Cagliari, 6 August 1998; See also ENEA's *Divisione Sistemi Ecosostenibili*, Technical Note, DT-SDA-00015 (1998).

[4] Baron, D., "About the Modelling Of Fuel Thermal Conductivity Degradation at High-burnup Accounting for Recovering Process with Temperature", *Proceedings of the Seminar on Thermal Performance of High Burn-up LWR Fuel*, Cadarache, France, 3-6 March 1998.

[5] Baron, D., "Fuel Thermal Conductivity: A Review of the Modelling Available for UO_2, (U-Gd) O_2 and MOX Fuel", *Proceedings of the Seminar on Thermal Performance of High Burn-up LWR fuel*, Cadarache, France, 3-6 March 1998.

[6] Ross, A.M., R.L. Stoute, "Heat Transfer Coefficient Between UO_2 and Zircaloy-2", AECL-1552 (1962).

[7] The RELAP5 Code Development Team, "RELAP5/MOD3 Code Manual, Volume I: Code Structure, System Models and Solution Methods", NUREG/CR-5535 (1995).

[8] Fink, J.K., "Thermophysical Properties of Uranium Dioxide", *Journal of Nuclear Materials*, Elsevier, 279, 1-18 (2000).

[9] Carbajo, J.J., G.L. Yoder, S.G. Popov, V.K. Ivanov, "A Review of Thermophysical Properties of MOX and UO_2 Fuels", *Journal of Nuclear Materials*, Elsevier, 299, 181-198 (2001).

TECHNICAL SESSION IV

Safety and Control of ADS

Chairs: J-M. Lagniel, P. Coddington

SAFETY ANALYSIS OF THE EU PDS-XADS DESIGNS

P. Coddington, K. Mikityuk
Paul Scherrer Institut, 5232 Villigen, Switzerland
E-mail: paul.coddington@psi.ch

M. Schikorr, W. Maschek
Forschungszentrum Karlsruhe, 76021 Karlsruhe, Germany

R. Sehgal
KTH Royal Institute of Technology, 100 44 Stockholm, Sweden

J. Champigny
FRAMATOME ANP, 69456 Lyon Cedex 06, France

L. Mansani
Ansaldo, 16161 Genova, Italy

P. Meloni
ENEA, 40129 Bologna, Italy

H. Wider
Joint Research Centre of the EC, Petten, Netherlands

Abstract

Within the Fifth Framework Programme of the European Union (EU), the PDS-XADS project is focused on Preliminary Design Studies of an Experimental Accelerator-driven Reactor System (ADS). Three basic designs are being studied in detail – two ADS design options, one with a lead-bismuth eutectic (LBE) cooled core (an 80 MWth unit and a smaller unit) and another (80 MWth) with a gas (helium) cooled core. One part of the PDS-XADS project involves the assessment of the safety of the two 80 MWth designs. The main objectives are as follows: develop an integrated safety approach common to both the LBE and the gas-cooled concepts; identify the main safety issues in an XADS with their phenomenology and develop an evaluation methodology for both alternatives; and perform transient analyses with the aim of producing safety analysis reports on the design features required to meet XADS safety objectives.

Introduction

Within the Fifth Framework Programme of the EU, the PDS-XADS project is focused on Preliminary Design Studies of an Experimental Accelerator-driven Reactor System (ADS). Two basic design options are being studied in detail – two ADS design options (an 80 MWth unit and a smaller unit), one with a lead-bismuth eutectic (LBE) cooled core and another (an 80 MWth unit) with a gas (helium) cooled core. Both designs are driven by a neutron spallation source coming from a 600 MeV proton accelerator beam impacting a heavy liquid metal (LBE), windowless target.

One part of the PDS-XADS project involves the assessment of the safety of the two 80 MWth designs. The main objectives are as follows:

- Develop an integrated safety approach common to both the LBE and the gas-cooled concepts.
- Identify the main safety issues in an XADS with their phenomenology and develop an evaluation methodology for both alternatives.
- Perform transient analyses with the aim of producing safety analysis reports on the design features required to meet XADS safety objectives.

The rationale for the integrated safety approach is quite similar to that practiced for current LWR plants, i.e. defence-in-depth, single failure criterion and specified safety goals. The PDS-XADS is a subcritical fast reactor and is cooled either with LBE or gas (helium). Thus, it has the inherent advantage that reactivity-initiated accidents (RIAs), which were the *bane* of fast reactors, may be prevented by an appropriate choice of subcriticality level. The safety evaluation approach required the specification of the design basis conditions (DBC) and the design extension conditions (DEC) for both the LBE-cooled and the gas-cooled designs. Again, guidance on the specifications was derived from the safety regulations for LWRs and fast reactors.

For the LBE-cooled XADS designed by Ansaldo/ENEA, a total of 26 transient initiators were identified for detailed analysis and categorised as follows: operational transients (3), protected transients (11) and unprotected transients (12). For the gas-cooled XADS designed by FANP and NNC/CEA, a total of 31 transient initiators were identified and categorised as follows: operational transients (3), protected transients (17) and unprotected transients (11). Many of the transient initiators were common to both designs (e.g. spurious beam trip, protected/unprotected loss of flow and loss of heat sink, unprotected subassembly blockage, etc.) while some of the initiators were specific to one particular concept (i.e. loss of coolant accidents and water/steam ingress into the reactor core for the gas-cooled design).

In order to perform the analysis, a review was made of the code systems available to the project partners, which could be adapted to the analysis of the PDS-XADS DBC and DEC transients. These codes include: 1) SIM-ADS code; 2) RELAP5 code modified for LBE by Ansaldo and the RELAP5/PARCS coupled code (with gas-cooled subcritical system kinetics models added by ENEA); 3) TRAC/AAA code of US NRC modified for LBE and gas coolants by the Los Alamos National Laboratory and further modified by PSI; 4) code EAC (European accident code) developed at JRC-Petten; 5) SAS4/SASSYS codes modified to include LBE; and 6) SIMMER code, which can model fast reactor hypothetical core disruption accidents (HCDA), and the STAR-CD code. The availability of a number of different codes able to analyse the same transients offers the capability of performing code-to-code comparisons, which is very important when analysing new reactor concepts in the absence of extensive experimental validation studies.

In this paper, representative results of the transient analyses performed using the different code systems for the different designs, including the code-to-code comparisons, are presented and discussed. The results showed for the LBE-cooled XADS that this design exhibits a very wide safety margin (for both protected and unprotected transients) as a consequence of very favourable safety characteristics. These safety characteristics included: excellent heat transfer properties and high boiling point of the coolant, favourable in-vessel and secondary system coolant natural circulation flow characteristics and large thermal inertia within the primary system as a result of large coolant mass (pool design). For the gas-cooled XADS, the results demonstrated the importance of core heat transfer, and the adequacy of the decay heat removal system for protected depressurisation and loss of flow transients. The results also helped to define the limited time window for backup proton beam shutdown systems in the event of an unprotected transient.

LBE and He-cooled XADS concepts

The main parameters of 80 MWth MOX-fuelled LBE and gas (He) cooled ADS demonstration facilities developed by Ansaldo [1,2] and by FRAMATOME [3,4] are given in Table 1.

Table 1. Main parameters of LBE and He-cooled XADS systems

Parameter	LBE	He
Nominal thermal power, MW	80	80
Multiplication factor k_{eff} at BOC	0.973	0.954
Number of FSAs/fuel pins per FSA	120/90	90/37
FSA flat-to-flat distance, mm	138	120
Fuel type/fuel mass, t	MOX/3.24	MOX/4.37
Plutonium content, %	23	35
Core inner/outer diameter, m	0.58/1.7	0.48/1.4
Fuel height, mm	900	1 500
Fuel pellet inner/outer diameter, mm	1.8/7.14	3.2/11.5
Clad outer diameter, mm	8.5	13
Pitch-to-diameter ratio	1.58	1.29
Average/peak power rating, W/cm	82/130	160/256
Primary coolant/pressure, MPa	PbBi/1	He/6
Inlet/outlet coolant temperature, C	300/400	200/450
Core mass flow rate, kg/s	5 460	61.6
Core pressure drop, kPa	25	100

The core diagrams of the two systems are presented in Figure 1(a) and 1(b), respectively. The subcritical core in both options had an annular configuration. The spallation neutron source unit was inserted in the core central void region. The diagrams of the two systems are shown in Figures 2(a) and 2(b), respectively.

In the LBE option, the primary system did not use traditional mechanical pumps. Instead, the natural circulation of the primary LBE was enhanced with gas lift pumps. Due to the high fuel pin pitch-to-diameter ratio in the core and the absence of mechanical pumps and low coolant velocities, the hydraulic resistance of the LBE primary circuit was very low (~0.3 bar), providing a high level of natural circulation in case of pump trip. This, along with a low core power rating, positive LBE properties, use of a passive decay heat removal system and external neutron source, provides a sound basis for a high level of safety with the LBE system. The gas-cooled XADS had a more compact core compared to the LBE-cooled system and in particular had a smaller number of thicker fuel pins, with the result that core average and peak linear ratings were about twice those of the LBE-cooled concept.

In the gas-cooled option, the coolant (at ~60 bar pressure) flowed out of the core [Figure 2(b)] into the large upper plenum volume, through the inner part of a concentric pipe and to the power conversion system (PCS), which consisted of a heat exchanger and blower unit. The blower drives the coolant along the outer region of the concentric pipe into the reactor vessel downcomer and from there into the lower plenum and the core inlet.

Figure 1. Diagrams of the LBE (a) and He (b) XADS core designs

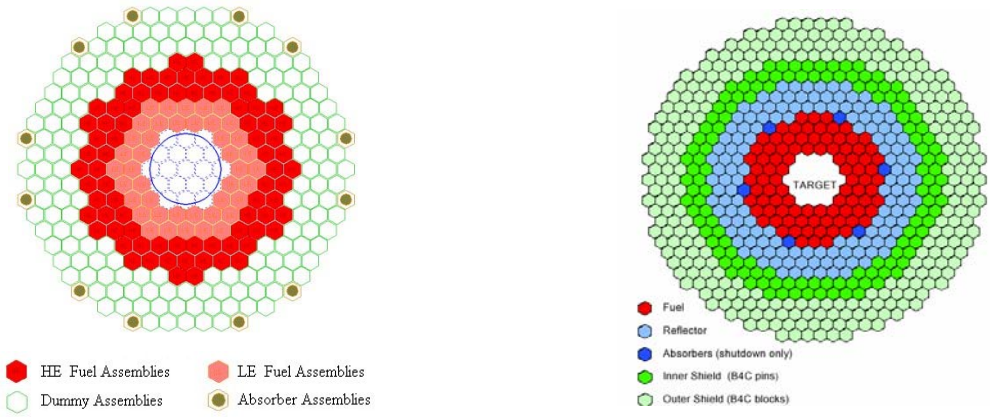

(a) (b)

Figure 2. Diagrams of the LBE (a) and He (b) XADS system designs

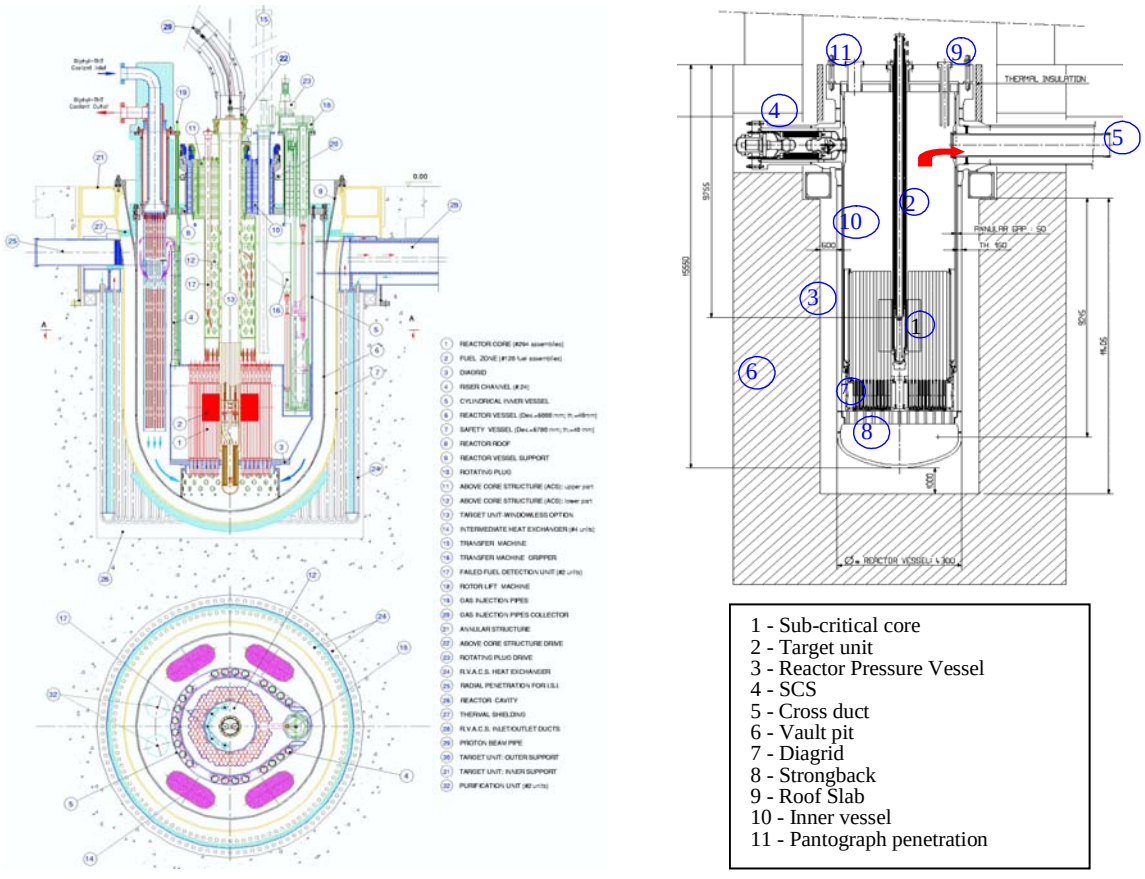

(a) (b)

For the gas-cooled XADS, the decay heat removal system consisted of two out of three heat exchangers [Figure 2(b)], each with a nominal heat removal capacity of 2 MW connected directly to the pressure vessel at the same elevation as the connection to the PCS. The heat exchangers had a natural circulation secondary side water coolant flow and were designed to operate on the primary side under natural circulation conditions at full reactor pressure; they also include blowers to circulate the primary coolant flow under low pressure (LOCA) conditions. Another feature of the decay heat removal system was a valve located just upstream of the cold side PCS connection to the pressure vessel, which when closed prevents coolant for a loss of coolant accident flowing directly out of the break without first flowing through the core.

LBE-cooled XADS transient analysis

The range of transients selected to be analysed as part of the project are listed in Table 2. These tansients can be divided into a number of groups; first (as shown), most of the transients were analysed in a protected (accelerator beam trip) and unprotected (no beam trip) mode. The transient initiators include failures in the primary and secondary system components [e.g. loss of flow, loss of heat sink, loss of inventory (LOCA), etc.], failures in the functioning of the accelerator (e.g. beam over power, beam trip, etc.), reactivity addition tansients and transients with the potential for local core melt [e.g. subassembly (SA) blockage]. Included in Table 2 is the expected analysis allocated to the various teams and code systems. As described above, one advantage of a project of this type is the ability to collect together different analytical tools, including such "system codes" as: TRAC/AAA and RELAP5 (suitably modified for LBE systems); special "fast reactor" codes (e.g. SIM-ADS and SIMMER) that include only limited modelling of the primary and secondary systems or are core-only codes; and computational fluid dynamics codes such as STAR-CD. The allocation of the analysis tried to take advantage of the different capabilities of the various code systems, while permiting some measure of code-to-code comparison to provide some benchmarking of the results.

An example of one of the more extensive comparisons is shown (in part) in Figure 3 for the unprotected loss of flow transient. Here, we see an example of two types of analysis, the first using the system codes (e.g. RELAP5 and TRAC) that include a full represenation of the primary and secondary systems. These show the evolution of the transition to thermally driven natural circulation. The remainder of the codes use as input either a simplified approach or a core input flow rate taken from one of the system codes. All of the codes that calculate the core flow show that because of the low system pressure loss, the natural circulation flow rate was between 40% and 50% of the nominal value. Most of the code systems calculate the change in core power using a point kinetics model. And here we see that because of subcriticality there was only a small reduction in the core power. Due to the high core flow under natural circulation conditions, the resultant core temperatures (in almost all of the codes) showed only a modest increase of typically 100 C (i.e. from 400-500 C) for the core exit coolant temperature. The results of this analysis highlight two important features – 1) that there is a large degree of agreement between the very different analytical tools and 2) this reactor (Ansaldo design) is able to accommodate an unprotected loss of flow transient with only a modest increase in core temperatures. This second feature can be applied to almost all of the transients analysed in Table 2, the only exception being U-5 and the unproteced loss of flow and heat sink (comparative results presented in Figure 4). In this figure, which shows the results from TRAC, RELAP5 and SIM-ADS, we see that even though there was a total loss of heat sink, there was still a substantial natural circulation flow rate of between 20% and 35% for the system code calculations. The natural circulation flow distributes the heat generation in the core over the whole of the primary system resulting in a relatively slow increase in the core temperatures. The maximum cladding temperature increase was 400 C to 500 C for the RELAP5/TRAC calculations in 1 000 s, which is a more than sufficient time window for the accelerator beam to be manually switched off. It should be noted that

for operational transients without accelerator beam trip (including ULOF presented above), which are equivalent to anticipated transients without scram (ATWS) in a critical reactor, it is important that the increase in the primary coolant temperature does not lead to coolant boiling in the secondary system. This has the potential to increase the severity of the event by leading to a loss of heat sink.

Table 2. LBE transients analysed

Transient Number	Transient	Description	Burnup State		Organisations analyzing Transient						Transient already analysed by ANSALDO
					ENEA	PSI	JRC	FzK	FzK	FzK	
Transients analyzed for LBE -XADS Design (ANSALDO)			BOC	EOC	RELAP5+ PARCS	TRAC-M	STAR-CD, CFD, EAC2	SIMMER	SAS4ADS	SIM-ADS	RELAP5
Operational Transients											
O - 1	Shutdown	plant taken to Ambient (30 C)	X	X						done	from HFP to HZP
O - 2	Shutdown with target flooded	target is flooded and then plant taken down to Ambient (30 C)	X	X			X			done	
O - 3	Startup	plant is taken from CZP to HFP	X	X						done	from HZP to HFP
Protected Transients											
P - 1	PLOF	complete loss of all forced / enhanced circulations in primary and secondary(oil) systems	X	X	BOC done	BOC done				done	X
P - 2	PTOP	300 pcm jump in reactivity at HFP	X	X		BOC done		BOC done		done	
P - 3	PTOP	300 pcm jump at CZP	X	X		BOC done				X	
P - 4	PLOH	complete loss of both secondary trains	X	X	BOC done	BOC done				done	
P - 5	PLOF+PLOH	loss of gas and secondary loops lost	X	X	BOC done	BOC done	BOC done			done	X
P - 6a	LOCA	primary vessel leaks, level in primary drops by 2 m, HX uncovered, (partial) loss of nat. circ. in primary	X	X		BOC done	open				X
P - 6b	LOCA	double vessel leak, level in primary drops, core remain covered, loss of nat. circ. in primary	X	X		BOC done	open				
P - 7	Over-cooling of primary side	core inlet temp. drops by 150 C in 450 sec	X	X		BOC done				X	X
P - 8 DEC	Inlet Blockage of SA w/o radial heat transfer	flow area of peak SA reduced to 2.5%, no radial heat transfer assumed	X	X	open		open			X	
P - 9 DEC	Blockage of SA with radial heat transfer	flow area of peak SA reduced to 2.5%, radial heat transfer assumed	X	X			open				X
P - 10	Spurious beam trips	beam trips for 1,2,3 ...10 sec intervals	X	X	BOC done	BOC done		BOC done	BOC done		X
P - 11	HX Tube rupture	secondary oil leaks into primary side, can happen only when sec. in natural circulation mode	X	X		BOC done					
Unprotected Transients											
U - 1	ULOF	complete loss of all forced / enhanced circulations in primary and secondary(oil) systems	X	X	BOC done	BOC done	BOC done	BOC done		done	various partial ULOFs
U - 2	UTOP	300 pcm jump in reactivity at HFP	X	X		BOC done	open	BOC done, EOC done		done	
U - 3	UTOP	300 pcm jump at CZP	X	X		BOC done	open			done	
U - 4 DEC	ULOH	complete loss of both secondary trains	X	X	BOC done	BOC done	BOC done			done	
U - 5 DEC	ULOF+ULOH	loss of gas and secondary loops lost	X	X	BOC done	BOC done	BOC done			done	
U - 6 DEC	Unprotected LOCA	primary vessel leaks, level in primary drops by 2m, loss of nat. circ. possible	X	X		BOC done	open				
U - 7	Unprotected over-cooling of primary side	core inlet drops by 150 C in 450 sec	X	X		BOC done				done	no feedbacks
U - 8 DEC	Unprotected blockage of SA w/o radial heat transfer	flow area of peak SA reduced to 2.5%, no radial heat transfer assumed	X	X	BOC done		open	BOC done		X	with radial heat transfer
U - 9 DEC	Unprocted inlet blockage of SA with radial heat transfer	flow area of peak SA reduced to 2.5%, no radial heat transfer assumed	X	X			open	BOC done			
U - 10	Unprotected HX Tube rupture	secondary oil leaks into primary side	X	X		BOC done					
U - 11	Beam Overpower to 200 % at HFP		X		BOC done	BOC done		BOC done	BOC done	X	X
U - 12	Beam Power Jump to 100% at HZP		X	X	BOC done	BOC done			BOC done	X	X

Figure 3. Comparison of code results for loss of flow transient

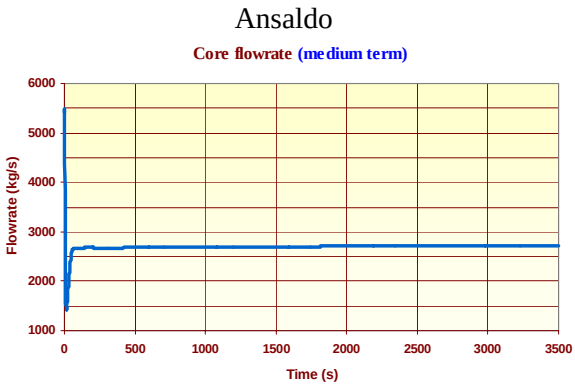

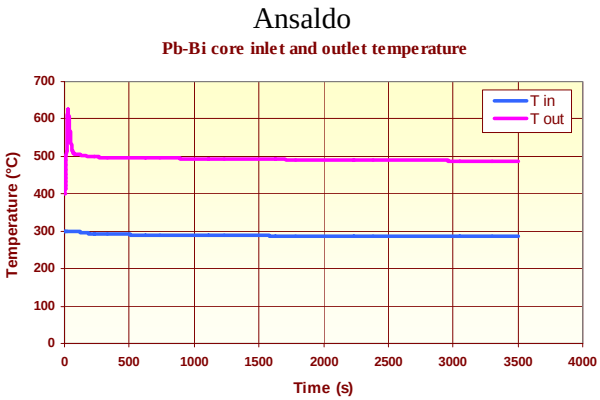

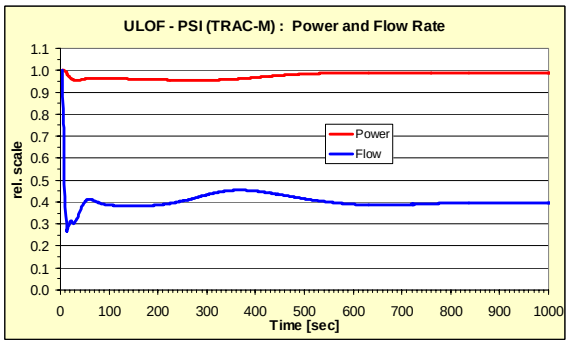

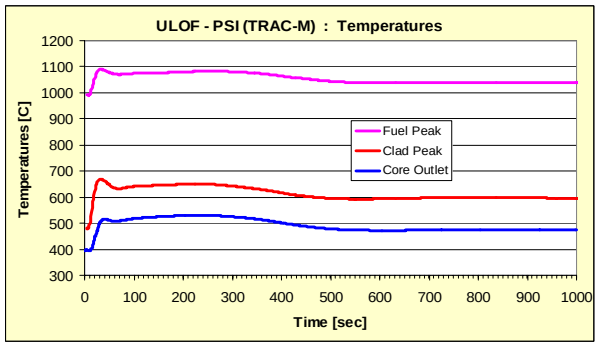

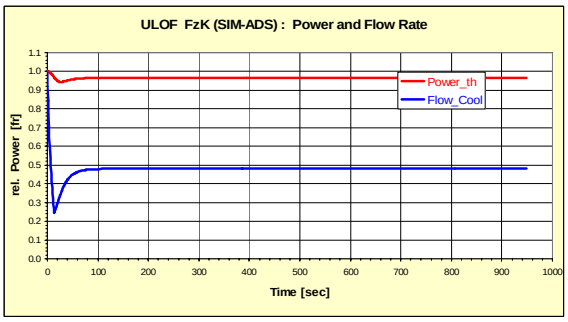

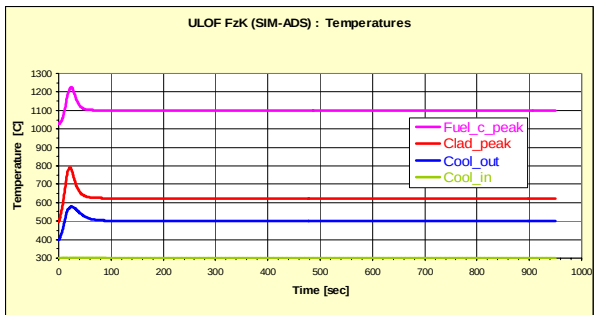

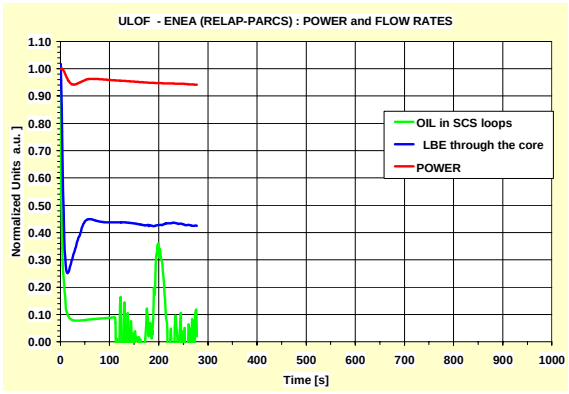

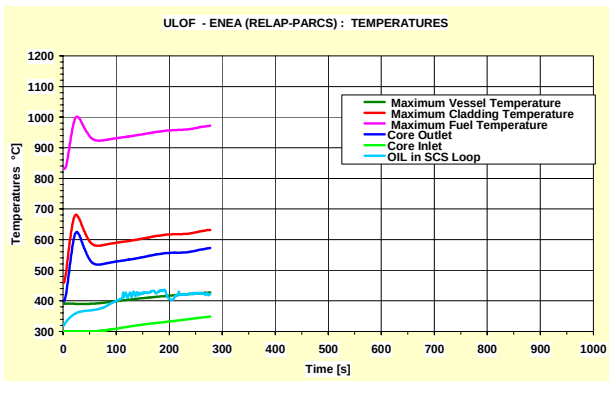

Figure 4. Comparison of code results for loss of flow and loss of heat sink transients

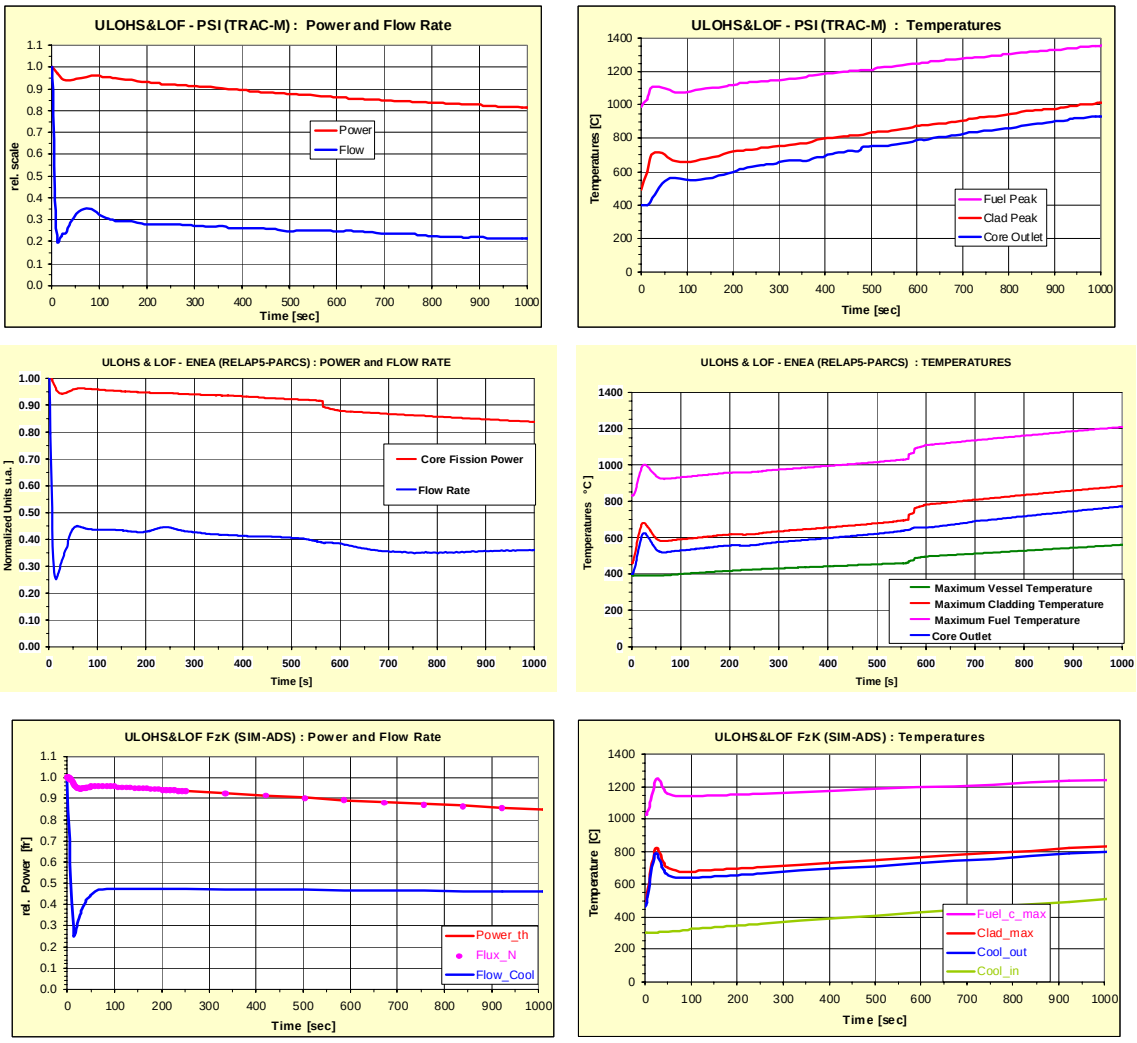

A transient that was considered of importance in the analysis of sodium-cooled fast reactors, was that of local subassembly blockage because of the potential for local fuel melting to go undetected with the result that it may spread into a core-wide problem. As a required condition in the PDS-XADS safety assessment, the impact of local coolant flow blockages, specifically the reduction of the flow area to 2.5% in the hottest assembly, was investigated using SIMMER (permits an analysis of core melt conditions) and STAR-CD (a CFD code). In the two-dimensional (2-D) SIMMER-III simulation framework, the flow area of the whole innermost subassembly ring was reduced. This is a pessimistic assumption because all surrounding subassemblies adjacent to the target unit would be blocked simultaneously and radial heat transfer limited to four flats. In the present study, three calculations were performed to examine the impact of hexcan gap flow (HGF) and radial heat transfer (RHT). The highest cladding temperatures in the innermost subassembly ring for the three calculations are presented in Figure 5. In case (1) with HGF and RHT, the cladding temperature stayed at ~200 K below the melting point and no clad melting was predicted. If only a single assembly is blocked in an actual three-dimensional (3-D) simulation, cladding temperatures can be expected to be much lower. In case (2), HGF was artificially suppressed but the cladding temperature still stayed at 100 K below the melting point. Case (3) was performed to investigate conditions if the core is *forced* into melting. For this case, a pin failure occurred at 31 s, while fuel sweep-out into the upper plenum region at 94 s

brought a strong reactivity reduction so that no severe power excursion would occur. Figure 6 shows the fuel particle distribution after the pin failure and the expanding damage in the innermost assembly, indicating that fuel particles could be swept away from the core region and that reactivity would be reduced as a consequence.

In Figures 7(a) and 7(b) below the STAR-CD steady state results with an unprotected inlet blockage in one subassembly are presented. The assumed blockage reduced the coolant flow rate in the concerned subassembly to 2.5% of nominal flow. [Note that this is a more severe restriction than that of the SIMMER analysis, which assumed a flow restriction of 2.5% and led to higher temperatures (as will be seen).] Figure 7(a) below shows the LBE temperatures in the blocked and the neighbouring intact subassembly at full flow. The neighbouring subassembly was locally heated much above the nominal 400 C outlet temperature. Since all six neighbouring SAs were at full flow, they removed nearly all the heat generated in the blocked assembly. In Figure 7(b), the cladding temperatures of the blocked subassembly and the neighbouring one with full flow are shown. It can be seen that the maximum cladding temperature in the blocked subassembly was 1 670 K, i.e. just a few degrees below the steel melting point but approximately 100 C higher than the equivalent SIMMER calculation. (This means rather certainly that many fuel pins have already ruptured and that fission gas release has occurred. But, since the maximum fuel temperature is only 1 900 K, few other radioisotopes will have been released from the fuel matrix.) However, given the uncertainty in these analyses and the different boundary condition assumptions (see above), the difference in fact is relatively modest.

The distribution of molten fuel within the primary system, which is not modelled by above codes, requires further analysis to determine if the fuel could migrate to heat exchanges leading to tube failure.

Figure 5. SIMMER-III clad temperatures for blockage case

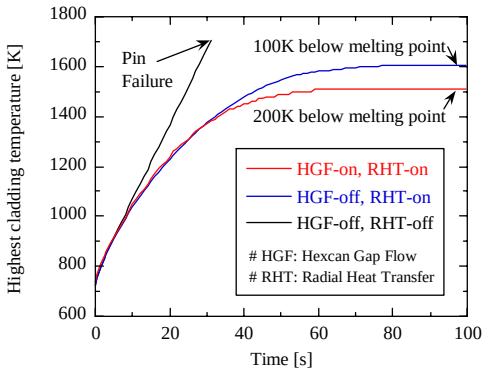

Figure 6. SIMMER-III fuel sweep-out for pin failure case

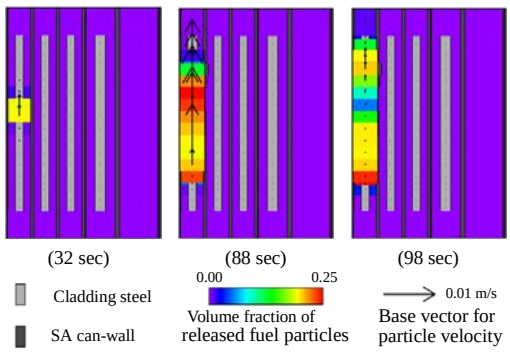

Figure 7. Coolant (a) and clad temperatures [K] (b) in blocked and neighbouring SA at full flow

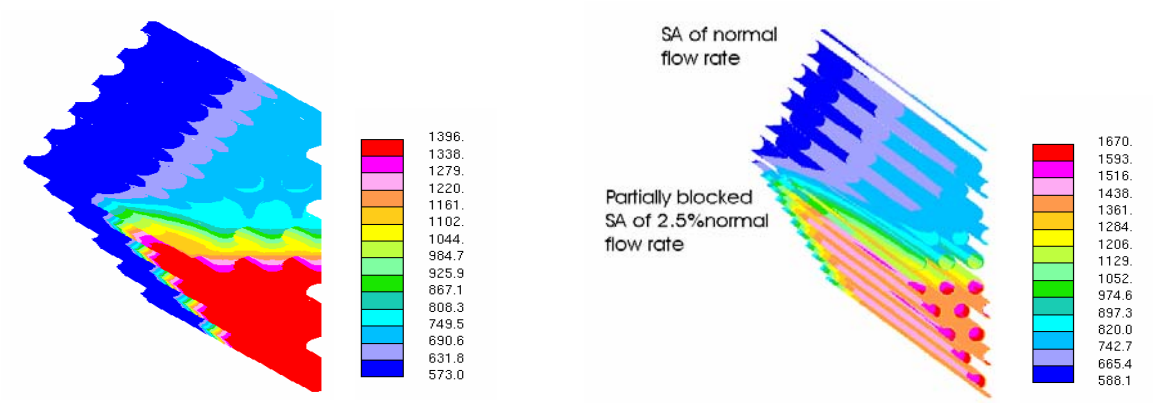

(a) (b)

Gas-cooled XADS transient analysis

The range of transients to be analysed for the gas-cooled XADS was reviewed and a table similar to that produced for the LBE design (see Table 2 above) was developed. The transients selected for analysis (as for the LBE) included core-driven events (e.g. beam over power, reactivity addition accidents) and system-driven events (e.g. failure of the main blower, loss of heat sink, loss of coolant, etc.), which were analysed assuming both protected (beam trip) and unprotected conditions. Of special interest are the two classes of events that are more relevant to gas-cooled systems. These are: 1) loss of coolant accidents and (2) the ingress of water into the core from a failure in the decay heat removal heat exchangers.

As part of the initial transient analysis of the gas-cooled concept, a number of critical features became apparent including: high clad temperatures were obtained even during normal operation; clad temperatures in excess of 1 200 C were obtained for a range of protected transients; and clad temperatures rose to the melting point in a few tens of seconds unless the accelerator beam was immediately tripped for more "severe" accidents (such as a large break in the pipe connecting the vessel to the power conversion unit).

In order to address the first two of the above-mentioned issues, the reactor core was redesigned to increase the fuel rod to coolant heat transfer and to redirect the coolant flow to the higher rated subassemblies. The first was achieved by introducing roughened fuel rods and the second by applying a gagging scheme to the inlet of the fuel assemblies based on their expected power. One of the consequences was that both increased the core pressure drop. Therefore, a goal of the subsequent analysis was to demonstrate the adequacy of the decay heat removal system to function (as designed) under natural convection conditions at full reactor pressure and with the use of the blowers following reactor depressurisation.

One of the first tasks of the revised analysis was to determine an adequate database and consequential heat transfer and pressure loss coefficients for the redesigned core. An example of the "correction factors" introduced into the analysis code systems is given below in Figure 8.

Figure 8. Effect of clad roughening on fuel rod heat transfer

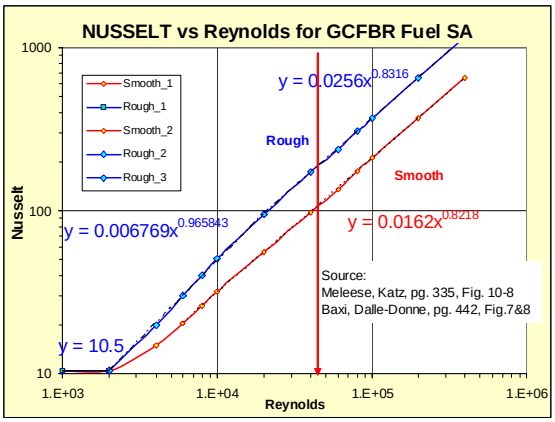

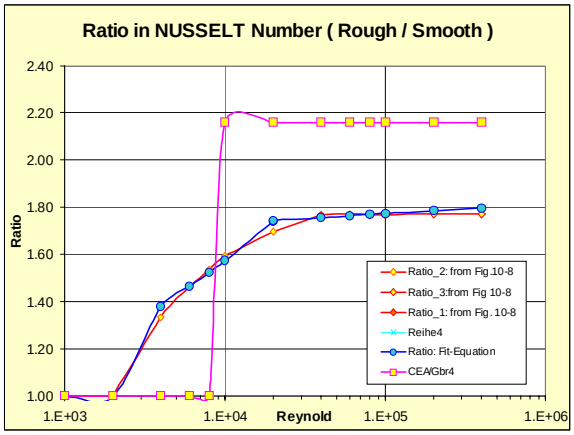

Recommended Correction Factor CF:

1000<Re<2000	CF_NUSSELT = 1
2000<Re<20,000	CF_NUSSELT = 0.4176*Re^0.144043
20.000<Re<E6	CF_NUSSELT = 1.58*Re^0.0102

An example of the results of the revised analysis is shown in Figure 9, which illustrates the core flow and peak clad temperatures for a TRAC/AAA calculation for a protected main blower trip transient. In this figure we see that in the long term (i.e. after ~200 s when the flow through the power conversion system falls to zero), natural circulation flow is established by the decay heat removal system at a flow rate of ~1.6 kg/s for two out of the three units. This is slightly higher than the nominal design value of 0.65 kg/s per unit. During this period, the clad temperatures slowly decrease to a value of ~600 C after ~2 000 s. However, the magnitude of the peak clad temperatures is primarily defined by the normal operational fuel-stored energy and the cooling during the early period of the transient following the trip of the accelerator beam (for this transient is based on a high core-exit coolant temperature set point). Thus, it is important for this and other system-driven transients to maintain the flow though the core from the PCS for as long as possible by careful design of the main blower and the PCS isolation valve placed just inside the cold side of the connection pipe from the vessel to the PCS. In the current analysis, as we see from Figure 9 (TRAC/AAA) and Figure 10 (SIM-ADS), the PCS flow rate reduces to zero over a period of 30 s due to closure of this valve. With these constraints [i.e. pump run down of up to 30 s, reduced fuel-stored energy due to increased normal operation heat transfer (use of roughened fuel pins) and fuel assembly gagging], and with the associated increased transient heat transfer (for high Reynolds numbers), we see that it is possible to reduce the peak clad temperatures to ~700 C for a main blower trip transient, which is considered the operational transient with a relatively high probability of occurrence.

In addition to the analysis presented, similar conclusions can be drawn for most of the protected system-driven transients. However, none of the above design changes have any significant impact on the response of the reactor to unprotected transients. With unprotected transients, the reactivity changes that occur as a result of the increase in fuel temperature, etc., have a minimal effect on core power of subcritical systems, and thus the core will continue to heat up to unacceptable temperatures.

The results of the transient calculations presented above were obtained using system codes in which the coolant temperature and flows are averaged over large volumes or nodes with the result that any information relating to the thermal and flow gradients (e.g. those exiting the core) was lost. This is important for both normal operation and accident situations if large gradients may occur. In order to address this concern, computational fluid dynamic (CFD) models are being developed using the STAR-CD code with the detailed mesh shown in Figure 11 as an example. As a first stage in the

analysis, thermal-hydraulic calculations for nominal conditions were performed to determine the helium temperature and the temperature in the different structural components (e.g. reactor main vessel, the inner vessel, cross duct, core assemblies and shielding, accelerator vessel, upper shielding plate, etc.). As a second step, the transient calculation of the helium and structural temperatures will be calculated. These calculations will provide the input for a detailed stress analysis of these components under normal and transient conditions.

Figure 9. TRAC/AAA analysis of pump trip transient for the gas-cooled XADS

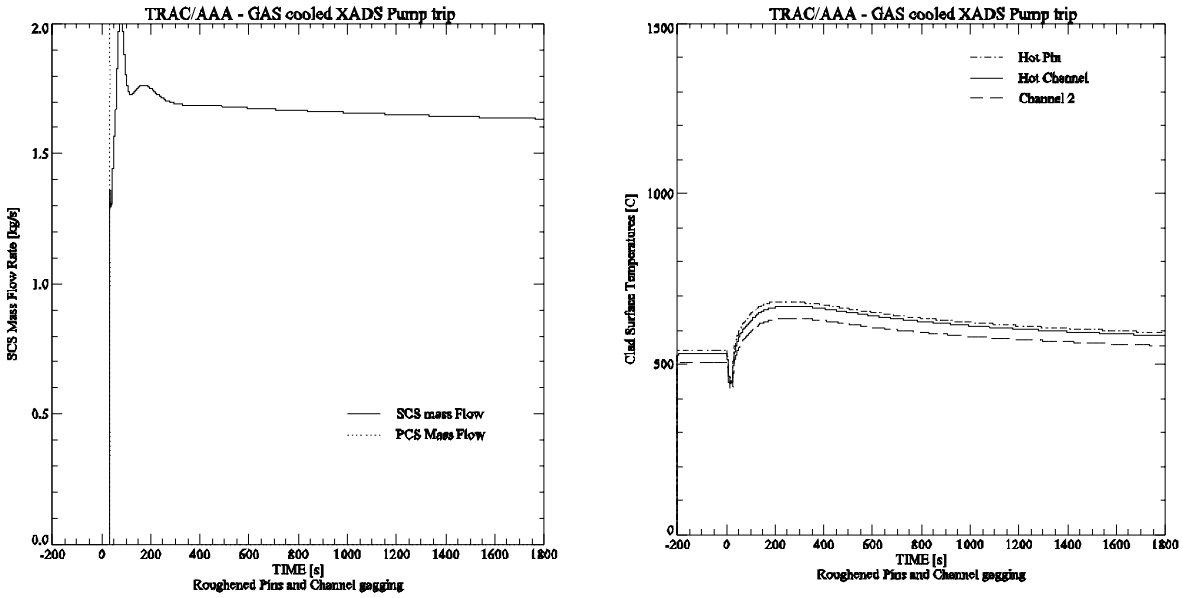

Figure 10. SIM-ADS results for peak fuel and clad temperatures, coolant inlet and outlet temperatures

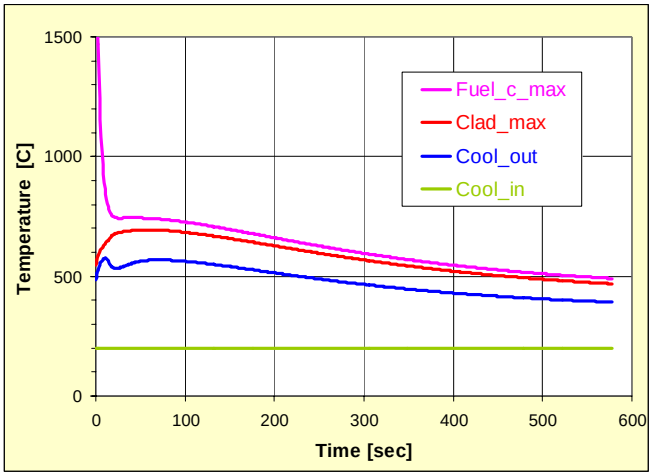

Figure 11. STAR-CD solid mesh and cross-section of the model at core midplane level

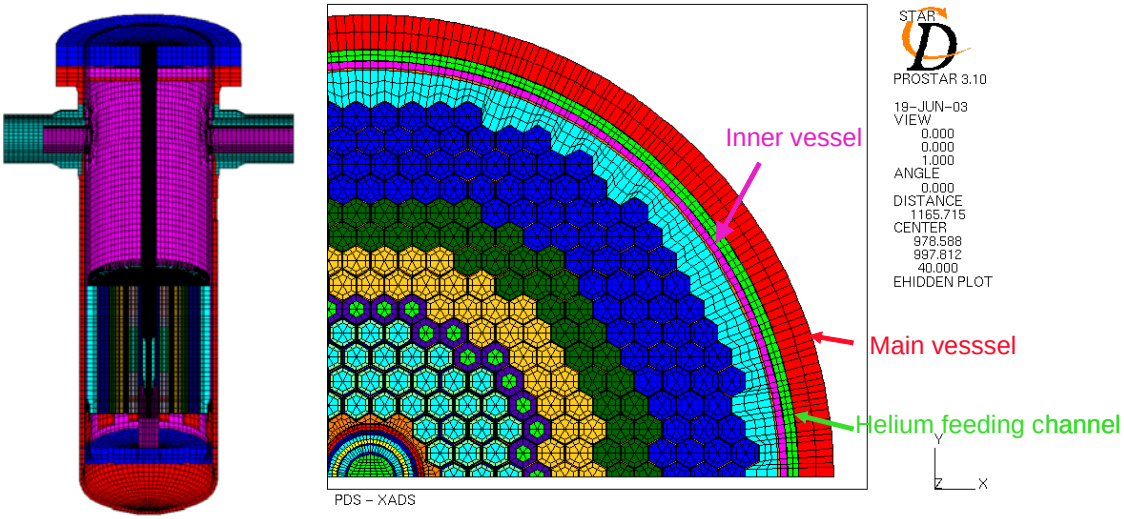

Conclusions

A general conclusion from the analysis performed and the transients presented (i.e. loss of flow, loss of heat sink, etc.) is that for the LBE-cooled reactor concept (as designed by Ansaldo), the reactor system is able to cool the core for all protected transients and almost all unprotected transients because of the high thermal inertia of the coolant, the excellent natural circulation properties and the modest power ratings. Even in the most severe case considered (unprotected loss of flow and complete loss of heat sink), there is a grace period between 30 and 60 minutes to switch off the beam before the cladding temperatures reach excessive levels. An additional benefit of analysis through the PDS-XADS project framework is the ability to provide code-to-code comparisons for a range of transients using a wide range of codes. In the context of the analysis of the LBE-cooled design, a high degree of agreement was obtained both for system-driven and local transients.

For the gas-cooled concept, the analysis performed indicated that for the long-term cooling of the core to be assured, the decay heat removal system needs to operate as designed at all of the different reactor states to be considered (namely, at nominal system pressure, under natural circulation conditions and with the reactor in a depressurised state). In addition, for most of the protected transients, it can be shown that with adequate consideration given to the system design (e.g. linear heat generation rate, fuel pellet diameter, sufficient operational heat transfer, fuel pin roughening and subassembly gagging, a slow main blower coast down characteristics, etc.), the energy stored in the fuel can be removed without encountering an excessive increase in the peak clad temperatures. However, none of the design changes made during the course of the analysis change the basic response of the gas-cooled system to unprotected transients. Since the reactivity changes that occur as a result of the increase in the fuel temperature, etc., have a minimal effect on the core power of subcritical systems, the core temperatures will quickly increase to unacceptable levels. This therefore places an increased emphasis on the reliability of the beam shutdown mechanisms in order to assure that these mechanisms function on demand to a very high degree of reliability.

Acknowledgements

The authors would like to thank the many people involved in the PDS-XADS project who contributed both directly and indirectly to this work. Our special thanks goes to all those who provided information on the design, system and core static analysis. The current study has been conducted in the framework of the PDS-XADS project under the Fifth Framework Programme of the European Commission (contract number FIKW-CT2001-00179). The authors would like to acknowledge the EU PDS-XADS project team, which provided financial support for this work.

REFERENCES

[1] Cinotti, L., *et al*., "Status of the Studies Performed by the European Industry on the LBE Cooled XADS", *Proceedings of the International Workshop on P&T and ADS Development*, InWor for P&T and ADS 2003, ADOPT'03, 6-8 October 2003 (2003).

[2] Cinotti, L., G. Gherardi, "The Pb-Bi Cooled XADS Status of Development", *Journal of Nuclear Materials*, 301, 8-14 (2002).

[3] Giraud, B., "Preliminary Design Study of an Experimental Accelerator Driven System – Overall Description of the Gas-cooled System", *Proceedings of the International Workshop on P&T and ADS Development*, InWor for P&T and ADS 2003, ADOPT'03, 6-8 October 2003 (2003).

[4] McDermott, M.F., *et al*., "Preliminary Design Study of a Helium-cooled Experimental Accelerator Driven System", *Proceedings of the International Workshop on P&T and ADS Development*, InWor for P&T and ADS 2003, ADOPT'03, 6-8 October 2003 (2003).

COMPARATIVE TRANSIENT ANALYSES OF ACCELERATOR-DRIVEN SYSTEMS WITH MIXED OXIDE AND ADVANCED FERTILE-FREE FUELS

X-N. Chen, T. Suzuki, A. Rineiski, C. Matzerath-Boccaccini, E. Wiegner, W. Maschek
Forschungszentrum Karlsruhe (FZK)
Institute for Nuclear and Energy Technologies, Postfach 3640
D-76021 Karlsruhe, Germany

Abstract

Comparative safety analyses and investigations were performed for a small-scale ADS with conventional MOX fuel and an 800 MWth power class ADT with advanced fertile-free fuels, both cooled by Pb/Bi. The analyses covered perturbations of the source [e.g. unprotected transient overcurrent (UTOC) and beam interruptions] as well as perturbations on the core side, protected/unprotected transient overpower (P/UTOP) induced by reactivity additions and unprotected loss of flow (ULOF) accidents. These showed that the small-scale ADS had a very good safety performance, while for the 800 MWth ADT with ZrO_2 and MgO matrix based fuels some safety problems were identified, mainly related to the large positive void feedback and high linear power rate. Further design and safety optimisations are under consideration.

Introduction

Accelerator-driven systems (ADS), which combine a subcritical reactor with a high-energy proton accelerator via a spallation target, are developed with the goal of efficient incineration/transmutation of minor actinides (MAs). Currently, the feasibility of ADS is being investigated within the Fifth Framework Programme (FP5) of the European Union, the so-called Preliminary Design Studies of an Experimental Accelerator-driven System (PDS-XADS) [1]. This work is devoted to both heavy metal cooled (Pb/Bi) and gas (He) cooled options. The chosen power level of this demonstrator is 80 MWth, k_{eff} is 0.97 at BOL and the core contains conventional fast reactor fuel (MOX). In parallel, FP5 FUTURE [2] investigates accelerator-driven transmuters (ADT) of the 800 MWth power class with advanced fertile-free cercer and cermet fuels. Inert matrices with high thermal conductivities are essential for these fuels because of low MA thermal conductivities. The main goal for designing the ADT was to investigate the feasibility of utilisation of these advanced fuels (details in Ref. [3]). One of the important issues was the demonstration of an adequate safety level for cores with these advanced dedicated fuels. As shown in Ref. [4], utilisation of such fertile-free fuels could lead to safety problems.

These new fuels significantly differ both in their thermal-physical/mechanical data and behaviour from conventional fast reactor fuels. In addition, due to their lack of U-238 and large MA content, these fuels have a significant impact on core safety parameters, represented by Doppler, void worth, clad worth, kinetics data, etc. Different core designs for these transmuters have been developed mainly using ZrO_2, MgO and Mo-92 as matrices for the Pu/Am/Cm fuels. All of these fuel/matrix combinations will be investigated step by step. Preliminary analyses showed that the most promising matrices from a safety point of view are those with MgO and Mo-92. To obtain a complete picture, the impact of ZrO_2-matrix based fuels on core safety was also investigated.

In this paper, comparative safety analyses and investigations were performed for the PDS-XADS with MOX fuel and the FUTURE-ADT with fuels embedded in ZrO_2 and MgO matrices, with both ADS and ADT cooled by Pb/Bi. The main differences between the ADS and ADT investigated in this paper refer both to the power class (size) and fuels utilised.

The current analyses cover perturbations of the target/source side and transients triggered on the core/nuclear system side. In this first round of investigations, the following transients were investigated:

- UTOC: Unprotected transient overcurrent.
- BI: Beam interruption.
- UTOP: Unprotected transient overpower.
- PTOP: Protected transient overpower.
- ULOF: Unprotected loss of flow**.**

Investigations of these advanced composite fuels reveal that especially for severe transients, new phenomena and scenarios must be expected and modelled. Severe accidents with fuel/clad melting and loss of core geometry are not investigated because the phenomenology under such conditions cannot be modelled adequately with the fuel and pin models in the current codes. New phenomena that might be expected under such conditions are discussed in Ref. [5] (e.g. fuel/matrix separation due to different melting points of the fuel/matrix system or high He production caused by Cm decay). The static neutronic analyses were performed by the ERANOS code system [6]. The transient analyses performed here use mainly the SIMMER-III code, a 2-D multi-phase, multi-component, three velocity field code coupled with space-time kinetics and using transport theory for the neutron flux shape calculation [7,8].

Core design and main parameters

The design of the PDS-XADS including neutronics, thermo-hydraulics, etc., was performed in detail within the PDS-XADS project [1,9]. On the other hand, in the FUTURE project a simpler core design was generated for the purpose of investigating the feasibility of an ADT with new fuels. The PDS-XADS core midplane and the FUTURE-ADT cross-sections are shown in Figures 1 and 2. The main geometric, thermal-hydraulic and neutronic data are given for PDS-XADS and FUTURE ZrO_2 and MgO matrix fuel ADTs in Tables 1, 2 and 3, respectively. For FUTURE-ADT core cross-sections, the target area is given in yellow, surrounded by three enrichment zones and reflectors.

Figure 1. Core cross-section of the PDS-XADS

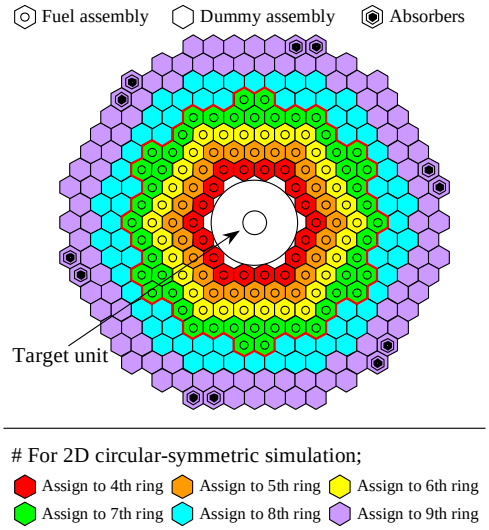

Figure 2. Core cross-sections of the FUTURE ZrO_2 and MgO ADTs

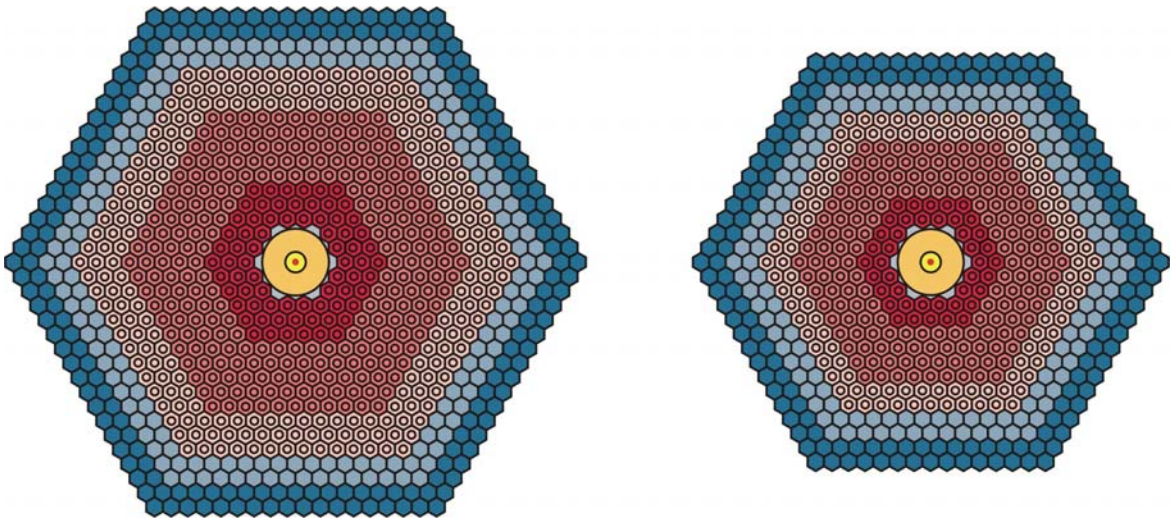

Table 1. Geometric parameters in the PDS-XADS and FUTURE-ADT designs

Parameter	PDS-XADS	FUTURE ZrO_2	FUTURE MgO
Core active height	0.87 m	1.00 m	1.00 m
Number of pins per SA	90	91	91
Number of fuel SAs	120	528	312
Subasssembly pitch	137.6 mm	112 mm	112 mm
Fuel pellet inner diameter	1.80 mm	0 mm	0 mm
Fuel pellet outer diameter	7.14 mm	5.85 mm	5.85 mm
Clad inner diameter	7.37 mm	6.00 mm	6.00 mm
Clad outer diameter	8.50 mm	6.80 mm	6.80 mm
Wrapper thickness	2.00 mm	2.00 mm	2.00 mm
P/D	1.57647	1.6	1.6

Table 2. Thermal-hydraulic parameters in the PDS-XADS and FUTURE-ADT designs

Parameter	PDS-XADS	FUTURE ZrO_2	FUTURE MgO
Total thermal power	80 MW	800 MW	800 MW
Peak linear power	153 W/cm	276 W/cm	479 W/cm
Mean velocity of coolant	0.42 m/s	1.00 m/s	1.86 m/s
Inlet coolant temperature	573 K	573 K	573 K
Outlet coolant temperature	673 K	723 K	710 K
Peak clad temperature	753 K	858 K	816 K
Peak fuel temperature	1 169 K	2 170 K	1 800 K

Table 3. Neutronic safety parameters (calculated by SIMMER) in the PDS-XADS and FUTURE-ADT designs

Parameter	PDS-XADS	FUTURE ZrO_2	FUTURE MgO
Enrichment zone	1	3	3
Enrichment/fuel fraction	23.25 at.%	38, 43, 53 vol.%	46, 50, 60 vol.%
K-eff at BOL	0.9655	0.9706	0.9781
Beta-eff	314 pcm	191 pcm	189 pcm
Neutron generation time Λ	$1.43 \cdot 10^{-6}$ s	$5.39 \cdot 10^{-7}$ sec	$5.34 \cdot 10^{-7}$ sec
Decay constant λ^{-1}	11.36 sec	13.16 sec	13.16 sec
Core void worth	-707 pcm	7 184 pcm	6 761 pcm
Doppler constant	-580 pcm	-19 pcm	-14 pcm

The neutronic safety parameters shown here are calculated by SIMMER and correspond to results obtained by other groups in the PDS-XADS and FUTURE projects. The most significant deviations of the ADT from ADS are that the ADT has very small negative Doppler feedback and a very large positive core void worth. The significant void worth introduces a positive reactivity feedback mechanism from thermal coolant expansion. A stabilising Doppler feedback is not available. Axial thermal expansion of the fuel pins and radial thermal expansion of the core subassemblies and grid plate will lead to

negative feedback, but they were not included in the analysis. Currently, only an insufficient database is available on these effects; however, they will be taken into account in future analyses. Note that the matrix volume fractions in the outer core zones are less than the required 50% [2,3]. The core design of the FUTURE-ADT has been updated to achieve this condition.

The large positive void worth of the cercer ADT is a result of the soft spectrum and relatively large core sizes. The ZrO_2 and MgO matrices have low thresholds for inelastic scatter, which leads to a relatively soft neutron spectrum and a significant proportion of neutrons below the americium fission threshold. A loss of coolant shifts the neutron spectrum to energies above the fission threshold of americium, which results in a large positive void worth. For the PDS-XADS and FUTURE ZrO_2 and MgO ADTs, ring-wise void worths of each fuel subassembly ring are shown in Figures 3, 4 and 5, respectively.

Figure 3. Void worth of the individual fuel SA rings in the PDS-XADS

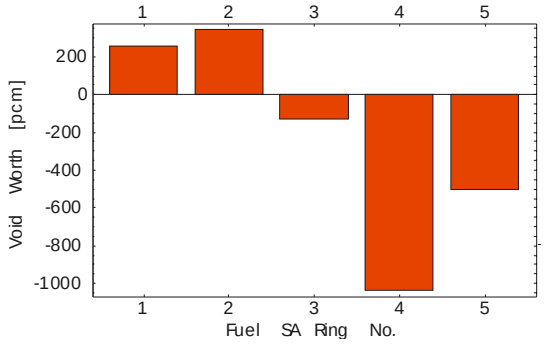

Figure 4. Void worth of individual fuel SA rings in the FUTURE ZrO_2 matrix fuel ADT

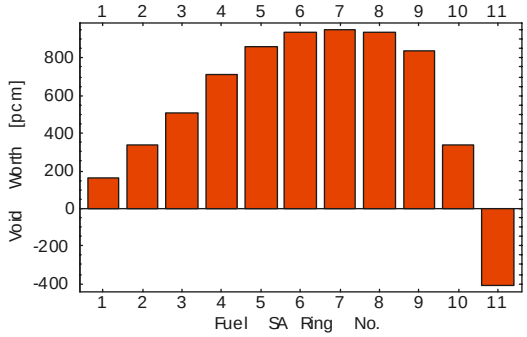

Figure 5. Void worth of individual fuel SA rings in the FUTURE MgO matrix fuel ADT

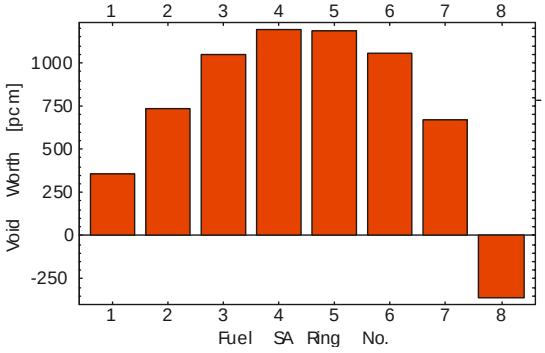

Fuel thermal conductivity has a large impact on fuel central temperature. Figure 6 shows thermal conductivities of MOX fuel and ZrO_2 matrix fuel, including experimental values and MgO matrix fuel. The curve for MOX fuel is based on the standard European fast reactor (EFR) recommendation with O/M = 2 and 5% porosity [10]. The curve for FUTURE ZrO_2 matrix fuel is a linear volume weighting of thermal conductivities of ZrO_2 [11] and EFR fuel with O/M = 1.88 and 10% porosity, where the volume ratio of matrix and fuel is 62/38. The curve for FUTURE MgO matrix fuel is obtained using Schulz's formula [12], where the volume ratio of matrix and fuel is 56/44. The experimental data were chosen from Ref. [13] for the Ca-stabilised ZrO_2 inert matrix UO_2 fuel with a composition of 72.9 wt.% ZrO_2, 8.1 wt.% CaO and 19 wt.% UO_2, and 10.1% porosity.

Figure 6. Fuel thermal conductivities of PDS-XADS MOX fuel; FUTURE MgO matrix fuel with 56 vol.% MgO and 10% porosity; FUTURE ZrO_2 matrix fuel with 62 vol.% ZrO_2 and 10% porosity; experimental data for ZrO_2 matrix UO_2 fuel [13] with 72.9 wt.% ZrO_2 and 10.1% porosity

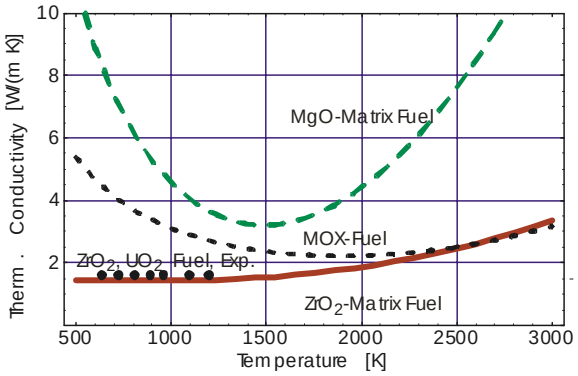

Results of transient analyses

For the small-scale PDS-XADS with good safety coefficients (negative void worth, large Doppler), the analyses revealed benign behaviour under design basis conditions (DBC) and strong resistance against severe transients [9]. Even under hypothetical conditions of core degradation and melting [design extension conditions (DEC)], defined with ad hoc assumptions, no severe accident scenario developed [14]. Such core melt scenarios were modelled with SIMMER [7,8] for MOX fuel and HLM coolant conditions.

For FUTURE-ADT with deteriorated safety parameters, a first picture of its behaviour [5] has begun to develop. Some problems include the lack of high temperature fuel data, the lack of knowledge regarding phenomenological behaviour under melt conditions and the lack of irradiation data. As previously described, for transients within the design basis, the fertile-free cores show virtually no feedback from Doppler but might reveal positive feedback from coolant expansion.

UTOC: Unprotected transient overcurrent

Power and reactivity traces of a beam overcurrent transient (where the beam strength is increased by 100% for 10 seconds) for the small-scale MOX ADS and the two ADTs are displayed in Figures 7, 8 and 9, respectively. It was observed that fuel centre temperatures in the hottest cell reached melting conditions at 9.5 s in the ZrO_2 ADT. In the MgO ADT, the peak fuel temperature was 2 277 K, which is just below the matrix fuel eutectic melting point. However, the coolant velocity in the hottest cell

reached values of 2 m/s, which is regarded as the LBE erosion limit. In contrast, for the small MOX ADS, the fuel temperatures stayed 1 440 K below the melting point. As an example, the fuel centre temperature distributions are shown in Figure 10 for the UTOC case of MgO ADT.

Figure 7. 100% beam overcurrent in small-scale PDS-XADS with conventional fast reactor fuel

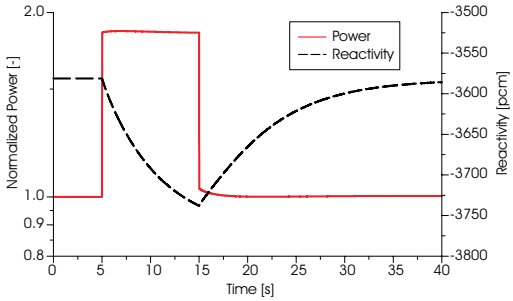

Figure 8. 100% beam overcurrent in the 800 MWth ADT with ZrO_2 matrix fertile-free fuel

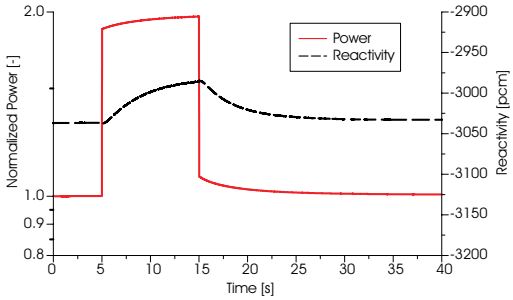

Figure 9. 100% beam overcurrent in the 800 MWth ADT with MgO matrix fertile-free fuel

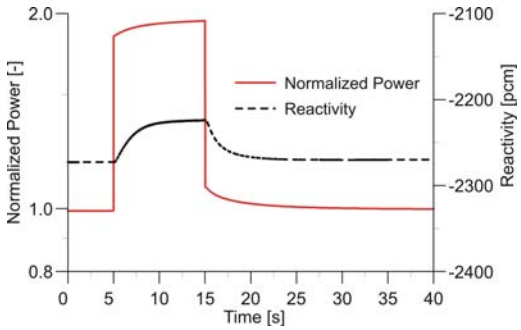

Figure 10. Fuel centre temperature distributions in the case of 100% beam overcurrent in the 800 MWth ADT with MgO matrix fertile-free fuel

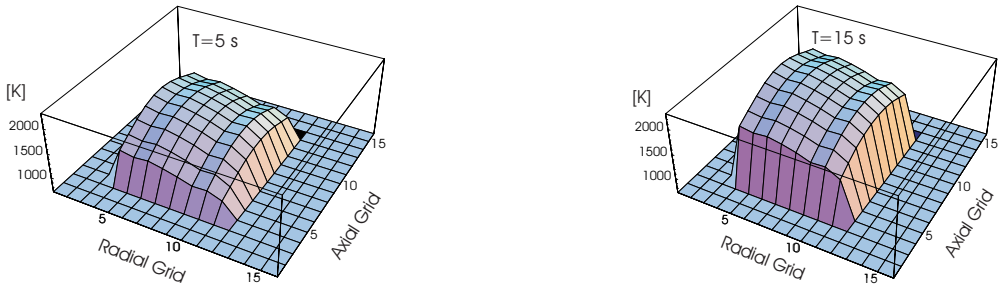

BI: Beam trip/interruption

Power and reactivity traces of beam trip transients (where the beam is interrupted for 10 seconds) for the small-scale ADS and ADT are displayed in Figures 11, 12 and 13, showing the difference in the reactivity development. The XADS had significant negative feedback, while the ADTs had slightly positive feedback. As described, the core expansion effects were not taken into account. Since the ADTs had higher fuel centre temperatures and the coolant inlet temperatures were the same, the fuel temperature drops in the ADTs were large (~1 000 K) compared to ~400 K in the XADS. Additionally, with the XADS, thermal conductivity increased as power decreased; whereas for the FUTURE ZrO_2 fuel conductivity decreased under such conditions. The thermal conductivity for MgO showed non-monotonous behaviour in this transient.

Figure 11. Beam trip (beam interruption) transient in the small-scale XADS with conventional fast reactor fuel

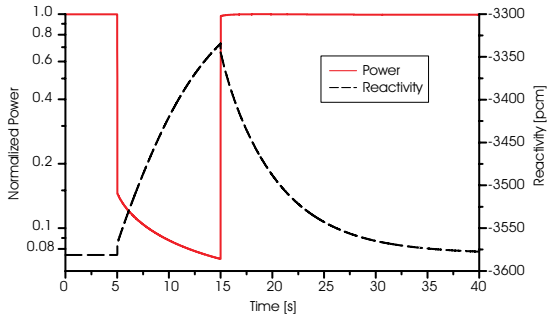

Figure 12. Beam trip transient in the 800 MWth ADT with ZrO_2 matrix fertile-free fuel

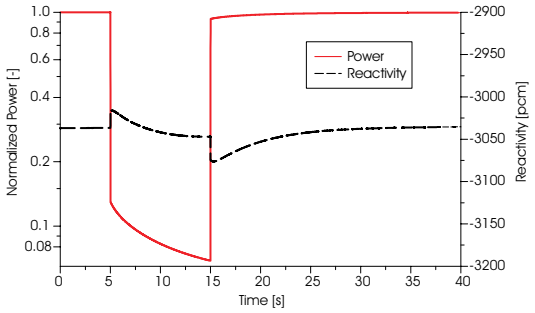

Figure 13. Beam trip transient in the 800 MWth ADT with MgO matrix fertile-free fuel

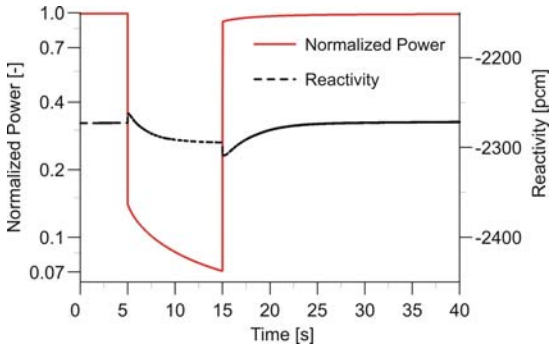

UTOP: Unprotected transient overpower

Power and reactivity traces of a UTOP transient [where the reactivity was increased by 314 pcm (corresponding to one beta in PDS-XADS, see Table 3) within 0.5 seconds] for the small-scale ADS and two ADTs are displayed in Figures 14, 15 and 16, respectively. A scenario that could introduce positive reactivity in the ADT is the blowdown of fission gases and helium after local pin failure and local voiding processes. This blowdown scenario was already studied using SIMMER [8]. An additional UTOP case was calculated for the ZrO_2 ADT, where the reactivity increase was 2 000 pcm. In the highly rated pins, fuel melting conditions were reached under such conditions.

Figure 14. Unprotected transient of overpower at a reactivity increase by 314 pcm (1 $) in the 80 MWth XADS with MOX fuel

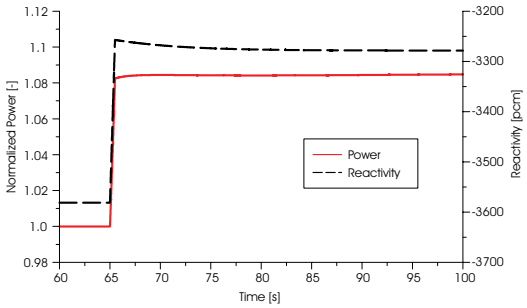

Figure 15. Unprotected transient of overpower at a reactivity increase by 314 pcm in the 800 MWth ADT with ZrO_2 matrix fertile-free fuel

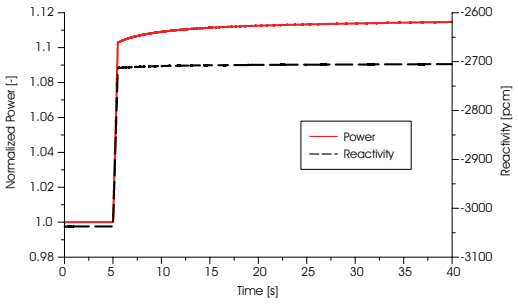

Figure 16. Unprotected transient of overpower at a reactivity increase by 314 pcm in the 800 MWth ADT with MgO matrix fertile-free fuel

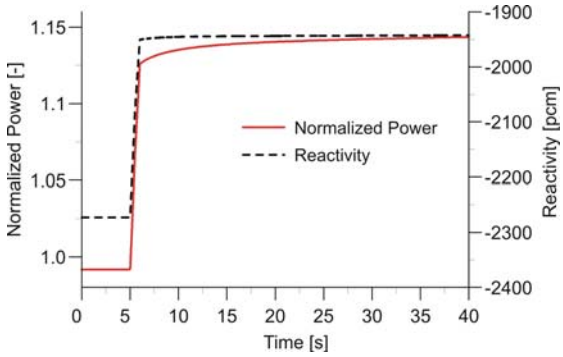

PTOP: Protected transient overpower

The 10 $ reactivity increase was also investigated but under the protected condition where the beam was shut off when reactivity began to increase. As expected, the power dropped to decay heat levels and all temperatures were reduced correspondingly. Power and reactivity traces of this PTOP transient are shown for both ZrO_2 and MgO ADTs in Figure 17.

Figure 17. Protected transients of overpower at a reactivity increase by 10 $ in the 800 MWth ADT with ZrO_2 and MgO matrix fertile-free fuels

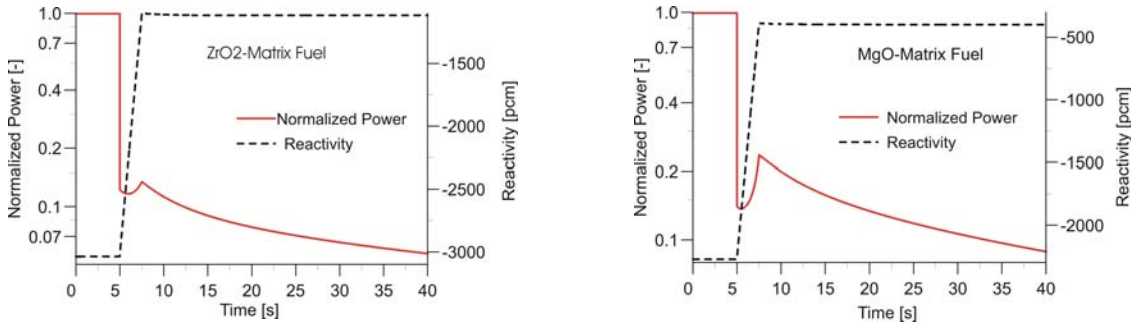

ULOF: Unprotected loss of flow

The ULOF condition meant a complete loss of forced coolant circulation in both the PDS-XADS and ADT. For the PDS-XADS, this corresponded to a coastdown of the gas lift pumps, whereas for the ADT, a conventional pump rundown was simulated. The coolant inlet temperatures were kept at steady state; as for the FUTURE-ADT, no primary/secondary side has been defined to date.

The transient of the coolant flow rate and the normalised power for the PDS-XADS are shown in Figure 18. After seizure of the gas lift pumps, a natural convection flow took over. Since the reactivity feedback caused by the Doppler effect and coolant thermal expansion was negative, the power levels were slightly below nominal. The highest cladding temperature at the top position of the core reached ~910 K, which was much lower than the cladding melting point (1 700 K). Coolant temperatures went up to 870 K. This result supported the high safety potential of the current XADS design. As previously mentioned, for the FUTURE-ADT design a forced convection cooling is envisaged. The pump coastdown was arbitrarily assumed with a pump characteristic, which would result in a flow-halving time of 5 s in the ZrO_2 core. Furthermore, beam-on conditions and constant coolant inlet temperatures were modelled. No axial structural expansion was modelled in this first set of investigations. The calculations showed that natural convection finally leads, after a flow dip, to a coolant velocity of 34% of nominal for the ZrO_2 ADT and 26% for the MgO ADT. (Note the higher MgO steady state power density and coolant velocity.) A significant difference to the PDS-XADS was, however, the positive feedback from coolant expansion. Thus, the core power levels off above nominal power. The power and reactivity traces are given in Figures 19 and 20 for both ADTs. The highest coolant temperatures in these calculations reached 1 160 K, peak clad temperature was ~1 250 K and the peak fuel temperature increased to 2 350 K for the ZrO_2 ADT; whereas, the peak temperatures of coolant, cladding and fuel were 1 257 K, 1 362 K and 2 038 K, respectively, for the MgO ADT. In the ULOF calculations, no clad or fuel melting was reached, for the MgO core fuel temperatures were already close to the eutectic melt limit. For both ADT cores, the transient coolant temperatures went beyond the limit set for corrosion prevention.

Figure 18. Coolant flow rate and power in the ULOF case of the small-scale PDS-XADS

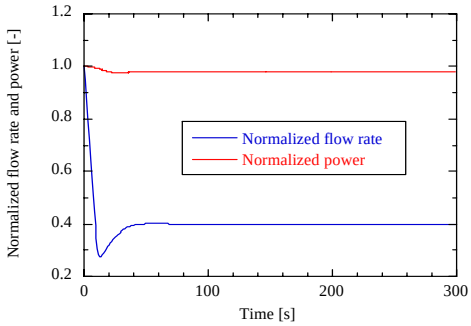

Figure 19. Power and reactivity traces in the ULOF case of the FUTURE ZrO_2 ADT

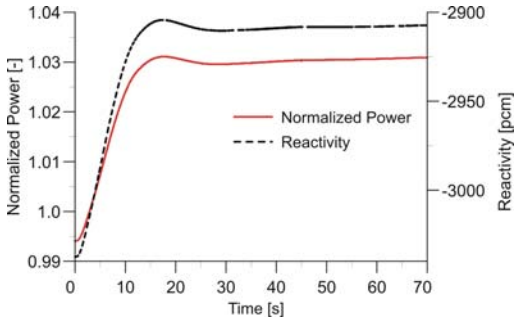

Figure 20. Power and reactivity traces in the ULOF case of the FUTURE MgO ADT

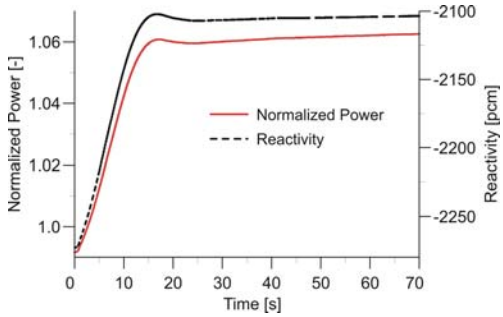

DEC Behaviour

The first qualitative analyses of the DEC behaviour show the importance of the clad worth of these cores, as steel melting advances any Pb/Bi boiling and leads to unclad pin stubs, which disrupt and may lead to sweep-out scenarios and reduction of reactivity (depending on the timing and amount of clad/fuel removal). Voiding can take place and add reactivity via the blowdown of He and fission gases from the fission gas plena. It can also be noted that the change of the reactivity level alters the flux and power shape, possibly leading to higher energy deposition into the peripheral regions of the core [15]. The application of space-time kinetics seems to be important to cover these effects, which might impact the propagation potential of an accident. Fuel break-up and sweep-out effects were simulated and results were presented in Ref. [14]. More detailed analyses of the DEC phenomena are planned in the future.

Conclusion

The transient behaviour of the 80 MWth PDS-XADS with conventional fast reactor fuel and good safety parameters (no MA content in the fuel, low power rating) was compared with an 800 MWth ADT using advanced fertile-free fuels with high MA load. Specifically, two options with ZrO_2 and MgO matrices were investigated. The analyses showed that the small Pb/Bi-cooled ADS has a very good safety performance. Analyses for the ADT with ZrO_2-matrix based fuel and strong positive feedback potentials revealed some safety problems. These were mainly related to the thermal conductivity of the fuel and the high positive void worth. The ZrO_2 fuel had a very low power-to-melt ratio of ~400 W/cm linear power. UTOCs and UTOPs might lead to local melting conditions. For the MgO matrix, the behaviour under overpower conditions was improved, since MgO fuel has higher thermal conductivity, and no melting conditions were noted for the transients analysed. But the highest fuel temperatures were quite close to the fuel melting point (eutectic point) that was assumed to be 2 300 K. Moreover, the core must be further optimised to cope with the requirements of the LBE erosion limit. In the ULOF cases of both ADTs, the natural convection potential of Pb/Bi could prevent immediate core damage. However, the coolant temperatures increased up to 1 160 K and 1 260 K, which are far beyond the permissible temperature limits for erosion control and prevention. For the MgO core, fuel temperatures were again close to the melting point. From the viewpoint of safety, it can be stated that both the ZrO_2 and MgO-based cores need further optimisation. The safety parameters of the ADT, especially the void worth, could be improved by reducing the core size and total power, for example. Further calculations are currently going on, reaching also into the DEC range with fuel melting and pin disruption. Additional code development is under way, which reveals the urgent need for a broader experimental basis related to the high temperature range of these fuels.

Acknowledgements

We are grateful to Dr. Rudy Konings at the Institute for Transuranium Elements in Karlsruhe for providing us with additional information on fuel thermal conductivities. The work was partly performed under the EU contracts, FIKW-CT-2001-00148 (FUTURE) and FIKW-CT-2001-00179 (PDS-XADS).

REFERENCES

[1] *PDS-XADS Preliminary Design Studies of an Experimental Accelerator-driven System*, EU contract number FIKW-CT-2001-00179 (2001).

[2] Maschek, W., Mg. Mori, P. Smith, R. Thetford, J. Wallenius, V. Sobolev, S. Pillon, *Preliminary Safety Ranking for the Investigated Candidate Fuels of Accelerator Driven Transmuter (ADT) – Fuels for Transmutation of Transuranium Elements (FUTURE)*, EU contract number FIKW-CT-2001-00148 (2003).

[3] Pillon, S., J. Wallenius, P. Smith, W. Maschek, "The European FUTURE Programme", *Global 2003*, New Orleans, LA, USA (2003).

[4] Maschek, W., A. Rineiski, M. Flad, K. Morita, P. Coste, “Analysis of Severe Accident Scenarios and Proposals for Safety Improvements for ADS Transmuters with Dedicated Fuel”, *Nuclear Technology*, 141, 2 (2003).

[5] Maschek, W., T. Suzuki, X-N. Chen, Mg. Mori, C. Matzerath-Boccaccini, M. Flad, K. Morita, “Behaviour of Transmuter Fuels of Accelerator Driven Systems Under Severe Accident Conditions”, *GENES3/ANP2003*, Kyoto, Japan (2003).

[6] Doriath, J.Y., E. Kiefhaber, U. Wehmann, J.M. Rieunier, “ERANOS, The Advanced European System of Codes for Reactor Ph. Calc.”, *International Conference on Math. Methods and Sup. Comp.*, Karlsruhe, Germany (1993).

[7] Kondo, S., H. Yamano, T. Suzuki, Y. Tobita, S. Fujita, X. Cao, K. Kamiyama, K. Morita, E.A. Fischer, D.J. Brear, N. Shirakawa, M. Mizuno, S. Hosono, T. Kondo, W. Maschek, E. Kiefhaber, G. Buckel, A. Rineiski, M. Flad, P. Coste, S. Pigny, L. Louvet, T. Cadiou, “SIMMER-III, A Computer Program for LMFR Core Disruptive Accident Analysis”, JNC TN9400 2001-002 (2000).

[8] Maschek, W., A. Rineiski, K. Morita, E. Kiefhaber, G. Buckel, M. Flad, P. Coste, S. Pigny, G. Rimpault, J. Louvet, T. Cadiou, S. Kondo, H. Yamano, T. Suzuki, Y. Tobita, S. Fujita, “SIMMER-III, A Code for Analyzing Transients and Accidents in Accelerator Driven Systems (ADS)”, *AccApp’00*, Washington, USA (2000).

[9] Chen, X-N., T. Suzuki, A. Rineiski, E. Wiegner, W. Maschek, M. Flad, “Unprotected Transients in a Small Accelerator Driven System”, *AccApp’03*, San Diego, USA (2003).

[10] Schimdt, H.E., C. Sari, K. Richter, “The Thermal Conductivity of Oxides of Uranium, Neptunium and Americium at Elevated Temperatures”, *Journal of the Less-common Metals*, 121, 621-630 (1986).

[11] Touloukian, Y., *et al*, *Thermophys. Prop. Mater. Vol. 1*, New York, Plenum (1970).

[12] Schulz, B., “Thermal Conductivity of Porous and Highly Porous Materials”, *High Temperatures – High Pressures*, 13, 649-660 (1981).

[13] Ronchi, C., J.P. Ottaviani, C. Degueldre, R. Calabrese, “Thermophysical Properties of Inert Matrix Fuels for Actinide Transmutation”, *Journal of Nuclear Materials*, 320, 54-65 (2003).

[14] Suzuki, T., X. Chen, A. Rineiski, W. Maschek (FZK), “Analyses of Unprotected Transients in the Lead/Bismuth-cooled Accelerator Driven System PDS-XADS”, *Proceedings of GLOBAL 2003*, Int. ANS/ENS 2003 Winter Meeting, New Orleans, US, 16-20 November 2003, pp. 1 725-1 732 (2003).

[15] Rineiski, A., W. Maschek, G. Rimpault, “Performance of Neutron Kinetics Models for ADS Transient Analyses”, *AccApp’01*, Reno, USA (2001).

COMPARATIVE TRANSIENT ANALYSIS OF Pb/Bi AND GAS-COOLED XADS CONCEPTS

P. Coddington, K. Mikityuk, R. Chawla
LRS, Paul Scherrer Institute, Villigen (PSI), Switzerland
paul.coddington@psi.ch

Abstract

In the field of waste management incorporating a transmutation option, accelerator-driven systems (ADS) represent an important alternative to conventional reactors due to their higher safety level when minor actinides (such as neptunium and americium) are loaded into the core. The Preliminary Design Study of an Experimental Accelerator-driven System (PDS-XADS) is being performed within the European Union's Fifth Framework Programme. The main goal of PDS-XADS is to demonstrate the feasibility of an ADS and to compare different coolant (Pb/Bi and gas) and power (50-80 MWth) options. At this stage, all options use MOX fuel. Comparative safety analyses were performed using the TRAC/AAA code for the 80 MWth Pb/Bi and gas-cooled designs. The analyses covered reactivity increase (as an example of perturbations of the core), transient overcurrent (as an example of perturbations of the source) and loss of coolant (as an example of transients coming from faults in the primary and secondary coolant systems).

Introduction

In the field of waste management incorporating a transmutation option, accelerator-driven systems (ADS) represent an important alternative to conventional reactors due to their higher safety level when minor actinides (e.g. neptunium and americium) are loaded into the core. Within the European Union Fifth Framework Programme (FP5), several ADS-related projects are being performed, one of which is the Preliminary Design Study of an Experimental Accelerator-driven System (PDS-XADS). The main goal of PDS-XADS is to demonstrate the feasibility of an ADS and to compare different coolant (Pb/Bi and gas) and power (50-80 MWth) options. At this stage, all options use MOX fuel.

Comparative safety analyses were performed using an adapted version of the TRAC/AAA code [1] for both the 80 MWth Pb/Bi and gas-cooled designs. The analyses presented in this paper cover reactivity increase (as an example of perturbations of the core), transient overcurrent (as an example of perturbations of the source) and loss of coolant (as an example of transients coming from faults in the primary and secondary coolant systems).

A detailed evaluation of reactor safety depends on a wide range of considerations, including possible initiating events, response of the reactor core, reactor coolant and mitigating effects, e.g. shutdown mechanisms, decay heat removal, etc. Many of these features are design specific, so that a simple one-to-one comparison between the two systems is very difficult. For example, the safety of a given XADS concept is a mixture of the response of the plant system (which would be similar to that in the corresponding critical reactor case and thus is unrelated to the subcritical nature of the ADS) and the response of the reactor core (where the individual core design and level of subcriticality are important). This is highlighted by comparing both system and core-initiated transients for the two XADS concepts.

Pb/Bi and He-cooled XADS concepts

The main parameters of 80 MWth MOX-fuelled Pb/Bi and gas (He) cooled ADS demonstration facilities developed by Ansaldo [2,3] and by FRAMATOME [4] are given in Table 1.

Table 1. Main parameters of Pb/Bi and He-cooled XADS systems

Parameter	Pb/Bi	He
Nominal thermal power, MW	80	80
Multiplication factor k_{eff} at BOC	0.973	0.954
Number of FSAs/fuel pins per FSA	120/90	90/37
FSA flat-to-flat distance, mm	138	120
Fuel type/fuel mass, t	MOX/3.24	MOX/4.37
Plutonium content, %	23	35
Core inner/outer diameter, m	0.58/1.7	0.48/1.4
Fuel height, mm	900	1 500
Fuel pellet inner/outer diameter, mm	1.8/7.14	3.2/11.5
Clad outer diameter, mm	8.5	13
Pitch-to-diameter ratio	1.58	1.29
Average/peak power rating, W/cm	82/130	160/256
Primary coolant/pressure, MPa	PbBi/1	He/6
Inlet/outlet coolant temperature, ºC	300/400	200/450
Core mass flow rate, kg/s	5 460	61.6
Core pressure drop, kPa	25	100

Diagrams of the two systems' core designs are presented in Figure 1(a) and 1(b). The subcritical core in both options has an annular configuration. A spallation neutron source unit is inserted in the core central void. In both cases, this source unit has its own circuit with circulating Pb/Bi eutectics used as a coolant and a target.

Figure 1. Diagrams of the Pb/Bi (a) and He (b) XADS core designs

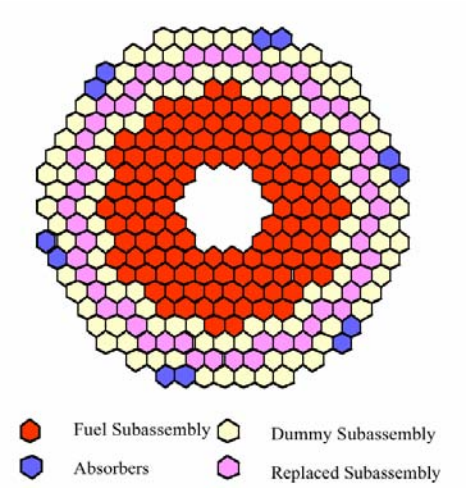

(a)

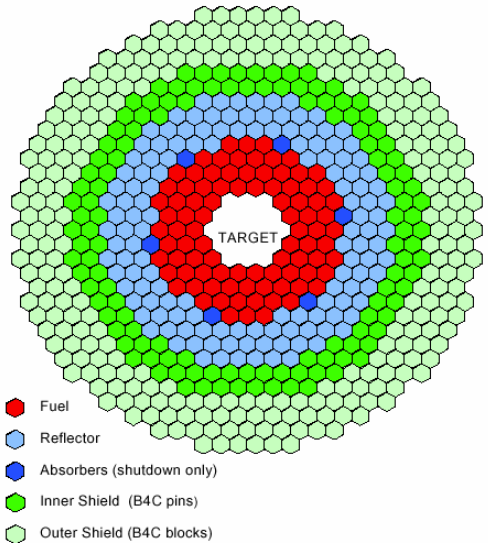

(b)

Diagrams of the two systems are shown in Figure 2(a) and 2(b). In the Pb/Bi option, the primary system does not use traditional mechanical pumps. Instead, the natural circulation of the primary Pb/Bi is enhanced with gas lift pumps. Due to the high fuel pin pitch-to-diameter ratio in the core, absence of mechanical pumps and low coolant velocities, the hydraulic resistance of the Pb/Bi primary circuit is very low (~0.3 bar), providing a high level of natural circulation in case of pump trip. This along with a low core power rating, positive Pb/Bi properties (especially, high thermal inertia, chemical inertness and low neutron absorption), use of the passive decay heat removal system and the external neutron source provide a sound basis for a high level of safety with the Pb/Bi system.

In the gas-cooled option, the coolant (at ~60 bar pressure) flows out of the core [Figure 2(b)] and into the large upper plenum volume, then through the inner part of a concentric pipe to the power conversion system (PCS), which consists of a heat exchanger and blower unit. The secondary side of the heat exchanger is water-cooled. The blower drives the coolant along the outer region of the concentric pipe, into the reactor vessel downcomer and then to the lower plenum and core inlet. The gas-cooled XADS has a more compact core compared to the Pb/Bi-cooled system and, in particular, has a smaller number of thicker fuel pins per assembly with the result that the core average and peak linear ratings are about twice those of the Pb/Bi-cooled concept. For the gas-cooled XADS, the decay heat removal system consists of two out of three heat exchangers [Figure 2(b)], each with a nominal heat removal capacity of 2 MW, connected directly to the pressure vessel and placed at the same elevation as the connection to the PCS. The heat exchangers have a natural circulation secondary side water coolant flow and are designed to operate on the primary side under natural circulation conditions at full reactor pressure. However, the heat exchangers include blowers to circulate the primary coolant flow under low pressure (LOCA) conditions. An other important feature of the decay heat removal system is that a valve is located just upstream of the cold side PCS connection to the pressure vessel, which for a loss of coolant accident when closed prevents coolant flowing directly out of the break without first flowing through the core.

Figure 2. Diagrams of the Pb/Bi (a) and He (b) XADS system designs

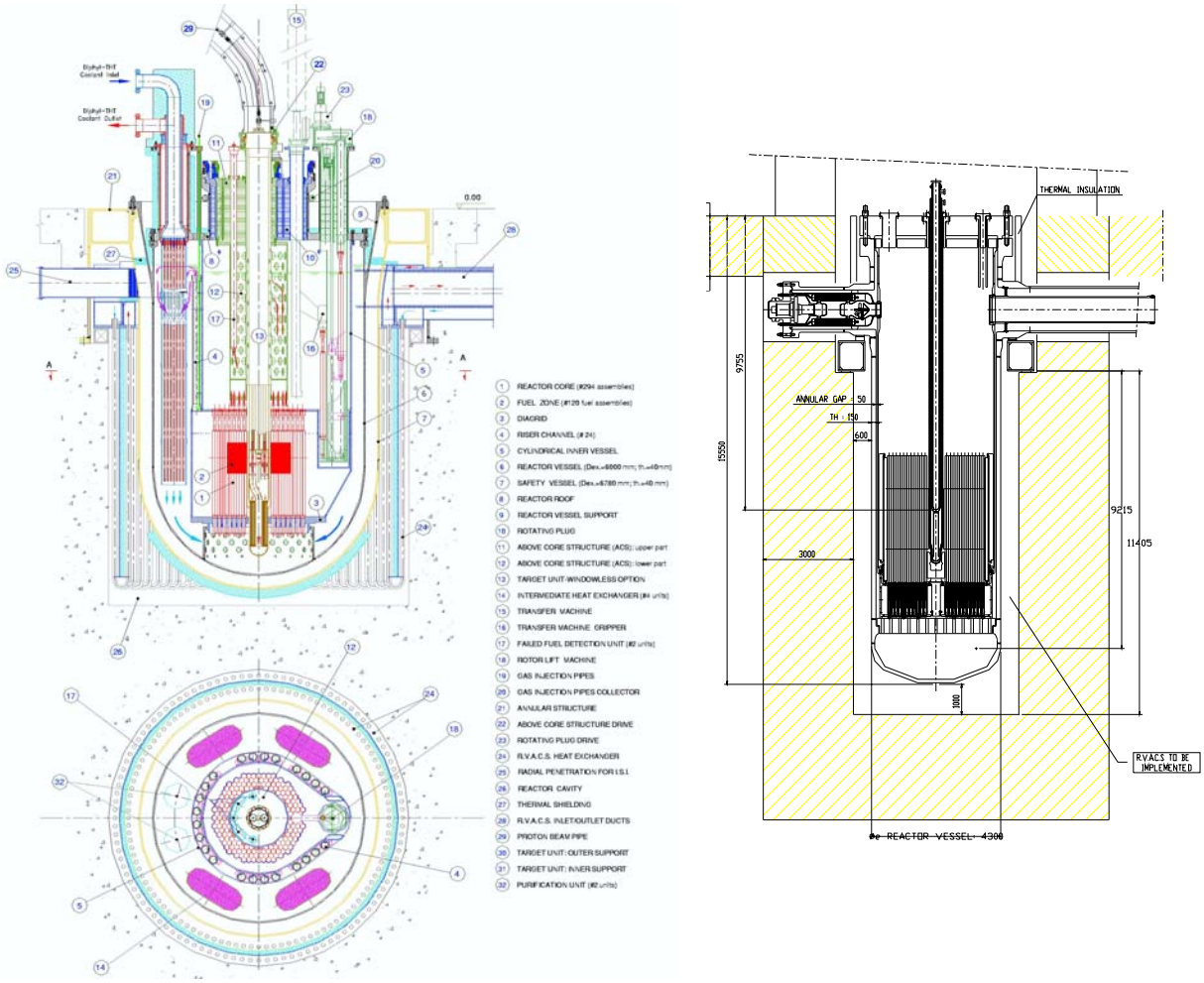

(a) (b)

TRAC/AAA models

The TRAC/AAA [1] code version was specially developed at Los Alamos National Laboratory (USA) on the basis of the standard TRAC-M code to simulate transient behaviour of fast spectrum reactor systems, in particular to simulate additional working fluids (including liquid metals and helium), to add liquid metal and gas heat transfer correlations, to simulate fluid power in the working fluid and to simulate conduction within the working fluid (important for liquid metal coolants). Further code developments have been performed at PSI, including the integration of the FRED [5] fuel model to better capture reactivity feedback effects due to the fuel and core structure thermal expansion.

A three-dimensional (3-D) R-Z-q representation with some 1 440 computational cells was elaborated for the TRAC/AAA simulation of the Pb/Bi primary vessel. The secondary and tertiary circuits of the Pb/Bi system were simulated using 1-D components. For the gas-cooled concept, a 1-D noding scheme of the pressure vessel, PCS and secondary coolant system (SCS) was used. A full set of plant protection controls and trips was included to control the accelerator beam trip, main blower trip, PCS isolation valve trip, opening of the SCS isolation valve and startup of the SCS blower.

Transient overpower (TOP) in Pb/Bi and gas-cooled systems

The results obtained for an unprotected (no beam trip) transient overpower accident (hypothetical addition of 2 000 pcm of reactivity) in the subcritical gas and Pb/Bi-cooled reactors are shown in Figure 3. Results [curves (2) for gas] are shown to provide a comparison of calculations for the two systems, beginning from the same subcriticality level of ~0.97 (chosen for the Pb/Bi-cooled system). The power jump to approximately 2.5· nominal was the same in both systems. However, due to the higher power rating in the gas-cooled system and the low thermal inertia of the coolant, the clad and fuel temperatures increased to much higher values. In fact, for this transient the calculation terminated as soon as fuel melting occurred. Curves (1) for the gas-cooled system show that this transient is mitigated when the initial (operating) reactivity level is reduced. In this calculation, the nominal value of ~0.954 for the gas-cooled design was used.

Figure 3. Calculation results for unprotected transient overpower in Pb/Bi and gas-cooled systems

(a) K-effective, (b) relative reactor power, (c) clad surface temperatures

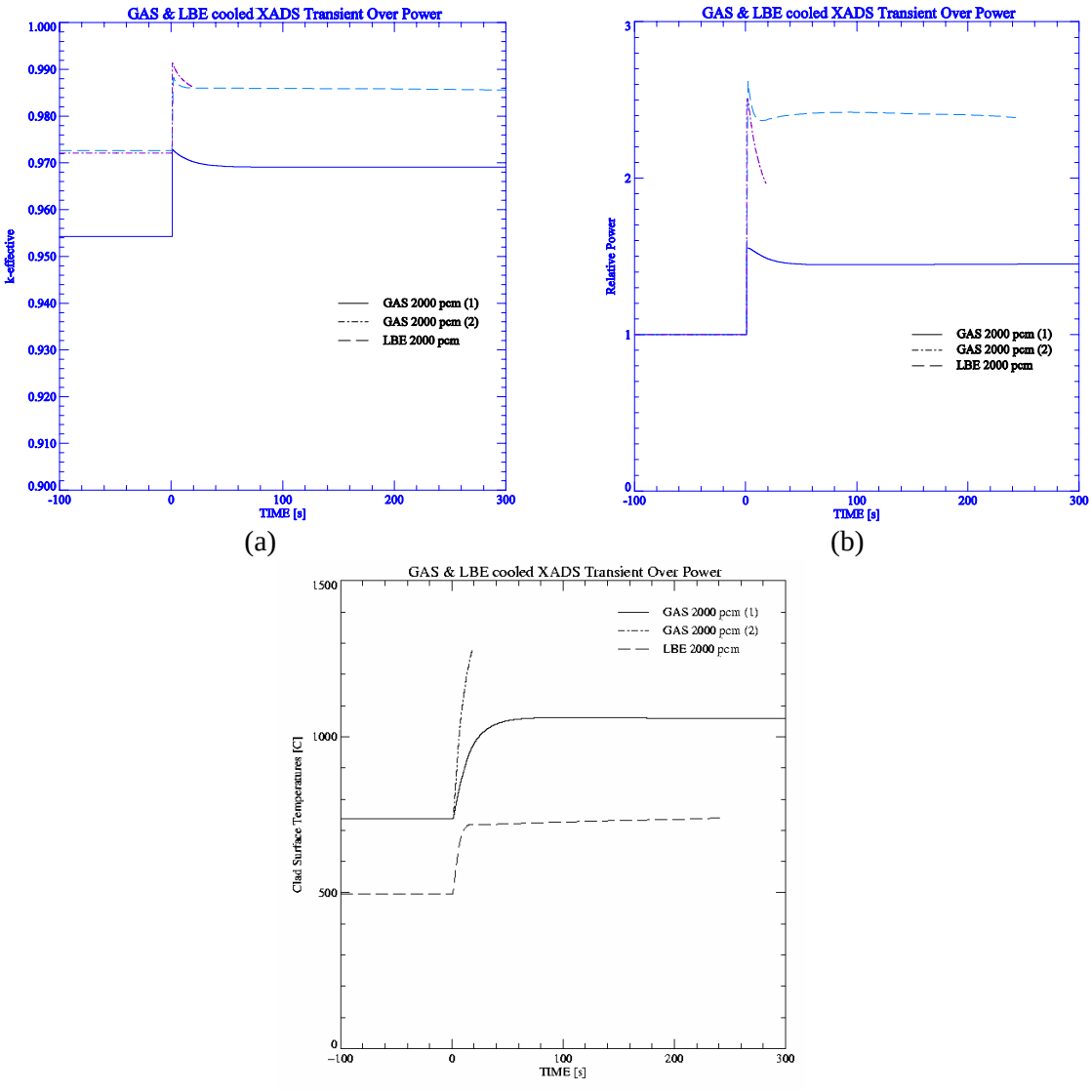

Beam overcurrent in Pb/Bi and gas-cooled systems

Since it is important in the analysed ADS for the beam current to be able to vary by over at least a factor of two to accommodate the reactivity swing expected during a reactor cycle, one transient that must be considered is the accidental increase in beam current to the maximum that the accelerator can deliver. Therefore, in order to examine this accident, the consequence of a beam overcurrent by a factor of two was considered.

The results obtained for three transients are presented in Figure 4. The transients examined are an unprotected beam overcurrent for the gas-cooled XADS, a protected beam overcurrent for the gas-cooled XADS and an unprotected beam overcurrent for the Pb/Bi-cooled XADS. The beam overcurrent transients were initiated from the design values of k_{eff}, i.e. the gas-cooled XADS transients start from a k_{eff} of ~0.954 and the Pb/Bi-cooled XADS from a k_{eff} of ~0.973.

For all transients, the $2\cdot$ beam overpower resulted in a rapid increase of the core power to ~1.8-1.9 of the initial value. The increase in core power produced an increase in the fuel and clad temperatures with the result that for the unprotected gas-cooled XADS transient [curves GAS (1) in Figure 4], clad melting occurred after ~20 s resulting in the termination of this calculation. This is similar to the situation for the TOP transient reported earlier with a k_{eff} value of 0.973 for the gas-cooled XADS, i.e. for the GAS (2) curves in Figure 3. (It should be noted that the initial peak cladding temperature for the gas-cooled system was lower in this calculation than that reported for the TOP transient. Also in this calculation the influence of increased clad to coolant heat transfer as a consequence of roughening the fuel pin surface was taken into account.) The effects of a subsequent trip of the accelerator are shown in the second gas transient [protected beam overcurrent, curves GAS (2) in Figure 4]. For this calculation, the accelerator was assumed to trip on high coolant (core exit) temperature. For this transient, as a consequence of the rapid reduction in the core power to the decay heat level, and the fact that at least initially the PCS blower and heat exchanger continue to operate, the clad and fuel temperatures fell rapidly.

The response of the Pb/Bi-cooled reactor was similar to that for the TOP accident, except with the beam overcurrent transient where the power jump was approximately $1.9\cdot$ nominal compared to $2.5\cdot$ nominal for TOP. Figure 4 shows that for the unprotected Pb/Bi-cooled reactor, due to the much greater thermal capacity of the coolant, there are only modest increases in the peak clad and fuel centre line temperatures.

Another interesting difference between the two reactor systems is shown in Figure 4. Due to higher peak linear rating and larger fuel pin diameter of the gas-cooled concept, normal operation fuel centre line temperature was significantly higher, making it more sensitive to “overpower” transients.

A general conclusion from the two overpower transients presented above (i.e. TOP and beam overcurrent) is that although the power increase is dependent upon the subcriticality of the system, the response of the reactor to this power increase is more related to the general design of the reactor (e.g. power level, linear rating) and the choice of coolant.

Figure 4. Calculation results for beam overcurrent accident in Pb/Bi and gas-cooled systems

(a) Clad surface temperature, (b) fuel centre line temperature, (c) relative reactor power, (d) k-effective

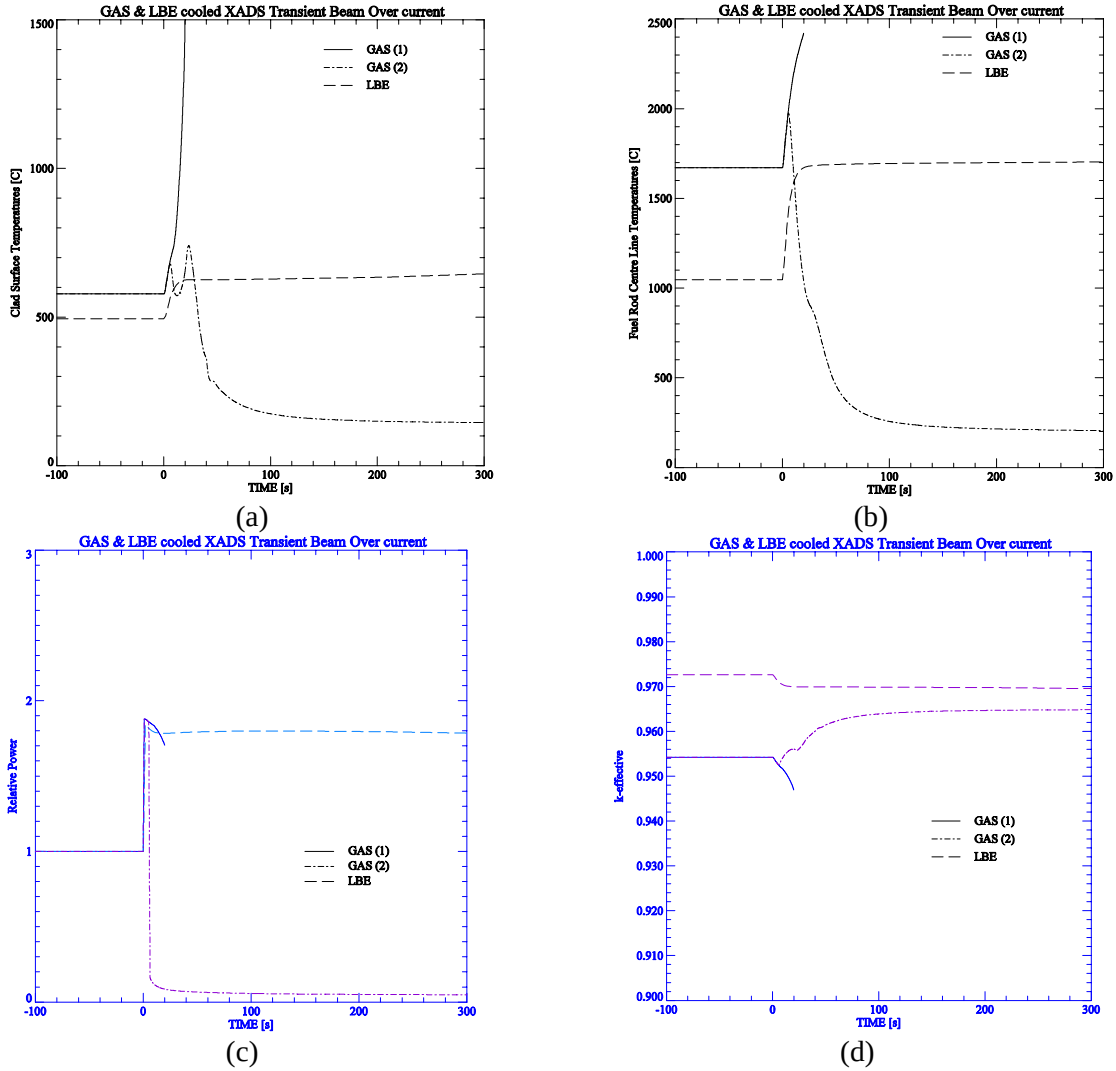

Loss of coolant accident (LOCA) in Pb/Bi-cooled system

The loss of primary coolant was simulated with a leak at the bottom of the primary vessel, the break area was assumed to be 50 cm^2 and the outer pressure was set equal to 1 bar. Results for the unprotected (no beam trip) accident with a loss of 74 m^3 of coolant are presented in Figure 5. The value of 74 m^3 corresponds to the free volume space between the main and safeguard vessels of the reactor system. In this case, due to the increased level swell of the Pb/Bi in the riser, the main circulation path remained unbroken and all the "gas lift" pumps remained in operation. The circulation flow rate was established via the main path at ~45% of the nominal value and so effectively removed the reactor power through the intermediate heat exchangers (IHX) even though the "collapsed" coolant level decreased by almost 3 m. As a consequence of the reduction in coolant flow rate, the fuel and clad temperatures increased in the transient to 1 115 C and 630 C, respectively, and stabilised at these levels. Thus, in case of a main vessel break, the system remained coolable even in the unprotected case.

Figure 5. Calculation results for unprotected LOCA in Pb/Bi-cooled system

(a) Relative core and IHX power, (b) relative primary and secondary coolant flow rate, (c) peak fuel and clad temperatures, core outlet coolant temperature, (d) collapsed coolant level above fuel top and integrated break flow

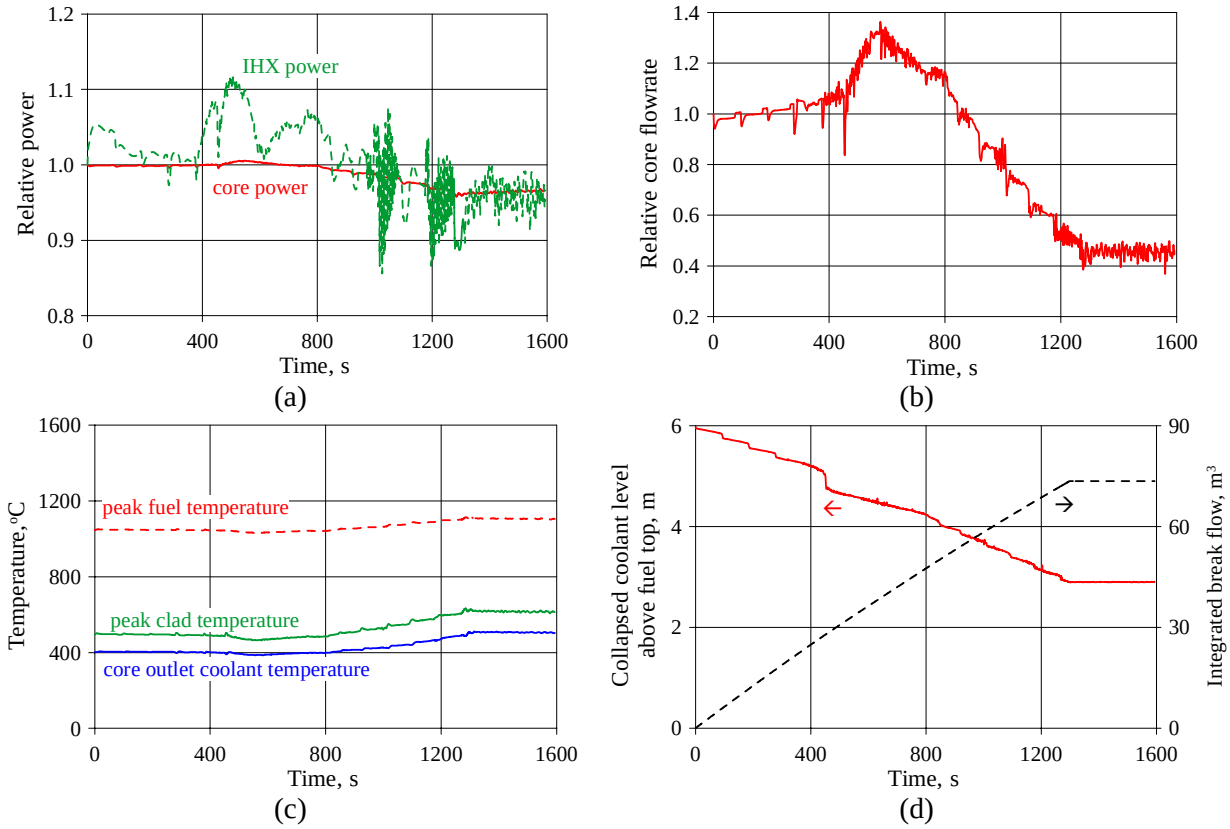

Loss of coolant accident in gas-cooled system

Since gas-cooled fast reactors, including the current subcritical XADS design, operate at high pressures during normal operation, they are susceptible to large and small break loss of coolant accidents. Breaks in the pressure vessel other than very small ones (e.g. instrument penetrations) are generally excluded from the list of design basis conditions (DBC) and are treated as residual risk. For this reason, for the analysis of DBC events, a range of breaks in the "outer skin" (i.e. cold side) of the pipe connecting the reactor pressure vessel to the power conversion system (PCS) was considered. As an example, the transient results of a large 300 cm^2 break loss of coolant accident are presented here.

As stated above, the gas-cooled XADS decay heat removal system consists of two out of three heat exchangers, each with a nominal heat removal capacity of 2 MW and connected to the pressure vessel at the same elevation as the connection to the PCS. The heat exchangers operate under natural circulation conditions at full reactor pressure but include blowers to circulate the coolant flow under low pressure (LOCA) conditions. The other important feature of the decay heat removal system is the valve located just upstream of the cold side PCS connection to the pressure vessel, which when closed prevents coolant flowing directly out of a break without first flowing through the core. Therefore, it is important that this valve closes early in any LOCA, i.e. before flow reversal occurs in the cold side of the PCS pipe.

In the "large" 300 cm^2 break accident, the reactor depressurises rapidly (i.e. within 30 s) to atmospheric conditions so that, during this time, the flow through the PCS quickly falls to zero, the PCS cold side valve closes and the SCS blowers are initiated. If the accelerator beam is not "shut off" during this period, then the clad and fuel temperatures will rise rapidly within the first 10 s and melting will result. This is similar to the overpower transients discussed above, where the low thermal inertia of the coolant in the gas-cooled XADS together with the higher linear heat generation rates and thicker fuel pellets means that rapid and redundant/independent accelerator beam trip mechanisms are required to prevent core melt. The results presented in Figure 6 (smooth fuel pins and no fuel channel gagging) and Figure 7 (roughened fuel pins and limited gagging) are therefore for protected transients, i.e. assuming accelerator beam trip on high coolant temperature occurs at ~5 s.

Figure 6 and Figure 7 show that following the rapid depressurisation and termination of the PCS flow, the SCS (two out of three units) flow is quickly established at about the design value of 0.65 kg/s per unit, and that the peak clad temperature increases as the coolant flow through the core decreases. During this period, the fuel and clad temperatures equalise to about the same value. The magnitude of the initial increase in the clad temperature is directly related to normal operation stored energy in the fuel, which is a function of the linear rating, fuel pin size and normal operation heat transfer. This latter dependency is clearly shown in Figure 6 and Figure 7. In the latter case, as a consequence of the increased heat transfer in normal operation due to roughening of the pin surface, the fuel stored energy was lower and the transient increase in the clad temperature was significantly reduced.

Following the initial equalisation of the clad and fuel temperatures, the clad and fuel temperatures increased as the coolant temperature increased to the level needed to match the SCS heat removal rate to the core decay heat. The coolant/clad and fuel temperatures then fell as the decay heat fell.

In summary, for a large break LOCA, due to the low thermal inertia of the coolant, it is not possible to protect the current gas-cooled XADS from clad and fuel melt unless the accelerator beam is tripped off within the first few seconds. For a protected LOCA, the SCS system was shown to work as designed, while the initial increase in the clad temperature was dependent upon the design parameters of the core, e.g. linear rating, fuel pellet diameter, normal operation heat transfer, etc. Through suitable design, the peak clad temperature could be reduced to an acceptable value.

Figure 6. Calculation results for LOCA in gas-cooled system with large (300 cm^2) break in the PCS connecting pipe (smooth fuel pins and without fuel channel gagging)

a) PCS and SCS mass flow rates, b) clad surface temperature

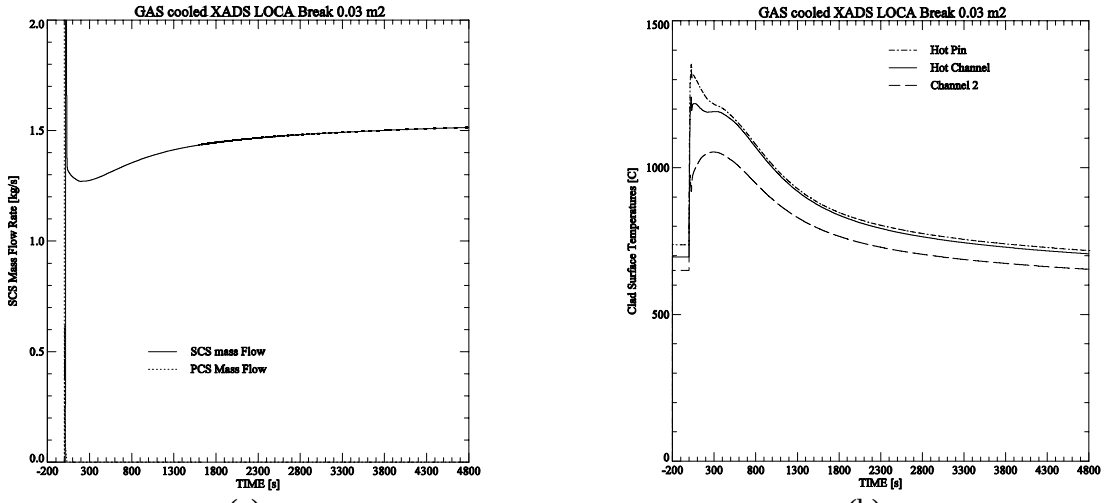

(a) (b)

Figure 7. Calculation results for LOCA in gas-cooled system with large (300 cm^2) break in the PCS connecting pipe (roughened fuel pins and limited gagging)

(a) PCS and SCS mass flow rates, (b) clad surface temperature

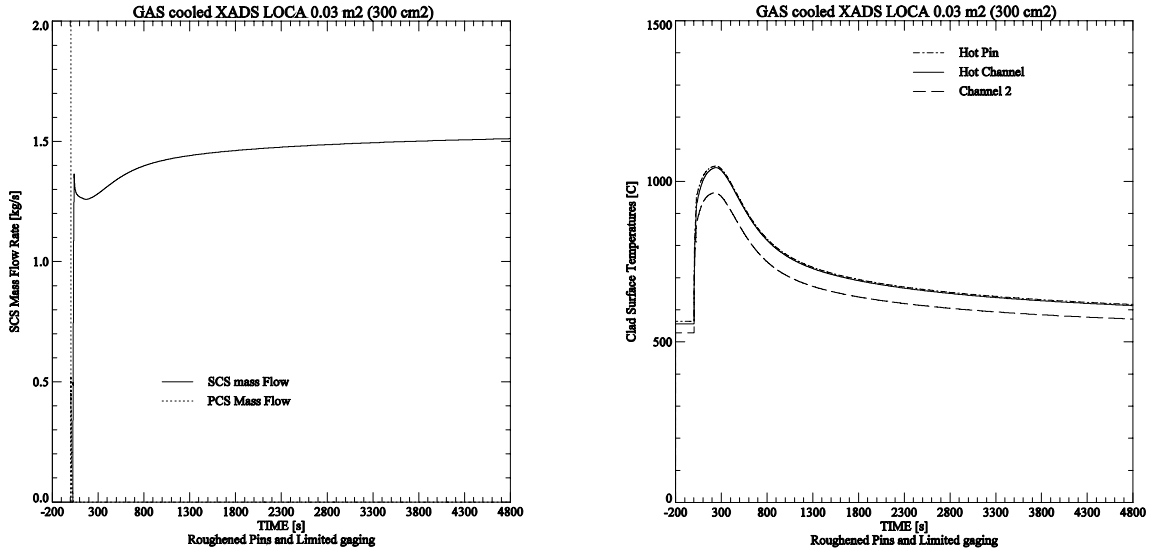

(a) (b)

Conclusions

A general conclusion from the two overpower transients presented (i.e. TOP and beam overcurrent) is that although the power increase is dependent on the subcriticality of the system, the response of the reactor to this power increase is more related to the general design of the reactor (e.g. power level, linear rating) and the choice of coolant. This conclusion is even more evident for transients coming from faults in the primary and secondary coolant systems (hydraulically driven transients). For instance, in the case of a main vessel break (LOCA), the Pb/Bi system remains coolable even in an unprotected case. However, for a large break LOCA in the gas-cooled XADS, it is not possible to prevent clad and fuel melt unless the accelerator beam is tripped off within the first few seconds because of the low thermal inertia of the coolant. For a protected LOCA, the SCS system was shown to work as designed, the initial increase in the clad temperature being dependent on design parameters of the core, e.g. linear heat generation rate, fuel pellet diameter, normal operation heat transfer, etc. Through suitable design, the peak clad temperature could be reduced to an acceptable value.

Acknowledgements

The current study was conducted in the framework of the PDS-XADS project during the Fifth Framework Programme of the European Commission (contract number FIKW-CT2001-00179). The authors would like to acknowledge the EU PDS-XADS project team, which provided financial support for this work.

REFERENCES

[1] Spore, J.W., P. Sadasivan, D.R. Liles, "Accelerator Transmutation of Waste Updates for TRAC-M", LA-UR-01-3660, Los Alamos National Laboratory (2001).

[2] Cinotti, L., *et al*., "Status of the Studies Performed by the European Industry on the LBE Cooled XADS", *Proceedings of the International Workshop on P&T and ADS Development – InWor for P&T and ADS 2003*, ADOPT'03, 6-8 October 2003 (2003).

[3] Cinotti, L., G. Gherardi, "The Pb-Bi Cooled XADS Status of Development", *Journal of Nuclear Materials*, 301, 8-14 (2002).

[4] McDermott, M.F., *et al*., "Preliminary Design Study of a Helium-cooled Experimental Accelerator Driven System", *Proceedings of the International Workshop on P&T and ADS Development – InWor for P&T and ADS 2003*, ADOPT'03, 6-8 October 2003 (2003).

[5] Mikityuk, K., P. Fomitchenko, "FRED: Calculational Model of Fuel Rod Behavior Under Accident Conditions Coupled with RELAP5/MOD3", *Proceedings of ICONE-8*, 8th International Conference on Nuclear Engineering, ICONE-8101, Baltimore, MD, USA, 2-6 April 2000.

THERMAL-HYDRAULIC EXPERIMENTS ON THE TALL LBE TEST FACILITY

B.R. Sehgal, W.M. Ma, A. Karbojian
Royal Institute of Technology (KTH)
10044 Stockholm, Sweden

Abstract

In order to support ADS-related technologies, the thermal-hydraulic ADS lead-bismuth loop (TALL) was designed and constructed at KTH to investigate the heat transfer performance of different heat exchangers, and the thermal-hydraulic characteristics of natural and forced circulation flow under steady and transient conditions. The LBE loop is of full height and was scaled such that the prototypic (power/volume) ratio would represent the main components. So far, the forced convection and heat transfer of LBE through a straight tube heat exchanger and a U-tube heat exchanger have been accomplished and documented [1]. Transient experiments in the test facility are being conducted with reference to safety issues of ADS under the following conditions: a) startup and shutdown, b) loss of heat sink, c) loss of external driving head, d) heater trips, e) sudden change in power, and f) blockage in pipe. Preliminary tests were encouraging given the agreement of experimental data with RELAP5 analysis. More transient experiments and RELAP5 analysis will be performed in the future.

Introduction

Accelerator-driven systems (ADS) have been proposed for the transmutation of long-lived actinides in nuclear waste. Lead-bismuth eutectic (LBE) is likely to be a leading candidate for both coolant and target of ADS because LBE has exceptional chemical, thermo-physical and neutronic properties, which are well-suited for nuclear coolant and spallation target applications. In particular, LBE has a low melting temperature (~125 C) and a very high boiling temperature (~1 670 C). It is chemically inert, does not react violently with air and water, and its spallation can yield close to 30 neutrons per 1 GeV proton. However, LBE is not compatible with common steels used in nuclear installations, which therefore, requires specific protective measures. Due to its high atomic number, the understanding of LBE flow and heat transfer is necessary for the thermal-hydraulic design of an ADS.

Motivated by the increasing interest in transmutation of nuclear waste by LBE-cooled ADS worldwide, a great amount of R&D activities have been or are being performed to address the basic aspects of LBE technology. The European Union is one of the key players in this campaign, with 13 projects in the area of P&T of the EURATOM Fifth Framework Programme (FP5). The Royal Institute of Technology (KTH) is actively participating in the activities concerned with R&D on ADS technologies. We are partners in both the PDS-XADS and TECLA projects of FP5. The project of Technology, Materials and Thermal-hydraulics for Lead Alloys (TECLA) aims to validate the choice of LBE as the spallation material in the target and/or the coolant in a hybrid reactor. The key objective of TECLA is to investigate the corrosion phenomenon of the structural material with LBE and the thermal-hydraulic performance for LBE. We were involved in the medium-scale TECLA experiments on heat exchangers. According to the task, the thermal-hydraulic ADS lead-bismuth loop (TALL) was designed and constructed at KTH. Our guidelines for the design were not only to perform the experiments for heat exchangers, but also to establish an experimental platform for natural circulation and safety concerns in an LBE or lead-cooled reactor. As a result, the TALL facility was designed to perform transient experiments with reference to the safety issues of ADS.

The present paper focuses on a description of the TALL test facility, an overview of the investigation on heat exchangers and an introduction to ongoing transient experiments.

Description of the TALL test facility

TALL is a medium-scale facility designed to perform investigations on LBE flow and heat transfer with prototypic thermal-hydraulic conditions (as in the conceptual ADS design). The flow can be forced convection or natural circulation in character. TALL can also be used to study the performance of a conceptual design during representative accident scenarios. The first objective of TALL was to perform experiments for TECLA, i.e. to investigate the heat transfer performance of different heat exchangers. The second objective was to investigate the thermal-hydraulic characteristics of LBE natural circulation and forced circulation flow under steady and transient conditions.

Specifications

The specifications of TALL are set and modified to simulate prototypic thermal-hydraulic conditions of an ADS reactor, with well-conditioned flow and controllable power for thermal-hydraulic tests. The facility consists of a primary loop (LBE loop) and a secondary loop (oil loop). The LBE loop consists of sump tank, core tank, expansion tank, heat exchanger, EM pump, EM flowmeter, electric heaters and instrumentation. It is 6.8-m tall and the placement of heaters and heat exchangers allows natural convection flow as should occur in the prototypic vessel. Scaling is based on two considerations – resources and conceptual ADS designs. The LBE loop is of full height and has been scaled to prototypic

(power/volume) ratio to represent all the components – their LBE volume, pressure drops, flow velocities and the heating rates corresponding to one tube of the chosen heat exchanger design. For the final design, partners and international collaborations provided the needed technological underpinning. The technical parameters are as follows.

- All parts in contact with LBE are made of 316 or 316 L stainless steel.
- The overall height of the facility is 6.8 m.
- Total electric power is 55 kW and can be increased.
- LBE flow velocity is up to 3 m/s in the heat exchanger.
- LBE volume flow rate is up to 2.5 m^3/h.
- Maximum LBE temperature is up to 500°C.
- Maximum temperature difference along the heat exchanger is 150°C.
- The pressure at the top is ~1 bar and the bottom pressure is ~8 bar.
- Design natural convection velocity is »50 cm/s.
- The LBE is eutectic alloy with the composition of 45% Pb and 55% Bi in weight.
- LBE purity is higher than 99.5%.
- Oxygen level in LBE is measurable.
- The working fluid in secondary loop is glycerol [$C_3H_5(OH)_3$] with a boiling point of 290°C.
- Configuration provides flexibility for different test sections.
- Data acquisition and control is provided.

Main components

TALL is composed of a primary loop and a secondary loop. The primary loop is a closed LBE loop consisting of a pump, flowmeter, oxygen meter, heaters, piping, heat exchangers and tanks. In addition, the facility has a data acquisition system, an oxygen measurement system, a cover gas system, a vacuum system and an exhaust system. The schema of the facility is depicted in Figure 1. The LBE operation and main components of the facility are described in detail in the text that follows.

For the first time only, LBE ingots are loaded into the melting tank, heated to 180°C and held 24 hours with argon flushing. Then, a scoop (fine mesh stainless steel) is used to clean the slag off the top of the LBE melt until the mirror surface shows and the molten LBE is transferred by drainage and argon pressure into the sump tank through the filter. During routine operation, the LBE is melted in the sump tank and pressurised to fill the loop. EM pump is used to circulate the molten LBE through the loop. After leaving the pump, the LBE flows through the core tank and is heated by immersion heaters to a specific temperature at the outlet, which is connected to a long vertical pipe. The LBE keeps travelling

up the long vertical pipe to the expansion tank where the LBE turns to the oxygen sensor and then through the heat exchanger where the LBE's temperature is decreased to a certain value. The LBE leaves the heat exchanger and keeps flowing down through the EM flowmeter, which is placed on the long vertical pipe between the heat exchanger and the pump. The LBE finally returns to the pump.

Figure 1. Schema of the TALL test facility

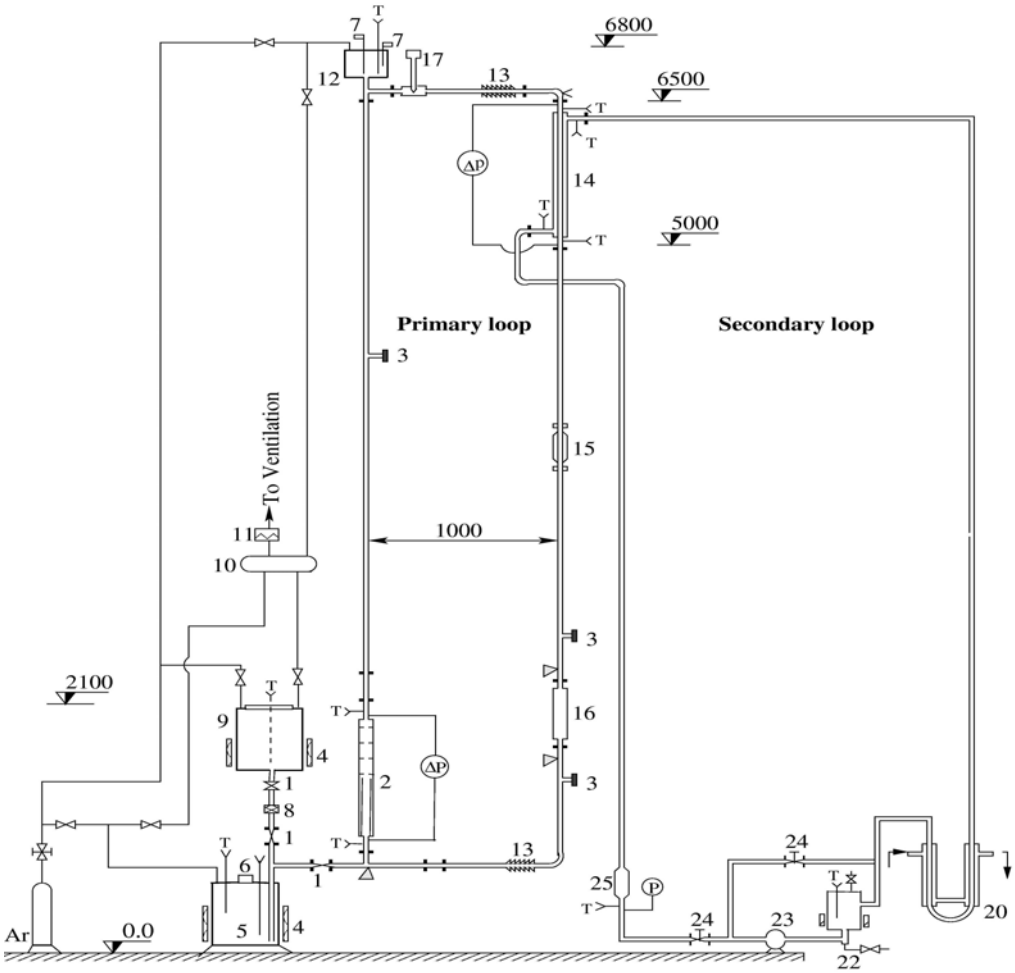

Primary loop:
Piping––33.4mm O.D. and 27.8mm I.D.
Material––AISI 316 stainless steel
Working fluid –– LBE
Max flowrate –– 15 liters/min
Preheating of piping –– Rope heater

1–Valve for LBE
2–Core tank & heater (28kW)
3–Blind flange
4–Melting heater (6kW)
5–Sump tank for LBE
6–Observing window
7–Level sensor
8–Filter
9–Melting tank
10–Exhaust gas tank
11–HEPA filter
12–Expansion tank

Secondary loop:
Piping––26.7mm O.D. and 23.3mm I.D.
Piping material––carbon steel
Working fluid –– Glycerol
Max flowrate –– 260 liters/min
Preheating of piping –– Band heater

13–Expansion tube
14–LBE–oil heat exchenger
15–EM Flowmeter
16–EM Pump
17–Oxygen meter

20–Oil–water heat exchenger
21–heater (3kW)
22–Sump tank for oil
23–Oil pump
24–Valve for oil
25–Flowmeter for oil

Tanks

The melting tank is designed to melt commercial LBE ingots and to remove impurities. For preparation of the LBE melt, a round vessel is used. The melting tank was designed so that it can contain 150% of the loop's total volume with a certain free volume for cover gas plenum.

The sump tank collects the melted LBE from the melting tank before circulation. It has the same volume and diameter as the melting tank. It is placed under the loop so that it can collect and hold the LBE when the loop drains. An observation window is available on the top of the sump tank. During the operation, the LBE is melted in the sump tank and then transferred by cover gas pressure into the loop.

Two band heaters are employed to melt the LBE in each tank. The heaters are mounted around the outside surface of the vessel and are well-insulated. The LBE's temperature is controlled automatically by the controllable power supply system.

The highest located component of the loop is the expansion tank, which is used to collect the extra LBE from the loop due to heat expansion and to balance the pressure variation. All three tanks mentioned above are made of 316 stainless steel.

The core tank is one of the complicated components in the loop. It holds the immersion heaters that provide the main electric power supply. The core tank was scaled so that it could represent the reactor core corresponding to one tube of the heat exchanger, especially from the aspects of flow resistance and coolant inventory. Multi-hole plates are placed in the tank in order to increase the flow resistance. The number of the multi-hole plates can be changed in order to obtain the prototypic ratio of the core tank resistance to the loop's resistance. The immersion heaters are located in the lower part and the multi-hole plates are located in the upper part.

Heat exchanger

According to a sub-task of TECLA, the thermal-hydraulic performance of different types of heat exchangers will be investigated.

As shown in Figure 2, straight tube and U-tube heat exchangers were designed to perform the TECLA experiments.

Geometrical scaling is done in order to preserve relevant non-dimensional parameters (Re for forced circulation and Gr for natural convection) and is based on resources (such as laboratory condition, instrumentation and budget). As a result, single tube heat exchangers were employed. Both heat exchangers are composed of an inner tube and an outer duct, with the primary fluid (LBE) flowing in the inner tube and the secondary fluid (glycerol) flowing in the annulus. For the ease of fabrication, a square duct is chosen as the outer duct of the U-tube heat exchanger.

A 10-mm I.D. and 1.5-mm thick steel tube is used as the inner tube in both the heat exchangers. LBE velocities and Re numbers similar to those in the heat exchanger of the conceptual ADS design are easy to reach in the experiments. The effective lengths of both heat exchangers are one meter, which was decided after comprehensive consideration of the inlet/outlet temperature, heat removal capacity, heat flux and flow resistance.

Figure 2. Schema of the heat exchangers

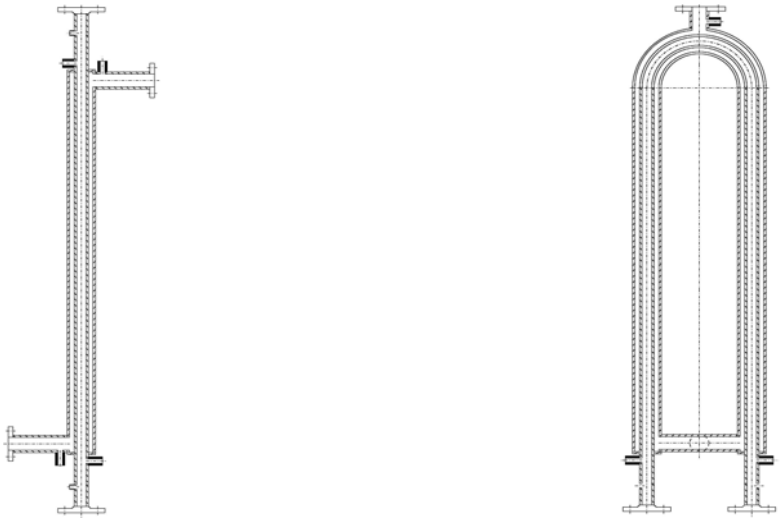

(a) Straight tube (b) U-tube

EM Pump

The electromagnetic (EM) pump provides the driving head for forced convection flow. The pump uses a system of rotating permanent magnets, which can withstand an LBE temperature of 300°C to 450°C as in our application. The LBE flows through the channel located in the gap between these magnets. An AC motor is employed to rotate the pump, on the shaft of which two magnetic disks are fixed.

The pump can develop 1.6 bar pressure at the flow rate of 0.6 L/s. Productivity of the pump is controlled by adjusting the rotation speed of the motor using a standard frequency converter.

Secondary loop

As shown in Figure 1, a secondary loop was designed to realise the heat transfer form LBE to an intermediate fluid, and finally to an oil-water heat exchanger. Glycerol [$C_3H_5(OH)_3$] was chosen as the working fluid (intermediate fluid) in the secondary loop because it has a high boiling point (290 C) and well known thermal properties. Glycerol's boiling point is much higher than the melting point of LBE (125 C), which can also allow a higher operational temperature (ǂ 125 C) so that solidification of LBE in the heat exchanger is avoided.

The secondary loop is an open circulation loop that consists of an oil pump, heat exchangers, sump tank, flowmeter, piping, valves and assorted temperature and pressure sensors. The oil pump is employed for the secondary loop to supply the flow driving head. During the operation, the glycerol leaves the oil sump tank due to suction of the pump. After leaving the pump, the flow is divided into two parts – one part returns to the sump tank via the bypass and the other part keeps flowing and turns up to a flowmeter where the flow rate is recorded. The bypass design is for easy control of the flow rate. The glycerol leaving the flowmeter travels through a long vertical pipe and arrives at the heat exchanger, where the glycerol's temperature is increased due to heat received from the LBE. The glycerol leaves the heat exchanger, keeps flowing and turns down through the long vertical pipe and comes to another heat exchanger (oil-water heat exchanger) where the glycerol is cooled down by tap water and finally returns to the oil sump tank.

Instrumentation

The EM flowmeter is designed for measuring the flow rate of liquid LBE in a 316 stainless steel pipe with a diameter of 30 mm. The flowmeter consists of a sensor, an electronic block and a cable connecting the sensor with the electronic block.

The sensor is mounted vertically around the cold leg under the heat exchanger. The signal from the sensor is processed by an electronic block and the reading is shown on a PC monitor. The liquid LBE's temperature at the sensor can reach up to 400 C. The measuring range of the flowmeter varies from 0.01 L/s to 1.0 L/s.

In order to monitor the oxygen level in LBE, an oxygen measurement system is employed. The system consists of an oxygen sensor (from Los Alamos National Laboratory, USA) and a Keithley 6 514 programmable electrometer.

A Rosemount 3 051 differential pressure transmitter in combination with the1 199 diaphragm seal system is employed to measure the pressure drop of LBE flow.

An Omega FLMH-1 040 (AL)-HT high temperature oil flowmeter is used to measure the glycerol flow rate. Its temperature limit is up to 204 C. The flowmeter utilises a spring-and-piston type assembly, which enables it to be mounted in any position and gives immunity from changes in viscosity.

Thermocouples and pressure transducers are used to measure temperature and pressure, respectively. Electrical panels are available to control all operations of heaters, pumps and valves. A data acquisition system (DAS) is realised using National Instruments data input instrumentation and a computer program written in LabVIEW. The readings are performed through two SCXI-1 102 32-channel amplifiers and a 6 035E analogue input DAQ card.

Tests on the heat exchangers

The facility came into operation in September 2003. Tests on a straight tube and a U-tube heat exchanger have since been conducted. The ranges of the main thermal-hydraulic parameters of LBE in a heat exchanger are: inlet temperature from 230 C to 450 C, temperature drop from 20 C to 100 C, and velocity from 0.5 m/s to 2.5 m/s. The pressure drop and heat transfer characteristics were obtained for the straight tube heat exchanger and the U-tube heat exchanger, respectively.

Figure 3 shows the variation of the pressure drop with the Reynolds number for the two tested heat exchangers. It is obvious that the pressure drop of the LBE flow through the U-tube is larger than that of the straight tube.

For LBE flow in a straight tube, it appears that the present measured values are on average 15% higher than those from the following Techo, *et al*., correlation, which is for fully developed turbulent flow and smooth surface conditions.

$$\frac{1}{\sqrt{f}} = 1.7372 \ln \frac{\mathrm{Re}}{1.964\,\mathrm{Re} - 3.8215} \tag{1}$$

For a commercial stainless steel tube, if roughness may be chosen as 0.018 mm, the pressure drop calculated by the following Moody correlation will be in reasonable agreement with experimental data.

$$f = 1.375 \cdot 10^{-3}\left[1 + 21.544\left(\frac{2e}{d} + \frac{100}{\mathrm{Re}}\right)^{1/3}\right] \quad (2)$$

For both heat exchangers, the overall heat transfer coefficient increases with the increasing LBE and glycerol flow rate (illustrated in Figures 4 and 5), but the glycerol flow rate has a more significant effect. Furthermore, the overall heat transfer coefficient of the U-tube heat exchanger is higher than that obtained in the straight tube heat exchanger under the same conditions. More details of tests on heat exchangers are documented in Ref. [1].

Figure 3. Pressure drops of LBE flow through the heat exchangers

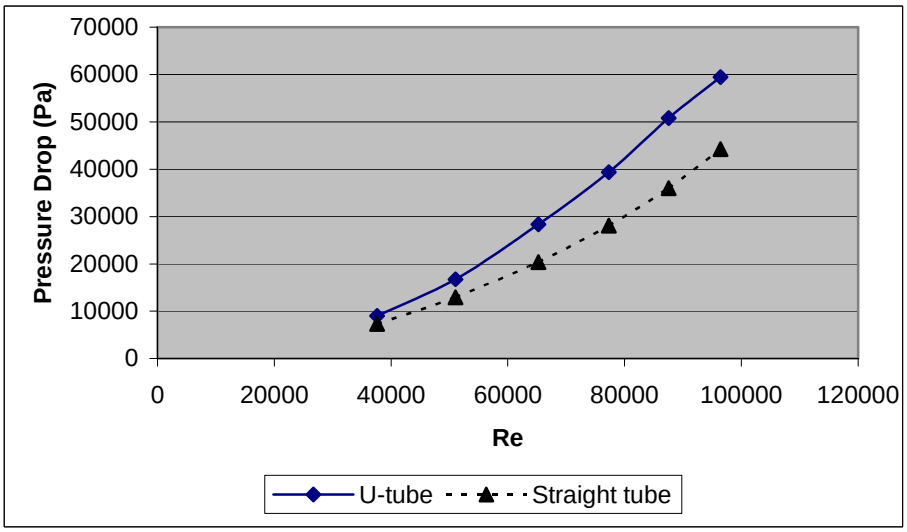

Figure 4. Effect of the glycerol flow rate on heat transfer

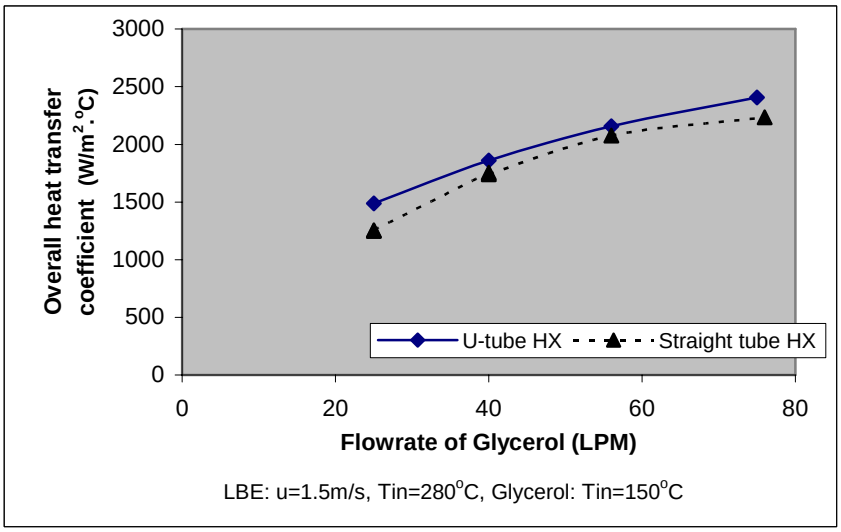

Figure 5. Effect of the LBE flow rate on heat transfer

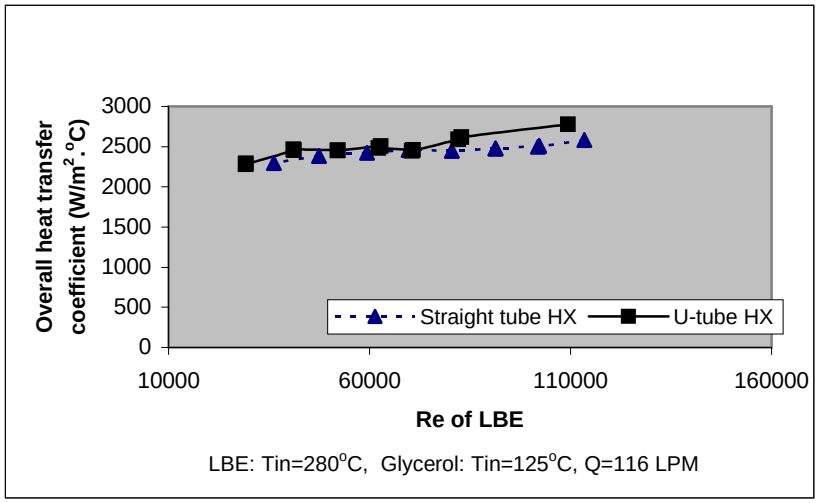

Transient tests

Transient experiments with reference to safety issues of ADS were started in May 2004. While simulating decay heat in the core tank, the temperature and flow rate characteristics will be measured during the following transients:

a) Startup or shutdown of the facility.

b) Loss of heat sink (switch off pump in secondary loop).

c) Loss of external driving head (switch off pump in primary loop) – completely passive mode of LBE loop operation.

d) Switch on and off the heater to simulate accelerator trips.

e) Blockage in pipes.

f) Sudden increase or decrease in power.

It was deemed important to find a way to measure low velocity during LOF transients. As a result, the flowmeter was recalibrated and the correlation between flow rate and pressure drop through the heat exchanger was obtained, which provides a sound basis to monitor the flow change during the transients.

Based on improved measurement, a loss of flow transient is shown in Figure 6. The transient was stopped at 628 seconds since the temperature was reaching the limit. The variations of flow rate and temperature were very similar to the RELAP5 calculations as shown in Figure 7, which provides an encouraging perspective on the experiment and calculations, though they started from different initial conditions. If a new model of an EM pump is taken into account and the same initial conditions are used, we believe that the experiment and calculations will show good quantitative comparison.

The transient experiments are just at the beginning. More experiments will be performed during the next few months. A RELAP5 analysis will also be performed.

Figure 6. The transient of loss of external driving head in the primary loop

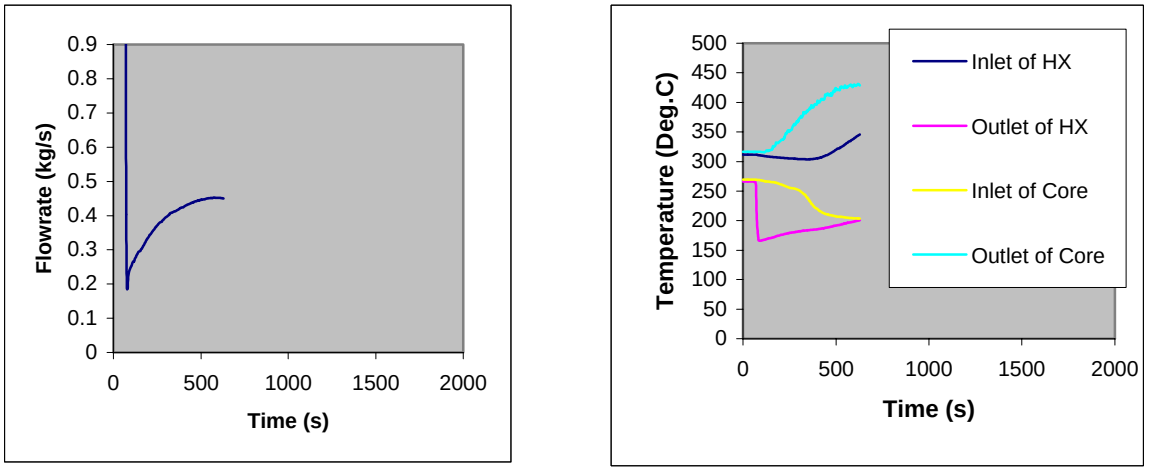

Figure 7. Calculation of the transient of loss of external driving head in the primary loop

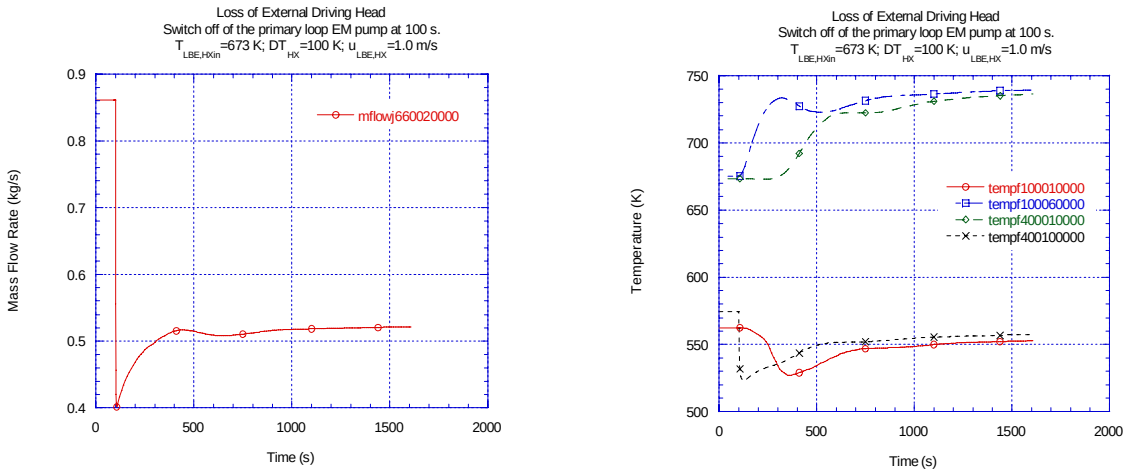

Concluding remarks

The TALL facility was designed to investigate transients with reference to safety issues as well as the thermal-hydraulic performance of heat exchangers in a conceptual ADS subcritical reactor design. Thus, it is a multi-purpose test platform. The facility came into operation in September 2003. So far, investigations have been performed on two different heat exchangers, one with a straight tube and one with a U-tube. Transient experiments addressing safety issues of the ADS are on the way. More data on transients and natural circulation will be obtained during the next several months. According to test progress, the main conclusions are as follows:

- The loop is well-controlled and the thermal-hydraulic conditions can be adjusted properly.
- The operational parameters, e.g. LBE flow rate and temperature level, meet design requirements.
- The LBE inlet temperatures of the heat exchangers are up to 450 C, with the outlet temperature of the core tank up to 500 C.

- Pressure drop through the straight tube appears to be higher than that calculated via the Techo, *et al*., correlation (1) for a smooth tube, but in good agreement with that calculated via the Moody correlation (2), which takes into account the effect of surface roughness.

- The heat transfer coefficient of secondary (glycerol) flow is much smaller than that of primary (LBE) flow, and hence dominates the determination of the overall heat transfer coefficient.

- In general, the U-tube heat exchanger has a better heat transfer performance than the straight tube heat exchanger, especially for secondary flow. In fact, the heat transfer resistance is very low for primary flow, thus any heat transfer enhancement design should be put on the secondary side.

- Preliminary tests are encouraging for the agreement of experimental data with RELAP5 analysis.

- More experiments, data check and analysis will be carried out.

Acknowledgements

This work was supported by the European Commission (EC), the Swedish Nuclear Power Inspectorate (SKI) and the Swedish Nuclear Fuel and Waste Management Company (SKB).

REFERENCES

[1] Sehgal, B.R., W. Ma, A. Karbojian, *Lead-bismuth Flow and Heat Transfer Performance in Heat Exchangers*, Technical Report for European Commission Fifth Framework Programme, Deliverable D39 of TECLA, December 2003.

[2] Sehgal, B.R., W. Ma, Z. Koszela, A. Karbojian, *Thermal-hydraulic ADS Lead-bismuth Loop (TALL) and Pre-test Analysis*, Technical Report for European Commission Fifth Framework Programme, KTH, March 2003.

[3] Kakac, S., *et al*., *Handbook of Single-phase Convective Heat Transfer*, John Wiley & Sons (1987).

[4] *Proceedings of the 2nd International Conference on Accelerator-driven Transmutation Technologies and Applications*, Kalmar, Sweden, 3-7 June 1996.

[5] *Proceedings of Heavy Liquid Metal Coolants in Nuclear Technology*, Obninsk, Russia, 5-9 October (1998).

[6] *XADS Pb-Bi Cooled Experimental Accelerator Driven System Reference Configuration*, Summary Report of Ansaldo Nucleare, ADS 1 SIFX 0500-Rev. 0 (2001).

[7] *Energy Amplifier Demonstration Facility Reference Configuration*, Summary Report of Ansaldo Nucleare, EA B0.00 1 200-Rev. 0 (1999).

[8] Buongiorno, J., *et al*., *Thermal Design of Lead-bismuth Cooled Reactors for Actinide Burning and Power Production*, Massachusetts Institute of Technology, MIT-ANP-TR-066 (1999).

ANALYSIS OF LEAD-BISMUTH EUTECTIC FLOWING INTO BEAM DUCT

Kenji Nishihara, Hiroyuki Oigawa
Japan Atomic Energy Research Institute, Japan

Abstract

Beam window breakage is one of the accidents under consideration for the operation of an accelerator-driven subcritical system (ADS). After the beam window breaks, the target material [lead-bismuth eutectic (LBE)] flows into the beam duct in liquid and gaseous phases. The inlet velocity of the liquid LBE and the pressure of gaseous LBE in the duct were analysed.

Introduction

Beam window breakage is one of the accidents under consideration for the operation of an accelerator-driven subcritical system (ADS). The issues that arise when a beam window breaks are as follows: detection of the fracture, stoppage of the proton beam, protection of the accelerator, etc. One of the detection methods is to detect the change in degree of vacuum in the beam duct. Once this has been detected, the ion source of the accelerator will be stopped. (The scheme of the beam stop is outside the scope of the present work.) Then, the beam duct will be closed with the fast-acting valve at the end of the transport portion of the accelerator to avoid the target material flowing into the upper portion of the accelerator.

In the present paper, behaviour of the target material [lead-bismuth eutectic (LBE) in our design] after beam window breakage is investigated without considering other elements such as polonium and spallation products in LBE. After the window breaks, LBE flows into the duct and goes over at the level of the cover gas if the diameter of the fracture is large. Since the volume of the vacuum portion in the duct decreases significantly, the degree of vacuum decreases. If the fracture is small, the amount of LBE flowing in the duct is balanced with the evaporation into the duct, supposing that heat insulation is maintained between LBE and duct. The time dependence of LBE flowing into the duct is analysed in the following sections for the two types of fracture.

Analysis conditions

The proposed ADS is a tank-type reactor cooled by lead-bismuth eutectic. The analysis model and parameters are shown in Figure 1 and Table 1, respectively. The beam duct is inserted at the depth of 6.5 m, which was determined from the design of a steam generator in the tank. The proton beam is accelerated and transported through a transport portion whose diameter is 5 cm. Then, the beam is expanded in a big expansion portion before the target widow. The fracture is supposed to occur at the centre of the window.

The phenomenon that occur after a breakage are divided into two cases according to the diameter of the fracture. In the first case, the large fracture has a hole size of more than 5 cm in diameter. LBE flows into the duct at a speed that is faster than evaporation. The time-dependent behaviour of the LBE level is obtained considering pressure losses at the fracture hole and friction with the sidewall of the duct. The degree of vacuum in the duct changes according to the volume of the vacuum portion.

In the second case, there is a small fracture of ~1 mm in diameter. Supposing heat insulation is maintained for LBE flowing into the duct, the amount of LBE flowing into the duct balances with the evaporation, and the LBE surface level becomes constant. The degree of vacuum decreases by LBE evaporation according to the saturated evaporation pressure at each position in the duct.

Figure 1. Analysis model

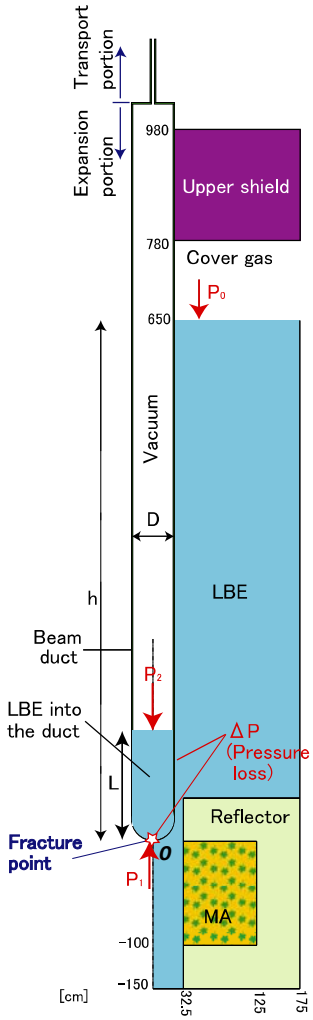

Table 1. Analysis conditions

Coolant/target material	Lead-bismuth
Temperature of LBE	430 C
Temperature of cover gas	200 C
Temperature of upper core	30 C
Diameter of the beam duct	
(Expansion portion) (*D*)	40 cm
(Transport portion*)	5 cm
Length of the duct	
(Expansion portion)	10 m
(Transport portion*)	200 m
Diameter of fracture (*d*)	10-40 cm
Window depth (*h*)	6.5 m
Degree of vacuum	10^{-4} Pa
Proton energy	1.5 GeV
Power	30 MW
Exothermic density in LBE near the window (*q*)	1 000 W/cm^3

*Containing the acceleration part

Large fracture

The amount of LBE flowing into the duct is determined from Eq. (1), which represents a balance of pressures to LBE in the duct.

$$\frac{L}{A}\frac{d^2(\rho AL)}{dt^2} = P_1 - P_2 - \Delta P - \rho gL \tag{1}$$

where L is the level of LBE [m], A is the cross-section of the beam duct [m^2], P_0 is the pressure of the cover gas [Pa], $P_1 = P_0 + \rho gh$ is the pressure at the fracture [Pa], P_2 is the pressure in the duct [Pa], ΔP is the pressure loss [Pa], h is the window depth [m], g is the gravity constant [m/sec^2] and ρ is the density of LBE [kg/m^3].

Pressure loss is caused by the hole and friction with the sidewall as in Eq. (2).

$$\Delta P = \left(\zeta + \lambda\frac{L}{D}\right)\frac{\rho v^2}{2} \tag{2}$$

where ζ is the pressure loss coefficient of the orifice, λ is the friction loss coefficient with the sidewall and v is the flow velocity [m/sec].

In the analysis of the LBE surface level, the limit of the length of the expansion portion (10 m) is ignored. A change of P_2 is also neglected.

The calculated results are shown in Figure 2 for fracture hole diameters of 40, 20, 10 and 5 cm. For the 40 cm case, which agrees with the diameter of the duct, the LBE surface level achieves 10 m at 1.4 seconds after the breakage. Since the limit of the length of the expansion portion is ignored, the maximum level of 14.2 m is obtained. The level oscillates and converges to 0.99 m. In other cases, the levels are not too much over 0.99 m.

Figure 2. Level of LBE after a large window fracture

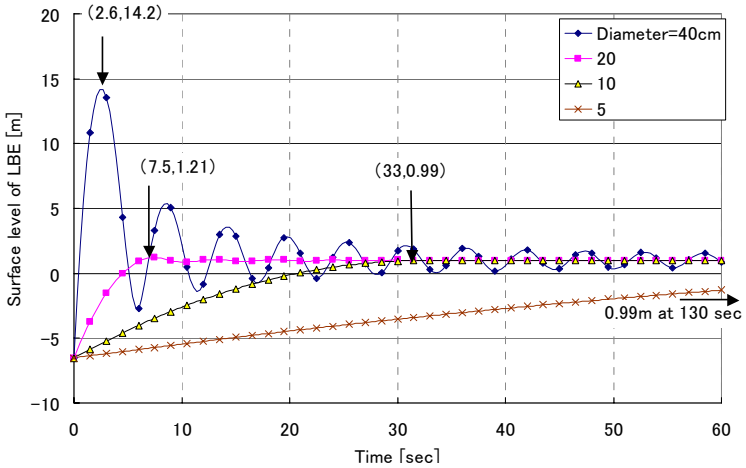

The variation of the degree of vacuum is shown in Figure 3 when the initial value is set at 1.0 10^{-4} Pa. It should be noted that this analysis is based on the volume of vacuum part in the duct, not considering the evaporation pressure of Pb-Bi and other elements contained in LBE. The degree becomes 1.1 10^{-4} Pa for an LBE surface level of -5.3 m and 2.0 10^{-4} Pa for the level of 0 m. Then, the variations converge to 2.34 10^{-4} Pa in all cases. The time intervals when the degree of vacuum achieves 1.1 10^{-4} and 2.0 10^{-4} Pa are shown in Table 2. Since the degree of vacuum minimally increases as shown in Table 2, the change is possibly detected by the pressure gauge.

Figure 3. Variation of the degree of vacuum

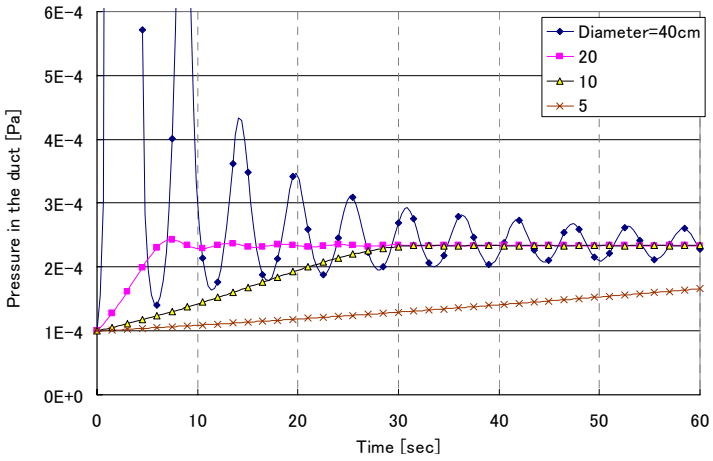

Table 2. Variation of the LBE level after a large fracture

Diameter of the fracture	40 cm	20 cm	10 cm	5 cm
Maximum level [m]	14.2	1.21	0.99	0.99
Time at the maximum level [sec]	2.6	7.5	33	130
Time for the degree of vacuum of 1.1E-4 Pa (when the level is -5.3 m) [sec]	0.075	0.6	2.7	10.8
Time for the degree of vacuum of 2.0E-4 Pa (when the level is 0.043 m) [sec]	0.43	4.55	21	86.45

Small fracture

In the case of the small fracture, the variation of LBE amount in the duct is determined by Eq. (3), which represents a balance of LBE flowing into the duct and evaporation, supposing heat insulation is maintained for LBE flowing into the duct with the wall. Although the temperature of the LBE may exceed the melting point of the window material, this effect is not considered.

$$\frac{dM}{dt} = \rho a v - \frac{qV}{r} \tag{3}$$

where M is the LBE amount in beam duct [kg], a is the cross-section of fracture hole area [m^3], v is the velocity at the fracture [m/s], q is the exothermic density [W/m^3], $V = M/\rho$ is the volume of LBE in beam duct [m^3] and r is the latent heat [J/kg].

LBE velocity at the fracture is given by:

$$\zeta \frac{\rho}{2} v^2 = \rho g h - P_0 - P_2 \tag{4}$$

The solution of Eq. (3) is as follows:

$$M = \frac{a \rho^2 \rho v}{q} \left(1 - e^{-\frac{q}{\rho \rho} t} \right) \tag{5}$$

Since $-q/(\rho\rho)$ is constant at 0.116/s, the time behaviour is unrelated to the diameter of the fracture hole as shown in Figure 4. The amount of LBE flowing in the beam duct and the amount of evaporation are almost proportional to the cross-section of the fracture area, a, in the balanced state.

Figure 4. Amount of LBE in the duct after a small fracture

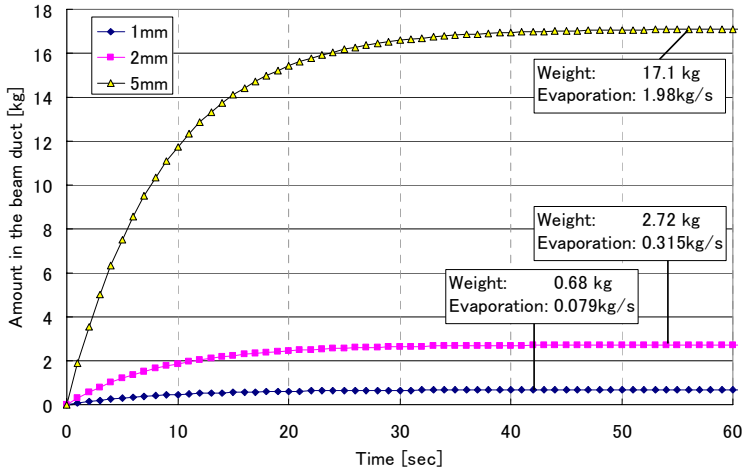

The gaseous LBE goes up to the beam duct and exists according to the saturated evaporation pressure at each position. Temperature of the sidewall changes from 430 C at the surface of LBE to 30 C at the upper shield (through 200 C at the cover gas) as shown in Figure 5. The saturated evaporation pressure corresponding to the temperature is given as follows:

$$P_{sat} = \exp\left\{40.304 - 26.474 \log(T) + 3.044 \left(\log(t)\right)^2\right\} \text{ by ENEA} \tag{6}$$

or

$$\log_{10} P_{sat} = 11.1 - \frac{10660}{T + 273.15} \text{ by MIT} \tag{7}$$

where P_{sat} is the saturated evaporation pressure [Pa] and T is the temperature [C].

The calculated values are plotted in Figure 6 for the cases of ENEA [1] and MIT [2]. The pressures are very small and between ENEA and MIT the pressures are different at low temperatures (~200 C). Almost all evaporated LBE adheres to the sidewall. The position of the detector to measure precise pressure variation is appropriate at the cover gas near the LBE surface whose temperature is 300-400 C, though the effect of irradiation to the detector should be taken into account.

Figure 5. Temperature of the sidewall

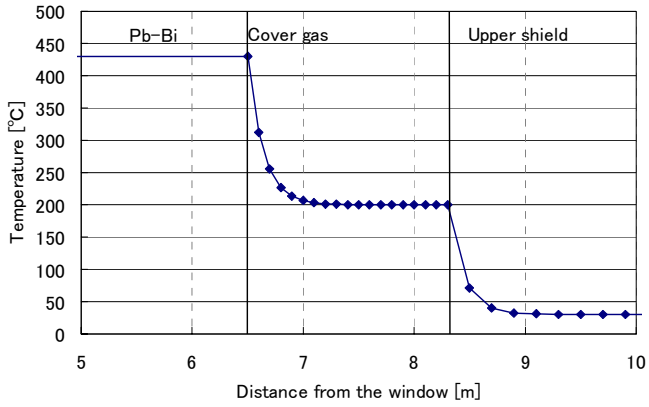

Figure 6. Saturated evaporation pressure

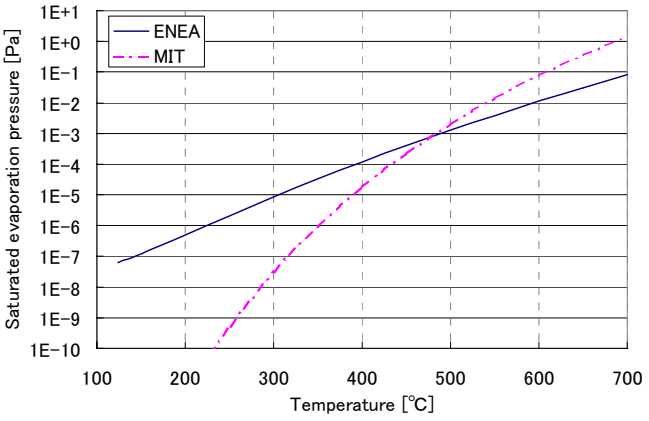

Discussions

The behaviour of the LBE in liquid and gaseous phases when beam window breakage occurs was analysed in the previous two sections. The detection method and the speed of a fast-acting valve, which avoid LBE flowing into the upper part of the accelerator, are considered based on the results. Sensitivity of a gauge for the degree of vacuum is ~10^{-7} Pa. A trigger pressure for a fast-acting valve is 10^{-6} to 10^{-1} Pa. The total closing time of the valve from detection is ~10 msec, which is short enough to stop liquid LBE since LBE flows into the duct at 16.3 m/sec (i.e. 16 cm for 10 msec even for the maximum fracture). In the case of a large fracture, detection is not difficult because the degree of vacuum becomes worse by 10% or 100% the volume change when LBE flows with the height of 120 cm or 650 cm into the duct, respectively.

For gaseous LBE in the case of the small fracture, detection depends on the evaporation pressure of LBE. The temperature of the sidewall near the coolant surface is 300-400 C and the corresponding saturated evaporation pressure is ~10^{-7} to 10^{-4} Pa, which is possibly detected. If the detector is set above the upper part of the cover gas portion, detection may be difficult. A study on the closing time necessary to stop gaseous LBE from getting into the upper part of the accelerator is work for the future.

Conclusion

We attempted to investigate the behaviour of LBE in two cases – a large and a small fracture after window breakage in the tank-type ADS. In the case of the large fracture, the level of liquid LBE oscillates according to the diameter of the fracture hole and then converges to the level of 0.99 m. In the case of the small fracture, the amount of liquid LBE flowing into the duct becomes constant because the LBE flowing into the duct balances with the evaporation by heat from the proton beam, supposing heat insulation is maintained between LBE and duct. Since the delay for the inlet of liquid LBE is more than a few seconds except for the largest fracture of 40 cm, detection of the fracture and closing of the fast-acting valve to avoid LBE following into the upper part of the accelerator can take place. The design study for reliable detection and closing systems are future work.

Gaseous LBE was also investigated for a small fracture simply via the saturated evaporation pressure. Evaporated LBE is considered to adhere immediately around the level of the cover gas and few gaseous LBE exists in the duct.

REFERENCES

[1] Cevolani, S., *et al.*, *Review of the Liquid Lead-bismuth Alloy Physical Properties*, ENEA-DT-SBD-00004 (1998).

[2] Buongiorno, J., *et al.*, *Advanced Nuclear Power Technology Program, Conceptual Design of a Lead-bismuth Cooled Fast Reactor with In-vessel Direct-contact Steam Generation*, MIT-ANP-TR-079 (2001).

ON THE SUPPLEMENTARY FEEDBACK EFFECT SPECIFIC FOR ACCELERATOR-COUPLED SYSTEMS (ACS)

Pavel M. Bokov, Danas Ridikas
DSM/DAPNIA/SPhN, CEA Saclay, F-91191 Gif-sur-Yvette, France
Email: pavel.bokov@cea.fr

Igor S. Slessarev
29, rés. Tivoli, allée des Peupliers, F-13090 Aix-en-Provence, France

Abstract

In this work a new approach to the realisation of an accelerator-coupled hybrid system (ACS) is proposed. A significant improvement of the feedback effect due to the particularities of the neutron production in a spallation target is expected. In the present study, we explain the principles of system functioning as well as the advantages and disadvantages of the proposed concept. The quantitative analysis of the innovative ACS operation is based on a generalised point kinetics approach. In the framework of this simplified model, we show that the particular dependence of the spallation neutron yield allows for the creation of a supplementary negative feedback effect (Doppler-like). Implementation of this concept should compensate, to some extent, the eventual feedback degradation in the cores dedicated to the transmutation of nuclear waste.

Introduction

In general, nuclear systems devoted to minor actinide (MA) transmutation may suffer from significant degradation of safety characteristics. In particular, such important parameters as delayed neutron fraction can decrease by several times compared to conventional nuclear reactors. Another serious problem arising in such systems is the reduction of the Doppler effect – the fastest and most important temperature feedback effect in the reactor core. This degradation of safety properties makes the control of such systems rather delicate.

An innovative solution to handle the above problem was proposed recently and consists of the artificial enhancement of system neutronics, which involves an external neutron source added to the core permitting the system to operate in subcritical mode (so-called hybrid nuclear reactor). In an accelerator-driven system (ADS) [1] where a subcritical core serves only to amplify the incident beam energy, a large subcriticality margin (k_{eff} ~0.95-0.97) mitigates the negative consequences of the degradation of safety parameters. However, this significant subcriticality level requires a powerful and expensive particle accelerator. Another way to deal with the problem is to employ the concept of the accelerator-coupled system (ACS) [2]. With an ACS, an external neutron source, which is coupled directly to the core power and is artificially or naturally delayed, can compensate the decrease of delayed neutron fraction. In this case, less powerful (and thus less expensive) particle accelerators may be applied. On the other hand, the ACS inherits some properties of a critical nuclear system. In particular, the degradation of feedback effects (e.g. Doppler) makes power and temperature excursions possible in the case of unprotected reactivity insertion.

In the present work, we propose a new approach for the realisation of ACS where a significant improvement of the feedback effect is expected due to the modification of the accelerator-core coupling mode and due to the particularities of neutron production in a spallation target.

Generalities of hybrid systems

In principle, core subcriticality will improve safety when feedback effects, the delayed neutron fraction or other safety-related parameters are degraded due to the presence of long-lived actinides that are subjected to transmutation. There are at least two different ways a subcritical core can function in combination with an external neutron source. In brief, this source can be independent of neutron (energy) production in the core [as in accelerator-driven systems (ADS)]. Or, the source can depend on neutron (energy) production in the core and in this way become “coupled” or “co-ordinated” by core power level [as in accelerator-coupled system (ACS [2])]. Each combination opens some new opportunities related to safety improvement. Major features of ADS and ACS are summarised below.

In the case of ADS, an *independent* mechanism of supplementary neutron production is used to achieve the desired power level and the accelerator power is supplied via an independent energy grid.

In the case of ACS, a source of “artificially delayed neutrons” consumes a portion of in-core released energy. In this way the external neutron source becomes “coupled” with the core power level. As a result, the supplementary neutron creation will be delayed to time required for fission energy transfer from the core to a chosen neutron production mechanism (e.g. spallation, nuclear fusion, *bremsstrahlung*-photonuclear, etc.). In other words, this intermediate process temporarily “hides” neutrons (of some neutron generation) in order to recover them later. This allows for the artificial increasing of neutron lifetime and for the slow down of dangerous transients [3].

Compared to conventional critical reactors, this particular property of the ACS can improve the reactor dynamics significantly. Moreover, the ACS operates in critical mode and, therefore, in contrast to the ADS, takes advantage of favourable temperature feedback, which might exist in these systems [3].

In terms of safety, ADS is *inherently* more favourable (compared with similar critical reactor) in regards to reactivity accidents where core subcriticality mitigates consequences of reactivity insertion. On the other hand, a system functioning in a critical regime (including ACS) is *intrinsically* safer in the case of thermo-hydraulic type transients. Therefore, it would be attractive to combine the inherent advantages of both ADS and ACS in a single installation. In other words, one needs to realise a system where the following occurs during *unprotected transients*:

a) The intensity of an external neutron source decreases with the decrease of core power.

b) The intensity of an external neutron source remains stable or even decreases with the increase of core power.

c) Conditions a) and b) must be *intrinsic*.

One possible solution to merge the above advantages is presented in the following section. It is based on the physical processes taking place in the neutron production target, which makes our approach inherent.

Accelerator-core coupling modes in ACS

Traditionally, it is assumed that in hybrid systems the current of a proton accelerator is the coupling parameter, which one can vary to change the neutron source intensity. In the case of ACS, at least two modes of coupling between the external neutron source and the core could be envisaged.

1. When it is supposed to modify the intensity of an external neutron source Q by varying the proton beam current I_p at a fixed nominal value of the proton energy, namely:

$$I_p = I_{p,0}\, P^{out} / P_0^{out} \tag{1}$$

   Here P^{out} is the output power of the installation and subscript "0" denotes nominal values of the corresponding variables. Hereafter, this method of "accelerator-core" coupling is designated as "*I*-mode" coupling.

2. When *any change of an output power leads to a proportional change of proton energy* ε_p at a fixed nominal value of the proton current, namely:

$$\varepsilon_p = \varepsilon_{p,0}\, P^{out} / P_0^{out} \tag{2}$$

   This coupling method is hereafter denoted as "*E*-mode" coupling.

In this work we propose *to utilise the proton energy as a coupling parameter* (*E*-mode ACS). The difference between *E*-mode and *I*-mode, of which we would like to make use, is based on the *non-linear behaviour of neutron yield* Y_n *with respect to the proton energy* ε_p *variation* (hereafter the "Y_n-effect").

As shown in a number of studies, when the energy of incident protons becomes higher than ~1 GeV, for example, the neutron yield normalised per incident proton energy becomes nearly constant and even slightly decreases with proton energy (see Refs. [4-6] and references contained therein). There are two major reasons for this decrease of neutron production efficiency with energy increase - 1) opening of new reaction channels and 2) escape of high-energy particles from the spallation target with finite geometry.

This neutron production dependence is illustrated qualitatively in Figure 1. The neutron yield, after protons passed the reaction threshold [zone (1')], grows rather rapidly with energy [zone (1")]; above a certain value of e_p, this dependence has a moderated quasi-linear behaviour [zone (2)]. Thus, there is a value of proton energy $e_p^{optimum}$, which is optimal with respect to neutron economy (i.e. neutron yield per one incident proton and per consumed energy reaches its maximal value). Therefore, it is generally considered nonsensical to increase the energy of protons beyond $e_p^{optimum}$ since the production of neutrons in the spallation target becomes less efficient compared with the equivalent increase of the proton current (accelerator power being constant).

Figure 1. Dependence of the spallation neutron yield Y_n (e_p) / e_p (solid line) and that of the source effectiveness $h_{Pfi\ Q}$ (e_p) (dash line)

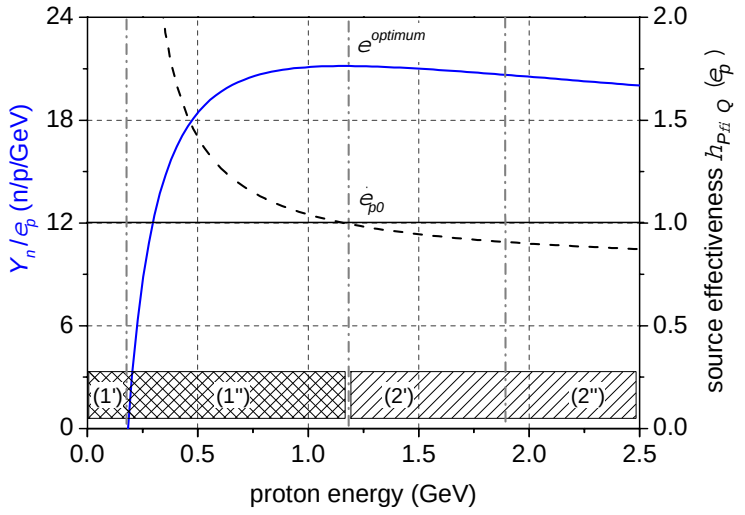

Quantitatively, the Y_n-effect as a function of proton energy can be described by an empirical formula proposed in Ref. [6] with the units of neutron yield per one incident proton interacting with a thick and heavy metal target:

$$Y_n(e_p) = -a + b(e_p)^a \qquad (3)$$

where parameters a, $b \neq 0$ and $0 \leq a \leq 1$ can be fitted to the experimental data depending on the target geometry and material. This particular dependence of the neutron yield on target geometry and material should not be neglected. Furthermore, one should make use of these particular situations. Indeed, our preliminary estimates have shown that some optimisation on the geometry of the spallation target might further strengthen the Y_n-effect. More quantitative calculations in this context are needed.

Principle of the operation – DENNY concept

In this work, we propose to utilise this particularity of neutron production to form quasi-linear dependence (Y_n-effect) between energy production in the core and external neutron production in the spallation target, aiming to get auto-regulating behaviour of the ensemble "accelerator-subcritical core". A proposed system (*E*-mode coupled ACS) would have the kinetics of a critical system with an artificial group of delayed neutrons as with a "standard" ACS. Also, its external neutron production would contain supplementary feedback, tending to stabilise installation power in its nominal state.

To elucidate this statement, we recall that ACS may be considered as a *critical* system with two types of neutrons contributing to the *global* neutron balance – "core neutrons" and "source neutrons". Despite the fact that this separation of neutrons is relatively artificial, it reflects their origin and, thus, the corresponding neutron production feedback for each case. In the same context, the Y_n-effect can be compared to the Doppler feedback effect but for the external source neutrons. Similarly, as with the Doppler feedback effect, the Y_n-effect is intrinsic. It would be quite advantageous for system safety to have this supplementary feedback acting on the entire neutron balance if the "standard" core feedback is degraded and cannot play a self-stabilising role, which is indispensable for inherent system safety.

The advantage of the above realisation of a coupled hybrid system can be illustrated by the "neutron production versus core power" [Figure 2(a)] as well as by the "core power versus accelerator power" [Figure 2(b)] diagrams during unprotected accidents. We note the equivalence between Figure 2(a) (*E*-mode ACS) and Figure 1 for the neutron yield Y_n dependence, which is possible to make use of only in the case of *E*-coupling. According to the new concept (proposed *E*-mode ACS), the power (and temperature) excursion would be less important than in the "standard" *I*-mode ACS, which is clearly seen in Figure 2(b). For the present work, the system with an accelerator coupled to the core in *E*-mode is named DENNY (delayed enhanced neutronics with non-linear neutron yield). Below we propose the principle of DENNY functioning.

Let us consider the *E*-mode ACS with a pre-defined subcriticality level $r_0 = (1 - k_{eff,0}) / k_{eff,0}$ and a fraction $f < 1$ of the produced core power, which is used to drive an external neutron source. External neutrons are created in the spallation target by incident protons accelerated up to the energy e_p. It is preferable to choose the nominal proton energy $e_{p,0} > e_p^{optimum}$ in order to avoid an eventual instability of the DENNY power with respect to negative reactivity insertions (power decrease). Hence, the proton energy must be chosen as follows: $e_{p,0} = e^{optimum} + De_m$ [zone (2") in Figure 1]. Here the margin De_m [zone (2') in Figure 1] makes the system more stable with respect to negative reactivity insertions. This is valid if during system operation the proton energy remains beyond the optimal energy, i.e. the condition $e_p \ddagger e^{optimum}$ is fulfilled.

Figure 2. Diagrams of intrinsic dependences

(a) Neutron production Q dependence on core power P and (b) equilibrium core power P_c dependence on accelerator power P_a for different concepts of a hybrid system

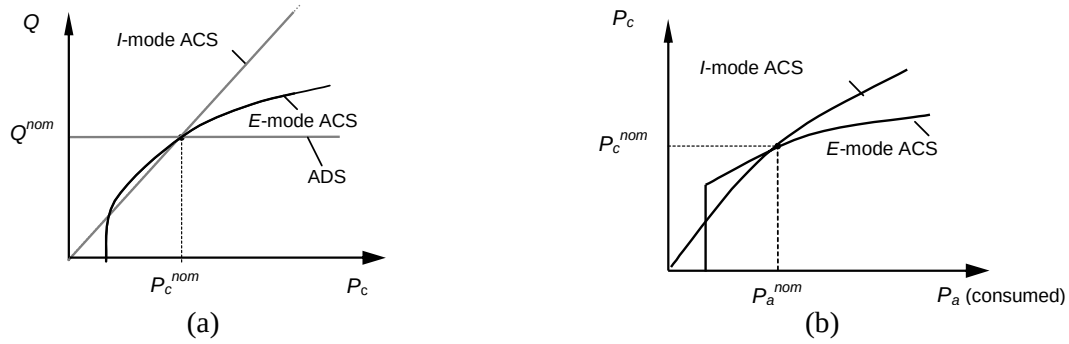

The nominal values of proton current ($I_{p,0}$) and of fraction of accelerator feed power (f_0) are chosen in such a way to sustain the power level P_0 in a nominal state (I_{p0} r_0P_0). The value of the proton current is fixed over all periods of the *E*-mode ACS functioning. On the contrary, the fraction f may be adjusted to compensate eventual reactivity swing (e.g. due to burn-up). In other words, for proton energy we write:

$$e_p = e_{p,0}\frac{fP}{f_0P_0} \tag{4}$$

Above we explained schematically the principle of DENNY functioning where some details are omitted with a view to simplify the description. For example, we suppose that accelerator efficiency is identical for all proton energies, importance of source neutrons does not depend on proton energy, etc. A detailed description of a hybrid system based on the *E*-mode coupling is outside the scope of this paper. However, in order to provide some quantitative illustration of the main principles, a simplified model of system operation with *E*-coupling is presented below.

Results and discussion

Let us study the response of the *E*-mode ACS to an accidental reactivity insertion in order to qualitatively describe the influence of the Y_n-effect on its kinetics. A new equilibrium power level $\overline{P}$ of the system after insertion of the reactivity Δr_{ext} can be found from the generalised reactivity-power balance equation [2,7,8], which follows from the stationary kinetic equation:

$$\Delta r_{ext} - r_0 + \Delta r_{feedback}\left(\overline{P}\right) + r_0 Q\left(\overline{P}\right)/\overline{P} = 0 \tag{5}$$

where the term $Q(P) = P_0 Y_n\left(e_p(P)\right)/Y_n\left(e_{p,0}\right)$ describes the external source and the proton energy e_p was already defined in Eq. (4). In *this* context, the last term in Eq. (5) may be considered as "source (feedback) reactivity" [i.e. $r_{source} = r_0 Q\left(\overline{P}\right)/\overline{P}$]. Equation (5) together with the feedback model and the neutron yield dependence describes the equilibrium states of the *E*-mode ACS after reactivity transients. In this case, a new power level $\overline{P}$ after the reactivity transients will be determined not only by core feedback but also by the ability of the external source to produce sufficient neutrons to sustain this power.

Equation (5) is non-linear with respect to the variable $\overline{P}$ and can be solved numerically. However, the linearisation of Eq. (5) allows us to characterise the Y_n-effect analytically with respect to an infinitesimal power fluctuation. Introducing the normalised power reactivity coefficients $A \equiv P_0 \left(dr_{feedback} \left(P_0\right)/dP_0\right)$ and $B \equiv P_0 \left(dr_{source} \left(P_0\right)/dP_0\right)$, we rewrite Eq. (5) in the linearised form:

$$dr_{ext} + d\overline{P} \left(A + B\right)/P_0 = 0 \tag{6}$$

Taking into account that $Q(P_0) = P_0$ (being the initial condition), and after some modifications, one obtains the following expression for the parameter B:

$$B = r_0 P_0 \left[\frac{d}{dP_0}\left(\frac{Q\left(P_0\right)}{P_0}\right)\right] = -r_0 \left(1 - h_{P\text{fi}\,Q}\left(P_0\right)\right) \tag{7}$$

with the function $h_{P\text{fi}\,Q}\left(P\right) \equiv dQ/dP$ being a measure of the local source effectiveness, i.e. a source response due to an infinitesimal power change in a nominal state. With respect to the global neutron balance in the E-mode ACS, Eq. (7) demonstrates that parameter B may be considered as a coefficient, being a measured supplementary neutron production feedback and arising in the system due to the Y_n-effect. As it follows from Eq. (7), coefficient B is proportional to the nominal subcriticality level r_0 and depends on the $h_{P\text{fi}\,Q}\left(P_0\right)$ functional behaviour.

Non-linear neutron production influences the equilibrium power level and its effectiveness $[h_{P\text{fi}\,Q}(P_0)]$ will depend on the choice of the nominal proton energy e_{p0}. The Y_n-effect increases the asymptotical power if $e_{p,0} < e_p^{optimum}$ [zone (1) in Figure 1] and, on the contrary, it reduces power growth if $e_{p,0} \ge e_p^{optimum}$ [zone (2) in Figure 1]. In fact, we can see from Eq. (7) that if the condition $(dQ / dP) < 1$ is fulfilled, the external neutron source is not able to support the increasing power, which will limit the consequential power growth $\Delta\overline{P} = \overline{P} - P_0$.

Let us suppose for simplicity that $f = f_0$. In this case the function $h_{P\text{fi}\,Q}$ can be expressed as follows:

$$h_{P\text{fi}\,Q}\left(e_p\right) = \left(\frac{e_p}{Y_n\left(e_p\right)}\right)\left(\frac{dY_n\left(e_p\right)}{de_p}\right) \tag{8}$$

As it follows from Eq. (3) and Eq. (8), at $\hat{e}_{p0} = \left(a/\left[\left(1 - a\right)b\right]\right)^{1/a}$ the function $h_{P\text{fi}\,Q}\left(\hat{e}_{p0}\right) = 1$. This energy point defines the limit between the "destabilising" area of the Y_n-effect (amplification of $\Delta\overline{P}$, similar to positive feedback) at $e_{p,0} < \hat{e}_{p,0}$ and the "stabilising" domain of the Y_n-effect (suppression of $\Delta\overline{P}$, similar to negative feedback) at $e_{p,0} \ge \hat{e}_{p,0}$ (Figure 1). It is important to note that in the present case, $\hat{e}_{p,0}$ is equal to the optimum energy $e_p^{optimum}$ with respect to neutron economy.

What is the real gain of the proposed DENNY concept? Below we perform a comparative analysis for the ACS case with I-mode coupling and E-mode coupling, which results in a linear $Q(P)$ dependence and a non-linear $Q(P)$ dependence, respectively [see Figure 2(a)]. The effectiveness of

the Y_n-effect for safety improvement can be described by the *transient suppression parameter D*. It is defined as the ratio of asymptotic power values of *E*-coupled and *I*-coupled systems after a certain reactivity insertion transient, namely:

$$D = \overline{P}^{(E\text{-}mode)} \Big/ \overline{P}^{(I\text{-}mode)} \tag{9}$$

If $D < 1$, it signifies that the Y_n-effect stabilises the system. The *D*-values at different r_0 and Δr_{ext} for the linear model of in-core feedback are presented in Figure 3(a). For a quantitative comparison we defined the parameters in Eq. (3), which we took from Ref. [6], namely $a = 8.2$, $b = 29.3$ and $\alpha = 0.75$. According to the discussion in the previous section, we chose nominal energy value $\varepsilon_{p,0} = 1.6$ GeV greater than $\hat{\varepsilon}_{p,0} = 1.16$ GeV for our comparative analysis, from which the following conclusions were drawn:

- The stabilising role of the Y_n-effect increases when both r_0 and Δr_{ext} increase. This effect can be quite significant (up to 27% at $r_0 = 15\beta$) even in the case of "good" in-core feedback (A = -488 pcm). Further growth of Δr_{ext} leads to the saturation of such a tendency.

- Augmentation of the nominal proton energy $\varepsilon_{p,0}$ enhances the stabilising impact of the Y_n-effect due to the reduction of the source effectiveness $\eta_{Pfi\,Q}(\varepsilon_{p0})$.

Figure 3. Transient suppression parameter *D* as a function of subcriticality level r_0

(a) At different values of the inserted reactivity Δr_{ext} (feedback coefficient A = – 488 pcm),
(b) at different values of the parameter A (the inserted reactivity Δr_{ext} = 350 pcm); β = 350 pcm

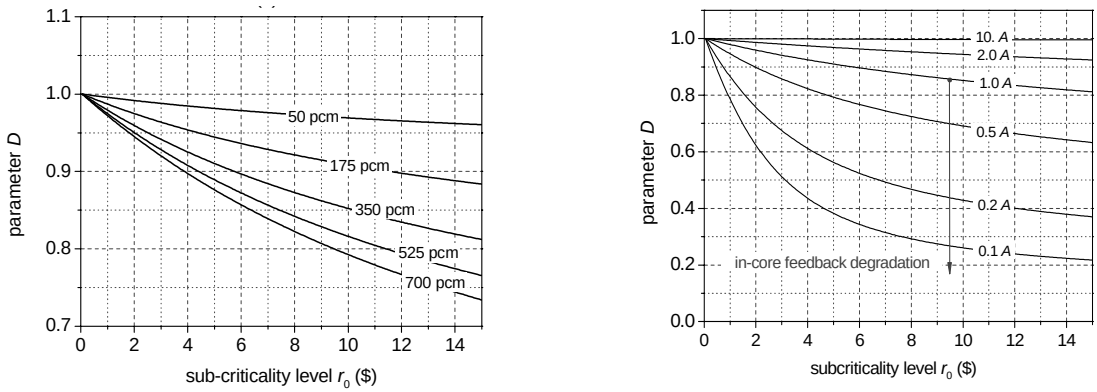

(a) (b)

Parameter *D* depends also on the feedback coefficient *A*, defined earlier in this work. We recall that this parameter reflects both the in-core feedback effects and the thermo-hydraulics of the system. Figure 3(b) demonstrates that the impact of the Y_n-effect on power stabilisation increases when the absolute value of feedback coefficient *A* decreases. This dependence of the transient suppression parameter *D* on parameter *A* was predictable. Indeed, if $A \to 0$, i.e. in-core feedback effects are absent, the *Y_n-effect becomes the only feedback effect, exiting in the system.*

Conclusions

In the present work, a new approach for the realisation of an accelerator-coupled hybrid system (ACS) was proposed and nominated as the DENNY system (delayed enhanced neutronics with

non-linear neutron yield). This concept is based on the particularity of neutron production forming a quasi-linear dependence between energy production (coupled to the proton energy) in the core and the external neutron yield Y_n in the spallation target (Y_n-effect). This particular dependence provides auto-regulating behaviour of the ensemble "accelerator-subcritical core". The proposed system has the kinetics of a critical system with an artificial group of delayed neutrons as with the "standard" ACS. In addition, its external neutron production contains supplementary feedback, which is able to stabilise the installation power in its nominal state.

We showed that significant improvement of the feedback effect due to this particular coupling between an accelerator and a subcritical core (*E*-mode coupling) could be achieved. The proposed Y_n-effect can be compared to the Doppler feedback effect but for external source neutrons. Similar to the Doppler effect, the Y_n-effect is intrinsic. Lastly, our qualitative estimates showed that implementation of this concept could compensate eventual feedback degradation in cores dedicated to the transmutation of nuclear waste. Further and more quantitative analysis is urgently needed. Such further studies should include feasibility estimates to show whether the *E*-mode ACS could be realised in practice.

REFERENCES

[1] Rubbia, C., *et al.*, *Conceptual Design of a Fast Neutron Operated High Power Energy Amplifier*, CERN/AT/ 95-44, Geneva, Switzerland (1995).

[2] Gandini, A., M. Salvatores, I. Slessarev, "Coupling of Reactor Power with Accelerator Current in ADS Systems", *Annals of Nuclear Energy*, 27(13), p. 1 147 (2000).

[3] Slessarev, I., P. Bokov, "Deterministic Safety Study of Advanced Molten Salt Nuclear Systems for Prospective Nuclear Power", *Nucl. Eng. Design*., 231(1), pp. 67-88 (2004).

[4] Andriamonje, S., *et al*., "Experimental Determination of the Energy Generated in Nuclear Cascades by a High Energy Beam", *Phys. Lett*., B 348, p. 697 (1995).

[5] Letourneau, A., J. Galin, F. Goldenbaum, *et al*., "Neutron Production in Bombardments of Thin and Thick W, Hg, Pb Targets by 0.4, 0.8, 1.2, 1.8 and 2.5 GeV Protons", *Nuclear Instruments and Methods in Physics Research*, B 170, pp. 299-322 (2000).

[6] Pankratov, D., *et al.*, "Secondary Neutron Yields from Thick Pb and W Targets Irradiated by Protons with Energy 0.8 and 1.6 GeV", *Proceedings of the 2nd International Conference on Accelerator-driven Transmutation Technologies and Applications*, V2, Kalmar, Sweden (1996).

[7] Wade, D., "LMR Core Design for Inherent Safety", *Proceedings of the NEA/CRP Meeting*, Paris, France (1986).

[8] Gandini, A., M. Salvatores, I. Slessarev, "Balance of Power in ADS Operation and Safety", *Annals of Nuclear Energy*, 27, pp. 71-84 (1999).

K_{eff} AND K_s BURN-UP SWING COMPENSATION IN MYRRHA

W. Haeck
Ghent University (UGent), Belgium
SCK•CEN, Belgium

H. Aït Abderrahim
SCK•CEN, Belgium

C. Wagemans
Ghent University (UGent), Belgium

Abstract

Burn-up for the reference core of MYRRHA over a single cycle of 90 days was estimated with MCNPX and SPECTRUM (an MCNPX postprocessor developed at SCK•CEN). Over this cycle, the source multiplication factor k_s dropped from 0.952 to 0.941 ($\Delta\rho_s$ = 1 263 pcm) while the effective multiplication factor k_{eff} dropped from 0.946 to 0.933 ($\Delta\rho$ = 1 484 pcm). A number of possible techniques have already been proposed and studied to minimise this burn-up swing such as proton current variation, use of burnable poisons, use of negative void coefficients and multi-batch core operation. We propose the concept of a realistic operational cycle in which voided boxes and/or burnable absorbers (with different levels of enrichment) are used to minimise the burn-up swing in the MYRRHA case. In this paper, we also make an initial assessment of the applicability of these operational cycles to the MYRRHA case.

Introduction

MYRRHA (multi-purpose hybrid research reactor for high-tech application) [1] is an ADS (accelerator-driven system) under development at the Belgian Nuclear Research Centre SCK•CEN in Mol, Belgium, which aims to serve as a basis for the European experimental ADS to provide protons and neutrons for various R&D applications including materials testing, transmutation experiments, etc. The system itself consists of a proton accelerator delivering a 350 MeV, 5 mA proton beam to a liquid Pb-Bi spallation target coupled with a Pb-Bi-cooled, subcritical fast core.

The configuration of the reference core [2] is shown in Figure 1. It consists of 39 fuel assemblies with 30% MOX (in red) and six assemblies with 20% MOX (in orange). The remaining channels are loaded with "dummy" assemblies, which are fuel assembly-like boxes filled with Pb-Bi coolant. The hexagonal fuel assembly for MYRRHA consists of 91 fuel pins, which are surrounded by a hexagonal shroud with an inner plate-to-plate width of 82.0 mm and a wall thickness of 1.75 mm. The cylindrical fuel pin itself has an outer diameter of 6.59 mm and an inner diameter of 5.55 mm. The fuel pellet contained within the pin has a diameter of 5.40 mm without an inner gap. The active length of the fuel is 600 mm. In this configuration, the source multiplication factor k_s is 0.95236 – 0.00028 and the effective multiplication factor k_{eff} is 0.94589 – 0.00020. The targeted operating regime for the system is three months (90 days) of operation followed by one month (30 days) of core reshuffling, loading and maintenance. It is foreseen to have two or three cycles per year (if necessary, followed by a longer maintenance period).

Figure 1. The MYRRHA reference core

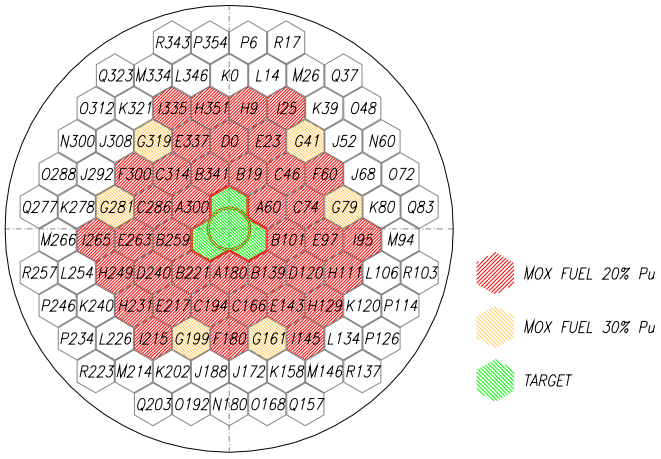

For the purpose of burn-up calculations, the active part of a fuel assembly is divided into five equally sized segments. Each cycle of 90 days is then divided into six steps of 15 days. At the beginning of each cycle, the neutron spectrum in the fuel of each assembly segment is calculated using MCNPX [3]. The code SPECTRUM [4] (developed at SCK•CEN as a postprocessor for MCNPX) uses these spectra to calculate ORIGEN libraries [5] for all fuel assembly segments. This way, every segment has a library associated with it specifically for the cycle that we are studying. It is possible to recalculate the library for every burn-up step, but the neutron spectrum and the resulting library do not change enough to justify this approach. For every burn-up step, MCNPX is used to calculate the total flux in every segment for the depletion calculation. The composition of the material after each burn-up step (accounting for 99.99% of absorption in the fuel) is calculated by SPECTRUM using ORIGEN 2.2. This new composition is then used in MCNX for the next burn-up step. The nuclear data used for all calculations is JEF2.2 (unless stated otherwise).

Concept of a realistic operational cycle for MYRRHA

In a normal critical system like a pressurised water reactor (PWR), control is achieved by compensating the excess reactivity of the fuel with anti-reactivity obtained through various means to obtain a total reactivity level of zero. Some of these sources of anti-reactivity are the result of operation and/or the dynamics of the reactor like the xenon and samarium effect, the various temperature feedback mechanisms and the Doppler effect. Some of these effects can actually change as the burn-up of the fuel increases. Other sources are actively varied in time to compensate the excess reactivity of the fuel and to keep the total reactivity of the reactor at zero. In the case of a PWR, this is done by adding boric acid to the coolant of the primary circuit and by using control rods. At beginning of life (BOL), a large amount of positive reactivity is invested in the fuel. The boric acid in the water at BOL compensates most of this positive reactivity. The rest is negated by various other effects. At the end of the cycle, the anti-reactivity associated with the boric acid becomes zero and it is no longer possible to maintain the reactor at a zero reactivity level. At this point, the fuel has lost ~40% of its reactivity due to burn-up. For the following cycle, the fuel elements are reshuffled and new elements are introduced. The entire cycle then repeats itself.

A similar strategy can be adopted for an ADS-like MYRRHA. However, instead of using the normal reactivity ρ associated with the effective multiplication factor k_{eff}, we will use the reactivity ρ_s associated with the source multiplication factor k_s. The definition of this reactivity ρ_s is similar to that of normal reactivity ρ:

$$\rho_s = \frac{k_s - 1}{k_s} \tag{1}$$

Because ADS is always subcritical, this reactivity ρ_s will always be negative. As such, we cannot speak of positive and negative reactivity without rescaling this reactivity to a certain operating level ρ_{s0}. This value is a reference value for the reactivity and can be chosen freely. A choice for the operating level could be the reactivity ρ_s of the core at the beginning of the cycle, or even the mean value of ρ_s over an entire cycle.

We must insure that the fuel for MYRRHA will at least be able to compensate for all possible reactivity effects and the burn-up of a few cycles. Contrary to the case of a normal reactor where the excess of normal reactivity can be quite high, the maximum amount of reactivity ρ_s introduced by the fuel above the operating level is limited to $|\rho_{s0}|$ and should even be less if we want a sufficient safety margin. If the amount of reactivity introduced by the fuel would be higher than this value, the core could become critical under certain situations. This excess reactivity must be compensated through different means. First of all, there will be the inherent mechanisms that introduce anti-reactivity like the Doppler effect, temperature feedback effects on fuel and moderator/coolant, etc. We also require sources of anti-reactivity that we can actively use to bring the total reactivity back to the operating level. Possibilities would include the use of burnable absorber (either integrated in a fuel assembly or as a separate assembly placed around the core), control rods or fuel assembly-like boxes filled with helium at low pressure (this uses the negative void coefficient of the Pb-Bi coolant to introduce anti-reactivity). These have been shown in the past to be viable options [6,7,8].

The reactivity balance for MYRRHA using some of these techniques would look like Figures 2(a) and 2(b). These balances assume a single year of operation with three cycles of 90 days followed by 30 days of maintenance, with the same configuration of the core. Please note that these figures are not exact and that they are provided to give a sense of how the system would evolve.

Figure 2. Reactivity balances for MYRRHA

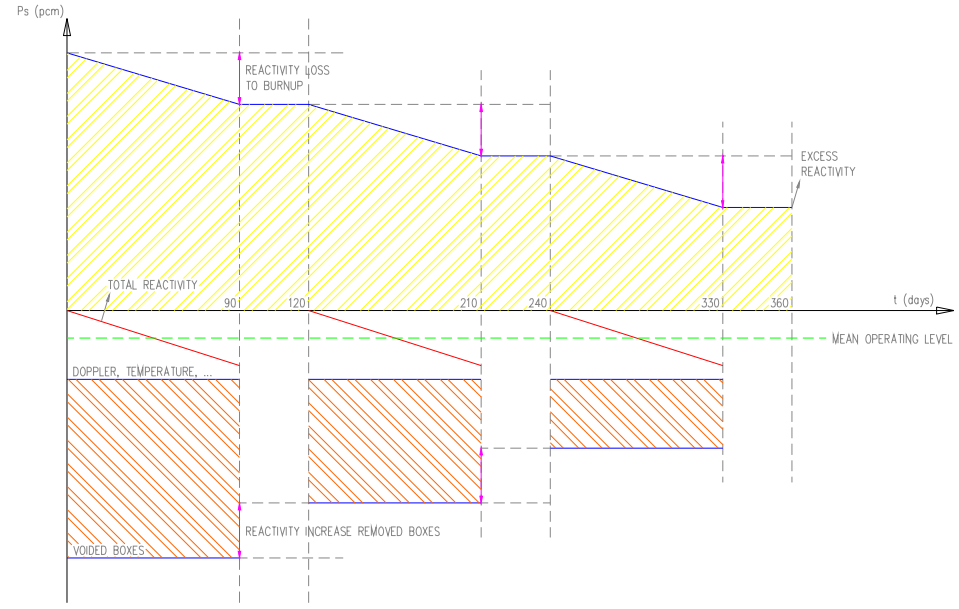

(a)

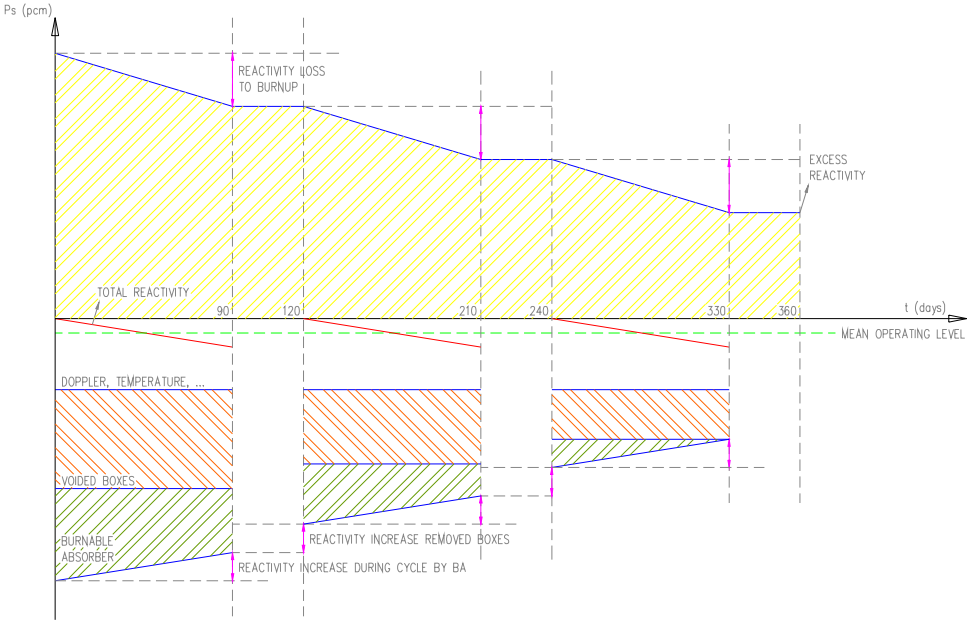

(b)

The first balance [Figure (2a)] depicts the situation in which only voided boxes are used. The voided boxes increase the radial and axial leakage from the core. As a result, fewer neutrons are scattered back into the core, hence lowering the reactivity of the core. It is important to note that these voided boxes are introduced in the reflector around the core. As the radius of the core increases, the effect of these boxes on the total reactivity will decrease (because the centre of the core will be unaffected by the increased leakage caused by the boxes). In the case of Figure 2(a), a number of boxes are added to the core resulting in an amount of anti-reactivity sufficient to compensate for a few cycles. The loss of reactivity during one cycle can now be compensated by removing a few boxes from the core. Because of this, the operating level will not drop below the initial level minus the reactivity loss of a single cycle.

We now obtain an average operating level over a single cycle of about the initial operating level minus half the reactivity lost over the cycle due to burn-up. It would also be possible to design the system so that the average operating level over a single cycle is the operating level we want to achieve over the cycle. We would only need to introduce some extra positive reactivity at the beginning of the cycle equal to half the amount of reactivity lost during a single cycle. This can be achieved by simply removing some voided boxes from the core or by increasing the excess reactivity in the fuel.

Figure 2(b) depicts the situation where voided boxes are used in combination with burnable absorber in the reflector. In this case, B_4C rods are introduced in the reflector (these are not control rods as they cannot be moved during a cycle). The amount of anti-reactivity decreases during the cycle, leading to a higher average operating level as compared to the voided boxes. When the configuration of the core changes a lot from cycle to cycle, the required composition of the rods will change from cycle to cycle (because the reactivity loss due to burn-up will differ from cycle to cycle). It would be necessary to custom-build the required rods for every cycle (the density of the burnable absorber must be adjusted so that the rod represents the right amount of anti-reactivity for that cycle). A solution to this problem would be the use of rods that represent a small amount of anti-reactivity for every cycle (e.g. half the reactivity loss of an average cycle, or 500 to 750 pcm for example). The rest could be compensated by a number of voided boxes. As a result, the total reactivity over a single cycle would only drop by one-half of the amount lost in the situation without burnable absorber [see Figure 2(b)]. Another method to compensate the burn-up swing would be the use of homogeneous poisoning of the core, preferably poisoning that can be adjusted during operation like boric acid in a PWR. A way to achieve homogeneous poisoning would be to incorporate small amounts of the poison in every fuel assembly (either in a single pin or by adding the poison to structural materials of an assembly). As with the rods in the reflector, we must take into account the different configurations of the core. This means that an amount of poison in an assembly that is just right for a given cycle will not necessarily be right for the next cycle. We also have to keep in mind that burnable absorber in the vicinity of the spallation source will have a negative effect on the source.

By using these operational cycles, we can keep operating value within a certain range and increase the residence time of fuel in the core. By using burnable absorbers, we can even reduce this range to half the range without burnable absorber. A compensation technique that can be altered during operation would be the most interesting for controlling the system. Using control rods would be the perfect solution but variation of the accelerator beam current is also an option. However, the latter will raise safety issues as we would need a beam current reserve. As a result, we would have to foresee the possibility of injection of the entire reserve at BOL of the core (represents the worst case scenario as the burn-up of the core is at its minimum). It should be noted that varying the beam current will not directly change the reactivity of the core; it will only allow us to maintain the same flux or power level during the cycle. This is because the power of the system is proportional to the beam current I_p:

$$P = I_p Y \frac{k_s}{1 - k_s} \frac{E_f}{\nu} = -I_p Y \Sigma_s \frac{E_f}{\nu} \tag{2}$$

In Eq. 2, Y is the neutron yield per proton, E_f is the mean energy released per fission (set to 210 MeV) and ν is the mean number of neutrons released (set to 2.94). As we can see, a reduction of the reactivity by 20%, for example, of its original value will cause the beam current to increase by 20% of its original value if the power over the cycle is to remain constant. So if a core loses 20% of its reactivity per cycle, and if it would operate during three cycles without any compensation of the reactivity loss, then the total amount of beam current required would be 160% of the initial value. When

the core uses only voided boxes, this would be only 120% of the initial value. For the case of voided boxes combined with burnable absorber, this becomes 110% (if the burnable absorber compensates for half the reactivity loss). Variation of the beam current can thus be seen as a finetuning technique used in conjunction with other compensating techniques.

All of the above methods (except beam current adjustment) are techniques that can be used to keep the global reactivity level and thus the multiplication of the system as constant as possible. Constant multiplication, however, is not enough. We still need to make sure that we obtain the foreseen flux levels at discrete positions of the core. This can be controlled by fuel element reshuffling during the shutdown period between two cycles. There are two distinctly different refuelling schemes available to us. The first one is the in-out strategy. This involves the loading of new elements in the outer zone of the core and the relocation of older elements towards the centre of the core. This scheme is widely used in PWRs as it flattens the radial flux distribution. It does, however, cause significant neutron leakage from the reactor (something that can be rectified by using an appropriate reflector). The second strategy is the in-out strategy in which new elements are added in the centre of the core and older elements are moved to the outside. This causes neutron leakage to drop drastically but will also cause a radial flux distribution with a large peak in the centre.

Burn-up in the reference core

Table 1 gives the evolution of the most important parameters (multiplication factors k_s and k_{eff}, reactivity and power of the system) of the reference core during one irradiation cycle. The upper part of Figure 3 shows the evolution of the total flux in the middle of three different assemblies (assembly A close to the source, assembly D in the middle of the core and assembly I on the outside of the core; see Figure 1). The lower part of Figure 3 shows the same for the fast flux ($E_n > 0.75$ MeV). Over this single cycle, the source multiplication factor k_s drops from 0.95236 to 0.94105 while the effective multiplication factor k_{eff} drops from 0.94589 to 0.93279. This equals a total reactivity loss of 1 263 pcm (associated with k_s) or a loss of 1 484 pcm of normal reactivity (associated with k_{eff}). As a result, the reference core of MYRRHA has lost almost 21.3% of its initial power during a single cycle. The total flux drops by ~20%. On the other hand, the fast flux drops by only ~15% compared to the values at the beginning of the cycle.

Table 1. Evolution of multiplication factors, reactivity values and power of the reference core

Time (days)	k_s	k_{eff}	ρ_s (pcm)	ρ (pcm)	P (MW)
0	0.95236 – 0.00028	0.94589 – 0.00021	-5 002 – 31	-5 721 – 23	42.80
15	0.94983 – 0.00038		-5 282 – 43		40.45
30	0.94806 – 0.00043		-5 478 – 48		38.87
45	0.94639 – 0.00045		-5 665 – 50		37.33
60	0.94417 – 0.00048		-5 913 – 54		35.87
75	0.94224 – 0.00048		-6 131 – 54		34.46
90	0.94105 – 0.00049	0.93279 – 0.00020	-6 265 – 55	-7 205 – 23	33.69

Figure 3. Flux evolution in the reference core

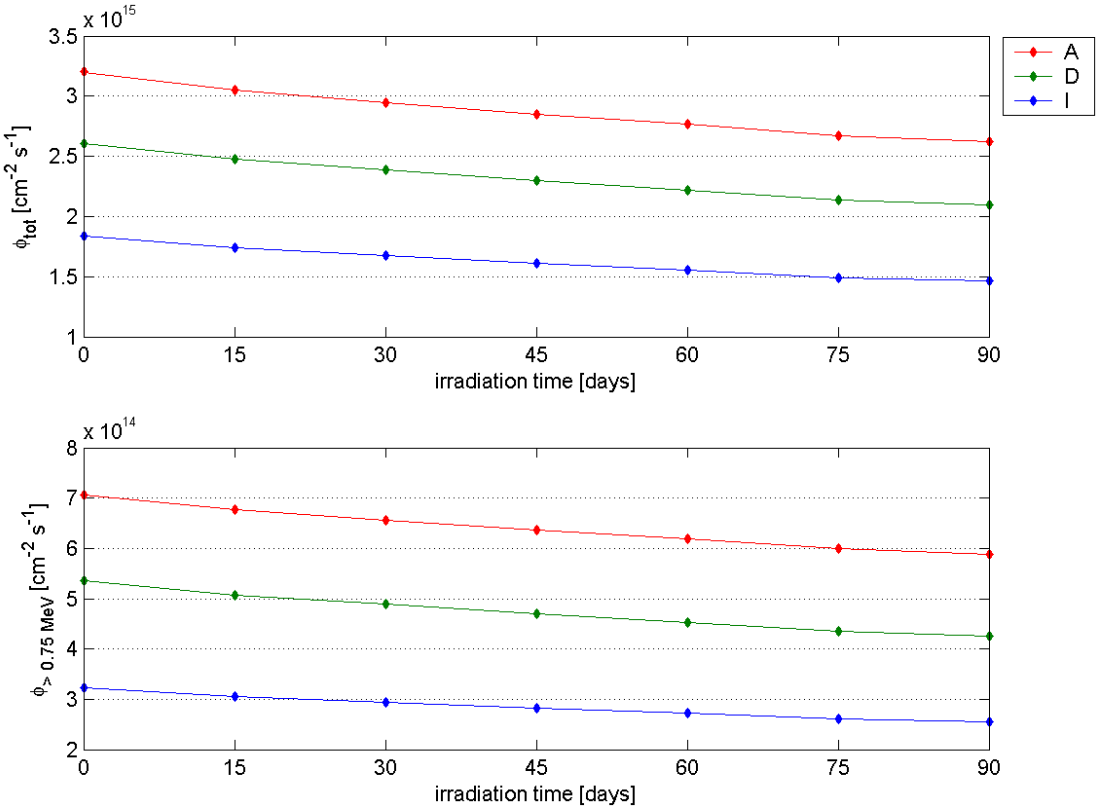

Modified core calculations

To demonstrate the feasibility of the operational cycles that we proposed earlier, we performed burn-up calculations over two cycles of a modified MYRRHA core (see Figure 4). This modified core was loaded with 45 assemblies with 30% MOX. The six assemblies with 20% MOX in the reference core were thus replaced by higher enriched assemblies providing us with 1 783 pcm of excess reactivity (which should more than suffice to compensate the reactivity loss over a single cycle). This excess reactivity was almost completely compensated by six voided boxes (accounting for 1 421 pcm of anti-reactivity) placed symmetrically around the core. The resulting modified core had slightly higher k_s and k_{eff} values compared to the reference core (see Table 2). The evolution of the multiplication factors k_s and k_{eff} as well as the reactivity and power of the system for this modified core during one irradiation cycle are given in Table 3. Figure 5 gives the evolution of total flux and fast flux (E_n > 0.75 MeV) in the middle of three different assemblies.

Table 2. Multiplication factors and reactivity values in the reference core and modified core

	Reference core	Full 30% MOX core	Adding voided boxes
k_{eff}	0.94589 – 0.00021	0.96614 – 0.00022	0.94969 – 0.00020
k_s	0.95236 – 0.00028	0.96881 – 0.00019	0.95565 – 0.00026
ρ (pcm)	-5 721 – 24	3 505 – 24	-5 298 – 22
ρ_s (pcm)	-5 002 – 31	-3 219 – 20	-4 640 – 29

Figure 4. The MYRRHA modified core

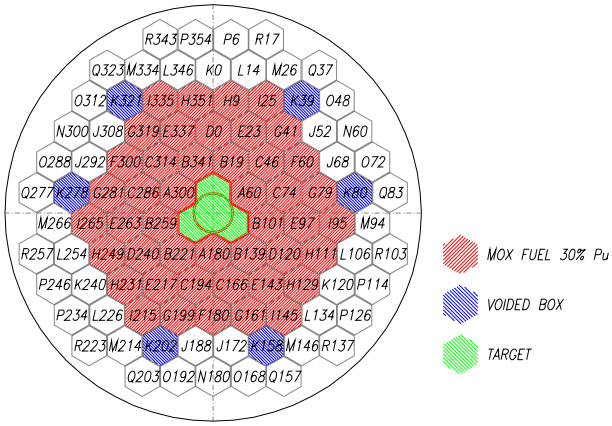

Table 3. Evolution of multiplication factors, reactivity values and power of the modified core

Time (days)	k_s	k_{eff}	r_s (pcm)	r (pcm)	P (MW)
0	0.95565 – 0.00026	0.94969 – 0.00020	-4 640 – 29	-5 298 – 22	46.21
15	0.95329 – 0.00048		-4 899 – 53		43.59
30	0.95053 – 0.00050		-5 204 – 56		40.83
45	0.94942 – 0.00051		-5 327 – 57		39.96
60	0.94762 – 0.00053		-5 528 – 59		38.23
75	0.94629 – 0.00054		-5 676 – 61		37.39
90	0.94367 – 0.00057	0.93611 – 0.00021	-5 969 – 64	-6 825 – 24	35.43
Cooling	-	-	-	-	-
120	0.95682 – 0.00033	0.95118 – 0.00021	-4 513 – 37	-5 133 – 23	47.55

During the first cycle, the source multiplication factor k_s of the modified core dropped from 0.95565 to 0.94367 while the effective multiplication factor k_{eff} dropped from 0.94969 to 093611. This equals a total reactivity loss of 1 329 pcm (associated with k_s) or a loss of 1 527 pcm of normal reactivity (associated with k_{eff}). As with the reference core, this modified core lost over 20% of its initial power during a single cycle. The total and fast flux dropped by ~20%.

At the beginning of the second cycle, the voided box assemblies were removed from the core. As a result, the reactivity of the core went up with 1 456 pcm, compensating the reactivity loss of the first cycle. The source multiplication factor went up to 0.95682 and the initial power of the system reached 48 MWth, which was somewhat higher than at the beginning of the first cycle. In other words, the system reached the power and flux level at the beginning of the first cycle without replacing or adding new fuel assemblies.

Conclusions

We have shown that the operational cycles proposed in this paper are realistic and that they can be applied to the MYRRHA case with ease. In the case studied (two cycles of 90 days using only voided box assemblies), it also appeared that adding new elements after the first cycle was not necessary to reach the operating level of the first cycle at the beginning of the second cycle. Further study will include the addition of burnable absorber to the core.

Figure 5. Flux evolution in the modified core

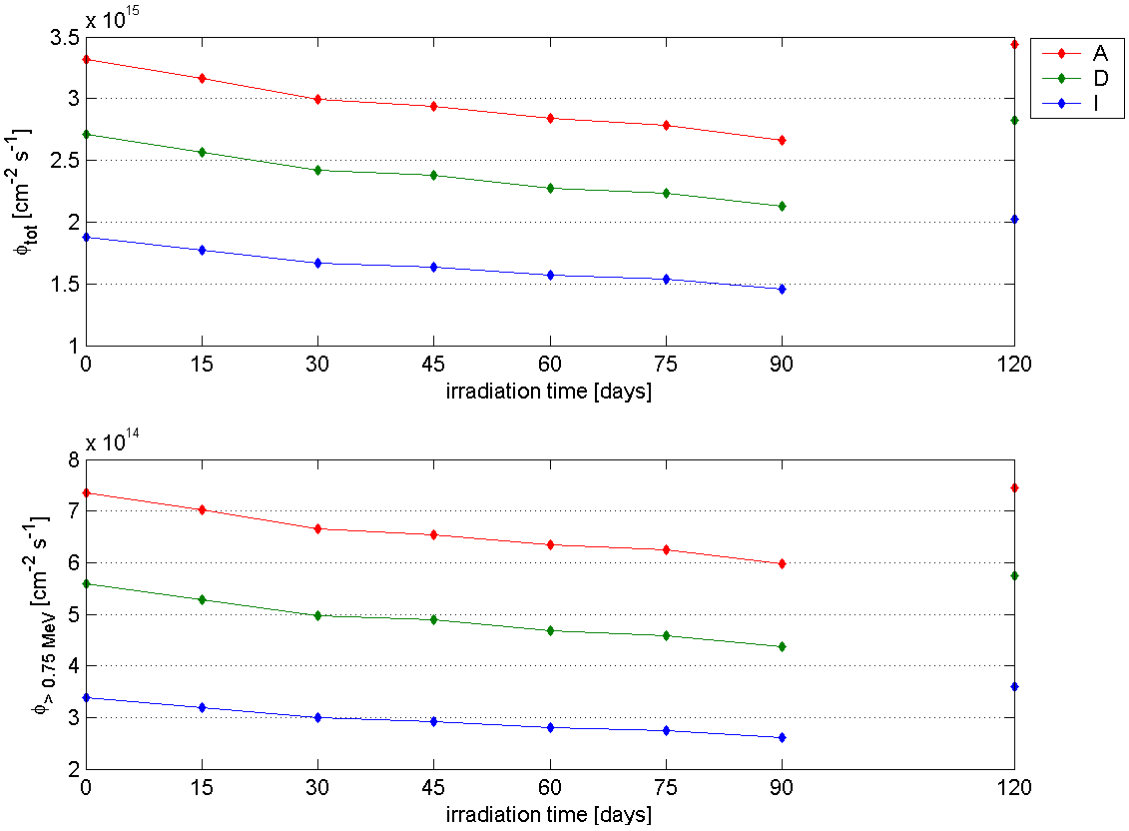

REFERENCES

[1] Aït Abderrahim, H., *et al.*, "MYRRHA, A Multipurpose Accelerator Driven System for R&D – State-of-the-art of the Project at Mid-2003", *Proceedings InWor P&T and ADS 2003*, October 2003.

[2] Sobolev, V., E. Malambu, *Sub-critical Core, Fuel Assembly and Fuel Rod of the Experimental ADS MYRRHA-II*, SCK•CEN Draft Technical Note, April 2004.

[3] Waters, L.S., ed., *MCNPX User's Manual, Version 2.4.0*, LA-CP-02-408, September 2002.

[4] Verboomen, B., W. Haeck, *SPECTRUM – Analysis of Spectral Data in Universal Multigroup Format – A Postprocessor for Continuous Energy Monte Carlo Calculations – Version 1.0a*, SCK•CEN BLG Report Nr 978 (2004).

[5] Croff, A.G., *ORIGEN2: A User's Manual for the ORIGEN2 Computer Code*, ORNL/TM-7175, July 1980.

[6] Malambu, E.M., Th. Aoust, N. Messaoudi, G. Van den Eynde, Ch. De Raedt, *Status of the Neutronic Analysis of the MYRRHA ADS – Progress Report November 2001*, SCK•CEN Internal Report R-3593 (2002).

[7] Van den Eynde, G., *Calculating the MYRRHA Core Using DIF3D 8.0*, SCK•CEN Technical Report RF&M/GVdE/gvde.34.B043200/MYRRHA/85–60, November 2003.

[8] Haeck, W., *Reactivity Values in MYRRHA – Comparison of Results from MCNPX 2.5.c and DIF3D 8.0*, SCK•CEN Technical Report RF&M/WH/wh.34.B043200/85/MYRRHA/03-61, November 2003.

TECHNICAL SESSION V

ADS Experiments and Test Facilities

Chairs: P. D'hondt, V. Bhatnagar

CONCEPT OF TRANSMUTATION EXPERIMENTAL FACILITY

Hiroyuki Oigawa, Toshinobu Sasa, Kenji Kikuchi, Kenji Nishihara, Yuji Kurata, Makoto Umeno, Kazufumi Tsujimoto, Shigeru Saito, Masatoshi Futakawa, Motoharu Mizumoto, Hideki Takano
Japan Atomic Energy Research Institute, Japan

Abstract

Under the framework of the High-intensity Proton Accelerator Project called J-PARC (Japan Proton Accelerator Research Complex), the Japan Atomic Energy Research Institute (JAERI) plans to construct the Transmutation Experimental Facility (TEF). The TEF consists of two facilities: the Transmutation Physics Experimental Facility (TEF-P) and the ADS Target Test Facility (TEF-T). The TEF-P is a critical facility that can accept a 600 MeV, 10 W proton beam. The TEF-T is a material irradiation facility using a 600 MeV, 200 kW proton beam and a Pb-Bi target; however, neutron multiplication by nuclear fuel will not be attempted. This report describes the purpose of the facility, the present status of the conceptual design and the expected experiments to be performed.

Introduction

To reduce the amount of minor actinide (MA) and long-lived fission products (LLFP) in high-level radioactive waste, the Japan Atomic Energy Research Institute (JAERI) proposed the "double-strata fuel cycle concept", i.e. the dedicated transmutation fuel cycle is established separately from the commercial power generation fuel cycle [1,2]. In the transmutation fuel cycle, nuclear fuel consisting mainly of MA is used to enhance transmutation efficiency. Using such MA fuel, the critical reactor would encounter many difficulties regarding safety and controllability. The accelerator-driven subcritical system (ADS) has potential advantages to manage these difficulties as compared to critical reactors: 1) varying fuel composition is acceptable (within reason) since the small Doppler effect does not seriously affect system safety and 2) a small value of delayed neutron fraction is also acceptable since the margin to prompt critical state and power control by the reactivity adjustment are not necessary. Therefore, the ADS is considered suitable to transmute MA in the transmutation fuel cycle.

The ADS proposed by JAERI is an 800 MWth, nitride fuelled Pb-Bi eutectic (LBE) cooled fast subcritical core driven by a spallation neutron source using an LBE target and 1.5 GeV, 20-30 MW proton accelerator [3]. To realise such a large-scale ADS, some technical issues need to be studied, developed and demonstrated. Issues include, for example, reliability of the accelerator, beam transport system, high-power spallation target technology, integrity of beam window, reactor physics and the controllability of a subcritical system, MA transmutation performance and fuel handling.

To promote research and development (R&D) for most of the above-mentioned technical issues, JAERI plans to build the Transmutation Experimental Facility (TEF) at Tokai Research Establishment under the framework of the joint project of a high-intensity proton accelerator called J-PARC (Japan Proton Accelerator Research Complex) with the High-energy Accelerator Research Organization (KEK) [4]. Figure 1 shows a site plan of the J-PARC facilities. Phase 1 of J-PARC consists of three accelerators (a 400 MeV linac, a 400 MeV - 3 GeV synchrotron and a 3-50 GeV synchrotron) and three experimental facilities (the Material and Life Science Facility, the Nuclear Physics Facility and the Neutrino Facility). The construction of these Phase 1 facilities is under way and is scheduled to be completed by 2007 (except a portion of the facilities). In Phase 2, construction of the TEF is planned along with an upgrade of the linac from 400 MeV to 600 MeV.

Figure 1. Site plan of the J-PARC facilities

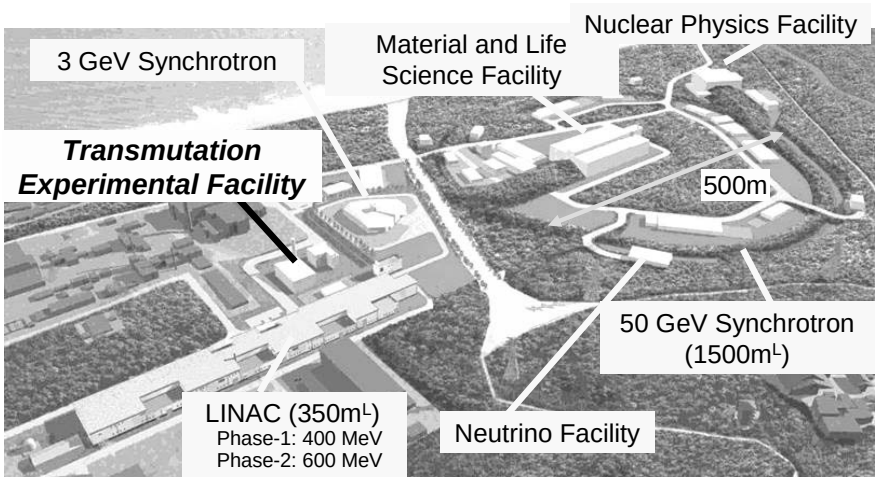

TEF consists of two buildings – the Transmutation Physics Experimental Facility (TEF-P) and the ADS Target Test Facility (TEF-T) as shown in Figure 2. TEF-P is a zero-power critical facility, which can be operated with a low-power proton beam to investigate reactor physics and ADS controllability. TEF-T is a material irradiation facility, which can accept a maximum 200 kW, 600 MeV proton beam into the spallation target of the LBE. In this paper, the purpose, the present status of the conceptual design and the expected experiments using the facility are reported.

Figure 2. Concept of the Transmutation Experimental Facility (TEF)

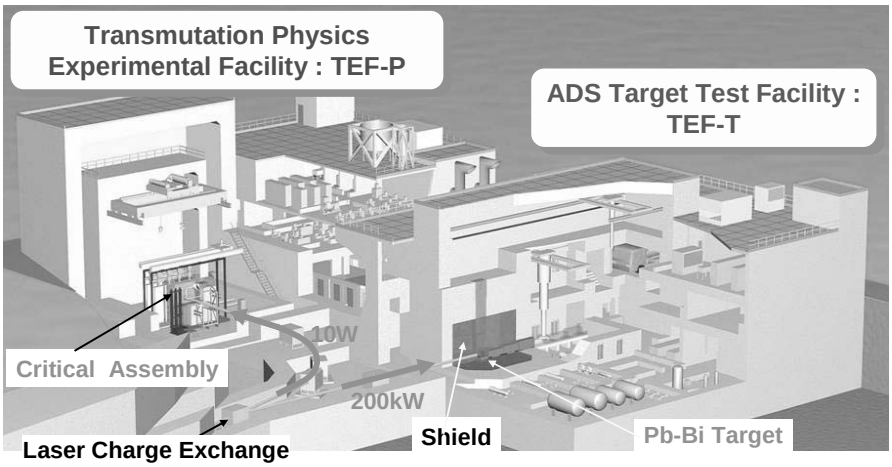

Background and purpose of TEF-P

Some experimental research on reactor physics aspects of ADS have been carried out using existing zero-power facilities worldwide. The most systematic is the MUSE program [5] at the Cadarache research centre of CEA (France) where the existing fast critical facility, MASURCA, is connected with a DT (and DD) neutron source called GENEPI. The purpose of the MUSE program is to investigate prediction accuracy of reactor physics parameters in a subcritical core (i.e. power distribution, subcriticality index and source importance in various core configurations). In Japan, basic experiments are underway on JAERI's FCA (fast critical assembly) for the fast neutron subcritical system using a ^{252}Cf neutron source and a DT neutron source [6]. Moreover, at the Kyoto University Critical Assembly (KUCA), an experimental program to connect the thermal neutron subcritical system with a proton accelerator (~150 MeV) is scheduled for a few years from now [7].

On the other hand, many experimental studies have been performed with proton accelerators worldwide to obtain the characteristics of a spallation neutron source using many kinds of target materials such as lead, tungsten and mercury.

However, there has been no experimental work implemented so far that involves research and demonstration of a fast subcritical system combined with a spallation source. Therefore, the main purpose of TEF-P is to research the reactor physics of a subcritical core that is driven by a spallation source using a 600 MeV proton beam. The second purpose is to demonstrate the controllability of a subcritical core; control of reactor power by adjustment of the proton beam current will be attempted in the experimental program. The third purpose is to research the transmutation performance of a subcritical core using a certain amount of MA and LLFP by installing proper shielding, cooling and handling devices.

Specifications of TEF-P

For the above-mentioned purpose, high thermal power is not necessary; a power level of critical experiments (i.e. 100 W) is preferable from the viewpoint of accessibility to the core. Although validation of core thermal feedback effects might be necessary, such experiments can be performed using an electrical heater that simulates reactor power without real fission energy and accompanying fission products. Maximum thermal power of TEF-P was tentatively set at 500 W.

The most important problem in building a new nuclear facility is how to prepare the fuel since tons of low enriched uranium or plutonium are necessary to make the core critical or near-critical (e.g. $k_{eff} = 0.95$) in a fast neutron system. We intend to use the plate-type fuel of the fast critical assembly (FCA) in JAERI/Tokai, or preferably to merge FCA into TEF-P. Metallic fuel of enriched uranium and plutonium will be available as well as natural and depleted uranium. Many kinds of simulation materials such as lead and sodium for the coolant, ZrH for the moderator, B_4C for the absorber and AlN for the nitride fuel will also be prepared.

Therefore, the TEF-P is designed with reference to FCA (the horizontal table-split type critical assembly with a rectangular lattice matrix). Figure 3 shows a conceptual view of the assembly. The fuel is loaded in the fixed and movable half assemblies. The movable assembly approaches the fixed one, and they contact each other for the operation. In the representative experimental configuration, two sets of control rods and six sets of safety rods are installed in total on both assemblies. These control and safety rods are not composed with absorber materials such as B_4C but with enriched uranium fuel to avoid disturbance of the experimental condition.

Low-current proton beam is extracted by a laser charge exchange technique from a high-intensity beam line of 200 kW (0.33 mA, 600 MeV), most of which is introduced into TEF-T. Figure 4 shows the concept of a beam transport system for TEF. The 200 kW proton beam is a pulsed one whose repetition rate and maximum pulse width are 25 Hz and 0.5 ms, respectively. The protons are accelerated as negative ions (H^-). The beam is exposed by a YAG laser, which can strip one of the two electrons so as to change a small amount (below 10 W) of H^- to neutral (H^0). The H^- and the H^0 are then separated by a bending magnet, where H^- is bent into TEF-T and H^0 goes straight/forward in the magnetic field. The other electron of the H^0 is finally stripped by a carbon foil so that the positive protons (H^+) are introduced into TEF-P. The time width of the proton pulse for TEF-P can be adjusted by changing the duration of the laser exposure; a 1 ns - 0.5 ms pulse is expected to be available. The proton beam intensity is controlled by a collimator.

Figure 3. Table-split type critical assembly (TEF-P)

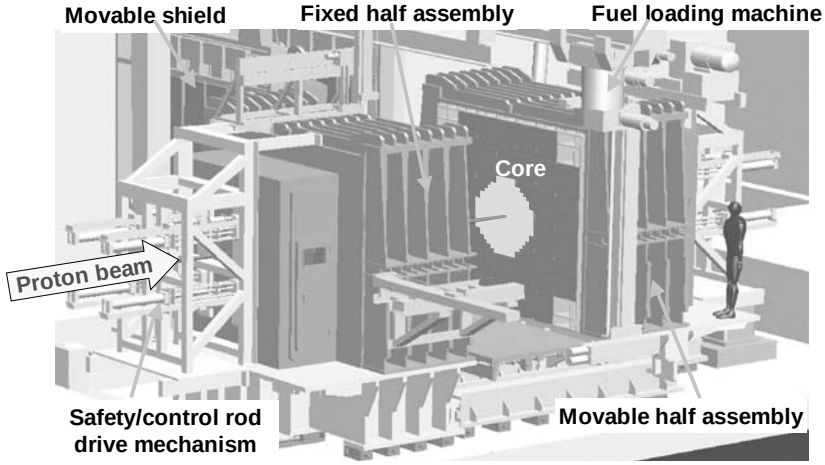

In the experiment with the proton beam, the effective multiplication factor k_{eff} of the critical assembly will be kept less than 0.98. One proton with 600 MeV produces ~15 neutrons via a spallation reaction with a heavy metal target such as lead. The 10 W proton beam corresponds to the source strength of 1.5×10^{12} neutrons/s, which is strong enough to measure power distribution even at a deep subcritical state such as $k_{eff} = 0.90$. A demonstrative test of the laser charge exchange technique is under way using an H^- ion source at JAERI/Tokai.

Safety aspects of the facility are being studied extensively because the TEF-P should be licensed as a nuclear reactor. As for a prompt critical accident, the power excursion can be terminated without fuel melting by the reactor scram system, which has multiplicity and diversity. Unexpected introduction of a 10 W beam into the critical state can also be terminated safely with reactor scram.

Figure 4. Concept of the beam transport system for TEF

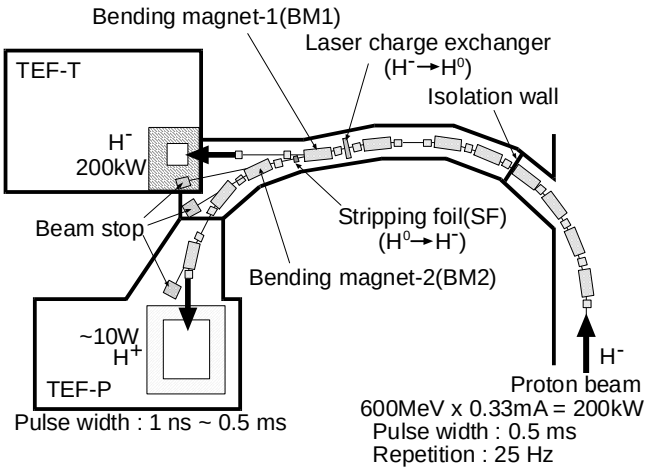

Experiments using TEF-P

Many experimental studies are planned using the TEF-P facility. The R&D to be performed is listed by item in Table 1.

Table 1. R&D items to be performed at TEF-P

Purpose	Experimental item
Validation of data and method to predict the neutronics in a fast subcritical system with a spallation source	Measurement of power distribution in subcritical system
	Determination of k_{eff} and effective source strength
	Evaluation of influence of high-energy particles
	Evaluation of influence of target, beam window, void in beam duct
Demonstration of controllability of a hybrid system driven by an accelerator	Feedback control of reactor power by beam intensity adjustment
	Investigation of system behaviour at beam trip and restart
	Determination of energy gain factor
Transmutation performance of MA and LLFP	Measurement of MA transmutation rate
	Measurement of MA and LLFP sample reactivity worth
	Study of moderated region for LLFP transmutation
	Simulation of MA-loaded nitride core
	Measurement of cross-section data by TOF technique

As for the neutronics in the subcritical system, power distribution, k_{eff}, effective neutron source strength and neutron spectrum are measured by parametrically changing the subcriticality and the spallation source position. The material of the target will be altered with Pb, Pb-Bi, W and so on. The reactivity worth is also measured for the case of the coolant void and the intrusion of the coolant into the beam duct. It is desirable to make the core critical in order to ensure the quality of experimental data of the subcriticality and reactivity worth.

As for the demonstration of the hybrid system, feedback control of the reactor power is examined by adjusting the beam intensity. Operating procedures at beam trip and restart are also examined.

Regarding the transmutation characteristics of MA and LLFP, fission chambers and activation foils are used to measure the transmutation rates. The cross-section data of MA and LLFP for the high-energy region (up to several hundreds of MeV) can be measured by the time-of-flight (TOF) technique with a short-pulsed proton beam. By coupling the 1 ns, 10 W proton beam and 5 m of flight path, the neutron flux of 4.7×10^5 n/cm^2/s can be obtained for TOF measurement with a good energy resolution (e.g. less than 1% at 1 MeV). Such cross-section measurements can be performed not only at the reactor room but also at the proton beam room and the experimental room (shown in Figure 5). Several kinds of MA and LLFP samples are also prepared to measure their reactivity worth, which is important for the integral validation of cross-section data.

Figure 5. Arrangement plan inside TEF-P

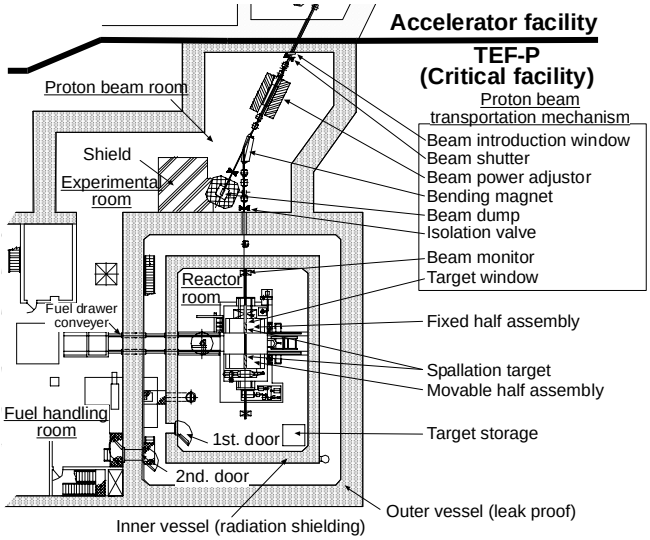

The ultimate target of the facility is to install a partial mock-up region of MA nitride fuel with air cooling to measure the physics parameters of the transmutation system. Figure 6 shows a schematic view of the partial loading of pin-type MA fuel around the spallation target. The central rectangular region ($28\ \text{cm} \times 28\ \text{cm}$) will be replaced with a hexagonal subassembly. Table 2 shows the heat generation and radioactivity in the central simulation zone with various fuel compositions. The first case in the table, MOX FBR, can be simulated by the existing critical assembly using an air blower to cool the decay heat and a simple radiological shielding for fuel loading by hand. It can be seen from Table 2 that if curium is not contained, decay heat and radioactivity can be managed by strengthening the capability of air blowers and by installing appropriate remote handling devices even for simulating the ADS with (MA + Pu + Zr) mono-nitride fuel. However, in the case with curium, decay heat and neutron emission seem too high to make the experiments.

Figure 6. Illustration of experimental configuration for partial mock-up using pin-fuelled zone

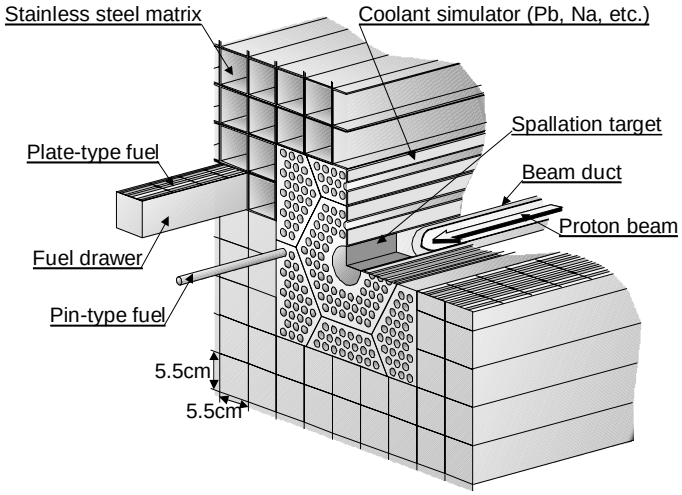

Table 2. Various fuel compositions and their heat and radioactivity

Fuel type to simulate	Actinide composition	Simulation zone: 28 cm × 28 cm × 60 cm		
		Decay heat (W)	γ-ray (γ/s)	Neutrons (n/s)
MOX FBR[a)]	Recovered from UO_2-LWR[d)]	7.1×10^2	3.1×10^{13}	7.5×10^6
MOX FBR with 5% MA[b)]	Recovered from UO_2-LWR[d),f)]	1.1×10^3	3.2×10^{14}	7.1×10^6
	Recovered from MOX-LWR[e),g)]	1.5×10^3	5.3×10^{14}	9.5×10^6
ADS with (MA + Pu + Zr) mono-nitride[c)]	Recovered from UO_2-LWR[d),f)]	1.6×10^3	8.3×10^{14}	3.4×10^6
	Recovered from MOX-LWR[e),g)]	2.6×10^3	1.5×10^{15}	4.5×10^6
	Recovered from MOX-LWR (with Cm)[e),h)]	1.3×10^4	1.3×10^{15}	1.5×10^{10}

a) Pu:U = 17:83, fuel volume ratio = 50.6%
b) MA:Pu:U = 5:16:79, fuel volume ratio = 50.6%
c) MA:Pu:Zr = 23:12:65, fuel volume ratio = 22.9%
d) Pu = 65% fissile
e) Pu = 55% fissile
f) ^{237}Np:^{241}Am:^{243}Am = 50:36:14
g) ^{237}Np:^{241}Am:^{243}Am = 5:63:32
h) ^{237}Np:^{241}Am:^{243}Am:$^{(244+245)}Cm$ = 4:53:28:14

The points that distinguish TEP-P from existing experimental facilities can be summarised as follows: 1) both high-energy proton beam and nuclear fuel are available, 2) the maximum neutron source intensity of ~10^{12} n/s is strong enough to perform precise measurements even in a deep subcritical state (e.g. k_{eff} = 0.90) and is low enough to easily access the assembly after irradiation, 3) a wide range of pulse width (1 ns - 0.5 ms) can be available by the laser charge exchange technique and 4) MA and LLFP can be used as a shape of foil, sample and fuel by installing an appropriate shielding and a remote handling device.

Background and purpose of TEF-T

The beam window of ADS plays an important role as a boundary between the accelerator and the subcritical core. However, it is situated under severe circumstances – heavy irradiation by both proton beam and neutrons, thermal stress by proton beam transients (i.e. startup, shutdown and beam trip),

mechanical stress from the pressure difference between the counter flow of the liquid metal target and the vacuum in the beam duct, and corrosion/erosion by Pb-Bi. Thus, feasibility of the beam window should be demonstrated as a top priority in ADS development. Some technical issues are also to be investigated for the high-power spallation target system (e.g. the purification system for spallation products and the polonium, the remote handling device for the Pb-Bi system, etc.).

From the above viewpoints, the demonstrative program called MEGAPIE [8] is under way at PSI, Switzerland, where a Pb-Bi spallation target will be operated using a 590 MeV, 1 MW proton beam for several months during 2006. Since this project uses existing accelerators, the duration of the experiment is restricted. Our proposed facility, TEF-T, aims at R&D on spallation target technologies as a proton-neutron irradiation facility dedicated to ADS.

Specification of TEF-T

TEF-T is the material irradiation facility with a 600 MeV, 200 kW proton beam and a Pb-Bi liquid eutectic target. To demonstrate the feasibility of the beam window, the proton beam density at the beam window should coincide with that of the future ADS plant. In the design of an ADS plant, a 30 MW proton beam of 1.5 GeV (20 mA) is assumed to be available, where the diameter of the beam is defocused to ~45 cm. The proton beam density at beam window becomes ~13 $\mu A/cm^2$ on average and the maximum density will be restricted to ~30 $\mu A/cm^2$. At TEF-T, the proton beam of 0.33 mA is focused to 40 mm in diameter, which results in the beam density of ~26 $\mu A/cm^2$ on average; this beam density is considered to be high enough for the demonstration.

The Pb-Bi eutectic is filled into a cylindrical vessel made by stainless steel. The size of the vessel is approximately 150 mm in diameter and 600 mm in length. The neutronics properties of the Pb-Bi target in TEF-T were calculated by the ATRAS code system [9]. The axial distribution of the neutron flux is shown in Figure 7. The neutron flux exceeds 10^{14} $n/cm^2/s$ at the centre of the target and 10^{13} $n/cm^2/s$ at the region of 300 mm in diameter and 300 mm in length, where various materials can be irradiated by fast neutrons.

Figure 7. Neutron flux distribution at the Pb-Bi target of TEF-T

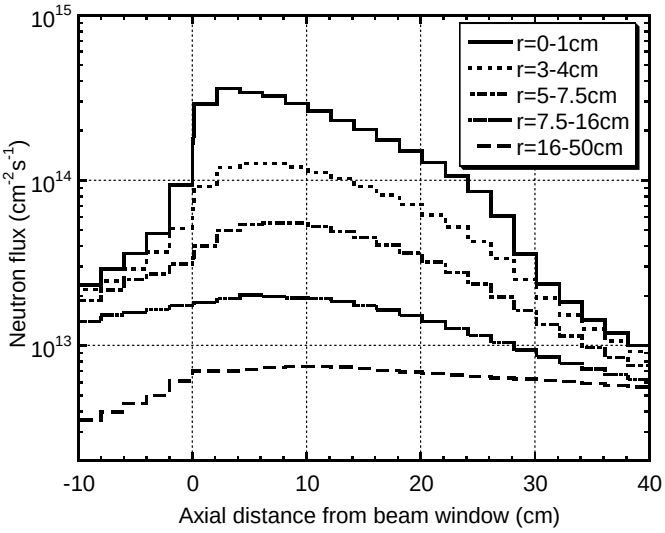

The maximum temperature and flow rate of the Pb-Bi target are designed as 450°C and 2 m/s, respectively. Other structural materials such as F82H steel will also be tested as the target vessel. The compatibility of the stainless steel (316SS) with flowing Pb-Bi eutectic is currently being tested by an experimental loop at JAERI/Tokai.

As for the target module, the "double-annular type" Pb-Bi target shown in Figure 8 is under consideration [10]. By this configuration, the electromagnetic (EM) pump and EM flowmeter can be separated from the Pb-Bi loop, and hence the target module can be easily withdrawn for the upper direction in the case of exchange. About 70% of the kinetic energy of the proton beam (140 keV) will be deposited in the target and this heat will be cooled by helium gas of the secondary loop.

Figure 8. Concept of double-annular type Pb-Bi target for TEF-T

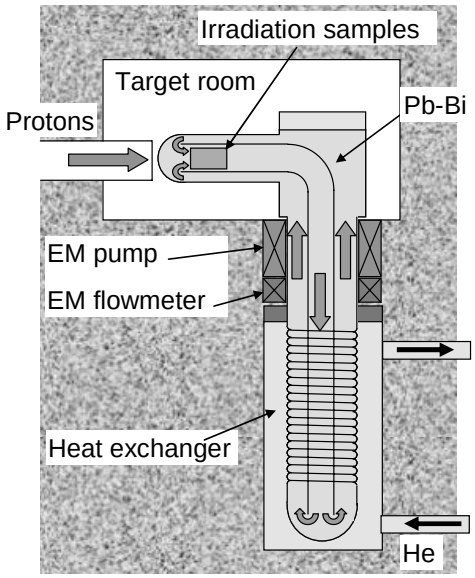

Experiments using TEF-T

The principal purpose of TEF-T is to demonstrate the feasibility of a high-power spallation target system and to research the material compatibility in the Pb-Bi with irradiated circumstances. The R&D program to be performed at TEF-T is summarised in Table 3.

Two kinds of target vessels are being considered – one is a "demonstration-type" and the other is an "irradiation-type" as shown in Figure 9. The demonstration-type vessel simulates the shape of the ADS beam window, where the Pb-Bi heated by the proton beam flows toward the beam window. On the other hand, the irradiation-type vessel is designed to optimise irradiation conditions for samples. The direction of the Pb-Bi flow will be opposite compared to the demonstration-type vessel.

The irradiated structural materials of the target vessel as well as the irradiated samples will be examined from the viewpoint of the following: tensile strength, ductility, fatigue, fracture toughness, DBTT (ductile-brittle transition temperature), etc. In addition to these tests, the effects of corrosion and erosion by Pb-Bi and the spallation products will be studied precisely by changing parameters such as temperature, irradiation period, flow speed and oxygen concentration in Pb-Bi. Plenty of experiences for operation and handling of a high-power spallation target can be accumulated at TEF-T.

Table 3. R&D items to be performed at TEF-T

Purpose	Experimental item
Serviceable lifetime of beam window and structural material under proton and neutron bombardment	Evaluation of soundness and lifetime of beam window
	Duplicated irradiation damage by protons and neutrons
	Establishment of material database for fast neutron irradiation
	Irradiation effect under stressed conditions
Compatibility of material with flowing liquid metal under high-power proton irradiation	Liquid metal corrosion and liquid metal embrittlement under proton and neutron irradiations
	Compatibility of materials with liquid metal as a function of temperature, velocity and oxygen concentration of the liquid metal
	Influence of spallation products
Operation and control of liquid metal spallation target system	Demonstration of performance of pump, flowmeter, heat exchanger and oxygen controller under actual liquid metal spallation target
	Transient behaviour of system at beam trip and restart
	Containment of spallation products and polonium
	Technical issues on system operation and maintenance

Figure 9. Two kinds of Pb-Bi target for TEF-T

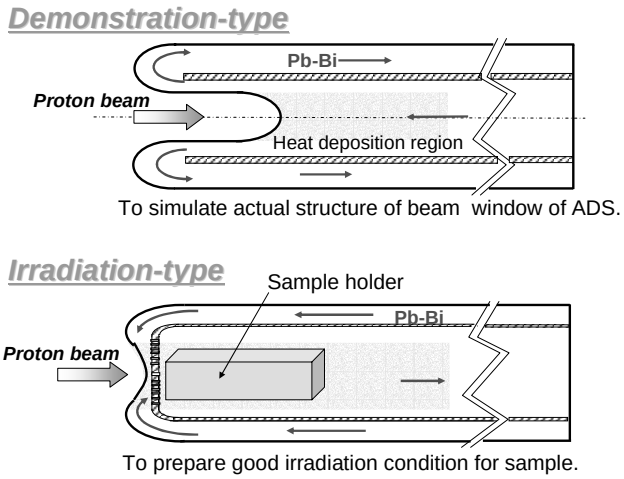

Conclusion

To perform R&D of an accelerator-driven transmutation system, the Transmutation Experimental Facility (TEF) was proposed under the J-PARC project. The TEF consists of two facilities – TEF-P and TEF-T. Outlines of the conceptual designs of both facilities were presented in this paper.

TEF-P is a critical assembly that can accept a low current 600 MeV proton beam for the spallation neutron source. The purpose of TEF-P includes experimental validation of the data and method to predict neutronics of the fast subcritical system with a spallation neutron source, demonstration of the controllability of a hybrid system driven by an accelerator, and basic research of reactor physics for transmutation of MA and LLFP. A horizontal table-split type assembly is proposed. The laser charge exchange technique will be used to introduce a 10 W proton beam into the facility.

TEF-T is the material irradiation facility using a 600 MeV, 200 kW proton beam and a Pb-Bi spallation target. The purpose of TEF-T includes R&D for the irradiation damage of the beam window, compatibility of the structural material with flowing liquid metal target and operation of the high-power spallation target. An outline of the target concept was presented.

Combining the experimental results and experiences obtained at both facilities, the feasibility of ADS can be evaluated and demonstrated.

REFERENCES

[1] Takano, H., *et al*., "Transmutation of Long-lived Radioactive Waste Based on Double-strata Concept", *Progress in Nuclear Energy*, 37, 371 (2000).

[2] Mukaiyama, T., *et al*., "Review of Research and Development of Accelerator-driven System in Japan for Transmutation of Long-lived Nuclides", *Progress in Nuclear Energy*, 38, 107 (2001).

[3] Tsujimoto, K., *et al*., "Neutronics Design for Lead-bismuth Cooled Accelerator-driven System for Transmutation of Minor Actinide", *J. Nucl. Sci. Technol*., 41, 21 (2004).

[4] The Joint Project Team of JAERI and KEK, "The Joint Project for High-intensity Proton Accelerators", JAERI-Tech 99-056 (KEK Report 99-4, JHF-99-3) (1999).

[5] González-Romero, E., *et al*., "The MUSE4 Pulsed Neutron Source Experiments", CD-ROM of PHYSOR 2004 – *The Physics of Fuel Cycles and Advanced Nuclear Systems: Global Developments*, Chicago, IL, 25-29 April 2004 (2004).

[6] Yamane, T., S. Okajima, "Subcritical Experiments in Uranium-fueled Core with Central Test Zone of Tungsten", CD-ROM of PHYSOR 2004 – *The Physics of Fuel Cycles and Advanced Nuclear Systems: Global Developments*, Chicago, IL, 25-29 April 2004 (2004).

[7] Misawa, T., *et al*., "Research on Accelerator Driven Subcritical System at Kyoto University Critical Assembly (KUCA) with the FFAG Proton Accelerator", to be presented in HPPA4 (2004).

[8] Bauer, G.S., *et al*., "MEGAPIE, A 1 MW Pilot Experiment for a Liquid Metal Spallation Target", *Proceedings of the 15th Meeting of the International Collaboration on Advanced Neutron Sources*, ICANS-XV, Tsukuba, Japan, 6-9 November 2000, JAERI-Conf 2001-002 (KEK Proceedings 2000-22), Vol. II, p. 1 146 (2001).

[9] Sasa, T., *et al*., "Accelerator-driven Transmutation Reactor Analysis Code System – ATRAS", JAERI-Data/Code 99-007 (1999).

[10] Kikuchi, K., *et al*., Private communication (2003).

EXPERIMENTAL VERIFICATION OF SELECTED TRANSMUTATION TECHNOLOGY AND MATERIALS FOR BASIC COMPONENTS OF A DEMONSTRATION TRANSMUTER WITH LIQUID FUEL BASED ON MOLTEN FLUORIDES (DEVELOPMENT OF NEW TECHNOLOGIES FOR NUCLEAR INCINERATION OF PWR SPENT FUEL IN THE CZECH REPUBLIC)

Miloslav Hron, Miroslav Mikisek, Ivo Peka
Nuclear Research Institute Rez plc, CZ 250 68 Rez, Czech Republic

Pavel Hosnedl
SKODA Nuclear Machinery plc, Orlik 266, CZ 316 06 Plzeň, Czech Republic

Abstract

Development of the project SPHINX (spent hot fuel incinerator by neutron flux) is based on the utilisation of a subcritical nuclear reactor system with liquid fuel based on molten fluorides. Existing experimental facilities have been used for experimental testing of the system, individual technological components and newly developed materials that should be resistant in the environment of molten fluorides at operational temperatures. Examples of facilities include the experimental reactors LR-0 and VR-1 with inserted zones for the investigation of neutronic characteristics of transmuter blanket cores, research reactor LVR-15 with instrumented probes for transmuter blanket sample testing in high neutron flux conditions, and experimental loops with molten fluoride salts for an investigation of transmuter system operational conditions. This paper describes some of the experiments performed and results obtained thus far.

Introduction

During the last decade, there have been new tendencies of significant decreasing of amount and potential danger of nuclear waste getting up in the world of nuclear power. The development of a convenient technology to resolve this issue has involved the rehabilitation of nuclear transmutation technologies, which have been well known since the beginning of the first nuclear era. However, at that time such technology was evaluated as unacceptably demanding from technological and economical perspectives. An attempt at the end of the first nuclear era to develop modifications of this technology under different conditions was supposed to be promising and acceptable for the efficient closing of the nuclear fuel cycle. The newly modified transmutation technologies should make it possible to return a fuel component, which is contained in nuclear fuel and burned up in conventional nuclear reactors, back to the nuclear fuel cycle and to turn a significant part of long-lived nuclear waste (heavy metals from the transuranium region) into useful energy without rests and in an irreversible way. Besides other positive features, this could be a way to exclude or at least minimise the undesirable misuse of such nuclear materials.

A series of national projects were started at the end of the 1980s and at the beginning of the 1990s. Of these projects, at least two should be mentioned – the Japanese OMEGA project and LANL's (USA) ADTT project. In the middle of the 1990s [1] in the Czech Republic, a similar project was begun following the tendencies established by Charles Bowman of LANL. The project, which was later on called SPHINX (spent hot fuel incinerator by neutron flux), has focused on the development of a burner for spent fuel from PWRs that have been operated in this and certain other central European countries. The principle feature of the adopted transmuter concept has been, since the very beginning of the project, the concept of liquid fuel based on molten fluorides. The proposal and organisation of the project was based on the activity of the national consortium, Transmutation, established in November 1996 by four leading institutions in nuclear research: Nuclear Research Institute Rez plc, the Nuclear Physics Institute of Academy of Sciences, SKODA Nuclear Machinery plc and the Faculty of Nuclear Sciences and Physical Engineering of the Czech Technical University in Prague [with whom the Technical University in Brno (specialised in secondary circuit problems) became associated in 2000].

The first stage of the project (mainly R&D) was proposed in 1997 and once approved, started under the acronym LA-0 in 1998. The focus was concentrated on broad computing analysis of the proposed system and elaboration of complex input for designing an experimental transmutation system on a zero power level. After successfully completing the first stage in 2000, the second stage was approved for the period of 2000 to 2003, which focused on experimental verification of selected transmutation technology for design development of basic components of the LA-10 demonstration transmuter at a 10 MW power level. This activity is based on the utilisation of existing experimental facilities as well as long-term experience and know-how, which include the following:

- Neutron source facility NG1 on external beam line of the isochronous cyclotron U-120M of the Nuclear Physics Institute (NPI) of the Czech Academy of Sciences in Rez (variable energy up to 35 and 17 MeV of protons and deuterons, respectively), which is based on the d (17 MeV) + Be (thick target) reaction.

- Experimental reactors LR-0 and VR-1 with inserted zones for the investigation of neutronic characteristics of transmuter blanket cores.

- Research reactor LVR-15 with instrumented probes for transmuter blanket sample testing in high neutron flux conditions.

- Experimental loops with molten fluoride salts for an investigation of transmuter system operational conditions.

- Know-how in the field of fluorine technology gained in the frame of long-term R&D activity on spent fuel reprocessing by dry method.

The governmental authorities of the Czech Republic as well as the future utilities of the developed technology have been providing the necessary funding. The utilities include: Radwaste Repository Authority, CEZ a.s. (Czech Electricity Generating Co.), SKODA Works Company Nuclear Machinery Branch plc and some other entities. A substantial part of the project has been incorporated in suitable forms of international collaboration such as the European Union's Framework Programmes, which are considered to be the most convenient. Individual parts of the project have been incorporated into corresponding tasks of the MOST (molten salt technology) project of the EU's Fifth Framework Programme. This collaboration began in November 2001 and lasted for three years. The convenient incorporation of the whole complex into the preliminarily proposed projects of the Sixth Framework Programme for a period of four years (2004-2008) as well as into other forms of multinational co-operation is desirable.

Principle features of the SPHINX project

The principle scheme of the SPHINX project is introduced in Figure 1. One of the main features of the project is the front end of its fuel cycle – the dry technology of reprocessing spent fuel from commercial reactors based on a fluoride volatility process is employed. This simultaneously represents the process of preparation of the transmuter fuel (in the form of molten fluorides) for the transmuter fuel cycle, supposing a continuous circulation of liquid fuel and at least quasi-continuous cleaning up during the transmuter operation. We should underline that the majority (~95%) of the inventory of spent fuel from the uranium-plutonium fuel cycle of conventional power reactors (nearly all uranium inventory as well as the majority of short-lived fission products) is supposed to be taken out for the remainder of the transmuter fuel cycle whereas all transuranium as well as long-lived fission products should remain in the mentioned forms of fluoride.

The second main feature of the SPHINX project is the developed concept of the transmuter and its blanket (Figure 2).

Figure 1. The principle scheme of the SPHINX project

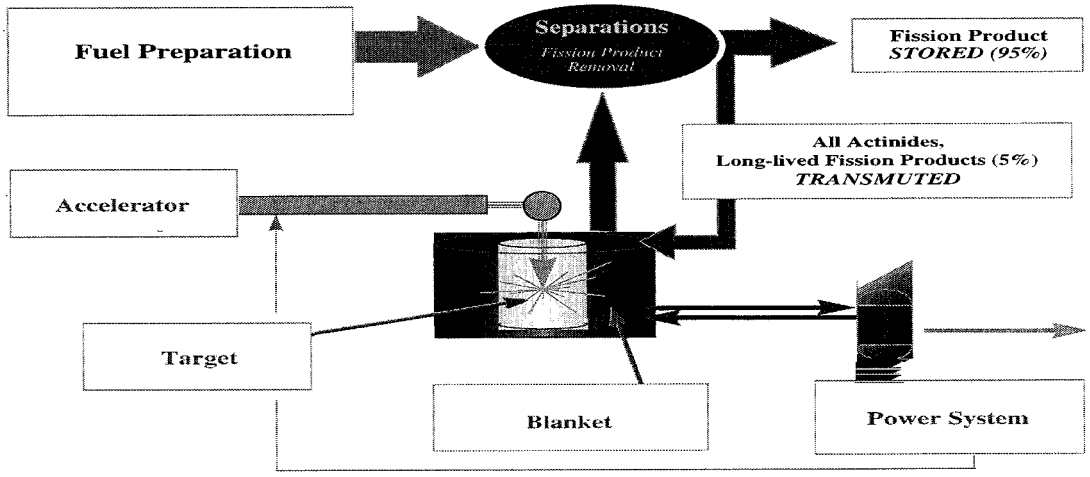

Figure 2. The schema of a transmuter elementary module with two primary circuits of molten fluorides

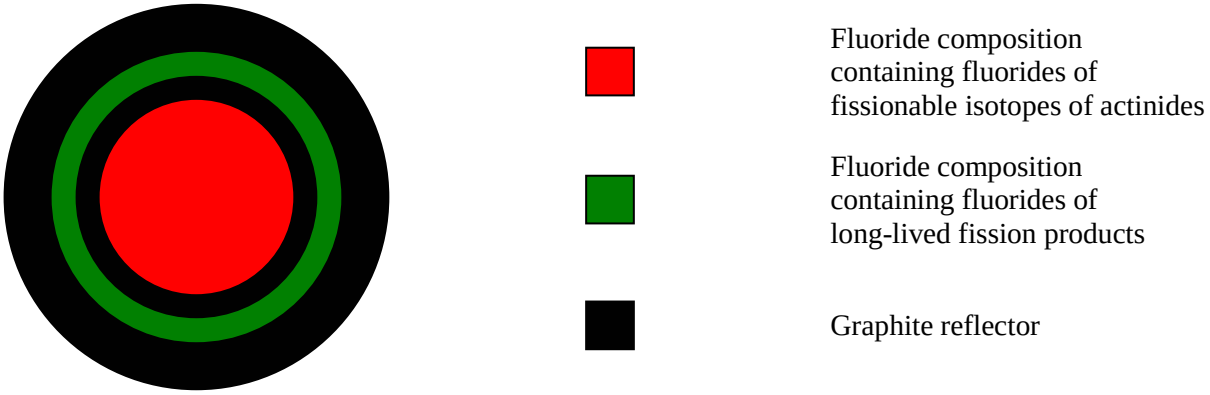

This concept is based on the idea of utilisation of efficient burning of transuranium nuclei in a large size fuel channel in the epithermal energy range where the majority of isotopes have resonances in their neutron cross-sections. It might be a critical system with reactivity and power controlled by specific flowing liquid fuel control systems (based on control of liquid fuel composition or its flow characteristics) or a subcritical system (with the subcriticality margin on the order of several betas) whose reactivity (keeping the prescribed level of subcriticality) is controlled in the same manner as in the above-described case of a critical system. Furthermore, the system is kept in a steady state and its power is controlled (driven) by an external neutron source or by a driving zone (part of a conventional reactor core).

The elementary module can be designed as a subcritical hexagonal fuel channel surrounded by six hexagonal graphite blocks, equipped with coaxial tubes (where molten fluorides of long-lived radionuclides may flow) that allow for efficient transmutation of long-lived radionuclides by an intensive flux of well-thermalised neutrons. These elementary modules represent an intensive source of energy and epithermal neutron flux that might be slowed down in graphite blocks and allow for very efficient incineration of at least some of the long-lived fission products in well-thermalised neutrons escaping the transmuter core. It should be noted that these elementary modules can be closely packed (joint) into a critical system or arranged in a complex of autonomous subcritical elementary modules that are driven by a set of external neutron sources or by a driving zone (a reactor core of another type surrounding the subcritical assembly of the molten fluoride elementary modules).

The two purposes of the proposed blanket system utilisation make usage possible as an efficient nuclear incinerator, actinide burner and, simultaneously, efficient energy source. Let us note that once such a system is developed and proven, it might serve as a new clean source of energy just by switching over from a uranium-plutonium fuel cycle to a thorium-uranium fuel cycle and thus excluding the generation of actinides. The main features of the SPHINX concept and the proof of individual processes as well as the corresponding technological and operational units of the nuclear “jeep” should be verified by the operation of a demonstration complex with power output on the order of 10 MWt. The concept of an experimental assembly of that type is introduced in Figure 3. Before we are able to design such a device, we must perform a broad experimental verification of design inputs for credible designing of a demonstration transmuter. The process of experimental verification recently (2002) began in the scope of the LA-10 project on the basis of preliminary preparation of an ideology of the experimental programme that was formulated earlier (in the scope of the LA-0 project in 1999 and 2000); some of its principle features were proven during this period. The experimental programmes and projects that have so far been developed/started will be described in the text that follows.

Figure 3. Subcritical dual-purpose experimental transmuter concept

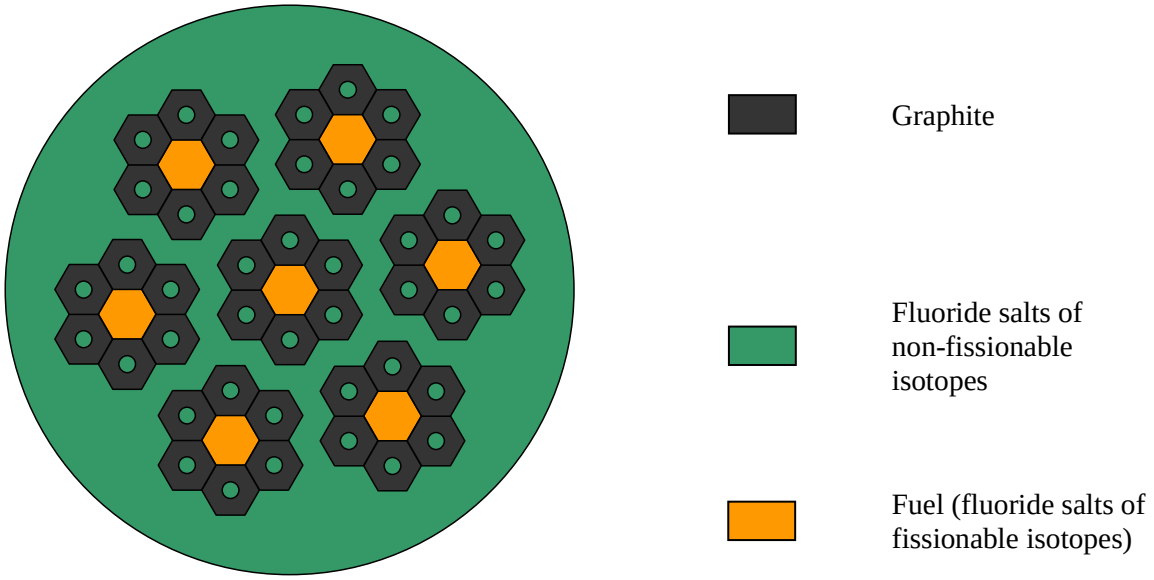

Main experimental programmes started in the scope of the SPHINX project

The two specific features of the SPHINX project mentioned above, namely the chemical technology of the front end of the fuel cycle process and the neutronics (both static and kinetic) of the multi-purpose blanket with flowing liquid fuel, represent sufficiently new concepts to be calculated by modified computer codes that should be experimentally verified. Regarding the fluoride volatility process, we use as a base the knowledge gained from experience accumulated during the 1980s when we worked in close collaboration with the Russian Kurchatov Institute (RKI) in Moscow. During this time, such technology was developed and a pilot line was built and prepared for testing by processing hot spent fuel from the BOR60 fast reactor in the Atomic Reactor Research Institute (ARRI) in Dimitrovgrad. During the 1990s, this line was innovated and installed at NRI Rez and the first stage of testing for the SPHINX project was begun.

The new blanket concept was developed and proven by broad computer analyses in the second half of the 1990s. In the same time period, experimental programmes for verification of main neutronic characteristics including time behaviour were proposed. For this purpose, there are several large experimental devices operated in the scope of the Transmutation consortium. First of all, the experimental reactor LR-0 at NRI Rez and VR-1 at FNSPE are at our disposal as well as the NPI cyclotron accelerator that was equipped with a new target serving as an intensive neutron source. The VR-1 experimental reactor was equipped with the oscillator for the purpose of SPHINX-type blanket testing (namely, time behaviour and important safety characteristics). The first stage of experimental verification of some basic neutronic characteristics, reactor equipment and materials technology, and measurement techniques has already begun and involves experiments with inserted zones containing materials typical of our blanket concept and simulating neutronic features in a simplified model.

Technology of the new non-traditional materials in the SPHINX blanket is the subject of a broad R&D programme including experimental testing. For this purpose, a series of technological loops was erected by SKODA Nuclear Machinery plc, starting with laboratory equipment and continuing in a semi-pilot scale. The same is valid for the development of a technology for continuous cleaning up of circulating liquid fuel in the transmuter internal fuel cycle based on electro separation methods.

In 2000, the Technical University in Brno (TUB) was associated into the Transmutation consortium for the studying and testing of secondary cooling circuits of the LA-10 transmuter. The first step in an experimental programme in that field, the measuring bench, was erected and will serve for both measurement of basic technological characteristics of fluoride compositions and verification of design input for an auxiliary circuit of a molten fluoride media pantry in large loop testing complexes, which are being developed jointly by SKODA NM and Energovyzkum (EVM) Ltd. (a daughter company of TUB), as well as for the LA-10 demonstration transmuter.

The most important experimental program was started in 2001 and was based on experimental irradiation of blanket samples in the high neutron flux of research reactors. This programme is being carried out in close contracted collaboration with the RKI project AMPOULE and involves the development and validation of a modified reactor computer code based on a stochastic Monte Carlo model of neutron field long-term time behaviour in a system with circulating liquid fuel based on molten fluorides. The experimental irradiations are simultaneously performed at NRI and RKI in the first stage. The second stage representing irradiation of samples containing fluorides of actinides (Np, Pu, Am and Cm) was agreed to be performed and finalised jointly at RKI in 2002/2003. Some of the results of the preparatory (first) stage of this programme, which have already been obtained in NRI Rez in the scope of the BLANKA project, will be briefly introduced in the following section. We note that the proposal to start broad experimental verification of design inputs for a demonstration transmuter of the mentioned type was already put forth at the Fourth International ADTT&A'01 Conference in Reno, Nevada at the end of 2001 [3]. All of these experimental programmes were also (just recently) proposed to the Sixth Framework Programme of the European Commission.

The programme of irradiated probes and BLANKA instrumented rigs

The very first idea for this programme was initiated by RKI as early as the late 1980s when some very preparatory irradiations and measurements were performed in the Tashkent research reactor. On the basis of the obtained experience, the project AMPOULE was developed at RKI in the 1990s. After a period of pre-contract negotiations in the second half of the 1990s, the bilateral contract was finally agreed upon and signed in July 2001. Immediately thereafter the first stage of the joint development of the modified reactor computer code ISTAR (based on a stochastic Monte Carlo model of neutron field long-term time behaviour in a system with circulating liquid fuel based on molten fluorides) started in autumn 2001. At the same time, preliminary irradiations, measurements and evaluations were performed on the LVR-15 research reactor at NRI with the aim to be able to design and perform the regular programme of irradiated BLANKA probes, serving as validation of the developed computer code.

During the same time frame, an elementary metallic probe and a complex of irradiated probes were performed, which lead to the realisation of BLANKA instrumented rigs. The first series, BLANKA 100 (identical in size to one fuel assembly of both the VR-1 experimental and LVR-15 research reactor), was designed and tested at NRI during 2001. Preliminary tests of the rig neutronic characteristics started in December 2001 on the experimental reactor VR-1 at the Czech Technical University in Prague. Then, a series of first irradiations were performed on the NRI research reactor LVR-15 in January and February 2002. The series of irradiation tests called BLANKA 101 were curried out with empty probes (no fluoride content), serving just for the tuning of all measuring channels and verification of design-predicted characteristics (temperature and pressure fields in particular).

After an evaluation of the obtained results, the first experiments were performed in April 2002 using probes containing pure NaF and/or NaF with an admixture of metallic Mo powder, modelling the presence of fission product. The probe, BLANKA 102, was inserted in the core of the research reactor at its very edge with a low value of neutron flux where heating of the probe is generated nearly

by gamma capture only. The temperature field was measured by a set of five independent thermocouples located in different positions in the elementary probe room. Figure 4 shows the results of a continuous measurement of gas pressures in individual layers of the BLANKA 102 probe during irradiation. The decrease of the pressure of the noble gas (Ar) filling the elementary probe at 11:30 on April 17 is caused by the testing of a controlled discharge of expected gaseous fission products in the case of the fluoride composition containing components of fluorides of fissionable metals.

Figure 4. Results of measurements of gas pressures in individual layers of BLANKA 102 probe

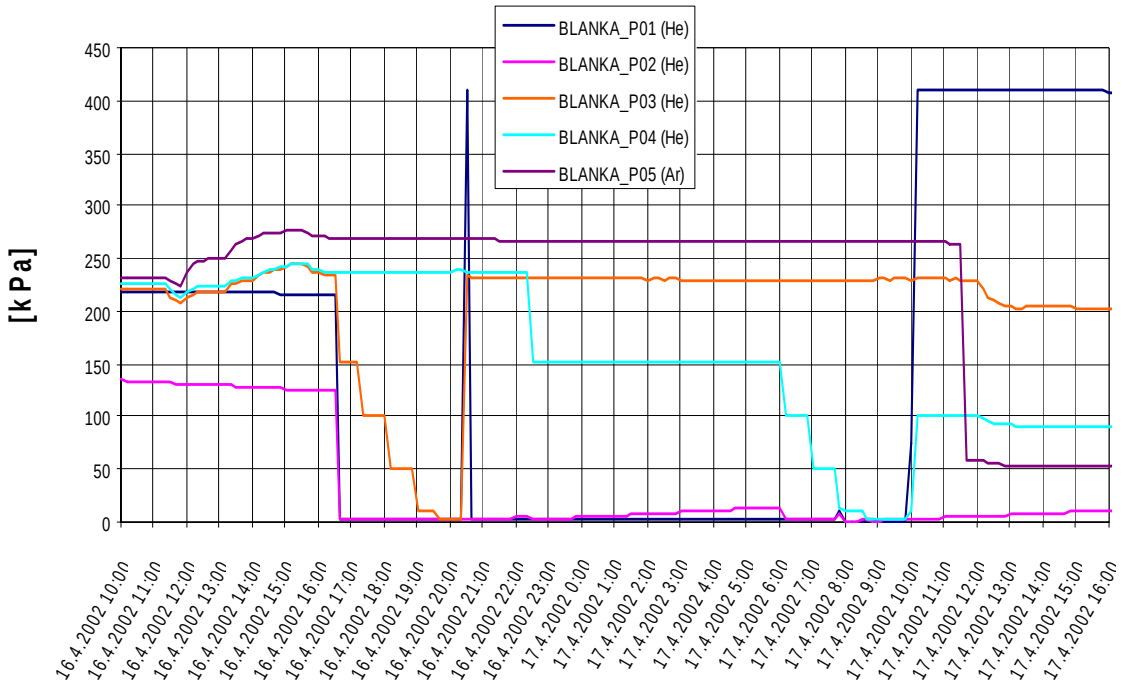

After evaluation of BLANKA 101 and 102 test results, some convenient small rearrangements were applied in the prepared new version of the BLANKA 103 probe, which were used in the experimental programme performed during the first half of 2003. The majority of the irradiated samples were based on a composition of ^{7}LiF + NaF. The admixture of modelling fission products and finally even an admixture of a small amount of UF_4 were incorporated into the individual sample compositions. An exact description of the BLANKA 103 sample content can be seen in Figure 5.

Figure 5. Contents of the BLANKA 103 sample pots

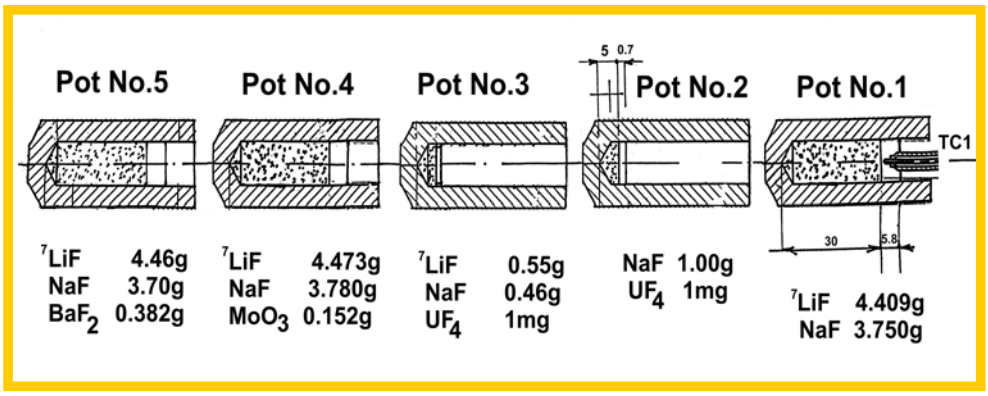

Figure 6. The simplified model of the BLANKA 400 rig for neutronic tests at room temperature

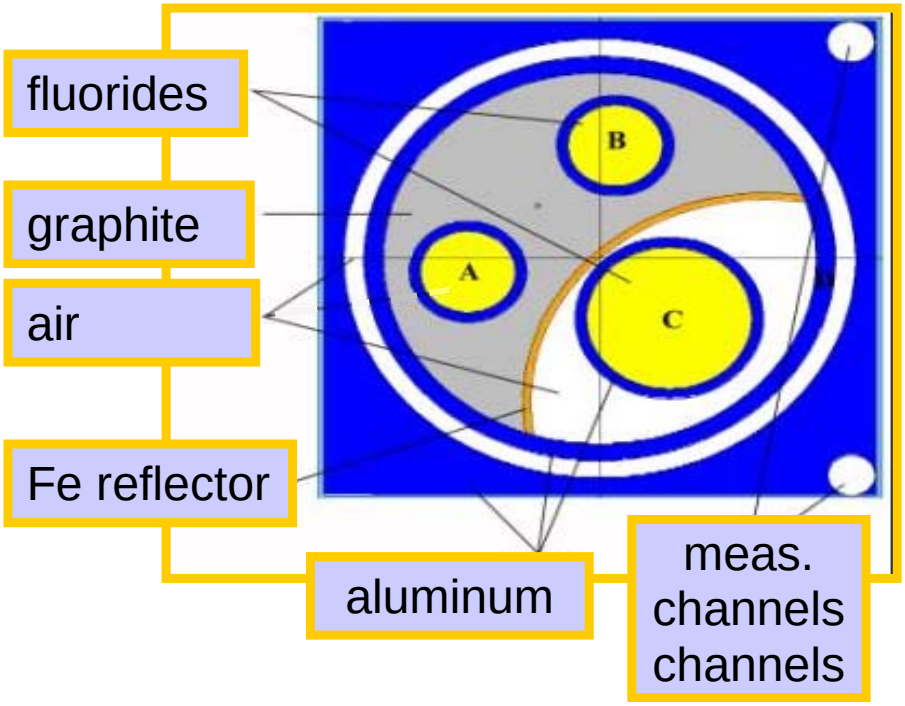

Following the experience accumulated during the BLANKA 100 instrumented rigs, the larger size series (identical to the area of four fuel assemblies) called BLANKA 400 was designed and preliminary tests started on the VR-1 experimental reactor at the end of 2003 under room temperature and low level of neutron flux conditions. For these neutronic tests, the simplified version manufactured from nuclear aluminium structural material (see Figure 6) was used. Once again, the first series of experiments was performed with pure NaF in tubes A, B and C, starting at the beginning of 2004 and due to finish by 31 May 2004. The same model was to serve for an adjustment of the testing facility with the external neutron source NG1 on external beam line of the isochronous cyclotron U-120M at NPI during the second half of 2004. During this time, neutronic experiments with BLANKA 400 filled in by LiF + NaF compositions in various ratios were forecast to take place at the VR-1 experimental reactor.

Conclusions

Principle features of the SPHINX project involving the development of a transmuter with liquid fuel based on molten fluorides and a connected R&D programme were described in necessary detail. The experimental part of the R&D programme of the SPHINX project was briefly introduced, which serves as verification of design inputs for designing a demonstration unit of a transmuter with liquid fuel based on molten fluorides. Due to the current status of the experimental programme, performance was focused on the irradiation of samples of molten salt systems as well as structural materials proposed for the blanket of the SPHINX transmuter in the field of high neutron flux of research reactors (attention focused on the latter part). We should underline that the main aims of this programme (called BLANKA irradiated probes) are the following:

- Experimental verification of long-time behaviour of transmuter blanket, which contains molten fluoride salts as fuel and graphite as moderator or reflector.

- Material research on behaviour of materials in neutron and gamma fields, and material interactions in high temperature conditions.Validation of computational codes (system of codes NJOY – preparation of data library for MCNP; MCNP – computation of cross-sections for the code ISTAR being developed for the computation of actinide concentration in long-term operation of the transmuter).

Preliminary experiments have been performed by irradiation of simplified samples of fluorides of non-fissionable metals since mid-2001. The first experiment with the instrumented rig BLANKA 101, which served for the tuning of measuring methods and channels, started in December 2001. In this experiment, the probe without fluorides was inserted into the core of the LVR-15 research reactor in NRI Rez for a few days of irradiation on different levels of the reactor power (neutron flux). The second BLANKA 102 experiment was conducted in April 2002 when two samples were irradiated – one containing pure NaF and another containing NaF with an admixture of Mo metallic powder (modelling a fission product). Measurements and experience collected in this stage fully confirmed the principle correctness of design and operational properties of the programme of BLANKA instrumented rigs, serving as irradiation tests of transmuter blanket material samples under conditions close to operational.

After the evaluation of BLANKA 101 and 102 test results, some convenient small rearrangements were applied in the prepared new version of the probe BLANKA 103 and they were used in the experimental programme performed during the first half of 2003. Nearly all of the irradiated samples were based on a composition of ^{7}Li + NaF. The admixture of modelling fission products and finally even an admixture of a small amount of UF_4 were incorporated into individual sample compositions. There was also the insertion of structural material samples (also a subject of broad non-active and pre-irradiation technological testing), which were supposed to be irradiated and preliminarily tested in these irradiations. At the same time, the preliminary neutronic tests of the larger sized version (equal to the area of four quadratic fuel assemblies of VR-1 or LVR-15 reactor) of the BLANKA 400 rig started using a simplified aluminium model at room temperature inserted into the VR-1 experimental reactor and into the testing facility with the external neutron source NG1 on the external beam line of the isochronous cyclotron U-120M in NPI. We will be able to report later this year on results obtained in these experimental programmes.

Acknowledgements

The SPHINX project was proposed at the end of 1996 by the Transmutation consortium established by four leading nuclear research bodies in the Czech Republic (Nuclear Research Institute Rez plc, SKODA Nuclear Machinery plc in Pilsen, the Nuclear Physics Institute of Academy of Sciences in Rez and the Technical University in Prague) to whom Technical University in Brno (specialised in secondary circuit problems) associated in 2000. The project has been supported by the Ministry of Industry and Trade of the Czech Republic, CEZ a.s. (Czech Power Company) and RAWRA (Radwaste Repository Authority). At present, two agreements on multi-national co-operation in this field have been signed – one with the European Commission (project MOST) and one with the Russian Kurchatov Institute. The experimental programme of project SPHINX was proposed to the Sixth Framework Programme of the European Commission for the period 2004-2008.

The authors would like to acknowledge all the support the project has received so far and to express their hope that understanding will continue as progress is made towards the efficient resolution of crucial issues on nuclear power and as successful development takes place in this new era.

REFERENCES

[1] Hron, M., "A Preliminary Design Concept of the Experimental Assembly LA-0 for Accelerator-driven Transmuter Reactor/Blanket Core Neutronics and Connected Technology Testing", Report LA-UR 95-3761, Los Alamos National Laboratory, New Mexico, USA (1995).

[2] Hron, M., "National R&D Program of Nuclear Incineration of PWR Spent Fuel in a Transmuter with Liquid Fuel as Being Developed in the Czech Republic", ADTT&A'99, Prague-Pruhonice, Czech Republic, 7-11 June 1999.

[3] Hron, M., "Experimental Verification of Selected Transmutation Technology for a Design Development of Basic Components of the Demonstration Transmuter LA-10 (Development of New Technologies for Nuclear Incineration of PWR Spent Fuel in the Czech Republic)", Fourth International Conference ADTT&A'01, Reno, Nevada, November 2001.

[4] Hron, M., *et al*., "Project SPHINX – Spent Hot Fuel Incineration by Neutron Flux (Experimental Verification of Design Inputs for Transmuter with Liquid Fuel Based on Molten Fluorides)", 11th International Conference on Emerging Nuclear Energy Systems, Albuquerque, New Mexico, 29 September – 4 October 2002.

APPLICATION OF THE HYPER SYSTEM TO THE DUPIC FUEL CYCLE

Yonghee Kim, Tae-Yung Song
Korea Atomic Energy Research Institute
150 Duckjin-Dong, Yuseong, Daejeon 305-353, Korea

Abstract

This paper is concerned with the transmutation of TRUs in DUPIC (direct use of spent PWR fuel in CANDU) spent fuel in the HYPER system, which is an LBE-cooled ADS. The DUPIC concept is a synergistic combination of PWR and CANDU, in which PWR spent fuels are directly re-utilised in CANDU reactors after a very simple refabrication process. The objective of this study is to investigate the TRU transmutation potential of the HYPER core for the DUPIC-HYPER fuel cycle. All the previously developed HYPER core design concepts were retained except those which involve fuel composed of TRUs from DUPIC spent fuel. The HYPER core characteristics were analysed using the REBUS-3/DIF3D code system.

Introduction

A lead-bismuth eutectic (LBE) cooled 1 000 MWth ADS, which is called HYPER [1,2] (hybrid power extraction reactor), is being studied in Korea for the transmutation of TRUs and LLFPs. This paper is concerned with neutronic design characteristics of the HYPER core and its transmutation capability. Previously, the HYPER system was devoted to the transmutation of TRUs and LLFPs from PWR spent fuels, where the PWR spent fuel was reprocessed with simple pyro-processing and the recovered TRUs were incinerated in the HYPER core [2]. In this paper, a different transmutation fuel cycle is studied in order to ameliorate the spent fuel issue in Korea.

Korea is the only country that has both commercial PWRs and CANDUs in operation. Currently, there are 14 PWRs and four CANDUs in Korea. Currently, the CANDU reactor utilises natural uranium and, consequently, the fuel discharge burn-up is fairly low (~7 500 MWD/MTU), producing much more spent fuel compared to PWRs. In order to mitigate the CANDU spent fuel issue and to improve uranium utilisation, a tandem fuel cycle is being studied/developed in Korea. The fuel cycle is called DUPIC (direct use of spent PWR fuel in CANDU) [3] and is indigenous to Korea. In the DUPIC fuel cycle, the PWR spent fuel is reused in CANDU after a very simple refabrication process, which consists only of oxidation, and reduction (OREOX) processes and sintering. In the dry OREOX processing, even fission gases are not fully removed from the spent fuel. Thus, the DUPIC cycle is considered to be extremely proliferation-resistant. For a 35 GWD/MTU PWR spent fuel, a DUPIC fuel can be reused up to 15 GWD/MTU in the CANDU core. Therefore, ~22% uranium savings is possible and the spent fuel production is reduced by ~67%. The DUPIC study shows that the DUPIC fuel cycle cost is comparable to conventional once-through fuel cycles.

In the DUPIC-HYPER fuel cycle, TRUs from DUPIC spent fuel are transmuted in the HYPER core. Basically, the fuel cycle for HYPER is the same as in the previous PWR-HYPER case. The objective of this study is to investigate the TRU transmutation potential of the HYPER core for the DUPCI-HYPER fuel cycle. All the previous HYPER design concepts are applied to the new core design except that the fuel is composed of DUPIC TRUs. The core characteristics of HYPER are analysed with the REBUS-3/DIF3D code system.

The major mission of the HYPER system is to transmute as much as possible the TRUs in such a way that the associated fuel cycle is as proliferation-resistant as possible. For a proliferation-resistant fuel cycle, the so-called pyro-processing of spent fuels is utilised in HYPER. In the front-end reprocessing of DUPIC spent fuel, the uranium and rare earth (RE) element removal rates were 99.9% and 99%, respectively. On the other hand, only fission products are removed from HYPER spent fuel, where 95% of REs are assumed to be removed without any separation of TRUs as in the previous PWR-HYPER case.

Design features of the HYPER core

Figure 1 shows a schematic configuration of the HYPER core with 186 ductless hexagonal fuel assemblies. As shown in Figure 1, the fuel blanket is divided into three TRU enrichment zones to flatten the radial power distribution. In HYPER, a beam of 1 GeV protons is delivered to the central region of the core to generate spallation neutrons. To simplify the core design, the LBE coolant is also used as a spallation target. In addition to the ultimate shutdown system (USS), six safety assemblies are placed in the HYPER core for use in an emergency. The safety rods are used conditionally to control the reactivity of the core. For a balanced transmutation of TRUs and LLFPs, ^{99}Tc and ^{129}I are incinerated in moderated LLFP assemblies loaded in the reflector zone.

A preliminary study on the optimal range of subcriticality showed that subcriticality of the HYPER core might be in the range $0.961 < k_{eff} < 0.991$, subject to the constraint of 20 MW maximum accelerator power [4]. (This is considered as the maximum allowable beam power for the target window design of the HYPER system). The maximum allowable k_{eff} of the HYPER core was set to 0.98 during a normal operation through an iterative analysis of system safety and its technical feasibility. In the HYPER target design, we introduced an LBE injection tube to maximise the allowable proton beam current. The injection tube controls the LBE flow rate in the target channel such that the central flow rate is higher than that in the peripheral zone. With the aid of the injection tube, the beam window can be very efficiently cooled and the LBE flow rate in the target channel can be substantially reduced, thereby reducing the coolant pumping power. It is important to note that the reduced LBE flow rate in the target channel increases the temperature of the target LBE. Preliminary analysis for a dual injection tube showed that a 20 MW beam power could be accommodated with a sufficient margin for a flat beam profile [5].

It is well known that the LBE coolant speed is limited (usually < 2 m/sec) due to its erosive and corrosive behaviour. Therefore, the lattice structure of the fuel rods should be fairly sparse. In fast reactors, a pancake-type core is typically preferred mainly to reduce coolant pressure drop. Unfortunately, it has been found that the multiplication of the external source is quite inefficient in a pancake-type ADS because of the relatively large source neutron leakage. Kim, *et al*. [6], have shown that the maximum source multiplication can be achieved when the core height is ~2 m. Taking into account the source multiplication and the coolant speed, the core height of HYPER was compromised at 150 cm, and the power density was determined such that the average coolant speed could be ~1.65 m/sec. The inlet and exit coolant temperatures in the core are 340°C and 490°C, respectively. To reduce core size and to improve neutron economy, a ductless fuel assembly is adopted in the HYPER system. An advantage of ductless fuel assembly is that the flow blockage of a subassembly is basically impossible and the production of activation products in the duct is avoidable.

In general, a non-uranium alloy fuel is utilised in a TRU transmuter to maximise the TRU consumption rate. Previously, a Zr-based dispersion fuel was used as the HYPER fuel since it was expected that a very high fuel burn-up could be achieved. However, we found that the dispersion fuel transforms to a metallic alloy during high temperature operation. Therefore, in the current design the metallic alloy of U-TRU-Zr is used as the HYPER fuel (where pure lead is the bonding material). As a result, a large gas plenum is placed above the active core.

Concerning a TRU-loaded ADS, which uses a fixed cycle length, one of the challenging problems is a very large reactivity swing, leading to a large change in the accelerator power over a depletion period. Even in an ADS loaded with MA (minor actinide) fuel, the burn-up reactivity swing is found to be fairly noticeable, although it is relatively smaller than that in a TRU-loaded core. The large burn-up reactivity swing results in several unfavourable safety features as well as deleterious impacts on the economics of the system. In the HYPER core, ^{10}B was used as a burnable absorber (BA) in a unique way so as to reduce the reactivity swing and to control the core power distribution [2].

Each fuel assembly has 204 fuel rods and the fuel rods are aligned in a triangular pattern with 13 tie rods. A fairly open lattice with a pitch-to-diameter (P/D) ratio of 1.49 is adopted in HYPER. Table 1 shows the major design parameters of the HYPER fuel assembly. In Figure 2, a schematic configuration of the ductless fuel assembly is shown. The ^{10}B burnable absorber is loaded into the tie rods with top and bottom cutbacks in order to enhance the ^{10}B depletion rate and also to flatten the axial power distribution of the core. The BA concept with the cutbacks can effectively mitigate the peak fast neutron fluence of the assembly. The peak fast neutron fluence is a limiting design criterion in LBE-cooled fast reactors.

Figure 1. Schematic configuration of the HYPER core (186 fuel assemblies)

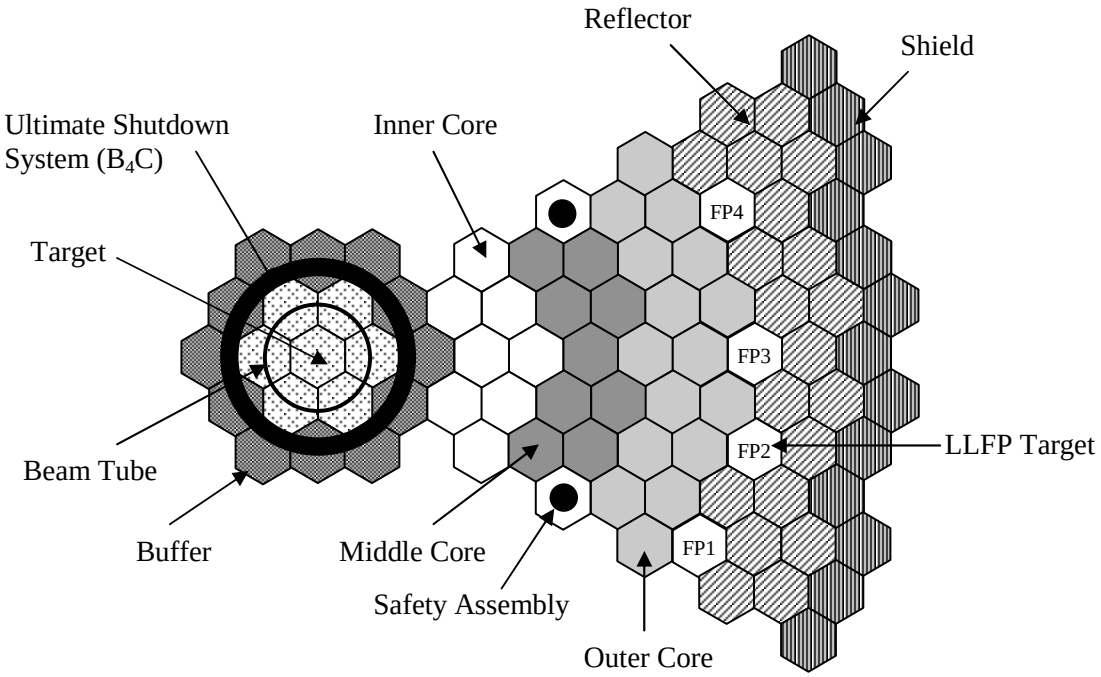

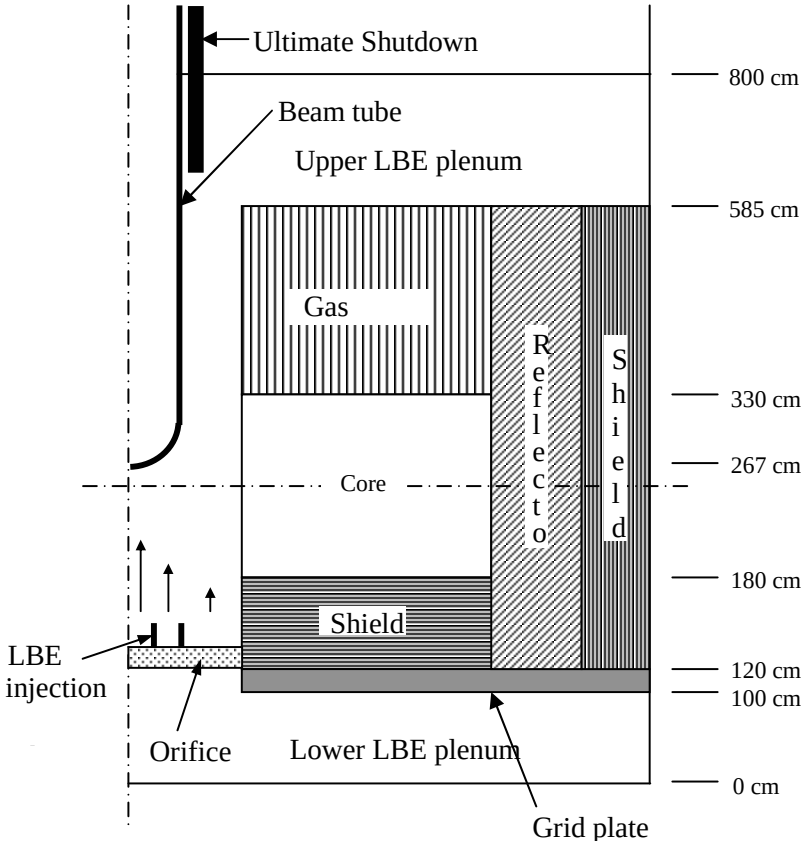

Table 1. Ductless fuel assembly design

Fuel material	Metallic alloy: U-TRU-Zr
Cladding and tie rod material	HT-9
Number of fuel pins per assembly	204
Number of tie rods	13
Pin diameter (cm)	0.77
Cladding thickness (cm)	0.060
Pitch/diameter ratio	1.49
Fuel smear density (% T.D.)	75
Outer radius of tie rod (cm)	0.44
Inner radius of tie rod (cm)	0.36
Active length (cm)	150
Interassembly gap [fuel-to-fuel] (cm)	0.34
Assembly pitch (cm)	17.0075

Figure 2. Configuration of the ductless fuel assembly with B_4C burnable absorber

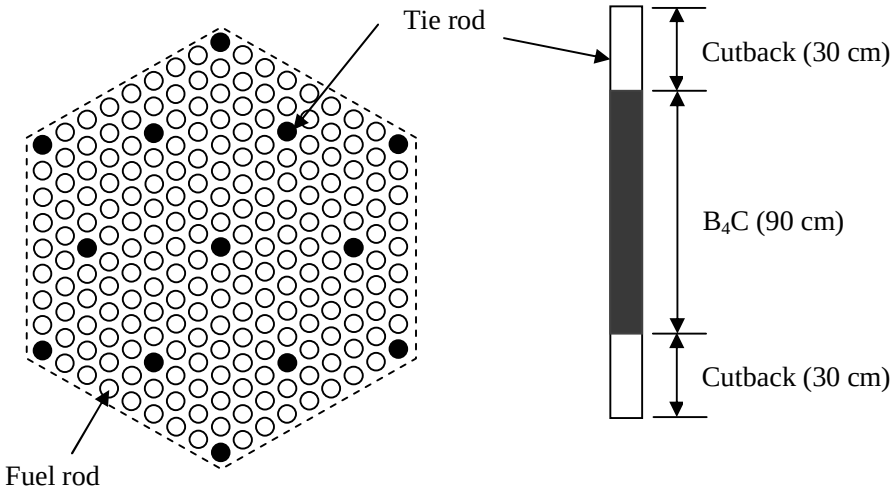

Neutronic performance of the HYPER core

In this section, we discuss the neutronic analysis of the HYPER core, which was performed with the REBUS-3 [7] code system. The core depletion analysis was based on the equilibrium cycle method of REBUS-3. The flux calculations were performed over a nine-group structure with hexagonal-Z models using a nodal diffusion theory option of the DIF3D code [8]. The region-dependent, nine-group cross-sections were generated using the TWODANT [9]/TRANSX [10] code system based on the data of ENDF/B-VI. For the external source in a central target zone, a pre-calculated generic source distribution was used.

In the REBUS-3 depletion analysis, it was assumed that 99.9% of the discharged fuel elements are recovered and recycled into the core after a one-year cooling time. In this work, 5% of the rare earth elements are carried over during the fuel reprocessing/fabrication processing since it is difficult to completely separate them from the fuel material.

Regarding fuel management, a scattered fuel assembly reloading is used as in conventional fast reactors since a whole-core fuel shuffling might be time-consuming in an LBE-cooled reactor and its effects would not be significant. A relatively short cycle length (half-year cycle with 146 EFPDs) is adopted in HYPER to reduce the burn-up reactivity swing. As a result, the batch size should be large to achieve a high fuel burn-up. For the inner zone, seven-batch fuel management is applied and an eight-batch scheme is applied to middle and outer zones. Consequently, the number of fuel assemblies to be reloaded in a cycle in each zone is six (inner), six (middle) and 12 (outer). In the actual scattered fuel reloading, the fuel enrichment of each fuel assembly in each zone needs to be adjusted to obtain the required subcriticality and acceptable power distribution. Thus, it is assumed that fuel enrichment is different depending on the fuel assemblies in each zone – the number of fuel enrichment splittings is four (inner core), five (middle core) and five (outer core). It is worthwhile to note that four types of fuel assemblies are needed for every reload cycle due to fuel management schemes.

In addition to the half-year cycle length, both the ^{10}B burnable absorber and control rods are used to further reduce the reactivity swing in the HYPER core. In the case of ^{10}B burnable absorber usage, B_4C is only loaded into the relatively high-flux zones to enhance burn-up rate since the burn-up penalty would be too serious if discharge burn-up were too low (see Figure 2). Also, it is important to note that BA is not applied to the inner core because an absorber near the external source significantly reduces the degree of source multiplication, hence increasing the required accelerator current. In the current design, natural enriched B_4C is used in the middle and outer cores. With the above fuel management schemes, the REBUS-3 analyses were performed for three different core designs in order to assess the effects of the burnable absorber and control rods on the core performance. The numerical results are summarised in Table 2 in terms of several important core parameters.

In Table 4, it is observed that burn-up reactivity swing in the ^{10}B-loaded core was reduced by ~33%, relative to the reference BA-free core design. However, fuel inventory is also increased by ~21% in the BA-loaded core due to the relatively slow depletion rate of the ^{10}B BA. The discharge burn-up of ^{10}B is ~55%. The increased fuel inventory in the BA-loaded core resulted in a reduced fuel discharge burn-up (from 21.2% to 17.9%). It is worthwhile to note that the power peaking factor is a little smaller in the BA-loaded core. This is because the ^{10}B BA was loaded with the top and bottom cutback zones, i.e. the axial power distribution is more flattened in the BA-loaded core. Consequently, the peak fast neutron fluence is significantly smaller in the BA-loaded core. The net fuel consumption rate is virtually independent of the BA loading, thus, the two cores have an almost identical TRU transmutation rate, 272 kg/year. However, the fuel mass, which should be reprocessed and refabricated, is larger in the BA-loaded core due to the increased fuel inventory.

Table 2 shows that the maximum proton current is still larger than 20 mA even in the BA-loaded core. Meanwhile, it is clear that the proton current is smaller than 20 mA when both BA and control rods are simultaneously utilised without compromising fuel discharge burn-up. This is because the inserted control rods are all fully withdrawn in the middle of the cycle. It is worthwhile to note that the k_{eff} value is still smaller than 0.99 when all the control rods are withdrawn at BOC, satisfying the subcriticality requirement of the HYPER core.

From Table 2 one can note that the source importance in HYPER cores is fairly high. High source importance is mainly attributed to the relatively high H/D ratio of the HYPER core. It is observed that source importance at EOC is just slightly lower than at BOC due to the accumulation of fission products. The BA-loaded cores have a slightly smaller source importance because of the presence of ^{10}B absorber.

It is observed that ^{10}B BA slightly reduces delayed neutron fraction and makes neutron generation time noticeably shorter. Table 2 also compares the coolant void reactivity of the three cores. In the void reactivity evaluation, it was assumed that all the coolant was voided only in the active core. It is clear that the BA-loaded cores have a much larger void reactivity. This is because the capture cross-section of the ^{10}B isotope decreases as the neutron spectrum becomes harder. We think that positive void reactivity would be acceptable since active-core-only voiding is basically impossible in an LBE-cooled reactor.

Table 2. Equilibrium cycle performance of the HYPER cores

Parameter		Without BA and CR	With BA only	With BA and CR
Average fuel weight fraction (%)	Inner zone	37.0	41.5	42.7
	Middle zone	41.7	46.6	47.3
	Outer zone	45.5	51.7	52.2
Effective full-power day [EFPD] (days)		146	146	146
Effective multiplication factor (k_{eff})	BOC	0.9801	0.9801	0.9804 (0.9898*)
	EOC	0.9504	0.9603	0.9701
Source importance (BOC/EOC)		(0.90/0.89)	(0.87/0.85)	(0.88/0.87)
Burn-up reactivity loss (% Δk)		2.97	1.98	1.03
Proton current [BOC/EOC] (mA)		(11.3/29.0)	(11.7/24.1)	(11.4/17.7)
β_{eff}, neutron generation time (μsec)	BOC	0.00288, 2.06	0.00280, 1.65	0.00279, 1.52
	EOC	0.00291, 2.21	0.00283, 1.76	0.00282, 1.68
Core average power density (kW/l)		143	143	143
3-D power peaking factor (BOC/EOC)		(1.60/1.77)	(1.52/1.71)	(1.54/1.60)
Linear power [average, peak] (kW/m)		(17.6, 31.2)	(17.6, 30.1)	(17.6, 28.2)
Average fuel discharge burn-up (a/o)		21.2	17.9	17.5
BOC ^{10}B inventory (kg)		-	13.9	13.9
Peak fast fluence (n/cm^2)		3.8×10^{23}	3.2×10^{23}	3.2×10^{23}
Fuel consumption [U/TRU] (kg/year)		(32/272)	(32/272)	(32/272)
Heavy metal inventory (kg)	BOC	5 007	6 075	6 210
	EOC	4 855	5 923	6 058
Active core void reactivity [BOC/EOC] (pcm)		(1 398/1 484)	(1 843/1 874)	(1 749/1 875)

k_{eff} in all-rod-out condition

In Figure 3, assembly power distributions are provided for both BOC and EOC of an equilibrium cycle for the three HYPER cores. One can see that the inner zone power increased while the outer zone power decreased as the core burn-up increased. This behaviour is generally observed in a TRU-loaded ADS core and is due to the reactivity loss of the core with burn-up. It is noteworthy that the change in the spatial power distribution is significantly mitigated in the core with the control rods, which is ascribed to the smaller reactivity swing in the core. Instead of using control rods, the maximum proton current could be reduced below 20 mA by simply increasing k_{eff} up to 0.99 at BOC. However, in this case, substantial slanting behaviour in the power distribution still occurs since the reactivity swing is fairly large. This is one of the motivations for using the control rods to compensate for reactivity change in HYPER.

Table 3 compares the fuel composition vectors at three fuel management stages (feed, charge and discharge) for an equilibrium cycle of the BA-loaded core with control rods. It is clearly seen that ^{240}Pu has the largest weight per cent in the equilibrium cycle while ^{239}Pu is the most dominant isotope in the feed fuel composition. One can find the ^{239}Pu fraction in the feed fuel relatively small compared with typical PWR spent fuel, where ^{239}Pu weight fraction is usually ~50%. This is because ^{239}Pu is burned most efficiently in the CANDU core. It is noteworthy that weight fractions of the higher actinides such as Am and Cm are significantly increased in the equilibrium core. Also, it is important to note that the weight fraction of the ^{238}U isotope almost doubled in the equilibrium core compared with the feed fuel. The RE fraction in the charging fuel is relatively noticeable.

Figure 3. Relative assembly power distributions in HYPER cores

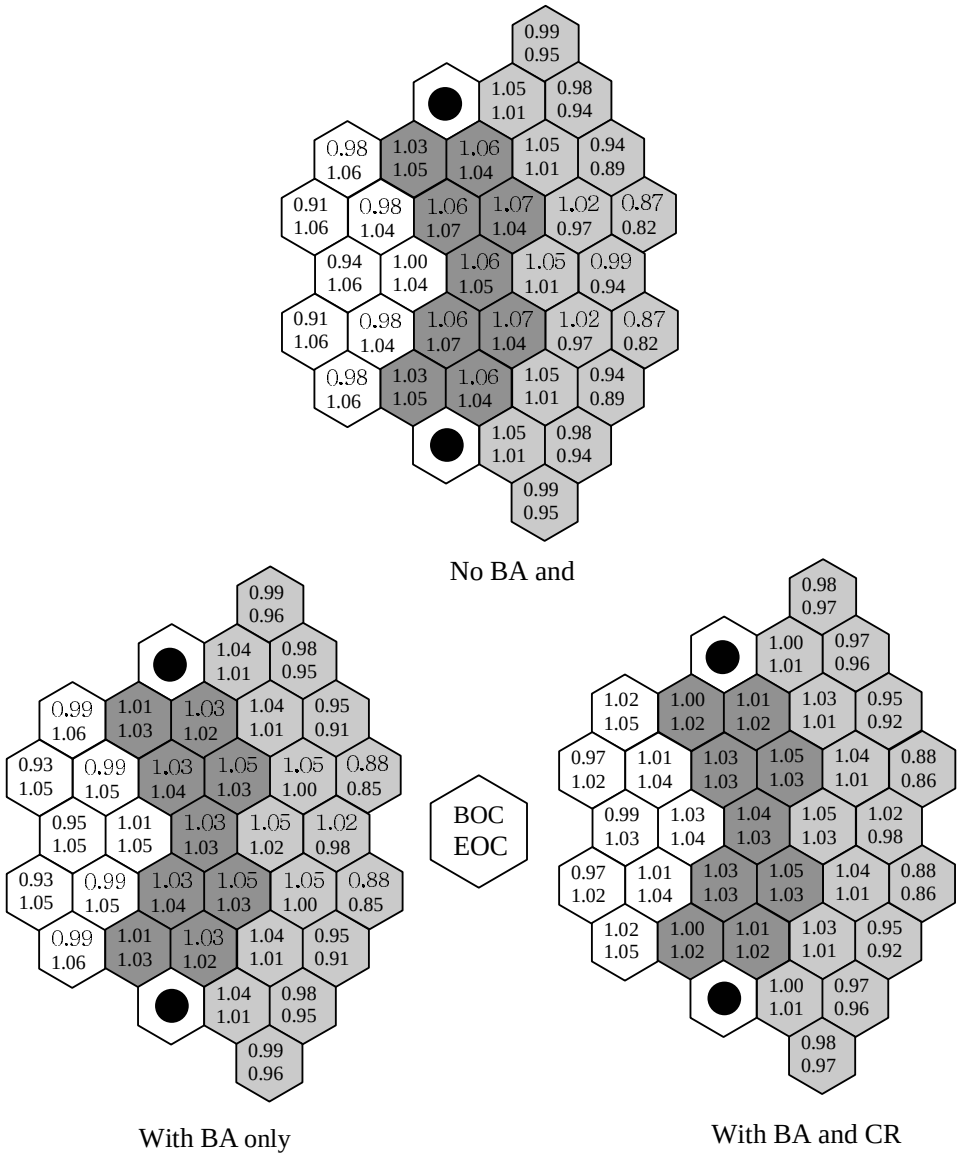

Table 3. Fuel composition in an equilibrium cycle core with BA and CR

Isotope	Feed	Charge	Discharge
^{234}U	2.47E-3	0.53	0.48
^{235}U	0.032	0.14	0.13
^{236}U	0.049	0.28	0.26
^{238}U	10.01	19.59	17.85
^{237}Np	4.55	2.07	1.27
^{238}Pu	3.53	4.43	3.69
^{239}Pu	33.72	15.82	9.86
^{240}Pu	27.28	28.95	23.96
^{241}Pu	3.06	4.07	3.82
^{242}Pu	8.66	11.46	9.92
^{241}Am	6.23	4.30	2.91
^{242}Am	0.0072	0.24	0.24
^{243}Am	1.32	3.52	3.29
^{242}Cm	1.73E-5	0.016	0.20
^{243}Cm	0.020	0.024	0.021
^{244}Cm	0.21	2.69	2.83
^{245}Cm	0.0050	0.87	0.87
^{246}Cm	0.0033	0.58	0.58
RE	1.33	0.41	3.56
FP*	0.0	0.0	14.27

**without RE*

Conclusions

A DUPIC-HYPER fuel cycle was studied to transmute TRUs contained in DUPIC spent fuel. It was found that fuel inventory is slightly larger in the DUPIC-HYPER fuel cycle due to a degraded plutonium vector than in the previous PWR-HYPER cycle. Consequently, burn-up reactivity swing is calculated to be a little smaller in the DUPIC-HYEPR case. However, without any design measure to reduce reactivity swing, the required maximum proton current was 29 mA, which is far beyond the targeted value of 20 mA. The reactivity swing was reduced by ~33% by introducing a B_4C burnable absorber with top/bottom cutbacks. Furthermore, conditional utilisation of control rods (CR) together with B_4C BA results in a maximum proton current of ~18 mA. It was confirmed that B_4C BA could substantially reduce fast fluence.

For a reference HYPER core without BA and CR, the core consumes ~272 kg of TRU per year with a fuel discharge burn-up of ~21 a/o. In the BA-loaded BA and CR cores, the TRU consumption rate is basically the same, but the fuel discharge burn-up is ~18 a/o due to the residual reactivity penalty of the B_4C BA. Also, it was found that control rods can be effectively utilised to mitigate the slanting behaviour of the radial power distribution in the HYPER core.

REFERENCES

[1] Park, W.S., *et al*., "HYPER (Hybrid Power Extraction Reactor): A System for Clean Nuclear Energy", *Nuclear Engineering and Design*, 199, p. 155 (2000).

[2] Kim, Y., *et al*., "Core Design Characteristics of the HYPER System", OECD/NEA 7th Information Exchange Meeting on Actinide and Fission Product Partitioning & Transmutation, Jeju, Korea, 14-16 October 2002.

[3] Ko, W.I., *et al*., "Economic Analysis on Direct Use of Spent Pressurized Water Reactor Fuel in CANDU Reactors – IV: DUPIC Fuel Cycle Cost", *Nuclear Technology*, 134, 167 (2000).

[4] Kim, Y., *et al*., "An Investigation of Subcriticality Level in Accelerator-driven System", *Proceedings of the PHYSOR 2002 International Conference on the New Frontiers of Nuclear Technology*, Seoul, Korea, 7-10 October 2002.

[5] Cho, C.H., *et al*., "The Introduction of a Double-annular Guide Tube for the Design of 20 MW Lead-bismuth Target System", OECD/NEA Fourth International Workshop on Utilization and Reliability of High Power Proton Accelerators, Daejeon, Korea, 16-19 May 2004.

[6] Kim, Y., *et al*., "Optimization of Height-to-diameter Ratio for an Accelerator-driven System", *Nuclear Science and Engineering*, 143, 141 (2002).

[7] Toppel, B.J., "A User's Guide to the REBUS-3 Fuel Cycle Analysis Capability", ANL-83-2, Argonne National Laboratory (1983).

[8] Derstine, K.L., "DIF3D: A Code to Solve One, Two, and Three-dimensional Finite Difference Diffusion Theory Problems", ANL-82-64, Argonne National Laboratory, April 1984.

[9] Alcouffe, R.E., *et al*., "User's Guide for TWODANT: A Code Package for Two-dimensional, Diffusion-accelerated Neutral Particle Transport", LA-10049-M, Los Alamos National Laboratory (1990).

[10] MacFralane, R.E., "TRANSX2: A Code for Interfacing MATXS Cross Section Libraries to Nuclear Transport Codes", LA-12312-MS, Los Alamos National Laboratory (1992).

NUMERICAL COMPARISONS BETWEEN NEUTRONIC CHARACTERISTICS OF MUSE4 CONFIGURATIONS AND XADS-TYPE MODELS

M. Plaschy[1], S. Pelloni[1], P. Coddington[1], R. Chawla[1,2], G. Rimpault[3], F. Mellier[3]
[1]Paul Scherrer Institute, Villigen (PSI), Switzerland; michael.plaschy@psi.ch
[2]Swiss Federal Institute of Technology (EPFL), Lausanne, Switzerland
[3]DEN/DER, CEA/Cadarache, Saint-Paul-lez-Durance, France

Abstract

The representativity of a specific MUSE4 configuration (M4SC2) was analysed from a nuclear data viewpoint, with respect to the current concepts of experimental accelerator-driven systems (XADSs) with gas (He), Na and Pb/Bi coolants. In this context, data sensitivity/uncertainty analyses based on first order perturbation theory calculations were performed using the deterministic code ERANOS (Version 2.0) in conjunction with its adjusted nuclear data library ERALIB-1, which lead to the determination of suitable representativity factors.

It was found that M4SC2 is quite representative of XADS with He and Na. However, in the case of a Pb/Bi system, the effects of significant uncertainties associated with the data for these two nuclides and their low content in M4SC2 were clearly highlighted, resulting in much lower representativity factors. Thus, the need for additional experiments was evident.

Introduction

In the field of waste management incorporating a transmutation option, accelerator-driven systems (ADS) represent an important alternative to conventional reactors due to their higher safety level when minor actinides such as Np and Am are loaded into the core. As a result, it is necessary to extend the validation domain of calculation methods for critical fast reactors to the analysis of source-driven subcritical configurations.

To reach this goal, the experimental program MUSE was launched in the MASURCA facility at CEA/Cadarache (France). Of particular interest, the MUSE4 phase consists of the coupling of a PuO_2/UO_2 + Na core with an external neutron source of high intensity [1]. Coupling has been achieved by employing a specially constructed pulsed neutron generator called GENEPI, which produces monoenergetic neutrons either via a $D(d,n)^3He$ reaction (2.7 MeV neutrons) or a $T(d,n)^4He$ reaction (14.1 MeV neutrons). The measurements being undertaken in the MUSE4 program constitute an important experimental database to be used for validating the calculation methods and data employed in the analysis of ADS (e.g. ERANOS and its associated data libraries).

In this context, specific investigations were conducted to assess (via data sensitivity/uncertainty analyses) representativity between MUSE4 and emerging concepts of experimental accelerator-driven systems (XADS). For this purpose, simplified RZ models for MUSE4 and different current XADS designs with gas (He), Na and Pb/Bi coolants (XADS_He, XADS_Pb/Bi, XADS_Na) were set up. The fuel considered throughout, for MUSE4 as well as for all the XADS, is 23-25% enriched PuO_2/UO_2 MOX fuel of the type used for the second SUPERPHENIX core. For the analyses, the deterministic code system ERANOS (Version 2.0) was used. The parameters studied include: the multiplication factor k_{eff}, a spectral index, F_5/F_8 (the fission rate of ^{235}U relative to that of ^{238}U at the centre of the fuel region) and a spatial index, $F_{5,1}/F_{5,2}$ (the ^{235}U fission rate at the interface between spallation module and core midplane relative to that at the centre of the fuel zone).

Deterministic calculation scheme

General description of ERANOS

ERANOS-2.0 is a deterministic code system consisting of a variety of dedicated modules. In the present analysis, we use the cell code ECCO [2], the RZ transport theory code BISTRO [3] and first-order perturbation theory modules [4] in conjunction with the adjusted nuclear data library ERALIB-1 [5]. The numerical approximations are P1 for the anisotropy of scattering and S8 for the angular discretisation of the flux being computed in 33 energy groups. BISTRO solves the Boltzmann equation by means of a standard finite difference method.

Representativity factors and general approach

Employing a recently applied methodology with ERANOS [4], representativity factors r_{RE} between MUSE4 and the three XADS configurations (with He, Na and Pb/Bi coolants) were evaluated for integral parameters such as the multiplication factor k_{eff} and specific reaction rate ratios on the basis of first-order perturbation theory. These factors, which quantify the impact of nuclear data uncertainties on the prediction of I, the parameter of interest (depend on cross-sections $P_1, \ldots, P_N$), are obtained as follows.

Sensitivity coefficients S_i for I (P_1, …, P_N) are computed according to Eq. (1):

$$S_i = \frac{\Delta I}{I} \Big/ \frac{\Delta P_i}{P_i} \tag{1}$$

The relative uncertainty σ_I of I is obtained by using a covariance matrix D as shown in Eq. (2):

$$\sigma_I^2 = S^t \, D \, S \tag{2}$$

It should be noted that D is associated with a specific nuclear data library.

For the parameter I, the representativity factor r_{RE} between two systems (e.g. MUSE and a given XADS) is determined from Eq. (3) [4], the covariance matrix being taken from the adjusted data library ERALIB-1:

$$r_{RE} = \frac{S_{XADS}^t \, D_{ERALIB} \, S_{MUSE}}{\sqrt{(\, S_{XADS}^t \, D_{ERALIB} \, S_{XADS} \,)(\, S_{MUSE}^t \, D_{ERALIB} \, S_{MUSE} \,)}} \tag{3}$$

The value of r_{RE} lies between 0.0 and 1.0. The closer r_{RE} is to 1.0, the more representative is MUSE of the XADS.

Representativity factors can also be used to quantify the uncertainty reduction possible for the prediction of I on the basis of suitable integral measurements. This occurs via Eq. (4):

$$\sigma_{I,XADS_reduced}^2 = \sigma_{I,XADS}^2 \left(1 - \frac{r_{RE}^2}{1 + \sigma_{I,exp}^2 \big/ \sigma_{I,MUSE}^2} \right) \tag{4}$$

Thereby, the experimental uncertainty of the parameter I [i.e. as measured in MUSE ($\sigma_{I,exp}$)] also plays a significant role. The smaller is the experimental uncertainty, the stronger is the uncertainty reduction for the predicted value of I in the system of interest, with the closeness of r_{RE} to 1.0 remaining an important aspect. Eq. (4) reflects the most optimistic case (zero experimental uncertainty):

$$\sigma_{I,XADS_reduced}^2 = \sigma_{I,XADS}^2 \left(1 - r_{RE}^2 \right) \tag{5}$$

In the current study, representativity between the MUSE4 experiments and the different XADS is evaluated based on the following scheme:

1. Assessment of nuclide-specific “integral sensitivities” on the basis of sensitivity coefficient (S_i) calculations [see Eq. (1)]. Integral sensitivity to a given nuclide is the uncertainty of I, which is obtained by assuming that a) there is no correlation between data for different nuclides, b) the individual reaction cross-sections for the nuclide considered are also not correlated and c) the relative uncertainty for each of the nuclide cross-sections is 100% over the whole energy range (< 20 MeV). Effectively, integral sensitivity is calculated on the basis of Eq. (2) while assuming that the matrix D is unity.

2. Determination of the uncertainty of I with the correct covariance matrix D from ERALIB-1 [see Eq. (2)].

3. Calculation of the representativity factor r_{RE} [see Eq. (3)].

4. Determination of the reduced uncertainty [see Eqs. (4,5)].

The reason for currently using the adjusted data library ERALIB-1 is to avoid the well known dominating effect of ^{239}Pu, which was observed in the analysis of MUSE3 in conjunction with the (unadjusted) JEF-2.2 library [4]. However, the resulting uncertainties may be somewhat small for the ADS situation, since the ERALIB adjustments were made solely on the basis of critical experiments. Also, it is necessary to underline the fact that method uncertainties, as well as uncertainties due to external source differences between MUSE4 and XADS, are not accounted for in the current analysis. Complementary studies, including method/data comparisons made in the framework of benchmark exercises, are certainly important in this context [6].

General description

Models

The simplified RZ models considered for XADS are based on current PDS-XADS designs [7]. These are described in Figure 1 and Table 1, where only the most important materials are indicated [8].

Figure 1. Definition of homogenised zones for three XADS models

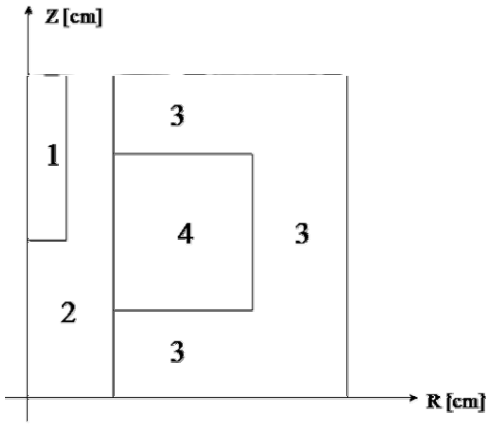

Table 1. Description of homogenised zones of three XADS models

Name	Zone 1	Zone 2	Zone 3	Zone 4
XADS_Pb/Bi	Void	Pb/Bi	Pb/Bi	PuO_2/UO_2 + Pb/Bi
XADS_He	Void	Pb/Bi	He + Steel	PuO_2/UO_2 + He
XADS_Na	Void	Pb/Bi	Na + Steel	PuO_2/UO_2 + Na

The basic principles for obtaining the models were that: a) the volume of the spallation source (void + Pb/Bi) and the volume of the fuel region (Zone 4) correspond to the PDS-XADS design, b) the outer radius of the reflector region (Zone 3) was adjusted to obtain a k_{eff} value of 0.97.

The reference experimental set-up considered is the second subcritical configuration investigated in the MUSE4 program, i.e. M4SC2 [8], the RZ model described in Figure 2 and Table 2. For the sake of consistency with XADS, the original outer radius of Zone 4 was modified slightly in order to achieve a k_{eff} value of 0.97.

Figure 2. Definition of homogenised zones for M4SC2 model

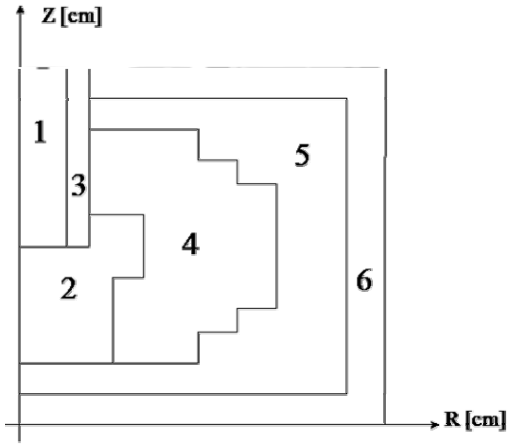

Table 2. Description of homogenised zones of M4SC2 model

Name	Zone 1	Zone 2	Zone 3	Zone 4	Zone 5	Zone 6
M4SC2	Void	Pb	Al	PuO_2/UO_2 + Na	Na + Steel	Steel

Parameters

As indicated earlier, representativity factors r_{RE} [see Eq. (3)] between M4SC2 and XADS_He, XADS_Na and XADS_Pb/Bi were considered for the three parameters listed below:

1. The multiplication factor k_{eff}.

2. F_5/F_8, i.e. the fission of ^{235}U relative to that ^{238}U at the centre of the fuel region. This provides useful spectral information due to the different nature of ^{235}U and ^{238}U fission, the latter being a threshold reaction and the former not being a threshold reaction.

3. $F_{5,1}/F_{5,2}$, i.e. the ^{235}U fission rate at the interface between spallation module and core midplane relative to that at the centre of the fuel zone. This spatial index is sensitive to the geometry and composition of the spallation module.

Numerical results and interpretation

Representativity for the multiplication factor k_{eff}

Relative "integral sensitivities" are presented in Table 3. It can be seen that the highest sensitivity in each case is to ^{239}Pu. The contributions of the other nuclides are much smaller and quite similar in magnitude, except for Pb_{nat} and ^{209}Bi, which have significant effects only in the XADS_Pb/Bi case.

K_{eff} uncertainties (again, only due to nuclear data uncertainties) are presented in Table 4, the main contributing nuclides being indicated for each case.

Table 3. Relative integral sensitivities (%) of k_{eff} with respect to the main isotopes

Isotopes	M4SC2	XADS_Na	XADS_Pb/Bi	XADS_He
^{235}U	0.8	1.9	1.7	1.8
^{238}U	3.1	2.6	3.7	0.4
^{239}Pu	83.0	84.6	78.3	85.5
^{240}Pu	4.8	4.6	4.7	6.2
^{241}Pu	1.6	4.6	4.1	4.4
^{56}Fe	3.2	0.3	1.3	0.2
^{52}Cr	1.4	0.5	0.1	0.7
^{23}Na	1.1	0.2	0.0	0.0
Pb_{nat}	0.0	0.1	2.8	0.1
^{209}Bi	0.0	0.1	3.0	0.1
Others	0.9	0.4	0.4	0.6

Table 4. K_{eff} uncertainties associated with the ERALIB-1 library

Name	Uncertainty on the k_{eff} (σ_I)	Main contributors
M4SC2	± 162 pcm	^{52}Cr, ^{239}Pu, ^{56}Fe …
XADS_Na	± 163 pcm	^{239}Pu, ^{240}Pu, ^{56}Fe …
XADS_Pb/Bi	± 1 021 pcm	^{209}Bi, Pb_{nat}, ^{239}Pu …
XADS_He	± 199 pcm	^{239}Pu, ^{58}Ni, ^{240}Pu …

The uncertainties are similar for M4SC2, XADS_Na and XADS_He (σ_I < 200 pcm), ^{239}Pu being one of the main contributors in each configuration. The structural material isotope ^{52}Cr is a major contributor for M4SC2, due to the larger quantity of this nuclide in the experimental set-up as compared to the XADS. One also notes that the situation is completely different for the XADS_Pb/Bi case, where Pb_{nat} and ^{209}Bi are the main contributors to the overall uncertainty (σ_I > 1 000 pcm) with the data for these nuclides not having been adjusted in ERALIB-1.

The corresponding representativity factors are provided in Table 5. It can be seen that for k_{eff} M4SC2 is quite representative of XADS_Na and XADS_He, the corresponding r_{RE} values being rather close to 1.0. On the contrary, the low presence of Pb_{nat} and the absence of ^{209}Bi in M4SC2 lead to a low-valued representativity factor for the XADS_Pb/Bi. This indicates the need for additional integral measurements related to the data of lead and bismuth.

Table 5. Representativity factors r_{RE} for k_{eff}

Compared systems	Representativity factor r_{RE}
M4SC2 ↔ XADS_Na	0.884
M4SC2 ↔ XADS_Pb/Bi	0.346
M4SC2 ↔ XADS_He	0.907

As indicated earlier, the degree to which the uncertainty of the prediction of a given parameter for an XADS can be reduced via an integral measurement depends on the corresponding representativity factor r_{RE} [see Eqs. (3,4)]. Thereby the experimental uncertainty associated with the measurement also plays a key role. To illustrate the point, Table 6 shows the k_{eff} uncertainty reduction for the case of the XADS_He, assuming different values of experimental uncertainty in M4SC2 [8].

Table 6. Example of k_{eff} uncertainty reduction for the XADS_He system

For the k_{eff} prediction	Value (with ERALIB-1)
$\sigma_{I,XADS}$: Uncertainty for XADS_He	± 199 pcm
$\sigma_{I,MUSE}$: Uncertainty for M4SC2	± 162 pcm
r_{RE}: Representativity factor	0.907
$\sigma_{I,XADS_reduced}$: Reduced uncertainty for XADS_He (with an $\sigma_{I,exp}$ experimental uncertainty of ± 0 pcm)	± 77 pcm
$\sigma_{I,XADS_reduced}$: Reduced uncertainty for XADS_He (with an $\sigma_{I,exp}$ experimental uncertainty of ± 100 pcm)	± 127 pcm
$\sigma_{I,XADS_reduced}$: Reduced uncertainty for XADS_He (with an $\sigma_{I,exp}$ experimental uncertainty of ± 200 pcm)	± 163 pcm

Once again, only uncertainties associated with nuclear data are being accounted for in the present analysis. Nevertheless, the sensitivity coefficients considered [see Eq. (1)] in determining corresponding representativity factors do allow the obtaining of important qualitative indications on the correlation between the compared systems. In the following sections, related to the two other integral parameters under consideration, the aspect of uncertainty reduction is not treated explicitly, the different XADS being compared with M4SC2 solely on the basis of integral sensitivities and representativity factors.

Representativity for F_5/F_8

The relative integral sensitivities to the main isotopes are given in Table 7 for the various cases. The contributions of ^{235}U and ^{238}U, these isotopes having a direct impact on the reaction rate ratio under consideration, are larger than in the previous (k_{eff}) case as expected. In addition, a significant contribution of ^{239}Pu is still observed for all the systems, while ^{23}Na, Pb_{nat} and ^{209}Bi have significant effects only in the systems in which they are present in an important way.

The corresponding representativity factors are given in Table 8. These are similar to the results for k_{eff}. The subcritical core of M4SC2 is representative of XADS_Na and XADS_He. Again, the low representativity with respect to XADS_Pb/Bi reflects deficiencies associated with the data for Pb_{nat} and ^{209}Bi, as well as the low content of these nuclides in the experimental configuration.

Table 7. Relative integral sensitivities (%) of the spectral ratio F_5/F_8 to the main isotopes

Isotopes	M4SC2	XADS_Na	XADS_Pb/Bi	XADS_He
^{235}U	37.3	33.6	32.8	38.6
^{238}U	33.1	33.1	33.0	35.4
^{239}Pu	13.3	11.7	10.7	11.7
^{240}Pu	0.8	1.3	1.2	1.2
^{241}Pu	0.2	0.5	0.5	0.5
^{56}Fe	6.3	7.2	5.4	8.4
^{52}Cr	2.0	0.9	0.5	1.6
^{23}Na	5.0	10.8	0.0	0.0
Pb_{nat}	0.4	0.1	6.8	0.2
^{209}Bi	0.0	0.1	8.5	0.2
Others	1.6	0.5	0.5	2.1

Table 8. Representativity factors r_{RE} for F_5/F_8

Compared systems	Representativity factor r_{RE}
M4SC2 ↔ XADS_Na	0.853
M4SC2 ↔ XADS_Pb/Bi	0.264
M4SC2 ↔ XADS_He	0.885

Representativity for $F_{5,1}/F_{5,2}$

Relative integral sensitivities for this spatial index are presented in Table 9. The contributions of the individual nuclides are significantly different from the previous two cases (see Tables 3 and 7), indicating the significant impact of the spallation module on this particular parameter. The contributions of Pb_{nat} and ^{209}Bi (except for M4SC2 where ^{209}Bi does not occur) increase quite markedly.

As to be expected, the representativity factors given in Table 10 are also significantly different from the corresponding values in the previous sections. Generally speaking, the r_{RE} factors are much smaller. This is due to the different source regions, which are quite dissimilar in terms of geometry and material composition (e.g. the source module of M4SC2 has no ^{209}Bi as mentioned above). Additional calculations for the three XADS, which were carried out assuming modified targets where ^{209}Bi is replaced by Pb_{nat}, indeed yielded significantly larger representativity factors (shown in Table 10).

Table 9. Relative integral sensitivities (%) to the main isotopes for $F_{5,1}/F_{5,2}$

Isotopes	M4SC2	XADS_Na	XADS_Pb/Bi	XADS_He
^{235}U	0.2	0.3	0.3	0.1
^{238}U	34.5	15.7	22.4	15.9
^{239}Pu	20.9	5.5	1.0	6.0
^{240}Pu	4.9	3.5	5.9	1.3
^{56}Fe	0.5	4.6	39.9	37.2
^{57}Fe	0.6	2.3	6.2	4.9
^{52}Cr	3.8	3.2	1.4	0.1
^{58}Ni	0.5	0.7	1.3	5.7
^{23}Na	16.8	23.2	0.0	0.0
Pb_{nat}	15.3	20.7	15.0	15.0
^{209}Bi	0.0	19.0	4.8	13.4
Others	1.8	1.3	1.9	0.3

Table 10. Representativity factors r_{RE} for $F_{5,1}/F_{5,2}$

Compared systems	Rep. factor r_{RE}	Rep. factor r_{RE} (no ^{209}Bi in XADS spallation module)
M4SC2 ↔ XADS_Na	0.258	0.552
M4SC2 ↔ XADS_Pb/Bi	0.066	0.383
M4SC2 ↔ XADS_He	0.259	0.556

Conclusions

Investigations related to k_{eff} and reaction rate ratios were conducted to assess the representativity between MUSE4 and various concepts of experimental accelerator-driven systems (XADS). In this context, sensitivity/uncertainty calculations were performed using deterministic code system ERANOS (Version 2.0) in conjunction with its adjusted data library ERALIB-1 based on the JEF-2.2 evaluation. Employing a recently applied methodology [4], representativity factors r_{RE} between the second subcritical MUSE4 core (M4SC2) and the three current PDS-XADS designs (with He, Na and Pb/Bi coolants) were evaluated for different integral parameters.

Specifically, it was found that the representativity between M4SC2 and an XADS with an Na or He coolant is, in general, quite satisfactory except for the region with the source module. In the case of an XADS with Pb/Bi coolant, the relatively low representativity results from the large uncertainties associated with the nuclear data for Pb_{nat} and ^{209}Bi, as does also the low content of these nuclides in the experimental configuration. This clearly indicates the need for additional integral experiments.

It is necessary to underline the fact that only data uncertainties were accounted for in the present study. Method uncertainties and combined method/data effects were not considered, nor were the effects of differences in the external neutron source [9]. Further investigations are called for in this context, for example detailed comparisons in the framework of specific benchmark exercises [6].

Acknowledgements

The authors would like to acknowledge the help provided by the EU PDS-XADS project team and the MUSE group of CEA/Cadarache in supplying various information related to the computational models employed.

REFERENCES

[1] Soule, R., *et al*., "Neutronic Studies in Support of ADS: The MUSE Experiments in the MASURCA Facility", Accepted for publication in *Nuclear Science and Engineering* (2004).

[2] Rimpault, G., "Algorithmic Features of the ECCO Cell Code for Treating Heterogeneous Fast Reactor Subassemblies", International Topical Meeting on Reactor Physics and Computations, Portland, USA (1995).

[3] Palmiotti, G., *et al*., "Optimized Two-dimensional Sn Transport (BISTRO)", *Nuclear Science and Engineering*, 104-26 (1990).

[4] Aliberti, G., *Caractérisation Neutronique des Systèmes Hybrides en Régimes Stationnaire et Transitoire*, Thèse de l'Université Louis Pasteur de Strasbourg (2001).

[5] Fort, E., *et al*., "Realisation and Performance of the Adjusted Nuclear Data Library ERALIB1 for Calculating Fast Reactor Neutronics", *Proceedings of PHYSOR'96*, Mito, Japan (1996).

[6] Villamarin, D., *et al*., "Benchmark on Computer Simulation of MASURCA Critical and Subcritical Experiments (MUSE4 Benchmark)", NEA/SEN/NSC/WPPT(2001)5, 2001.

[7] "XADS Pb-Bi Cooled Experimental Accelerator Driven System Reference Configuration", Summary report, Ansaldo Energia SpA, ADS 1 SIFX 0500 (2001).

[8] Plaschy, M., *Études Numériques et Expérimentales de Caractéristiques d'un Système Rapide Sous-critique Alimenté par une Source Externe*, Thèse de l'École Polytechnique Fédérale de Lausanne (EPFL), No. 2953 (2004).

[9] Pelloni, S., "PDS-XADS LBE and Gas Cooled Concepts: Neutronic Parameters Comparisons", *Proceedings of PHYSOR'04*, Chicago, USA (2004).

THERMAL STABILITY OF THE U-Zr FUEL AND ITS INTERFACIAL REACTION WITH LEAD

B-S. Lee, Y. Kim, J-H. Lee, T-Y. Song
Korea Atomic Energy Research Institute
P.O. Box 105, Yuseong, Daejeon, 305-600 Korea

Abstract

The effect of heat treatment on fuel rods at 630°C and 700°C and the interfacial reaction between fuel and lead were investigated. The U-Zr metallic fuel was fabricated by mixing, pressing, sintering and extrusion. There were two kinds of phases – α-Zr precipitates and a δ-UZr_2 matrix in the U-Zr metallic fuel. After heat treatment of the extruded rod at 630°C and 700°C, the volume changes of the samples increased slightly and the density variation was negligible. Therefore, it is evident that U-Zr fuels have good thermal stability. The interface between U-55Zr fuel and Pb according to annealing time at 650°C consisted of two distinctive regions – a reaction zone in the vicinity of the surface and an initial zone in the inner area. It should be noted that the thickness of the reaction zone was 26 μm, 36 μm and 46 μm at 100 hrs, 200 hrs and 1 000 hrs, respectively. Also, the reaction zone consisted of an α-Zr layer and a Zr-depleted area.

Introduction

The blanket fuel assembly for HYPER (hybrid powder extraction reactor) contains a bundle of pins arrayed in a triangular pitch, which has a hexagonal bundle structure. The reference blanket fuel pin consists of the fuel slug of the TRU-xZr (x = 50-60 wt.%) alloy and is immersed in lead for thermal bonding with the cladding. The blanket fuel cladding material is ferritic-martensitic steel HT9.

Although there are lots of experimental data on the metallic alloys of U-Pu-Zr and U-Zr, they are for fuel types with a Zr fraction of less than 20 wt.%. Therefore, little data is available for the HYPER system fuel where the Zr fraction is higher than 30 wt.%. As a basic study on HYPER fuel, we fabricated U-55 wt.% Zr fuel instead of the actual TRU-Zr fuel. It appeared that no experimental data pertinent to the TRU-xZr (x = 50-60 wt.%) alloy existed. The U-55 wt.% Zr metallic fuel was fabricated by mixing, pressing, sintering and extrusion. This work was performed in order to investigate the microstructures and the thermal stability of the U55 wt.% Zr metallic fuel and the interfacial reaction between U-55 wt.% Zr fuel and Pb according to annealing time at 650°C.

Experimental procedure

The uranium powder was manufactured by a centrifugal atomiser and the zirconium powder (Sejong materials Co. Ltd, Korea) was prepared via the hydride-dehydride process.

The U-Zr metallic fuel was performed by mixing, pressing and sintering in optimum compaction and sintering conditions [1]. The sintered U-60 wt.% Zr was extruded by an indirect extrusion machine at 760°C and with a 13:1 extrusion ratio. Specimens of 25 mm in length were cut, vacuum-sealed in quartz tubes and annealed in a box furnace at 630°C and 700°C for up to 1 500 hrs. Sample swelling as a function of temperature and time was determined from dimensional changes. The densities of the annealed samples were calculated from the weights and dimensions. The microstructures and phase identification of the extruded rod and the annealed rod were examined by SEM and EDS. The area fraction of each phase obtained by SEM was analysed by a BMI plus ver. 4.0 (Winatech, Korea).

In order to clarify interfacial reaction between fuel and lead, a series of experiments were executed with fuel in Pb melt at 650°C for 100, 200 and 1 000 hrs. The composition of diffusion layers and the diffusion depth were analysed using SEM/EDS.

Results and discussion

Figure 1 shows uranium and zirconium particles. The mean particle sizes of the uranium and zirconium powders are 55 μm and 60 μm, respectively. Most of the uranium particles have a smooth surface and a generally near-perfect spherical shape with a few attached satellites. On the other hand, the zirconium particles fabricated by the hydride-dehydride process have an irregular morphology.

Figure 2 shows the back-scattered electron (BSE) image of the sintered sample. As can be seen in phase diagrams, the α-Zr phases are distributed in the δ phase, which is observed as a white matrix [2]. Also, small amounts of pores are found throughout the sample.

Figure 1. Photographs of the atomised (a) U powder and (b) Zr powder

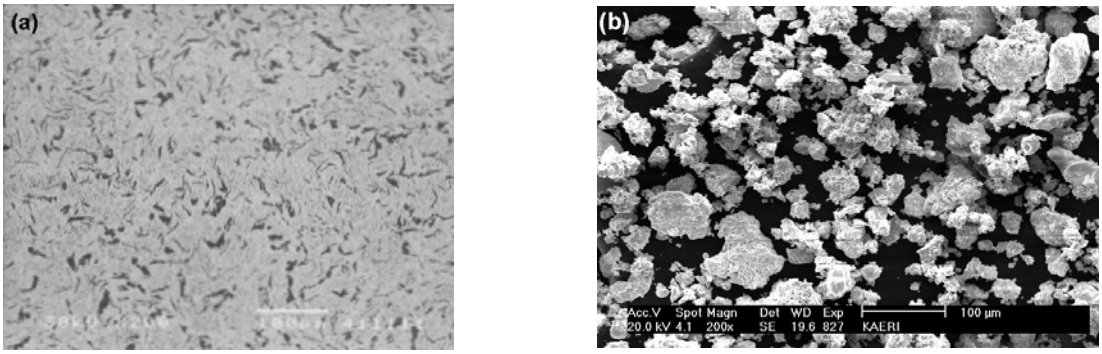

Figure 2. SEM micrograph and EDS analysis results for U-60 wt.% Zr sintered sample

(a) δ-UZr_2 matrix, (b) α-Zr phase

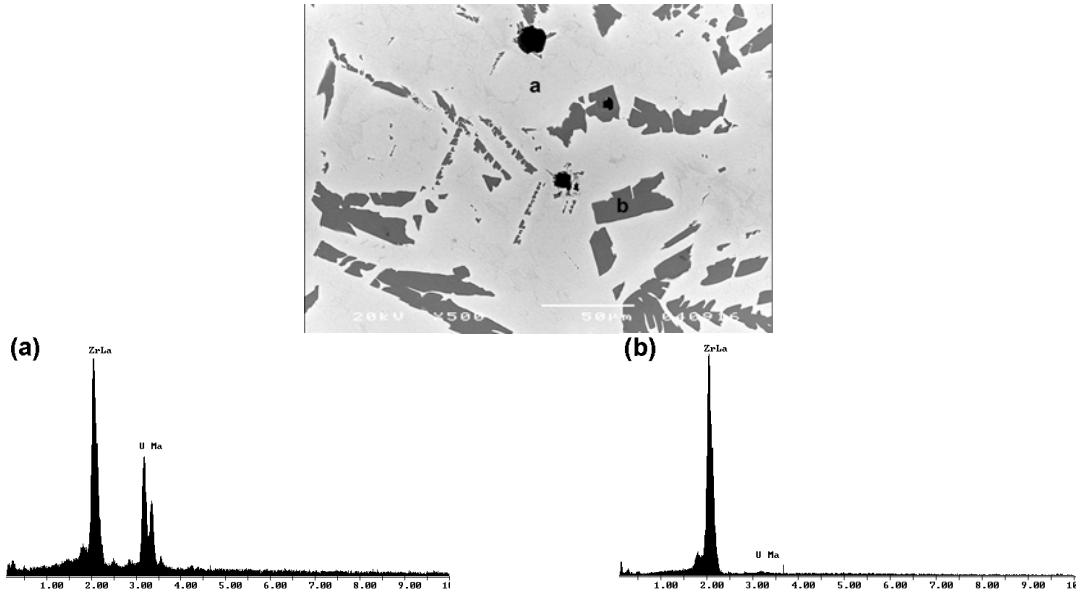

BSE images of the hot extruded rod are shown in Figures 3 and 4. In the sintered samples mentioned above, the α-Zr phases were also distributed (homogenously) in the white δ phase matrix and the porosity was drastically decreased because of the densification by the extrusion process. It was confirmed that the U-55 wt.% Zr alloy with a high melting point could be fabricated via a sintering process at a relatively low temperature in lieu of a conventional casting process.

Figure 5 shows the dependency of swelling behaviour and the density changes of temperature and time for the samples. The volume changes of the samples increased slightly and the density variation was negligible. Therefore, it is evident that U-55 wt.% Zr fuel has good thermal stability.

Figure 3. SEM micrographs of the extruded rod

(a) Transverse direction, (b) longitudinal direction

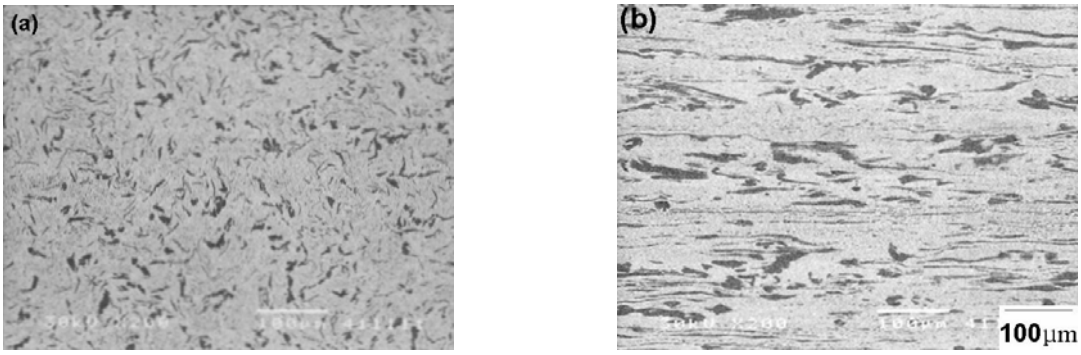

Figure 4. SEM micrograph and EDS analysis results for the extruded rod

(a) δ-UZr_2 matrix, (b) α-Zr phase

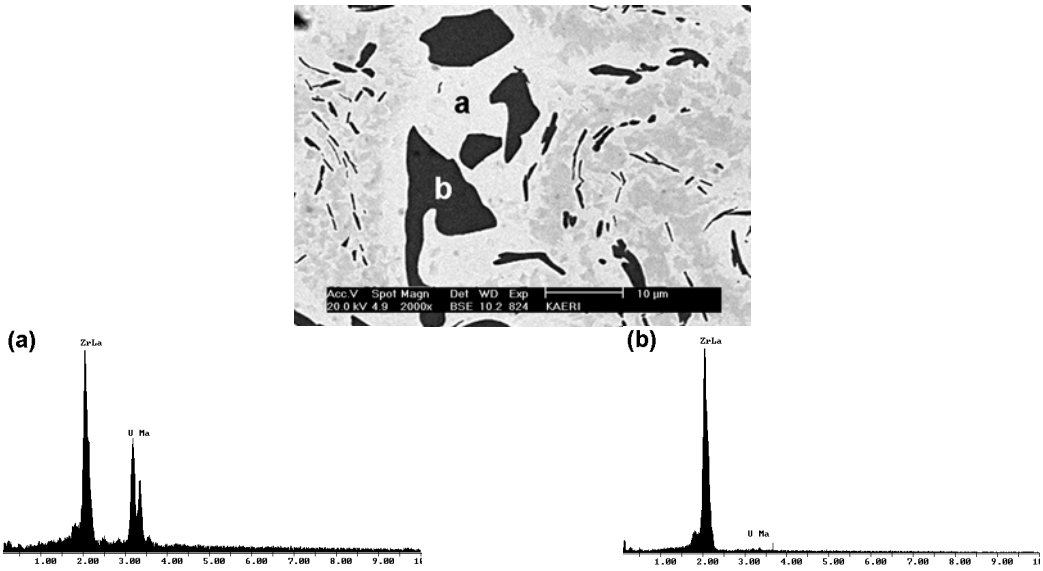

Figure 5. Volume and density changes of the extruded rod on temperature and time

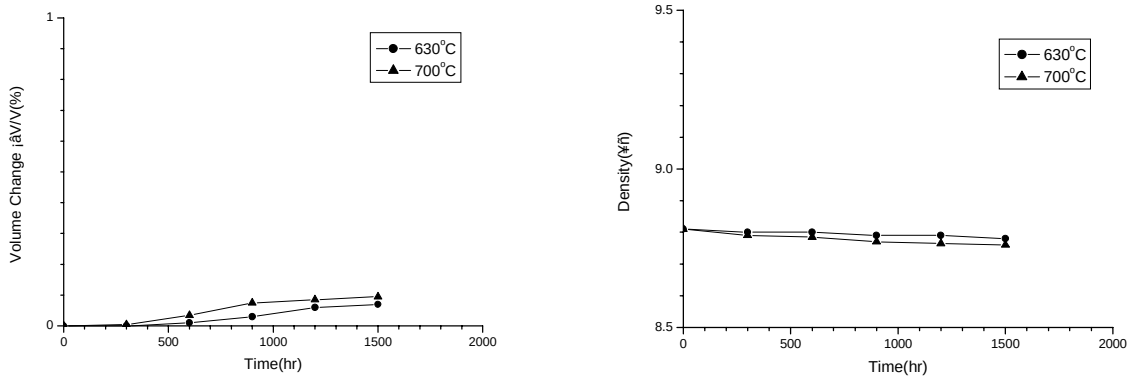

Figure 6 shows BSE images of the rod annealed at 630°C and 700°C for 600 hrs and 1 500 hrs. These figures show that as the annealing time increased, the lathed α-Zr phases began to break into pieces and grow into spherical particles. As the annealing temperature increased, spheroidising of the α-Zr phases was accelerated, with transformation to a spherical shape. We can interpret that the geometrically unstable lathed α-Zr phase transformed to the spherical phase with a lower surface area by coalescence. In addition, we think that the α-Zr and δ-UZr_2 phases dissolved and formed a solid solution at an annealing temperature above 617°C, and that the spheroidised α-Zr and δ phases appeared again during cooling.

As the annealing time increased, the hardness decreased and the decreasing rate of the hardness was much higher at 700°C than at 630°C (Figure 7). This is attributed to the increase of the area fraction of the δ phase and the decrease of the area fraction of the relatively hard α-Zr phase as the annealing temperature and time increased.

Figure 8 shows the area fraction of the α-Zr phase according to the annealing time at 630°C and 700°C. In the case of 630°C of annealing time, the area fraction of the α-Zr phase gradually decreased as the annealing time increased, whereas the area fraction of the α-Zr phase sharply decreased at the early stage of annealing time and then the decreasing rate declined at 700°C. This phenomenon agreed with the results on hardness values vis-à-vis annealing time as shown in Figure 7. When the U-55 wt.% Zr alloy is annealed at above 617°C, which is the unstable region of α-Zr phase, the alloy is diffused into the uranium matrix and finally forms δ phase at a lower temperature. Hence, it can be interpreted that the drastic decrease of area fraction of the α-Zr phase at the early stage of annealing time was due to the higher concentration gradient of Zr, which is the driving force of Zr diffusion.

Figure 6. SEM micrographs of the U-55 wt.% Zr fuel annealed at 630°C and 700°C for 600 hrs and 1 500 hrs

(a)(b) 630℃, (c)(d) 700℃, (a)(c) 600 hrs, (b)(d) 1 500 hrs

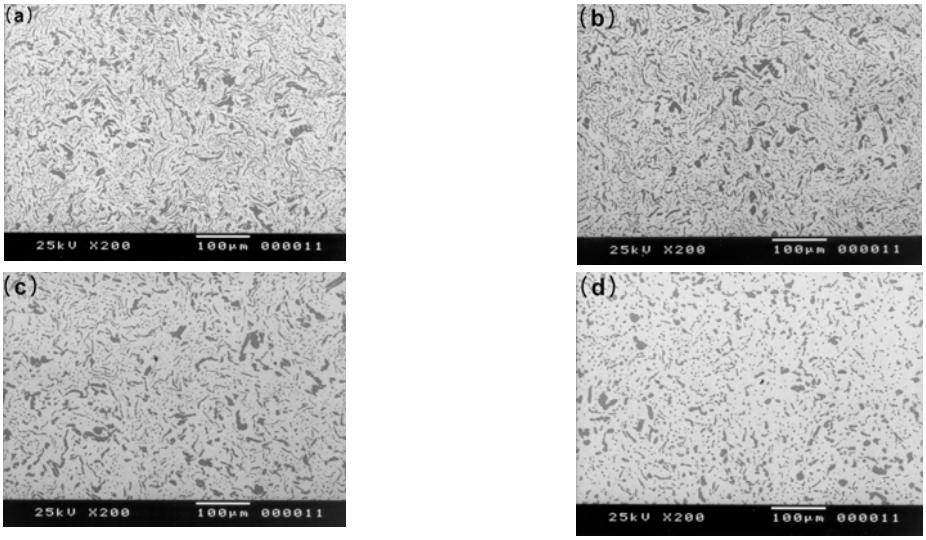

Figure 7. Variation of room temperature hardness of rods after annealing at 630°C and 700°C

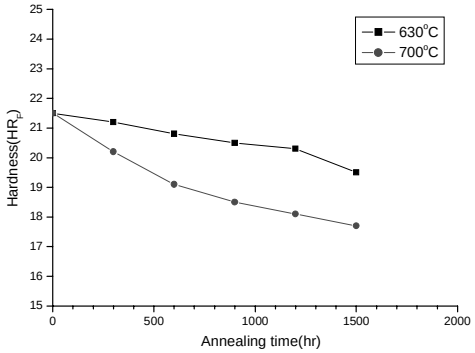

Figure 8. Variation of area fraction of α-Zr phase with annealing times at 630°C and 700°C

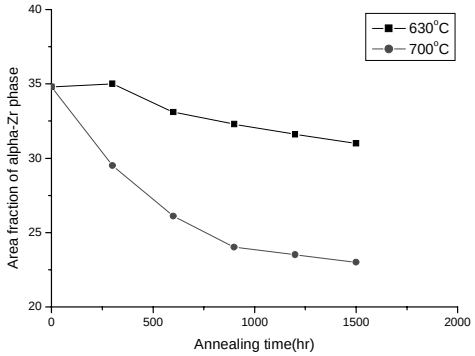

Figure 9 shows EDS line profile results on the interface between U-55Zr and Pb according to annealing time at 650°C. The microstructures of each sample consisted of two distinctive regions – a reaction zone in the vicinity of the surface and an initial zone in the inner area. It should be noted that the thickness of the reaction zone was 26 μm, 36 μm and 46 μm at 100 hrs, 200 hrs and 1 000 hrs, respectively, as the annealing time increased. The reaction zone also consisted of two regions – an α-Zr layer and a Zr-depleted area. The α-Zr layer may be formed by a diffusivity difference between U and Zr atoms (i.e. Zr atom diffuses into the Pb melt during annealing while U is relatively intact due to lower diffusivity). The TRU in the metallic fuel is reported to react with stainless, as a cladding material then forms eutectic at a low temperature. Thus, it is anticipated that the α-Zr layer should effectively act as a reaction barrier with the cladding material.

In order to closely investigate the reaction layer, EDS analysis was performed as shown in Figure 10. The analysis shows that a negligible amount of Pb is present in the very outer layer of the reaction zone with Zr-rich phase (region A). And the α-Zr phase forms a thick layer of ~10 μm underneath the surface (region B). Region C consists of U-rich phase and Zr formed by the decomposition of δ phase. As the annealing time increased, the thickness of the reaction layer from A to C increased to the direction of as-extruded area, region D.

Figure 9. Line profiles of interface of U-55Zr fuel with Pb bonding according to annealing time at 650°C

(a) 100 hrs, (b) 200 hrs, (c) 1 000 hrs

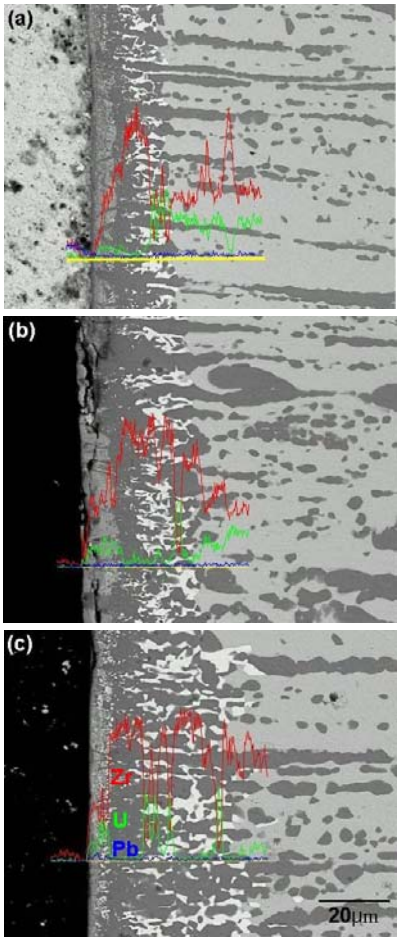

Figure 10. SEM/EDS results of U-55Zr with Pb bonding for 1 000 hrs at 650°C

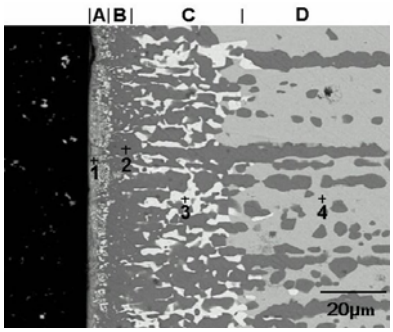

Mark	Pb	U	Zr
1	0.76	19.11	80.13
2		0.37	99.63
3		95.11	4.89
4		31.82	68.18

Figures in at.%.

Conclusions

- The α-Zr phases were distributed in the white δ-UZr_2 phase matrix and the porosity was drastically decreased due to densification from the extrusion process.

- The volume changes of the samples increased slightly and the density variation was negligible. Therefore, it is evident that U-55 wt.% Zr fuel has good thermal stability.

- As annealing time increased, hardness decreased and the decreasing rate of hardness was much higher at 700°C than 630°C. This is attributed to the increase of area fraction of δ phase and the decrease of area fraction of relatively hard α-Zr phase as annealing temperature and time increased.

- The interface between U-55Zr fuel and Pb at annealing time and 650°C consisted of a reaction zone and an initial zone in the inner area. The reaction zone consisted of a α-Zr layer and a Zr-depleted area with thicknesses of 26 μm (100 hrs), 36 μm (200 hrs), 46 μm (1 000 hrs).

REFERENCES

[1] Cho, H.S., *et al*., *Proceedings of the Korean Nuclear Society Spring Meeting*, Jeju, Korea, May 2001.

[2] *Phase Transformation in Materials*, 2nd Ed., D.A. Porter, K.E. Easterling (1992).

SUMMARIES OF TECHNICAL SESSIONS

Chairs: R. Sheffield, B-H. Choi

The summaries contained in this section reflect the views of the respective Chairperson(s) and do not necessarily reflect the views of the technical session group members.

SUMMARY OF TECHNICAL SESSION I: ACCELERATOR RELIABILITY

Chairs: A.C. Mueller, P. Pierini

A huge session – 11 contributions

ADS – Accelerator system designs (4)

- PDS-XADS reference accelerator, D. Vandeplassche.
- Japan SC ADS accelerator, N. Ouchi.
- LANL SC ADS accelerator, R. Garnett.
- FFAG at Kyoto University, M. Tanigaki.

Report on subcomponent operation (4)

- Spoke cavities, C. Mielot.
- China proton source + RFQ, X-L. Guan.
- PSI transport lines, P. Schmeltzbach.
- TRIPS source, G. Ciavola.

Beam dynamics aspects (2)

- Fault tolerance in RF and magnets, J.L. Biarrotte.
- Sensibility studies to errors, I. Shumakov.

Report on SNS commissioning (1), S. Henderson.

ADS accelerator design

Three out of four designs presented are based, to the largest possible extent, on a superconducting linac solution. *Is that a pattern?*

PDS-XADS

Explored cyclotron vs. linac capabilities.

- Performances, reliability, fault tolerance and extrapolation.
- Ruled out cyclotrons.

Designed a linac using reliability/availability guidelines.

- Technology chosen for injector (source + RFQ) and high energy section.
- Still a few options in intermediate energy stage.

Issuing "paper" deliverables but technological activities to present only supported by national programs.

JAERI-KEK

Today, the system design is slightly less developed (will need to further integrate availability issues) ***YET*** amazing technological effort has been made to provide real one-to-one components.

- *Clear focus on development of SC cavity technology* of bulk Nb electropolished cavities that drives most of the program choices.
- *SC linac cryomodule test bench.*
- *Significant tests in near future.*

LANL

All SC linac (after LEDA) fully based on spoke structures.

- Very sound beam dynamics studies.
- Work based on LANL spoke experience.
- Simpler 4 k operation. (Simplicity for reliability?)
- Looking towards 5-cell spokes. (We hope to hear about it!)

In the end 280 m/176 cavities, PDS-XADS has 250 m/190 cavities. Continuing the comparison is worthwhile.

FFAG

A concept from the 1950's (University consortium US) but feasible only as of today (complexity of B-fields). Actual intensities similar to synchrocyclotron (1 mA) but order of magnitude gain predicted. We need to have a comparative assessment following the guidelines of the HPPA3 report, which showed the limits of the reliability characteristics that can be achieved by a cyclotron vs. linac potential.

Subcomponent operation

Proton sources

There now exist at least four sources that clearly satisfy the ADS performance goals.

- [LEDA, SILHI], TRIPS and CIAE.

- Runs in 100-200 h range have confirmed high availability.
- Last thing to check – long (three-month) runs.
- A priori, a twin-source design (PDS-XADS) seems acceptable.

RFQs

- LEDA operation record (more than needed for ADS).
- IPHI, CIAE status reported (we also have TRASCO). ***Big technological effort!***
- Though none is currently operational.

PSI beam lines (0.2->2 mA)

Summary of about 20 years of HPPA beam line operation, including maintenance and reliability considerations.

Spoke cavities

- Tests have been reported with cavity exceeding ADS expectations.
- CNRS has a b = 0.15 under construction.
- Towards full engineering of a structure with all ancillary components (power coupler, CTS) – a cyromodule is planned by CNRS.
- *Importance of international access and collaboration around "regional" technological pole of excellence – Ile de France SUPRATECH.*

Beam dynamics aspects

Fault tolerance

- RF faults: can tolerate cavity loss (!) but need procedures for a fast reset of the linac to allow beam transmission, followed by a slower tuning to minimise beam losses.
- Magnet faults: the doublet focussing scheme (plus large linac SC cavity bore) can accept a full quadrupole doublet fault maintaining beam specs on target.

Sensitivity to fabrication tolerances

- Analytical and numerical methods can be used to assess the sensitivity to fabrication tolerances in devices such as RFQ or periodic beam lines.

SNS – A (pulsed) 1.4 MW SC proton HPPA

1 GeV 6% d.f., 1.4 mA average current (77% as of 01/2004)

Front end has been commissioned with beam.

- Source, RFQ, DTL 1-3 to 40 MeV, nominal parameters.

Installation and commissioning is steadily proceeding.

- Cavities tested with higher than expected gradients.
- DTL 4-6 and CCL 1-3 by August.
- Cryogenics system cooldown very soon.
- Start SC linac commissioning at the beginning of 2005.
- ***81% energy gain from SC RF*.**
- Budget figures of interest for XADS.

Plan availability increase from 50% to 90% in five years.

We are eager to know the results of the SC linac commissioning.

Significant set-up that will demonstrate it is possible to transfer the digital RF controls used in TESLA to a SC proton machine.

- It is needed for the Lorentz force detuning of the pulsed cavities.
- Very important test bench for the path towards fault tolerance capabilities.

Long-term upgrade plan to 2-4 MW!

- Space already allocated for upgrade in high-beta section.

Conclusion

A lot of information and lessons learned from experimental accelerator development programmes in other fields of physics…

…but need for identified resources for XADS reliability programmes (US, Europe) and

…the availability/reliability requirements are unique for ADS.

Better situation in Asia (but present designs not optimised for fault tolerance).

SUMMARY OF TECHNICAL SESSION II: TARGET, WINDOW AND COOLANT TECHNOLOGY

Chairs: X. Cheng, T-Y. Song

"Research & Development on Lead-bismuth Technology for Accelerator-driven Transmutation System in JAERI" by Y. Kurata (JAERI), *et al.*

JAERI's corrosion loop (JLBL-1) test (350/400-450°C, 1 m/s).

- Corrosion depth of 316SS at high temperature part: ~100 μm/3 000 h.
- At low temperature part: deposition of Pb/Bi and Fe-Cr, plugging (needed filter).

MES (Mitsui Engineering and Shipbuilding Co., Ltd.) loop (350- 450°C, 0.4-0.6 m/s).

- 1.0×10^{-5} wt.% oxygen, 1 000 h, F82H/JPCA sample: no significant corrosion.

Static corrosion test (F82H, Mod. 9Cr-1Mo 316ss, etc.)

- 450°C, 3.2×10^{-4} wt.% oxygen, 3 000 h: increasing Cr $\rightarrow$ decreasing corrosion depth.
- 550°C, 1.2×10^{-3} wt.% oxygen, 3 000 h: Si added steel shows good corrosion resistance.

"Vacuum Gas Dynamics Investigation and Experimental Results on the TRASCO-ADS Windowless Interface" by P. Michelato (INFN), *et al.*

- Windowless interface system is being developed as part of the TRASCO program. TRASCO program is to develop ADS. INFN, ENEA and Italian companies are involved in TRASCO.
- Pumping, vacuum and cold trap systems were investigated.
- LBE evaporation rate was measured and model was validated.
- Source terms of hydrogen isotopes and noble gases were investigated.
- Te was used for Po evaporation measurement and Hg experiment is under study.

"Corrosion Test in the Static Condition and Installation of Corrosion Loop at KAERI for Lead-bismuth Eutectic" by J-E. Cha (KAERI), *et al.*

KAERI installed Pb-Bi static corrosion test facility in 2003.

- Filtering samples for loop test.
- Oxygen control by H_2/H_2O, max. 800°C.
- Test performed at 650°C, $< 10^{-8}/10^{-6}$ wt.%, < 500 h for 316L/HT-9/T91.
  - Need to repeat the test to see consistency of data.

KAERI's corrosion loop.

- Completed design and fabrication of components in 2003.
- Plan to complete construction of the loop by September 2004.

"The Vacuum Interface Compatibility Experiment (VICE)" by P. Schuurmans (SCK•CEN), *et al.*

MYRRHA adopts windowless target system.

Problem: Gas/vapour emanation at windowless target surface.

- Outgassing.
- Spallation product.
- LBE evaporation.

VICE: Realistic geometry of lower beam line.

- Spallation product mix assessment was performed.
- Pre-conditioning vessel tested.
- Pb-Bi evaporation experiment performed.

"The Introduction of a Dual Injection Tube for the Design of a 20 MW Lead-bismuth Target System" by C-H. Cho (KAERI), *et al.*

DIT (dual injection tube) was introduced to improve KAERI's HYPER target design.

- Reduce target flow rate: lower pumping power, reduce thermal stripping.

Introduction of DIT (1 GeV, beam diameter 30 cm).

- Max. allowable beam current: 14 mA (parabolic), 21 mA (uniform).

Parabolic beam: smaller diameter of inner injection tube is recommended.

- Uniform beam: larger diameter of inner injection tube is recommended.

"Design Study Around Beam Window of ADS" by H. Oigawa (JAERI), *et al.*

Target and beam window design were performed for JAERI's ADS system.

- 1.5 GeV, Pb-Bi target, k_{eff} (0.97), 800 MWth.

A 30 MW beam was studied.

- Beam duct(45 cm), inlet temperature (300°C).
- Window: HCM12A (thickness: 2-4 mm).

Max. temperature of window outer surface: 490°C.

Max. stress: 106 MPa.

"Primary Isotope Yields for MSDM Calculations of Spallation Reactions on ^{208}Pb with Proton Energy of 1 GeV" by S. Fan (CIAE), *et al.*

- MSDM code is a high-energy transport code used to simulate spallation reaction.
- Original MSDM code was modified to take into account effects related to level densities.
- After the modification, new calculation results turned out to agree with some experimental data of 1 GeV spallation reaction on a ^{208}Pb target.
- But new MSDM results do not agree well when compared with the experimental data of neutron-rich nuclides.

"CFD Analysis on the Active Part of the Window Target Unit for LBE-cooled XADS" by N.I. Tak (FZK), *et al.*

CFD analysis was performed for XADS target.

- Target (Pb-Bi), natural convection cooling, inlet temperature (233°C).
- 600 MeV, 6 mA.

Steady-state case.

- Reduction in window thickness (at centre) to 2 mm leads to allowable max. temperature of outer window surface (limit: 500°C).

Transient case.

- At 1 s beam trip conditions, max. temperature drop is 207°C (412°C/s).

"Optimisation of a Code to Improve Spallation Yield Predictions in an ADS Target System" by T. Sawada (TIT), *et al.*

- PHITS: General purpose particle and heavy ion transport code system.
- Tried to optimize PHITS so that it can be used for ADS-related calculations with precision.

- Calculation prediction can be improved by:
  - Increasing the excited energy for the evaporation stage.
  - Reducing the pre-equilibrium stage.
  - Changing the timescale or cut-off energy for the intra-cascade stage.

SUMMARY OF TECHNICAL SESSION III: SUBCRITICAL SYSTEM DESIGN AND ADS SIMULATIONS

Chairs: W. Gudowski, H. Oigawa

Categories of presentations

- Research/demo facility design described or referenced to:
  - Kyoto, MYRRHA, TRADE.
- Conceptual design of full-scale transmuter:
  - Burn-up swing and CSMSR.
- Design of ADS – components:
  - MYRRHA vessel studies, accelerator and BTL for TRADE.
- Benchmark on beam interruptions.

Research/demo facility design

- More international harmonisation would be beneficial for many parties (the same is valid for Pb/Bi technology experiments):
  - Similar experiments are under preparation or planned – better focus and task distribution would be desirable (*probably not easy to agree upon).*
  - *Real accelerators are going to be coupled with subcritical cores in the near future.*
  - **ADS, demo, PoP, etc. facilities should have clear objectives, *internationally harmonised*, in order to focus on investigation of important parameters for a real transmutation facility without unnecessary duplications.**
    - *RACE experiment in US not reported.*
    - *SAD (Russia, ISTC) not reported.*

Conceptual design of full-scale transmuter

- Visible convergence for Pb/Bi system design concerning:
  - Power (800 MWth).
  - K_{eff} (0.97).
  - Fuel options (nitride intensively studied but not exclusively).
- Big variety of core designs, we consider that there is great potential to optimise ADS performance.
- Variety of fuel compositions and fuel cycle.

- Fast information exchange between different groups is definitely beneficial for the progress of ADS concepts.

- Interesting alternative options for ADS under investigation; we would like to have a bit more clarity on CSMSR.

Design of ADS – components

Very interesting engineering work taking us closer to practical solutions.

- Even if the choice of accelerator is still an open question, it is clear that first PoP experiments will be done with cyclotron (Kyoto, TRADE, SAD, etc.).

Benchmark on beam interruptions

Easy conclusions:

- Everybody happy with benchmarks so time for validation activity.

- Time for an international ***validation experiment***? Should it have been planned already? Can we use existing facilities? Should we take into account facilities under advanced planning/ construction?

- Any role for OECD/NEA?

Final conclusions

- Interesting session covering very different topics with direct links to other sessions.

- Final recommendations/advice to participants and OECD/NEA should be done based on synthesis of all sessions.

SUMMARY OF TECHNICAL SESSION IV: SAFETY AND CONTROL OF ADS

Chairs: J-M. Lagniel, P. Coddington

Two papers – very design specific – were presented describing the results of WP2 of the PDS-XADS project and covering the two 80 XADS designs. The conclusions reached were: a) a Pb-Bi reactor ADS has significant safety characteristics, particularly if it has a low Δp and a high natural circulation flow rate, and b) a gas-cooled system has a short space period for beam-shut off end. Any pump-driven system will lie between these two.

We heard about the new Pb-Bi loop, which provides neutral circulation, etc., and is useful for only Pb-Bi system.

An interesting paper was presented describing a proposal for dynamic control of an ADS by linking.

The intriguing use of void boxes with mini cycles to control reactivity swings was discussed as well as plans to look at burnable poisons.

A paper compared the PDS-ADS Pb-Bi 80 MW and the reactor design considered as part of the EU FUTURE project.

- This has oxide fuels with Am and Cm, leading to different fuel thermal properties and reduced ≥/ and large positive void worth.

- Compensation results presented for TOP.

  – UTOP results sensitive to fuel properties – providing small in comparison to the subcriticality level. Power change is the same.

  – ULOF because of high subcriticality margin. Power remains ~1.0 so response is function of flow reduction, i.e. system behaviour.

- *Results are sensitive* to the change in fuel thermal properties.

SUMMARY OF TECHNICAL SESSION V: ADS EXPERIMENTS AND TEST FACILITIES

Chairs: P. D'hondt, V. Bhatnagar

Summary

- Five (5) papers were presented.
- One (1) paper was not presented: "Core Neutronics Assessment for TRADE Experiments" by D.G. Naberezhnev, *et al*. (ANL, USA).

Paper 1

- Presented by H. Oigawa (JAERI, Japan).
- Entitled "Concept of Transmutation Experimental Facility".
- Remarks – within the J-PARC complex:
  - **TEF-P**: Physics experiments with MA nitride fuel (600 MeV, 10 W), H^- beam as a mock-up of subcritical facility.
  - Validation of neutronics, performance test of ADS and transmutation of MA and LLFP.
  - **TEF-T**: Material irradiation tests (200 kW beam, dia. = 4 cm, 10^{14} n/cm^2/s) in flowing LBE without nuclear fuel.
  - Test lifetime of window, structural material under (n, p) irradiation, compatibility of materials with LBE, operation and control of spallation target system
  - Decision and operation 2008 onwards?

Paper 2

- Presented by M. Hron (NRI, Czech Republic).
- Entitled "Experimental Verification of Selected Transmutation Technology and Materials for Basic Components of a Demonstration Transmuter with Liquid Fuel Based on Molten Fluorides".
- Remarks:
  - **SPHINX**: spent hot fuel incinerator by neutron flux project.
  - **Accelerator-driven concept** of MA transmutation demonstrator with molten salt using dry processing.
  - **BLANKA 1**: fluoride material testing probe irradiated in research reactor at NRI, Rez (T, p measurements).
  - **BLANKA 4**: Larger assembly also installed.
  - EC project: **MOST** and Russian **AMPULA.**

Paper 3

- Presented by Y.H. Kim (KAERI, Korea).
- Entitled “Application of the HYPER System to the DUPIC Fuel Cycle”.
- Remarks:
  - DUPIC: PWR spent fuel recycled in CANDU reactor after a simple refabrication process.
  - After pyroprocessing, this spent fuel can be transmuted in HYPER system.
  - Proliferation resistance cycle, uranium resource saving.
  - Fuel cycle cost comparable to once-through cycle.
  - HYPER system preliminary design features and performance analysis presented.
  - Utilities still have to show interest in this cycle.

Paper 4

- Presented by P. Coddington (PSI, CH).
- Entitled “Numerical Comparisons Between Neutronic Characteristics of MUSE4 Configurations and XADS-type Models”.
- Remarks:
  - Aim was to make representativity calculations between MUSE4 and XADS concepts for Na, He and LBE-cooled systems.
  - Results do not show good representation in LBE case.
  - There were comments from the audience regarding the utility of the calculations as configurations do not match.
  - Pb-loaded MUSE4 system could be better for these calculations.
  - Suggestion for TRADE simulation was made but not found to be of great value.

Paper 5

- Presented by B.S. Lee (KAERI, Korea).
- Entitled “Reaction of Pb Bonding Between Fuel and Cladding”.

- Remarks:
  - Presentation included the fabrication process and a study of thermal stability of U-Zr fuel.
  - U-55 wt.% Zr fuel has good thermal stability.
  - A significant interaction between U-55 wt.% Zr and Pb is observed at 650°C.
  - Thickness of the interaction zone is 26, 36, 46 μm when the sample is immersed in liquid Pb for 100, 200, 1 000 hrs, respectively.

SUMMARIES OF WORKING GROUP DISCUSSION SESSIONS

Chairs: R. Sheffield, B-H. Choi

The summaries contained in this section reflect the views of the respective Chairperson(s) and do not necessarily reflect the views of the working group members.

SUMMARY OF WORKING GROUP DISCUSSION ON ACCELERATORS

Chair: P.K. Sigg

Discussion

Suggestions (Y.L. Cho) on chosen topics – availability, reliability, high intensity and efficiency:

- Define ***observation period***; Suggestion (A. Mueller): For three months of operation, followed by one month shutdown period (maintenance, restocking).

  – Comment (T. Mukaiyama): For future industrial applications (burners), observation period should be greater than one year!

Beam trips: Neglect events < 1 sec. ⟶ **goal: only five trips/month, > 1 sec.**!

- Comment (R. Sheffield): Trip of > 10 sec. ⟶ reactor will shut down!

Reliability culture: Suggestion is to **go to industrial standards** (e.g. aerospace industry).

- Comment (P. Schmelzbach): There is a trade-off between system complexity and redundancy!

- Definition (P. Pierini): Differentiate component vs. system reliability; this should be clearly identified in specs.

- Comment: Recording (data logging) is not sufficient ⟶ (H. Aït Abderrahim, A. Mueller) interpretation is essential, affects the quality of the available database.

Suggestion: Agree upon/introduce common standards or guidelines! (But WHO will do that?)

- Comment: Safety increases reliability (!?)

- Comment (R. Sheffield): Diagnostics can be failure cause – false alarms can be frequent (see P. Schmelzbach).

- Comment (several speakers): Aside from well known "trouble areas" (vacuum, RF systems), many interruptions are caused by support system failures (power grid, cooling systems, etc.), and are not directly influenced by accelerator design).

- Observation: Many machines are "experimental", that is to say, prototypes (one of a kind), so reliability is not the same as in industrial plants (including reactors).

- Comment (D. Vandeplassche): Commercial cyclotrons (e.g. for medical applications) are "finished" at one time ⟶ *no more tinkering*!

Energy efficiency; Question (T. Mukaiyama): Can anyone give a number for overall electrical efficiency?

- Discussion: You can expect a maximum of ~50% (based on several opinions – R. Sheffield, A. Mueller...)

- Comment (R. Sheffield): There exists a trade-off between availability and efficiency ⟶ redundancy (like hot spares) is detrimental to energy efficiency!

Question (L. Ponomarev): What amount of beam power is desired for ADS? Or, how much power can reactors reasonably take? (The question has been asked before.)

Answer (H. Aït Abderrahim, A. Mueller, others): 10-20 MW is sufficient!

Non-technical issues

Funding: What can be done to increase funding for ADS? On the accelerator side (A. Mueller), accelerator community seems to get short changed. Suggestion: Widen the spectrum of applications offered for accelerator development!

Manpower: There seems to be a shortage of qualified, experienced accelerator scientists. Question: What can be done to alleviate the problem in view of the increasing demand for new/existing projects?

Suggestions: More aggressive advertising in universities, career planning, etc. More effort is needed!

Conclusion

Questions yet to be resolved (T. Mukaiyama): After having worked out solutions to some of the key questions (such as: what accelerator type is "best" → try SC linac; what are the costs → first estimates available for prototype machines; what is the energy consumption → see above discussion on energy efficiency), there are still a few open questions. At present, trying to answer them is only guesswork. Typically, questions such as "When will what accelerator be fully operational?" and "When will the trip rate reach the desired value?" are still waiting to be answered in the future. The prototypes now under construction will help us in providing answers to these questions and many smaller issues.

SUMMARY OF WORKING GROUP DISCUSSION ON SUBCRITICAL SYSTEMS AND INTERFACE ENGINEERING

Chair: W. Gudowski

What are the expected results of our discussion?

- Understanding where we are internationally with ADS programmes and to clarify the details.
- Understanding to where different projects are heading.
- Finding synergies and benefits in international collaboration and a good balance between COMPETITION and COLLABORATION.
- Agreement on what message we should convey to nuclear utilities and to the nuclear community as a whole on ADS and P&T issues.
- Some important technical issues not yet answered:
  - What is the maximum beam power accepted by a reactor? (Reactor perspective is not only beam trips!)
- Advise OECD/NEA on priorities in its P&T and ADS activities.

Good starting point – conclusions of M. Salvatores' presentation regarding putting an international perspective on the future of ADS

"The perceived role of P&T has evolved from an optional strategy aiming to reduce the burden on deep geological storage, to an integral component of future nuclear systems. In this new perspective, 'transmutation' is achieved in an optimum manner in a fast neutron reactor, with the homogeneous recycling of not separated TRU."

The main reactions to this statement are:

- The perception by the geological disposal community is not in line with the statement especially perceived in EURADWASTE 2004. P&T is perceived for the moment as a burden for geological disposal. **Thus, there is a real need for communication between the two communities**.
- In an electricity market open for competition it will be difficult to make a dirty fuel cycle acceptable to the utilities. **This will be jeopardizing the competitiveness of nuclear electricity generation** (one of the Gen. IV criteria).
- Multiple recycling needed within P&T is unacceptable to utilities as considered in the homogeneous burning.
- Transmutation is achieved in an optimum manner in a fast neutron system, be it a critical reactor or an ADS system.

"Specialized devices, like ADS, can have a role in a transition scenario between the present LWR-dominated to a future FR-dominated situation."

The main reactions to this statement are:

- ADS is a dedicated system for waste burning but not simply for the transition period between the LWR era and the FR-dominated era. **ADS will be a dedicated waste burner also when the FR will be deployed for economical reasons**.

- Even if ADS will be for a transition period, this will be a long one (**around one century**).

- Why such a huge effort for a transition period if limited to 20 to 30 years as claimed by the Gen. IV community?

"In any case, ADS deployment can hardly be considered by a single country in isolation and a 'regional' approach is needed, where countries with rather different policies in terms of nuclear power development can join efforts to develop shared facilities."

The main reactions to this statement are:

- **This is true at the Asian level as a Japan-China-Korea initiative** has begun to join the effort related to the R&D support programme for ADS and even to join the effort for ADS facilities in the J-PARC ADS part (the latest statement on the wishes of Japan; enlargement to world collaboration).

- A joint effort in R&D support can also be achieved through the ISTC initiatives.

- This is true at European level under the EC FP (4, 5, 6) programmes for R&D support but a step further would be needed in terms of realisation.

Target issues

"The best solution issue – window or windowless."

The main reactions to this statement are:

- Windowless can be a favoured design under the condition that after a hydraulic demonstration and a vacuum interface compatibility demonstration, the realisation of an experimental testing is realised.

- Scale 1/1 experiment is needed.

- If windowless can be accepted, one should not avoid a cold window to protect the accelerator from eventual contamination.

- The technology of cold windows, even used in other applications, needs to be demonstrated at the high-power proton beams considered for ADS accelerators.

- An assessment of the maximum power acceptable in the windowless design should be established.

- The optimum acceptable proton energy for ADS application is 600 to 800 MeV; thus one cannot relax more on the energy to avoid high currents.

"Can we envisage an experiment in the near future to help us resolve this issue? A WINDOWLESS MEGAPIE? Where and when?"

The main reactions to this statement are:

- Yes such an experiment should be prepared and performed.

- An attempt was done during the FP6 project IP EUROTRANS but due to budget shorting this is not taken in the present programme.

- PSI and SCK•CEN are thinking about such an experiment.

"Too little work has been done on the consequences of a window break."

The main reactions to this statement are:

- For the first time, work on this topic has been reported by JAERI and the group recommends an increase in this effort.

SUMMARY OF WORKING GROUP DISCUSSION ON SAFETY AND CONTROL OF ADS

Chair: P. Coddington

Points of discussion

We thought of a good idea to propose to OECD/NEA/NSC. There should be a safety-related benchmark to follow the beam trip benchmark.

- Eight-hundred (800) MW transmuters with Pb-Bi coolant with **MA load** fuel and typical beta, reactivity, $\mathbf{k_{eff}}$.
- **Both at beginning and end of cycle**.
- Also during hot standby conditions.

Safety activities

Licensing challenge.

Subcritical:

New concept	Length of time to get CSR	> ABWR
New coolant		> AP600/AP1000
New fuel		

Do not try all three at once.

Safety guideline – DEC

Core melt – DEC

Two realistic analyses of core melt/recriticality is thought too difficult (at this time) to analyse.

Therefore, the **core melt frequency** needs to be so low to be in the residual risk category.

- For **detectable** transients, if beam trip is the only barrier then the failure rate needs to be $\mathbf{10^{8}}$.
- For **undetectable** transients, these have to be designed out. For example, open core design from JAERI to avoid SA blockages.

Safety

Much discussion

ADS offers advantages over critical systems for **reactivity accidents**.

However, **beam trip** (without shutdown system) is the first and only shutdown mechanism.

- All system transients/design must be analysed to **define** GRACE PERIOD for beam shut off to determine:
  - Nature and location response of detection system for all possible accidents.
  - Processing logic.
  - Definition of signal that goes to the accelerator.

All this needs a high reliability since this may be the only barrier to **core melt**.

This means that a review needs to be made on **safety-related instrumentation**.

Temperature increases:

- Thermocouples where/**each SA, core exit**.
- Response time – core exit – problems with flow mixing, etc.
- Power monitor.
- Subcriticality monitor.

For DBs – safety guidelines

Goal – no off-site release. Based on analysis of PDS-XADS, there will be limited clad failures.

But this is **not obvious** since we saw for the gas reactor. DBs may lead to pin failure and therefore activity release to the containment.

This will then help to define the requirements for the **containment** – an issue **not discussed**.

ADS reactivity control

Shutdown

Discussion relating to an alternative shutdown mechanism.

Conclusion that a **set of "safety" shutdown rods** should be considered, these being most relevant when k_{eff} becomes close to 1.0.

Burn-up control

Discussion on the presentations:

- Use of burnable poisons.
- Limited use of control rods.
- Void boxes (for mini cycles).
- Link to the beam power, to the core power.
- Generally, there are safety considerations for constant (fixed) beam power.

Definition of optimum subcriticality level

This needs to be better quantified rather then left to guesswork and big margin.

Annex 1

LIST OF WORKSHOP ORGANISERS

Honorary co-chairs

Luis Echávarri, Director-General of OECD/NEA
Chung-Won Cho, Director-General of Nuclear Energy, Ministry of Science and Technology (Korea)

General co-chairs

Byong-Ho Choi, Director, High Power Proton Accelerator Development, KAERI (Korea)
Richard Sheffield, Los Alamos National Laboratory (USA)

Scientific secretary

Byung-Chan Na (OECD/NEA)

International scientific advisors

Richard Sheffield (LANL, USA), Chair
Pierre D'hondt (SCK•CEN, Belgium)
Yves Jongen (IBA, Belgium)
Alex Mueller (CNRS Orsay, France)
Dominique Warin (CEA, France)
Guy Laffont (CEA, France)
Jean-Marie Lagniel (CEA, France)
Concetta Fazio (FZK, Germany)
Guenter Bauer (FZJ, Germany)
Joachim Knebel (FZK, Germany)
Alberto Negrini (Ansaldo, Italy)
Carlo Pagani (INFN, Italy)
Stefano Monti (ENEA, Italy)
Hideki Takano (JAERI, Japan)
Minoru Takahashi (Tokyo Institute of Technology, Japan)
Nobuo Ouchi (JAERI, Japan)
Yuji Kurata (JAERI, Japan)
Byong-Ho Choi (KAERI, Korea)
Tae-Yung Song (KAERI, Korea)
Won-Seok Park (KAERI, Korea)
Dolores Gomez-Briceno (CIEMAT, Spain)
Enrique Gonzalez (CIEMAT, Spain)

Marcus Eriksson (RIT, Sweden)
Waclaw Gudowski (RIT, Sweden)
Thomas Stammbach (PSI, Switzerland)
Colin Zimmerman (BNFL, UK)
David Hill (ORNL, USA)
Eric Pitcher (LANL, USA)
George Lawrence (LANL, USA)
Jordi Roglans (ANL, USA)
Michael Cappiello (LANL, USA)
Phillip Finck (ANL, USA)
Kemal Pasamehmetglu (LANL, USA)
Rusi P. Taleyarkhan (ORNL, USA)

Local organising committee

In-Soo Ko, POSTECH, local organising committee Chair
Yong-Sub Cho, KAERI
Sang-Hoon Nam, Pohang Accelerator Laboratory (PAL)
Seung-Jeong Noh, Dankook University
Moo-Hyun Cho, POSTECH
Yong-Seok Hwang, Seoul National University
Jong-Bum Choi, Chonbuk National University
Sung-Oh Cho, KAIST
Jae-Hyung You, KAERI
Won-Seok Park, KAERI
Tae-Yung Song, KAERI
Chang-Sup Lee, KEPRI
Seong-Man Bae, KEPRI
Jae-Won Park, KAERI, local organising committee Co-ordinator

Annex 2

LIST OF PARTICIPANTS

BELGIUM

AÏT ABDERRAHIM, Hamid
SCK•CEN, Reactor Physics & Myrrha Dept.
200 Boeretang
B-2400 MOL
Tel: +32 14 33 22 77
Fax: +32 14 32 15 29
Eml:haitabde@sckcen.be

D'HONDT, Pierre
SCK•CEN
Boeretang 200
B-2400 MOL
Tel: +32 14 33 22 00
Fax: +32 14 32 15 29
Eml:pdhondt@sckcen.be

HAECK, Wim
SCK•CEN
Boeretang 200
B-2400 MOL
Tel: +32 14 33 22 71
Fax: +32 14 32 15 29
Eml:whaeck@sckcen.be

VANDEPLASSCHE, Dirk
IBA, Chemin du Cyclotron 3
B-1348 LOUVAIN-LA-NEUVE
Tel: +32 10 47 58 49
Fax: +32 10 47 58 47
Eml:dirk@iba.be

CHINA (PEOPLE'S REPUBLIC OF)

FAN, Sheng
China Institute of Atomic Energy
P.O. Box 275 (41)
BEIJING 102413
Tel: +86 10 693 57 670
Fax: +86 10 693 57 008
Eml:sfan@iris.ciae.ac.cn

GUAN, Xialing
China Institute of Atomic Energy
Institute of High Energy Physics
P.O. Box 918
BEIJING 100039
Tel: +86 10 693 58 804
Fax: +86 10 693 57 787
Eml:guanxl@mail.ihep.ac.cn

HAN, Yinlu
China Institute of Atomic Energy
P.O. Box 275-41
BEIJING 102413
Tel: +86 10 693 57 275
Fax: +86 10 693 57 787
Eml:han@iris.ciae.ac.cn

LI, Jigen
China Institute of Atomic Energy
P.O. Box 275-56
BEIJING 102413

Tel: +86 10 693 58 284
Fax: +86 10 693 57 787
Eml:jigen@iris.ciae.ac.cn

SHI, Yongqian
China Institute of Atomic Energy
P.O. Box 275-45
BEIJING 102413

Tel: +86 10 693 58 028
Fax: +86 10 693 57 787
Eml:shiyq@iris.ciae.ac.cn

XIA, Haihong
China Institute of Atomic Energy
P.O. Box 275-80
BEIJING 102413

Tel: +86 10 693 58 798
Fax: +86 10 693 57 787
Eml:xiahh@iris.ciae.ac.cn

CZECH REPUBLIC

HOSNEDL, Pavel
SKODA Nuclear Machinery Ltd.
Orlik 266
CZ-316 06 PLZEN

Tel: +420 6 05 22 16 66
Fax: +420 3 78 04 27 49
Eml:Pavel.Hosnedl@skoda-js.cz

HRON, Miloslav Joseph
Nuclear Research Institute Rez, plc
CZ-250 68 REZ

Tel: +420 7 28 53 01 92
Fax: +420 2 66 17 23 98
Eml:hron@nri.cz

PEKA, Ivo
Nuclear Research Institute
Rez 130
CZ-250 68 REZ

Tel: +420 6 02 18 59 44
Fax: +420 2 66 17 23 98
Eml:hro@ujv.cz

FRANCE

BOKOV, Pavel
CEA Saclay
DSM/DAPNIA/SPhN Bât. 703
F-91191 GIF-SUR-YVETTE

Tel: +33 1 69 08 78 47
Fax: +33 1 69 08 75 84
Eml:pavel.bokov@cea.fr

LAGNIEL, Jean-Michel
CEA DAM
DPTA-SP2A, BP 12
F-91680 BRUYÈRES-LE-CHÂTEL

Tel: +33 1 69 26 52 49
Fax: +33 1 69 26 70 24
Eml:jean-michel.lagniel@cea.fr

MIÉLOT, Christophe
IPN Orsay
IPNO Bât. 106, 15 rue G. Clémenceau
F-91406 ORSAY CEDEX

Tel: +33 1 69 15 71 27
Fax: +33 1 69 15 77 35
Eml:mielot@ipno.in2p3.fr

MIÉLOT-WIRATKASEM, Worachina
5 rue G. Clémenceau
F-91406 ORSAY

Tel: +33 1 69 15 71 27
Fax: +33 1 69 15 77 35
Eml:worachina@yahoo.com

MUELLER, Alex
Dept. Head, R&D Accelerators/Exotic Beams
Institut de Physique Nucléaire
Bât. 106, 15 rue G. Clémenceau
F-91406 ORSAY CEDEX
Tel: +33 1 69 15 62 40
Fax: +33 1 69 15 77 35
Eml:mueller@ipno.in2p3.fr

SALVATORES, Massimo
Commissariat à l'Énergie Atomique
DEN/DIR/AFF-INT Bldg. 101
CEA Cadarache
F-13108 SAINT-PAUL-LEZ-DURANCE
Tel: +33 4 42 25 33 65
Fax: +33 4 42 25 41 42
Eml:massimo.salvatores@cea.fr

GERMANY

CHEN, Xue-Nong
Forschungszentrum Karlsruhe
Inst. for Nuclear and Energy Technologies
Hermann-von-Helmholtz-Platz 1
D-76344 EGGENSTEIN-LEOPOLDSHAFEN
Tel: +49 72 47 82 59 85
Fax: +49 72 47 82 38 24
Eml:xchen@iket.fzk.de

CHENG, Xu
Forschungszentrum Kalrsruhe
Inst. for Nuclear and Energy Technologies
Hermann-von-Helmholtz-Platz 1
D-76344 EGGENSTEIN-LEOPOLDSHAFEN
Tel: +49 72 47 82 48 97
Fax: +49 72 47 82 48 37
Eml:xu.cheng@iket.fzk.de

INDONESIA

MUKAIYAMA, Takehiko
Director, Jakarta Liaison Office
Japan Atomic Industrial Forum, Inc.
MidPlaza 1, 12th Floor
JL. Jend. Sudirman Kav. 10-11
JAKARTA 10220
Tel: +62 21 570 7571
Fax: +62 21 570 7577
Eml:mukaiyamat@biz.net.id

ITALY

BURGAZZI, Luciano
FIC-NUC ENEA
Via Martiri di Monte Sole, 4
I-40129 BOLOGNA
Tel: +39 051 60 98 556
Fax: +39 051 60 98 279
Eml:burgazzi@bologna.enea.it

CIAVOLA, Giovanni
Group Leader
Istituto Nazionale de Fisica Nucleare – LNS
Via S. Sofia, 44
I-95123 CATANIA
Tel: +39 095 54 22 62
Fax: +39 095 54 23 02
Eml:celona@lns.infn.it

COMUNIAN, Michele
INFN-Legnaro National Laboratories
Viale dell'universita, 2
I-35020 Legnaro, PADOVA
Tel: +39 049 806 85 01
Fax: +39 049 806 88 29
Eml:michele.comunian@lnl.infn.it

FAGOTTI, Enrico
INFN-LNL
Viale dell'universita, 2
I-35020 Legnaro, PADOVA
Tel: +39 049 806 84 13
Fax: +39 049 806 88 29
Eml:enrico.fagotti@lnl.infn.it

MICHELATO, Paolo
INFN-Milano-LASA
Via Fratelli Cervi, 201
I-20090 Segrate, MILANO
Tel: +39 02 503 19 562
Fax: +39 02 503 19 543
Eml:Paolo.Michelato@mi.infn.it

PICARDI, Luigi
ENEA
Via E. Fermi, 45
I-00044 FRASCATI
Tel: +39 069 40 05 774
Fax: +39 069 40 05 334
Eml:picardi@frascati.enea.it

PIERINI, Paolo
INFN-Milano-LASA
Via Fratelli Cervi, 201
I-20090 Segrate, MILANO
Tel: +39 02 23 92 560
Fax: +39 02 23 92 543
Eml:paolo.pierini@mi.infn.it

JAPAN

KOBAYASHI, Hiroshi
Tokyo Institute of Technology
N1-459, Ninokata Laboratory
2-12-1 Ookayama Megro
Tel: +81 3 5734 3062
Fax: +81 3 5734 3062
Eml:hkobayas@geo.titech.ac.jp

KURATA, Yuji
Nuclear Transmutation Group
Center for Neutron Science, JEARI
Tokai-mura, Naka-gun, Ibaraki-ken 319-1195
Tel: +81 29 282 5059
Fax: +81 29 282 6489
Eml:ykurata@popsvr.tokai.jaeri.go.jp

MISAWA, Tsuyoshi
Research Reactor Institute
Kyoto University
Kumatori, Sennan, Osaka 590-0494
Tel: +81 724 51 2376
Fax: +81 724 51 2603
Eml:misa@kuca.rri.kyoto-u.ac.jp

MISHIMA, Kaichiro
Research Reactor Institute
Kyoto University
Kumatori-cho, Sennan-gu, Osaka 590-0494
Tel: +81 724 51 2449
Fax: +81 724 51 2637
Eml:mishima@rri.kyoto-u.ac.jp

NISHIHARA, Kenji
Center for Neutron Science, JAERI
2-4 Shirakata-shirane
Tokai-mura, Naka-gun, Ibaraki-ken 319-1195
Tel: +81 029 282 6935
Fax: +81 029 282 5671
Eml:nishi@omega.tokai.jaeri.go.jp

NOGUCHI, Shuichi
KEK Accelerator Laboratory
1-1 Oho
Tsukuba-shi, Ibaraki-ken 305-0801
Tel: +81 29 864 5230
Fax: +81 29 864 3182
Eml:shuichi.noguchi@kek.jp

OIGAWA, Hiroyuki
Nuclear Transmutation Group
Center for Proton Acc. Facilities, JAERI
Tokai-mura, Ibaraki-ken 319-1195
Tel: +81 29 282 6935
Fax: +81 29 282 5671
Eml:oigawa@omega.tokai.jaeri.go.jp

OUCHI, Nobuo
Accelerator Group, JAERI
Tokai-mura, Naka-gun, Ibaraki-ken 319-1195
Tel: +81 29 282 5461
Fax: +81 29 282 5663
Eml:ouchi@linac.tokai.jaeri.go.jp

TAKANO, Hideki
Deputy Director
Center of Neutron Science, JAERI
Tokai-mura, Naka-gun, Ibaraki-ken 319-1195
Tel: +81 29 282 6151
Fax: +81 29 282 5996
Eml:takano@cens.tokai.jaeri.go.jp

TANIGAKI, Minoru
Research Reactor Institute
Kyoto University
2-1010 Asashiro-nishi
Kumatori-cho, Sennan-gun
Tel: +81 724 51 2476
Fax: +81 724 51 2620
Eml:tanigaki@rri.kyoto-u.ac.jp

KOREA (REPUBLIC OF)

BAE, Young-Soon
POSTECH
San 31, Hyoja-Dong
Namgu, POHANG 790-784
Tel: +82 54 279 1136
Fax:
Eml:ysbae7@postech.ac.kr

CHA, Jae-Eun
HYPER Team, KAERI
P.O. BOX 105
Yuseong, DAEJEON 305-600
Tel: +82 42 868 2065
Fax: +82 42 868 2080
Eml:jecha@kaeri.re.kr

CHAI, Jong-Seo
KIRAMS
215-4 Gongneung-Dong
Nowon-Ku, SEOUL 139-709
Tel: +82 11 9132 2239
Fax:
Eml:jschai@kcch.re.kr

CHANG, In-Soon
President, KAERI
150 Duckjin-Dong
Yuseong, DAEJEON 305-353
Tel: +82 42 868 82 46
Fax: +82 42 861 75 21
Eml:ischang@kaeri.re.kr

CHO, Chung-Ho
KAERI
P.O. Box 105
Yuseong, DAEJEON 305-600
Tel: +82 42 868 2914
Fax: +82 42 868 2080
Eml:ex-chcho@kaeri.re.kr

CHO, Yong-Sub
KAERI
P.O. Box 105
Yuseong, DAEJEON 305-600
Tel: +82 42 868 2975
Fax:
Eml:choys@kaeri.re.kr

CHOE, Wonho
KAIST
373-1 Kusong-Dong
Yuseong, DAEJEON 305-701
Tel: +82 42 869 2539
Fax:
Eml: wcho@kaist.ac.kr

CHOI, Byung-Ho
KAERI
150 Duckjin-Dong
Yuseong, DAEJEON 305-353
Tel: +82 02 2299 1732
Fax:
Eml: bhchoi@kaeri.re.kr

CHOI, Han-Woo
KIGAM
30 Gajeong-Dong
Yuseong, DAEJEON 305-350
Tel: +82 42 868 3664
Fax:
Eml: starlove@kigam.re.kr

CHOI, M.
KISTI
52 Eoeun-Dong
Yuseong, DAEJEON 305-353
Tel: +82 11 9902 9619
Fax:
Eml: mcho@reseat.re.kr

GIL, Choong-Sup
Nuclear Engineering Dept., KAERI
P.O. Box 105
Yuseong, DAEJEON 305-600
Tel: +82 42 868 8104
Fax: +82 42 868 8103
Eml: csgil@kaeri.re.kr

GWON, Saang-Won
Ministry of Science & Technology (MOST)
Government Complex
Gwacheon City, Gyeonggi-Do 427-715
Tel: +82 2 503 7651
Fax:
Eml: swgwon@most.go.kr

JANG, Ji-Ho
KAERI
150 Duckjin-Dong
Yuseong, DAEJEON 305-353
Tel: +82 42 868 8952
Fax:
Eml: jangjh@kaeri.re.kr

JOO, Po-Kook
Project Manager
Ind. Technology Coop. Grp., KAERI
P.O. BOX 105
Yuseong, DEAJEON 305-600
Tel: +82 42 868 82 73
Fax: +82 42 861 11 84
Eml:

JUNG, Il-Lae
KAERI
150 Duckjin-Dong
Yuseong, DAEJEON 305-353
Tel: +82 42 868 8036
Fax:
Eml: ex-jil714@kaeri.re.kr

JUNG, Ki-Jung
Director
Planning Division, KAERI
P.O. Box 105
Yuseong, DAEJEON 305-600
Tel: +82 42 868 2060
Fax: +82 42 861 1015
Eml: kjjung@kaeri.re.kr

JUNG, Y.S.
RLC Networks Inc.
111-5 Eoeun-Dong
Yuseong, DAEJEON 305-807
Tel: +82 42 365 2115
Fax:
Eml:yssystems@hanmir.com

KIM, Bo-Young
KAERI
P.O. Box 105
Yuseong, DEAJEON 305-600
Tel: +82 42 868 2998
Fax:
Eml:ex-midas@kaeri.re.kr

KIM, Do-Heon
Nuclear Data Evaluation Laboratory
KAERI
P.O. Box 105
Yuseong, DAEJEON 305-600
Tel: +82 42 868 8651
Fax: +82 42 868 2636
Eml:kimdh@kaeri.re.kr

KIM, Hee-Soo
Dankook University
147 Hannam-Dong
Hougsan, SEOUL 140-714
Tel: +82 02 995 2974
Fax:
Eml:kong010@hotmail.com

KIM, Hyung-Duk
KAERI
150 Duckjin-Dong
Yuseong, DAEJEON 305-353
Tel: +82 42 868 8133
Fax:
Eml:ex-hdgim@kaeri.re.kr

KIM, In-Gyu
KAERI
P.O. Box 105
Yuseong, DAEJEON 305-600
Tel: +82 42 868 8031
Fax:
Eml:igkim@kaeri.re.kr

KIM, Jae-Keun
KAERI
P.O. Box 105
Yuseong, DAEJEON 305-600
Tel:
Fax:
Eml:ex-kjg@kaeri.re.kr

KIM, Jaehang
KIRAMS
215-4 Gongneung-Dong
Nowon, SEOUL 139-709
Tel: +82 2 970 1357
Fax:
Eml:jhkim68@kcch.re.kr

KIM, Joonkon
KIGAM
30 Gajeong-Dong
Yuseong, DAEJEON 305-350
Tel: +82 42 868 3663
Fax:
Eml:kimacc@kigam.re.kr

KIM, Jun-Yeon
KAERI
P.O. Box 105
Yuseong, DAEJEON 305-600
Tel:
Fax:
Eml:jykim2@kaeri.re.kr

KIM, K.P.
KAERI
P.O. Box 105
Yuseong, DEAJEON 305-600
Tel: +82 42 868 2747
Fax:
Eml:KPKIM@kaeri.re.kr

KIM, Kye-Ryung
KAERI
P.O. Box 105
Yuseong, DAEJEON 305-600
Tel: +82 42 868 8602
Fax:
Eml:kimkr@kaeri.re.kr

KIM, Mi-Hye
KAERI
150 Duckjin-Dong
Yuseong, DAEJEON 305-353
Tel: +82 42 868 2836
Fax:
Eml:ex-namihy@kaeri.re.kr

KIM, Seong-Yun
KAERI
150 Duckjin-Dong
Yuseong, DAEJEON 305-353
Tel: +82 42 868 2126
Fax: +82 42 861 8292
Eml:sykim@kaeri.re.kr

KIM, Yonghee
KAERI
P.O. Box 105
Yuseong, DAEJEON 305-600
Tel: +82 42 868 2067
Fax:
Eml:yhkim@kaeri.re.kr

KIM, Yong-Hwan
KAERI
P.O. Box 105
Yuseong, DAEJEON 305-600
Tel:
Fax:
Eml:ex-yhkim@kaeri.re.kr

KIM, Yong-Nam
Department of Nuclear Engineering
Hanyang University
17 Haengdang-Dong
Sungdong, SEOUL 133-791
Tel: +82 02 2299 1732
Fax:
Eml:captin@nural.hanyang.ac.kr

KIM, Yu-Seok
KAERI
P.O. Box 105
Yuseong, DAEJEON 305-600
Tel: +82 02 970 1364
Fax:
Eml:unison@kcch.re.kr

KOH, S.K.
Ulsan University
San 29, Muger 2-Dong
ULSAN 680-749
Tel: +82 52 259 2321
Fax:
Eml:skkoh@ulsan.ac.kr

KONG, Young-Jo
Dankook University
147 Hannam-Dong
Hougsan, SEOUL 140-714
Tel: +82 02 995 29 74
Fax:
Eml:0010k@hanmail.net

KWON, Hyeok-Jung
KAERI
P.O. Box 105
Yuseong, DAEJEON 305-600
Tel: +82 42 868 86 65
Fax:
Eml:hjkwon@kaeri.re.kr

KWON, Hyuk-Il
KAERI
P.O. Box 105
Yuseong, DAEJEON 305-600
Tel: +82 42 868 28 10
Fax:
Eml:hikwon@kaeri.re.kr

LEE, Bong-Sang
KAERI
P.O. Box 105
Yuseong, DAEJEON 305-600
Tel: +82 42 868 29 71
Fax: +82 42 868 20 80
Eml:ex-lbs@kaeri.re.kr

LEE, Chan-Young
KAERI
P.O. Box 105
Yuseong, DAEJEON 305-600
Tel: +82 42 868 89 53
Fax:
Eml:ex-ley@kaeri.re.kr

LEE, Hwa-Ryun
KAERI
150 Duckjin-Dong
Yuseong, DAEJEON 305-353
Tel: +82 42 868 28 81
Fax:
Eml:ex-hrlee@kaeri.re.kr

LEE, Jae-Hyung
KAERI
P.O. Box 105
Yuseong, DAEJEON 305-600
Tel: +82 42 868 29 11
Fax:
Eml:jhlee3@kaeri.re.kr

LEE, Jae-Sang
KAERI
P.O. Box 105
Yuseong, DAEJEON 305-600
Tel: +82 42 868 27 94
Fax:
Eml:jslee8@kaeri.re.kr

LEE, Il-Soo
First Secretary
Delegation of the Rep. of Korea to OECD
2-4, rue Louis David
75782 PARIS CEDEX 16
Tel: +33 1 44 05 24 10
Fax: +33 1 47 55 86 70
Eml:islee@most.go.kr

LEE, Sang-Hee
KAERI
P.O. Box 105
Yuseong, DAEJEON 305-600
Tel: +82 42 868 87 34
Fax:
Eml:ex-leesh@kaeri.re.kr

LEE, Seok-Kwan
Dankook University
147 Hannam-Dong
Hougsan, SEOUL 140-714
Tel: +82 02 792 60 81
Fax:
Eml:Vodcall@lycos.co.kr

LEE, Seok-Ki
KAERI
P.O. Box 105
Yuseong, DAEJEON 305-600

Tel: +82 42 868 87 40
Fax:
Eml:ex-sklee@kaeri.re.kr

LEE, Seung-Hyun
KAERI
P.O. Box 105
Yuseong, DAEJEON 305-600

Tel: +82 42 868 87 41
Fax:
Eml:

LEE, Soo-Yeon
KAERI
P.O. Box 105
Yuseong, DAEJEON 305-600

Tel: +82 42 868 22 80
Fax:
Eml:ex-syli22@kaeri.re.kr

LEE, Young-Il
KAERI
P.O. Box 105
Yuseong, DAEJEON 305-600

Tel: +82 41 857 56 55
Fax:
Eml:Mutanty@korea.com

MIN, Kyoung-Wook
KAIST
373-1 Kusong-Dong
Yuseong, DAEJEON 305-701

Tel: +82 42 869 25 25
Fax:
Eml:kwmin@space.kaist.ac.kr

NAM, J.W.
KAERI
P.O. Box 105
Yuseong, DAEJEON 305-600

Tel: +82 42 868 89 58
Fax:
Eml:ex-jwnam@kaeri.re.kr

NO, Yong-Oh
KAERI
P.O. Box 105
Yuseong, DAEJEON 305-600

Tel:
Fax:
Eml:ex-siren746@kaeri.re.kr

NOH, Seung-Jung
Dankook University
147 Hannam-Dong
Hougsan, SEOUL 140-714

Tel:
Fax:
Eml:snjoj@dankook.ac.kr

PARK, Jae-Won
Proton Engineer Frontier Project
KAERI
150 Duckjin-Dong
Yuseong, DAEJEON 305-353

Tel: +82 868 29 70
Fax: +82 868 81 31
Eml:ex-pjw@kaeri.re.kr

PARK, Mi-Young
KAERI
P.O. Box 105
Yuseong, DAEJEON 305-600

Tel: +82 42 868 89 52
Fax:
Eml:ex-mypark@kaeri.re.kr

PARK, Mum-Sik
KAERI
P.O. Box 105
Yuseong, DAEJEON 305-600
Tel: +82 42 868 28 82
Fax:
Eml:ex-bspark@kaeri.re.kr

PARK, Won-Seok
Head of Project Operation Team
Nuclear Hydrogen Prod. Project, KAERI
P.O. Box 105
Yuseong, DAEJEON 305-600
Tel: +82 42 868 83 75
Fax: +82 42 868 20 80
Eml:wonpark@kaeri.re.kr

SANG, Hyo-Han
KAERI
P.O. Box 105
Yuseong, DAEJEON 305-600
Tel: +82 42 868 27 16
Fax:
Eml:twios96@hananet.net

SEOL, Kyung-Tae
KAERI
P.O. Box 105
Yuseong, DAEJEON 305-600
Tel: +82 02 970 13 64
Fax:
Eml:unison@kcch.re.kr

SHIM, Chan-Bo
KAERI
P.O. Box 105
Yuseong, DAEJEON 305-600
Tel:
Fax:
Eml:ex-ldshim@kaeri.re.kr

SHIN, Min-Jae
KAERI
P.O. Box 105
Yuseong, DAEJEON 305-600
Tel:
Fax:
Eml:ex-mjshin@kaeri.re.kr

SHIN, Uncheol
KIPO, Government Complex – Daejeon
Dunsan-Dong
Seo-Gu, DAEJEON 302-701
Tel: +82 19 406 14 55
Fax:
Eml:sinuc1@kipo.go.kr

SOHN, Chang-Won
KAERI
P.O. Box 105
Yuseong, DAEJEON 305-600
Tel: +82 42 868 29 98
Fax:
Eml:ex-cwsohn@kaeri.re.kr

SONG, Tae-Yung
KAERI
P.O. Box 105
Yuseong, DAEJEON 305-600
Tel: +82 42 868 89 24
Fax: +82 42 868 20 80
Eml:tysong@kaeri.re.kr

SONG, Young-Ki
KAERI
P.O. Box 105
Yuseong, DAEJEON 305-600
Tel: +82 42 868 85 92
Fax:
Eml:ygsong@kaeri.re.kr

YANG, D.Y.
Kepco
58-2 Sungsan-Dong
Mapo, SEOUL 121-250
Tel: +82 2 332 60 11
Fax:
Eml:kepyang@prosyscon.co.kr

YANG, Maeng-Ho
KAERI
P.O. Box 105
Yuseong, DAEJEON 305-600
Tel: +82 42 868 21 50
Fax:
Eml:mhyang@kaeri.re.kr

YOO, Ki-Suk
Pro-System
58-2 Sungsan-Dong
Mapo, SEOUL 121-250
Tel: +82 2 332 60 11
Fax:
Eml:ksyoo111@yahoo.co.kr

YOON, Dae-Soo
Director-General
Ministry of Science & Technology (MOST)
Government Complex – Gwacheon
Gwacheon City, Gyeonggi-Do 427-715
Tel:
Fax:
Eml:

RUSSIAN FEDERATION

DEGTYAREV, Alexey M.
Head of Laboratory
RRC Kurchatov Institute
Nuclear Safety Institute
Kurchatov Sq. 1
MOSCOW 123182
Tel: +7 095 196 9530
Fax: +7 095 196 7270
Eml:amd@nsi.kiae.ru

PONOMAREV, Leonid
RCC MUCATEX
ul. Rogova 9-2
MOSCOW 123098
Tel: +7 095 947 2772
Fax: +7 095 947 2787
Eml:mucatex.leonid@g23.relcom.ru

SHUMAKOV, Igor
Head of Linear Accelerator Department
Moscow Radiotechnical Institute (MRTI)
Warshawskoe shosse, 132
MOSCOW 117519
Tel: +7 095 315 6313
Fax: +7 095 314 1053
Eml:ishumakov@mtu-net.ru

SWEDEN

GUDOWSKI, Waclaw
Nuclear and Reactor Physics
Royal Institute of Technology
Center for Physics, Astronomy and Biotech
Roslagstullsbacken 21
S-106 91 STOCKHOLM
Tel: +46 8 5537 82 00/73 656 0887
Fax: +46 8 5537 84 65
Eml:wacek@neutron.kth.se

SWITZERLAND

CODDINGTON, Paul
Lab. for Reactor Physics & System Behaviour
Paul Scherrer Institute
CH-5232 VILLIGEN – PSI
Tel: +41 56 310 27 38
Fax: +41 56 310 23 27
Eml: Paul.Coddington@psi.ch

GROESCHEL, Friederich
Alternate TG Metal Member
Head Sect. Str. Mat. & Corrosion
Paul Scherrer Institute, WHGA/246
CH-5232 VILLIGEN – PSI
Tel: +41 56 310 21 96
Fax: +41 56 310 31 31
Eml: friedrich.groeschel@psi.ch

SCHMELZBACH, Pierre A.
Head of the Accelerator Division
Paul Scherrer Institute, WBGA/C22
CH-5232 VILLIGEN – PSI
Tel: +41 56 310 40 73
Fax: +41 56 310 33 83
Eml: Pierre.Schmelzbach@psi.ch

SIGG, Peter
Head, RF Section
Paul Scherrer Institute, WLGA/C25
CH-5232 VILLIGEN – PSI
Tel: +41 56 310 32 34
Fax: +41 56 310 32 94
Eml: peter.sigg@psi.ch

UNITED STATES OF AMERICA

CHO, Yanglai
Argonne National Laboratory
9700 S. Cass Ave.
Argonne, IL 60439
Tel: +1 630 252 6616
Fax:
Eml: yc@aps.anl.gov

HENDERSON, Stuart D.
Accelerator Physics Group Leader
Spallation Neutron Source Project
701 Scarboro Road
Oak Ridge, TN 37830
Tel: +1 865 241 6794
Fax: +1 865 574 6617
Eml: shenderson@sns.gov

SHEFFIELD, Richard
Los Alamos National Laboratory
LANSCE-DO, MS H851
Los Alamos, NM 87545
Tel: +1 505 667 1237
Fax: +1 505 667 7443
Eml: sheff@lanl.gov

INTERNATIONAL ORGANISATIONS

BHATNAGAR, Ved
European Commission
Nuclear Fission & Radiation Protection
DGRTD J.4, CDMA 1/46
B-1049 BRUSSELS
Tel: +32 2 299 58 96
Fax: +32 2 299 49 91
Eml: Ved.Bhatnagar@cec.eu.int

MARCUS, Gail H.
Deputy Director-General
OECD Nuclear Energy Agency
12 boulevard des Iles
F-92130 ISSY-LES-MOULINEAUX

Tel: +33 1 45 24 10 02
Fax: +33 1 45 24 11 10
Eml:gail.marcus@oecd.org

NA, Byung Chan
OECD Nuclear Energy Agency, Data Bank
12 boulevard des Iles
F-92130 ISSY-LES-MOULINEAUX

Tel: +33 1 45 24 10 91
Fax: +33 1 45 24 11 28
Eml:na@nea.fr

OECD PUBLICATIONS, 2, rue André-Pascal, 75775 PARIS CEDEX 16

PRINTED IN FRANCE

(66 2005 15 1) – No. 54409 2005

OECD, 1999.

Software: 1987-1996, Acrobat is a trademark of ADOBE.

All rights reserved. OECD grants you the right to use one copy of this Program for your personal use only. Unauthorised reproduction, lending, hiring, transmission or distribution of any data or software is prohibited. You must treat the Program and associated materials and any elements thereof like any other copyrighted material.

All requests should be made to:

Head of Publications Service,
OECD Publications Service,
2, rue André-Pascal, 75775 Paris
Cedex 16, France.

OCDE, 1999

Logiciel, 1987-1996, Acrobat, marque déposée d'ADOBE.

Tous droits du producteur et du propriétaire de ce produit sont réservés. L'OCDE autorise la reproduction d'un seul exemplaire de ce programme pour usage personnel et non commercial uniquement. Sauf autorisation, la duplication, la location, le prêt, l'utilisation de ce produit pour exécution publique sont interdits. Ce programme, les données y afférantes et d'autres éléments doivent donc être traités comme toute autre documentation sur laquelle s'exerce la protection par le droit d'auteur.

Les demandes sont à adresser au :

Chef du Service des Publications,
Service des Publications de l'OCDE,
2, rue André-Pascal,
75775 Paris Cedex 16, France.